

Particle Size Measurement

Volume 1

Powder sampling and particle size
measurement

Fifth edition

TERENCE ALLEN

*Formerly Senior Consultant
E.I. Dupont de Nemour and Company
Wilmington, Delaware, USA*



CHAPMAN & HALL

London · Weinheim · New York · Tokyo · Melbourne · Madras

Chapman & Hall, 2-6 Boundary Row, London SE1 8HN, UK

Chapman & Hall GmbH, Pappelallee 3, 69469 Weinheim, Germany

Chapman & Hall USA, 115 Fifth Avenue, New York, NY 10003, USA

Chapman & Hall Japan, ITP-Japan, Kyowa Building, 3F, 2-2-1 Hirakawacho,
Chiyoda-ku, Tokyo 102, Japan

Chapman & Hall Australia, 102 Dodds Street, South Melbourne, Victoria 3205,
Australia

Chapman & Hall India, R. Seshadri, 32 Second Main Road, CIT East, Madras 600 035,
India

First edition 1968

Second edition 1975

Third edition 1981

Fourth edition 1990

Fifth edition 1997

© 1968, 1975, 1981, 1990, 1997 T. Allen

Printed in Great Britain at T.J. Press (Padstow) Ltd., Padstow, Cornwall

ISBN 0 412 72950 4

0 412 75350 2 (2 volume set)

Apart from any fair dealing for the purposes of research or private study, or criticism or review, as permitted under the UK Copyright Designs and Patents Act, 1988, this publication may not be reproduced, stored, or transmitted, in any form or by any means, without the prior permission in writing of the publishers, or in the case of reprographic reproduction only in accordance with the terms of the licences issued by the Copyright Licensing Agency in the UK, or in accordance with the terms of licences issued by the appropriate Reproduction Rights Organization outside the UK. Enquiries concerning reproduction outside the terms stated here should be sent to the publishers at the London address printed on this page.

The publisher makes no representation, express or implied, with regard to the accuracy of the information contained in this book and cannot accept any legal responsibility or liability for any errors or omissions that may be made.

A catalogue record for this book is available from the British Library

Library of Congress Catalog Card number: 96-86676



Printed on permanent acid-free text paper, manufactured in accordance with
ANSI/NISO Z39.48-1992 and ANSI/NISO Z39.48-1984 (Permanence of Paper).

Powder Technology Series

EDITED BY

BRIAN SCARLETT and
Delft University of Technology
The Netherlands

GENJI JIMBO
Chubu Powtech Plaza Lab
Japan

Many materials exist in the form of a disperse system, for example powders, pastes, slurries, emulsions and aerosols. The study of such systems necessarily arises in many technologies but may alternatively be regarded as a separate subject which is concerned with the manufacture, characterization and manipulation of such systems. Chapman & Hall were one of the first publishers to recognize the basic importance of the subject, going on to instigate this series of books. The series does not aspire to define and confine the subject without duplication, but rather to provide a good home for any book which has a contribution to make to the record of both the theory and the application of the subject. We hope that all engineers and scientists who concern themselves with disperse systems will use these books and that those who become expert will contribute further to the series.

Chemistry of Powder Production

Yasuo Arai
Hardback (0 412 39540 1), 292 pages

Particle Size Analysis

Claus Bernhardt
Translated by H. Finken
Hardback (0 412 55880 7), 428 pages

Particle Classification

K. Heiskanen
Hardback (0 412 49300 4), 330 pages

Powder Surface Area and Porosity

S. Lowell and Joan E. Shields
3rd edn, hardback (0 412 39690 4), 256 pages

Pneumatic Conveying of Solids

R.D. Marcus, L.S. Leung, G.E. Klinzing and F. Rizk
Hardback (0 412 21490 3), 592 pages

Principles of Flow in Disperse Systems

O. Molerus
Hardback (0 412 40630 6), 314 pages

Particle Technology

Hans Rumpf
Translated by F.A. Bull
Hardback (0 412 35230 3), 216 pages

Processing of Particulate Solids

J.P.K. Seville, U. Tuzan and R. Clift
Hardback (0 751 40376 8), 384 pages

Contents

Acknowledgements	xv
Preface to the the fifth edition	xvii
Preface to the the first edition	xix
Editor's foreword	xxi
1 Powder sampling	1
1.1 Introduction	1
1.2 Sample selection	2
1.3 Sampling stored material	4
1.3.1 Sampling stored non-flowing material	5
1.3.2 Sampling stored free-flowing material	7
1.4 Sampling flowing streams	8
1.4.1 Sampling from a conveyor belt	9
1.4.2 Point samplers	10
1.4.3 Sampling from falling streams	12
1.4.4 Stream sampling ladles	13
1.4.5 Traversing cutters	14
1.4.6 Sampling dusty material	16
1.4.7 Moving flap sampler	17
1.5 Sample reduction	19
1.5.1 Scoop sampling	19
1.5.2 Cone and quartering	20
1.5.3 Table sampling	20
1.5.4 Chute splitting	22
1.5.5 The rotary sample divider	23
1.5.6 Miscellaneous sampling devices	23
1.6 Slurry sampling	24
1.7 Reduction of laboratory sample to measurement sample	27
1.8 Number of samples required	28
1.9 Theoretical statistical errors on a number basis	31
1.10 Practical statistical errors on a number basis	33
1.11 Theoretical statistical errors on a weight basis	35
1.12 Practical statistical errors on a weight basis	36
1.13 Experimental tests of sampling techniques	37
1.14 Weight of sample required	38
1.14.1 Gross sample	38
1.14.2 Sampling by increments	40

2	Data presentation and interpretation	44
2.1	Introduction	44
2.2	Particle size	45
2.3	Average diameters	50
2.4	Particle dispersion	54
2.5	Particle shape	54
	2.5.1 Shape coefficients	55
	2.5.2 Shape factors	56
	2.5.3 Shape regeneration by Fourier analysis	58
	2.5.4 Fractal dimensions characterization of textured surfaces	59
	2.5.5 Other methods of shape analysis	62
	2.5.6 Sorting by shape	62
2.6	Determination of specific surface from size distribution data	62
	2.6.1 from a number count	63
	2.6.2 from a surface count	63
	2.6.3 from a volume (mass) count	64
2.7	Tabular presentation of particle size distribution	65
2.8	Graphical presentation of size distribution data	68
	2.8.1 Presentation on linear graph paper	68
2.9	Standard forms of distribution functions	69
2.10	Arithmetic normal distribution	69
	2.10.1 Manipulation of the normal equation	71
2.11	The log-normal distribution	72
	2.11.1 Relationship between number mean sizes for a log-normal distribution	74
	2.11.2 Derived mean sizes	77
	2.11.3 Transformation between log-normal distributions	78
	2.11.4 Relationship between median and mode of a log-normal equation	79
	2.11.5 An improved equation and graph paper for log-normal evaluations	80
	2.11.6 Application	80
2.12	Johnson's S _B distribution	81
2.13	Rosin-Rammler, Bennet-Sperling formula	83
2.14	Other distribution laws	84
	2.14.1 Simplification of two-parameter equations	85
	2.14.2 Comments	86
2.15	The law of compensating errors	86
2.16	Evaluation of non linear distributions on log-normal paper	88
	2.16.1 Bimodal intersecting distributions	93
	2.16.2 Bimodal non-intersecting distributions	93
	2.16.3 Other distributions	94
	2.16.4 Applications of log-normal plots	94
	2.16.5 Curve fitting	94

2.17	Alternative notations for frequency distribution	98
2.17.1	Notation	98
2.17.2	Moment of a distribution	98
2.17.3	Transformation from $q_t(x)$ to $q_r(x)$.	99
2.17.4	Relation between moments	99
2.17.5	Means of distributions	100
2.17.6	Standard deviations	101
2.17.7	Coefficient of variation	102
2.17.8	Applications	102
2.17.9	Transformation of abscissae	104
2.18	Phi-notation	108
3	Particle size by image analysis	112
3.1	Introduction	112
3.2	Optical microscopy	113
3.2.1	Upper size limit	114
3.2.2	Lower size limit	114
3.3	Sample preparation	115
3.4	Measurement of plane sections through packed beds	117
3.5	Particle size	117
3.6	Calibration	118
3.6.1	Linear eyepiece graticules	118
3.6.2	Globe and circle graticules	120
3.7	Training of operators	120
3.8	Experimental techniques	121
3.9	Determination of particle size distribution by number	122
3.10	Conditions governing a weight size determination	124
3.10.1	Illustrative example of the calculation of a size distribution by weight	125
3.11	Quantitative image analysis	128
3.11.1	Calibration of image analyzers	128
3.11.2	Experimental procedures	128
3.11.3	Commercial quantitative image analysis systems.	137
3.11.4	On-line microscopy	140
3.12	Electron microscopy	140
3.13	Transmission electron microscopy	141
3.13.1	Specimen preparation for TEM	142
3.13.2	Replica and shadowing techniques	145
3.13.3	Chemical analysis	145
3.14	Scanning electron microscopy	146
3.15	Other scanning electron microscopy techniques	148
3.16	Errors involved in converting a number to a volume count	148
4	Particle size analysis by sieving	156
4.1	Introduction	156
4.2	Woven-wire and punched plate sieves	158
4.3	Electroformed micromesh sieves	159

4.2	Woven-wire and punched plate sieves	158
4.3	Electroformed micromesh sieves	159
4.4	Standard sieves	162
4.5	Mathematical analysis of the sieving process	163
4.6	Calibration of sieves	167
4.7	Sieving errors	169
4.8	Methods of sieving	171
4.9	Amount of sample	172
4.10	Hand sieving	172
4.11	Machine sieving	175
4.12	Wet sieving	176
4.12.1	Manual	176
4.12.2	Wet sieving by machine	177
4.13	Air-Jet sieving	178
4.14	The Sonic Sifter	180
4.15	The Seishin Robot Sifter	181
4.16	Automatic systems	181
4.16.1	The Gradex particle size analyzer	181
4.16.2	Labcon automatic sieve system	182
4.17	Ultrasonic sieving	182
4.18	The sieve cascadograph	182
4.19	Felvation	183
4.20	Self organized sieves (SORSI)	184
4.21	Shape separation	185
4.22	Correlation with light scattering data	185
4.23	Conclusions	186
5	Fluid classification	190
5.1	Introduction	190
5.2	Assessment of classifier efficiency	190
5.3	Systems	197
5.4	Counter-flow equilibrium classifiers in a gravitational field-elutriators	198
5.5	Cross-flow gravitational classification	200
5.5.1	The Warmain Cyclosizer	200
5.5.2	The Humboldt particle size analyzer TDS	201
5.6	Counter-flow centrifugal classifiers	201
5.7	Cross-flow centrifugal classifiers	202
5.8	Zig-zag classifiers	202
5.9	Cross-flow elbow classifier	202
5.10	Fractionation methods for particle size measurement	202
5.11	Hydrodynamic chromatography	203
5.12	Capillary hydrodynamic fractionation	206
5.13	Capillary zone electrophoresis	207
5.14	Size exclusion chromatography	208
5.15	Field flow fractionation	208
5.15.1	Sedimentation field flow fractionation	209

5.15.2	Time-delayed-exponential SF3	211
5.15.3	Thermal field flow fractionation	213
5.15.4	Magnetic field flow fractionation	213
5.15.5	Flow field flow fractionation	213
5.15.6	Steric field flow fractionation	214
5.16	The Matec electro-acoustic system EAS-8000	215
5.17	Continuous SPLIT fractionation	215
5.18	Classification by decantation	216
6	Interaction between fluids and particles	223
6.1	Introduction	223
6.2	Settling of a single homogeneous sphere under a gravitational force	225
6.2.1	Relationship between settling velocity and particle size	225
6.2.2	Calculation of particle size in the laminar flow region	227
6.3	Size limits for gravity sedimentation	228
6.3.1	Upper size limit	228
6.3.2	Lower size limit	229
6.4	Time for terminal velocity to be attained	232
6.5	Wall effects	234
6.6	Errors due to discontinuity of the fluid	235
6.7	Viscosity of a suspension	236
6.8	Non-rigid spheres	236
6.9	Non-spherical particles	237
6.9.1	Stokes region	237
6.9.2	Transition region	240
6.10	Relationship between drag coefficient and Reynolds number in the transition region	242
6.11	The turbulent flow region	245
6.12	Concentration effects	246
6.13	Hindered settling	251
6.13.1	Low concentration effects	251
6.13.2	High concentration effects	252
6.14	Electro-viscosity	254
6.15	Dispersion of powders	255
6.15.1	Dry powder dispersion	255
6.15.2	The use of glidants to improve flowability of dry powders	256
6.15.3	Wet powder dispersion	256
6.15.4	Role of dispersing agents	257
6.15.5	Wetting a powder	257
6.15.6	Determination of contact angle (θ)	259
6.15.7	Deagglomerating wetted clumps	260
6.15.8	Suspension stability	260
6.15.9	Tests of dispersion quality	262

7	Sedimentation theory	269
7.1	Powder density	269
7.2	Liquid viscosity	271
7.3	Resolution of sedimenting suspensions	272
7.4	Concentration changes in a suspension settling under gravity	273
7.5	Relationship between density gradient and concentration	274
7.5.1	Hydrometers	275
7.6	Theory for the gravity photosedimentation technique	277
7.6.1	The Beer-Lambert law	277
7.6.2	The extinction coefficient	280
7.7	Theory for concentration determination with the x-ray gravitational sedimentation technique	281
7.8	Theory for mass oversize distribution determination for cumulative, homogeneous, gravitational sedimentation	281
7.9	Stokes equation for centrifugal sedimentation	283
7.9.1	General theory	283
7.10	Stokes diameter determination for cumulative and incremental line-start techniques	284
7.10.1	Incremental, line-start, centrifugal technique	284
7.10.2	Homogeneous, cumulative, centrifugal technique	284
7.10.3	Sedimentation distance small compared with distance from centrifuge axis	284
7.11	Line-start technique using a photocentrifuge	285
7.11.1	Introduction	285
7.11.2	Homogeneous mode	285
7.11.3	Line-start mode	285
7.12	Theory for mass oversize distribution determination for cumulative, homogeneous, centrifugal sedimentation	287
7.13	Theory for mass oversize distribution determination for incremental, homogeneous, centrifugal sedimentation	289
7.13.1	General theory	289
7.13.2	Variable time method	290
7.13.3	Variable inner radius (pipette withdrawal)	295
7.13.4	Variable measurement radius (scanning x-ray centrifuge)	297
8	Sedimentation methods of particle size measurement	300
8.1	Introduction	300
8.2	Homogeneous incremental gravitational sedimentation	304
8.2.1	The pipette method of Andreasen	304
8.2.2	The photosedimentation technique	306
8.2.3	X-ray sedimentation	308
8.2.4	Hydrometers and divers	309
8.3	Homogeneous cumulative gravitational sedimentation	310

8.3.1	Introduction	310
8.3.2	Balances	311
8.3.3	Sedimentation columns	312
8.4	Line-start incremental gravitational sedimentation	312
8.4.1	Photosedimentation	312
8.5	Line-start cumulative gravitational sedimentation	312
8.5.1	Introduction	312
8.5.2	Methods	312
8.6	Homogeneous incremental centrifugal sedimentation	313
8.6.1	Introduction	313
8.6.2	The Simcar pipette disc centrifuge	314
8.6.3	The Ladal pipette disc centrifuge	314
8.6.4	The Ladal x-ray disc centrifuge	314
8.6.5	The Du Pont/Brookhaven scanning x-ray disc centrifugal sedimentometer (BI-XDC)	315
8.6.6	The BI-DCP disc (photo)centrifuge	317
8.7	Cuvet photocentrifuges	317
8.8	Homogeneous cumulative centrifugal sedimentation	318
8.8.1	Methods	318
8.9	Line-start incremental centrifugal sedimentation	320
8.9.1	Disc photocentrifuges	320
8.10	Line-start cumulative centrifugal sedimentation	322
8.10.1	MSA analyzer	322
8.11	Particle size analysis using non-invasive dielectric sensors	323
8.12	Conclusions	323
9	Stream scanning methods of particle size measurement	327
9.1	Introduction	327
9.2	The electrical sensing zone method (The Coulter Principle)	329
9.2.1	Introduction	329
9.2.2	Operating principle	330
9.2.3	Theory for the electrical sensing zone method	331
9.2.4	Effect of particle shape and orientation	334
9.2.5	Pulse shape	334
9.2.6	Effect of coincidence	335
9.2.7	Multiple aperture method for powders having a wide size range	338
9.2.8	Calibration	339
9.2.9	Carrying out a mass balance	339
9.2.10	Oversize counts on a mass basis using the Coulter Counter	341
9.2.11	Apparatus	342
9.2.12	Limitations of the method	344
9.2.13	Coulter Multisizer mass balance calculation for BCR 70 standard quartz powder	345
9.3	Fiber length analysis	349

9.4	Optical particle counters	350
9.4.1	Aerometrics Eclipse particle size analyzer	354
9.4.2	Hiac/Royco	354
9.4.3	Kratel Partascope	356
9.4.4	Kratel Partograph	356
9.4.5	Climet	356
9.4.6	Particle Measuring Systems	358
9.4.7	Flowvision	360
9.4.8	Polytec HC (high concentration optical counter)	361
9.4.9	Lasentec	362
9.4.10	Galai CIS	363
9.4.11	Spectrex Prototron	364
9.4.12	Spectrex PCT-1 laser particle counter	365
9.4.13	Procedyne	365
9.4.14	Kane May	366
9.4.15	Met One	368
9.4.16	Erdco acoustical counter	368
9.4.17	Micro Pure Systems acoustic particle monitors (Monitek)	368
9.4.18	Rion laser based liquidborne particle counter	369
9.4.19	Faley Status 8000	369
9.4.20	Kowa Nanolyzer™ PC-30 and PC-500	369
9.4.21	Malvern Autocounters	370
9.4.22	Particle Sizing Systems Accusizer™ 770	370
9.4.23	AWK electronic sieve analyzer	371
9.4.24	PMT universal size distribution measuring systems	371
9.4.25	Canty Vision System	371
9.4.26	Contamination Control Systems	373
9.5	Aerodynamic time-of flight measurement	373
9.5.1	Amherst API Aerosizer	373
9.5.2	The TSI Aerodynamic Particle Sizer APS 33B	373
9.6	Laser phase/Doppler principle	374
9.6.1	BIRAL PD-Lisatek and L2F	375
9.6.2	Hosokawa Mikropul E-Spart Analyzer	375
9.6.3	Aerometrics phase/Doppler particle analyzer (APDPA)	377
9.6.4	Dantec Particle Dynamic Analyzer	378
9.7	Interferometers	378
9.7.1	The TSI Liquitrak™ interferometer	379
9.8	Flow ultramicroscope	380
9.8.1	ISPA image analysis system	381
9.9	Measurement of the size distribution of drops in dispersions	381
9.10	Dupont electrolytic grain size analyzer	383
9.11	TSI condensation particle counter	383
9.12	TSI diffusion battery	383

9.13	TSI diffusional particle sizer	384
9.14	Differential mobility analyzer (DMA)	384
9.15	Scanning mobility particle sizer (SMPS)	385
9.16	Atmospheric particle counters	386
10	Field scanning methods of particle size measurement	392
10.1	Introduction	392
10.2	Effect of comminution on particle size distribution	393
10.3	Single point analyzers	395
	10.3.1 Static noise measurement	395
	10.3.2 Ultrasonic attenuation.	395
	10.3.3 β -ray attenuation	396
	10.3.4 X-ray attenuation and fluorescence	396
	10.3.5 Counter-flow classifiers	398
	10.3.6 Hydrocyclones	399
	10.3.7 The cyclosensor	400
	10.3.8 Automatic sieving machines	401
	10.3.9 Gas flow permeametry	403
	10.3.10 Correlation techniques	404
10.4	Low angle laser light scattering (LALLS)	404
	10.4.1 Introduction	404
	10.4.2 Theoretical basis for LALLS instruments	406
	10.4.3 Commercial instruments	411
10.5	Optical incoherent space frequency analysis	419
10.6	Small angle x-ray scattering (SAXS)	420
10.7	Ultrasonic attenuation	420
10.8	Photon correlation spectroscopy (PCS)	426
	10.8.1 Introduction	426
	10.8.2 Principles	426
	10.8.3 Through dynamic light scattering	427
	10.8.4 Particle size	428
	10.8.5 Concentration effects	429
	10.8.6 Particle interaction	429
	10.8.7 Particle size effects	430
	10.8.8 Polydispersity	430
	10.8.9 The controlled reference method	432
	10.8.10 Commercial equipment	433
	10.8.11 Discussion	436
	10.8.12 Diffusion wave spectroscopy (DWS)	436
10.9	Insitec Ensemble Particle Concentration-Size (EPCS) Systems	436
10.10	Turbo-Power Model TPO-400	439
10.11	Turbidity	439
10.12	Transient turbidity	441
10.13	Concentration monitors	441
10.14	Shape discrimination	441

11	Industrial applications of particle size measurement	449
11.1	Introduction	449
11.2	Industrial diamonds	453
11.3	Control of oversize particles	454
11.4	Starry night	457
11.5	Control of adhesive additives	459
11.6	Video-tape	461
11.7	Curve fitting	461
11.8	Effect of size distribution on filter efficiency	461
11.9	Predicting pigment gloss and hiding power	461
11.10	Strength of engineering plastics	467
11.11	Homogeneity control of ceramic paste	467
11.12	Flowability	469
11.13	Elimination of intra-lot variability by mixing	471
11.14	Mixing and segregation	472
11.15	Comminution	475
11.16	Attrition	476
11.17	Instrument evaluation	477
11.17.1	Introduction	477
11.17.2	Evaluation procedure	480
11.17.3	Definition of accuracy	480
11.17.4	Definition of reproducibility	484
11.17.5	Mean accuracy and reproducibility	486
11.17.6	Discussion	486
11.18	Summary	486
Appendix	Manufacturers and suppliers	488
Author index		503
Subject index		517

Acknowledgments

I would like to express my grateful thanks to Dr Brian H. Kaye for introducing me to the fascinating study of particle characterization. After completing a Masters degree at Nottingham Technical College under his guidance I was fortunate enough to be offered a post at the then Bradford Institute of Technology. At Bradford, Dr John C. Williams always had time for helpful advice and guidance. John became a good friend and, eventually, my PhD supervisor. After more than twenty years at what eventually became the University of Bradford, I retired from the academic life and looked for other interests. It was then I met, once more, Dr Reg Davies who had been a student with me at Nottingham. Reg was working for the DuPont Company who were in need of someone with my background and I was fortunate enough to be offered the position. In my ten years at DuPont I have seen the development of the Particle Science and Technology (PARSAT) Group under Reg's direction. It has been my privilege to have been involved in this development since I consider this group to be pre-eminent in this field. I have learnt a great deal from my thirty or so PARSAT colleagues and particularly from Reg.

My special thanks go to my colleague Dr John Boughton who gave advice on the electron microscopy section. I also wish to thank the DuPont Company for granting permission to publish the industrial applications section. Several, of these applications were work carried out by Reg and I am pleased to acknowledge his considerable contribution to this chapter.

My thanks are also due to holders of copyright for permission to publish and to many manufacturers who have given me details of their products.

Terence Allen

Hockessin, DE, USA

Powder sampling

1.1 Introduction

It is usually not feasible to characterize a bulk powder or a process stream in its entirety, so sampling is carried out to obtain samples of the bulk which are representative of the bulk in some particular property.

Whenever a powder is analyzed, whether for physical or chemical assay, the quality of the measurement depends upon how representative the sample is of the bulk from which it is drawn. The measurement may be made on a few milligrams taken from a bulk of many tonnes so the chances of measuring a non-representative sample are considerable. This results in the rejection of good product and acceptance of bad, which can strain customer loyalty. It can also result in needless expensive investigations [1].

The total error is made up of errors due to the primary sampling, subsequent sample dividing and errors in the analysis itself. Sampling is said to be accurate when it is free from bias, that is, the error of sampling is a random variable about the true mean. Sampling is precise when the error variation is small irrespective of whether the mean is the true mean or not.

Errors in particle size analysis may be due to:

- instrument limitations;
- improper procedure e.g. inadequate dispersion;
- operator errors e.g. improper instrument set-up or poor calibration;
- incorrect sampling.

Two types of sampling errors are possible [2].

- Errors due to segregation of the bulk; this depends upon the previous history of the powder and can be minimized by suitable mixing and building up a sample from a large number of increments.
- Statistical errors which cannot be prevented. Even for an ideal random mixture the quantitative distribution in samples of a given magnitude is not constant but is subject to random fluctuations. It is the only sampling error which cannot be suppressed and occurs in ideal

2 Powder sampling and particle size measurement

sampling. It can be estimated beforehand and reduced by increasing the sample size.

1.2 Sample selection

Samples are withdrawn from a population in order to *estimate* certain characteristic of that population and to establish confidence limits for that characteristic. The characteristic may be particle size, composition or quality; a measure of the spread of the distribution may also be required. The objective may be to set up limits between which the quality of a final product is acceptable or to decide whether the characteristics of a given lot meets preset criteria, or it may be to estimate the variability within a lot or between lots.

If the material comes in containers, or can be viewed as discrete units, the objective may be to estimate the number of units outside of specification. The value of the estimate is largely dependent on the sampling technique adopted. It is of little value, and could impart false information, if it is biased or imprecise.

It is usually impossible to measure the size distribution of a bulk powder and so it is necessary to carry out measurements on a sample extracted from the bulk. This sample is itself frequently too large and has to be further sub-divided. The stages, in reducing from bulk to measurement samples are:

bulk or process stream	gross sample	laboratory sample	test sample	measurement sample
(10^n kg)	(> kg)	(< kg)	(g)	(mg)

The gross sample is either one of a series of spot samples which have been extracted in order to determine the variability of the bulk or process stream with location or time or it is made up of sub-samples to be representative of the bulk as a whole.

In some cases the gross sample is too large to send to the laboratory and has to be reduced in quantity. This reduction needs to be carried out in such a way that the laboratory sample is fully representative of the gross sample. When this reduction is unnecessary the gross sample is also the laboratory sample.

The laboratory sample may be required for a number of tests, so it is sometimes necessary to further sub-divide it into test samples.

Finally, the test sample may be used in its entirety or further sub-divided to form the measurement sample.

The object of sampling is to gain knowledge of the characteristics of the whole from measurements impracticable to apply to the whole; bias, at any of the reduction stages, adversely affects the final analysis. Problems arise due to inhomogeneities in the parent distribution. If the

bulk powder is homogeneous, or can be mixed prior to sampling in order to generate a homogeneous powder, sampling problems do not arise. In order to establish homogeneity it is necessary to examine samples taken from the bulk, either at random or according to some pre-determined pattern. If homogeneity is established a single sample is representative of the bulk. The definition of homogeneity requires specification of the portion or sample size between which the variability is sufficiently small to be neglected.

Temporal or spatial variability of inhomogeneous powders may be random, i.e. there is no discernible pattern and it is impossible to predict the value at any one point from a knowledge of the value at any other point. In this case it is necessary to examine a number of samples in order to establish a mean and a standard deviation [3]. Non-random variation may be regular cyclic, which can cause problems if the sampling sequence follows the same cycle, or irregular cyclic, in which case the larger the portion the greater the smoothing out of irregularities.

Handling of non-cohesive powders can result in size segregation, hence the distribution of particle size in a powder depends upon its previous history. If free-flowing powder is poured into a heap there is a tendency for the fine particles to percolate through the coarse and for the coarse particles to roll on the fines. This leads to an excess of fines in the center of the heap and an excess of coarse on the outside. (Figure 1.1) shows a cross-section through a heap of binary powder with the fine particles tending to remain in the center. Sizes; coarse (black) approximately 1 mm diameter, fine (white) approximately 0.2 mm diameter. For markedly greater disparities in size the segregation seems to be size independent.

For powders that are vibrated, the percolation process lifts larger particles to the powder surface (Figure 1.2). i.e. vibration causes small particles to percolate under large ones thus lifting them. A recent computer modeling study [4,5] with 50,000 small spheres and 250 larger spheres whose diameters were four times as great, showed that 60 vibrations are enough to bring most of the larger spheres to the surface.

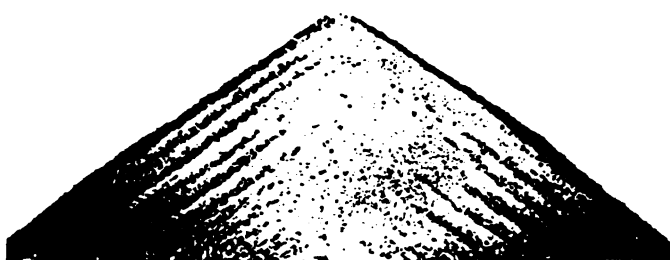


Fig. 1.1 Segregation of powders when poured into a heap.

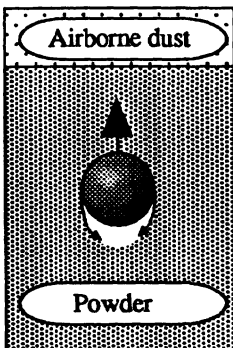


Fig. 1.2 Segregation due to vibration.

Further, the process seems to function provided the ratio of diameters is greater than 2.8:1.

The situation can however be quite complex, since material is often fed into containers or on to belt conveyors from the side, hence the feeding itself can generate both vertical and horizontal segregation. Generally little is known in advance concerning the homogeneity of a system and uniformity is rarely constant and often non-random.

For these reasons, it is recommended that, wherever possible the golden rules of sampling should be followed:

- A powder should always be sampled when in motion.
- The whole of the stream of powder should be taken for many short increments of time in preference to part of the stream being taken for the whole of the time.

Observance of these rules, coupled with an understanding of the manner in which segregation takes place, leads to the best sampling procedure. Any method that does not follow these rules should be regarded as a second-best method liable to lead to errors. Finally, the need for care and skill in abstracting samples cannot be over-emphasized.

1.3 Sampling stored material

There are a very large number of possible systems from which a gross sample has to be extracted, so it is impossible to lay down instructions which will meet all situations. Essentially, the solution depends on whether the powder is stationary or moving and whether it is cohesive or free-flowing. It is usual to assume that the powder was mixed before storage. If this assumption is not true then the homogeneity of the powder will depend on its previous history. Thus, a non-flowing

material which has been segregated during manufacture, or prior to storage, will remain segregated. For a free-flowing material, segregation can occur during transfer from the mixer to the storage container.

1.3.1 Sampling stored non-flowing material

Non-flowing material is composed of very fine cohesive powders, sticky material, moist material or fibrous solids. These may be stored in small containers such as drums or bags or large containers such as trucks or railway wagons. Surface sampling is usually carried out with a scoop because of its simplicity; a pre-supposition is that the powder at the sampling point is representative of the bulk i.e. that the powder was mixed before storage. Accuracy is increased by taking more than one sample and these should be analyzed separately and combined in later analyzes if the variation between samples is at an acceptable level.

(a) *Sampling spears*; Sampling accuracy is improved if samples from the body of the material is included and this may be carried out with the aid of a sampling spear (thief). Three types are available (Figure 1.3); in type 1 the sampling chamber runs the full length of the spear, in type 2 the sampling chamber is at the end of the spear and in type 3 there are separate chambers along the length of the spear. The spear is thrust into the powder with the inside chamber closed off and, when in position, the outer tube is rotated to allow powder to fall into the inner chamber. When the chamber is full, the inner tube is turned to the closed position and the spear withdrawn. Possible segregation throughout the bed may be investigated with type 3, an average value for the length of the spear with type 2 and a spot sample with type 3. Frequently the spears are vibrated to facilitate filling and this can lead to an unrepresentative quantity of fines entering the sample volume. The sampling chambers also have a tendency to stick if coarse particles are present. *Self-burrowing probes* (Figure 1.4) are also available for sampling stored powder.

In industry it is common to sample small heaps by coning and quartering. The heap is first flattened at the top and then separated into four equal segments with a sharp-edged board or shovel. The segments are drawn apart and, frequently, two opposite quadrants are recombined and the operation repeated until a small enough sample has been generated. This practice is based on the assumption that the heap is symmetrical and, since this is rarely so, the withdrawn sample is usually non-representative. This method is no more accurate than scoop or thief sampling, which are simpler to carry out, but gross errors are to be expected (Figure 1.5). Coning and quartering should never be used with free-flowing powders.

(b) *Sampling from trucks and wagons*; In sampling from a truck or a wagon it is recommended that eight samples be extracted [6]. No increment should be taken at less than twelve inches below the surface;

6 Powder sampling and particle size measurement

this avoids the surface layer in which segregation can have occurred due to vibration (Figure 1.6). Care needs to be taken to prevent powder sliding down the slope created due to removal of surface material.

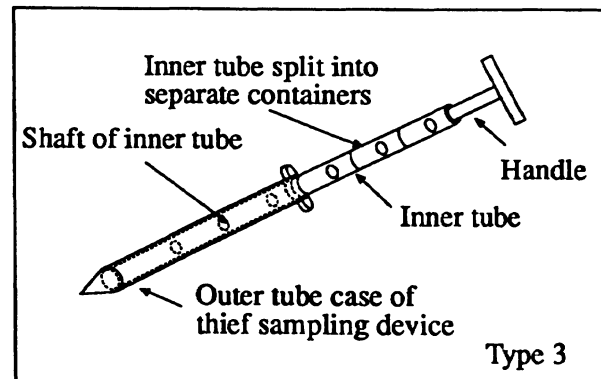
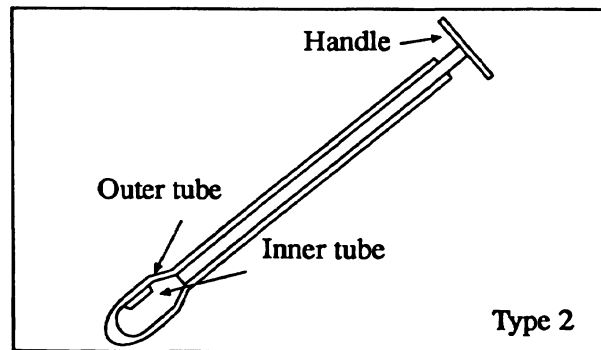
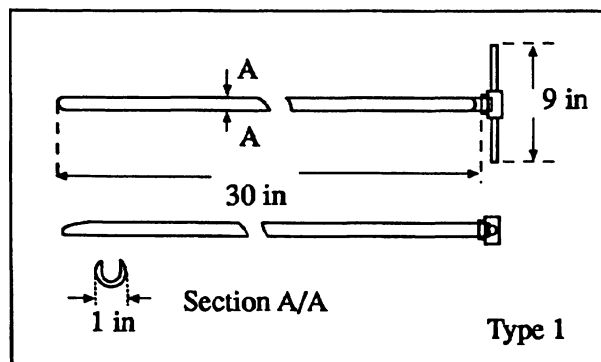


Fig. 1.3 Sampling spears.

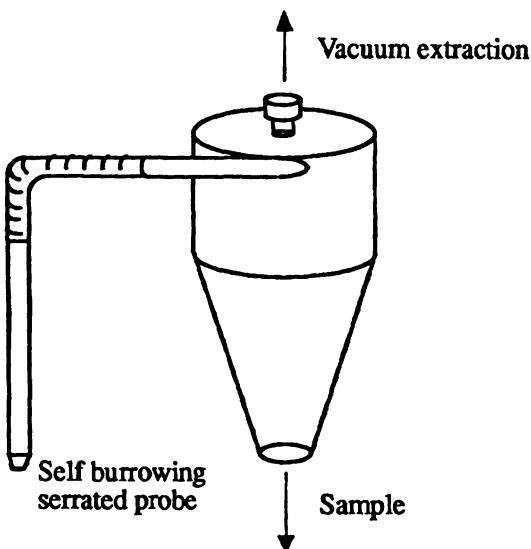


Fig. 1.4 Self-burrowing sampler for stored powders.

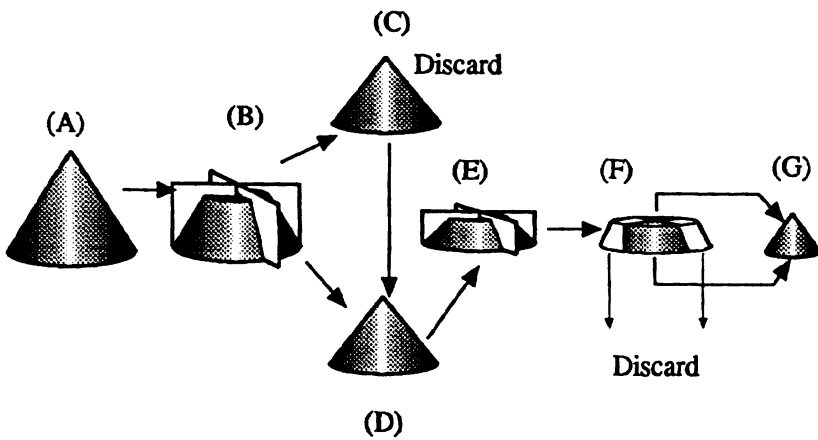


Fig. 1.5 Coning and quartering process.

1.3.2 Sampling stored free-flowing material

It is practically impossible to sample representatively stationary free-flowing powder because of the severe segregation that has almost certainly occurred. There is only one sound piece of advice to give regarding sampling such material. Don't! Never! Well hardly ever! If

8 Powder sampling and particle size measurement

there is no alternative several samples should be taken and analyzed separately so that an estimate can be made of the degree of segregation. The act of forming a heap will result in segregation and the distribution of particle sizes within the powder will depend upon how the the heap was formed. Examination of the cross-section of a heap of free-flowing powder reveals marked segregation, fine particles being concentrated in a region near the axis and coarse particles in the outer part. The nature of segregation within containers will depend upon how the containers were filled and whether they have been transported i.e. upon the previous history of the powders.

Suppose an analysis is required from several tons of material which is available in bags or small containers. Several of these containers should be selected systematically or, preferably, using a table of random numbers. The whole of each bag should then be sampled using a full stream or Vezin type splitter so that the golden rules of sampling are obeyed. This is the only way of obtaining a representative sample from each bag. It would probably have been easier and certainly preferable to have obtained a sample as the containers were being filled.

1.4 Sampling flowing streams

Most powder systems are transported at some time during their manufacture as flowing streams: Hoppers are emptied by screw or belt conveyors. Powders are transferred to bagging operations by screw or pneumatic conveyors and many solids are transported through pipes. A general rule in all sampling is that whenever possible the sample should be taken when the powder is in motion. This is usually easy with continuous processes; with consignment sampling it may be possible during filling and emptying of storage containers.

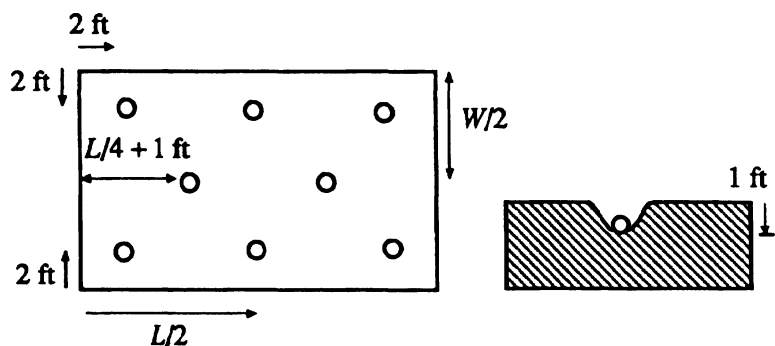


Fig. 1.6 Sampling points for a wagon or a truck.

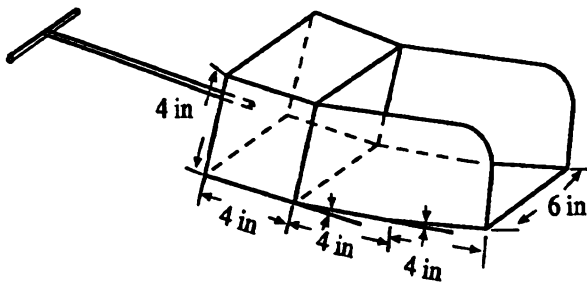


Fig. 1.7 Scoop suitable for sampling coal, with a 2 in maximum size, from a moving belt (BS 1017).

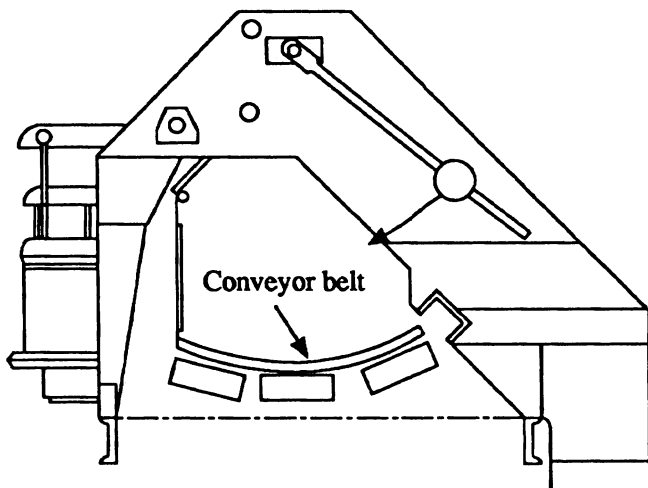


Fig. 1.8 Automatic sampler for belt conveyor.

1.4.1 Sampling from a conveyor belt

When a sample is to be collected from a conveyor belt, the best position for collecting the increments is where the material falls in a stream from the end of the belt. If access at such a point is not possible the sample must be collected from the belt. The whole of the powder on a short length of the belt must be collected and, again, it must be borne in mind that the particles at the edge of the belt may not be the same as those at the center, and particles at the top of the bed may not be the same as those at the bottom. If the belt can be stopped, the sample may be collected by inserting into the stream a frame consisting of two parallel plates shaped to fit the belt; the whole of the material between the plates is then swept out. A scoop, such as the one shown in Figure 1.7, can be

used to scoop out an increment, but this operation can be hazardous if the belt is moving.

Bristol Engineering Company manufacture a belt conveyor system which has only one moving part in contact with the material. An arm sweeps across the belt to remove the sample (Figure 1.8).

When sampling from a continuous stream, the sampling may be continuous or intermittent. In continuous sampling a portion of the flowing stream is split off and frequently further divided subsequently. In intermittent sampling the whole stream is taken for many short increments of time at fixed time intervals. These increments are usually compounded and samples for analysis taken from this gross sample. Consignment sampling is carried out on a single consignment (e.g. a truck or wagon load).

1.4.2 Point samplers

Samples can be extracted from the product stream by the projection of a sample tube, containing a nozzle or orifice, into the flow. The particles impact on the tube and fill the open cavity. The sampling head is out of stream when not sampling. The snorkel type sampler (Figure 1.9) is available for vertical or inclined applications and can be pre-programmed on sampling frequency. It is not possible to sample non-homogeneous streams representatively with this type of device.

With the auger type sampler (Figure 1.10) a slot inside the process stream is rotated to capture a cross-section of the process stream which is then delivered by gravity into a sample container. This type of device does not collect a representative sample unless the stream is homogeneous and has the added disadvantage that it obstructs flow.

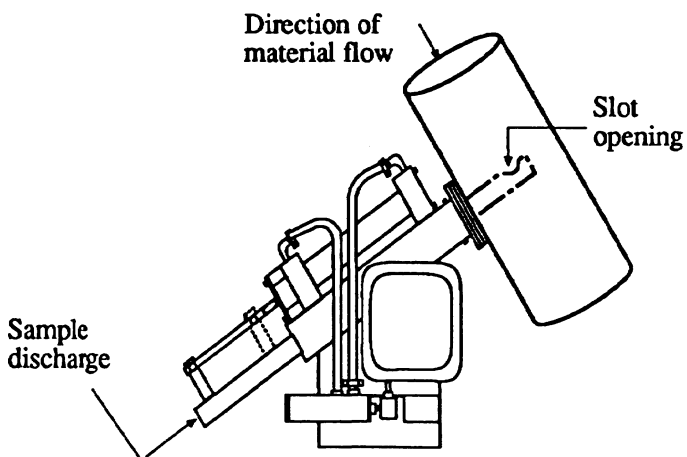


Fig. 1.9 Snorkel type point sampler.

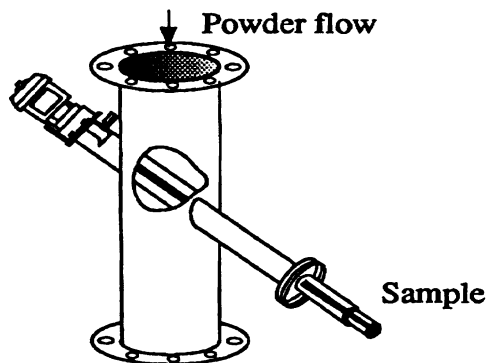


Fig. 1.10 Auger sampler.

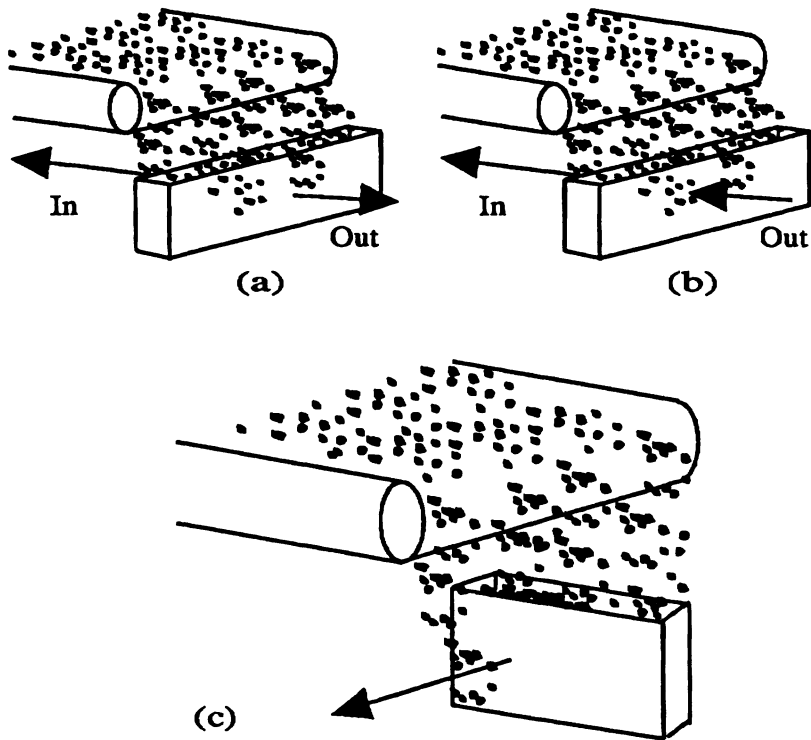


Fig. 1.11 Sampling from falling streams. (a) bad sampling technique, (b) good sampling technique, (c) sampling procedure to be adopted for high mass flow rate.

12 Powder sampling and particle size measurement

1.4.3 Sampling from falling streams

In collecting from a falling stream of powder, care should be taken to offset the effects of segregation. Each increment should be obtained by collecting the whole of the stream for a short time. Care must be taken in putting the sampler in and out of the stream. Figure 1.11 shows correct and incorrect ways of doing this. Unless the time during which the receiver is stationary in its receiving position is long compared with the time taken to insert and withdraw the sampler, the method shown in Figure 1.11a will lead to an excess of coarse particles as the surface region of the stream, usually rich in coarse particles, is sampled for a longer time than the rest of the stream. The method shown in Figure 1.11b is not subject to this objection. If this method is not possible due to some obstruction, the ratio of stationary to moving time for the receiver should be made as large as possible. In many cases it is not possible to collect the whole of the stream as this would give too large an amount to be handled. The best procedure is to pass a sample collector of the form shown in Figure 1.11c through the stream.

The width of the receiver, b , will be chosen to give an acceptable weight of sample but must not be made so small that the biggest particles have any difficulty in entering the receiver. Particles that strike the edges of the receiver are likely to bounce out and not be collected so that the effective width is $(b - d)$, where d is the particle diameter. The effective width is therefore greater for small particles than for large ones. To reduce this error to an acceptable level the ratio of box width to the diameter of the largest particle should be made as large as possible with a minimum value of 3:1. The depth (a) must be great enough to ensure that it is never full of powder. If the receiver fills before it finishes its traverse through the powder, a wedge shaped heap will form and this will be size selective: As more powder falls on top of the heap the fine particles will percolate through the surface and be retained, whereas the coarse particles will roll down the sloping surface and be lost. The length of the receiver (c) should be sufficient to ensure that the full depth of the stream is collected.

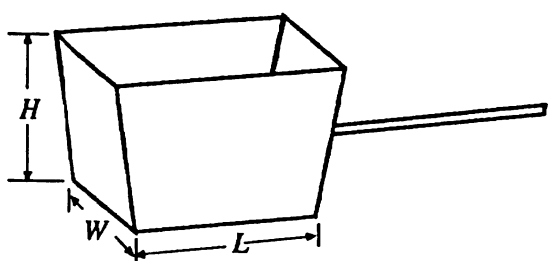


Fig. 1.12 Ladle suitable for sampling from a falling stream of powder.

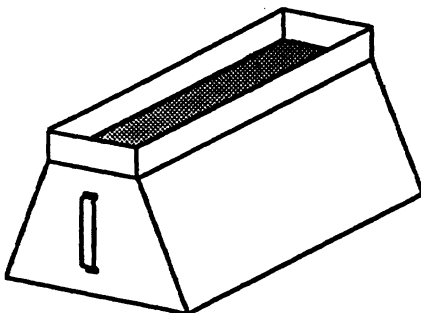


Fig. 1.13 Stream sampling cup.

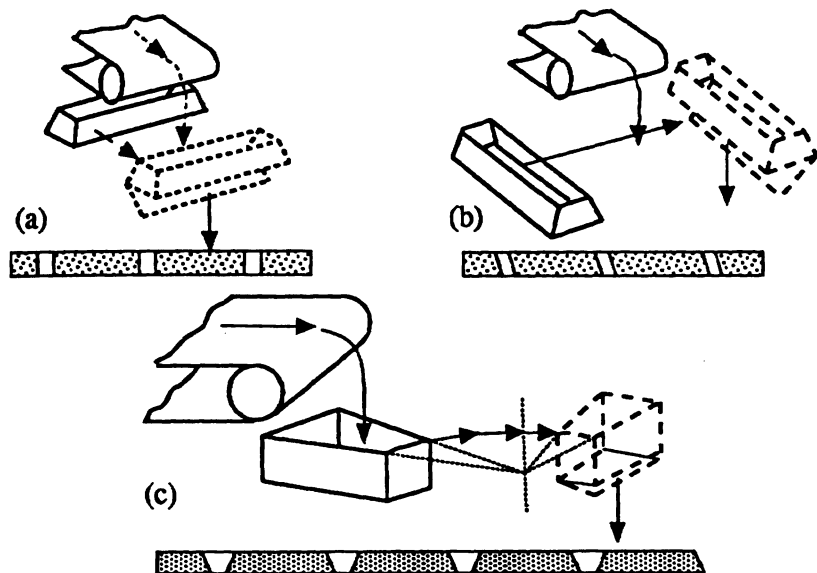


Fig. 1.14 (a) Cross-sectional sampler, straight path action, in line; (b) cross-line; (c) oscillating or swinging arc path.

1.4.4 Stream sampling ladles

Figure 1.12 shows a ladle designed for manual withdrawal of samples from a moving stream of coal (BS1017). The recommended dimensions for different sizes lumps are $W = 4.5$ in; $H = 6$ in; $L = 6, 7.25$ and 8.5 in for lumps of size 2, 2.5 and 3 in respectively. An alternative design is shown in Figure 1.13.

With the designs shown in Figure 1.14a and 1.14b uniform increments are withdrawn to give a representative sample but the design shown in Figure 1.14c will give a biased sample if the inner and outer arcs of the container are significantly different in length and the powder is horizontally segregated across the belt. Several commercial on-line samplers, based on these principles, are available.

1.4.5 Traversing cutters

With large tonnages, samples taken from conveyors can represent large quantities of material which need to be further reduced. Often, a traversing cutter is used as a primary sampler, and the extracted sample is further cut into a convenient quantity by a secondary sampling device. It must be borne in mind that the secondary sampler must also conform with the golden rules of sampling.

This equipment is satisfactory for many applications but it has limitations which restrict its use. These are:

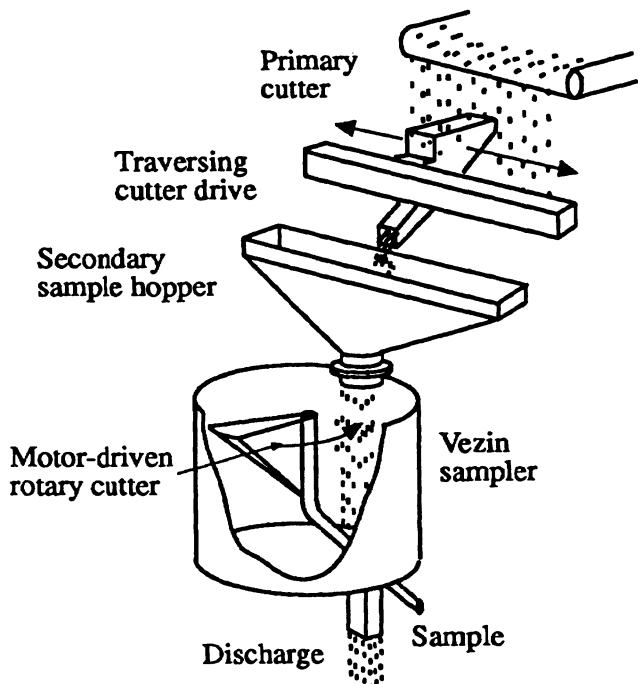


Fig. 1.15 Schematic of a primary and secondary system based on Denver Equipment Company's type C and Vezin samplers.

- Although comparatively readily designed into new plant it is frequently difficult and expensive to retrofit an existing plant. The main reason for this is due to space requirements.
- The quantity of sample obtained is proportional to product flowrate and this can be inconvenient when the plant flow-rate is subject to wide variations. On the other hand, where a plant's daily average is required, this is a necessary condition.
- It is difficult to enclose the sampler to the extent required to prevent the escape of dust and fume when handling dusty powders.

Commercial samplers are available which combine a traversing type sampler with an unacceptable table sampler. An alternative design is the radial cutter or Vezin sampler shown in Figure 1.15. These samplers vary in size from a 15 cm laboratory unit to a 152 cm commercial unit.

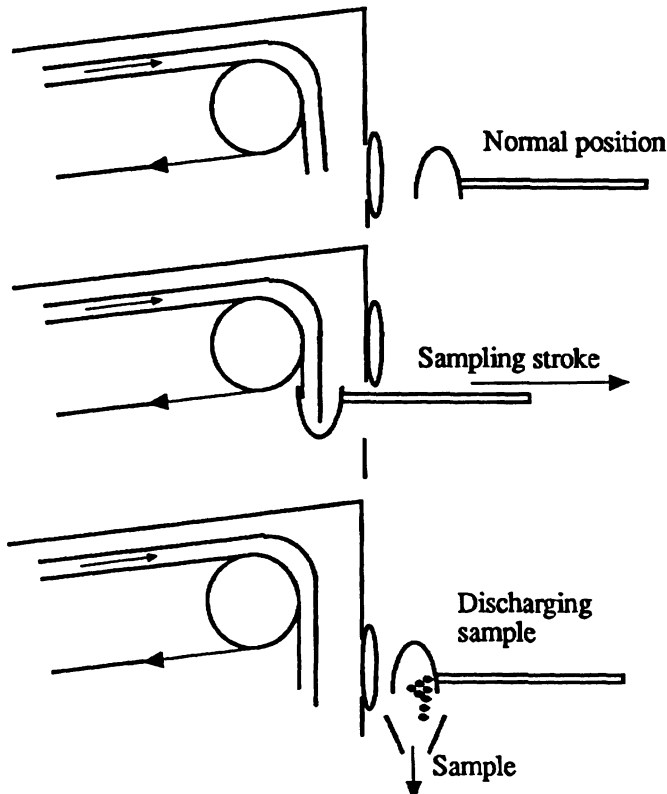


Fig. 1.16 Full-stream trough sampler.

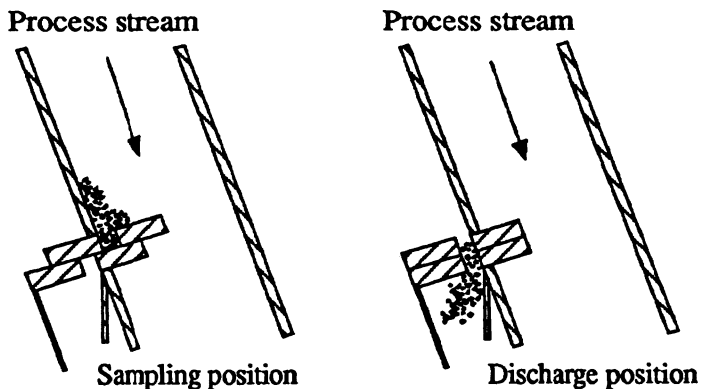


Fig. 1.17 The constant volume sampler.

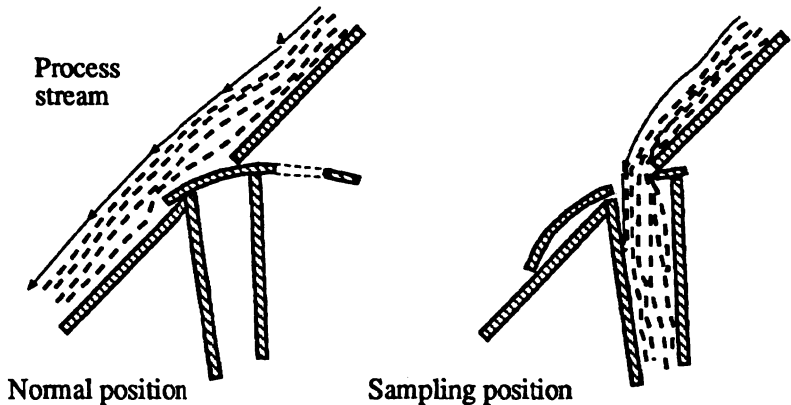


Fig. 1.18 The slide valve sampler.

1.4.6 Sampling dusty material

Figure 1.16 shows a sampler designed to sample a dusty material, sampling taking place only on the return stroke. This is suitable provided the trough extends the whole length of the stream and does not overfill. The sampler shown in Figure 1.17 was designed to extract a constant volume of homogeneous granular material for chemical assay and cannot be recommended when a physical assay is required [7]. The slide valve sampler (Figure 1.18) is suitable for collecting size - representative samples [8].

A variant of this problem is encountered in sampling from pre-weighed batches (Figure 1.19). The sampler is, essentially, a screw conveyor which extracts a sample continuously while the container is

being filled. This system suffers from two drawbacks in that it limits the discharge opening thus reducing throughput and takes part of the stream for the whole of the time thus contravening the golden rules of sampling. Similar samplers are available to sample flowing streams continuously; these are essentially Archimedean screws (Figure 1.20). Many variations of this design are possible and the reader is referred to Cornish *et al.* [3] for a comprehensive treatment. Figure 1.21 shows an industrial sampler for free-flowing material including granules, powders and pellets. This can be mounted on screw conveyors, drag conveyors or angular gravity chutes with manual or automatic control.

1.4.7 Moving flap sampler

The diverter valve shown in Figure 1.22a was used for extracting a sample from a pilot plant granulator operation. The sample was fed to a hopper and thence, by a vibratory feeder, to a low-angle laser light scattering instrument. The granules were then returned to the process stream. This system allowed on-line analyses every minute so that the process could be optimized. A more substantial design was required for continuous plant operation (Figure 1.22b) with a moving piston operated rectangular flap weighing around 50 lb.

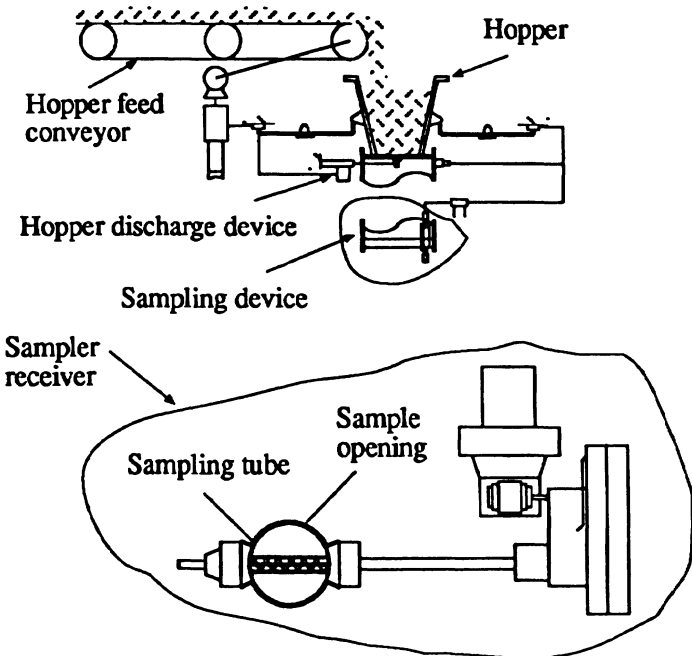


Fig. 1.19 Sampling from a hopper.

18 Powder sampling and particle size measurement

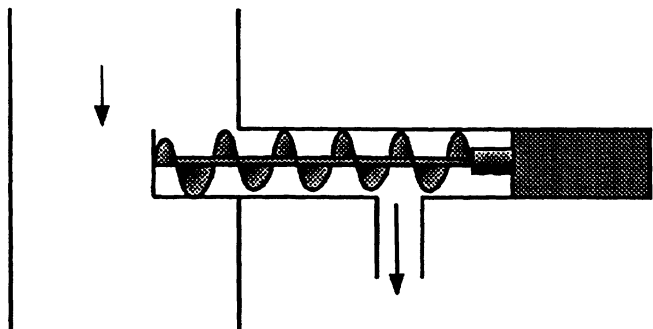


Fig. 1.20 Archimedian screw sampler.

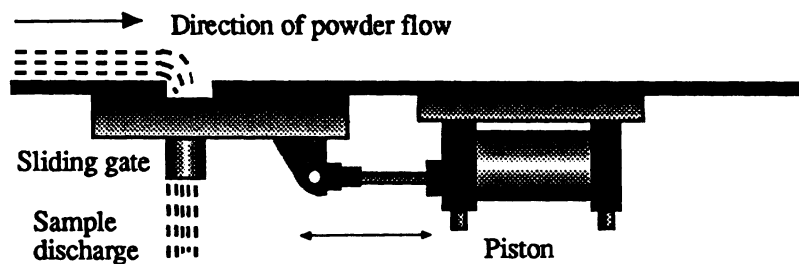


Fig. 1.21 Sampler for screw conveyor.

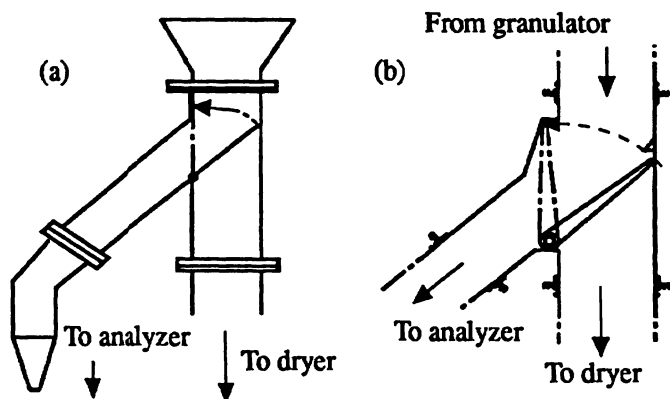


Fig. 1.22 Sampler for on-line particle size measurement: (a) diverter valve sampler; (b) a moving flap sampler.

1.5 Sample reduction

The gross sample is frequently too large to be handled easily and may have to be reduced to a more convenient weight. Obviously the method employed must conform with the two golden rules mentioned earlier. Usually the amount of material to be handled is small enough that getting it in motion poses no great difficulty. There is a natural tendency to remove an aliquot with a scoop or spatula and this must be avoided since it negates the effort involved in obtaining a representative sample from the bulk. Placing the material in a container and shaking it to obtain a good mix prior to extracting a scoop sample is not recommended. To obtain the best results, the material should be made as homogeneous as possible by pre-mixing. It is common then to empty the material into a hopper and this should be done with care. A homogeneous segregating powder, when fed to a hopper from a central inlet, will segregate since, in essence, it is being poured into a heap. In a core flow hopper the central region, which is rich in fines, empties first, followed by the material nearer the walls which has an excess of coarse.

The walls of the hopper should have steep sides (at least 70°) to ensure mass flow and should be filled in such a way that size segregation does not occur. This can best be done by moving the pour point about so that the surface of the powder is more or less horizontal. Several sample-dividing devices are available and these are discussed briefly below.

1.5.1 Scoop sampling

The method consists of plunging a scoop into the powder and removing a sample (Figure 1.23). This is particularly prone to error since the whole of the sample does not pass through the sampling device, and since the sample is taken from the surface, where it is not representative of the mass.

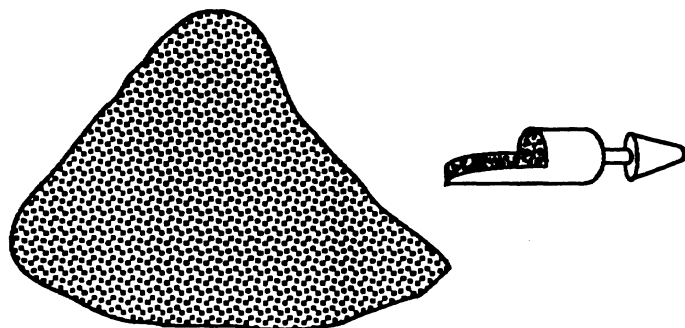


Fig. 1.23 Scoop sampling.

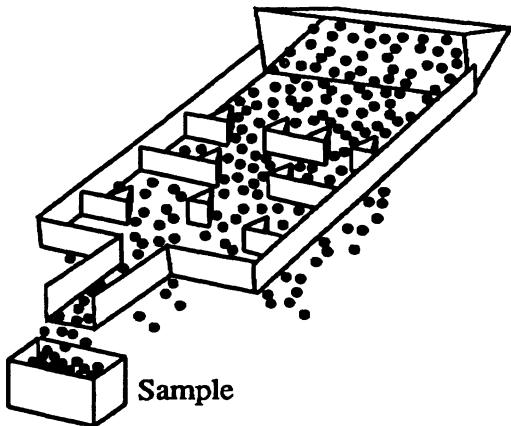


Fig. 1.24 Table sampling.

For powder in a container, it is usual to shake the sample prior to sampling in an attempt to achieve a good mix. However, the method of shaking can promote segregation.

1.5.2 Cone and quartering

This method consists of pouring the powder into a heap and relying on its radial symmetry to give identical samples when the heap is flattened and divided by a cross-shaped cutter. This method is particularly prone to selective sampling and should be avoided (Figure 1.5).

1.5.3 Table sampling

In a sampling table the material is fed to the top of an inclined plane in which there is a series of holes. Prisms placed in the path of the stream break it into fractions. Some powder falls through the holes and is discarded, while the powder remaining on the plane passes on to the next row of holes and prisms, and more is removed, and so on. The powder reaching the bottom of the plane is the sample (Figure 1.24). The objection to this type of device is that it relies on the initial feed being uniformly distributed, and a complete mixing after each separation, a condition not in general achieved. As it relies on the removal of part of the stream sequentially, errors are compounded at each separation, hence its accuracy is low. Its advantages are its low price and its lack of moving parts.

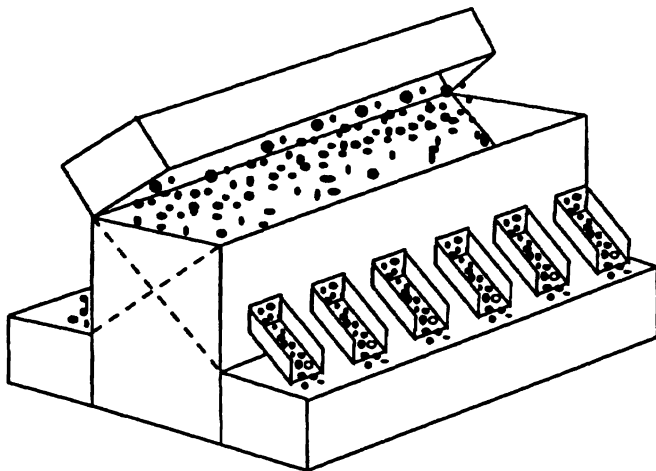


Fig. 1.25 Line diagram of chute splitter.

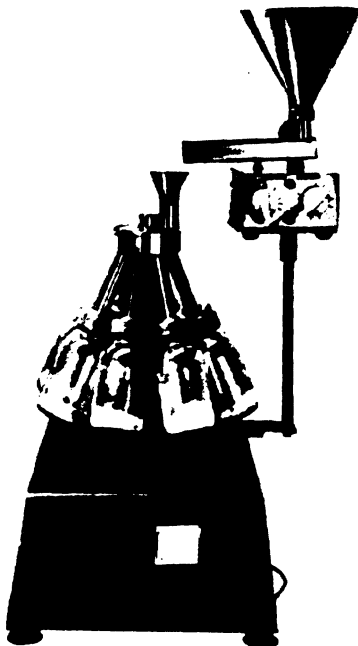


Fig. 1.26 The Retsch rotary sample divider.

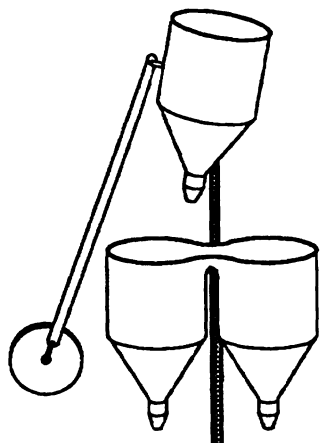


Fig. 1.27 Oscillating hopper sampler divider.

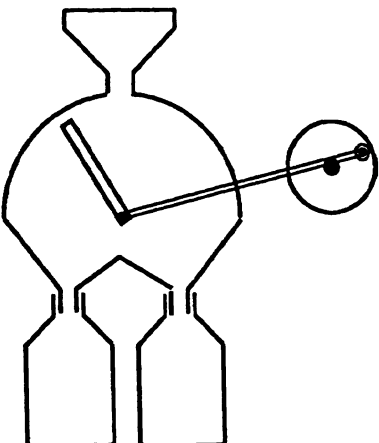


Fig. 1.28 Oscillating paddle sampler divider.

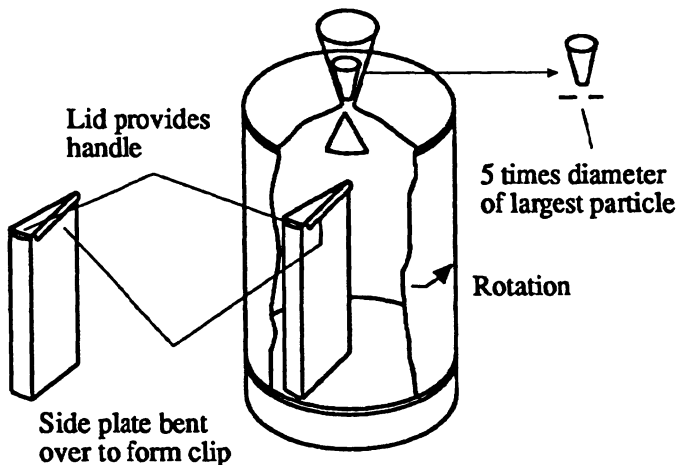


Fig. 1.29 Pascal turntable sample divider.

1.5.4 Chute splitting

The chute splitter consists of a V-shaped trough along the bottom of which is a series of chutes alternately feeding two trays placed on either side of the trough (Figure 1.25). The material is repeatedly halved until a sample of the desired size is obtained. When carried out with great care this method can give satisfactory sample division but it is

particularly prone to operator error, which is detectable by unequal splitting of the sample.

1.5.5 The rotary sample divider

The rotary sample divider conforms to the golden rules of sampling. The preferred method of using this device is to fill a mass flow hopper in such a way that segregation does not occur. The table is then set in motion and the hopper outlet opened so that the powder falls into the collecting boxes. The use of a vibratory feeder is recommended to provide a constant flowrate (Figure 1.26). Several versions of this instrument are available, some of which were designed for free-flowing powders, some for dusty powders and some for cohesive powders. They handle quantities from 40 liters down to a few grams.

1.5.6 Miscellaneous sampling devices

In the oscillating hopper sample divider [9] (Figure 1.27), the feed hopper is pivoted about a horizontal axis so that it can oscillate while emptying. Two collectors are placed under the hopper outlet so that the powder falls into them alternately so that at each step the sample is halved. The instrument are available, some of which were designed for free-flowing Imperial Chemical Industries (ICI) oscillating paddle sample divider (Figure 1.28) works in a similar way.

The Pascal turntable sampler recommended in BS 3406 is very similar to the spinning riffler. In this instrument the powder falls through a hopper outlet on to a cone whose position can be varied in order to alter the hopper outlet size. The powder slides down the cone into containers on a revolving table (Figure 1.29).

The Glen Creston rotary divider (Figure 1.30) consists of an internal inclined pipe which is rotated by a geared motor. The powder is fed into this pipe and with each revolution a proportion falls into the

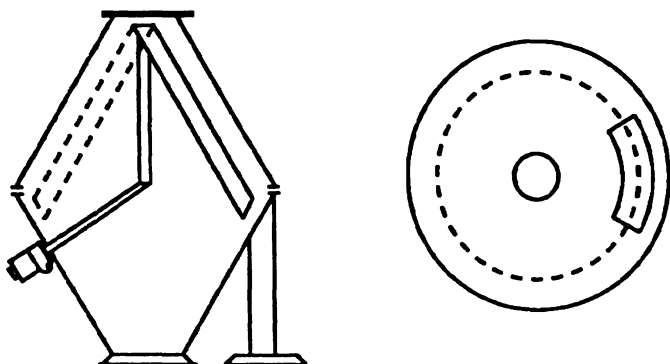


Fig. 1.30 The Glen Creston rotary sampler.

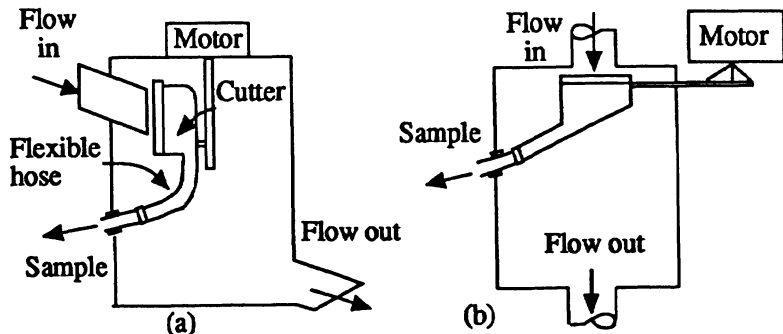


Fig. 1.31 (a) Sloping trough cutter. (b) Vertical pipe cutter.

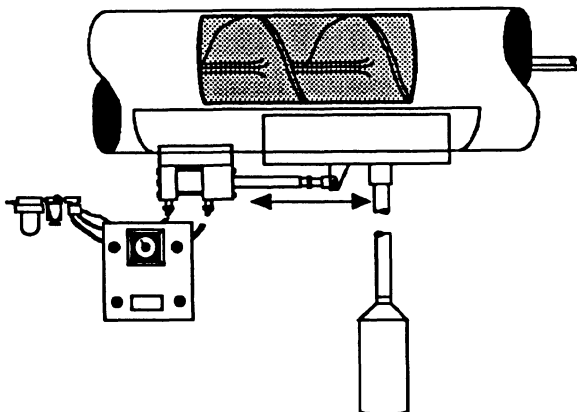


Fig. 1.32 Sampling from screw or drag conveyors.

sample column. The opening in the sample column can be adjusted from outside the divider by means of a sliding plate. By this method it is possible to vary the ratio of sample to total throughput. Appropriate dividers are available for different particle sizes and sampling volumes.

Denver Equipment Company manufacture a sloping trough cutter (Figure 1.31a) and a vertical pipe cutter (Figure 1.31b). Gustafson manufacture an automatic sampler for free flowing materials from screw or drag conveyors (Figure 1.32).

1.6 Slurry sampling

Slurry process streams vary in flowrate, solids concentration and particle size distribution. Any sampling technique must be able to cope with these variations without affecting the representativeness of the

extracted sample. For batch sampling, automatic devices are available where a sampling slot traverses intermittently across a free-falling slurry. Unfortunately it is difficult to improvise with this technique for continuous sampling, since such samplers introduce pulsating flow conditions into the system. Osborne [10] described a sampler which consists of a narrow slot continuously rotated on an axis parallel to the slurry flow (Figure 1.33a). Cross [11] used a slotted pipe mounted vertically in the overflow compartment next to the vortex finder of a hydrocyclone (Figure 1.33c). Since most continuous size analyzers require a constant volume flowrate, further subdivision is often necessary. Osborne's solution (Figure 1.33b) was to feed the sample stream to a well agitated tank and withdraw a representative sample at a constant flow-rate.

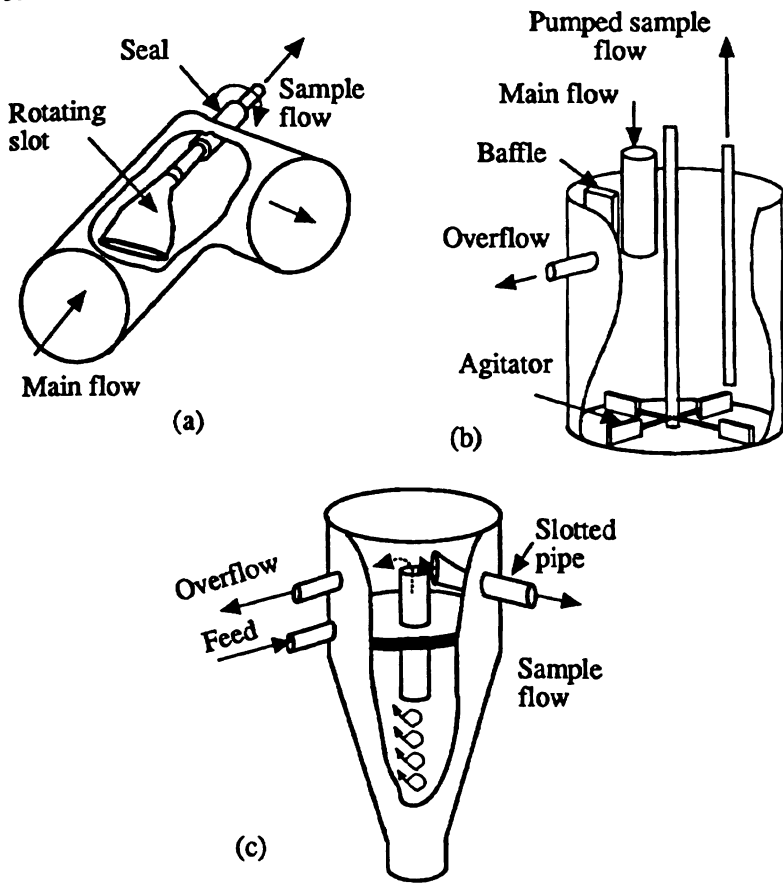


Fig. 1.33 (a) Osborne's rotating slot slurry sampler. (b) Osborne's sampling tank. (c) Cross's slotted pipe slurry sampler.

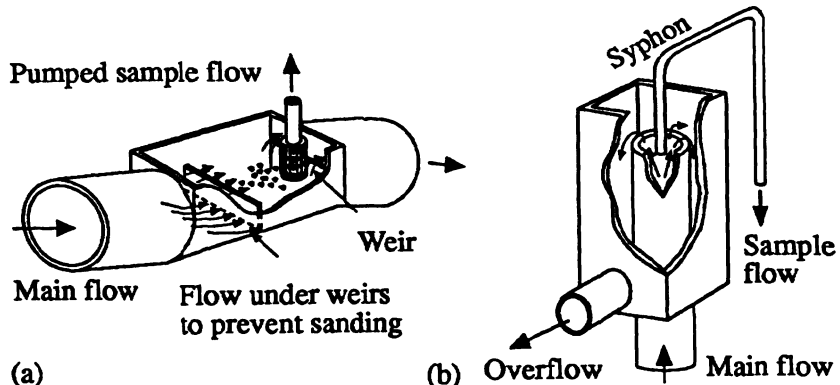


Fig. 1.34 (a) Autometrics' design for direct sampling (b) Autometrics' design for extracting a small sample.

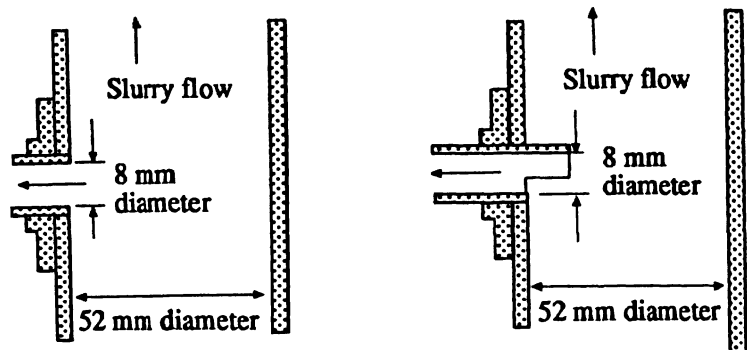


Fig. 1.35 Schematic diagram for side-wall sampling of slurries.

Autometrics [12] analyze the whole of the extracted sample (Figure 1.34a). Gaps are left below the weirs to prevent sanding. Sub-division of the sample stream, for calibration purposes, can be accomplished very successfully by siphoning from a vertical fast-flowing stream (Figure 1.34b).

Side-wall sampling. Due to their simplicity side-wall samplers are superficially attractive (Figure 1.35) but serious errors in concentration and particle size distribution can arise unless the particles are fine, the concentration is high and a very high sampling velocity is used. A projection extending from the pipe wall only marginally improves sampling efficiency [13].

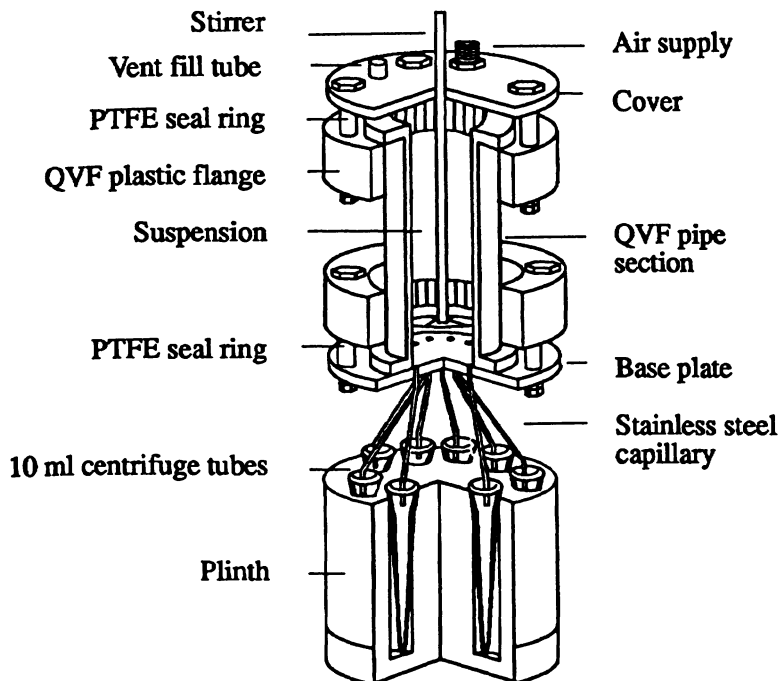


Fig. 1.36 The Microscal suspension sampler, 100 mL to 10 mL.

1.7 Reduction of laboratory sample to measurement sample

The methods described in section 1.5 are capable of reducing the gross sample of many kilograms down to a laboratory sample of up to about 1 kg and further reducing this to a few grams. In many cases this reduction is sufficient to generate a measurement sample whilst for some analytical techniques a further reduction is required. Coning and quartering a paste is often used for preparing samples down to 20 mg in weight but the efficiency of the method is operator dependent. Sampling an agitated suspension with a syringe or pipette is a good method for fine powders but, with coarse powders, concentration gradients and particle segregation due to settling may lead to selective sampling.

The Microscal suspension sampler [14] (Figure 1.36) is designed to eliminate these errors. It consists of a glass cylinder closed at either end by stainless steel plates. Around the periphery of the base plate are ten equidistant holes leading to ten centrifuge tubes via stainless steel capillary tubes. The cover plate has a central hole through which passes a stirrer, a sealable inlet for introduction of the suspension, and a gas orifice which enables the gas pressure to be varied. The suspension is

placed in the cylinder and, whilst undergoing agitation, gas is introduced under pressure in order to blow the suspension into the centrifuge tubes. Tests indicate that this system gives significantly less variation than syringe withdrawal, i.e. 1.0% standard deviation as opposed to 3.0%.

Since the spinning riffler proved far superior to the other methods it was examined further in order to determine its optimum operating conditions. It was found that a minimum of 35 presentations is required to give optimum results. If the speed of rotation is made too great the efficiency will fall off due to air currents which result in powder loss. It has also been found [15] that $\text{Var}(P_n) \propto (1 + L/V)^{0.5}$ where $\text{Var}(P_n)$ is the square of the standard deviation, L is the linear flow rate of the feed and V the peripheral velocity of the spinning disc.

1.8 Number of samples required

The basic assumption, in analyzing data statistically, is that the samples are representative of the populations from which they are withdrawn. However, there is an uncertainty associated with any measured property and this can be estimated using the confidence interval (CI). This can be expressed in general terms as:

$$\text{CI} = \text{estimate} \pm M(\text{standard deviation of the estimate})$$

where M is a multiplier that is determined by the chosen confidence interval (usually 90, 95 or 99%) and the amount of information available to calculate the standard deviation of the estimate.

Given a random set of n samples with a measured mean x_m withdrawn from a powder whose standard deviation σ is known, the true mean will lie in the interval [16]:

$$\mu = x_m \pm \frac{M\sigma}{\sqrt{n}} \quad (1.1)$$

At the 95% confidence level $M = 1.96$, i.e. there is a five in one hundred chance that the true mean lies outside these limits. The 90% confidence interval is smaller ($M = 1.645$) and is less likely to have the true value of x within its limits. The 99% confidence interval is larger ($M = 2.576$) but is more likely to contain the true value of x within its limits.

For pharmaceutical applications, a value $t = 2$ is used to denote working quality and a value $t = 3$ (99.9% confidence level) is used for total quality [1].

The statistical reliability of analytical data can be improved by increasing the homogeneity of the sample (reducing σ), which can be done by mixing, increasing the size of the sample, or increasing the number of samples taken (increasing n).

In most instances the population standard deviation is not known and must be estimated from the sample standard deviation (s). Substitution of s for σ in equation (1.1) with $M = 1.96$ does not result in a 95% confidence interval unless the sample number is infinitely large (in practice $n > 30$). When s is used, multipliers, whose values depend on sample number, are chosen from the t -distribution and the denominator in equation (1.1) is replaced by $\sqrt{n - 1}$.

Assuming a normal distribution of variance, the number of samples required, to assume at the 95% confidence level that the median is known to $\pm A$, is given by

$$n = \left\lceil \frac{ts}{A} \right\rceil^2 \quad (1.2)$$

where $A = |\mu - x_m|$ is the maximum allowable difference between the estimate to be made from the sample and the actual value.

Example 1

In many sampling procedures, sub-samples are taken at different levels and locations to form a composite sample. If historical evidence suggests that the standard deviation between samples is 0.5, and it is necessary to know the average quality of the lot to within 0.3, the number of sub-samples required, at the 95% confidence level, is given by equation (1.2) [17]:

$$n = \left(\frac{2 \times 0.5}{0.3} \right)^2 = 11.1 = 12$$

Example 2

16 samples, withdrawn at random from an unmixed powder, gave a median $x_m = 3.13 \mu\text{m}$ by low-angle laser light scattering (LALLS) with a standard deviation of $s = 0.80 \mu\text{m}$. Then, in microns, the median lies between the limits:

$$\mu = 3.13 \pm 2.14 \frac{0.8}{\sqrt{(16-1)}}$$

$$\mu = 3.13 \pm 0.44$$

The multiplier $t = 2.14$ is obtained from a t table for $n = 16 - 1$ degrees of freedom at the 95% confidence level. Thus we are 95% confident that the median lies in the confidence interval (CI):

$$\text{CI} = 2.69 \leq 3.13 \leq 3.57$$

30 Powder sampling and particle size measurement

Based on this data, the number of samples required to give an estimate to within ± 0.10 , ($E = 0.10$) is:

$$n = \left(\frac{2.14 \times 0.8}{0.10} \right)^2$$

$$n = 293$$

After mixing, 16 samples gave a median x_m of $3.107 \mu\text{m}$ with a standard deviation s_t of $0.052 \mu\text{m}$. Then:

$$\mu = 3.107 \pm 2.14 \left(\frac{0.052}{\sqrt{15}} \right)$$

$$\mu = 3.107 \pm 0.029$$

Thus we are 95% confident that the true median lies in the confidence interval:

$$\text{CI} = 3.078 \leq 3.107 \leq 3.136$$

i.e. the mixing step increases the measurement precision by a factor of fourteen.

A single sample, run 16 times on a LALLS instrument gave a median of $3.11 \mu\text{m}$ with a standard deviation of $s_s = 0.030 \mu\text{m}$.

The total variation (s_t^2) is the sum of the variation due to the measuring procedure (s_s^2) and the variation due to the sampling procedure (s_n^2).

$$s_t^2 = s_s^2 + s_n^2 \quad (1.3)$$

$$s_s = 0.042$$

It is possible to isolate the sampling error from the measurement error. The standard deviation due to sampling (s_s) is $0.042 \mu\text{m}$ and the standard deviation of the measurement technique (s_n) is $0.030 \mu\text{m}$ giving a total standard deviation (s_t) of $0.052 \mu\text{m}$. As can be seen from this example, there is little to be gained in using a measurement technique substantially more accurate than the sampling that preceded it.

Further, the number of samples required, after mixing, in order to assume at the 95% confidence level that the median is known to $0.1 \mu\text{m}$ is:

$$n-1 = \left(\frac{2.14 \times 0.052}{0.10} \right)^2$$

$n = 2.2$ i.e. 3 samples. The same accuracy can be attained by compounding increments from the unmixed powder in motion, for example, by riffling in a spinning riffler.

In the pharmaceutical industry there has been a tendency by federal agencies to request that blending validation be carried out using samples the size of a dosage unit. A theoretical experiment using random numbers was carried out to assess the effect of changing sample size [18]. A set of assays of a dosage weighing 1 g containing 100 mg of drug substance was extracted from a bulk of 100 g. Four

1 g samples were averaged for each of 10 measurements and the standard deviation for each group of four determined. The experiment was repeated with 3 g, 5 g and 9 g samples. The means and averages for each set of 10 groups are given in Table 1.1.

$0.10 \mu\text{m}$ is:

The expected standard deviation is based on the premise that it is inversely proportional to the square root of sample size. Assuming the 5 g sample gives accurate data it can be seen that the 9 g sample is slightly worse than expected and the 1 g sample is much better than expected.

1.9 Theoretical statistical errors on a number basis

The ultimate that may be obtained by representative sampling may be called the 'ideal' sample. A powder may be considered as made up of two components *A* and *B*. The probability that the number fraction (*p*) of the bulk in terms of *A* shall be represented by the corresponding composition (*p_i*) of an ideal sample can be computed from the number of particles of *A* and *B* in the sample (*n*) and the bulk (*N*).

Table 1.1 Means and standard deviations of active ingredients in simulated sampling trials

Sample weight (g)	Mean (mg)	Standard deviation (mg)	Expected standard deviation (mg)
1	98.20	5.78	8.31
3	99.45	4.78	4.83
5	99.50	3.74	3.74
9	100.20	3.10	2.79

$$\sigma_i = \sqrt{\frac{p(1-p)}{n} \left[1 - \frac{n}{N} \right]} \quad (1.4)$$

where σ_i is the theoretical standard deviation, [the variance $\text{Var}(\sigma_i)$ is defined as the square of the standard deviation].

For a normal distribution of variance, the spread of data about the mean is described by the probability equation

$$\frac{d\phi}{dp} = \frac{1}{\sigma_i \sqrt{2\pi}} \exp\left[-\frac{(p-\bar{p})^2}{2\sigma_i^2}\right] \quad (1.5)$$

Using the transformation $\sigma_i y = (p - \bar{p})$ (1.6)

$$\frac{d\phi}{dy} = \frac{1}{\sqrt{2\pi}} \exp\left[-\frac{y^2}{2}\right] \quad (1.7)$$

This differential equation is presented graphically in Figure 1.37 and the integrated version in Figure 1.38. From Table 1.2, 68.26% of all occurrences lie within $\pm 1\sigma_i$ (between $y = -1$ and $y = +1$) from the mean, 95.44% within $\pm 2\sigma_i$ and 99.94% within $\pm 3\sigma_i$.

Table 1.2 Cumulative normal distribution

y	ϕ (%)	y	$\frac{d\phi}{dx}$
-4.0	0.003	-3.50	0.28
-3.0	0.13	-2.50	2.00
-2.0	2.28	-1.75	8.80
-1.5	6.68	-1.25	18.38
-1.0	15.87	-0.75	29.96
-0.5	30.85	-0.25	38.30
0.0	50.00	0.00	39.89
+0.5	69.15	0.25	38.30
1.0	84.13	0.75	29.96
1.5	93.32	1.25	18.38
2	97.72	1.75	8.80
3	99.87	2.50	2.15
4	99.997	3.50	0.13

Example 3

Consider a bulk made up of 8000 white balls and 4000 black balls from which 750 are extracted. Substituting in equation (1.4):

$$\sigma_i = \sqrt{\frac{\left(\frac{1}{3} \times \frac{2}{3}\right)}{750}} \left[1 - \frac{750}{12000} \right]$$

$$\sigma_i = 0.0167$$

Hence:

$$n \pm n\sigma_i = (2/3 \pm 0.0167 \text{ of } 750) \text{ for the white balls}$$

$$n \pm n\sigma_i = n \pm 12.5$$

where $n = 500$ or 250 for the white and black balls respectively. Thus 68 times out of 100 there will be between 487.5 and 512.5 white balls in the sample; 95 times out of 100 there will be between 475 and 525 and 26 times out of 10,000 there will be either more than 537.5 or less than 462.5.

1.10 Practical statistical errors on a number basis

The mean, on a number basis, can be calculated from experimental data using the following equation:

$$\bar{x} = \frac{\sum \Delta nx}{\sum \Delta n} \quad (1.8)$$

The standard deviation can also be calculated using the following equation:

$$\sigma_n = \sqrt{\frac{\sum \Delta n(x - \bar{x})^2}{n}} \quad (1.9)$$

If the true mean is not known, the experimental mean, determined using equation (1.8), must be used. In this case the denominator in equation (1.9) is replaced by $(n - 1)$, which has a negligible effect when n is large.

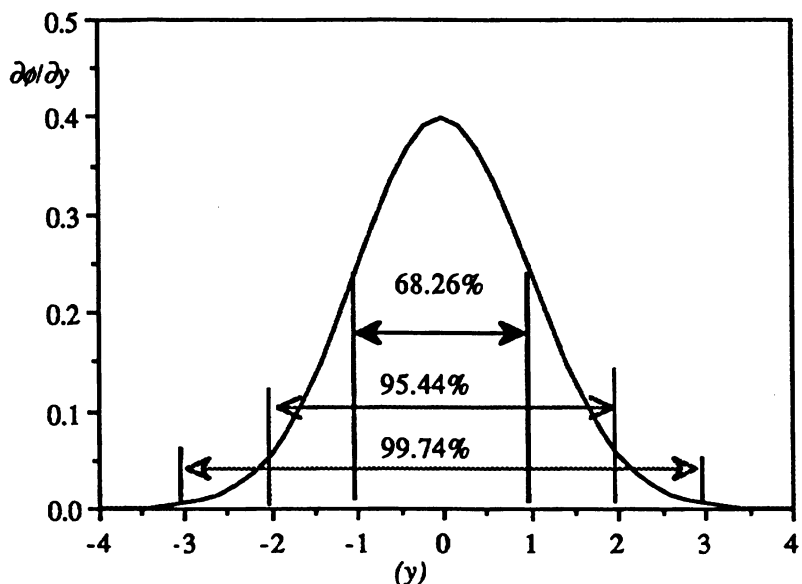


Fig. 1.37 Normal probability function (relative).

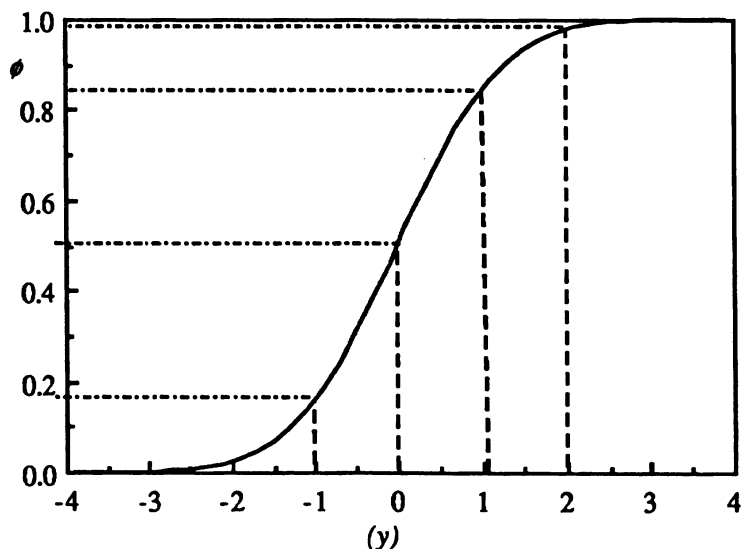


Fig. 1.38 Normal probability function (cumulative).

Table 1.3 Variation in the number of black balls in samples taken from a bulk containing 4000 black balls and 8000 similar white balls

Number of black balls			Frequency of occurrence (Δn)
Upper limit	Lower limit	Median value (\bar{x})	
3857	3872	3864	0
3873	3888	3880	1
3889	3904	3896	6
3905	3920	3912	10
3921	3936	3928	43
3937	3952	3944	103
3953	3968	3960	141
3969	3984	3976	195
3985	4000	3992	185
4001	4016	4008	160
4017	4032	4024	90
4033	4048	4040	37
4049	4064	4056	17
4065	4080	4072	11
4081	4096	4088	1

Example 4

Assume that the sampling operation described in example 1 is carried out $n = 1000$ times with the results presented in Table 1.3. Then, from equation 1.9, the standard deviation $\sigma_n = 35.9$, which is 2.87 times the theoretical value. If the true mean (4000) is not known the experimental mean, which equals 3985 by equation (1.8), must be used.

In this case the denominator in equation (1.9) is replaced by $(n - 1)$ but this has a negligible effect since n is so large. The resulting standard deviation $\sigma_i = 32.4$ is very similar to the previous value due to the large number of samples taken.

1.11 Theoretical statistical errors on a weight basis

Instead of the number fraction it is more convenient to assess sample and bulk composition in terms of weight fractions P and P_i giving [19]:

$$\text{Var}(P_i) = \frac{P(1-P)}{w} \left[P_B w_A + (1-P_B) w_B \right] \left(1 - \frac{w}{W} \right) \quad (1.10)$$

w_A and w_B are the average weights of individual grains of components A and B.

The standard deviation (σ_i) of the sample is given by the square root of the variance, and the weight of the sample divided by the weight of the bulk, (w/W), in many practical cases tends to zero. This function may be used as a basis from which to assess the efficiency of a real, non-ideal sampling device. In this case the variance of the ample assay $\text{Var}(P_n)$ will be greater than $\text{Var}(P_i)$ due to experimental deficiencies. The experimental variance is given by:

$$\text{Var}(P_n) = \sum \frac{(P - \bar{P})^2}{n} \quad (1.11)$$

where \bar{P} is the true fraction by weight of component A or B, P is the fraction obtained after sampling and n is the number of observations. The efficiency of a non-ideal sampler can be defined as:

$$C = \frac{\text{Var}(P_i)}{\text{Var}(P_n)} \quad (1.12)$$

and should approximate to unity when experimental sampling errors are low. The maximum sample error can be expressed as [20]:

$$E = \pm 100 \frac{2\sigma_n}{P} \quad (1.13)$$

Example 5

Consider a binary powder with a bulk of 800 g made up of a 40:60 mixture of particles of weight 0.05 g and 0.10 g. Determine the required gross sample weight, assuming perfect sampling, for a 2% standard deviation

$$w = \frac{0.40 \times 0.60}{w} [0.40 \times 0.10 + 0.60 \times 0.05] \left(1 - \frac{w}{800}\right)$$

$$w = 40 \text{ g}$$

1.12 Practical statistical errors on a weight basis

The percentage standard deviation can be calculated from experimental data using the following form of equation (1.9):

$$\sigma_n = \sqrt{\frac{\sum \Delta n_i (P_i - \bar{P})^2}{n}} \quad (1.14)$$

where \bar{P} is the true (known) percentage by weight of component A or B, Δn_i is the number of samples in a narrow weight percentage range

centered on P_i obtained by sampling and n the total number of samples taken. If \bar{P} is not known it can be determined using equation (1.9) with x replaced by P , it being assumed that n is large otherwise it would be necessary to replace the denominator in equation (1.14) with $n-1$.

Table 1.4 Sampling of a 60:40 binary sand mixture using a spinning riffler

Coarse percentage (P_i)	Frequency (Δn_i)	$\Delta n_i(P_i - \bar{P})$
59.8	3	0.12
59.9	3	0.03
60.0	5	0.00
60.1	2	0.02
60.2	2	0.08
60.3	1	0.09

Experimental data	Calculated data using equations (1.10) and (1.11)	
$W = 800\text{g}$	$Var(P_i) = 0.0057$	$\sigma_i = 0.075\%$
$w_A = 2.84 \times 10^{-4} \text{ g}$	$Var(P_n) = 0.0213$	$\sigma_n = 0.146\%$
$w_B = 0.214 \times 10^{-4} \text{ g}$		

Maximum sample error [equation (1.13)]	$E = 0.486\%$
Sampling effectiveness [equation (1.12)]	$C = 2.7$

1.13 Experimental tests of sampling techniques

Example 6

Binary mixtures of coarse and fine sand (60:40 ratio) were examined [21] with a spinning riffler to give the data in Table 1.4. The experiment was repeated using other sampling techniques to give the data in Table 1.5. In every case 16 samples were examined to give the

Table 1.5 Reliability of selected sampling methods using a 60:40 sand mixture

Sampling technique	Standard deviation
Cone and quartering	6.81
Scoop sampling	5.14
Table sampling	2.09
Chute slitting	1.01
Spinning riffling	0.146
Random variation	0.075

standard deviations shown in column 2. It may be deduced that very little confidence can be placed in the first three techniques and that the spinning riffler is so superior to all other methods that it should be used whenever possible.

1.14 Weight of sample required

1.14.1 Gross sample

Particle size analysis is carried out on a sample extracted from the bulk which, irrespective of the precautions taken, never represents the bulk exactly. The limiting (minimum) weight of the gross sample may be calculated, using a simple formula to give an error within pre-designated limits, provided the weight of the gross sample is much smaller than that of the bulk.

The limiting weight is given by:

$$M_s = \frac{1}{2} \left(\frac{\rho}{\sigma_i^2} \right) \left(\frac{1}{w_l} - 2 \right) d_l^3 \times 10^3 \quad (1.15)$$

where:

- M_s is the limiting weight in (g);
- ρ is the powder density (g cm^{-3});
- σ_i^2 is the variance of the tolerated sampling error;
- w_l is the fractional mass of the coarsest size class being sampled;
- d_l^3 is the arithmetic mean of the cubes of the extreme diameter in the size class (cm^3).

Table 1.6. Minimum sample mass required for sampling from a stream of powder

Upper sieve size (cm)	Lower sieve size (cm)	Mass % in class ($100w_i$)	Sample weight required
0.0600	0.0420	0.1	37.5 kg
0.0420	0.0300	2.5	0.474 kg
0.0300	0.0212	19.2	14.9 g
0.0212	0.0150	35.6	1.32 g

This equation is applicable when the coarsest class covers a size range of not more than $\sqrt{2}:1$ and w_i is less than 50% of the total sample.

Example 7

Determine the minimum sample of quartz ($\rho = 2.65 \text{ g cm}^{-3}$) to give an expected sampling error $\sigma_i = 0.05$ (= 5%) if the coarsest size range of 105 to 75 μm contains 10% of the total weight.

$$M_s = \frac{1}{2} \left[\frac{2.65}{0.05^2} \right] \left[\frac{1}{0.10} - 2 \right] \left[\frac{(0.0105^3 - 0.0075^3)}{2} \right] \times 10^3$$

$$M_s = 1.56 \text{ g}$$

Since M_s is proportional to d^3 it increases rapidly with increasing particle size.

Example 8

Assume that a sieve analysis of the above powder is carried out, with the results shown in Table 1.6 and the tolerable sampling error for each fraction is $\pm 5\%$. The amount required for each fraction, in order to keep within this limit, equation (1.15) is given in column 4.

For a sieve analysis; in order to reduce the errors at the coarse end of the distribution, repeat analyses should be made using only the coarsest sieves. For the example above an error of 100% in the coarsest size range may be acceptable, i.e. (0.1 ± 0.1) g; this reduces the required weight to 94 g.

1.14.2 Sampling by increments

For sampling a moving stream of powder the gross sample is made up of increments. In this case the minimum incremental weight is given by:

Table 1.7. Minimum incremental mass required for sampling from a stream of powder

Maximum particle size (mm)	Minimum mass of increment (kg)
250 – 150	40.0
150 – 100	20.0
100 – 50	12.0
50 – 20	4.0
20 – 10	0.8
10 – 0	0.3

$$M_i = \frac{\mu_0 w_0}{v_0} \quad (1.16)$$

where:

- M_i is the average mass of the increment,
- μ_0 is the average rate of flow,
- w_0 is the cutter width for a traversing cutter,
- v_0 is the cutter velocity.

If w_0 is too small, a biased sample deficient in coarse particles, results. For this reason w_0 should be at least $3d$ where d is the diameter of the largest particle present in the bulk.

ISO 3081 suggest a minimum incremental mass based on the maximum particle size in mm. These values are given in Table 1.7. Secondary samplers then reduce this to analytical quantities.

Example 9

Determine the minimum increment weight for a powder falling from a belt conveyer at a rate of 3 metric tons per hour if the size of the largest particle is 1.0 mm and the sampling cutter speed is 6 cm s^{-1}

$$M_i = \left[\frac{3 \times 10^3 \text{ kg h}^{-1}}{3600 \text{ s h}^{-1}} \right] \left[\frac{3 \times 10^{-3} \text{ m}}{0.06 \text{ m s}^{-1}} \right]$$

$$M_i = 42 \text{ g}$$

Since the flowrate is 833 g s^{-1} this is not a practical amount, hence a two stage sampler is required. Sampler 1, say, can sample for 2 s to generate 1.67 kg of powder, which is fed to a hopper to provide a feed to a second sampler which reduces it by a factor of 40 to generate the required 42 g.

The minimum number of increments required to give an acceptable accuracy for the sampling period is 35, hence, the gross sample weight is given by:

$$M_s = 1.47 \text{ kg}$$

The gross sample can be reduced to a laboratory sample of about 10 g, using a Vezin type sampler for example, and finally to a measurement sample of about 1 g using a rotary riffler. If the particle size analysis is carried out on less than 1 g the final reduction is usually effected by dispersing the powder in a liquid and pipetting out the required aliquot.

Gy [22] proposed an equation relating the standard deviation, which he calls the fundamental error σ_F , to the sample size:

$$\sigma_F^2 = \left(\frac{1}{w} - \frac{1}{W} \right) C d^3 \quad (1.17)$$

where W is the mass of the bulk and $w = n\omega$ is the mass of n increments, each of weight ω which make up the sample, C is the heterogeneity constant for the material being sampled and d is the size of the coarsest element.

For the mining industry [23], he expressed the constant C in the form $C = clfg$ where:

$$c = \frac{1-P}{P} \rho \quad (1.18)$$

P is the investigated constant; ρ is the true density of the material; l is the relative degree of homogeneity, for a random mixture $l = 1$, for a perfect mixture $l = 0$; f is a shape factor assumed equal to 0.5 for irregular particles and 1 for regular particles; g is a measure of the width of the size distribution, $g = 0.25$ for a wide distribution and 0.75 for a narrow distribution (i.e. $d_{max} < 2 d_{min}$).

For the pharmaceutical industry Deleuil [1] suggested $C = 0.11c$, with the coarsest size being replaced by the 95% size.

For $W \gg w$ equation (1.17) can be written:

$$w\theta^2 = 0.1l \left(\frac{1-P}{P^3} \right) \rho t^3 d^3 \quad (1.19)$$

where $\theta = t \frac{\sigma_F}{P}$ and $t = 3$, (99.9% confidence level) for total quality.

- For $d_{95} = 100 \mu\text{m}$, $\rho = 1.5$, $P = 10^{-3}$ (1000 ppm) $\theta = 0.2$, $l = 0.03$ (random), $w = 1000 \text{ g}$.
- For $d_{95} = 100 \mu\text{m}$, $\rho = 1.5$, $P = 0.05$ $\theta = 0.05$, $l = 1$ (homogeneous), $w = 4 \text{ g}$.
- For $d_{95} = 20 \mu\text{m}$, $\rho = 1.5$, $P = 10^{-4}$ (100 ppm) $\theta = 0.05$, $l = 0.03$ (random), $w = 8000 \text{ g}$.

Deleuil [1] points out that a sample of this weight is never prepared because the lot is considered to be perfectly homogeneous ($l = 1$).

The product from industrial grinding circuits oscillates due to variation in hardness and particle size distribution of feed. Heiskanen and Niemelia [24] demonstrated that, using automatic sampling, on-line analysis and autocorrelation procedures, they could map out a frequency of oscillation.

References

- 1 Deleuil, M. (1994), Handbook of Powder Technology, No. 9, *Powder technology and pharmaceutical processes*, Ch. 1, eds. D. Chulia, M. Deleuil and Y. Pourcelot, Elsevier, 1, 42
- 2 Sommer, K. (1981) *Aufbereit Tech.*, 22(2), 96–105, 1
- 3 Cornish, D.C., Jepson, G. and Smurthwaite, M.J. (1981), *Sampling for Process Analyzers*, Butterworth, 3, 17
- 4 Julien, R., Meakin, P. and Pavlovich, A. (1992), *Phys. Rev. Let.*, 69, 640, 3
- 5 Maddox, J. (1992), *Nature*, 358, 3, 535, 3
- 6 ASTM D451-63 (1963), *Sieve Analysis of Granular Mineral Surfacing for Asphalt Roofing and Shingles*, 5
- 7 Hulley, B.J. (1970), *Chem. Eng.*, CE 410 - CE 413, 16
- 8 Clarke, J.R.P. (1970), *Measurement and Control*, 3, 241–244, 16
- 9 BS 3406 (1961): *Methods for the determination of particle size of powders*, Part I, sub-division of gross sample down to 0.2 mL, 22
- 10 Osborne, B.F. (1972), *C.I.M. Bull.*, 65, 97–107, 25
- 11 Cross, H.E. (1967), *Mining Congress J.*, 62–67, 25
- 12 Hinde, A.L. (1973), *J. South Afr. Inst. Min. Metall.*, 73, 256–268, 26
- 13 Nasr-el-Din, H., Shook, C.A. and Esmail, M.N. (1985), *Can. J. Chem. Eng.*, 63, 746–753, 26

- 14 Burt, M.W.G., Fewtrel, C.A. and Wharton, R.A. (1973), *Powder Technol.*, 7(6), 327–330, 27
- 15 Hatton, T.A. (1978), *Powder Technol.*, 19, 227–33, 28
- 16 Herdan, G. (1960), *Small particle statistics*, Butterworths, 28
- 17 Davies, R. (1982), *Encyclopedia of chemical technology*, Kirk-Othmer, 3rd ed., p. 528, John Wiley, 29
- 18 Carstensen, J.T. and Rhodes, C.T. (1993), *Drug Dev. Ind. Pharm.*, 19(20), 2699–2708, 31
- 19 Stange, K. (1954), *Chem. Eng. Tech.*, 26, 331, 35
- 20 Hawes, R. and Muller, L.D. (1960), A.E.R.E. R3051, Harwell, UKAEA, 36
- 21 Allen, T. and Khan, A.A. (1970), *Chem. Eng.*, 238, CE108–CE112, May, 37
- 22 Gy, P. (1953), *R. Ind. Min.* (French), 36, 311–345, 41
- 23 Gy, P. (1982), *Sampling of Particulate Material, Theory and Practice*, Elsevier, Amsterdam, 2nd ed., 41
- 24 Heiskanen, K. and Niemelia, O. (1993), *Part. Part. Syst. Charact.* 10, 70–73, 42

Data presentation and interpretation

2.1 Introduction

The behavior and properties of particulate material are, to a large extent, dependent on particle morphology (shape, texture etc.) size and size distribution. Therefore proper measurement, informative data presentation and correct data interpretation are fundamental to an understanding of powder handling and end-use properties.

In this chapter the following questions will be addressed:

- What is meant by particle size?
- What is meant by particle diameter?
 - For a single particle?
 - For an assembly of particles?
- How is the average size of an assembly of particles defined?
- What is meant by particle shape?
- What is meant by particle size distribution?

As well as answering these questions, methods of presenting data will be covered together with data analysis and interpretation.

Physical characterization differs from chemical assay in that frequently a unique value does not exist. The determined amount of copper in an ore sample should not depend upon the analytical procedure employed whereas the measured size distribution is method dependent. Only homogeneous, spherical particles have an unambiguous size.

The following story illustrates the problem. Some extra terrestrial beings (ETB) were sent to earth to study humans. Their homes were spherical and the more important the ETB the bigger the sphere. The ETB who landed in the Arctic had no problem in defining the shape of the igloos as hemispherical with a single (base) diameter. The ETB who landed in North America classified the wigwams as conical but required two dimensions, height and base diameter, to describe their size. The ETB who landed in New York classified the skyscrapers as cuboid with three dimensions mutually perpendicular. The one who landed in London gazed about him despairingly before committing

suicide. One of the purposes of this chapter is to reduce the possibility of similar tragedies.

2.2 Particle size

The size of a spherical homogeneous particle is uniquely defined by its diameter. For regular, compact particles such as cubes or regular tetrahedra, a single dimension can be used to define size. With some regular particles it may be necessary to specify more than one dimension: For a cone the base diameter and height are required whilst for a cuboid three dimensions are needed.

Derived diameters are determined by measuring a size-dependent property of the particle and relating it to a single linear dimension. The most widely used of these are the equivalent spherical diameters. Thus, a unit cube has the same volume as a sphere of diameter 1.24 units, hence this is the derived volume diameter. The diameter therefore depends upon the measured property.

Consider a cube of side 1 cm; its volume $V = 1 \text{ cm}^3$ and its superficial surface area $S = 6 \text{ cm}^2$. d_v is the diameter of a sphere having the same volume as the cube and d_s is the diameter of a sphere having the same surface area.

$$V = \frac{\pi}{6} d_v^3 \quad \text{so that} \quad d_v = \left(\frac{6}{\pi} \right)^{1/3} = 1.241$$

$$S = \pi d_s^2 \quad \text{so that} \quad d_s = \left(\frac{6}{\pi} \right)^{1/2} = 1.382$$

The surface to volume ratio is of fundamental importance since it controls the rate at which the particle reacts with its surroundings. This is given by:

$$\frac{S}{V} = \frac{\pi d_s^2}{\frac{\pi}{6} d_v^3} \quad \text{Thus } \frac{S}{V} = \frac{6d_s^2}{d_v^3} \quad \text{i.e. } S_v = \frac{6}{d_{sv}}$$

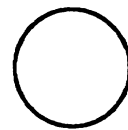
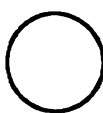
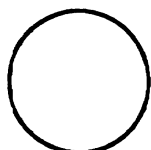
Hence, for a unit cube $d_{sv} = 1$. Thus a sphere of diameter 1.241 cm has the same volume as the cube, a sphere of diameter 1.382 cm has the same superficial surface area and a sphere of diameter 1 cm has the same surface to volume ratio. Definitions of the symbols used are given in Table 2.1.

If one is dealing with crystals of known shape it would be more sensible to relate the dimension to that shape, but this is not common practice; for the unit cube this procedure would make all the above derived diameters equal to unity.



$$d_{St,min} = 236 \mu\text{m}$$

$$d_{St,max} = 277 \mu\text{m}$$



$$d_{a,max} = 252 \mu\text{m} \quad d_v = 204 \mu\text{m} \quad d_{a,min} = 225 \mu\text{m}$$

Fig. 2.1 Stokes diameter for an irregular particle of volume diameter 204 μm . With maximum resistance to drag the particle will fall at the same speed as a sphere of diameter 236 μm . With minimum resistance to drag the particle will fall at the same speed as a sphere of diameter 277 μm .

A small, spherical, homogeneous particle settling in a fluid, rapidly reaches a constant 'terminal' velocity which is uniquely related to the diameter of the sphere. If an irregularly shaped particle is allowed to settle in a liquid, its terminal velocity may be compared with the terminal velocity of a sphere of the same density settling under similar conditions. The size of the particle, defined as its Stokes diameter, is then equated to the diameter of that sphere. In the laminar flow region particles settle in random orientation and a single particle generates a range of equivalent diameters depending on its orientation (Figure 2.1). The Stokes diameter is some average of these. Outside the laminar flow region particles orientate themselves to give maximum resistance to motion and the free falling diameter that is generated will be the smallest of these diameters.

Microscopy is the only widely used particle sizing technique in which individual particles are observed and measured. A single irregular particle has an infinite number of linear dimensions and it is only when they are averaged that a meaningful value results. For an assembly of particles each measurement quantifies the particle size in only one direction. If the particles are in random orientation, and if sufficient particles are counted, the size distribution of these measurements reflect the size distribution of the projected areas of the particles perpendicular to the viewing direction. Because of the need to

count a large number of particles in order to generate meaningful data these diameters are called statistical diameters.

If the projected areas of the particles are compared with the areas of series of circles the projected area diameters generated describe the particles in two dimensions for the orientation in which they are measured. In microscopy this is usually the projected area in stable orientation but in certain cases the particles may be in a less stable orientation to generate a lower value (Figure 2.2).

For a single particle the expectation of a statistical diameter and its coefficient of variation may be calculated from the following equations [1] (Figure 2.3).

$$E(d_R) = \frac{1}{\pi} \int_0^\pi d_R d\theta_R \quad (2.1)$$

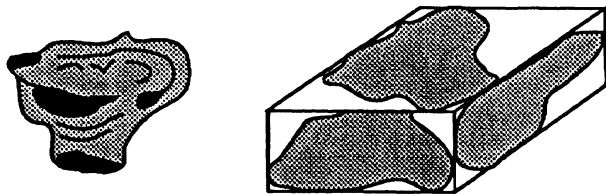


Fig. 2.2 The projected area of a particle is orientation dependent. Martin's diameter (d_M) is 246 μm , the Feret diameter (d_F) is 312 μm and the projected area diameter in stable orientation ($d_{a,\max}$) is 252 μm (the particle is the same as in Figure 2.1).

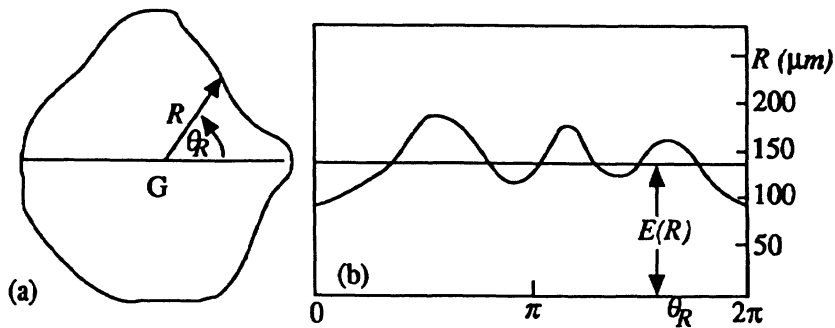


Fig. 2.3 (a) Definition of unrolled diameter d_R [radius $R = (d_R/2)$]; (b) unrolled curve.

Table 2.1 Definitions of particle diameters

Symbol	Name (diameter)	Definition	Formula
d_v	Volume	Diameter of a sphere having the same volume as the particle	$V = \frac{\pi d_v^3}{6}$
d_s	Surface	Diameter of a sphere having the same surface as the particle	$S = \pi d_s^2$
d_{sv}	Surface-volume	Diameter of a sphere having the same external surface to volume ratio as the particle	$d_{sv} = (d_v^3/d_s^2)^{1/3}$
d_d	Drag	Diameter of a sphere having the same resistance to motion as the particle in a fluid of the same viscosity and at the same velocity (d_d approaches d_s when Re is small)	$F_d = 3\pi d_d \eta v$
d_f	Free-falling	Diameter of a sphere having the same free-falling speed as a particle of the same density in a fluid of the same density and viscosity	
d_{St}	Stokes	Free-falling diameter in the laminar flow region	$d_{St} = \sqrt{(d_v^3/d_s^2)}$
d_a	Projected area	Diameter of a circle having the same projected area as the particle in stable orientation	
d_p	Projected area	Diameter of a circle having the same projected area as the particle in random orientation [mean value of $d_p = d_s$ for convex particles]	
d_c	Perimeter	Diameter of a circle having the same perimeter as the projected outline of the particle	$P = \pi d_c$
d_A	Sieve	Width of the minimum square aperture through which the particle will pass	
$\cdot d_F$	Feret	The distance between pairs of parallel tangents to the projected outline of the particle in some fixed direction	
$\cdot d_M$	Martin	Chord length, parallel to some fixed direction, which divides the particle projected outline into two equal areas	
d_R	Unrolled	Chord length through the centroid of the particle outline	

- statistical diameters, often defined in terms of the mean value for a particular particle.

$$\sigma_{d_R}^2 = \left[E(d_R^2) - \frac{E^2(d_R)}{E(d_R)} \right] \quad (2.2)$$

$$E(d_F) = \frac{1}{\pi} \int_0^\pi d_F d\theta_F \quad (2.3)$$

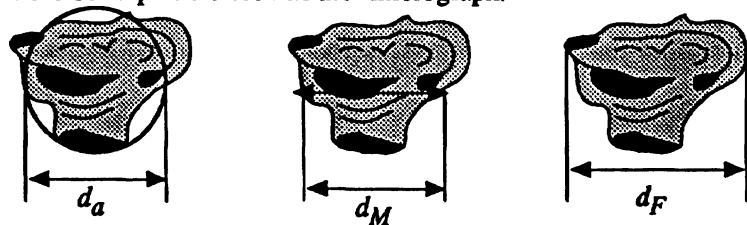
$$\sigma_F^2 = \left[E(d_F^2) - \frac{E^2(d_F)}{E(d_F)} \right] \quad (2.4)$$

$$E(d_M) = \frac{1}{\pi} \int_0^\pi d_M d\theta_M \quad (2.5)$$

$$\sigma_M = \sqrt{\left[E(d_M^2) - \frac{E^2(d_M)}{E(d_M)} \right]} \quad (2.6)$$

An illustration of two statistical diameters, Feret and Martin, and the projected area diameter is given in Figure 2.4.

Anomalies can occur due to the state of aggregation of the particles. Figure 2.5a shows a single particle of Prussian blue about 1 µm in diameter. The nitrogen adsorption surface area is 61.3 m² g⁻¹ from which the surface-volume mean diameter is 0.051 µm. This is the diameter of the primary particles of which the aggregate is made up. Similarly the micronised Prussian blue Figure 2.5b has approximately the same surface-volume mean diameter. With the red oxide Figure 2.5c the diameter is 0.21 µm which is approximately the same as the solid particle seen in the micrograph.



Projected area diameter
(stable orientation)
252 µm

Martin diameter
246 µm

Feret diameter
312 µm

Fig. 2.4 Particle size of a quartz particle by microscopy using Feret, Martin and projected area diameter.

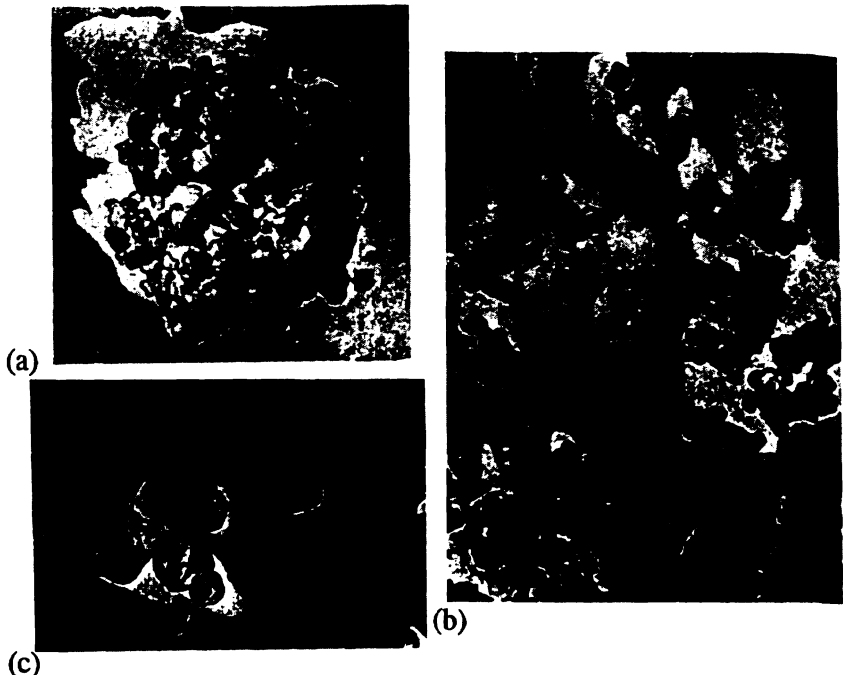


Fig. 2.5 Electron microscope photo-micrographs of two paint pigments showing how particles can be aggregates of finer particles [2]. (a) A single particle of Prussian blue about $1\mu\text{m}$ in diameter. (b) the primary particles, which combine to make up (a) of mean size $0.051\mu\text{m}$. (c) a red oxide of diameter $0.021\mu\text{m}$ which is approximately the same diameter as the solid particle seen in the micrograph.

2.3 Average diameters

The purpose of an average is to represent a group of individual values in a simple and concise manner in order to obtain an understanding of the group. It is important therefore that the average should be representative of the group. All averages are a measure of central tendency, which is unaffected by the relatively few extreme values in the tails of the distribution.

The *mode*, the most commonly occurring (most popular) value in a distribution, passes through the peak of the relative distribution curve, i.e. it is the value at which the frequency is a maximum (Figure 2.6). More than one high density region may be present in which case the distribution is said to be multi-modal, i.e. bimodal, trimodal and so on.

The *median* divides the distribution into two equal parts, i.e. it is the 50% size on the cumulative distribution curve.

The *mean* (\bar{x}) is the center of gravity of the distribution (Figure 2.7):

$$\sum_0^{\bar{x}} (x - \bar{x}) \frac{d\phi}{dx} dx = \sum_0^{\bar{x}} (\bar{x} - x) \frac{d\phi}{dx} dx$$

$$\bar{x} \sum_0^{\bar{x}} d\phi = \sum_0^{\bar{x}} x d\phi$$

i.e. For the mean, the moment of the sums of the elementary areas of the relative distribution, of width dx , about the ordinate, equals the sum of the moments of the elements about the ordinate:

$$\bar{x} = \frac{\sum x d\phi}{\sum d\phi} \quad (2.7)$$

For a number distribution $d\phi = dN$ and:

$$\bar{x} = \frac{\sum x dN}{\sum dN} = x_{NL}$$

For a mass (volume) distribution $d\phi = dV = x^3 dN$ giving:

$$\bar{x} = \frac{\sum x dV}{\sum dV}$$

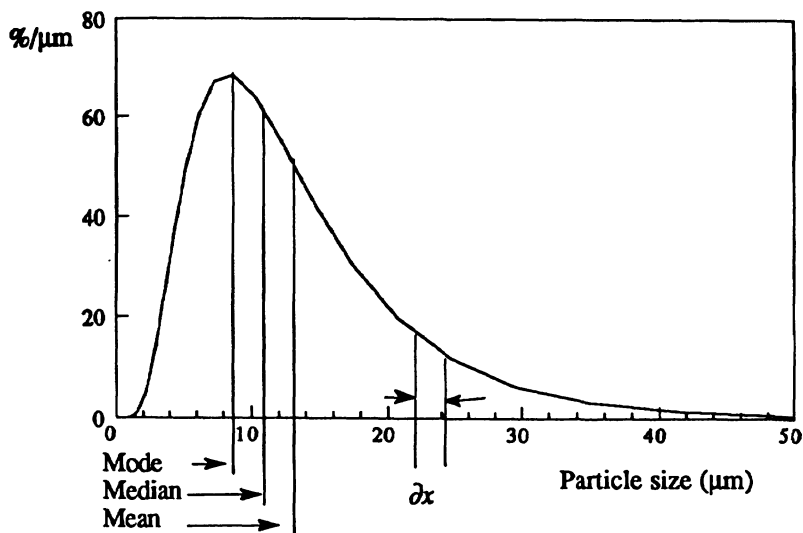


Fig. 2.6 Definitions of some average diameters.

$$\bar{x} = \frac{\sum x(x^3 dN)}{\sum x^3 dN}$$

$$\bar{x} = \frac{\sum x^4 dN}{\sum x^3 dN} = x_{VM} \quad (2.8)$$

These means represent the distribution in only two of its properties. The characteristics of a distribution are its total number, length, surface, volume (mass) and moment. Note that:

A system of unequally sized particles may be represented by a system of uniform particles having two, and only two, characteristics of the original distribution.

As a simple illustration, consider a system of particles containing one particle of each size from one to ten; this distribution can be represented in number and length by a mean size of 5.5 (i.e. the number-length mean diameter $x_{NL} = 5.50$) but ten particles each of size 5.5 will not have the same surface or volume as the original distribution.

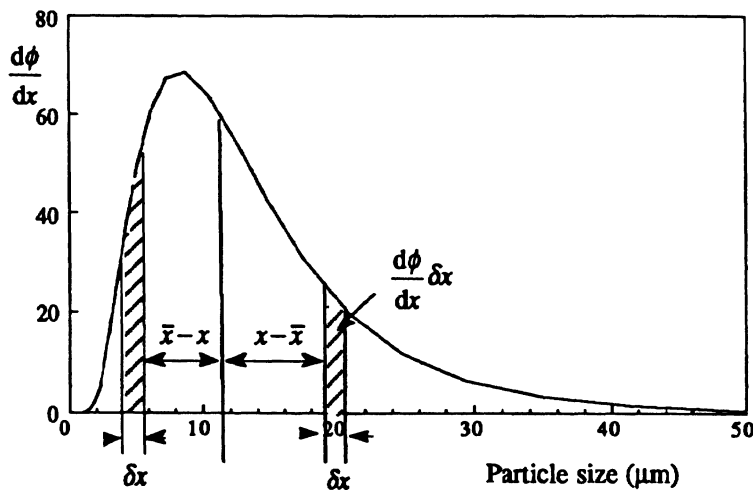


Fig. 2.7 Finding the center of gravity of a distribution by taking moments.

Table 2.2 Definitions of mean diameters

Number, length	x_{NL}	=	$\frac{\sum dL}{\sum dN}$	=	$\frac{\sum xdN}{\sum dN}$
Number, surface	x_{NS}	=	$\sqrt{\frac{\sum dS}{\sum dN}}$	=	$\sqrt{\left(\frac{\sum x^2 dN}{\sum dN}\right)}$
Number, volume	x_{NV}	=	$\left[\frac{\sum dV}{\sum dN}\right]^{1/3}$	=	$\left[\frac{\sum x^3 dN}{\sum dN}\right]^{1/3}$
Length, surface	x_{LS}	=	$\frac{\sum dS}{\sum dL}$	=	$\frac{\sum x^2 dN}{\sum xdN}$
Length, volume	x_{LV}	=	$\sqrt{\frac{\sum dV}{\sum dL}}$	=	$\sqrt{\frac{\sum x^3 dN}{\sum xdN}}$
Surface, volume	x_{SV}	=	$\frac{\sum dV}{\sum dS}$	=	$\frac{\sum x^3 dN}{\sum x^2 dN}$
Volume moment	x_{VM}	=	$\frac{\sum dM}{\sum dV}$	=	$\frac{\sum x^4 dN}{\sum x^3 dN}$
Weight moment	x_{WM}	=	$\frac{\sum dM}{\sum dV}$	=	$\frac{\rho \sum x^4 dN}{\rho \sum x^3 dN}$

ρ = powder density

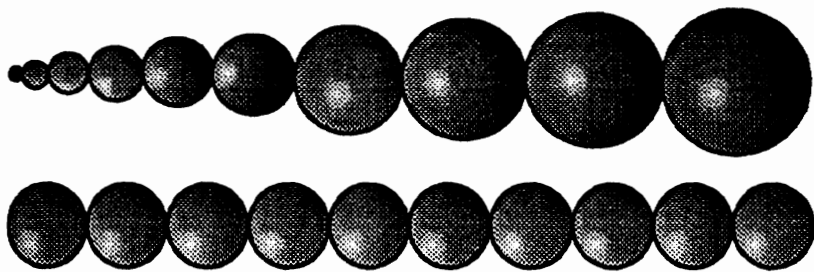


Fig. 2.8 The homogeneous distribution that represents in number and length a heterogeneous distribution of 10 particles of size 1 to 10 with unit separation in size.

Similarly the volume-moment mean diameter (i.e. the mean of the mass distribution) is:

$$x_{VM} = 8.37$$

Mean diameters are defined in Table 2.2 and values for the example above are given in Table 2.3. The size increases systematically with the order of the distribution i.e. the mean of the volume distribution is greater than the mean of the surface distribution is greater than the

mean of the length distribution is greater than the mean of the number distribution.

Table 2.3 Calculated values of mean diameters for a selection of particles of diameter 1 to 10 with 1 particle in each size class

Number (N)	Length (L)	Surface (S)	Volume (V)	Moment (M)
	$L = \sum_{1}^{10} x dN$	$S = \sum_{1}^{10} x^2 dN$	$V = \sum_{1}^{10} x^3 dN$	$M = \sum_{1}^{10} x^4 dN$
$N = 10$	$L = 55$	$S = 385$	$V = 3\ 025$	$M = 25\ 333$
$x_{NL} = 5.50$ $x_{LS} = 7.00$ $x_{SV} = 7.86$ $x_{VM} = 8.37$	$x_{NS} = 6.20$ $x_{LV} = 7.42$ $x_{SM} = 8.11$	$x_{NV} = 6.71$ $x_{LM} = 7.72$	$x_{NM} = 7.09$	

2.4 Particle dispersion

The spread of a distribution may be expressed in terms of a range, i.e. the difference between its minimum and maximum sizes; the inter-quartile range is the difference between the 25% and 75% size ($x_{75} - x_{25}$); the inter-percentile range between two percentages, usually 10 and 90 ($x_{90} - x_{10}$). The standard deviation and geometric standard deviation are statistical measures of spread.

The least significant of these is the first, since a stray undersize or oversize particle can greatly affect its value. The most significant are the standard deviations.

2.5 Particle shape

Particle shape is a fundamental powder property affecting powder packing and thus bulk density, porosity, permeability, cohesion, flowability, caking behavior [3], attrition, interaction with fluids and the covering power of pigments, although little quantitative work has been carried out on these relationships. Davies [4] gives other examples where information on shape is needed to describe powder behavior.

Many papers have been written on shape determination but there are few articles which relate the measurements to powder behavior and end-use properties. Hawkins [5] in a recent book, however, critically reviews nearly 300 articles on particle shape measurement.

Qualitative terms [6] may be used to give some indication of particle shape but these are inadequate as a measure of particle properties.

Heywood [7] recognized that the word 'shape' in common usage refers to two distinct characteristics of a particle, form and proportions. The former refers to the degree to which a particle approaches a definite form, such as a cube, tetrahedron or sphere, and the latter by the relative proportions of the particle which distinguish one cuboid, tetrahedron or spheroid from another of the same class (Figure 2.9).

Macroscopically, shape may be derived using shape coefficients or shape factors. Microscopically particle texture may be defined using fractals or Fourier transforms. The introduction of quantitative image microscopy has made such approaches to particle texture analysis practical.

2.5.1 Shape coefficients

The surface area and volume of a particle are given by the following equations:

$$\text{Surface of a particle, } S = \pi d_s^2 = \alpha_{s,a} d_a^2 = x_a^2$$

$$\text{Volume of a particle, } V = \frac{\pi}{6} d_v^3 = \alpha_{v,a} d_a^3 = x_a^3 \quad (2.9)$$

where α_s and α_v are the surface and volume shape coefficients, the additional suffix denoting that the measured diameter is the projected area diameter, (for a sieve analysis for example, $S = \alpha_{s,A} d_A^2$ and so on). The symbol x denotes size, as opposed to diameter, and includes the shape coefficient. This artifact is found to be very useful for general treatment of data. It must be noted that, in general, particles do not have a unique surface area, the measured surface depending on the method of measurement. Similarly, unless the particles are homogeneous, their measured volume depends on the measurement technique. The surface area per unit volume (volume-specific surface) is the ratio of S to V : For example:

$$S_v = \frac{S}{V} = \frac{6d_s^2}{d_v^3} = \frac{6}{d_{sv}} \quad (2.10)$$

$$S_v = \frac{\alpha_{s,a} d_a^2}{\alpha_{v,a} d_a^3} = \frac{\alpha_{sv,a}}{d_a} \quad (2.11)$$

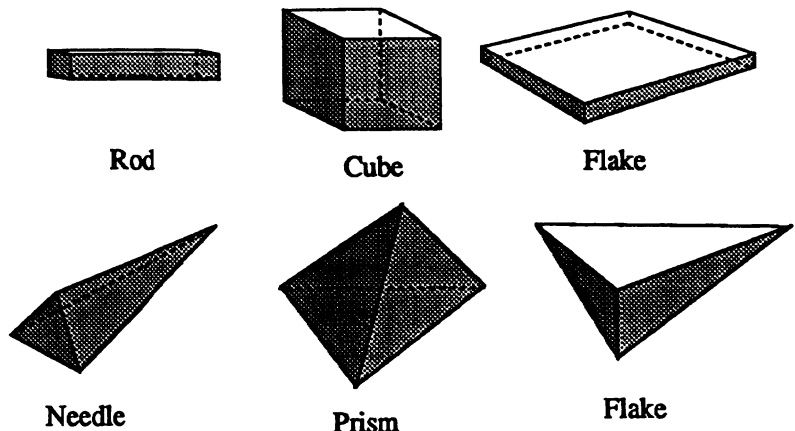


Fig. 2.9 Form and proportions.

where d_{sv} , the surface-volume diameter is the diameter of a sphere having the same surface to volume ratio as the particle. $\alpha_{sv,a}$ is the surface-volume shape coefficient by microscopy.

Similarly the volume specific surface by microscopy is:

$$S_{v,a} = \frac{6}{d_a} \quad (2.12)$$

and the volume-specific surface by sieving is defined as:

$$S_{v,A} = \frac{6}{d_A} \quad (2.13)$$

Thus, the manner in which the surface area changes from sample to sample can be investigated on the assumption that shape is size independent.

2.5.2 Shape factors

The size of a particle may be expressed by a single dimension using one of the diameters defined in Table 2.1. The differences between these dimensions increases as the particle diverges in shape from a sphere. For a population of particles whose shape is not size dependent, distributions obtained using different methods of analysis will be homologous. Multiplying the sizes of one distribution by a constant factor will therefore generate the other distribution.

One of the earliest defined shape factors is the sphericity ψ_W , which was defined by Wadell as [8 – 11]:

$$\psi_W = \frac{\text{surface area of a sphere having the same volume as the particle}}{\text{surface area of the particle}}$$

$$\psi_W = \left(\frac{d_v}{d_s} \right)^2 \quad (2.14)$$

For two-dimensional images the proximity of the image to the outline of a circle is defined by circularity where:

$$\text{circularity} = \frac{(\text{perimeter of particle outline})^2}{4\pi(\text{cross-sectional or projection area of particle outline})}$$

As an illustration of the application of shape coefficients and shape factors consider a cuboid of side x, x, kx , where k is a variable.

$$\text{In this case: } \psi_W = \frac{(4.5\pi k^2)^{1/3}}{(1 + 2k)}$$

and, assuming $d_{St} = \sqrt{d_v^3 / d_s}$, (see Table 2.1 and equation 2.16)

$$\frac{\alpha_{sv,St}}{6} = \frac{(1 + 2k)^{0.75}}{(4.5\pi k^2)^{0.50}} \quad (2.15)$$

$\alpha_{sv,St}$ is the surface-volume shape coefficient by Stokes diameter (d_{St}). Both $(1/\psi_W)$ and α_{sv} are plotted against k in Figure 2.10; the shape of the curve will vary according to the ordinate units employed, e.g. if Stokes diameter were chosen for the ordinate instead of k .

The ratio of Stokes diameter to Coulter diameter for particles of cuboid form is given by the relationship below (i.e. the median size by sedimentation is 29.2 μm and the median size by Coulter is 32.0 μm):

$$\frac{d_{St}}{d_C} = \frac{29.2}{32}$$

Thus the shape factor for this powder, relating Stokes and Coulter diameter is 0.913.

It can be shown that, for non-re-entrant particles, where the drag diameter equals the surface diameter:

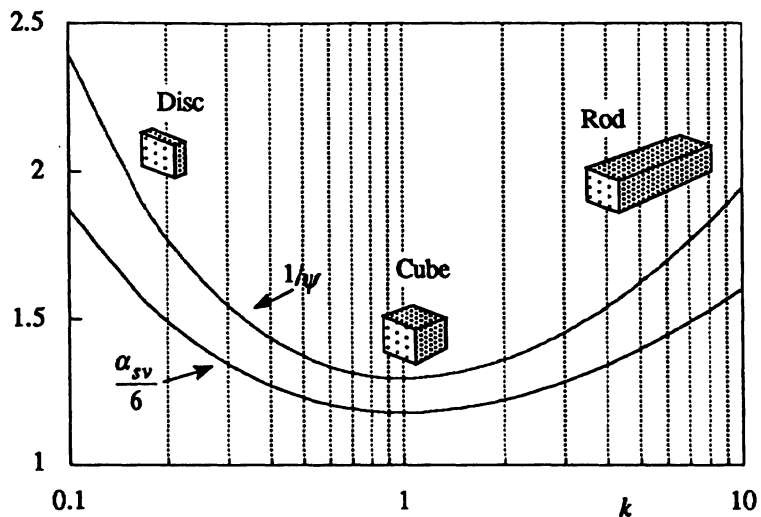


Fig. 2.10 Relationship between shape factors and particle dimensions.

$$\frac{d_{St}}{d_C} = \sqrt{\frac{(d_v)^3}{d_s}} = \psi_W^{0.25}$$

Thus the particles are discs ($k = 0.327$) or cylinders ($k = 3.56$) (Figure 2.10). It can be deduced from this that unless the particles are grossly irregular, the difference between Stokes diameter and Coulter diameter is very small.

2.5.3 Shape regeneration by Fourier analysis

Briefly, this method consists of finding the center of gravity of a particle and its perimeter, from which a polar coordinate system is set up. A fixed angular coordinate interval, say $2\pi/N$ radians, is chosen and the distances of the origin to the boundary at these N points are determined so that the shape of the particle is represented by these distances and their angular coordinates. Thus for N (= 8, 16, 32) measurements, determined on the image of the particle, the Fourier coefficients can be estimated. For each particle a Fourier representation is obtained, giving pattern vectors of 8, 16 or 32 elements, which are subject to feature extraction, classification and recognition [12]. The shape of individual particles can be characterized using Fourier grain analysis or morphological analysis [13–15]. The method has been extended to measuring the shape mix in powders [16]. It has been used to relate attrition rate in a milling

operation to particle shape [17,18]. Particle shape grouping by the co-ordinate detection function with Fourier analysis was discussed by Shibata *et al.* [19].

2.5.4 Fractal dimensions characterization of textured surfaces

Rough (textured) particles do not have a unique surface. The measured surface depends upon the method of measurement and will increase as the degree of scrutiny increases. For example, corrugating a one acre field by plowing it will increase its superficial area to $\sqrt{2}$ acres.

Texture is difficult to define and quantify. Davies [4], for example, defined texture as the number of asperities possessed by a particle outline. He generated a shape distribution histogram by plotting asperity frequency against particle perimeter and defined a mean texture for a powder in terms of asperities per mm. Using these definitions it is possible to monitor particle abrasion and quantify the potential of conveyed powders to generate dust [20]. Texture has also been defined in terms of roughness or rugosity where the rugosity coefficient is defined as the perimeter of the particle outline divided by the perimeter of the convex hull [21].

Mandelbrot introduced a new geometry in a book, which was first published in French in 1975, with a revised English edition [22] in 1977. In 1983 he published an extended and revised edition which he considered to be the definitive text [23]. Essentially he stated that there are regions between a straight line which has a dimension of 1, a surface which has a dimension of 2 and a volume which has a dimension of 3, and these regions have fractional dimensions between these integer limits. An excellent review of the importance of fractal geometry in particle characterization has been presented by Kaye [24].

If an irregular outline is enclosed by a polygon of constant side length λ , the perimeter P_λ will increase as the side length decreases.

For a polygon with n sides: $P_\lambda = n\lambda$ (2.16)

Mandelbrot showed that: $P_\lambda = k\lambda^{1-D}$ (2.17)

Hence a plot of $\log P_\lambda$ against $\log \lambda$ will have a slope of $1-D$. The parameter D is characteristic of the texture of the particle and was called by Mandelbrot the fractal dimension. The fractal dimension for the outline of a particle lies between 1 and 2, the more irregular the outline, the higher the value.

As an illustration of the technique consider a map of the British coastline (Figure 2.11). The fractal dimension is found to depend upon the degree of scrutiny [25,26] (Figure 2.12), having a dual value of 1.41 for large step lengths decreasing to 1.28 for short step lengths.

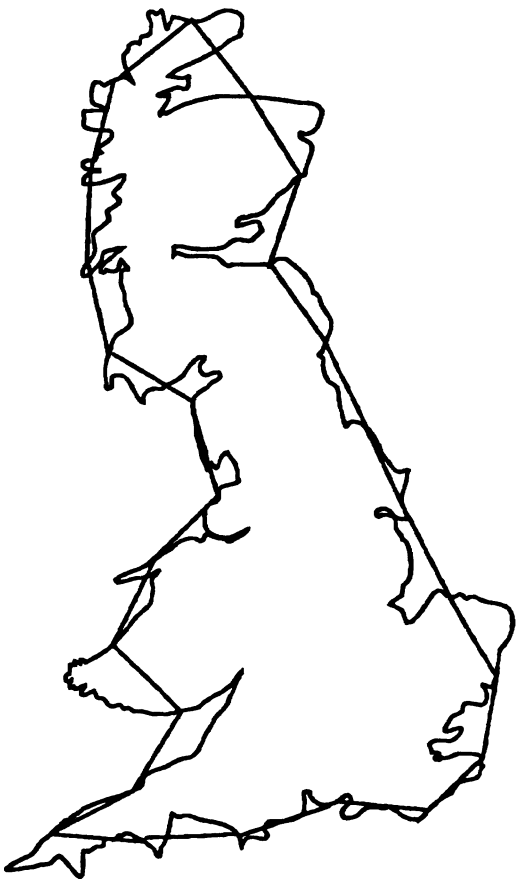


Fig. 2.11 Fractal analysis of the British coastline.

The method has found applications in determining the ruggedness of particle profiles and can be modified for use with image analyzers.

Fractals may also be used to describe the texture of surfaces with values lying between 2 and 3, the more irregular the surface, the higher its fractal dimension; a fractal surface is defined as being a surface in which increasing and similar detail is revealed with increasing magnification, i.e. the dimension is scale invariant [27]. This parameter has been used to examine rice hull (husk) [28]. Because of its high energy content, rice hull can be a source of energy for the rice milling process. The major obstacle has been its non-uniform flow in the reactor attributable in part to its irregular geometry. Kaupp [29] fitted a polynomial to describe the surface irregularities as observed with an

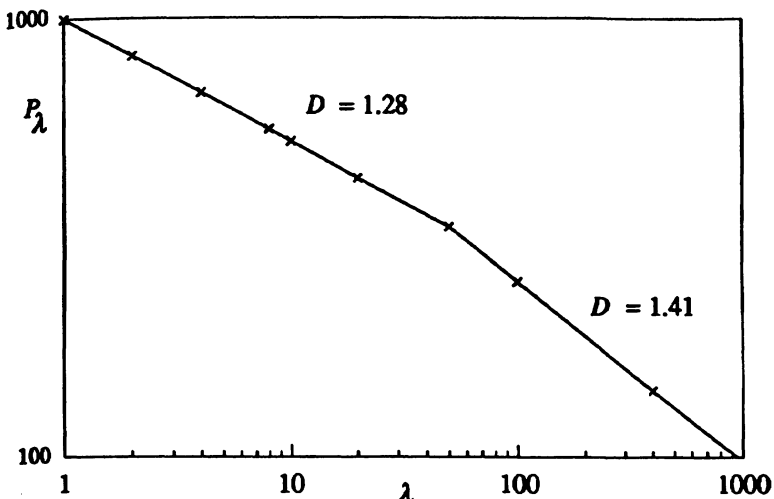


Fig. 2.12 Relationship between step length (λ) and perimeter (P_λ) for the British coastline.

electron microscope by tracing the circumference with a computer guided image analyzer.

Fan *et al.* [28] determined surface area by nitrogen gas adsorption; they stated that the fractal dimension could be determined by adsorbing

different sized molecules on similar surfaces, or keeping the adsorbate the same but changing the size of the adsorbent. They adopted the latter procedure by using between sieve fractions. In the first case the specific surface S is related to the fractal dimension D_{sf} by equation (2.18) and in the second the relationship given in equation (2.19) applies.

$$S = \sigma^{-0.5}(D_{sf}^f - 2) \quad (2.18)$$

$$S = r^{-(D_{sf}^f - 3)} \quad (2.19)$$

where σ is the cross-sectional area of the adsorbate molecule and r is the particle radius. Avnir *et al.* [30] used molecules of different sizes and found $1 < D < 2$. Pore wall roughness has also been determined by fractal geometry using mercury intrusion/retraction [31].

Fractal analysis is also being applied to computer modeling of aerosol agglomeration [32] and the reaction kinetics of pigment

formation [33,34]. The fractal surface of particles has been linked to their shedding propensity [35] and to erosion during pneumatic conveying [36]. For a recent review of the application of fractals to particle morphology readers are referred to [37].

2.5.5 Other methods of shape analysis

Gotoh and Finney [38] proposed a mathematical method for expressing a single, three dimensional body by sectioning as an equivalent ellipsoid with the same volume, surface area and average projected area as the original body.

Micro-cuboids in three dimensional turbulent flow have been examined using Fraunhofer diffraction [39]. Both dynamic and static three dimensional particle shape features could be obtained and served as a basis for particle shape analysis by pattern recognition.

The use of wedge-shaped photodetectors to measure forward light scattering intensity has also been explored for determination of crystal shape [40].

2.5.6 Sorting by shape

Particle may be sorted by shape by taking advantage of their behavior on a sloping, vibrating surface. Rounded particle tend to roll, granular particles to hop and flaky particles to shuffle. Ridgeway and Rupp [41,42] used a table designed for sorting industrial diamonds (Jeffrey – Galion) for their work whereas others used a rotating disc [43,44]. Slotted sieves have also been used for shape sorting. These have the advantage that they sort quantitatively on the basis of two of the particles' principal dimensions and they sort more selectively than a sorting table [45]. Identical square mesh sieves have also been used to sort different shaped particles by residence time [46]. The Jeffrey – Galion table has also been used to sort milled pasta and milled gelatin by shape [47].

2.6 Determination of specific surface from size distribution data

Surface to volume (or mass) ratio is a fundamental property of a powder since it governs the rate at which the powder interacts with its surroundings. As examples, small crystals in a mother liquor, with high surface to volume ratios, dissolve or grow more rapidly than large ones. Medication, in powder form, can pass through the body relatively unadsorbed if the active ingredients are composed of large particles, whereas fine particles are rapidly adsorbed; in the former case there is little reaction to the medication whereas in the latter it could be toxic.

Specific surface can be determined directly by permeametry, gas diffusion, gas adsorption and adsorption from solution and can also be calculated from size distribution data.

2.6.1 Determination of specific surface from a number count

Consider a number count carried out by microscopy, where the measured diameter is the projected area diameter ($d_{a,r}$).

For an assembly of particles equation (2.11) becomes:

$$S_v = \frac{S}{V} = \frac{\sum_{r=\min}^{r=\max} \alpha_{sv,a_r} \Delta n_r d_{a,r}^2}{\sum_{r=\min}^{r=\max} \alpha_{v,a_r} \Delta n_r d_{a,r}^3} \quad (2.20)$$

where there are Δn_r particles of projected area diameter $d_{a,r}$.

Assuming that the surface-volume shape coefficient by projected area, $\alpha_{sv,a}$, is size independent over the size range under consideration:

$$S_v = \alpha_{sv,a} \frac{\sum_{r=\min}^{r=\max} \Delta n_r d_{a,r}^2}{\sum_{r=\min}^{r=\max} \Delta n_r d_{a,r}^3} \quad (2.21)$$

Thus if S_v is determined by some independent procedure, the manner in which the surface-volume shape coefficient by microscopy, $\alpha_{sv,a}$ changes with projected area diameter can be investigated. Alternatively, assuming $\alpha_{sv,a} = 6$, the volume-specific surface by microscopy, $S_{v,a}$, can be determined.

2.6.2 Determination of specific surface from a surface count

Consider a size distribution obtained by a surface analysis method, e.g. photosedimentation, where the measured diameter is the Stokes diameter ($d_{St,r}$) and the surface fraction between two diameters centered on $d_{St,r}$ is S_r .

Let $p_r = \frac{S_r}{S}$

where $S = \sum_{r=\min}^{r=\max} S_r$

Then $S_r = p_r S = \alpha_{sp,r} \Delta n_r d_{St,r}^2$

and

$$V_r = \alpha_{vp,r} \Delta n_r d_{St,r}^3$$

Therefore $S_r = \left(\frac{\alpha_{sp,r}}{p_r} \right) \left(\frac{V_r}{\alpha_{vp,r} d_{St,r}} \right)$

Assuming that $\alpha_{sv,p}$, the surface-volume shape coefficient by photosedimentation, is size independent over the size range under consideration:

$$S_v = \frac{\alpha_{sv,p}}{\sum_{r=\min}^{\max} p_r d_{St,r}} \quad (2.22)$$

2.6.3 Determination of specific surface from a volume (mass) count

Consider a particle size distribution determination by mass where the fractional masses (volume = V_r) of particles of mean diameters (d_r) are determined. For a sieve analysis, for example, the measured diameters are sieve diameters ($d_{x,r} = d_{A,r}$) and the fractional volume residing between two sieves of mean aperture $d_{A,r}$ is V_r .

Let $q_r = \frac{V_r}{V}$ where $V = \sum_{r=\min}^{\max} V_r$

$$V_r = q_r V = \alpha_{v,x,r} \Delta n_r d_{x,r}^3$$

$$S_r = \alpha_{s,x,r} \Delta n_r d_{x,r}^2$$

Therefore

$$S_r = \alpha_{sv,x,r} \frac{q_r V}{d_{x,r}}$$

$$S_v = \alpha_{sv,x} \sum_{r=\min}^{\max} \frac{q_r}{d_{x,r}} \quad (2.23)$$

Example Determination of specific surface from sieve analysis data

Table 2.4 Calculation of mass specific surface from sieve analysis data

Sieve size (μm)	Mean sieve size (d_{Ar})	Mass fraction residing on sieve (q_r)	Surface area factor ($\text{cm}^2 \text{cm}^{-3}$) (q_r/d_{Ar})
105	89	0.30	33.7
150	125	0.50	40.0
210	178	0.20	11.2

From the data in Table 2.4, the volume specific surface by sieving is $509 \text{ cm}^2 \text{cm}^{-3}$. For a powder of density 2500 kg m^{-3} this becomes $204 \text{ cm}^2 \text{g}^{-1}$.

2.7 Tabular presentation of particle size distribution

Having defined the relevant particle size the frequency of occurrence of each size can be found. Number distributions can be determined by microscopy, electrical and light sensing zone methods; surface distributions by photosedimentation and mass distributions by sieving and x-ray sedimentation.

Table 2.5 shows an example of size analysis data (ϕ can be number, surface or weight). Column 1 gives the interval of the size classes; column 2 gives the mean size of each of these classes; column 3 gives the percentage frequency of occurrence within these classes; these sets of data are accumulated in column 4; percentage/ μm is presented in column 5, percentage/ $\log(\mu\text{m})$ (base 10) in column 6 and percentage/ $\ln(\mu\text{m})$ (base e) in column 7.

For narrow size distributions it is usually preferable to use an arithmetic size progression (as in Table 2.5) and present the frequency data in the manner given in column 5.

For wide size ranges a geometric size progression (e.g. 2, $2\sqrt{2}$, 4) is usually preferred with frequency data as presented as in column 6.

For data manipulation the presentation in column 7 is preferred. The relationships between these data are as follows:

$$\frac{d\phi}{d \ln(x)} = x \frac{d\phi}{dx} = \log(e) \frac{d\phi}{d \log(x)} = \left[0.434 \frac{d\phi}{d \log(x)} \right] \quad (2.24)$$

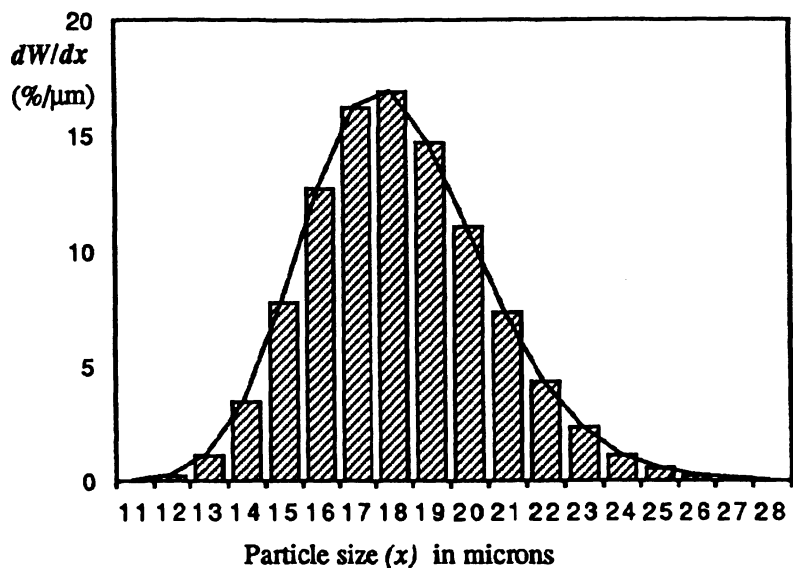


Fig. 2.13 Frequency distribution presented as a histogram and as a continuous curve. The ordinate is presented as percentage per micron so that the area under the curve is 100.

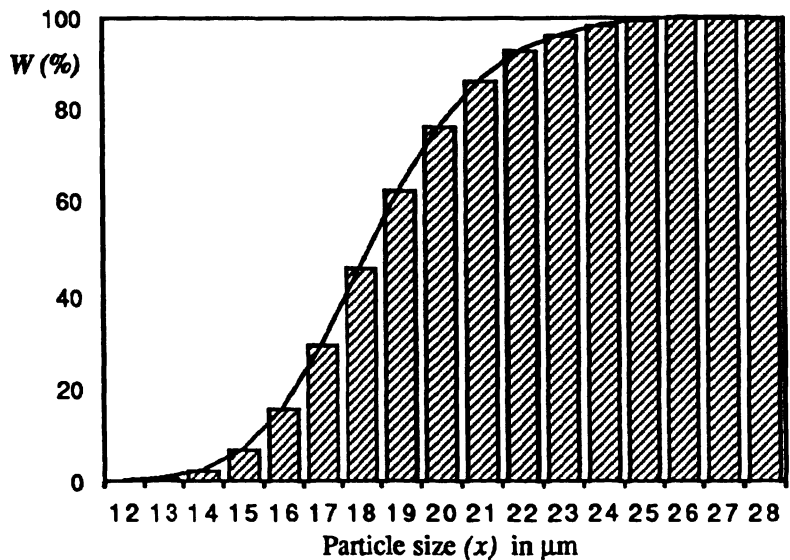


Fig. 2.14 Cumulative percentage undersize curve.

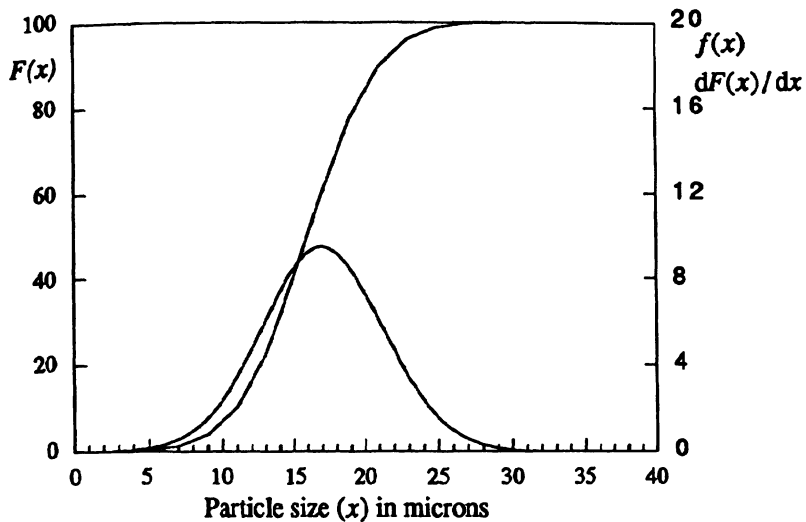


Fig. 2.15 Frequency distribution presented as continuous curve with the abscissa on a linear scale. The right ordinate is presented as percentage/micron so that the area under the curve is 100.

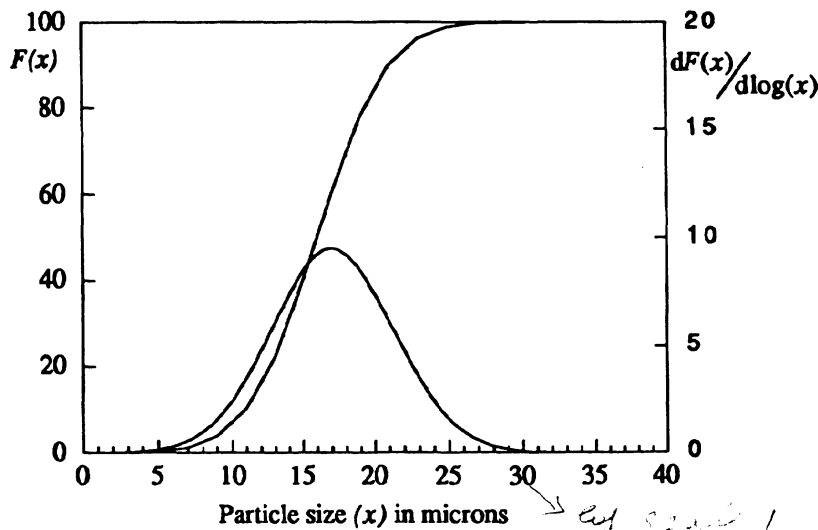


Fig. 2.16 Frequency distribution presented as continuous curve with the abscissa on a logarithmic scale. The right ordinate is presented as percentage log-micron so that the area under the curve is 100.

Table 2.5 Tabular presentation of size distribution data

Size limits (μm)	Mean size (μm)	Relative frequency (%) ($d\phi$)	Cumulative frequency (%) (ϕ)	% per μm $(\frac{d\phi}{dx})$	% per $\log(\mu\text{m})$ $(\frac{d\phi}{d\log x})$	% per $\ln(\mu\text{m})$ $(\frac{d\phi}{d\ln x})$
1 - 3	2	0.00	0.00	0.00		
3 - 5	4	0.04	0.04	0.02	0	0
5 - 7	6	0.22	0.27	0.12	1	2
7 - 9	8	0.88	1.14	0.44	3	8
9 - 11	10	2.70	3.84	1.35	13	31
11 - 13	12	6.48	10.32	3.24	39	89
13 - 15	14	12.10	22.42	6.05	85	195
15 - 17	16	17.60	40.02	8.80	141	324
17 - 19	18	19.95	59.97	9.98	179	413
19 - 21	20	17.60	77.57	8.80	176	405
21 - 23	22	12.10	89.67	6.05	133	306
23 - 25	24	6.48	96.15	3.24	78	179
25 - 27	26	2.70	98.85	1.35	35	81
27 - 29	28	0.88	99.72	0.44	12	28
29 - 31	30	0.22	99.95	0.12	3	8
31 - 33	32	0.04	99.99	0.02	1	1
33 - 35	34	0.01	100.00	0.01	0	0

2.8 Graphical presentation of size distribution data

2.8.1 Presentation on linear graph paper

The simplest presentation of this data is in the form of a histogram on a relative and/or cumulative basis (Figures 2.13 and 2.14). Since the distribution is continuous, straight lines can be drawn through the histogram to produce one of two curves: frequency/micron and cumulative percentage distribution (either undersize or oversize). It is common practice to normalize particle size distributions (i.e. summate to 100%). In order to compare distributions it is equally essential to normalize the frequency distribution so that the area under this curve is 100%. The ordinate should always be plotted as percentage per micron if the size is plotted on a linear scale (Figure 2.15). For the linear scale, the relationship between size and frequency may be written:

$$f(x) = \frac{dF(x)}{dx} \text{ so that } \int_0^x F(x) = \int_0^x f(x)dx \quad (2.25)$$

[$\phi = F(x)$] may be replaced by W for a mass distribution, S for a surface distribution and N for a number distribution.

Alternatively, the frequency can be plotted with a logarithmic scale for the abscissa. In this case the ordinate is calculated as percentage per log(micron) in order to normalize the area under the frequency curve to 100 (Figure 2.16). This type of presentation is particularly useful for size analysis data since many powders are logarithmically distributed and many instruments present data with sizes in a geometric progression. A linear plot of geometrically tabulated data compresses the data points at the fine end of the distribution so that detail is lost.

If further data manipulation is envisaged Naperian logarithms are preferred (i.e. to base e rather than base 10) since data in this form lend themselves to computer manipulation, particularly if the notation popular in Germany is used [48]. If a log to the base 10 abscissa is used the area under the frequency curve decreases from 100 to 43.4 units in this case [see equations (2.24)].

It is common practice to plot size distribution data in such a way that a straight line results, with all the advantages that follow from such a presentation. Some of the mathematical expressions for achieving this are given below.

2.9 Standard forms of distribution functions

Particle size, like other variables in nature, tends to follow well-defined mathematical laws in its distribution. This is not only of theoretical interest since data manipulation is made much easier if the distribution can be described by a mathematical law. Experimental data tends to follow the Normal law or Gaussian frequency distribution in many areas of statistics and statistical physics. However, the log-normal law is more frequently found with particulate systems. These laws suffer the disadvantage that they do not permit a maximum or minimum size and so, whilst fitting real distributions in the middle of the distribution, fail at each of the tails.

2.10 Arithmetic normal distribution

The normal law or Gaussian frequency distribution occurs when the measured value of some property of a system is determined by a large number of small effects, each of which may or may not operate. If a large number of the measurements of the value are made and the results plotted as a frequency distribution the well known Gaussian bell-shaped curve results. The equation representing the normal distribution is:

$$y = \frac{1}{\sigma \sqrt{2\pi}} \exp \left[-\frac{(x - \bar{x})^2}{2\sigma^2} \right] \quad (2.26)$$

$$\text{where } y = \frac{d\phi}{dx}$$

and

$$\phi = \int_{-\infty}^{+\infty} f(x) dx = 1 \quad (2.27)$$

i.e. the distribution is normalized (sums to unity or 100%)

- σ is the standard deviation,
- \bar{x} is the mean size,
- ϕ is the general term for the frequency; number, length, surface or volume (mass).

The mean size (\bar{x}) is defined as:

$$\bar{x} = \frac{\sum x \Delta \phi}{\sum \Delta \phi} \quad (2.28)$$

The standard deviation (σ) is defined as:

$$\sigma = \sqrt{\frac{\sum (x - \bar{x})^2 \Delta \phi}{\sum \Delta \phi}} \quad (2.29)$$

Let $t = \frac{(x - \bar{x})}{\sigma}$, then $\sigma dt = dx$ and equation (2.26) becomes:

$$\frac{d\phi}{dt} = \frac{1}{\sqrt{2\pi}} \exp\left(-\frac{t^2}{2}\right) \quad (2.30)$$

Hence

$$\int_0^\phi d\phi = \frac{1}{\sqrt{2\pi}} \int_{-\infty}^t \exp\left(-\frac{t^2}{2}\right) dt \quad (2.31)$$

And

+ 4.2

$$\int_\phi^{+\infty} d\phi = \frac{1}{\sqrt{2\pi}} \int_t^{-\infty} \exp\left(-\frac{t^2}{2}\right) dt \quad (2.32)$$

2.10.1 Manipulation of the normal equation

The fraction undersize the mean size (\bar{x}) is obtained by inserting the limits $x = -\infty$, $x = \bar{x}$, i.e. $t = -\infty$, $t = 0$, in equation (2.31) to give $\phi = 0.5$, i.e. the mean and median are coincident. Similarly it can be shown that the mode is the same as the median. Writing $X^2 = (-t^2/2)$:

$$\exp(-X^2) = \lim_{n \rightarrow \infty} \left[1 - \frac{(-X)^2}{n} \right]^n$$

$$\exp(X^2) = 1 + n \left(\frac{-X^2}{n} \right) + \frac{n(n-1)}{2!} \left(\frac{-X^2}{n} \right)^2 + \frac{n!}{(n-r)!r!} \left(\frac{-X^2}{n} \right)^r + \dots$$

The fraction lying within one standard deviation of the mean is obtained by inserting the integral limits $x = x_g$, $x = x_g + \sigma_g$, i.e. $X = 0$, $X = 1/\sqrt{2}$. Therefore:

$$\int_0^{1/\sqrt{2}} \exp(X^2) dX = \left[X - \frac{X^3}{3} + \frac{1}{2!} \frac{X^5}{5} - \frac{1}{3!} \frac{X^7}{7} + \frac{(-1)^{r+1}}{(r-1)!} \frac{X^{2r-1}}{2r-1} \dots \right]$$

Thus:

$$\begin{aligned} \phi(x_g) - \phi(x_g + \sigma) &= \frac{1}{\pi} \left[\frac{1}{\sqrt{2}} - \frac{1}{3} \left(\frac{1}{\sqrt{2}} \right)^3 + \frac{1}{2!} \frac{1}{5} \left(\frac{1}{\sqrt{2}} \right)^5 - \frac{1}{3!} \frac{1}{7} \left(\frac{1}{\sqrt{2}} \right)^7 + \dots \right] \\ &= 0.3413 \end{aligned}$$

The fractional area under the curve between the mean size and one standard deviation from the mean, $0.8413 - 0.5000 = 0.3413$. 68% of the distribution falls within one standard deviation from the mean (see Table 2.6) and all but 0.26% lies within two standard deviations from the mean. Therefore the standard deviation equals the difference between the 84.13% size and the mean (median) size. Equation 2.31 is the basis for arithmetic probability graph paper and the solution is widely available in tabular form.

Table 2.6 Tabular solution to the normal probability equation

t	Integral (ϕ)
0	0.5000
0.5	0.6915
1.0	0.8413
1.5	0.9332
2.0	0.9987
3.0	0.9997

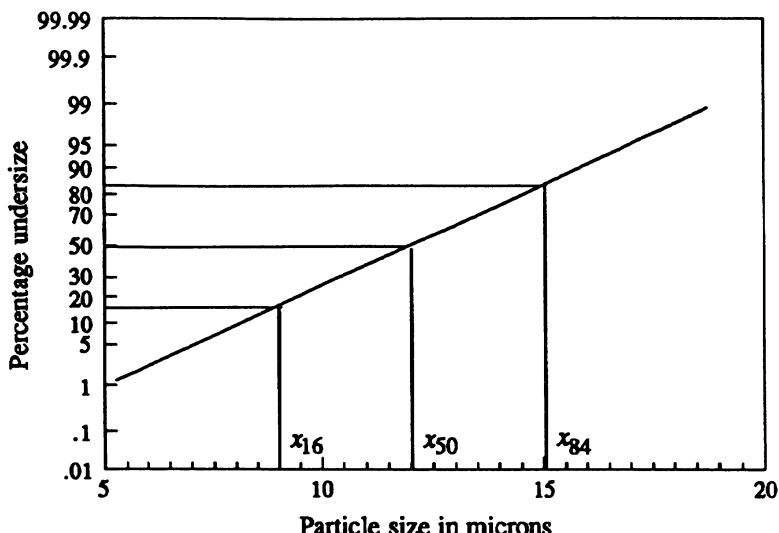


Fig. 2.17 Graphical presentation of size analysis data on normal probability paper.

A fundamental property of the normal distribution is that differences from the mean are equally likely. i.e. the probability of finding particles 10 units larger than the mean is the same as finding particles 10 units smaller. An example, plotted on probability axes, is shown in Figure 2.17 with a mean of 12 μm and a standard deviation of 3 μm so that the (84% - 50%) size interval equals the (50% - 16%) size interval = 3 μm . The distribution is completely described by these two parameters. Although it might be expected that this type of distribution would be common, it seems to occur only for narrow size ranges of classified material. Most distributions are skewed, usually to the right.

2.11 The log-normal distribution

According to the normal law, differences of equal amounts in excess or deficit from a mean value are equally likely. With the log-normal law, it is ratios of equal amounts which are equally likely. In order to maintain a symmetrical bell-shaped curve, it is therefore necessary to plot the relative frequency against size in a geometric progression. The equation of the log-normal distribution is obtained by replacing x with $z = \ln x$, in equation (2.27). Then:

$$y = \frac{1}{\sigma_z \sqrt{2\pi}} \exp\left(-\frac{(z - \bar{z})^2}{2\sigma_z^2}\right)$$

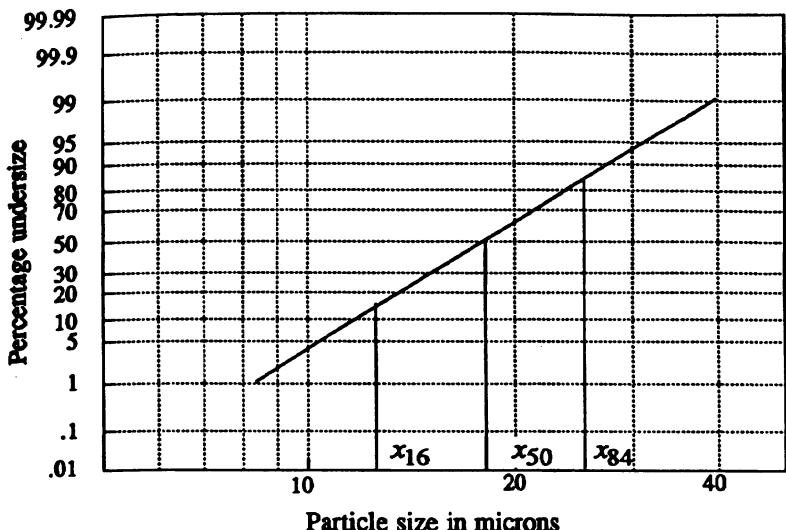


Fig. 2.18 Graphical presentation of size analysis data on log-normal probability paper.

$$\text{or: } \frac{d\phi}{d \ln x} = \frac{1}{\sqrt{2\pi} \ln \sigma_g} \exp \left[-\frac{(\ln x - \ln x_g)^2}{2 \ln^2 \sigma_g} \right] \quad (2.33)$$

x_g is the geometric mean of the distribution (i.e. the arithmetic mean of the logarithms) and σ_g is the geometric standard deviation, σ_z is the standard deviation of z .

$\prod x^{d\phi}$ is the product of the group data in which the frequency of particles of size x is $d\phi$:

$$x_g^\phi = x_1^{d\phi_1} \cdot x_2^{d\phi_2} \cdots x_r^{d\phi_r} \cdots x_n^{d\phi_n}$$

$$\bar{z} = \frac{\sum z d\phi}{\sum d\phi} \quad \{ \phi = N \text{ (number)}, S \text{ (surface)} \text{ or } W \text{ (weight)} \}$$

$$\bar{z} = \frac{\sum z d\phi}{\phi}$$

$$\ln x_g = \frac{\sum \ln x d\phi}{\phi}$$

$$\text{Thus: } x_g = [\sqrt{\prod x^{d\phi}}]^{\phi} \quad (2.34)$$

Since the particle size is plotted on a logarithmic scale, the presentation of data on a log-probability graph is particularly useful when the range of sizes is large (Figure 2.18). The geometric standard deviation can be read from the graph, as with the arithmetic distribution, and is given by:

$$\log \sigma_g = \log x_{84} - \log x_{50} = \log x_{50} - \log x_{16} = \sqrt{\log \frac{x_{84}}{x_{16}}} \quad (2.35)$$

The geometric mode, the geometric mean and the median coincide for a log-normal distribution.

In Figure 2.18 the median size x_g is 18 µm, the 84% size $\sigma_g x_g$ is 25.2 µm and the 16% size x_g/σ_g is 12.86 µm: The ratio of the 84% size to the 50% size is the same as the ratio of the 50% size to the 16% size and equals the geometric standard deviation $\sigma_g = 1.40$. The distribution is completely described by the two numbers (18 and 1.40).

2.11.1 Relationship between number mean sizes for a log-normal distribution

Consider a log-normal distribution by number such that:

$$\int_{-\infty}^{+\infty} d\phi = \sum_{r=0}^{r=\infty} dN_r = \frac{1}{\ln \sigma_g \sqrt{2\pi}} \int_{-\infty}^{+\infty} \exp \left[-\left(\frac{\ln x - \ln x_g}{\sqrt{2 \ln \sigma_g}} \right)^2 \right] d \ln x = 1 \quad (2.36)$$

i.e. the distribution is normalized. dN_r is the number of particles in a narrow size range of mean size x_r , x_0 and x_∞ are the smallest and largest particles present in the distribution and σ_g is the geometric standard deviation [which is the same for number, length, surface and volume (mass) distribution].

The number-length mean diameter is defined as:

$$x_{NL} = \frac{\sum_{r=0}^{r=\infty} x_r dN_r}{\sum_{r=0}^{r=\infty} dN_r}$$

Normalizing i.e. equating the denominator to unity gives:

$$x_{NL} = \sum x_r dN_r$$

$$x_{NL} = \frac{1}{\ln \sigma_g \sqrt{2\pi}} \int_{-\infty}^{+\infty} \exp \left[-\left(\frac{\ln x - \ln x_{gN}}{\sqrt{2 \ln \sigma_g}} \right)^2 \right] x d \ln x$$

$$x_{NL} = \sum x_r dN_r = \frac{1}{\ln \sigma_g \sqrt{2\pi}} \int_{-\infty}^{+\infty} \exp \left[-\left(\frac{\ln x - \ln x_{gN}}{\sqrt{2 \ln \sigma_g}} \right)^2 \right] x d \ln x \quad (2.37)$$

Also

$$x_{NS}^2 = \frac{\sum_{r=0}^{r=\infty} x_r dN_r}{\sum_{r=0}^{r=\infty} dN_r} = \frac{\sum_{r=0}^{r=\infty} x^2 dN_r}{\sum_{r=0}^{r=\infty} dN_r}$$

$$x_{NS}^2 = \frac{1}{\ln \sigma_g \sqrt{2\pi}} \int_{-\infty}^{+\infty} \exp \left[-\left(\frac{\ln x - \ln x_{gN}}{\sqrt{2 \ln \sigma_g}} \right)^2 \right] x^2 d \ln x \quad (2.38)$$

$$x_{NV}^3 = \frac{\sum_{r=0}^{r=\infty} x_r dN_r}{\sum_{r=0}^{r=\infty} dN_r} = \frac{\sum_{r=0}^{r=\infty} x^3 dN_r}{\sum_{r=0}^{r=\infty} dN_r}$$

$$x_{NV}^3 = \frac{1}{\ln \sigma_g \sqrt{2\pi}} \int_{-\infty}^{+\infty} \exp \left[-\left(\frac{\ln x - \ln x_{gN}}{\sqrt{2 \ln \sigma_g}} \right)^2 \right] x^3 d \ln x \quad (2.39)$$

Making the substitution:

$$X = \frac{\ln x - \ln x_{gN}}{\sqrt{2 \ln \sigma_g}}$$

so that $x = \exp(\sqrt{2 \ln \sigma_g} X + \ln \sigma_g)$ and $x \sqrt{2 \ln \sigma_g} dX = dx$, then:

$$x_{NL} = \frac{x_g N}{\sqrt{\pi}} \int_{-\infty}^{+\infty} \exp(\sqrt{2} \ln \sigma_g X - X^2) dX \quad (2.40)$$

$$x_{NS}^2 = \frac{x_g^2 N}{\sqrt{\pi}} \int_{-\infty}^{+\infty} \exp(2\sqrt{2} \ln \sigma_g X - X^2) dX \quad (2.41)$$

$$x_{NV}^3 = \frac{x_g^3 N}{\sqrt{\pi}} \int_{-\infty}^{+\infty} \exp(3\sqrt{2} \ln \sigma_g X - X^2) dX \quad (2.42)$$

Making the transformations:

$$Y_1 = X - \frac{\sqrt{2}}{2} \ln \sigma_g \quad \text{in equation (2.40)}$$

$$Y_2 = X - \sqrt{2} \ln \sigma_g \quad \text{in equation (2.41)}$$

$$Y_3 = X - \frac{3\sqrt{2}}{2} \ln \sigma_g \quad \text{in equation (2.42)}$$

$$x_{NL} = \frac{x_g N}{\sqrt{\pi}} \exp\left(\frac{1}{2} \ln^2 \sigma_g\right) \int_{-\infty}^{+\infty} \exp(-Y_1^2) dY_1 \quad (2.43)$$

$$x_{NS}^2 = \frac{x_g N}{\sqrt{\pi}} \exp(2 \ln^2 \sigma_g) \int_{-\infty}^{+\infty} \exp(-Y_2^2) dY_2 \quad (2.44)$$

$$x_{NV}^3 = \frac{x_g N}{\sqrt{\pi}} \exp\left(\frac{9}{2} \ln^2 \sigma_g\right) \int_{-\infty}^{+\infty} \exp(Y_3^2) dY_3 \quad (2.45)$$

The integration yields a value $I = \sqrt{\pi}$ giving:

$$\ln x_{NL} = \ln x_g N + 0.5 \ln^2 \sigma_g \quad (2.46)$$

$$\ln x_{NS} = \ln x_g N + 1.0 \ln^2 \sigma_g \quad (2.47)$$

$$\ln x_{NV} = \ln x_{gN} + 1.5 \ln^2 \sigma_g \quad (2.48)$$

Similarly

$$\ln x_{NM} = \ln x_{gN} + 2.0 \ln^2 \sigma_g \quad (2.49)$$

2.11.2 Derived mean sizes

If the number size distribution of a particulate system is found to be log normal, equations (2.47) to (2.49) can be used to determine other mean sizes. For example, the volume-moment mean size is the mean size of a volume (mass) distribution:

$$x_{VM} = \frac{\sum_{r=0}^{r=\infty} x_r^4 dN_r}{\sum_{r=0}^{r=\infty} x_r^3 dN_r}$$

$$x_{VM} = \frac{x_{NM}^4}{x_{NV}^3}$$

Therefore:

$$\ln x_{VM} = 4 \ln x_{NM} - 3.0 \ln x_{NV} \quad (2.50)$$

Substituting from equations (2.48) and (2.49):

$$\ln x_{VM} = \ln x_{gN} + 3.5 \ln^2 \sigma_g \quad (2.51)$$

Similarly, the mean size of a surface distribution is given by:

$$\ln x_{SV} = \ln x_{gN} + 2.5 \ln^2 \sigma_g \quad (2.52)$$

Using this equation, the volume specific surface of the particulate system may be determined since:

$$S_V = 6/x_{SV}$$

2.11.3 Transformation between log-normal distributions

If the number distribution is log-normal, the mass distribution is also log-normal with the same geometric standard deviation. Using the same treatment as was used to derive equation (2.46) gives, for a mass analysis:

$$\ln x_{VM} = \ln x_{gV} + 0.5 \ln^2 \sigma_g \quad (2.53)$$

Comparing with equation (2.51) gives:

$$\ln x_{gV} = \ln x_{gN} + 3.0 \ln^2 \sigma_g \quad (2.54)$$

Since the relations between the number average sizes and the number geometric mean are known [equations (2.46) to (2.49)], these can now be expressed as relationships between number average sizes and the weight geometric mean x_{gV} .

$$\ln x_{NL} = \ln x_{gV} - 2.5 \ln^2 \sigma_g \quad (2.55)$$

$$\ln x_{NS} = \ln x_{gV} - 2.0 \ln^2 \sigma_g \quad (2.56)$$

$$\ln x_{NV} = \ln x_{gV} - 1.5 \ln^2 \sigma_g \quad (2.57)$$

$$\ln x_{NM} = \ln x_{gV} - 1.0 \ln^2 \sigma_g \quad (2.58)$$

Other average sizes can be derived from the above using a similar procedure to that used to derive equations (2.53) and (2.54) to give:

$$\ln x_{SV} = \ln x_{gV} - 0.5 \ln^2 \sigma_g \quad (2.59)$$

Similarly, for a surface distribution, the equivalent equation to equation (2.54) is:

$$\ln x_{gS} = \ln x_{gN} + 2.0 \ln^2 \sigma_g \quad (2.60)$$

Substituting this relationship into equations (2.55) to (2.58) yields the equivalent relationships relating surface average sizes with the surface geometric mean diameter.

2.11.4 Relationship between median and mode of a log-normal equation

The log-normal equation may be written:

$$\frac{d\phi}{dx} = \frac{1}{x\sqrt{2\pi}\ln\sigma_g} \exp(-X^2) \quad (2.61)$$

where

$$\sqrt{2\ln\sigma_g}X = (\ln x - \ln x_g)$$

so that

$$\sqrt{2\ln\sigma_g} \frac{dX}{dx} = \frac{1}{x}$$

At the mode ($x = x_m$), and:

$$\frac{d^2\phi}{dx^2} = 0 \text{ i.e. } \frac{d}{dx} \left[\frac{1}{x_m} \right] \exp(X^2) = 0$$

$$\frac{1}{x_m} \left[-2X \frac{dX}{dx} \right] - \frac{1}{x_m^2} = 0$$

$$\left[\frac{2(\ln x_m - \ln x_g)}{\sqrt{2\ln\sigma_g}} \right] \left(\frac{1}{x_m \sqrt{2\ln\sigma_g}} \right) + \frac{1}{x_m^2} = 0$$

Table 2.7 Relationships between average sizes for log normal equations

$\ln x_{NL} = \ln x_{gN} + 0.5 \ln^2 \sigma_g$	$\ln x_{LS} = \ln x_{gN} + 1.5 \ln^2 \sigma_g$
$\ln x_{NS} = \ln x_{gN} + 1.0 \ln^2 \sigma_g$	$\ln x_{LV} = \ln x_{gN} + 2.0 \ln^2 \sigma_g$
$\ln x_{NV} = \ln x_{gN} + 1.5 \ln^2 \sigma_g$	$\ln x_{LM} = \ln x_{gN} + 2.5 \ln^2 \sigma_g$
$\ln x_{NM} = \ln x_{gN} + 2.0 \ln^2 \sigma_g$	$\ln x_{VM} = \ln x_{gN} + 3.5 \ln^2 \sigma_g$
$\ln x_{SV} = \ln x_{gN} + 2.5 \ln^2 \sigma_g$	$\ln x_m = \ln x_g - 1.0 \ln^2 \sigma_g$
$\ln x_{SM} = \ln x_{gN} + 3.0 \ln^2 \sigma_g$	
$\ln x_{gS} = \ln x_{gN} + 2.0 \ln^2 \sigma_g$	
$\ln x_{gV} = \ln x_{gN} + 3.0 \ln^2 \sigma_g$	

$$\ln x_m = \ln x_g - \ln^2 \sigma_g \quad (2.62)$$

These relationships are summarized in Table 2.7.

2.11.5 An improved equation and graph paper for log-normal evaluations [49]

Using equation (2.33) and the relationship:

$$\frac{1}{x} = \exp(-\ln x) \quad (2.63)$$

the log-normal equation can be written:

$$\frac{d\phi}{dx} = \frac{1}{x_m \ln \sigma_g \sqrt{2\pi}} \exp\left(-\frac{1}{2} \ln^2 \sigma_g\right) \exp\left[-\frac{\ln^2(x/x_m)}{2 \ln^2 \sigma_g}\right] \quad (2.64)$$

This form of the log-normal equation is more convenient for use since the variable (x) only appears once.

Equation (2.64) may be written in the simplified form:

$$\frac{d\phi}{dx} = A \exp\left[-b \ln^2(x/x_m)\right] \quad (2.65)$$

The relationship between geometric mean and mode (equation (2.62)) takes the form:

$$C = \frac{x_m}{x_g} = \exp\left(-\frac{1}{2b}\right) \quad (2.66)$$

This modified form of the log-normal equation simplifies parameter determination from log-probability plots of experimental data. The graph paper may be furnished with additional scales of b and C both being determined by drawing a line parallel to the distribution through the pole (0.25 μm , 50%).

2.11.6 Application

Consider a log-normal equation with a geometric mean $x_g = 6.75 \mu\text{m}$ and a standard deviation $\sigma_g = 1.64$. According to equation (2.62) the mode x_m will be 5.27 μm making:

$$\frac{d\phi}{dx} = 0.1344 \exp \left[-2.02 \ln^2 \left(\frac{x}{5.27} \right) \right]$$

This form is particularly useful when further mathematical computation is envisaged, such as for grade efficiency $G_c(x)$ since:

$$G_c(x) = E_T \frac{dF_c(x)}{dF(x)}$$

$$G_c(x) = E_T \frac{d\phi_c}{dx} \quad (2.67)$$

where $(d\phi_c/dx)$ is the frequency of the coarse stream, $(d\phi/dx)$ is the frequency of the feed and E_T is the total efficiency (see Chapter 5).

2.12 Johnson's S_B distribution

The Johnson's S_B distribution is a bounded log-normal distribution, i.e. a truncated log-normal equation with a minimum and maximum size so that the whole size distribution is directly considered. This differs from conventional correlation analysis as summarized by Herdan [50]. It has been presented, in a series of papers by Yu and Standish [51–55], as a function that can represent all unimodal size distributions of particles. It may be written:

$$y = \frac{df(z)}{dz}$$

$$y = \frac{\sigma_z}{\sqrt{2\pi}} \frac{(z_{\max} - z_{\min})}{(z - z_{\min})(z_{\max} - z)} \exp \left\{ - \left[\frac{\mu_z + \sigma_z \ln \frac{(z - z_{\min})}{(z_{\max} - z)}}{2} \right]^2 \right\} \quad (2.68)$$

$(z_{\min} < z < z_{\max})$

The log-normal distribution is a special case of the S_B distribution which can be obtained by extending the size limits to $\pm\infty$.

$$\text{If we let } t = \mu_z + \sigma_z \ln \frac{(z - z_{\min})}{(z_{\max} - z)}$$

$$\text{so that } dt = \frac{\sigma_z(z_{\max} - z_{\min})}{(z - z_{\min})(z_{\max} - z)} dz,$$

Table 2.8 The properties of some commonly used density distribution functions

Name	Equation	Range of x
Normal	$\frac{1}{\sqrt{2\pi}\sigma} \exp\left[-\frac{(x-\bar{x})^2}{2\sigma^2}\right]$	$[-\infty, +\infty]$
Log-normal	$\frac{1}{\sqrt{2\pi} \ln \sigma_g} \exp\left[-\frac{(\ln x - \ln x_g)^2}{2\ln^2 \sigma_g}\right]$	$[0, +\infty]$
Rosin-Rammler [56]	$Cx^{n-1}e^{-bx^n}$	$[0, +\infty]$
Gaudin-Schuman [57-59]	Cx^{n-1}	$[0, x_{\max}]$
Gaudin-Meloy [60]	$C[1 - n(1-Cx)^{n-1}]$	$[0, x_{\max}]$
Roller [61-63]	$C\left[\frac{0.5}{\sqrt{x}} + \frac{b}{\sqrt[3]{x^2}}\right]$	$[0, x_{\max}]$
Harris [64]	$Cx^{s-1}[1 - bx^s]$	$[0, x_{\max}]$
Martin [65]	Cx^3e^{-bx}	$[0, +\infty]$
Gamma function [66,67]	$Cx^{P-1}e^{-x}$	$[0, +\infty]$
Weinig [68]	$Cx^a e^{-bx^2}$	$[0, +\infty]$
Heywood [69]	$Cx^3e^{-bx^n}$	$[0, +\infty]$
Griffith [70]	$Cx^{-a}e^{-bx^{-1}}$	$[0, +\infty]$
Klimpel-Austin [71]	$Cx^2[1 - n(1-Cx)^3]$	$[0, x_{\max}]$
Beta function [72]	$Cx^{P-1}(1 - n(1-Cx)^{a-1})$	$[0, x_{\max}]$

then: $y = \frac{df(z)}{dz} = \frac{df(x)}{dt} = \frac{1}{\sqrt{2\pi}} \exp\left(-\frac{t^2}{2}\right)$

If the fraction smaller than the actual smallest size is small it is usually safe to assume that $z_{\min} = 0$ so that:

$$F(z) = \frac{1}{\sqrt{2\pi}} \int_{-\infty}^{\xi} \exp\left(-\frac{t^2}{2}\right) dt$$

where $\xi = \sigma_z \left[\ln \frac{(z - z_{\min})}{(z_{\max} - z)} - \ln \frac{(z_g - z_{\min})}{(z_g - z_{\max})} \right]$

This reduces to the log-normal equation if ξ is simplified to:

$$\xi = \sigma_z (\ln z - \ln z_g)$$

Distributions which fit the S_B distribution will also fit the log-normal distribution but differences will occur in the end regions. These differences arise since the log-normal distribution does not admit a minimum or maximum size which must exist in any real system [73]. These small discrepancies can lead to large differences in their transformed size distributions.

2.13 The Rosin - Rammler - Bennett - Sperling formula

This formula was derived originally for broken coal and has since been found to apply to many other materials [74]. The equation may be written:

$$R = 100 \exp(-bx^n) \quad (2.69)$$

where R is the weight percentage retained on a sieve of aperture x .

Differentiating gives $\log(\frac{100}{R}) = bx^n \log_{10} e$

$$\log [\log(\frac{100}{R})] = \log b + \log(\log_{10} e) + n \log x$$

i.e. $\log [\log(\frac{100}{R})] = n \log x + \text{constant}$

A plot of the log of the reciprocal percentage weight retained against the log of particle size generates a straight line. The slope n is a measure of the particle size dispersion (size range) of the powder.

The peak of the frequency curve for $n = 1$ is at $(100/e) = 36.8\%$ and, denoting the mode by x_m equation 2.69 gives $b = 1/x_m$

The sieve aperture for $R = 36.8\%$ is used to characterize the degree of comminution of the material and, since the slope of the line on the Rosin-Rammler graph depends on the particle size range, the ratio of $\tan^{-1} n$ and x_m is a form of variance.

This equation is useful for monitoring grinding operations for highly skewed distributions, but should be used with caution since the device of taking logs always reduces scatter hence, taking logs twice is not to be recommended. An alternative form of the Rosin-Rammler equation is :

$$R = 100 \exp \{ -(x/x_0)^n \} \quad (2.70)$$

2.14 Other distribution laws

Yu and Standish [53] list the following distribution laws (Table 2.8) which have been used for particulate systems:

The cumulative form of the above distributions may also be presented as cumulative two-parameter equations:

$$\text{Gates-Gaudin-Schumann [57-59]} \quad F(x) = (bx)^n \quad (2.71)$$

$$\text{Gaudin-Meloy [60]} \quad F(x) = [1 - (1 - bx)^n] \quad (2.72)$$

$$\text{Roller [61-63]} \quad F(x) = a \sqrt{x} \exp\left(-\frac{b}{x}\right) \quad (2.73)$$

$$\text{Svensson [75]} \quad F(x) = x Ep(y) \quad (2.74)$$

$$\text{where: } Ep(y) = \frac{\int_0^y \exp(-y)(1/p)Ep(y)dy}{\int_0^y \exp(-y)(1/p)dy}$$

$y = \left(\frac{x}{x_\mu}\right)^n$ and x_μ is the mode of the distribution.

Three and four parameter equations have also been proposed, e.g.:

$$\text{Harris [64]} \quad F(x) = 1 - [1 - bx^s]^n \quad (2.75)$$

For $s = 1$ this degenerates to the Gaudin-Meloy equation.

2.14.1 Simplification of two parameter equations

Tarjan [76] converted a two-parameter size distribution function from the form $\phi = f(x)$ to the form $\phi = f(x/x_{0.5})$, where $x_{0.5}$ is the median. The result is an easy to handle function with a high degree of correspondence to the more complicated logarithmic function ϕ_K below:

$$\phi_K = \phi \ln(bx)^n \quad (2.76)$$

where

$$\phi = \frac{1}{\sqrt{2\pi}} \int_{-\infty}^u \exp\left(-\frac{u^2}{2}\right) du \quad (2.77)$$

Let the parameter b in equations (2.69), (2.71) and (2.72) be expressed in terms of $x_{0.5}$ when $\phi = 0.50$

$$\text{Gates-Gaudin-Schuman (GGS):} \quad 0.50 = (bx_{0.5})^n$$

$$\text{Rosin-Rammler (RR):} \quad 0.50 = \exp(-bx_{0.5}^n)$$

$$\text{Gaudin-Meloy (GM):} \quad 0.50 = (1 - bx_{0.5})^n$$

Substituting back for b gives:

$$\text{GGS} \quad \phi_{GGS} = 0.5 \left(\frac{x}{x_{0.5}} \right)^n \quad (2.78)$$

$$\text{RR} \quad \phi_{RR} = 1 - \exp \left[\left(\frac{x}{x_{0.5}} \right)^n \ln 2 \right] \quad (2.79)$$

$$\text{GM} \quad \phi_{GM} = 1 - \left[1 - \left(\frac{x}{x_{0.5}} \right) \left(1 - \sqrt[n]{0.5} \right) \right]^n \quad (2.80)$$

2.14.2 Comments

All the above equations are attempts to fit a straight line relationship to a frequency distribution. This procedure is worthwhile only if some benefit is derived. Narrow range size distributions are usually best presented as cumulative percentage undersize by mass or number on linear graph paper. The curve should then be differentiated (rather than using raw data) in order to smooth out experimental error. A simple visual presentation of this kind is preferred, for reasons of clarity, for presenting information to non-mathematicians.

These distributions can also be plotted on arithmetic normal probability paper to examine deviations from normality. Wide size distributions are best plotted using a logarithmic scale for the size axis. Log-probability paper is extremely useful for examining data. Multi-modality is easy to discern as is the removal of fines (by classification) from a grinding process. Grinding processes often generate parallel distributions on log-probability paper and the time to reach a desired endpoint can be predicted. Simple mathematical relationships exists for log-normal distributions so that size distributions may be rapidly converted from number to surface to volume, and any of the statistical mean diameters may be calculated.

As demonstrated by Yu and Standish [53], distribution transformations can lead to unacceptable errors, particularly with distribution laws with no limiting maximum or minimum sizes. Even direct transformation of a number count to a volume count for example is unacceptable, unless the distribution is narrow, the count is excessively high or special procedures are employed, as with carrying out volume counts in microscopy.

2.15 The law of compensating errors

In any method of particle size analysis it is always possible to assign the wrong size to some of the particles. If this error is without bias, possibility of assigning too great a size is equally as probable as assigning too small a size. This will modify the distribution but will have little effect on the central region. An illustration is shown, in Table 2.9 and Figure (2.19), with 25% in each size category wrongly placed in the size category below and 25% in the size category above, together with a biased distribution in which 25% in each size interval is displaced to the adjacent finer interval above. These are plotted as percentage per ln (μm) against particle size in Figure (2.20).

The original log-normal distribution has a median size of 7.29 μm with a geometric standard deviation of 1.78; the unbiased distribution has a median size of 7.29 μm with a geometric standard deviation of 1.80

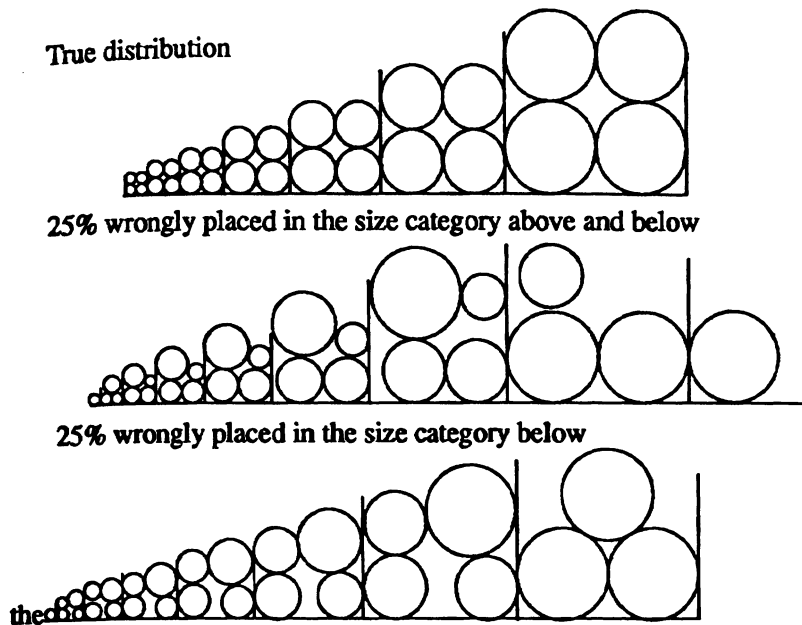


Fig. 2.19 Illustrations of the law of compensating errors:

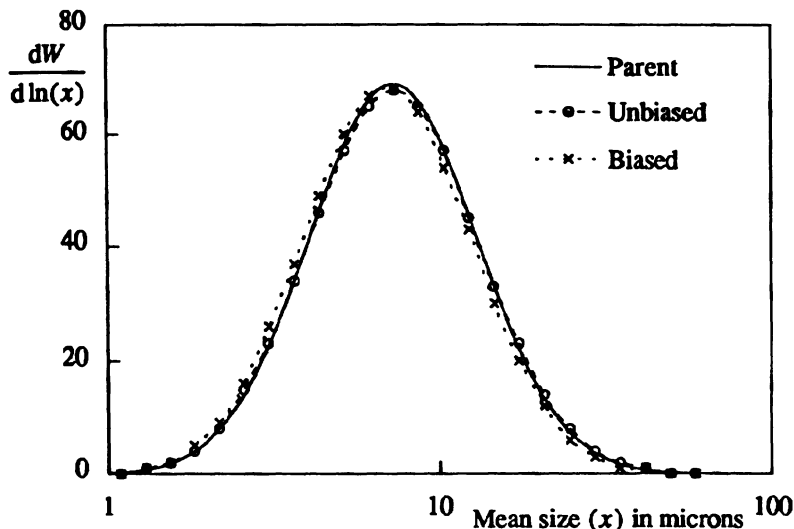


Fig. 2.20 Effect of displacing half the distribution, without bias, in each size interval, together with misplacing 25% in each size interval into the next finest interval.

Table 2.9 Illustration of the law of compensating errors

Mean size (c1)	% in interval (c2)	0.5c2 (c3)	0.25 × coarse (c4)	0.25 × fine (c5)	Unbiased error % (c6) = c2+c3+c4	Biased error % (c7) = 0.75c2 +c4
	0.00	0.00	0.00	0.02		0.00
0.84	0.02	0.01	0.01	0.00	0.02	0.03
1.09	0.05	0.03	0.03	0.01	0.07	0.07
1.30	0.14	0.07	0.08	0.01	0.16	0.18
1.54	0.32	0.16	0.17	0.03	0.36	0.41
1.83	0.68	0.34	0.34	0.08	0.76	0.85
2.18	1.34	0.67	0.60	0.17	1.44	1.61
2.59	2.41	1.20	0.99	0.34	2.52	2.79
3.08	3.94	1.97	1.47	0.60	4.05	4.43
3.67	5.90	2.95	2.02	0.99	5.95	6.44
4.36	8.06	4.03	2.52	1.47	8.02	8.57
5.19	10.07	5.04	2.87	2.02	9.93	10.43
6.17	11.50	5.75	3.00	2.52	11.26	11.62
7.34	11.99	5.99	2.86	2.87	11.72	11.85
8.72	11.42	5.71	2.49	3.00	11.19	11.05
10.37	9.94	4.97	1.98	2.86	9.80	9.43
12.34	7.91	3.95	1.44	2.49	7.87	7.37
14.67	5.74	2.87	0.95	1.98	5.80	5.26
17.45	3.81	1.91	0.58	1.44	3.92	3.44
20.75	2.31	1.16	0.32	0.95	2.43	2.06
24.68	1.28	0.64	0.16	0.58	1.38	1.12
29.34	0.65	0.32	0.08	0.32	0.72	0.56
34.90	0.30	0.15	0.03	0.16	0.34	0.26
41.50	0.13	0.06	0.01	0.08	0.15	0.11
49.35	0.05	0.02	0.00	0.03	0.06	0.04
58.69	0.02	0.01	0.00	0.01	0.02	0.01

and the biased distribution has a median size of 6.99 μm (an error of 4%) with a standard deviation of 1.79. For measurements in arithmetic progression of sizes the effect is small, provided sizing is carried out at 10 or more size intervals, and for a log-normal distribution the position of the mode is only slightly affected.

2.16 Evaluation of nonlinear distributions on log-normal paper

A bimodal distribution is detectable when plotted on log-probability axes by a change in the slope of the line. It is also possible to deduce other features.

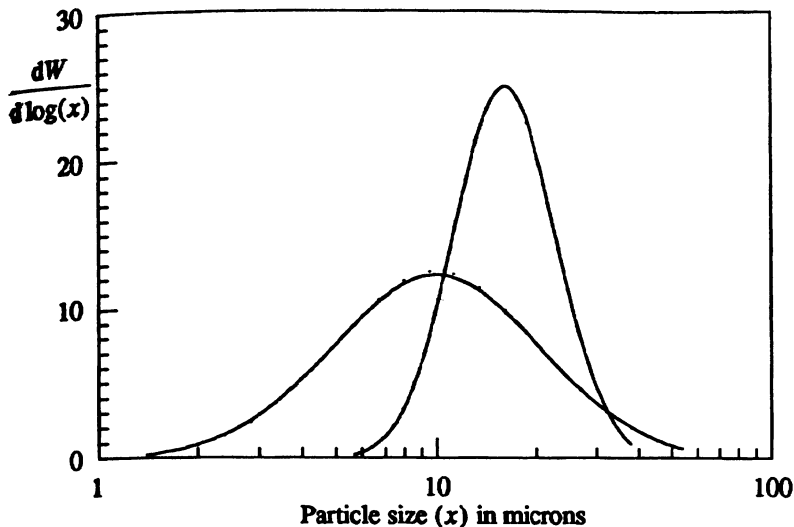


Fig. 2.21 Parent distributions for bimodal intersecting mixtures.

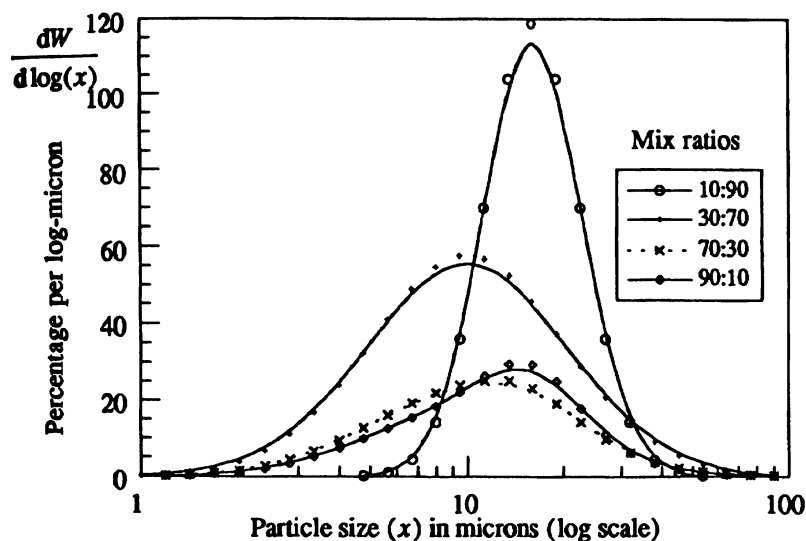


Fig. 2.22 Frequency plots of bimodal intersecting log-normal distributions in various mix ratios.

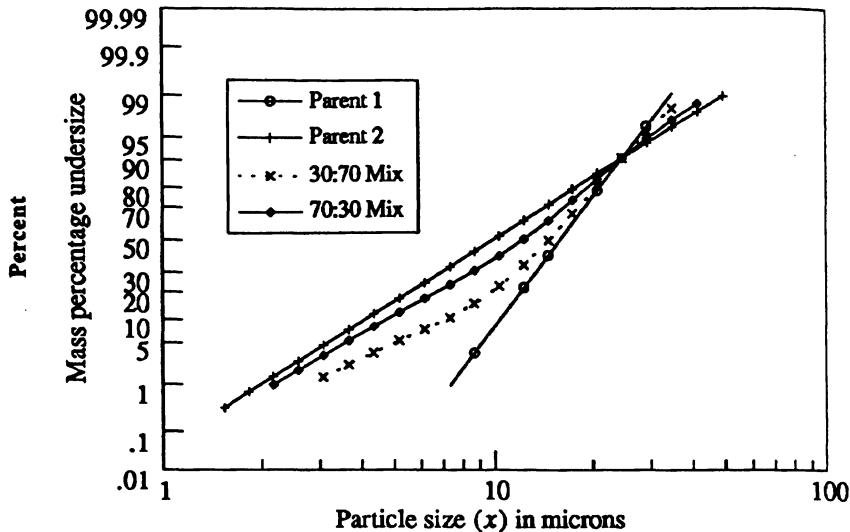


Fig. 2.23 Cumulative plots of bimodal intersecting log-normal distributions

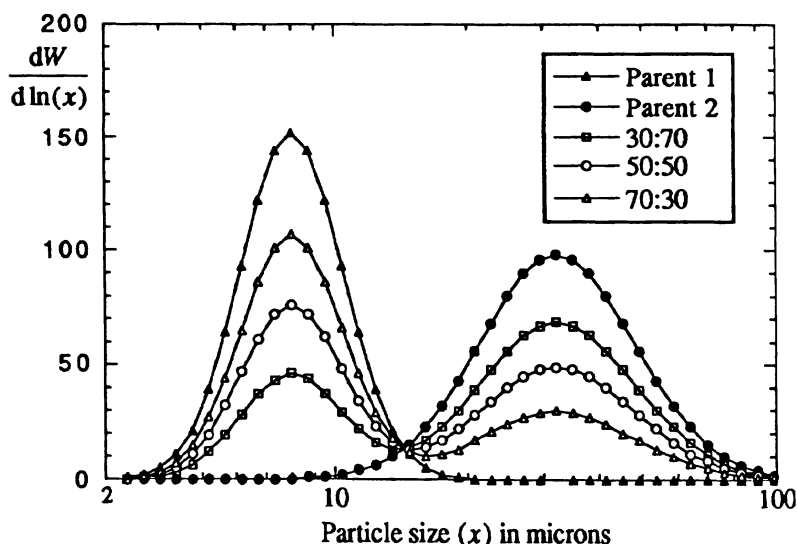


Fig. 2.24 Frequency plots of bimodal non-intersecting distribution in the ratios 30:70, 50:50 and 70:30.

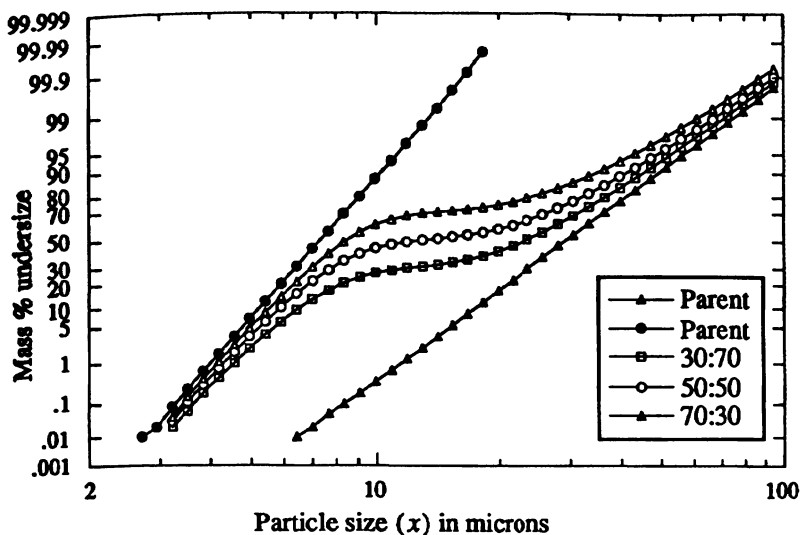


Fig. 2.25 Log-probability plots of mixtures of two non-intersecting log-normal distributions.

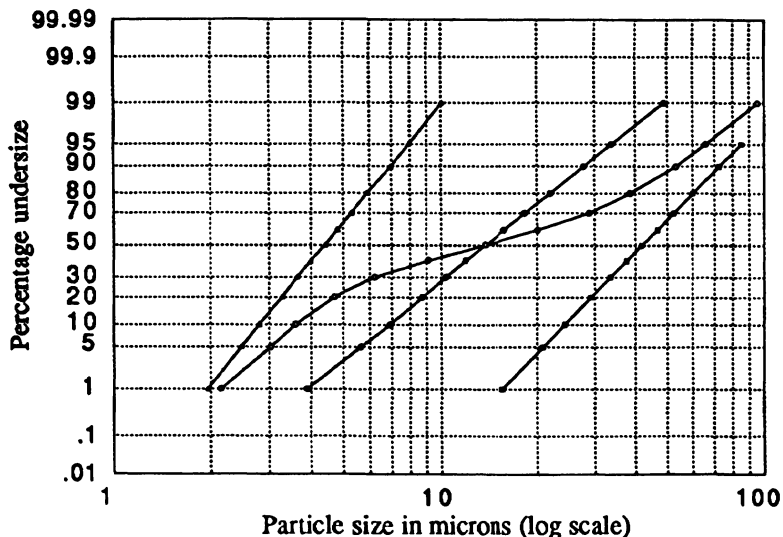


Fig. 2.26 Cumulative plots of trimodal non-intersecting log-normal distribution together with parent distributions (1:1:1 mixture).

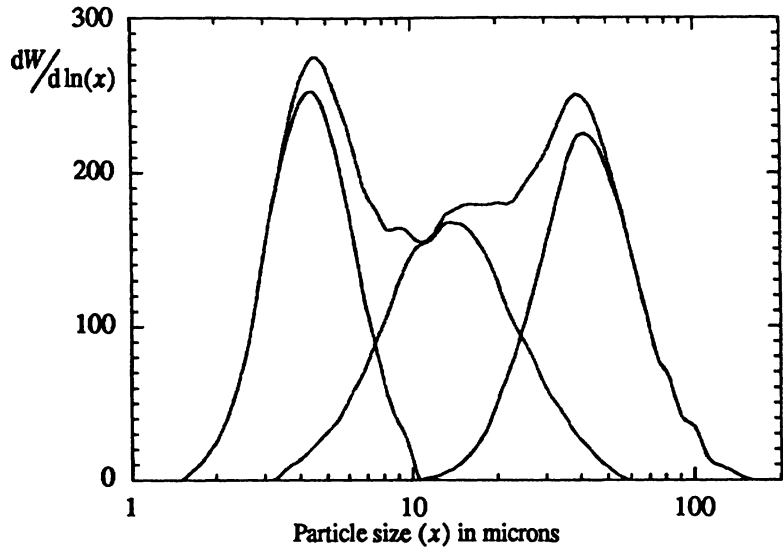


Fig. 2.27 Relative plot of trimodal non-intersecting log-normal distribution together with parent distributions (1:1:1 mixture).

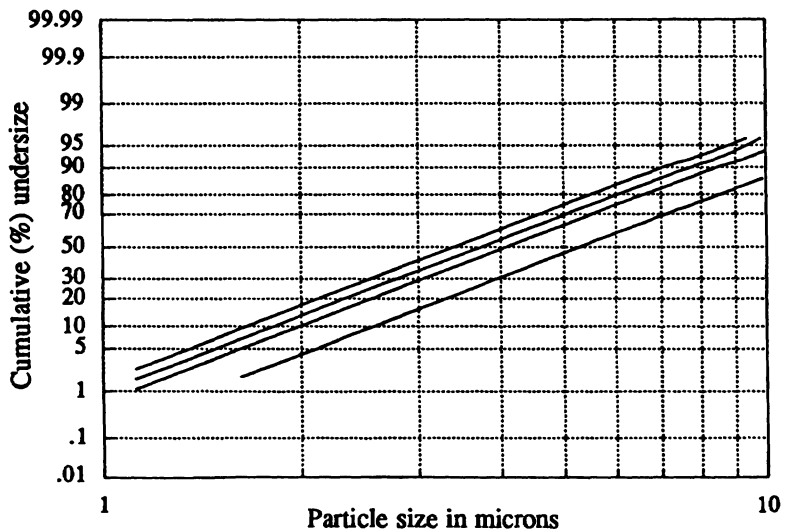


Fig. 2.28 Andreasen analyses monitoring a grinding operation.

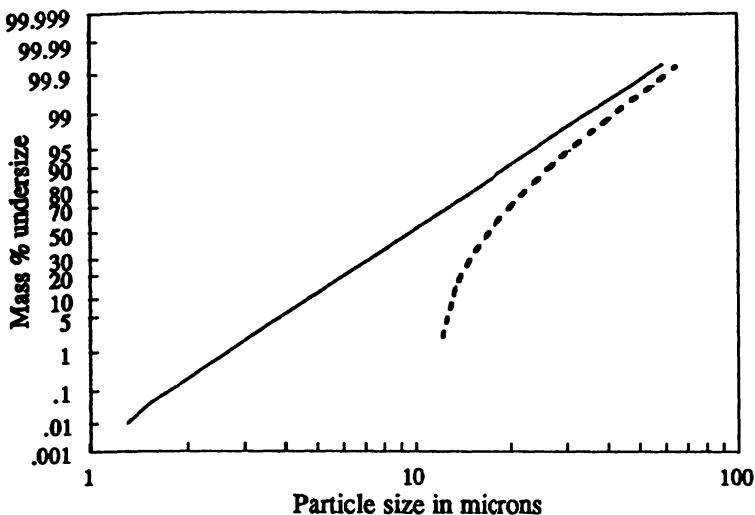


Fig. 2.29 Effect of classification on a log normal distribution. (Full line = parent distribution, dotted line = sub 6 μm particles removed).

2.16.1 Bimodal intersecting distributions

Figure 2.21 shows relative plots of two intersecting (overlapping), log-normal distributions with medians of 16 and 10 μm and standard deviations of 1.4 and 2.0 respectively. Relative plots of blends of these parent distributions are shown in Figure 2.22 and these look to be mono-modal distributions. A log-probability plot (Figure 2.23) shows the parent distributions together with mixtures. It can be seen that the mixtures generate curves which are asymptotic to the parent with the wider distribution (spread). Thus a log-probability plot picks out bimodalities which would not otherwise be detected.

2.16.2 Bimodal non-intersecting distributions

Figure 2.24 presents relative plots of blends of two non-intersecting, log-normal distributions with medians of 8 and 13 μm and standard deviations of 1.3 and 1.5 respectively. The areas under the two quite distinct curves give the proportions of the two components. On a log-probability plot (Figure 2.25), the mixtures are asymptotic to both parents and have a point of inflection where the two distributions overlap.

2.16.3 Other distributions

Figure 2.26 shows a trimodal distribution together with the parent distributions (1:1:1 mixture). This may be easily resolved into its component parts if the parent distributions do not intersect (Figure 2.27).

2.16.4 Applications of log-normal plots

Figure 2.28 shows Andreasen analyses monitoring a grinding operation. Since, in this case, the product of the median and the grinding time approaches a constant value it is possible to predict the grinding time required to attain a desired end point median size (Table 2.10).

Figure 2.29 shows a log-normal distribution of geometric mean size 10 μm . The distribution is deficient in sub - 6 μm particles, probably due to classification during a comminution operation, and is asymptotic to this size. If $(x-6)$ is taken as the particle size the parent distribution is obtained. A similar sort of plot occurs when there is a deficiency of coarse particles.

Table 2.10 Andreasen analyses monitoring a grinding operation

Grinding time (T hours)	Median size (x_g μm)	Tx_g
9	5.30	47.7
13	4.10	53.3
15	3.75	56.3
16	3.42	54.7

2.16.5 Curve fitting

An application of curve fitting using Kalaidograph [77] is shown in Figure 2.30. The experimental data are plotted as a differential log-probability graph and the program asked to fit the following equation:

$$\begin{aligned}
 y = & m1 * \exp(-((\ln(m0) - \ln(m2))^2) / (2 * ((\ln(m3))^2))) + \\
 & m4 * \exp(-((\ln(m0) - \ln(m5))^2) / (q2 * ((\ln(m6))^2))) + \\
 & m7 * \exp(-((\ln(m0) - \ln(m8))^2) / (2 * ((\ln(m9))^2)))
 \end{aligned} \quad (2.81)$$

The usual form of equation (2.81) is:

$$\begin{aligned}
 \frac{dW}{d \ln(x)} = & \frac{P_1}{\sqrt{2\pi} \ln(\sigma_{g1})} \exp \left[-\frac{(\ln(x) - \ln(x_{g1}))^2}{2 \ln^2(\sigma_{g1})} \right] \\
 & + \frac{P_2}{\sqrt{2\pi} \ln(\sigma_{g2})} \exp \left[-\frac{(\ln(x) - \ln(x_{g2}))^2}{2 \ln^2(\sigma_{g2})} \right] \\
 & + \frac{P_3}{\sqrt{2\pi} \ln(\sigma_{g3})} \exp \left[-\frac{(\ln(x) - \ln(x_{g3}))^2}{2 \ln^2(\sigma_{g3})} \right]
 \end{aligned} \quad (2.82)$$

Table 2.11 Curve fitting a trimodal log-normal equation to experimental data

	Definition	Estimate	Definition	Fit
m1	Height of first mode	36	$\frac{P_1}{\sqrt{2\pi} \ln(\sigma_{g1})}$	35.55
m2	Location of first mode	0.17	x_{g1}	0.178
m3	34% width of first mode	1.4	σ_{g1}	1.387
m4	Height of second mode	55	$\frac{P_2}{\sqrt{2\pi} \ln(\sigma_{g2})}$	55.52
m5	Location of second mode	0.45	x_{g2}	0.450
m6	34% width of second mode	1.4	σ_{g2}	1.389
m7	Height of third mode	30	$\frac{P_3}{\sqrt{2\pi} \ln(\sigma_{g3})}$	29.74
m8	Location of third mode	0.88	x_{g3}	0.871
m9	34% width of third mode	1.5	σ_{g3}	1.460

Regression coefficient = 0.9988

Estimates are made of the nine variables and the curve fitting procedure determines the true values. The time to carry out this iteration depends upon how near the estimates are to the true values. The 34% widths of the modes are obtained by estimating the ratios of the two sizes having

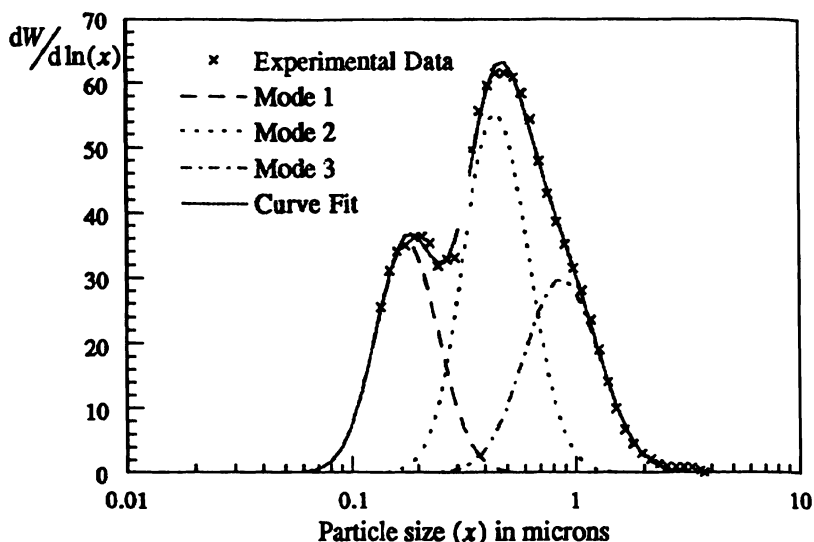


Fig. 2.30 Curve fitting a trimodal log-normal equation to Microtrac SPA data.

8% of the distribution above and 8% below so that these two sizes contain 84% of the distribution. The geometric standard deviation is the square root of the ratio of these sizes. The estimate for the first mode, for example, is $0.24 \mu\text{m}$ and $0.12 \mu\text{m}$ making $m_3 = \sqrt{2} = 1.4$.

Thus, the percentages under each mode can be determined by comparison of the final two columns of Table 2.11. $P_1 = 29.1\%$; $P_2 = 45.7\%$; $P_3 = 28.2\%$ hence $P_{Total} = 103\%$ ($=100\%$ within expected tolerances). The program can be used for other distributions having nine or less variables.

2.16.6 Data interpretation

The curve fitting procedure is a useful aid in data interpretation. It has been used, for example, to demonstrate that a unimodal log-normal distribution with a substantial sub-micron fraction appears as a bimodal log-normal distribution when measured using a gravitational sedimentation technique; this bimodality being due to the effects of thermal diffusion (Brownian motion) [78].

Figure 2.30 gives the data from a product having a tri-modal log-normal distribution. Figures 2.31 illustrates the differences in the size distribution of a product pumped at different flow rates. Increasing the flow rate caused the slurry to plug on-line filters more rapidly. The differences are subtle: The main effect of increasing the flow rate is to decrease the size of the coarse mode (agglomerates) from $1.65 \mu\text{m}$ to

$1.22 \mu\text{m}$ while the mode remains constant at $0.47 \pm 0.01 \mu\text{m}$ and the spread (σ_g) decreases from 2.17 to 2.12. The percentage under the fine mode remains constant at $58\% \pm 1\%$, the mode remains constant at $0.47 \pm 1 \mu\text{m}$ and the spread decreases from 1.39 to 1.38.

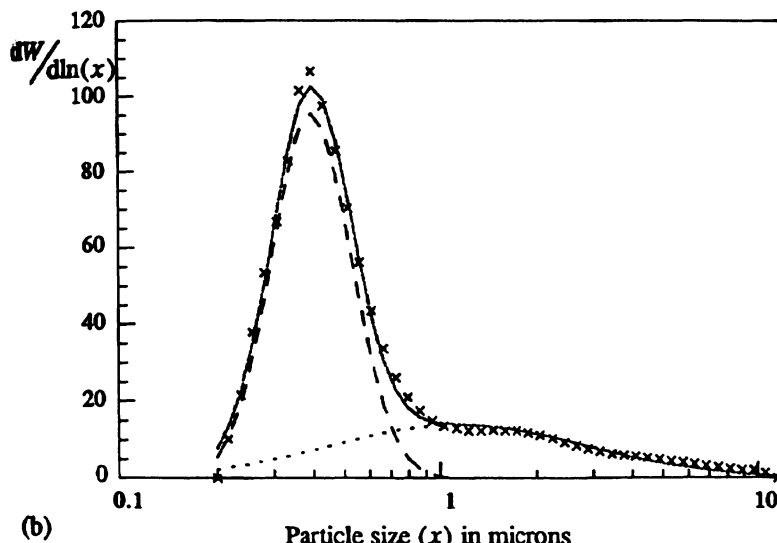
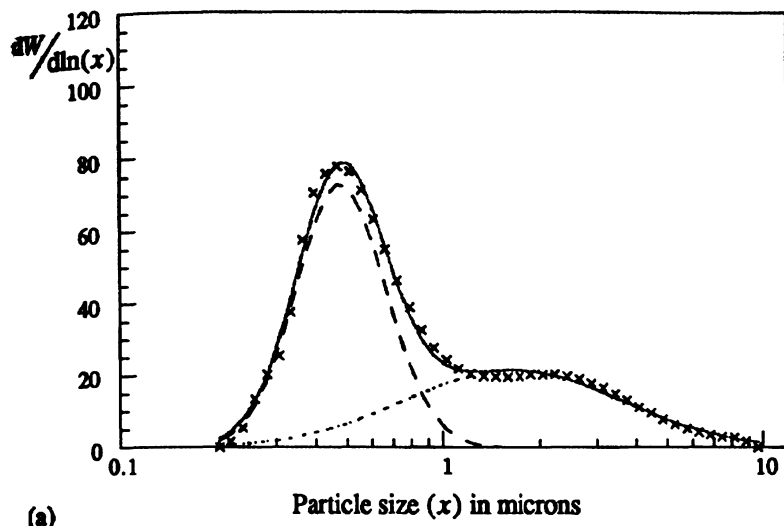


Fig. 2.31 (a) Size distribution of a slurry pumped at 25 gpm (b) size distribution of a slurry pumped at 100 gpm.

2.17 Alternative notations for frequency distribution

The notation given here is widely used but alternative notations have also been developed [German Standard DIN 66141, (1974)] [79–83]. Although elegant, the German notation requires memorization and is most suitable for frequent usage and computer applications.

2.17.1 Notation

Let the fractional number smaller than size x be:

$$Q_0(x) = \int_{x_{\min}}^x q_0(x) dx \quad (2.83)$$

$$\text{or } q_0(x) = \frac{dQ_0(x)}{dx}$$

Hence $q_0(x)$ is the fractional number in the size range x to $x + dx$. Further:

$$Q_0(x)_{\max} = \int_{x_{\min}}^{x_{\max}} q_0(x) dx = 1 \quad (2.84)$$

The subscript may be varied to accommodate other distributions, namely q_r and Q_r where: $r = 0$ for a number distribution; $r = 1$ for a length distribution; $r = 2$ for a surface distribution; $r = 3$ for a volume distribution.

2.17.2 Moment of a distribution

The moment of a distribution is written as:

$$M_{k,r} = \int_{x_{\min}}^{x_{\max}} x^k q_r(x) dx \quad (2.85)$$

$$\left[\text{Note } M_{0,r} = \int_{x_{\min}}^{x_{\max}} q_r(x) dx = 1 \right]$$

For an incomplete distribution:

$$M_{k,r}(x_e, x_u) = \int_{x_e}^{x_u} x^k q_r(x) dx \quad (2.86)$$

2.17.3 Transformation from $q_t(x)$ to $q_r(x)$

If $q_t(x)$ is known $q_r(x)$ may be determined using the following:

$$\frac{x_{\max}}{\int_{x_{\min}}^{x_{\max}} q_t(x) dx} = \frac{x_{\max}}{\int_{x_{\min}}^{x_{\max}} x^r q_0(x) dx} = \frac{x_{\max}}{\int_{x_{\min}}^{x_{\max}} x^{r-t} q_t(x) dx}$$

Hence
$$q_r(x) = \frac{x^{r-t} q_t(x)}{\int_{x_{\min}}^{x_{\max}} x^{r-t} q_t(x) dx}$$

$$q_r(x) = x^{r-t} \frac{q_t(x)}{M_{r-t,t}} \quad (2.87)$$

The denominator is necessary to normalize the distribution function.

Examples.

To convert from a number to a volume (mass) distribution put $t = 0$, $r = 3$. To convert from a surface to a mass distribution put $t = 2$, $r = 3$.

(a) Effect of particle shape

This transformation is derived with the assumption that particle shape does not change with size. More correctly, a shape coefficient $\alpha(x)$ needs to be introduced:

$$q_r(x) = \frac{\alpha(x) x^{r-t} q_t(x)}{\int_{x_{\min}}^{x_{\max}} \alpha(x) x^{r-t} q_t(x) dx} \quad (2.88)$$

2.17.4 Relation between moments

Substituting $q_0(x)$ for $q_r(x)$ in equation (2.85) and putting $t = 0$ in equation (2.87) gives:

$$\int_{x_{\min}}^{x_{\max}} x^k q_r dx$$

$$M_{k,r} = \frac{\int_{x_{\min}}^{x_{\max}} x^k q_r dx}{M_{r,0}}$$

$$M_{k,r} = \frac{\int_{x_{\min}}^{x_{\max}} x^{k+r} q_0 dx}{\int_{x_{\min}}^{x_{\max}} x^r q_0 dx}$$

$$M_{k,r} = \frac{M_{k+r,0}}{M_{r,0}} \quad (2.89)$$

More generally, substituting $q_r(x)$ from equation (2.87) in equation (2.85) gives:

$$M_{k,r} = \frac{M_{k+r-t,t}}{M_{r-t,t}} \quad (2.90)$$

Examples. To determine the surface-volume mean diameter from a number distribution, put $t = 0, r = 2, k = 1$.

$$M_{1,2} = \frac{M_{3,0}}{M_{2,0}} \quad (= x_{sv})$$

To determine the surface-volume mean diameter from a surface distribution, put $t = 2, r = 2, k = 1$.

$$M_{1,2} = \frac{M_{1,2}}{M_{0,2}}$$

2.17.5 Means of distributions

(a) Distribution means:

$$\int_{x_{\min}}^{x_{\max}} x q_r(x) dx$$

$$\bar{x}_{1,r} = \frac{\int_{x_{\min}}^{x_{\max}} q_r(x) dx}{\int_{x_{\min}}^{x_{\max}} x q_r(x) dx}$$

$$\bar{x}_{1,r} = \frac{M_{1,r}}{M_{0,r}} = \frac{M_{r+1,0}}{M_{r,0}} = M_{1,r} \quad (2.91)$$

(b) Arithmetic means:

$$(\bar{x}_{k,0})^k = \left[\frac{\int x^k q_0(x) dx}{\frac{\int q_0(x) dx}{x_{\min}}} \right]$$

$$[\bar{x}_{k,0}]^k = \frac{M_{k,0}}{M_{0,0}}$$

$$x_{k,0} = \sqrt[k]{M_{k,0}} \quad (2.92)$$

(c) More generally:

$$(\bar{x}_{k,r})^k = \frac{\int x^k q_r(x) dx}{\frac{\int q_r(x) dx}{x_{\min}}}$$

$$(\bar{x}_{k,r})^k = M_{k,r} \quad (2.93)$$

2.17.6 Standard deviations

For a number distribution, the variance is defined by:

$$\sigma_0^2 = \frac{\int_{x_{\min}}^{x_{\max}} (x - \bar{x}_{1,0})^2 q_0(x) dx}{x_{\min}}$$

$$\sigma_0^2 = \frac{\int_{x_{\min}}^{x_{\max}} x^2 q_0(x) dx - \bar{x}_{1,0}^2 \int_{x_{\min}}^{x_{\max}} q_0(x) dx}{x_{\min}}$$

$$\sigma_0^2 = M_{2,0} - (M_{1,0})^2 \quad (2.94)$$

More generally:

$$\sigma_r^2 = \int_{x_{\min}}^{x_{\max}} (x - \bar{x}_r)^2 q_r(x) dx$$

$$\sigma_r^2 = M_{2,r} - (M_{1,r})^2 \quad (2.95)$$

Alternatively:

$$\sigma_r^2 = M_{1,r} \left[\frac{M_{2,r}}{M_{1,r}} - M_{1,r} \right]$$

Replacing r by $r + 1$, putting $t = r + 1$ and $k = 1$ in equation (2.90) gives:

$$\sigma_r^2 = M_{1,r} [M_{1,r+1} - M_{1,r}] \quad (2.96)$$

From equation (2.93):

$$\sigma_r^2 = \bar{x}_{1,r} [\bar{x}_{1,r+1} - \bar{x}_{1,r}] \quad (2.97)$$

2.17.7 Coefficient of variation

$$C_r^2 = \frac{\sigma_r^2}{(\bar{x}_{1,r})^2} \quad (2.98)$$

$$C_r^2 = \frac{\bar{x}_{1,r+1}}{\bar{x}_{1,r}} - 1 \quad (2.99)$$

2.17.8 Applications

(a) Calculation of volume-specific surface

$$S_v = \frac{\text{surface area}}{\text{volume}}$$

$$\nu = \frac{\int_{x_{\min}}^{x_{\max}} \alpha_s(x) x^2 q_0(x) dx}{\int_{x_{\min}}^{x_{\max}} \alpha_v(x) x^3 q_0(x) dx}$$

where α_s and α_v are the surface and volume shape coefficients. Assuming that these are independent of particle size and defining the ratio of α_s to α_v as α_{sv} , the surface-volume shape coefficient,

$$S_v = \alpha_{sv} \frac{M_{2,0}}{M_{3,0}} = \frac{\alpha_{sv}}{M_{1,2}} = \alpha_{sv} M_{1,3} \quad (2.100)$$

Also, since $M_{1,2} = \bar{x}_{1,2}$

$$S_v = \frac{\alpha_{sv}}{\bar{x}_{1,2}} \quad (2.101)$$

(b) Calculation of the surface area of a size increment

$$S_v(x_e, x_u) = \frac{\int_{x_{\min}}^{x_u} \alpha_s(x) x^2 q_0(x) dx}{\int_{x_{\min}}^{x_u} \alpha_v(x) x^3 q_0(x) dx}$$

$$S_v(x_e, x_u) = \alpha_{sv} \frac{M_{2,0}(x_e, x_u)}{M_{3,0}(x_e, x_u)}$$

$$S_v(x_e, x_u) = \alpha_{sv} \left[\frac{M_{2,0}(x_e, x_u)}{M_{3,0}} \times \frac{M_{3,0}}{M_{3,0}(x_e, x_u)} \right]$$

Now:

$$Q_r(x_i) = \int_{x_{\min}}^{x_i} q_r(x) dx$$

$$\int_{x_i}^{\infty} x^r q_0(x) dx$$

$$Q_r(x_i) = \frac{x_{\min}}{M_{r,0}}$$

$$Q_r(x_i) = \frac{M_{r,0}(x_{\min}, x_i)}{M_{r,0}}$$

so:

$$Q_3(x_u) - Q_3(x_e) = \frac{M_{3,0}(x_e, x_u)}{M_{3,0}}$$

Hence:

$$S_v = \alpha_{sv} \left[\frac{M_{3,0}(x_e, x_u)}{M_{3,0}} \times \frac{1}{Q_3(x_u) - Q_3(x_e)} \right] \quad (2.102)$$

The application of this equation enables a surface area to be calculated from a summation of increments, i.e.

$$S_v = \alpha_{sv} \frac{M_{2,0}}{M_{3,0}}$$

$$S_v = \frac{\alpha_{sv}}{M_{3,0}} \left[\frac{\int_{x_{\min}}^{x_{u_1}} x^2 q_0(x) dx}{x_{u_1}} + \frac{\int_{x_{u_1}}^{x_{u_2}} x^2 q_0(x) dx}{x_{u_2}} + \dots \right]$$

$$S_v = \frac{\alpha_{sv}}{M_{3,0}} \sum_{i=1}^{i=n} M_{2,0}(x_{e_i}, x_{u_i}) \quad (2.103)$$

$$e_i = \text{min}, u_n = \text{max.}$$

2.17.9 Transformation of abscissae

Suppose, in an analysis, ξ , which is a function of x , is measured e.g. $\xi = \ln(x)$. Since the amount of material between sizes x and $x + dx$ is constant, there must be a simple relationship between $q(\xi)$ and $q(x)$.

Let $x = f(\xi)$ so that $\xi = \phi(x)$; then:

$$q_r^*(\xi) d\xi = q_r(x) dx$$

i.e. the quantity in the interval $d\xi$ is the same as the quantity in the interval dx . The new ordinate $q_r^*(\xi)$ is calculated from $q_r(x)$ and the differential ratio $dx/d\xi$.

$$q_r^*(\xi) = q_r(x) \frac{dx}{d\xi} \quad (2.104)$$

For example, suppose the following relationship holds: $\xi = x^k$

$$\frac{d\xi}{dx} = kx^{k-1}$$

and

$$q_r^*(\xi) = \frac{1}{kx^{k-1}} q_r(x) \quad (2.105)$$

Similarly for $\xi = \ln(x)$

$$\frac{d\xi}{dx} = x^{-1} \quad [\text{i.e. } d\ln(x) = \frac{dx}{x}]$$

$$\text{and } q_r^*[\ln(x)] = x q_r(x)$$

$$q_r^*[\log(x)] = \frac{x}{\log(e)} q_r(x)$$

In general, suppose we have the $q_u(x)$ distribution and wish to find the $q_r(x^k)$ distribution. From equation (2.87):

$$q_r(x) = \frac{x^{r-u} q_u(x)}{M_{r-u,u}}$$

Substituting in equation (2.105) gives:

$$q_r^*(\xi) = \frac{x^{r-u} q_u(x)}{M_{r-u,u}} \frac{1}{kx^{k-1}} \quad (2.106)$$

Example. In a Coulter Counter analysis, the pulse height V is proportional to particle volume, i.e.

$$\xi = V = p^3 x^3$$

(a) Calculation of $M_{r,0}$ ($= [\bar{x}_{r,0}]^r$)

By definition:

$$M_{r,0} = \int_{x_{\min}}^{x_{\max}} x^r q_0(x) dx$$

Using the transformation from the above equation:

$$Q_r(x) = \frac{\int_{x_{\min}}^{x_{\max}} x^r q_0(x) dx}{M_{r,0}}$$

$$M_{r,0} = \frac{1}{p_r} \int_{x_{\min}}^{x_{\max}} p^r x^r q_0(x) dx$$

$$M_{r,0} = \frac{1}{p^r} \int_{\xi_{\min}}^{\xi_{\max}} \xi^{r/3} q_0^*(\xi) d\xi$$

$$M_{r,0} = \frac{M_{r/3,0}(\xi)}{p^r} \quad (2.107)$$

Also, since $q_r(x) = \frac{x^r q_0^*(x)}{M_{r,0}}$, substituting in equations (2.104) and (2.107):

$$q_r(x) = x^r q_r^*(\xi) \frac{d\xi}{dx} \cdot \frac{p^r}{M_{r/3,0}(\xi)}$$

$$q_r(x) = \frac{3pq^{(r+2)/3} q_0^*(\xi)}{M_{r/3,0}(\xi)} \quad (2.108)$$

Ib) Calculation of $M_{k,r}$

From equation (2.85):

$$M_{k,r} = \int_{x_{\min}}^{x_{\max}} x^k q_r(x) dx$$

$$M_{k,r} = \frac{1}{p^k} \int_{\xi_{\min}}^{\xi_{\max}} \frac{\xi^{(k+r)/3} q_0^*(\xi) d\xi}{M_{r/3,0}(\xi)}$$

$$M_{k,r} = \frac{M_{(k+r)/3,0}(\xi)}{M_{r/3,0}(\xi)} \quad (2.109)$$

C) Calculation of volume specific surface

$$\theta = \alpha_{sv} \frac{M_{2,0}}{M_{3,0}}$$

which, using equation (2.109), can be written:

$$S_y = \alpha_{sv} p \frac{M_{2/3,0}(\xi)}{M_{1,0}(\xi)} \quad (2.110)$$

Thus, specific surface can be determined from moments calculated directly from Coulter Counter data.

D) Calculation of mean size $x_{k,r}$

Equation (2.93) may be written:

$$\bar{x}_{k,r} = k \sqrt[p]{M_{k,r}}$$

Substituting for $M_{k,r}$ from equation (2.109):

$$\bar{x}_{k,r} = \frac{1}{p} k \sqrt[p]{\frac{M_{(k+r)/3,0}(\xi)}{M_{r/3,0}(\xi)}} \quad (2.111)$$

- 11 Wadell, H. (1934), *Physics*, **5**, 281–91, 57
 12 Massacci, P. and Bonifazi, G. (1990), *Proc. Second World Congress Particle Technology*, Sept., Kyoto, Japan, Part 1, 265–271, 58
 13 Beddow, K. and Philip, G. (1975), *Plansbeer*, **23**(1), 58
 14 Meloy, T.P., Clark, N., Durney, T.E. and Pitchumani, B. (1985), *Chem. Eng. Sci.*, **1077–1084**, 58
 15 Alderliesten, M. (1991), *Part. Part. Charact.*, **231–241**, 58
 16 Fairbridge, C., Ng, S.H. and Palmer, A.D. (1986), *Fuel*, **65**, 1759–1762, 58
 17 Shibata, T. and Yamaguchi, K. (1990), *Proc. Second World Congress Particle Technology*, Sept., Kyoto, Japan, Part 1, 257–264, 59
 18 Schwartcz, H.P. and Shane, K.C. (1969), *Sedimentology*, **13**, 213–31, 59
 19 Shibata, T., Tsuji, T., Uemaki, O. and Yamaguchi, K. (1994), *First International Particle Technology Forum, Am. Inst. Chem. Engrs.*, Part 1, 95–100, 59
 20 Johnston, J.E. and Rosen, L.J. (1976), *Powder Technol.*, **14**, 195–201, 59
 21 Hawkins, A.L. (1993), *The Shape of Powder-Particle Outlines*, John Wiley, p. 58, 59
 22 Mandelbrot, B.B. (1977), *Fractals, Form, Chance and Dimension*, W.H. Freeman & Company, San Francisco, 59
 23 Mandelbrot, B.B. (1983), *The Fractal Geometry of Nature*, W. H. Freeman & Company, 59
 24 Kaye, B.H. (1991), *PSA '91, Proc. 25th Anniversary Conf. Particle Characterization Group, Analyt. Div. Royal Soc. Chem.*, ed N. Stanley-Wood and R. Lines, 59
 25 Mandelbrot, B.B. (1967), *Science*, **155**, 636–638, 59
 26 Kaye, B.H. and Clark, G.G. (1989), *Part. Part. Charact.*, **6**(1), 1–12, 59
 27 Fairbridge, C., Ng, S.H. and Palmer, A.D. (1986), *Fuel*, **65**, 1759–1762, 1986, 60
 28 Fan, L.T., Boateng, A.A. and Walawender, W.P. (1992), *Can. J. Chem. Eng.*, **70**, 388–390, April, 60, 61
 29 Kaupp, A. (1984), *Gasification of Rice Hulls, Theory and Practice*, Friedr. Vieweg & Son, Braunschweig/Weisbaden, Germany, 112–138, 60
 30 Avnir, D., Farin, D. and Pfeifer, P. (1993), *J. Chem. Phys.*, **79**, 3566, 61
 31 Tsakiraglou, C.D. and Pasyatakis, A.C. (1993), *J. Colloid Interf. Sci.*, **159**, 287–301, 61
 32 Richter, R., Sander, L.M. and Cheng, Z. (1984), *J. Colloid Interf. Sci.*, **100**(1), 203–209, 61
 33 Hurd, A.J. and Flower, W.L. (1988), *J. Colloid Interf. Sci.*, **122**(1), 62

2.18 Phi-notation

In geological literature dealing with particle size distribution [84,85], a very advantageous transformation of particle size is commonly used. This transformation replaces scale numbers based on linear millimeter values by the logarithms of these values. Because it is a logarithmic transformation it simplifies computation. The transformation is:

$$\phi = -\log_2 X_i \quad \text{or} \quad X_i = 2^{-\phi} \quad (2.112)$$

where X_i is a dimensionless ratio of a given particle size, in millimeters, to the standard particle size of 1mm.

Phi - values can be found if the common decadic logarithms of X_i are multiplied by $(\log 10^2)^{-1} = 3.322$. For easy manipulation a conversion chart [86] or a conversion table [87,88] can be used. The standard deviation σ_ϕ used in this notation is defined as:

$$\sigma_\phi = 0.5(\phi_{84} - \phi_{16}) \quad (2.113)$$

The skewness is defined as:

$$\phi = \frac{\phi_{84} + \phi_{16} - 2\phi_{50}}{\phi_{84} - \phi_{16}} \quad (2.114)$$

Other statistical measurements used in geology for particle size distribution characterization (moment, quartile and others) have been defined [89,90].

References

- 1 Tsubaki, J. and Jimbo, G. (1979), *Powder Technol.*, 2(2), 161–70, 47
- 2 Crowl, V.T. (1963), Paint Research Station Report, No. 325, Teddington, Middlesex, London, 50
- 3 Heyd, A. and Dhabbar, D. (1979), *Drug, Cosmet. Ind.*, 125, 42–45, 146–147, 54
- 4 Davies, R. (1975), *Powder Technol.*, 12, 111–124, 54, 59 ^{shape}
- 5 Hawkins, A.E. (1993), *The Shape of Powder-Particle Outlines*, John Wiley, 54
- 6 British Standard 2955 (1958), *Glossary of terms relating to powders*, 55
- 7 Heywood, H. (1947), *Symposium on particle size analysis, Inst. Chem. Eng.*, Suppl. 25, 14, 55
- 8 Wadell, H. (1932), *J. Geol.*, 40, 250–80, 57
- 9 Wadell, H. (1935), *J. Geol.*, 43, 459, 57
- 10 Wadell, H. (1934), *J. Franklin Inst.*, 217, 459, 57

- 34 Schaeffer, D.W. (1989), *Science*, **243**, 1023–1027, 62
35 Kasper, G., Chesters, S., Wen, H.Y. and Lundin, M. (1989), *Appl. Surface Sc.*, **40**, 185–192, 62
36 Zaltash, A., Myler, C.A., Dhodapkar, S. and Klinzing, G.E. (1989), *Powder Technol.*, **59**, 199–207, 62
37 Allen, M., Brown, G.J. and Miles, N.J. (1995), *Powder Technol.*, **84**, 1–14, 62
38 Gotah, K. and Finney, J.L. (1975), *Powder Technol.*, **12**(2), 125–130, 62
39 Neese, Th., Dück, J. and Thaufelder, T. (1995), *6th European Symp. Particle Size Characterization*, Partec 95, Nurenberg, Germany, publ. NürnbergMesse GmbH 315–325, 62
40 Heffels, C., Heitzmann, D., Kramer, H. and Scarlett, B. (1995), *6th European Symp. Particle Size Characterization*, Partec 95, Nurenberg, Germany, publ. NürnbergMesse GmbH 267–276, 62
41 Ridgeway, K. and Rupp, R. (1969), *J. Pharm., Pharmac. Suppl.*, **21**, 30–39, 62
42 Ridgeway, K. and Rupp, R. (1970/71), *Powder Technol.*, **4**, 195–202, 62
43 Riley, G.S. (1968/69), *Powder Technol.*, **2**(6), 315–319, 62
44 Viswanathan, K., Aravamudhan, S. and Mani, B.P. (1948), *Powder Technol.*, **39**, 83–91, 62
45 Whiteman, M. and Ridgeway, K. (1988), *Powder Technol.*, **56**, 83–94, 62
46 Meloy, T.P. and Makino, K. (1983), *Powder Technol.*, **36**, 253–258, 62
47 Lenn, C.P. and Holt, C.B. (1982), *Proc. Fourth Particle Size Analysis Conf.* 1981, publ. John Wiley, pp. 233–240, ed. N.G. Stanley-Wood and T. Allen, 62
48 Anon. *German Standard DIN 66141* (1974), Representation of particle size distribution, 69
49 Svarovsky, L. (1973), *Powder Technol.*, **7**(6), 351–2, 80
50 Herdan, G. (1968), *Small Particle Statistics*, Butterworths, 81
51 Yu, A.B. and Standish, N. (1987), *Powder Technol.*, **52**, 233, 81
52 Wu, A.B. (1989), PhD thesis, Univ. Woolongong, Australia, 81
53 Yu, A.B. and Standish, N. (1990), *Powder Technol.*, **62**, 101–118, 81, 84
54 Yu, A.B. and Standish, N. (1990), *World Congress Powder Technology*, Part 1, Soc. Powder Techn. Japan, Kyota, 81
55 Yu, A.B. (1994), First Int. Powder Technology Forum, Am. Inst. Chem. Eng., Denver, 120–125, 81
56 Rosin, P. and Rammler, E. (1933), *J. Inst. Fuel*, **7**, 29, 82
57 Gaudin, A.M. (1926), *Trans. AIME*, **73**, 253, 82
58 Gates, A.O. (1915), *Trans. AIME*, **52**, 875–909, 82, 84
59 Schumann, R. (1940), *Trans. AIME, Techn. Publ.* **1189**, 82, 84
60 Gaudin, A.M. and Meloy, T.P. (1962), *Trans. AIME*, **43–50**, 82, 84

- 61 Roller, P.S. (1937), *Proc. ASTM*, **37**, 675, 82, 84
 62 Roller, P.S. (1937), *J. Franklin Inst.*, **223**, 609, 82, 84
 63 Roller, P.S. (1941), *J. Phys. Chem.*, **45**, 241, 82, 84
 64 Harris, C.C. (1969), *Trans. AIME*, **244**, 187–90, 82, 85
 65 Martin, G. (1924), *Trans. Ceram. Soc.*, **23**, 61, 82
 66 Svensson, J. (1955), *K. Tekn. Hpgsk. Handl.*, No. 88, 82
 67 Evens, I. (1958), *Proc. Sci. in the Use of Coal, Inst. Fuel*, London,
 Paper 14, 82
 68 Weinig, A.J. (1933), *Col School of Mines Quarterly*, **28**, 57, 82
 69 Heywood, H. (1933), *Proc. Inst. Mech. Eng.*, **125**, 383, 82
 70 Griffith, L. (43), *Can. J. Res.*, **21**, 57, 82
 71 Klimpel, R.R. and Austin, L.G. (1965), *Trans. AIME*, **232**, 82,
 72 Popplewell, L.M., Campanella, O.H. and Peleg, M. (1988),
 Powder Technol., **54**, 119, 82
 73 Harris, C.C. (1968), *Trans. Am. Inst. Mech. Eng.*, **241**, 343, 83
 74 Rosin, P. and Rammler, E. (1933), *J. Inst. Fuel*, **7**(29), 83
 75 Svensson, J. (1955), *Acta Polytec. Scand.*, **163**, 53, 84
 76 Tarjan, G. (1974), *Powder Technol.*, **10**, 73–76, 86
 77 Kalaidograph, Abelbeck Software, Synergy Software, 2457
 Perkiomen Ave., Reading, PA 19606–9976, 94
 78 Allen, T. and Nelson, R.D. Jr. (1994), *First Int. Techn. Forum,*
 Am. Inst. Chem. Eng., Denver, Part 1, 113–119, 96
 79 Rumpf, H. and Ebert, K.F. (1964), *Chem. Ingr. Tech.*, **36**, 523–
 37, 98
 80 Rumpf, H. and Debbas, S. (1966), *Chem. Eng. Sci.*, **21**, 583–607,
 98
 81 Rumpf, H., Debbas, S. and Schonert, K. (1967), *Chem. Ingr.*
 Tech., **39**,(3), 116–9, 98
 82 Rumpf, H. (1961), *Chem. Ingr. Tech.*, **33**, 7, 502–508, 98
 83 Leschonski, K., Alex, W., and Koglin, B. (1974), *Chem. Ingr.*
 Tech., **46**, 3, 23–6, 98
 84 McManus, D.A. (1963), *J. Sediment. Petrol.*, **33**, 670, 108
 85 Krumbein, W.C. (1964), *J. Sediment. Petrol.*, **34**, 195, 108
 86 Krumbein, W.C. and Pettyjohn, F.J. (1938), *Manual of*
 Sedimentary Petrology, p. 244, Appleton-Century-Crofts, New
 York, 108
 87 Page, H.G. (1955), *J. Sediment. Petrol.*, **25**, 285, 108
 88 Griffiths, J.C. and McIntyre, D.D. (1958), *A Table for the*
 Conversion of Millimeters to Phi Units, Mineral Ind. Exp. Sta.,
 Penn. State University, 108
 89 Folk, R.L. (1966), *Sedimentology*, **6**, 108
 90 Griffiths, J.C. (1962), *Sedimentary Petrography*, (ed. H.B.
 Milnes) Macmillan, New York, Ch. 16, 108

Particle size analysis by image analysis

3.1 Introduction

A microscope examination should always be carried out whenever a sample is prepared for particle size analysis. Such an examination allows an estimate of the particle size range of the powder under test and its degree of dispersion. If the dispersion is incomplete it can be determined whether this is due to the presence of agglomerates or aggregates and, if agglomeration is present, may indicate the need for an alternative dispersing procedure.

Microscopy is often used as an absolute method of particle size analysis since it is the only method in which the individual particles are observed and measured [1-3]. It is particularly useful in aerosol science where particles are often collected in a form suitable for subsequent optical examination. It is useful not only for particle size measurement but also for particle shape and particle texture evaluation, collectively called morphology, with a sensitivity far greater than other techniques. Reports have also been presented of the use of microscopy to relate particle size to processing characteristics of valuable mineral ores [4,5].

Particle shape may be defined either qualitatively or quantitatively. The former includes the use of such terms as acicularity, roundness and so on. The latter, more definitively, compares perpendicularly oriented diameters, for example, to obtain shape factors. The introduction of automatic image analyzers allows for the determination of complex shape factors which were previously unobtainable. These factors are of great value in defining crystal morphology and relating this to operating (attrition during conveying, compaction and so on) and end-use properties.

A size analysis by number is simpler to perform than an analysis by mass since, in the former, the statistical reliability depends solely on the number of particles measured. For a mass analysis the omission of a single 10 µm particle leads to the same error as the omission of a thousand 1 µm particle since they both have the same volume. For a particle size analysis by mass, in order to obtain an estimated standard

error of less than 2%, 25 particles in the largest size category have to be counted. If all the particles in this area were counted the final count would run into millions. It is obvious therefore that the area to be examined must decrease with decreasing particle size and the results obtained must be presented as particles per unit area.

The problem may be likened to determining the size distribution of a number of differently sized homogeneous balls in a container. If the balls are of size $2, 2\sqrt{2}, 4, 4\sqrt{2} \dots 64, 64\sqrt{2}$, in line with the size ratios often adopted in optical microscopy, and the frequency of the top size category is found to be 8 in 1000, particles this can be readily converted to a mass frequency when the number of balls in the other size categories is known.

With a size analysis by mass, the accuracy is improved if 25 of the largest size category particles are counted. If the estimated mass of the 25 particles is 10% of the sample then the forecasted standard error is $(10/\sqrt{25})$ i.e. 2%. If, on completing the analysis, the mass percentage of the coarsest fraction is greater than 10% then it is necessary to count more coarse particles in order to maintain this level of accuracy.

The errors in converting from a number to a volume (mass) distribution are greatest when the size range is wide. For a narrowly classified powder, ranging in size from say 10 to 30 μm , it is necessary to use an arithmetic grading of sizes, probably a 2 μm interval in this case, but the same rules still apply and the direct conversion of a number distribution to a weight distribution can still give rise to considerable error at the coarse end of the size distribution. Using closer size intervals adds little to analytical accuracy but can greatly increase the computation time.

Examples of determining both a number and a mass distribution are given. Although the examples relate to manual counting, the conditions also govern size analyses by automatic image analyzers.

Light microscopy [6] is suitable for the measurement of particles in the size range from 3 μm to 1 mm. Scanning electron microscopy (SEM) from 20 nm to 1 mm and transmission electron microscopy (TEM) from 2 nm to 1 μm . Back scattered electrons and x-rays contain information on the chemistry and average atomic number of the material under the beam.

3.2 Optical microscopy

Optical microscopy is most often used for the examination of particles from about 3 μm to 150 μm . The theoretical lower limit is approximately 0.2 μm but the diffraction halo around the particle gives a gross overestimation of particle size. Above 150 μm a simple magnifying glass is suitable.

Its most severe limitation is its small depth of focus so that, for a sample having a wide range of sizes, only a few particles are in focus in any field of view. The surface of particles larger than about 5 μm can

be studied by reflected light, but only transmission microscopy, with which silhouettes are seen, is suitable for smaller particles.

3.2.1 Upper size limit

The method is preferably limited to sub-200 mesh sieve size (75 µm) but larger particles may be counted and sized provided their fractional weight is less than 10% of the total weight of the powder. When the fractional oversize weight exceeds 10%, these particles should be removed and a sieve and microscope analyses merged. Alternatively such large particles can be sized using a simple magnifying glass.

3.2.2 Lower size limit

The limit of resolution of an optical microscope is expressed by the fundamental formula:

$$d = \frac{f\lambda}{NA} \quad (3.1)$$

where d is the limit of resolution, i.e. particles in closer proximity than this appear as a single particle, λ is the wavelength of the illuminant, the numerical aperture of the objective $NA = \mu \sin\theta$, where μ is the refractive index of the immersion medium, θ is the angular aperture of the objective and f is a factor of about 0.6 to allow for the inefficiency of the system.

For $\lambda = 0.6 \mu\text{m}$ the resolving power is a maximum with $NA = 0.95$ (dry) and $NA = 1.40$ (wet) giving $d_{min} = 0.38 \mu\text{m}$ and $0.26 \mu\text{m}$ respectively. The images of particles having a separation of less than this merge to form a single image.

The resolution of the human eye is around 0.3 mm, therefore the maximum effective magnification with white light is:

$$\frac{0.30 \text{ mm}}{0.28 \mu\text{m}} = 1000$$

Particles smaller than the limit of resolution appear as diffuse circles; image broadening occurs, even for particles larger than d_{min} , and this results in oversizing. Some operators routinely size down to this level but a more realistic lower size is 0.8 µm with limited accuracy below 3 µm. It is recommended that monochromatic light be used for sizing below 3 µm. BS 3406 [6] for example, does not recommend optical microscopy for particles smaller than 3 µm. Powders containing material smaller than this are usually imaged by transmission or scanning electron microscopy and the resulting negatives or prints examined.

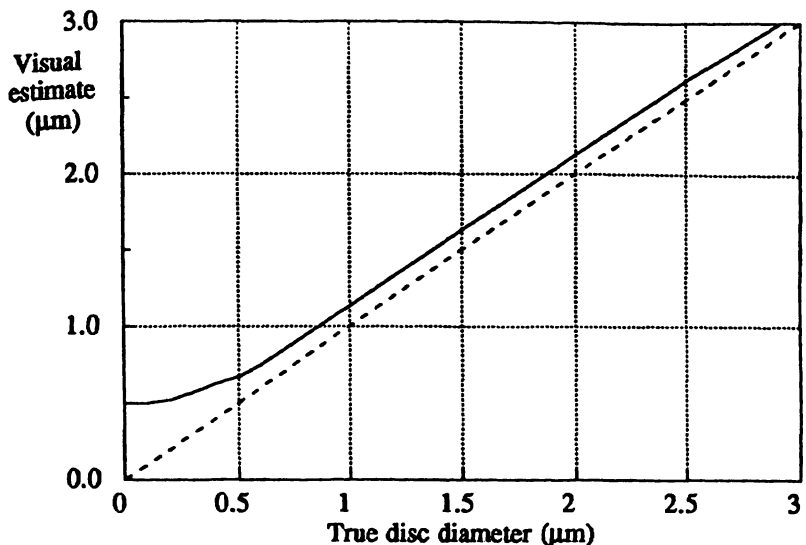


Fig. 3.1 Oversizing of small discs by optical microscopy [7]

Figure 3.1 plots visual estimates of disc sizes against their geometrical size. The measurements were made with the circular discs immersed in oil. Discs smaller than 0.25 μm in diameter generate diffuse images of diameter 0.5 μm ; at 0.5 μm the image has a diameter of 0.65 μm and discs of diameter greater than 1 μm generate an image that is 0.10 μm oversize. Due to less precise focusing with three dimensional particles, real particles are subject to greater errors.

3.3 Sample preparation

Great care has to be taken in slide or grid preparation since the measurement sample is so small that it is difficult to make it representative of the bulk. Many particulate systems contain agglomerates and aggregates and, if it is necessary that they retain their integrity, the dispersing procedure needs to be very gentle. Further, the sample under visual examination has to be dispersed uniformly since it is usually impossible to measure every particle; small regions selected at random or according to some predetermined plan are, therefore, examined. The simplest procedure is to extract samples from an agitated suspension; for less robust materials a procedure detailed in reference [3] may be used in which an air jet circulates the suspension through a sampling tube which can be closed and withdrawn to provide samples for analysis. The analysis is suspect if the regions in one area of the measurement sample give a very different size distribution to those in another area. Slides may be of three main types: dry,

temporary and permanent. For very easily dispersed material, the particles may be shaken from a fine brush or the end of a spatula on to a slide. Humphries [8] describes a microsample splitter that assists the free flow of grains in order to provide the very small samples needed for microscopy; a diagram of the device is reproduced in a book by Hawkins [9]. Hawkins also describes a moving pavement version of the spinning riffler designed for preparation of representative samples of free flowing particles on microscope slides [9,10]. A novel method of mounting particles on regularly spaced adhesive circles has recently been developed. This method of mounting results in ordered array rather than the random chaos of usual methods and greatly facilitates particle analysis [11-13].

For a temporary slide the powder can be incorporated into a viscous liquid, such as glycerin or oil, in which it is known to disperse completely. Some operators work the powder into the liquid with a flexible spatula, others roll it in with a glass rod. Either of these procedure can cause particle fracture and a preferable alternative is to use a small camel hair brush. A drop of this liquid can then be transferred to a microscope slide and a cover slip gently lowered over it. Rapid pressing of the cover slip must be avoided as it causes preferential transfer of the larger particles to the edge of the cover slip. It is undesirable for liquid to spread outside the limits of the cover slip; improved spreading is best effected with highly viscous liquids by pre-warming the microscope slide. Sealing the cover slip with amyl acetate (nail varnish is a good substitute) makes the slide semi-permanent. If low viscosity liquids are used it is necessary to have a well, or depression, on the slide to contain the dispersion.

Permanent slides may be produced by incorporating the powder into a 2% solution of colloidon in amyl acetate, canada balsam or polystyrene in xylol or gelatin in water. A drop of this is then placed on the still surface of distilled water in a large beaker. The resulting film is picked up on a microscope slide and completely dried. For gelatin the suspension is allowed to fall directly on to the slide; spreading is accelerated if the slide is first washed in a detergent. Sometimes this technique may also be used successfully with volatile liquids.

A dilute suspension may be filtered through a 0.2 µm PTFE membrane filter. The filter is then exposed to acetone vapor which renders it transparent.

Automatic and quantitative microscopes tend to give erroneous results for transparent particles. To overcome this problem, Amor and Block [14] used a silver staining technique to make the particles opaque. The particles are dry mounted on to a thin film of tacky collodion on a microscope slide. Silver is then deposited from solution using the silver mirror reaction. Preliminary sensitizing the crystalline surface ensures that much more silver is deposited on the particles than

on the collodion. A method of staining particles in aqueous solution prior to deposition on a membrane filter for analysis is also given.

Hamilton and Phelps [15] adapted the metal shadowing technique for the preparation of transparent profiles of dust particles. The process consisted of evaporating *in vacuo* a thin metal film in a direction normal to a slide containing particles. The particles are then removed by a jet of air or water, leaving sharp transparent profiles.

3.4 Measurement of plane sections through packed beds

When the size distribution of particles embedded in a continuous solid phase is required, the general approach is to deduce the distribution from the size of particle cross-section in a plane cut through the particle bed. The problem has occupied the attention of workers in diverse fields of science, who have tended to work in isolation and this has led to much duplication of effort.

The historical development of this technique has been reviewed by Eckhoff and Enstad [16] and the relevant theory of Scheil by Dullien *et al.* [17]. A theoretical analysis [18] has been criticized on several grounds [19]. Dullien *et al.* [20–22] examined salt particles embedded in a matrix of Wood's metal using the principles of quantitative stereology. They then leached out the salt particles and examined the matrix using mercury porosimetry. Poor agreement was obtained and this they attribute to the mercury porosimetry being controlled by neck diameter. Nicholson [23] considered the circular intersections of a Poisson distribution of spherical particles to estimate the particle size distribution. Saltzman *et al.* generated a computer based imaging system for slices through a packed bed and found good experimental agreement [24].

3.5 Particle size

The images seen in a microscope are projected areas whose dimensions depend on the particles' orientation on the slide. Particles in stable orientation tend to present their maximum area to the microscopist, hence the sizes measured by microscopy tend to be greater than those measured by other methods; that is, the smallest dimension of the particles are neglected. Any one particle has an infinite number of linear dimensions hence, if a chord length is measured at random, the length will depend upon the particle orientation on the slide. These orientation dependent measurements are known as statistical diameters, acceptable only when determined in such numbers as to typify a distribution. They are measured parallel to some fixed direction and are acceptable only when orientation is random; i.e. the distribution of diameters measured parallel to some other direction must give the same size distribution. Since they are representative of the two largest particle dimensions – the smallest is perpendicular to the viewing plane

if the particles are in stable orientation – the diameters will generally be larger than the Stokes diameters.

Acceptable statistical diameters are:

- *Martin's diameter (d_M)* being the length of the line which bisects the area of the particle's projected area. The line may be in any direction, which must be maintained constant throughout the analysis.
- *Feret's diameter (d_F)* is the distance between two tangents on opposite sides of the particle parallel to some fixed direction.
- *The projected area diameter (d_a)* takes into account both dimensions of the particle in the measurement plane, being the diameter of a circle having the same projected area as the particle. It is necessary to differentiate between this diameter and the projected area diameter for a particle in random orientation (d_p) since, in this case, the third and smallest dimension of the particle is also included.

The simplest diameter to measure is the Feret diameter but this is significantly larger than the other two diameters for most powders. It is probably best to reserve this diameter for comparison purposes and for rounded particles. Of the other two diameters, the projected area diameter is preferred since two dimensions are included in one measurement and the projected area is easier to estimate using globe and circle graticules than the length of the chord that bisects the image.

3.6 Calibration

It is necessary to use an eyepiece graticule when carrying out a microscope analysis; this is calibrated against a stage micrometer placed in the object plane; typically this is a microscope slide with ruled lines drawn in the central area. Linear eyepiece graticules labeled 0 to 100 may be used to scan the sample so that the linear dimensions yields a size distribution as a function of Feret diameter. Special graticules are also available containing globes (opaque images) and circles (transparent images).

3.6.1 Linear eyepiece graticules

These are linear scales, typically 10 mm, divided into 100 divisions of 100 μm , or 2 mm divided into 100 divisions of 20 μm each. These are placed in the focus of the microscope eyepiece so that they are coincident with the image of the microscope slide on the microscope stage. Calibration is effected using a stage graticule, 10 mm (100 \times 100

μm), 1 mm ($100 \times 10 \mu\text{m}$) or 100 mm ($50 \times 2 \mu\text{m}$), which is placed in the object plane. Köhler illumination should be used [6] to give uniform illumination of the viewing plane. Using an oil immersion objective, it is possible to resolve down to about $1 \mu\text{m}$, although a 15% oversizing is to be expected at this level due to diffraction effects.

A two dimensional array of latex spheres is often used for measuring more or less uniformly sized lattices. Hartman [25–27] investigated the errors in this method which comprise focusing, image distortion, misreading of photomicrographs, distortions in the photographic material, anisotropy, other array defects, non-uniformity of particle size, coating of solutes on the lattices and contact deformation. Hartman introduced a new method, the center finding technique in which the latex spheres acts as lenses enabling the center-to-center distance to be determined with high accuracy ($10 \pm 0.4 \mu\text{m}$ for $10 \mu\text{m}$ particles).

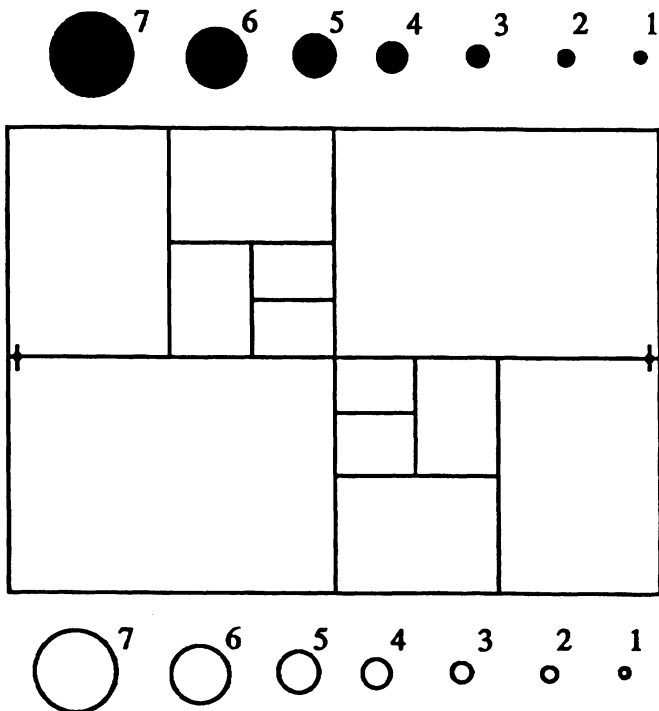


Fig. 3.2 The British Standard Graticule (Graticules Ltd). Diagram from BS 3406 (1963), Confirmed April 1993: *Methods for the Determination of the Particle Size of Powders: Part 4, Optical Microscope Method*. (Reproduced by permission from British Standards Institution, 2 Park Street, London W1, from whom copies of the complete standard may be obtained.)

3.6.2 *Globe and circle graticules*

The Patterson and Cawood graticule has 10 globes and circles ranging in diameter from 0.6 to 2.5 μm with a +2 mm \times 100 objective-eyepiece combination and is suitable for thermal precipitator work. May's graticule, with the same arrangement, covers 0.25 to 32 μm in a root two progression of sizes. (In both cases the lower limit is highly suspect).

The British Standard graticule is an improvement on Fair's graticule with seven globes and circles in a root two progression of sizes (Figure 3.2). With a +2 mm objective and a $\times 20$ eyepiece combination the minimum measurable size is about 1 μm . Circle 7 has a diameter eight times greater than circle 1; the grid has dimensions of 64 by 45.3 units with fiduciary marks at 60.4 units (circle 1 has diameter 1 unit). The graticule is divided into halves, quarters, eighths and sixteenths.

Detailed setting up procedures are given in BS 3406 but, as an example, if the distance between the fiduciary marks is 566 μm the diameter of circle 7 is equal to 75 μm .

3.7 Training of operators

Although the use of linear diameters such as Martin's or Feret's give the most reproducible analyses, the projected area diameter is more representative; hence the globe and circle graticule is the most popular. When comparing an irregular profile with a circle, untrained operators have a tendency to oversize the profile. A method of correcting this is to compare the analysis of a trained operator with that of a trainee. When the trainee recognizes the bias he readily corrects it. Heywood [28] produced a set of hand-held test cards pre-calibrated by counting squares. The trainee is required to compare each of the profiles with reference circles and assign it to a size group. Watson and Mulford [29] extended the technique by inscribing a number next to each profile and reducing them photographically so that they could be examined under a reversed telescope, giving more realistic conditions. In a series of tests with nine operators, four were over estimating and five were under estimating, seven of the nine being badly biased. The nine operators were trained microscopists who were aware of the natural tendency to oversize and mentally corrected. The nine observers were consistent with their bias but reduced it only slightly on a second test. Fairs [30] used a projection microscope for training purposes. This technique can also be used for size analysis [31] but is not recommended for particles smaller than 2 μm . Holdsworth *et al.* [32] demonstrated the need to train operators and showed that gross count differences on the same samples at different laboratories were much reduced after inter-laboratory checks.

Nathan *et al.* [33] compared three commonly used microscopic measurement techniques and confirmed oversizing by untrained

operators. They suggested that unskilled operators produced the best results with a line graticule and that experienced operators perform best with an image splitting device [34].

3.8 Experimental techniques

The microscope should be set up using Köhler illumination; monochromatic illumination produces a better image if small particles are to be measured.

The microscope needs a vernier stage capable of moving the slide in two directions at right angles. The limits of the uniformly dispersed field are determined using a low magnification objective. Since it is impracticable to examine every particle on the slide, a sample is selected. Either isolated fields areas or strips are selected from the whole of the viewing area in order to smooth out local concentration variations (Figure 3.3). For a number count at least five strips 5 to 20 mm long are examined, the length of the strips depending on the density of particles on the slide, the whole area being such that at least 625 particles are counted. For a weight count, the requirement is that

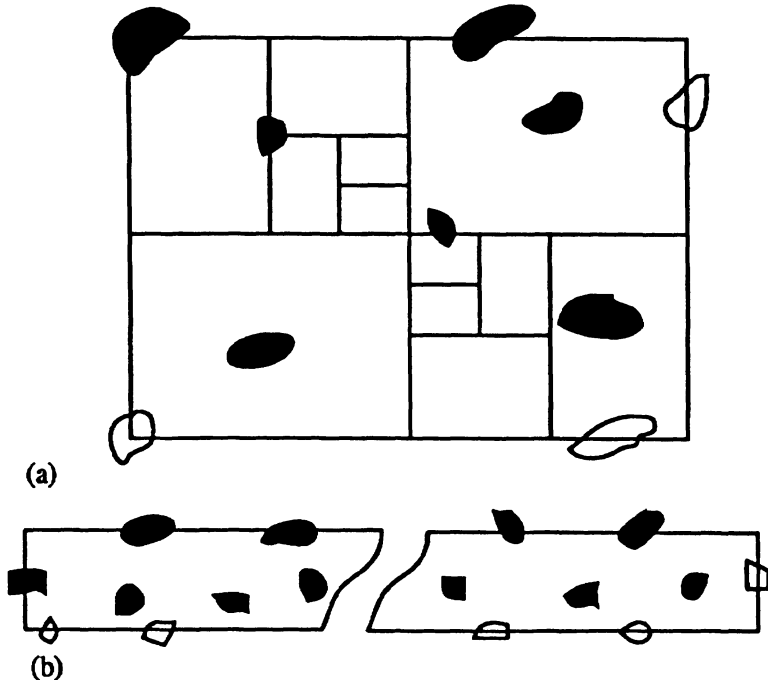


Fig. 3.3 Treatment of edge particles; (a) counting isolated fields, (b) counting strips.

the area contains at least 25 particles in the largest size category. If these are few in number it is advisable to use strip scanning for counting the coarsest size categories. For particles that are present in quantity, the use of an eyepiece graticule containing a field area, as opposed to a linear scale, is recommended. In either case the total area scanned must be determined in order that particle density on the slide (counts per mm²) may be calculated.

When counting isolated fields, particles overlapping two adjacent sides are not counted. With strip counting particles overlapping one of the edges are ignored; i.e. in Figure 3.3, shaded particles are included in count, unshaded particles are excluded otherwise the measured distribution will be weighted to the coarse sizes.

3.9 Determination of particle size distribution by number

Little difficulty is likely to be experienced in carrying out a number count since the same total area is used for all size classes and the minimum number of particles, namely 625, that it is necessary to count is specified in advance [equation (3.3)].

The number size distribution is calculated from the recorded values of the number m_r of particles in j size classes of mean size d_r found in sample areas $n_r a_r$. The percentage by number in each size class is then:

$$p_r = 100 \frac{(m_r n_r a_r)}{\sum_{r=1}^j (m_r n_r a_r)} \quad (3.2)$$

The use of the British Standard graticule is illustrated in Table 3.1. The magnification is set so that the largest particle present in the field of view is smaller than circle 7. The magnification is then increased in order to size accurately the smaller particles. If there are particles present which are smaller than the smallest circle on the graticule, a second increase in magnification may be necessary. Particles smaller than 2.3 µm are usually considered below the limit of the technique although this limit can be extended with loss of precision in the smaller size ranges. Sizes are often selected as an extension of sieve sizes i.e. 75, $75\sqrt{2}/2$, 37.5 and so on.

The class that contains the highest number concentration of particles (usually the smallest size class) is taken as the control size class. The dispersion technique should give about 3 particles per field of view for these particles and at least 96 fields of view should be examined. At lower magnifications it is usual both to increase the area of the field of view and decrease the number of fields examined.

Table 3.1 Illustrative example of the calculation of a size distribution by number using the British Standard globe and circle graticule

Circle number	Size limits (μm)	Total area examined (mm^2)	Number of particles counted (m_r)	Cumulative number	Number frequency undersize	Expected standard error $s(p_r)$
>7	>75		0	630	100.0	
7-6	75-53	$32 \times 0.25 \times (75/8)^2 \times 0.064 \times 0.0453 = 2.039$	4	630	100.0	0.32
6-5	53-37		8	626	99.4	0.45
5-4	37-27		6	618	98.1	0.40
>7			19*			
7-6	27-19	$128 \times 0.50 \times (26.52/8)^2 \times 0.064 \times 0.0453 = 2.039$	18	612	97.1	0.66
6-5	19-13		47	594	86.8	1.05
5-4	13-9.4		39	547	86.8	0.96
4-3	9.4-6.6		154	508	80.6	1.71
3-2	6.6-3.3		248	354	39.4	1.95
<2	<3.3		106	106	16.8	1.49

At high magnification, circle 7 is made equal to $26.52 \mu\text{m}$ ($= 75 \times \sqrt{2}/4$) making field area $= \left(\frac{26.52}{8}\right)^2 \times 0.064 \times 0.0453 = 0.0319 \text{ mm}^2$.

It is necessary to examine at least 100 fields and count over 625 particles and a quick check reveals that this can be done using half this area.

At low magnification, circle 7 is made equal to $75 \mu\text{m}$ making field area $= (75/8)^2 \times 0.064 \times 0.0453 = 0.2548 \text{ mm}^2$ and in order to examine at least 25 fields of total area 2.039 mm^2 it is necessary to examine 32 fields using a quarter of the graticule area.

* This is an oversize check which should roughly agree with the count at low magnification.

The expected standard error $s(p_r)$ of the percentage p_r by number in each size class, out of the total number in all size classes, is given by:

$$s(p_r) = \sqrt{\frac{p_r(100-p_r)}{\Sigma m_r}} \quad (3.3)$$

where Σm_r is the total number of particles of all size classes. The standard error is a maximum when $p_r = 50$, hence $s(p_r)$ will always be less than 2% if $m_r \geq 625$.

3.10 Conditions governing a weight size determination

The percentage by weight in each class is:

$$q_r = 100 \frac{\sum_{i=1}^j (m_i d_i^3 / n_i a_i)}{\sum_{i=1}^r (m_i d_i^3 / n_i a_i)} \quad (3.4)$$

Direct conversion of a number count to a mass count leads to unacceptable errors. The omission of a single particle, in the largest size class, in the previous example is equivalent to the omission of 12,000 particles in the smallest class i.e. the mass of a 63 μm particle is 12,000 times as great as the mass of a 2.9 μm particle.

The expected standard error $s(q_r)$ of the percentage q_r in each size class, out of the total weight in all size classes, is given by:

$$s(q_r) = \frac{q_r}{\sqrt{m_r}} \sqrt{1 - \frac{q_r}{50}} \quad (3.5)$$

q_r is usually a maximum for the coarsest size range. Assuming this contains 10% by weight of the material and that a standard error of 2% is satisfactory, then $m_r = 20$ particles. This should be calculated for each size class to confirm that in no case does it exceed 2%.

For a weight distribution the number of particles to be counted is governed by the number in the control size class. The number to be counted to achieve a given accuracy is:

$$s(M_g) = \frac{M_g}{\sqrt{m_r}} \quad s(M_g) = \frac{M_g}{\sqrt{m_r}} \quad (3.6)$$

$s(M_g)$ is the standard deviation expressed as a percentage of the total by weight;

M_g is the percentage by weight in the given size range;

m_r is the number of particles counted in the size range

If 10% by weight of particles lie in the top size range and an accuracy $s(M_g)$ of 2% is required then it is necessary to count 25 particles in the top size range. The number density (N_r) is then calculated

(particles mm^{-2}). The total count is maintained at about 700 by reducing the area examined for the smaller sizes. Briefly, the sample area required for particles of size d_r is:

$$A = N_0 A_0 \left(\frac{d_r}{d_0}\right)^6 \left(\frac{N_r}{N_0}\right) \quad (3.7)$$

where suffix '0' denotes the control class (the class containing the most particles by weight), which is usually the top size class.

3.10.1 Illustrative example of the calculation of a size distribution by weight

This example is based on using the British Standard procedure [6]. Preliminary scan: at minimum magnification (circle 7 = 75 μm) the number of scans required to give 150 particles in the three top size categories is determined (Table 3.2).

Number of scans $n_r = 5$

Length of scan = 10 mm

Width of scan (64/8) \times 75 μm = 0.60 mm

Number of particles recorded = m_r

Area scanned $n_r a_r = 5 \times 10 \times 0.60 = 30 \text{ mm}^2$

Table 3.2 Preliminary examination of 5 scans, area 30 mm^2

Class	Size limits (μm)	Number of particles (m_r)	Number density $N_r = (m_r/n_r a_r)$
1	106–75	9	0.300
2	75–53	47	1.567
3	53–37.5	103	3.433

Number of scans required in order to count 25 particles in the top size class (25/9) \times 5 = 14.

For other classes $n_r a_r = N_0 A_0 \left(\frac{d_r}{d_1}\right)^6 \left(\frac{N_r}{N_1}\right) n_1 a_1$

class 2: $n_2 a_2 = \left(\frac{1}{\sqrt{2}}\right)^6 \left(\frac{1.567}{0.300}\right) \times 14 = 10 \text{ scans}$

class 3: $n_3 a_3 = \left(\frac{1}{2}\right)^6 \left(\frac{3.433}{0.300}\right) \times 14 = 3 \text{ scans}$

Nine more scans are completed for the top (control) class size, during five of which particles in the second size class are recorded. The modified N values are determined and the above calculations repeated to ensure that a sufficient area has been scanned.

Table 3.3 Preliminary examination of 25 fields of total area 1.59 mm²

Class	Size limits (μm)	Number counted (m_r)	$N = \frac{m_r}{n_r a_r}$	Required area (mm) ² [equation (3.7)] (A_r)
4	37.5 - 26.5	21	13.2	6.6 = 107 fields
5	26.5 - 18.8	44	27.7	1.77 = 28 fields
6	18.8 - 13.3	79	99.4	0.79 = 25 x (0.5) fields

The process is then repeated at a higher magnification (Table 3.3). Calibration for class 4 is that 60.4 units = 283 μm making the diameter of circle 7 equal to: $(8/60.4) \times 283 = 37.5 \mu\text{m}$.

$$\text{Area of graticule: } \frac{64}{60.4} \times \frac{45.3}{60.4} \times (0.283)^2 = 0.0636 \text{ mm}^2$$

In class 6 particle density is high, hence half the graticule is examined. The requisite number of fields are examined and the calculations carried out to ensure a sufficient area has been covered.

The process is repeated at a higher magnification (Table 3.4). Circle 7 is made equal to 13.25 μm making the distance between the calibration marks 100 μm and the field area 0.00795 mm². 75 more fields need to be examined for class 7 only.

Table 3.4 Preliminary examination of 25 x (1/4) fields of total area 0.0497 mm²

Class	Size limits (μm)	Number counted (m_r)	$N_r = \frac{m_r}{n_r a_r}$	Required area (mm) ² [equation (3.7)] (A_r)
7	13.3 - 9.4	9	181	0.193
8	9.4 - 6.6	8	161	0.020
9	6.6 - 4.7	7	141	< 0.020
10	4.7 - 3.3	6	121	< 0.020
11	3.3 - 2.3	4	81	< 0.020

The data are tabulated and the standard error of the control size class determined to ensure that it is less than 2%. An accuracy factor is calculated for each size class and provided it is always less than the value for the control size class the standard error for the other size classes will be better than this. The completed table is shown as Table 3.5. Although the technique appears onerous, a skilled microscopist can carry out a weight analysis in about an hour.

Table 3.5 Illustrative example of a size distribution by weight using a British Standard graticule

Circle	Size of class limits (mm)	Area of sample field (mm^2) (a)	Number of sample fields (n)	Total sample area (mm^2) (na)	Number counted in class (m)	Number come. in class/ (mm^2) ($N = m/na$)	Weight factor	Relative weight in class (Nd^3)	Weight % in Class	Accuracy factor for class	Weight size (μm)	Size dist. % incl.
>7	+75	14x10 x.6	-	84	27	0.321	741 000	241 000	9.6	*464400	106	100.0
7-6	75 - 53	7x10x.6	-	42	66	1.571	262 000	412 000	16.4	*50700	75	90.4
6.5	53 - 37	5x10x.6	-	30	103	3.433	92 700	318 000	12.7	30900	53	74.0
7-6	37 - 27	0.0636	120	7.62	98	12.86	32 800	422 000	16.8	42600	37	61.3
6.5	27 - 19	0.0636	30	1.91	53	27.75	11 600	334 000	13.3	45800	27	44.5
5.4	19- 13.3	0.0636/2	25	0.795	79	99.4	4 100	417 000	16.2	45800	19	31.2
7-6	13.3- 9.4	0.25 x	100	0.199	36	181	1 450	262 000	10.4	30900	13	15.0
		0.00795										
6.5	9.4- 6.6	0.25 x	25	0.050	8	161	512	82 000	3.3	10300	9.4	4.6
5-4	6.6- 4.7	0.25 x	25	0.050	7	141	181	25 400	1.0	3400	6.6	1.3
4-3	4.7- 3.3	0.25 x	25	0.050	6	121	64	7 700	0.3	1100	4.7	0.3
3-2	3.3- 2.3	0.0159	25	0.050	4	80	23	1 800	0	200	3.3	0
				487				2512 900	100.0			

* Control size class. Standard error of control size class $s(q_0) = \frac{9.6}{\sqrt{27}} \sqrt{1 - \frac{9.6}{50}} = 1.66\%$.

- This should be smaller than the control size class for $s(q_0) < s(q_1)$. However the calculated standard error for this class is still less than 2% so this value is acceptable. If the error was too great more particles would have to be counted in this class.

3.11 Quantitative image analysis

Manual methods of obtaining data from images are slow and tedious and this can give rise to considerable error. The introduction of fully automated image analysis systems has virtually eliminated manual methods and also supplanted semi-automatic systems. All image analysis systems use scanning techniques for converting images into electrical signals which are processed to yield data on the images. If the microscope is fitted with an automatic stepping stage and autofocus, it is possible to measure large numbers of fields of view, thus greatly improving the statistical accuracy. However, image analysis systems cannot discriminate artifacts as readily as human operators and are unable to adjust focus during measurements in the field of view, which can cause problems with particulate systems having a wide size range. With automatic image analysis, not only is it necessary for particles to be singly dispersed, they should also be clearly separated from each other so that the analyzer is not confused by touching particles [35].

3.11.1 Calibration of image analyzers

The procedure for calibration of image analyzers varies from machine to machine. It usually involves indicating on a screen the dimensions of an imaged artifact of known dimensions. This may be a grid, grating, micrometer or ruler and the dimensions are usually expressed as pixels per unit length. The calibration should be carried out both parallel to, and perpendicular to, the scan direction. Image analyzers may also suffer from localized distortion, which may be detected by comparing a square grid with an overlaid software generated pattern.

The National Physical Laboratory [36] introduced a certified graticule to test the linearity of a scanner over the whole field, the resolution obtained and the effect of gray level detection on the measured size distribution. It has four separate fields: A major field divided into smaller proportional fields, an array of equidistant monosize circles, a root-two by diameter array and a log-normal number/diameter distribution in an equi-centered array. The value of this, commercially available [37], graticule has been illustrated by its use on a Quantimet 900. Polystyrene spheres (5, 7, 10 and 15 μm) have also been used for calibration and the results compared with SEM and Coulter data. [38].

3.11.2 Experimental procedures

Automatic image analysis is a six step process (Figure 3.4); (1) image formation, (2) image scanning, (3) feature detection, (4) feature analysis by count, shape, size or other selected parameter, (5) data processing and analyzing, (6) data presentation.

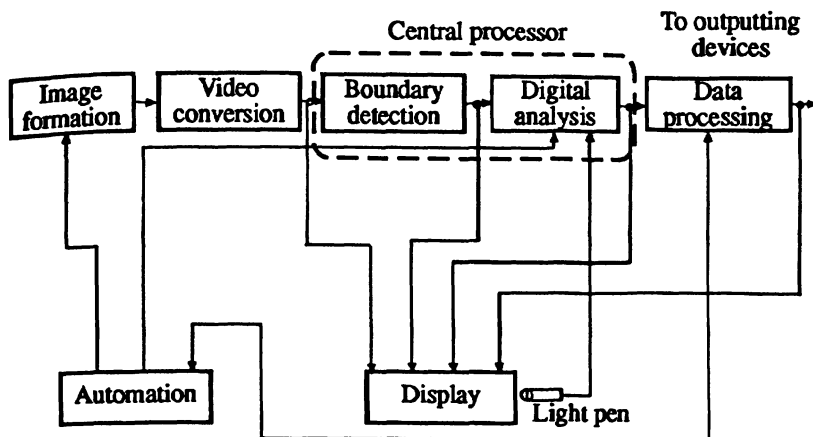


Fig 3.4 Block diagram of image analysis system, indicating the six major functions [44].

Image formation is a crucial step in image analysis. Quantitative image analyzers consist of a high linearity television camera which can be interfaced with a microscope, macroviewer or videotape. An electron probe interface can be used to accept image inputs from scanning electron microscopes, microprobes or acoustic microscopes [39–41].

On-line systems, covered more fully in Chapter 9, have been developed for measuring particle contamination in molten polymers [42] and for measuring particle size and shape [43]. Microscopy is combined with a light scanning device for particle size and shape determination in the Galai instrument. Castellini *et al.* [43] use a pulsed semiconductor laser as a light source to illuminate a flowing stream of particles, in the 2 to 400 µm size range, and determine their shape using a shadowgraph technique.

The macroviewer is used to analyze large objects such as 8 in by 10 in photographs. Large objects and photographs can be illuminated with incident light; transparencies and slides by transmitted light. The electron probe stores whole images generated by the SEM and converts them into a proper form for analysis.

Signals from the image received by the camera are processed by a central processing unit which contains circuits for measuring areas of features, number counts and size distributions based on selected diameters. Parameters such as ratio of maximum to minimum diameters may also be determined. The area under examination is displayed on a screen and interaction is either via a teletype keyboard or menu driven. Using this unit, objects can be selected for examination, objects can be deleted and touching particles can be separated. Image editing and classification features such as picture

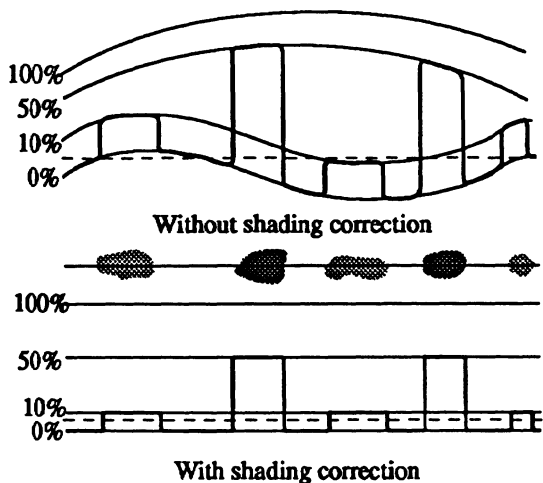


Fig. 3.5 Gray level shading correction: the objective of the gray level detection function is to define in the images the boundaries of features that are to be counted and measured (Bausch & Lomb, Omnicron).

enhancement using gray level detection to enhance contrast are often available (Figure 3.5). Surface texture analysis, fractal dimension determination, shape regeneration using Fourier analysis, angularity and roundness measurement may also be carried out. The resulting distributions are presented graphically in a wide variety of modes and the data may be stored for further interrogation.

Images require a great deal of computer memory because an image is actually an array of numbers; i.e. intensity at every location $I = f(x,y)$. For a 512 by 512 digital image, over a quarter of a million numbers must be stored. Consequently, until recently, most image analysis was done on large computers or with dedicated image processing hardware. It is now possible to do a great deal of processing on a workstation computer.

Most digital image operations fall into one of two categories [45], namely image processing and image analysis. Image processing operations turn one image into another image; for example, edge finding or crispening. Operations that quantify some aspect of the image, such as area fraction or average particle size, are called image analysis. In general one would prefer to do little or no processing in order to save time and not alter the original image. However it is often necessary to do some processing to prepare an image for analysis [46]. An image can be digitized from a video camera attached to a light microscope or on a copy stand to digitize either the particles themselves or a photomicrograph. Images can also be digitized from one of the

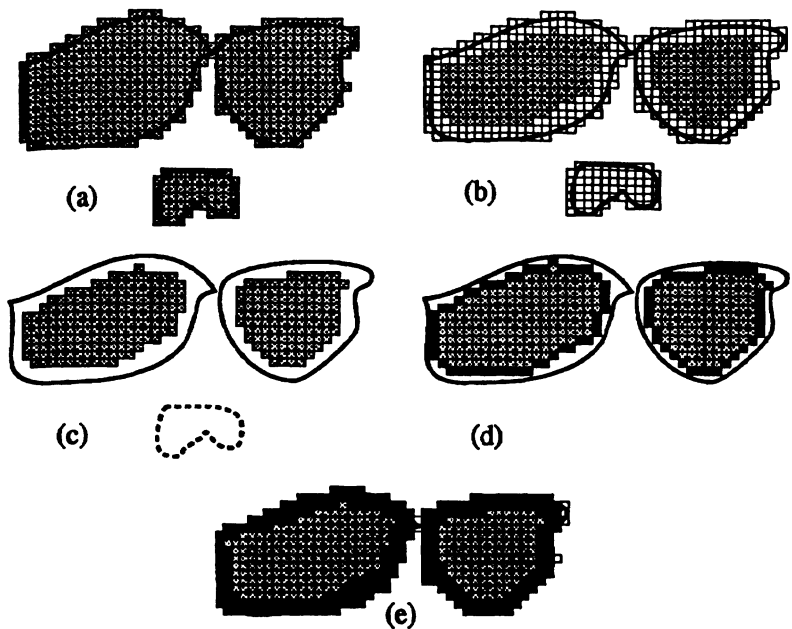


Fig. 3.6 Separating overlapping images using erosion and dilation.

contrast-bearing signals from a microscope. Once digitized the images can be stored for later analysis and processing or for archival purposes.

A digital image has a discrete number of pixels (picture elements), each of which contains an intensity value, usually scaled from 0 – 255. The number of pixels determines the resolution with 512 by 512 being the most common. Theoretically, image resolution is limited only by computer memory however it is usually not possible to display more than 1024 by 1024 and PC class computers may not be able to display 512 by 512. For most practical purposes 512 by 512 is adequate but higher resolution is useful for analyzing large and small features at the same time.

Each pixel in the image is digitized to a limited number of gray levels depending on the hardware used. The human eye has a range of 10^{10} brightness levels that it can adapt to but it can only discriminate about 20 levels at a time. Older image systems provide 64 or fewer levels but newer ones commonly provide 256. Such a large number of gray levels is necessary for discriminating phases on the basis of their brightness but may not be necessary for particle characterization.

The computer compares several focal planes and the sharpest image selected. The brightness is then corrected by the software until it is approximately constant over the whole image. The image is then

binarized: All pixels below a certain gray level become white and the rest become black or viceversa; with this procedure particles can be differentiated from background. The height of the binarization threshold has an influence on the number of black pixels and its selection is a multiple step procedure [47].

Some of the binary particles may contain bright spots. This happens especially with transparent particles in transmission microscopy. These spots have to be closed.

Although the human eye can only discriminate about 20 levels of intensity simultaneously, it can distinguish about 350,000 different shades of color. The significance of this is that pseudocolor can be used in an image to convey details that would otherwise be lost in a gray scale image.

In general, the goal of image processing is improving the image, but the only thing certain is that the image is changed. No information can be extracted that was not present in the original image and artifacts can be introduced. One example of a need for image processing would be separating overlapping particles (Figure 3.6).

- **Resolution** is determined by the number of pixels (picture elements): The measured area is the number of elements multiplied by the elemental area; the perimeter is the number of edge element multiplied by the length of the sides.
- **Erosion** In order to separate touching images, the edge pixels are removed together with any touching pixels within the image.
- The residual pixels make up smaller non-touching images; the smaller image disappears completely.
- **Dilation** In order to create new non-touching images a peripheral layer of pixels is applied.
- When a second layer of pixels is added, the original image is reformed with some loss of detail and the two touching images are separated.

Erosion and **dilation** results in some loss of information. Simple operations such as erosion and dilation or complex operations such as artificial intelligence can accomplish this task. If these fail, features can be cut apart by the operator using a light pen.

Other forms of image processing operate on the entire gray scale image and transform the contrast. Some uses for these operations include background smoothing, crispening, edge detection, noise removal and the enhancement or suppression of periodic information. The systems available today are both more sophisticated and simpler than before. The trend is towards more automation, greatly increased speed, more sensitivity and improved camera technology, particularly the use of CCDs. Specifically, many systems are based around or incorporate parallel processing hardware so that image pixels can be processed simultaneously, providing faster throughput and allowing

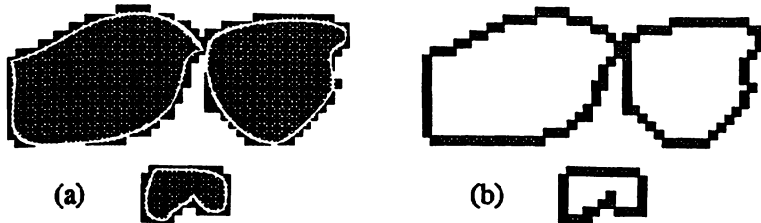


Fig. 3.7 (a) Area and (b) perimeter measurements by quantitative image microscopy.

highly complex algorithms to be supported. Fibers can be aligned, touching particles can be separated, particles can be selected for measurement and deleted holes can be filled. A light pen is often provided so that features can be selected for acceptance or rejection. Particles can be dilated or eroded for image enhancement, and fibers may be stretched or shrunk to create a better image.

The application of quantitative image analysis to size (area) and perimeter determination is demonstrated in Figure 3.7. The image analyzer sees only two images since the larger images overlap. The larger image (Figure 3.7a) has an area of 552 square units made up of 325 LHS (left hand side) and 227 RHS (right hand side) and the smaller image has an area of 66 square units (assuming the area occupied by one pixel is one square unit). The pixels that overlap the edges of the image define the perimeters (Figure 3.7b). The larger particle(s) have a perimeter of 134 units LHS and 73 units RHS and the smaller particle has a perimeter of 36 units. Thus, as in fractal geometry, the smaller the pixel the greater the perimeter. The contour following algorithm depends upon the chosen connectivity of the pixels (i.e. the number of touching pixels within the image).

Some other parameters that can be measured by quantitative image microscopy are illustrated in Figure 3.8; shape factors are illustrated in Figure 3.9 and editing features in Figure 3.10. Serra [48–50] developed the method of mathematical morphology in image analysis and the theory was extended by Matheron [51,52]. The basic operation involves erosion and dilation procedures to produce a modified image picture from the original. The major disadvantage of this procedure is the requirement for large memory space. This problem was resolved by use of a compressed data technique for binary image pictures [53].

Davidson *et al.* [54] compare image analysis to other methods of particle size measurement. They used a Magiscan image analyzer with Genias™ particle sizing software. The images were generated with a Zeiss universal microscope equipped with Optovar and bright field

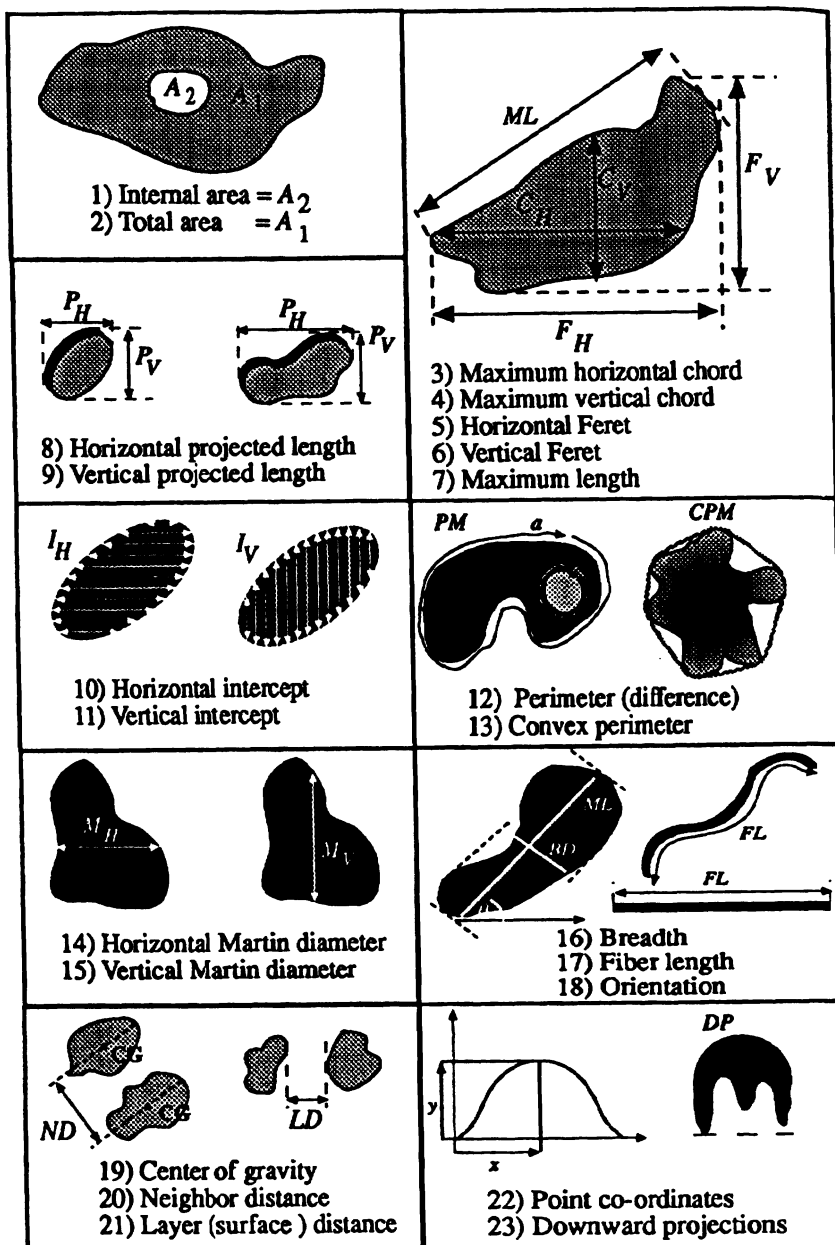


Fig. 3.8 Measured parameters by quantitative image microscopy.

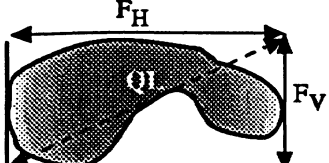
 <p>24) Pythagorean diameter (QL)</p>	 <p>$HD = \sqrt{(4A/\pi)}$</p> <p>25) Heywood diameter</p>
 <p>$SF_1 = (ML)^2/A$</p> <p>26) Shape factor (1)</p>	 <p>$SF_2 = (PM)^2/A$</p> <p>27) Shape factor (2)</p>

Fig. 3.8 (Cont.) Measured parameters by quantitative image microscopy.

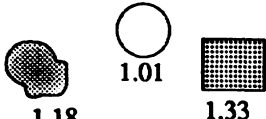
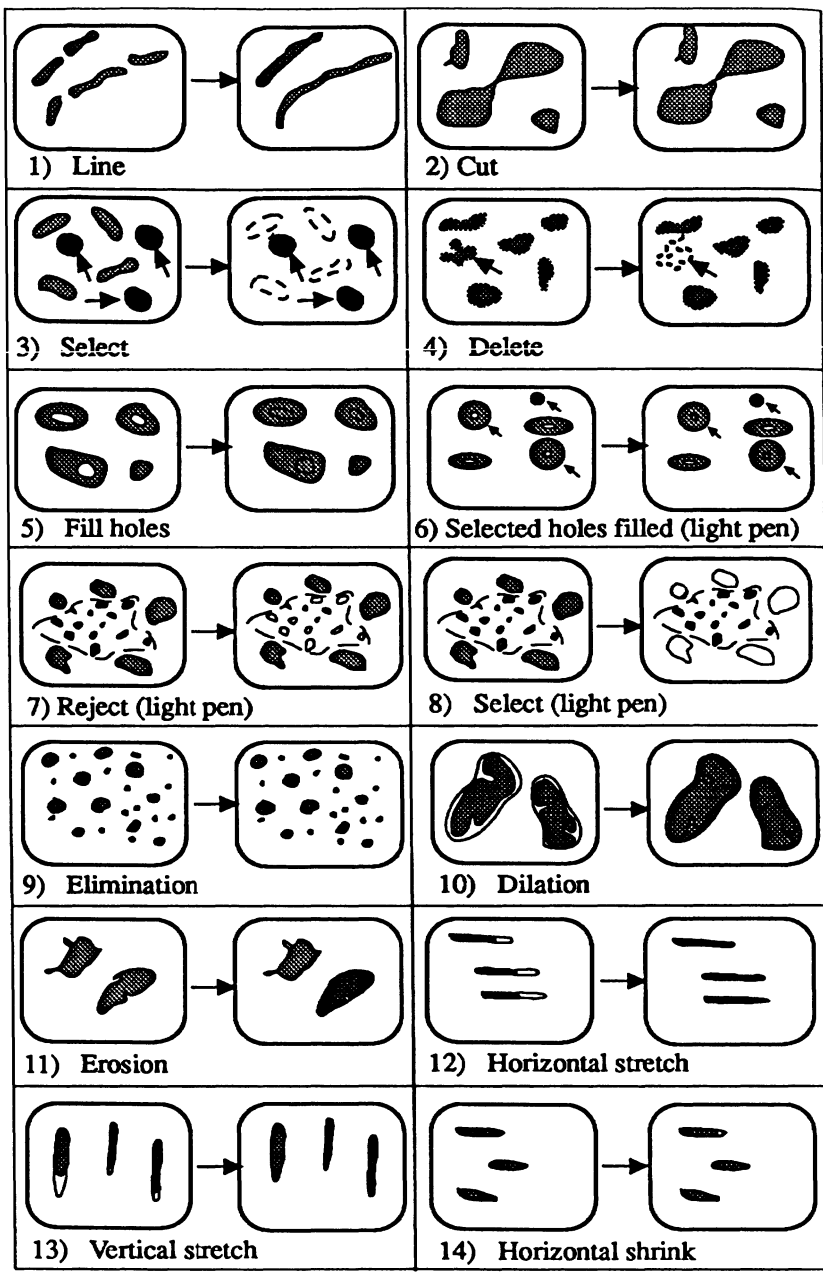
 <p>1) Roundness = $(P^2/4\pi A)$</p>	 <p>2) Aspect ratio = (L/B)</p>
 <p>3) Horizontal projection. with or without hole</p>	 <p>4) Area, A, area with or without a hole</p>
 <p>5) Vertical projection. with or without hole</p>	 <p>6) Perimeter, P, perimeter with or without hole</p>
 <p>7) Topological counts. tops (T), bottoms (B), joins (J), forks (F) and feature counts (FC)</p>	 <p>8) Integrated brightness and optical density</p>

Fig. 3.9 Shape factors of image analysis system.

**Fig. 3.10** Editing features of image analysis systems.

optics and acquired using a Dage-MTI camera model 70 with a green filter. Calibration was with a Bausch & Lomb ruled stage graticule. The gray levels were converted to binary and touching particles were separated manually. Various parameters were measured and data compared with data generated by sieving, using a Hiac PA 720 (operated with dry powder) and the Coulter Counter TA II. It was deduced that the cut size for the sieves was controlled by the breadth of the particle (as expected) and the measured parameter by Hiac was also controlled by breadth rather than equivalent spherical diameter as one would expect. If multiple pictures of the particles, taken from different directions, are available then a three dimensional image can be reconstructed and the 3-D convex hull reconstructed [55].

For automatic image analysis of fibers it is necessary to generate an image with a limited number of overlapping fibers. A method of generating such a distribution with dry fibers by impacting the particles on an inclined plate and subsequent sedimentation on to a microscope slide has been described [56]. For wet sample preparation the suspension was first dispersed, then deposited on a membrane filter for examination by reflected light or transmitted light after first making the filter transparent by a chemical agent. An alternative method of preparation by allowing the fibers to settle out of suspension on to a microscope slide was also used.

3.11.3 Commercial quantitative image analysis systems

The American Innovation Videometric 150 readily measures and counts specific features in an image. The system incorporates threshold monitoring so that images within selected brightness levels are selected. Editing is provided with the use of an adjustable paintbrush with the mouse to include or exclude any parts of the image. In this way objects which appear separated may be connected or objects which wrongly appear as one may be separated. The erosion routine reduces every detected feature by one pixel at a time over the entire boundary. This process breaks bridges and opens pores. During dilation pixels are added one at a time to smooth surfaces and fill in bays.

Analytical Measuring Systems features *Quickstep*, a sophisticated control system for precise positioning of microscope stages and macrostages in X, Y and Z axes with the added facility for automatic focus. As a 'stand-alone' system it offers versatile semi-automatic and fully automatic control for scanning selected areas of a specimen. Alternatively it can be used in conjunction with a microcomputer to run application programs or as an integral part of an AMS image analysis system. *VIDS V* is an interactive image analyzer which provides a means of quantifying images not suitable for gray level analysis. An image which can be viewed in color or monochrome may be analyzed by tracing around, or along, features; or by placing dots across them using a digitizing pad and cursor. The standard software provides all

the measurements and statistical tests. A low cost alternative to VIDS V is found in Measuremouse, which features a high resolution CCD camera to view the sample and display the image on its graphic monitor. Objects selected for measurement are inscribed using a mouse-driven cursor and their size and shape determined via an Amstrad personal computer. Comparison of measured parameters and the generation of size or shape distributions are carried out using spreadsheets such as Super Calc and the results provided via a high speed dot matrix printer. Optomax V is a fully automated image analysis system with a high spatial precision of 704 by 560 pixels. These systems are available in the USA from *Optomax Inc.*

Artek market a range of image analyzers. The *Artek Omnicon 3600* is an advanced, easy to use system with turnkey application software. A precision scanner converts optical images into video signals which are presented on a high resolution monitor screen. The required measurement is selected from more than 20 parameters. The measure key is pushed and the answer appears ready to be printed out, saved or exported to any of a wide range of data bases and spreadsheet programs.

Automatix produces automated image analysis packages comprising data collection, spreadsheet analysis and charting to be used with the Macintosh computer. This has been used, in conjunction with ancillary equipment, to produce a computer digital analysis system [57] for around \$4,000 [58]. Later, a more sophisticated system, costing around \$20,000, was described for digital examination of film defects [59].

Boeckeler manufacture simple systems which require more operator input but are less expensive than more automated systems. The VIA-20 Video Image Marker can be used to mark details on a video image; the VIA-50 includes a more varied array of positionable markers with an option for multiple overlay storage; the VIA-100 can perform horizontal, vertical and point-to-point measurements, and the VIA-150 combines the capabilities of the VIA-50 and VIA-100. The VIA-160A1 video area measurement system can be combined with a video microscopy system to give cell areas, chord lengths and number counts.

Buehler Omnimet II is a high resolution automatic image analysis system.

Compix C-Imaging 1280 System has an image input of 1024 x 1024 resolution and uses the latest hardware to achieve high speed processing and analysis. The 1280 x 1024 non-interlaced 19 in. color monitor provides viewing quality for user comfort. The system is complemented by *Simple*® imaging software to give user flexibility in an uncomplicated framework. The system can enhance, identify and count 1000 objects in less than 1 s, measure the data and perform summary statistics in less than 3 s, and provide histograms at the touch of a button. The *C-Imaging 640* system has a color or monochrome input with a resolution of 640 x 640. The system benefits from high speed processing and analysis hardware.

Data Translation market *Global Lab Image* which captures and digitizes images, then displays, processes and analyzes them. A complete set of algorithms are provided which work with any imaging device. The programs are used with Microsoft Windows™ for scientific word processing, statistics, spreadsheet analysis or data plotting.

Hamamatsu C-1000 is a computer compatible video camera which can be mounted on a microscope, macroviewer, optical bench or tripod. The number of particles can be tabulated based on specified parameters. Information can be input and analyzed by the computer.

Hitech Olympus Cue-3 is a color image analysis system with a wide range of image enhancement and processing capabilities.

The *Joyce Loebl Magiscan* is a total image analysis system which can be interfaced to a wide range of optical and electron microscopes. The general purpose menu and results programs provide flexible means of extracting particle size and shape information [60].

Leco offer several image analysis systems. The AMF-100 is dedicated to microhardness measurement and the 2005 is a top of the line, high performance system. The 2001 is a mid-range general purpose image analyzer. The 3001 operates using Microsoft® Windows™. The system can interface with a broad range of peripherals and has the ability to archive images for later processing.

The *Leica Quantimet 500* costs less than \$15,000 complete and can be used with any microscope. The single display combines menus and images through PC based Windows™ graphical user interface.

The *LeMont Oasys* image analysis system acquires, enhances, measures and classifies images. The Omega system forms a high quality bridge between a PC and SEM.

Millipore nMC System offers speed and precision in counting particles, determining size distributions and characterizing shapes.

The *Nachet 1500* is a processor specifically designed for image analysis. The image is acquired with a TV camera and directed to the Nachet 1500 for image processing and measurements. The results are sent to an Apple IIe type computer to drive the various peripheral devices associated with the topic being studied. The microcomputer is also used for setting up the instruction sequence for image processing and for running programs.

Nikon analytical microscopy workstation Microphot SA is adaptable for complex multi-imaging requirements run from a host computer.

Oncor Instrument Systems (formerly *American Innovision*) designs and manufactures its own hardware and software which incorporates multiple true color analysis models, multiple thresholds and low light true color CCD cameras.

Optomax V is a simple to use automatic image analysis system employing dual microprocessors combined with high speed measurement circuitry. The system uses up to four high performance TV cameras to provide direct viewing of macroscopic or microscopic

images. It counts and measures image features such as area, perimeter, Feret diameters, horizontal and vertical intercepts and so on.

Outokumpu Imagist is a medium priced unit which bridges the gap between the limited capability PC systems and the high cost, hardware based systems.

Shakespeare Corporation's Juliet features single particle size and shape measurement together with fractal analysis as well as conventional classical measurements. It also measures size and shape distributions for sets of particles with image manipulation and data graphing capability.

Tracor Northern manufacture complete x-ray microanalysis systems with video image collection and storage. The *TN-8500 Image Analysis System* features dedicated imaging hardware and software combined in an integrated system for advanced applications from the simplest particle size analysis to the most complex imaging applications such as fast Fourier transformation and 3-D reconstruction.

Carl Zeiss offer a family of upgradeable products including parallel processing software. The Videoplan-Vidas-Ibas line of digital image processing systems offers three different levels of automation. The videoplan takes advantage of the user's experience in recognizing complex structures. Measurements are performed by tracing contours with a cursor on a digitizing tablet or on a TV on-line image. The evaluation is supported by automatic data processing which includes data management. The Vidas system digitizes the images, which are then processed by Ibas. The Ibas system supports advanced procedures such as texture analysis and pattern recognition.

3.11.4 On-line microscopy

The Danfoss QueCheck Vision System performs a continuous analysis directly from the production line, typically at 0.5 s intervals. The final results of the measurement are available after 100–300 frames so that an equivalent sieve analysis is completed every 3 min. The particle size distribution is documented via an interface with data base and printer. The material is fed in a fine stream, by means of a vibratory feeder, past a vision camera which calculates the size distribution as they fall. The system has been applied to measuring the size distribution of sugar crystals. On-line image processing has also been applied to monitoring granule size distribution and shape in fluidized bed granulation [61].

3.12 Electron microscopy

When a solid is bombarded with high energy electrons the interaction produces secondary electrons (elastic), back-scattered electrons (inelastic), low loss electrons, Auger electrons, photo electrons, electron diffraction, characteristic x-rays, x-ray continuum, light, hole electron

pairs and specimen current. These interactions are used to identify the specimen and elements of the specimen and can also be used to physically characterize particulate systems.

Transmission electron microscopy (TEM) is used for very fine particles or thin specimens of crystalline materials. The elastically scattered electrons give amplitude contrast which is proportional to mass thickness. The inelastically scattered electrons suffer small energy losses and give high phase contrast. Bright field images form when electrons, which are inelastically scattered through small angles, combine with unscattered electrons, whereas dark field images are formed only from the scattered electrons. Scanning transmission electron microscopy (STEM) allows simultaneous viewing of both images and this is one of its major advantages.

For scanning electron microscopy (SEM) the two most important interactions are:

The generation of secondary electrons, which are the result of elastic collisions and typically less than 50 eV. The images formed by these are the most common and are marked by great depth of field;

Backscattered electrons, which are less applicable to particle sizing but have niche uses; the contrast is closely related to the atomic number of the sample and typically the voltage is greater than 50 eV.

3.13 Transmission electron microscopy (TEM)

TEM is used for the direct examination of particles in the 0.001 to 5 μm size range [62]. The TEM operates by flooding the sample with an electron beam, most commonly at 100–200 keV, and generating an image on a fluorescent screen or a photographic plate beyond the sample. Analyses can be performed directly on the screen images, but this ties down the instrument for long periods of time, hence it is more usual to analyze the photographic images.

TEMs operate in the magnification range from about 600 \times to 1,000,000 \times . Many particle size studies can be carried out at magnifications of less than 4,000 \times and several relatively inexpensive instruments are available giving magnifications up to 10,000 \times . Resolution capability of the best instrument currently available is sub-0.2 nm for line-to-line and approximately 0.2 to 0.3 nm for point-to-point.

Calibration is usually effected with narrowly classified polystyrene lattices available from Dow Chemicals or Duke Scientific, but diffraction gratings are necessary for high accuracy work. Single crystals of stable, well-characterized materials such as gold may be used as diffraction gratings and lattice fringe imaging can give direct calibration.

Some TEMs have a closed circuit television system fitted so that the images can be fed directly to an automatic image analysis system.

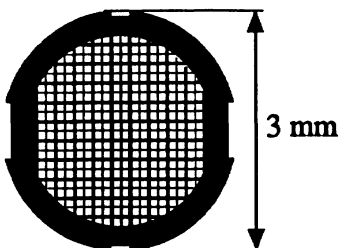


Fig. 3.11 Electron microscope grid.

3.13.1 Specimen preparation for TEM

Specimens for TEM are often deposited on or in a thin (10 to 20 nm) membrane which rests on a grid. These grids are usually made of copper and form a support for the film, which is usually only self-supporting over a small area (Figure 3.11). Specialty grids are available from a number of suppliers to fit particular needs. Examples would be nylon or beryllium grids for special characterization needs, or locator grids with numbered and/or lettered field markers.

Since most materials are opaque to the electron beam, even when only a few hundred nanometers thick, special problems arise in the production of suitable mounted specimens. Specimen support films are usually made of plastic or carbon, though other materials have also been used. Suitable film solutions may be made up of 2% w/v formvar (polyvinyl formal) in ethylene dichloride or chloroform.

Films may be produced in the following manner [63,64]. A dish about 20 cm in diameter is filled with clean distilled water and a large circle of 200-mesh steel gauze is placed on the bottom of the dish. A number of grids are placed on the wire gauze, then two drops of the film solution are dropped on to the surface of the water and the film that results after the solvent has evaporated is removed with a needle; this ensures that the water surface is clean. A second film, formed the same way, is removed by raising the wire gauze containing the grids which are then allowed to dry. A pre-examination of the grids in the electron microscope is desirable as this enables dirty films to be rejected, and the film polymerizes in the electron beam, thus greatly increasing its strength.

An alternative procedure is to clean a microscope slide with detergent and polish with a clean cloth without rinsing away the detergent, so as to form a hydrophilic layer at the surface, which facilitates stripping. The slide is dipped in a solution of formvar in ethylene dichloride (0.3% to 0.7% depending on the film thickness required) and allowed to drain dry. The film may be floated on to a water surface and mounted on grids as before. If individual grids are required, the film may be cut into small squares with a needle or razor

blade. The mounting operation is easier if a special jig is used [65]. The jig is a brass cylinder about 1 in. long and $\frac{1}{2}$ in. diameter with a hole of the same diameter as the specimen drilled and tapped through its axis. A set screw in the threaded hole is adjusted so that its end is flush with the face of the plug and withdrawn slightly to leave a shallow recess. The specimen grid is held in this recess and the membrane is lifted from the water surface with a wire loop of slightly larger diameter than the jig, surplus water being carefully removed with blotting paper. The wire loop is then lowered over the jig and, when the membrane is dry, the grid is raised by means of the screw, surplus membrane being removed by scoring round the grid with a needle. Special apparatus has also been described for producing plastic films of uniform thickness suitable for the preparation of replicas [66].

Carbon films are prepared under vacuum (10^{-3} mmHg) by electrical discharge from two pointed hard graphite rods [67]. Films are best deposited on microscope slides cleaned with detergent and placed about 10 to 15 cm from the source. A thickness indicator, consisting of a drop of vacuum oil on a piece of white glazed porcelain, is placed beside the slide. During the discharge, the porcelain not covered with oil takes on a brownish color, changing to a light chocolate shade as the film thickness increases from 5 to 10 nm, the latter being a suitable thickness for general use. Evaporation is completed in about half a second with a current of 50 A. The film may then be floated on to the surface of distilled water and picked up as a whole or scored into small squares. A simple method of producing a suitable specimen is to place a few milligrams of the powder on a microscope slide, add a drop of 1% to 2% w/v suspension of formvar in a suitable solvent and rub out the slide with a glass rod. Further solvent is added if required and the dispersion is spread over the slide and allowed to dry. The film is removed from the slide and mounted on the grid as before.

Another method of preparing the sample is to disperse it in linseed oil, which is then thinned with white spirit. The dispersion is spread over a microscope slide which is immersed in white spirit for a few minutes to remove the oil. After drying the slide a thin layer of carbon is deposited on the specimen to form a supporting film. Finally, this is floated off on water, as before, and picked up on a grid for examination [67].

A dispersed sample may also be obtained by means of an aerosol sampling device. A suitable technique is to form a sandwich of plastic film particles and 20 nm thick carbon. The underlying plastic may then be washed away with solvent and the specimen examined after shadowing [63,64,68].

A suspension of the powder may be made up and a drop placed on a grid by means of a pipette or hydrometer syringe. However, this often produces an uneven deposit. A more uniform deposit is often

produced by spraying the suspension on to the grid; several suitable spray guns have been described [62,69].

Timbrell [70] modified the Hamilton and Phelps [71] method for the preparation of transparent profiles to facilitate electron microscopy. The metal film is floated on to a water surface and picked up on a grid. In cases of difficulty, the slide is first dipped into 1% hydrofluoric acid to release the edge of the film and the process is completed in water. Although the metal film is strong enough to be floated off whole, it is preferable to score it into small squares as described earlier and then remove the separate pieces. In order to obtain reliable results for particle size analysis, as many separate grids as possible should be prepared and a large number of electron micrographs taken from each. Many other methods have been used and the preparation of the particle dispersion is the most important aspect of sizing by electron microscopy.

In an analysis of the errors involved in electron microscopy, Cartwright and Skidmore [72] examined the optical microscopy specimens produced by thermal precipitation. The specimens were then stripped from the microscope slides and the fines were counted, using an electron microscope. Good agreement was obtained by examining 1000 particles in the electron microscope using about 60 fields of view (60 micrographs) and almost 4000 particles in the optical microscope. To obtain accurate magnification calibration, four overlapping micrographs along the bar of a readily identifiable grid square were taken and the total length of the image of the grid bar was measured from the micrographs directly, using an optical microscope.

The surface areas of dust samples as determined by optical and electron microscope have also been compared [73]. Pore size distributions of thin films of Al_2O_3 , as measured by TEM, have also been compared with those determined by gas adsorption/desorption [74]. It has also been suggested that electron microscope gives a truer estimate of surface area than gas adsorption techniques [75]. Further information can be obtained in a recent review of specimen preparation for TEM [76].

Two other effects, which may influence apparent particle size, relate to the effect of the flooding electron beam on the particles. One of these is charging of non-conducting particles, which spreads the beam around the particles and makes sharp focusing impossible. The other is the gradual accumulation of vacuum pump oil (and other things) on the charged sample in the sample chamber. This often appears as a slowly developing skin around the particle thus increasing its apparent size. A view at reduced magnification will reveal a discolored region. This effect limits the time one can spend in a particular field of view, but the contamination is usually slow enough to not seriously jeopardize the study. The higher vacuum systems found in newer instruments reduce this effect.

3.13.2 Replica and shadowing techniques

Replicas are thin films of electron-transparent material which are cast on opaque specimens in order that their surface structure may be studied. The basic procedure is to form a film on the substance to be examined, separate the two and examine the film. If a reverse of the original is unsatisfactory, a positive replica may be obtained by repeating the process. One method is to deposit the specimen on a formvar-covered grid, vacuum-deposit about 10 nm of carbon, remove the formvar by rinsing with chloroform and finally remove the specimen with a suitable solvent [77]. Instead of a backing film, it is sometimes possible to prepare a carbon replica of a dried suspension deposited on a microscope slide, the replica being washed off the slide in a water bath or a bath of hydrofluoric acid. The carbon film may be strengthened immediately after being deposited by dipping the slide in a 2% w/v solution of Bedacryl 122X in benzene, which is removed by a suitable solvent after the film has been deposited on a grid[62]. Numerous variations of these techniques have been used [62,64,78-82].

In order to determine surface characteristics and particle thickness, it is usual to deposit obliquely a film of heavy metal on to a specimen or its replica. The metal is applied by deposition in a hard vacuum by a small source in order that a nearly parallel beam may reach the specimen. The technique was originated by Williams and Wyckoff [83] in 1946 and has been used extensively since.

Surface topography can also be studied using 3-D imaging. Two successive photographs of the same field are made with the specimen tilted by 11° to 14° between photographs. This stereo-pair can then be viewed with stereo viewing lenses for a remarkable sense of the third dimension.

3.13.3 Chemical analysis

When particles are bombarded with electrons, they emit radiation which depends upon their chemical composition. The Auger process [84,85] is a secondary electron process which follows the ejection of an electron from an inner shell level. The hole is filled by an electron falling to the vacant level, which provides the energy for another electron to be emitted. The energy of this Auger electron is characteristic of the molecule involved. The process can be studied by using monochromatic or polychromatic radiation or electron beams.

There have been many studies on metal surfaces using vacuum ultra violet techniques and the energy distribution curves (EDCs) obtained give information on the band structure of the metals.

The use of soft x-rays is known as electron spectroscopy for chemical analysis (ESCA), or x-ray photo-electron spectroscopy (XPS). In addition to ejecting electrons from the valence shell orbits, the x-rays have sufficient energy to eject electrons from some of the inner shells.

These are essentially atomic in nature and the spectra produced are characteristic of the atom concerned, rather than the molecule of which it forms a part [86].

These, and other techniques, may be applied in electron microscopy to permit chemical assay and particle size analysis to be run concurrently [87].

3.14 Scanning electron microscopy

In SEM a fine beam of electrons of medium energy (5–50 keV) is caused to scan across the sample in a series of parallel tracks [88]. These electrons interact with the sample, producing secondary electron emission (SEE), back-scattered electrons (BSE), light cathodoluminescence and x-rays. Each of these signals can be detected and displayed on the screen of a cathode ray tube like a television picture. Examinations are generally made on photographic records of the screen, although the images can be processed on-line [89]. The SEM is considerably faster and gives more three-dimensional detail than the TEM.

Some instruments can take samples as large as 8 in. square and parts viewed at magnifications varying from 20 \times to 100,000 \times at resolutions of 5 to 7 nm. The latest instruments are capable of resolutions down to 0.7 nm. The depth of focus is nearly 300 times that of the optical microscope. Because of its great depth of focus the SEM can give considerable information about the surface texture of particles.

In both the SEE and BSE modes, the particles appear as being viewed from above. In the SEE mode the particles appear to be illuminated diffusely, and particle size and aggregation behavior can be studied but there is little indication of height. In the BSE mode the particles appear to be illuminated by a point source of light and the resulting shadows give a good indication of height. Several of the current methods of particle size analysis can be adapted for the measurement of images in SEM photographic records. There is also active interest in the development of analysis techniques that will make use of the three-dimensional image presentation.

Many of the image modification procedures associated with automatic image analysis are applicable also with images based on back-scattered electrons. This permits thresholding, classification, boundary enhancement, separation of touching particles, etc. to be carried out before the image is measured [90].

There are three ways of producing a stereographic image in an SEM: horizontally shifting the object, tilting the object and leaning the electron beam. The first is the method used for stereography of aerial photographs, though it is the viewpoint that shifts in this case. The second method suffers the defect that it is difficult to position the object accurately after tilting. Kolendik [91] examined both these methods

and preferred the former whereas Kramarenko [92] stated that the first method was more effective and easier for high accuracy measurement. The tilting method has been described by Shoji *et al.* [93]; essentially it generates a binocular image by striking the specimen at oblique angles.

The Le Mont Scientific B-10 system features an energy-dispersive x-ray detector. Particles are loaded and interrogated to find size and shape; various software options are available. The Bausch and Lomb system has also been applied to electron beam microscopy [44,94]. Tracor Northern describe an integrated system for the collection and processing of analytical and image data from SEM and STEM [95,96].

Various sample preparation methods have been described. Krinsley and Margolis [97] mounted sand grains in Duco cement on the SEM target stub; this technique is not suitable for size analysis and cannot be used for fine particles [98]. Willard and Hjelmstad [99] tried to improve this technique in order to mount fine coal, by using double-backed adhesive tape. They had limited success with particles smaller than 30 µm and found that the method was unsuitable for larger particles. White *et al.* [100] prepared specimens of alumina by aspirating droplets of alumina suspension in NH₄OH solution on to aluminized glass slides and the fixing the slides to the SEM stub. This procedure is very slow and has been criticized as being unsuitable for particles which readily agglomerate or which swell in aqueous solutions. Turner *et al.* [97] prepared an adhesive layer by immersing about 3ft. of Scotch Tape in 150 cm³ of carbon tetrachloride or chloroform, agitating long enough for the adhesive layer to be dissolved and then removing the tape. A few drops of the solution were deposited on the SEM stub, the thickness of the adhesive layer on the stub being controlled by adjusting the concentration and the number of drops applied. A suitable amount of powder was dispersed in acetone (0.5% w/v) and a drop taken on a glass rod and dropped on to the stub. The mounted specimen was then coated with a 15 nm layer of aluminum. They also describe a method for studying agglomerates by freeze drying.

Once the images are recorded; the quality of the analysis depends on the quality of the particle dispersion, the contrast and focus (sharpness of image). From this point on, the particle sizing proceeds as in the optical process described earlier.

King and Schneider [101] state that the available commercial image processing and image analysis software systems do not usually include adequate algorithms for the effective analysis of multi-phase mineralogical textures. Filtering algorithms are usually inadequate for the accurate removal of image noise without compromising the integrity of phase edges. Although most systems offer good algorithms for the analysis of binary images, algorithms for higher order images are almost non-existent and these are essential for mineralogical analysis. They describe the development of an image analysis system which overcomes these limitations. It is based on SEM equipped with

secondary electron and back-scattered electron detectors, an image memory for the storage of digital images captured at slow scan speeds and a SUN workstation for image processing and image analysis.

3.15 Other scanning electron microscopy techniques

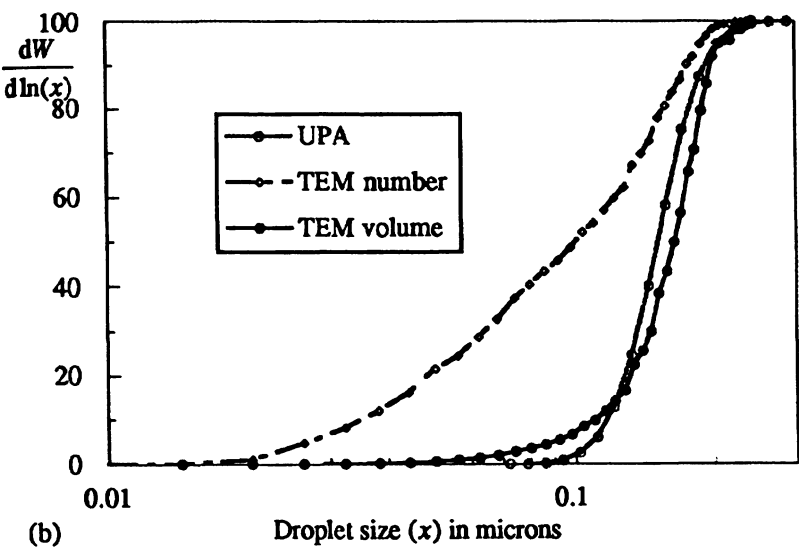
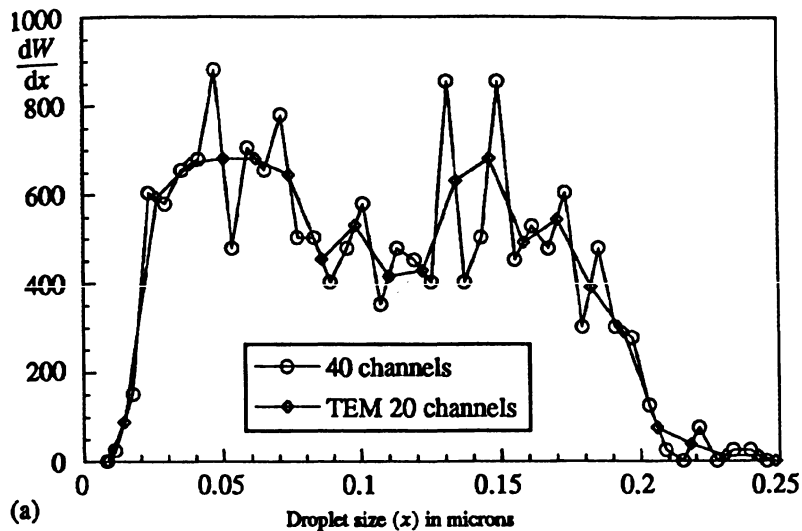
The scanning transmission electron microscope (STEM) uses a fine beam of electrons to scan the specimen as with the SEM, but detects transmitted electrons for display on a cathode ray tube (CRT). The performance is similar to the TEM, but with certain advantages. Since the sample is irradiated with a scanning beam, there is less beam damage to sensitive samples. In addition, for easily damaged samples, focusing can be done on a small region of the sample and instantly "transplanted" to an undamaged part for image recording. The CRT display of the image usually gives more flexibility in manipulating data, transforming it and so on. Use of the annular dark field detector also allows simultaneous bright field and dark field imaging of the same sample field.

Additional advantages enjoyed by the dedicated STEM units are their clean, high vacuum systems in use and their very bright electron source in the field emission gun. The high vacuum (10^{-11}) torr in the gun chamber and 10^{-8} to 10^{-9} torr in the sample chamber) allows prolonged observation of the sample without contamination, and the bright source allows viewing of data collection at TV scan rates.

The scanning tunneling microscope (STM), invented in 1981, allows examination of non-conductive surfaces [102] down to atomic resolution and can operate in ambient and aqueous environments [103,104]. Early references to the instrument use the acronym STEM, which produced confusion with the scanning transmission electron microscope. More recently, the consensus has been to use STM, as the acronym for the tunneling instrument. Since the introduction of the STM a number of variations have been devised, such as ATM (atomic force microscope), MFM (magnetic force microscope), LFM (lateral force, or friction force microscope), etc. None of the above find wide use for particle size determination. A detailed review of the capabilities of this technique has been published by Springer [105].

3.16 Errors involved in converting a number to a volume count

This example consists of TEM number count data on 662 droplets in 40 size classes linearly spaced between 0.015 and 0.250 μm . The resulting number distribution is noisy (Figure 3.12a), due to the large number of size classes and the linear presentation of what is essentially a log-normal distribution.



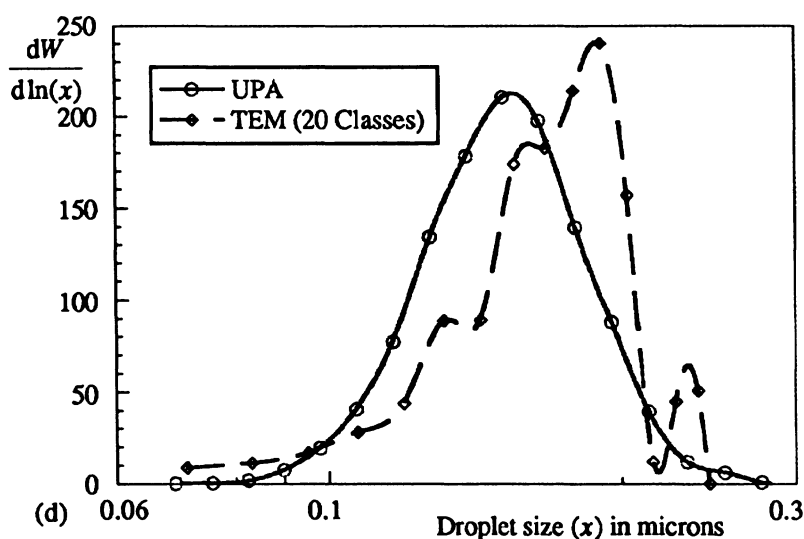
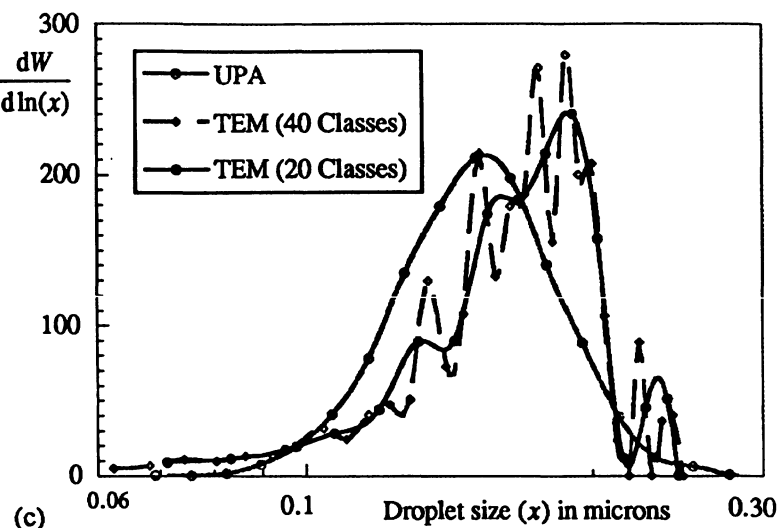


Fig. 3.12 Presentation and interpretation of microscope data.

The conversion to a volume distribution and comparison with Microtrac UPA data are shown in Figure 3.12b. The poor agreement is due, in part, to the errors generated when converting a number distribution of a wide ranging population into a volume distribution. A single 0.25 µm droplet has the same volume as 4630 droplets of size 0.015 µm, hence overcounting by a single large particle is equivalent to overcounting 4630 small particles.

Reducing the number of classes to 20, and plotting logarithmically, greatly reduces the noise (Figure 3.12c).

Comparison between UPA and TEM data (Figure 3.12d) illustrates that the difference between the two sets of data is due to overcounting large particles in the TEM analysis. This error occurs when all droplets in the photomicrograph are counted. It is essential that droplets overlapping two adjacent boundaries be neglected since the probability of large droplets overlapping is greater than the probability for small droplets.

This example illustrate four points:

1. Number distributions, for powders having a wide size range, should never be converted into volume distributions unless a statistically acceptable number of particles in the largest size category have been counted. For a microscope count, the correct procedure for carrying out a size distribution by weight should be followed.
2. Dividing the distribution into too many size categories can result in a noisy distribution unless sufficient particles are measured. The size ranges should be arranged logarithmically for powders having a wide size range.
3. When sizing photomicrographs, a frame should be drawn in the photograph, displaced from the edge by a distance equal to the radius of the largest particle in the distribution. All particles overlapping two adjacent sides of the frame should be left uncounted, otherwise the large particles are over-counted.
4. Data should be presented in such a way as to highlight the required information. Incorrect presentation can completely hide relevant information.

References

- 1 Schmidt, F., Schmidt, K.G. and Fissan, H. (1990), *J. Aerosol Sci.*, **21**, Suppl. 1, S535–538, 112
- 2 McCrone, W.C. (1991), *Phys. Methods Chem.*, 2nd ed., Rossiter, B.W. and Hamilton, J.F. eds., Wiley, N.Y., 112
- 3 Mayette, D.C., McMahon, B. and Daglian, C.P. (1992), *Ultrapure Water*, **9**(4), 20, 22–24, 26–29, 32, 34, 112, 115
- 4 Sutherland, D.N. (1993), *Part. Part. Charact.*, **10**(5), 271–274, 112

- 5 Lane, G.S. and Richmond, G.D. (1993), *Proc. 18th Int. Min. Proc. Congr.*, Sydney, 897–904, 112
- 6 British Standard BS 3406: Part 4 (1993), 113 114, 125
- 7 Charman, W.N. (1961), PhD thesis, University of London, 115
- 8 Humphries, D.W. (1961), *J. Sediment. Petrol.*, 31, 471–473, 116
- 9 Hawkins, A.E. (1993), *The Shape of Powder-Particle Outlines*, John Wiley, 116
- 10 Hawkins, A.E. and Davies, K.W. (1984), *Part. Part. Charact.*, 4, 22–27, 116
- 11 Cairncross, A., Flaherty, D.M. and Klabunde, U. (1993), *Proc. Microsc. Soc. America*, 51st A.G.M., August, Cincinnati, Ohio, 116
- 12 Allen, T. (1994), *Powder Technol.*, 79, 61–68, 116
- 13 Cairncross, A. or Klabunde, U. For further information, Du Pont Company, Central Research and Development, Experimental Station, PO Box 80328, Wilmington, DE 19880–20328, 116
- 14 Amor, A.F. and Block, M. (1968), *J. R. Microsc. Soc.*, 88(4), 601–605, 116
- 15 Hamilton, R.J. and Phelps, B.A. (1956), *Brit. J. Appl. Phys.*, 7, 186, 117
- 16 Eckhoff, R.K. and Enstad, G. (1975), *Powder Technol.*, 11, 1–10, 117
- 17 Dullien, F.A.L., Rhodes, E. and Schroeter, S.R. (1969–70), *Powder Technol.*, 3, 125–135, 117
- 18 Barberry, G. (1974), *Powder Technol.*, 9,(5/6), 231–240, 1176
- 19 Sahu, B.K. (1976), *Powder Technol.*, 13, 295–296, 117
- 20 Dullien, F.A.L., and Mehta, P.N. (1972), *Powder Technol.*, 5, 179–194, 117
- 21 Dullien, F.A.L. (1973) *Am. Chem. Soc. Div. Org. Coat. Plast. Chem.*, Paper 33, 2, 516–524, 117
- 22 Dullien, F.A.L. and Dhawan, G.K. (1974), *J. Colloid Interf. Sci.*, 47(2), 337–349, 117
- 23 Nicholson, W.L. (1976), *J. Microsc.*, 107(3), 323–324, 117
- 24 Saltzman, W.M., Pasternak, S.H. and Langer, R. (1987), *Chem. Eng. Sci.*, 42, 8, 1989–2004, 117
- 25 Hartmann, A.W. (1984), *Powder Technol.*, 39.49, 119
- 26 Hartmann, A.W. (1985), *Powder Technol.*, 42, 269, 119
- 27 Hartmann, A.W. (1986), *Powder Technol.*, 46, 109, 119
- 28 Heywood, H. (1946), *Bull. Inst. Min. Metall.*, No. 477, 488, 120
- 29 Watson, H.H. and Mulford, D.F. (1954), *Brit. J. Appl. Physics*, Suppl. 3, S105, 120
- 30 Fairs, G.L. (1954), Discussion, *ibid*, S108, 120
- 31 ASTM (1951), E20-SIT, 1539, 120
- 32 Holdsworth, J.F. et al. (1973), *Harold Heywood Memorial Symposium*, Loughborough Univ., England, 120
- 33 Nathan, I.F., Barnet, M.I and Turner, T.D. (1972), *Powder Technol.*, 5(2), 105–110, 120

- 34 Allen, T. (1990), cit. *Particle Size Measurement*, Chapman & Hall, 121
- 35 Fath, R., Enneking, U. and Sommer, K. (1986), *First World Congress Part. Technol.*, PARTEC, Nurenberg, 49, 128
- 36 Elkingdon, D.A. and Wilson, R. (1985), *Int. Conf., Royal Soc. Chem., Particle Size Analysis*, ed. P.J. Lloyd, Wiley, Chichester, England, publ. (1987), 61, 128
- 37 National Physical Laboratory, *Reference stage graticule for image analyzer calibration*, Teddington, England, 128
- 38 Blackford, D.B. (1987), *Aerosol Sci. Technol.*, 6, 85–89, 128
- 39 Smith, G.C. (1986), *NPL (National Physical Laboratory) News*, 365, 17, 129
- 40 Issouckis, M. (1986), *Nature*, 322, 91, 129
- 41 Issouckis, M. (1987), *Tappi J.*, 70, 156, 129
- 42 Kilham, L.B. (1987), *Tappi J.*, 70, 156, 129
- 43 Castellini, C., Francini, F., Langobardi, G and Papaloni, E. (1993), *Part. Part. Charact.* 10(5), 7–10, 129
- 44 Morton, R.R.A. and Martens, A.E. (1972), *Res. Develop.*, 23, 1, 24–26, 28, 129, 147
- 45 Anon *Outokompu Technical Bulletin* Digital image analysis of materials, 130
- 46 Gonzales, R.C. and Wintz, P. (1987), *Digital Image Processing*, 2nd ed. Addison-Wesley, 130
- 47 Weichert, R. (1992), Image analysis in particle technology, *Partec*, 5th European Symposium in Particle Characterization, Nurenberg, Germany, 1–12, 132
- 48 Serra, J. (1982), Academic Press Inc., New York, 133
- 49 Serra, J. (1972), *J. Micr. Part* 1, 93–103, 133
- 50 Serra, J. (1976), cit. 10, 133
- 51 Matheron, G. (1975), *Random Sets and Integral Geometry*, Wiley, New York, 133
- 52 Matheron, G. (1972), *J. Micr. Part* 1, 15–23, 133
- 53 Ma, X., Huang, T. and Yu, L. (1990), *Proc. World Congress Particle Technology*, Kyota, Japan, Part 1, 273–280, 133
- 54 Davidson, J.A., Etter, A.A., Thomas, T.R. and Butler, R.S. (1992), *Part. Part. Syst. Charact.*, 9, 94–108, 133
- 55 Huller, D. (1984), *VDI-Fortschrittsberichte*, Reihe 3, Verfahrenstechnik No 101, VDI-Verlag Dusseldorf, 137
- 56 Beck, M.S. and Sommer, K. (1995), *6th European Symp. Particle Size Characterization*, Partec 95, Nurenberg, Germany, publ. NürnbergMesse, GmbH, 79-84, 137
- 57 Keeler, R. (1991), *Res. and Develop. Magazine*, March, 48–52, 138
- 58 Cohen, E.D. and Grotovsky, R. (1991), 44th Annual Conf., *Soc. for Imaging Sci. and Technol.*, St Paul, Minn., 138
- 59 Cohen, E.D. and Grotovsky, R. (1992), personal communication,, 138

- 60 Davidson, J.A. (1993), *Part. Part. Charact.*, 9(2), 94–104, 139
61 Watano, S and Sparks, R. (1995), *Powder Technol.*, 83, 55–60,
140
62 Kay, D.H. (1965), *Techniques for electron microscopy*, 2nd ed.,
Blackwell Scientific Publications. Oxford, U.K., 141, 143, 145
63 Drummond D.G. ed. (1950), *The Practice of Electron
Microscopy*, Royal Microscopy Society, London, 142, 143
64 Walton, W.H. (1947), *Trans. Inst. Chem. Engrs.*, Suppl. 25, 64–76,
142, 143, 145
65 Cartwright, J. and Skidmore, J.W. (1953), Report Number 79,
Safety in Mines Research Establishment, Sheffield, U.K., 143
66 Revell, R.S.M. and Agar, A.W. (1955), *Brit. J. Appl. Phys.*, 6, 23,
143
67 Bradley, D.E. (1954), *Brit. J. Appl. Phys.*, 5, 65, 143
68 Crowl, V.T. (1961), *Paint Research Station*, Teddington, U.K.
Report No. 291, 143
69 Backus, R.C. and Williams, R.C. (1950), *Brit. J. Appl. Phys.*, 21,
11, 144
70 Timbrell, V. (1973), *proc. Harold Heywood Memorial Symp.*,
Loughborough, U.K., 144
71 Hamilton, R.J. and Phelps, B.A. (1956), *Brit. J. Appl. Phys.*, 7,
186, 144
72 Cartwright, J. and Skidmore, J.W. (1953), Report Number 79,
Safety in Mines Research Establishment, Sheffield, U.K., 144
73 Joffe, A.D. (1963), *Brit. J. Appl. Phys.*, 14, 7, 429, 144
74 Chu, Y.F. and Ruckenstein, E. (1976), *J. Catalysis*, 41, 3, 373–
383, 144
75 Ruzek, J. and Zbuzeck, B. (1975), *Silikaty*, 19, 1, 49–66, 144, 154
76 Anderson, R., Tracy, B. and Bravman, J. (1992), *Mat. Res. Soc.*,
V254, 144
77 Bradley, D.E. and Williams, D.J. (1957) *J Gen. Microbiol.* 17, 75,
145
78 Orr, C. and Dalleville, J.M. (1959), *Fine Particle Measurement*,
Macmillan, N.Y., 145
79 Herdan, G. (1960), *Small Particle Statistics*, Butterworths, 145
80 Bailey, G.W. and Ellis, J.R. (1954), *Microscope*, 14, 6, 217, 145
81 Corcoran, J.F. (1970), *Fuel*, 49, 3, 331–334, 145
82 Eckert, J.J.D. and Caveney, R.J. (1970), *Brit. J. Phys. E*, 413–414,
145
83 Williams, R.C. and Wyckoff, R.W.G. (1946), *Brit. J. Appl. Phys.*,
17, 23, 145
84 Chang, C.C. (1971), *Surface Sci.*, 25, 23, 145
85 Taylor, N.J. (1969), Ph.D. Thesis, London Univ., 145
86 Brundle, C.R. (1972), *Surface and Defect Properties of Solids*,
Chem. Soc. London, Ch 6, 146
87 Szalkowski, F.J. (1977), *J. Colloid Interf. Sci.*, 58, 2, 199–215,
146

- 88 Hay, W. and Sandberg, P. (1967), *Micropaleontology*, **13**, 407–418, 146
- 89 McCarthy, J.J. and Ferrara, P.R. (1982), *Microbeam Analysis*, 125–125, 146
- 90 Petruk, W. (1988), *Scanning Micr.*, **2**, 1257–1256, 146
- 91 Kolendik, O. (1981), *Practical Metallogr.*, **18**, 562–573, 147
- 92 Kramarenko, I.B. (1985), *Probl. Proch.*, **3**, 84–87, 147
- 93 Shoji, T., Okaya, K., Goto, K. and Otsuka, S. (1987), *Fine Particle Soc. Meeting*, Boston, 146
- 94 Morton, R.R.A. (1972), *Measurement and Analysis of Electron Beam Microscope Images*, Form 7050, Bausch and Lomb, 146
- 95 McCarthy J.J. and Benson, J.P. (1984), Form No. XR 2112A, Tracor Northern, 147
- 96 McCarthy, J.J., Fisher, R.M. and Lee, R.J. (1982), *Ultramicroscopy*, **8**, 351–360, 147
- 97 Krinsley, D. and Margolis, S. (1969), *Trans. N.Y. Acad. Sci.*, **31**, 457–477, 147
- 98 Turner, G.A., Fayed, E. and Zackariah, K. (1972), *Powder Technol.*, **6**, 33–37, 147
- 99 Willard, R.J. and Hjelmstad, K.E. (1969/70), *Powder Technol.*, **3**, 311–313, 147
- 100 White, E.W. et al. (1970), *Proc. 3rd Ann. SEM Symp.*, Illinois Inst. Technol. Res. Inst., Chicago, pp 57–64, 147
- 101 King, R.P. and Schneider, C.I. (1993), Kona, Powder and Particle, No. 11, Council of Powder Testing, Japan, pp. 165–178, 147
- 102 Sarid, D. (1992), *Scanning Force Microscopy with Applications to Electric, Magnetic and Atomic Forces*, Oxford Univ. Press, N.Y., 148
- 103 Binnig, G., Rossiter, B.W. and Hamilton, J.F. (1981), *Eur. Patent Appl.* **27**, 517, 148
- 104 Binnig, G., Rohrer, H., Gerber, Ch. and Weibel, E. (1982), *Phys. Rev. Letters*, **49**, 57, 148
- 105 Wiesendanger, R. and Güntheradt, H.J. (1992), *Scanning Tunneling Microscopy I and II*, pp 246 and 308 resp., Springer Series in Surface Science, 20 and 28, Springer Verlag, N.Y., 148

Particle size analysis by sieving

4.1 Introduction

Sieving has been used since early Egyptian times for the preparation of foodstuffs. The simplest sieves were made of woven fabric but punched plate sieves are recorded in early Egyptian drawings and, by 1556, Agricola is illustrating woven wire sieves [1]. Such sieves were used for powder classification and the inception of test sieving dates back to Rittinger [2] who, in 1867, proposed a $\sqrt{2}$ progression of aperture sizes based on 75 μm . Modern standards are based on a fourth root of two progression, apart from the French AFNOR series which is based on a tenth root of ten.

The technique is particularly useful since particles are sorted into categories solely on the basis of size, independently of other properties (density, surface, etc.). Sieving can be used to classify dry or wet powders and generates narrowly classified fractions. With micromesh sieves, near-monodisperse powders can be generated in the 1 to 10 μm size range [3].

Sieving consists of placing a powder sample on a sieve containing openings of a fixed size and agitating the sieve in such a way that particles that can pass through the openings do so. To speed up the analysis, several sieves are stacked on top of each other, with the sieve containing the coarsest openings on top. This 'nest' of sieves is vibrated until the residue on each sieve contains particles which can pass through the upper sieve and cannot pass through the lower sieve.

A variety of sieve apertures are currently available, ranging in size from around 20 μm to mm sizes for woven wire sieves, down to 5 μm or less for electroformed sieves, and above 1 mm for punched plate sieves. Woven wire sieves generally have pseudo-square apertures (i.e. the weaving process generates trapezoidal apertures in three dimensions) but punched plate and electroformed sieves are available with round and rectangular apertures. A variety of other shapes are also readily available.

Sieving is probably the most used and abused method of particle size analysis because the equipment, analytical procedure and basic concepts are so deceptively simple.

Sieve analysis presents three major difficulties. (1) With woven wire sieves the weaving process produces three dimensional apertures with considerable tolerances, particularly for fine-woven mesh. (2) The mesh is easily damaged in use. (3) The particles must be efficiently presented to the sieve apertures.

Fractionation by sieving is a function of two dimensions only, maximum breadth and maximum thickness for, unless the particles are excessively elongated, the length does not affect the passage of particles through the sieve apertures (Figure 4.1). Particles having two dimensions smaller than the openings will pass through when the sieve is vibrated, whereas larger particles will be retained. The sieve size d_A is defined, on the basis of woven wire sieves, as the minimum square aperture through which a particle can pass (Figure 4.2).

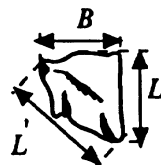
The sieve surface consists of a go, no-go barrier; particles much smaller in size pass through rapidly and larger particles pass through more slowly. Since the apertures have a range of sizes, the final particle that can pass through will pass through the largest opening when its two smaller dimensions are in a preferred direction. Since this will take a very long time sieving is usually deemed complete when not more than 0.2% of the original weight of sample passes through in a 2min sieving operation [4].

Sieves are often referred to by their mesh size, which is the number of wires per linear inch. The American Society for Testing Materials (ASTM) standards range from 635 mesh ($20\text{ }\mu\text{m}$) to 5 mesh (125 mm). The apertures for the 400 mesh are $37.5\text{ }\mu\text{m}$, hence the wire thickness is $26\text{ }\mu\text{m}$ and the percentage open area is 35.

Sieve analyses can be highly reproducible even when using different sets of sieves. Although most of the problems associated with



Plane of maximum stability



Limiting particle dimensions



Spheres of equal volume and surface

Fig. 4.1 Equivalent particle diameters (after Heywood).

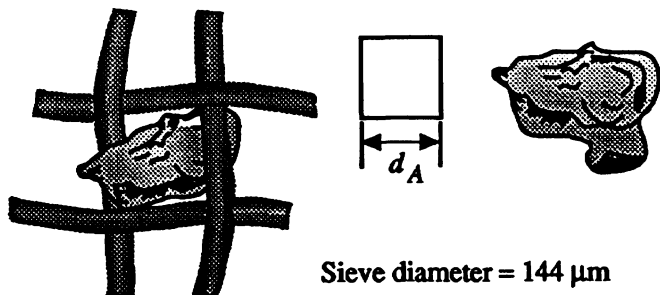


Fig. 4.2 Sieve size of particle shown in Figure 2.1.

sieving have been known for many years and solutions proposed, reproducibility is rarely achieved in practice due to the failure to take cognisance of these problems [5]. An overview of recent developments in fine sieving in Japan have been presented in two reviews [6,7].

4.2 Woven-wire and punched plate sieves

Sieve cloth is woven from wire and the cloth is soldered and clamped to the bottom of cylindrical containers [8,9]. Although the apertures are described as square, they deviate from this shape due to the three-dimensional structure of the weave. Heavy duty sieves are often made of perforated plate, giving rise to circular holes [10]. Various other shapes, such as slots for sieving fibers, are also available. Fine sieves are usually woven with phosphor bronze wire, medium with brass, and coarse with mild steel. Special purpose sieves are also available in stainless steel and the flour industry uses nylon or silk. A variety of electroformed sieves are also available.

Bates discusses screen mesh fabric selection and how the material should be fixed to the frame, particularly with regard to stretching the material and adjusting the tension [11].

Wahl [12] describes the production of highly wear resistant sieves in soft annealed plates of chromium steel by punching, plasma cutting or mechanical working followed by heating and strain hardening.

A method of preparing a metal sieve cloth holder has been described in which parallel grooves were cut on a metal mandrel [13]. These were filled with an insulating material to produce a network of conducting and non-conducting lines. After passivating the mandrel, copper wire was wound perpendicular to the linear net to give the pattern, and the whole immersed in a nickel plating bath; two thousand five hundred holes per cm^2 were produced with a nickel deposition of 25 to 30 μm .

The cylindrical sieve cloth containers (sieves) are formed in such a way that they will stack, one on top of another, to give a snug fit (Figure 4.3).

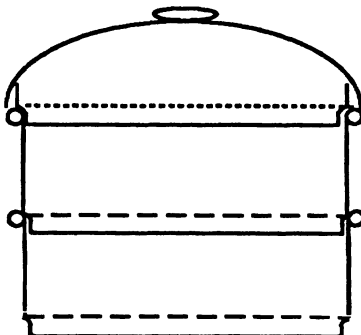


Fig. 4.3. Stacking of sieves.

A variety of sieve aperture ranges are currently used and these may be classified as coarse (4 to 100 mm), medium (0.2 to 4 mm) and fine (less than 0.2 mm). The fine range extends down to 20 μm with woven wire mesh and to 5 μm or less with electroformed sieves.

Large scale sieving machines, to take a charge of 50 to 100 kg, are needed for the coarse range [14]. A wide range of commercial sieve shakers are available for the medium range and these usually classify the powder into five or six fractions with a loading of 50 to 100 g. Special sieving techniques are used with the finer micromesh sieves.

Due to the method of manufacture, woven wire sieves have poor tolerances, particularly as the aperture size decreases. Tolerances are improved and the lower size limit extended with the electroformed micromesh sieves.

4.3 Electroformed micromesh sieves

Micromesh sieves [15] were first described by Daescher *et al.* [16] and are available in a wide range of sizes and aperture shapes from Buckbee Mears, Veco and Endecottes down to aperture sizes of 1 μm [17].

Basically, the photo-etching process is as follows. A fully degreased metal sheet is covered on both sides with a photosensitive coating and the desired pattern is applied photographically to both sides of the sheet. Subsequently the sheet is passed through an etching machine and the unexposed metal is etched away. Finally the photosensitive coating is removed. A supporting grid is made by printing a coarse line pattern on both sides of a sheet of copper foil coated with photosensitive enamel. The foil is developed and the material between the lines etched away. The mesh is drawn tautly over the grid and nickel-plated on to it. The precision of the method gives a tolerance of 2 μm for apertures from 300 to 500 μm reducing to 1 μm for apertures from 5 to 106 μm . For square mesh sieves the pattern is ruled on to a wax-coated glass plate with up to 8000 lines per inch, with

each line 0.0001 in wide, and the grooves are etched and filled. The lower limit for off-the-shelf sieves is about 5 µm but apertures down to 1 µm have been produced. Apertures are normally square or round. The percentage open area decreases with decreasing aperture size, ranging from 2.4% for 5 µm aperture sieves to 31.5% for 40 µm aperture sieves; this leads to greatly extended sieving time when using the smaller aperture sieves. These were originally available only in 3 in diameter frames but this has been extended to 8 in and 12 in frames. Buckbee Mears also make 20 cm diameter frames with apertures down to 3 µm.

Veco manufacture round and square aperture sieves. The apertures for the former are in the shape of truncated cones with the small circle uppermost. This reduces blinding but also reduces the open area and therefore prolongs the sieving time. Where thicker sieves are required, the Veco sieves are subjected to further electrodeposition on both sides to produce biconical apertures.

The tolerances with micromesh sieves are much better than those for woven-wire sieves, the apertures being guaranteed to ± 2 µm of nominal size except for the smaller aperture sieves [18]. Each type of sieve has advantages and disadvantages; e.g. sieves having a large percentage open area are structurally weaker but measurement time is reduced.

Size and shape accuracy are improved by depositing successive layers of nickel, copper and nickel on a stainless steel plate, followed by etching through a photolithographic mask additional layers of copper and nickel. The holes are filled with dielectric, after which the additional nickel is removed down to the copper layer [19]. A description of electroforming methods for making multilayer matrixes for precision screens has been patented [20].

Niklas discusses edge weaknesses in nickel electroformed sieves due to acute angle corners [21]. Additives used during photo-etching increases [22]. Stork [23] also describe sieve preparation by electrodepositing a thin metal skeleton on a substrate, removal of the skeleton from the substrate, followed by deposition of two or more layers of metal on both sides of the substrate. Additives encourage growth perpendicular to the surface of the skeleton.

Dry sieving is often possible with the coarser micromesh sieves, and this may be speeded up and the lower limit extended, with air jet and sonic sifting. Agglomeration of the particles can sometimes be reduced by drying or adding about 1% of a dispersant such as stearic acid or fumed silica. If this is unsuccessful, wet methods may have to be used [24].

Several variants of microsieving (5–30 µm) using ultrasound have been examined [25]. Efficient sieving was only possible by using a liquid column and high suspension transport. The required conditions were determined for quartz and chalk to give an undersize free residue.

Ultrasonics are frequently used as an aid to sieving or for cleaning blocked sieves; the danger of rupturing the delicate mesh is possible under these conditions, readily occurring at low frequencies c. 50 Hz and sometimes at frequencies as high as 20 kHz. Colon recommends an upper limit of 40 kHz though Crawley [26] reports damage to an 11 µm sieve at a frequency of 80 kHz and a power level of 40 W and subsequently recommends a frequency of 800 kHz and a power level of 20 W. Daescher [27] confirmed Rosenberg's [28] findings that the rate of cavitation is less in hydrocarbons than in alcohol and about six times greater in water than in alcohol. Saturating the alcohol with carbon dioxide was found to reduce the rate. He tested three ultrasonic cleaners, 40 kHz, 60 W; 40 kHz, 100 W; 90 kHz, 40 W, and found that the higher frequency cleaner produced the least amount of erosion. Veco recommend 15 to 20 s at a time with a low power 40 kHz ultrasonic bath containing an equi-volume mixture of isopropyl or ethyl alcohol and water with the sieve in a vertical position, and this is in accord with ASTM E161-70. Alpine recommend a cleaning time varying from 10 to 20 min for 10 µm sieves down to 2 to 4 min for sieves in the size range 50 to 100 µm. In a comparison between round and square hole micromesh sieves [29] it was found that the effective apertures of the round mesh sieves, using sand, was 21% greater than the square mesh apertures.

Table 4.1 Nominal apertures and permissible variations for a selection of US woven wire sieves

Standard (mm)	Alternative (in)	Tolerance (± mm)	Intermediate (mm)	Maximum (mm)
(µm)	(in)	(µm)	(µm)	(µm)
125.0	5	3.7	130.0	130.9
63.0	2.500	1.9	65.6	66.2
31.5	1.250	1.0	32.9	33.2
16.0	0.625	0.5	16.7	17.0
8.0	0.312	0.25	8.41	8.58
4.0	0.157	0.13	4.23	4.35
2.0	0.0787	0.070	2.135	2.215
1.0	0.0394	0.040	1.080	0.135
850	0.0331	35	925	970
300	0.0117	14	337	363
150	0.0059	8	174	192
125	0.0049	7	147	163
106	0.0041	6	126	141
90	0.0035	5	108	122
75	0.0029	5	91	103
38	0.0015	3	48	57
20	0.0008	3	29	35

4.4 Standard sieves

The U.S. Standard Sieve Series as described by the American Society for Testing and Materials (ASTM) Standards [30] ranges from 20 µm to 5 in. The apertures for the 400 mesh are 38 µm with a nominal wire thickness of 30 µm. On the basis of Table 4.1, in which a selection of sieve dimensions are shown, the (nominal) 75 µm sieve has a median aperture size in the range 70–80 µm and not more than 5% of the apertures shall fall in the (intermediate to maximum) size range of 91–103 µm. This implies that there is a probability of having a 103 µm aperture in a nominal 75 µm sieve. The relative tolerance increases with decreasing nominal size leading to poor reproducibility when analyses are carried out using different nests of (uncalibrated) sieves. Electroformed sieves with square or round apertures and tolerances of ± 2 µm, are also available. Complete instructions and procedures on the use and calibration of testing sieves are contained in ASTM STP447B [31]. This publication also contains a list of all published ASTM standards on sieve analysis procedures for specific materials or industries. Standard frames are available with nominal diameters of 3, 6, 8, 10 or 12 in. Non-standard frames are also available.

British Standard Specifications [32] adopted a primary size of 75 µm (200 mesh) with a fourth root of two progression in size and suggest that alternate sieves should normally be used for an analysis (i.e. a root two progression of sizes). Thus the specific surface area of particles on consecutive sieves is in a 2:1 progression.

The French AFNOR Standard NFX 11-501, (1957) first adopted in 1938 and known as the R10 or Renard series, is based on a sieve opening of 1 mm in a tenth root of ten progression of size.

$$\text{Now: } (10^{0.1})^3 = 1.259^3 \approx 2 \quad (4.1)$$

Hence, similarly shaped particles passing consecutive apertures are in a 2:1 volume ratio as opposed to the 2:1 surface ratio in the British Standard.

Series R20 form intermediate sieves to give a twentieth root of ten progression and may be included for narrow size distributions.

Most test sieves are certified and manufactured to ISO 9002 standards. Woven wire sieves, having apertures ranging from 20 µm to 125 mm, are readily available in 100, 200, 300 and 450 mm diameters as well as 3, 8, 12 and 18 in diameters. Microplate sieves are available in 100 and 200 mm diameters with round or square apertures ranging from 1 to 125 mm. Endecottes test sieves have at least five intermediate and one final inspection in which wirecloth dimensions are inspected by projector.

Micro-mesh electroformed sieves are available in 3, 8 and 12 in diameter frames, as well as custom made sizes. Sieves have apertures

ranging from 5 to 500 μm , other apertures are also available; etched sieves have round apertures ranging from 500 to 1200 μm .

4.5 Mathematical analysis of the sieving process

The tolerances on sieve cloth are extremely wide, particularly for small aperture cloth. For example, the British Standard Specification (BS 410) for a 200 mesh sieve requires a median diameter of 75 plus or minus 33 μm . It is clear that oversize apertures are more undesirable than undersize, since the latter are merely ineffective whilst the former permit the passage of oversize particles. In order to reduce differences between analyses using different sets of sieves (differences of up to 42% have been recorded) manufacturers such as ATM make specially selected sieves [33] available which can reduce the differences by a factor of 10.

The nominal wire thickness for a 75 μm sieve is 52 μm hence, at the commencement of a sieving operation, the nominal open area comprises 35% of the total area [i.e. $(75/127)^2$] with apertures ranging in size from 42 to 108 μm (Figure 4.4). As sieving progresses, the number of particle that can pass through the smaller aperture decreases, and with it the percentage of available open area. At the same time the effective sieve size increases, rising, in the example given above, to 84 μm and then to 94 μm and, eventually to the largest aperture in the sieve cloth. Thus the mechanism of sieving can be divided into two regions with a transition region in between [34]; an initial region which relates to the passage of particles much finer than the mesh openings and a second region which relates to the passage of near-mesh particles (Figure 4.5). Near-mesh particles are defined as particles which will pass through the sieve openings in only a limited number of ways, and the ultimate particle is the one that will pass only through the largest aperture in only one orientation.

The first region is governed by the law

$$P = at^b \quad (4.2)$$

where P is the cumulative weight fraction through the sieve, t is the sieving time, a is the fraction passing through the sieve in unit time or per tap for hand sieving and b is a constant nearly equal to unity.

Whitby assumed a to be a function of several variables; total load on sieve (W), particle density (ρ_s), mesh opening (S), percentage open area (A_0), sieve area (A), particle size (d) and bed depth on sieve (T).

This function reduces to:

$$a = f\left(\frac{W}{\rho_s S A_0}, \frac{S}{d}, \frac{A_0}{A}, \frac{T}{d}, \frac{A}{S^2}\right) \quad (4.3)$$

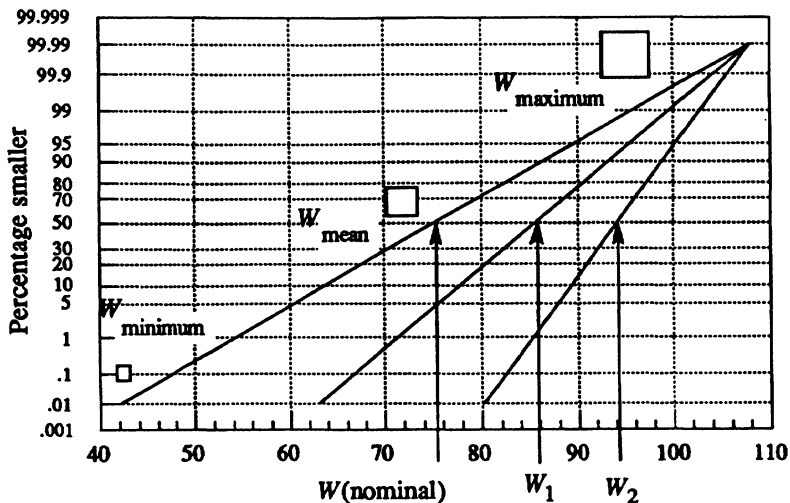


Fig 4.4 Effective aperture width distribution with increasing sieving time.

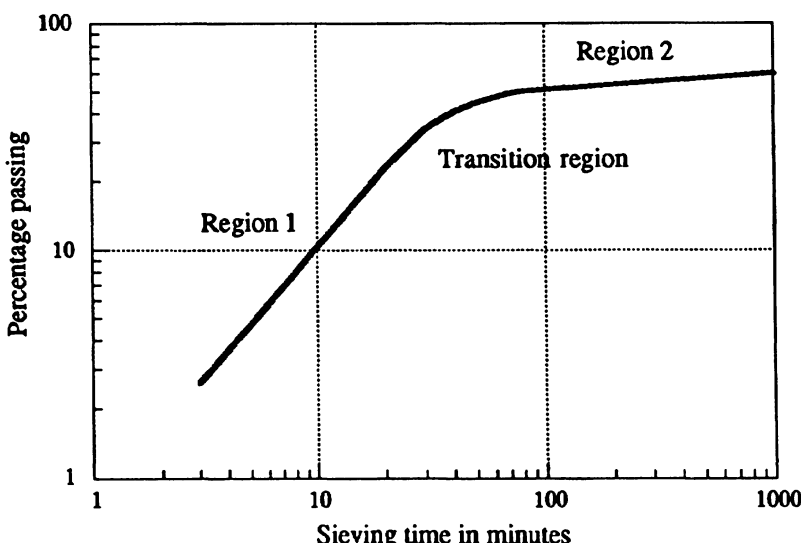


Fig. 4.5 The rate at which particle pass through a sieve.

an identity with seven variables and two dimensions; hence a is a function of five dimensionless groups.

Since A_0/A is constant for any sieve, A/S^2 is so large that it is unlikely to have any appreciable effect, and the effect of variation in T/d is negligible so that the equation reduces to:

$$a = f\left(\frac{W}{\rho_s S A_0}, \frac{S}{d}\right) \quad (4.4)$$

Whitby found:

$$\frac{aW}{A_0 S} = C_1 \left[\left(\frac{S}{k_s \bar{d}_m} \right) \left(\frac{h}{\log \sigma_{gp}} \right) \right] \quad (4.5)$$

where $k_s \bar{d}_m$ is a linear function of the geometric mass mean of the particle size distribution, C_1 and h are constants and σ_{gp} is the geometric standard deviation at a particular size on the distribution curve. This expression was found to hold for wheat products, crushed quartz, St Peter's sand, glass beads and other similar materials.

Whitby suggested that the end-point of sieving be selected at the beginning of region 2. This can be done by plotting the time-weight curve on log-probability paper and selecting the end point at the beginning of region 2. It is difficult to do this in practice and an alternative procedure is to use a log-log plot and define the end-point as the intersection of the extrapolation for the two regions (Figure 4.5).

Using the conventional rate test, the sieving operation is terminated some time during region 2. The true end-point, when every particle capable of passing through a sieve has done so, is not reached unless the sieving time is unduly protracted.

The second region refers to the passage of 'near-mesh' particles. These are defined as particles which will pass through the sieve openings in only a limited number of ways relative to the many possible orientations with respect to the sieve surface. The passage of such particles is a statistical process, that is, there is always an element of chance as to whether a particular particle will or will not pass through the sieve. In the limit, the sieving process is controlled by the largest aperture through which the ultimate particle will pass in only one particular orientation. In practice there is no 'end-point' to a sieving operation, so this is defined in an arbitrary manner.

The rate method is fundamentally more accurate than the time method but it is more tedious to apply in practice and, for most routine purposes, a specified sieving time is adequate.

Several authors have derived equations for the rate of sieving during region 2 where the residual particles are near mesh. The general relationship is of the form:

$$\frac{dR}{dt} = k(R_t - R_\infty)^m \quad (4.6)$$

where R_t is the residue on the sieve at time t and R_∞ is the ultimate end point.

Kaye [35] and Jansen and Glastonberry [36] assumed $m = 1$ and plotted $\log(R_t - R_\infty)$ against t , which yields a straight line if the (assumed) value for R_∞ is correct.

In practice this value of R is of limited practical value, since it cannot apply to the nominal aperture of the sieve. As sieving progresses, the smaller apertures become ineffective since all the particles finer than these apertures will have passed through the sieve. The sieving operation is therefore controlled by the largest aperture in the sieve and the final particle to pass through the sieve will only do so when presented to this aperture in its most favorable orientation. i.e. for a 75 µm sieve the true end-point could be 100 µm or more.

Conventional dry sieving is not recommended for brittle material since attrition takes place and an end-point is difficult to define. If the rate of passage of particles does not decrease with sieving time it may be due to particle attrition, de-agglomeration or a damaged sieve [37].

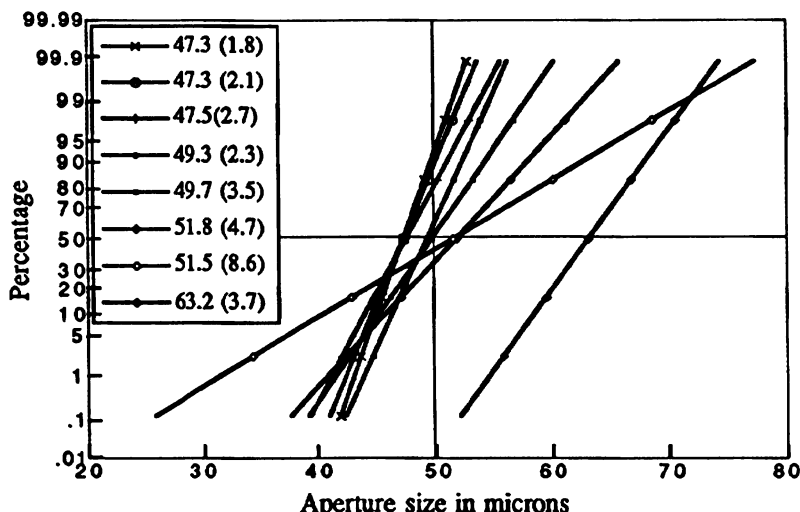


Fig. 4.6 Cumulative distribution by number of aperture widths of eight 50 µm woven wire sieves. The included table gives the median width with the standard deviation in brackets.

4.6 Calibration of sieves

It is not widely realized that analyses of the same sample of material by different sieves of the same nominal aperture size are subject to discrepancies which may be considerable. These discrepancies may be due to non-representative samples, differences in the time the material is sieved, operator errors, humidity, different sieving actions and differences in the sieves themselves.

Ideally, sieves should have apertures of identical shape and size. However, due to the methods of fabrication, woven wire sieves have a range of aperture sizes and weaving gives a three dimensional effect. Fairly wide tolerances are accepted and specified in standards but even these are sometimes exceeded in practice. Leschonski [38] examined eight 50 µm woven wire sieves with the results presented in Figure 4.6. The median varied between 47.3 and 63.2 µm (almost certainly an incorrectly labeled 63µm sieve) and the standard deviation between 1.8 and 8.6 µm. Ilantzis [39] gave a rigorous statistical analysis of microscopic measurements on a set of 13 different sieves (Table 4.2). Most of the sieves had rectangular openings with wider variations on the warp than the weft, and with a coefficient of variation rising from 3–5% with large aperture sieves up to 10% with small apertures. Only four of the sieves met the standard specifications.

All aperture widths shown in Figure 4.6 are for nominal 50 µm sieves but comparative tests on the same material using these sieves could yield enormous differences in the residual weight. In order to obtain

Table 4.2 Means and standard deviations of 13 different sieves as reported by Ilantzis [39]

Nominal aperture width (µm)	Warp		Weft	
	Median (µm)	Standard deviation	Median (µm)	Standard deviation
40	44.1	4.85	45.2	4.56
50	53.2	6.12	50.8	5.19
63	62.9	4.20	64.0	3.75
80	82.6	5.68	84.3	4.02
100	103.2	4.44	106.1	2.91
125	121.5	4.89	123.8	5.59
160	167.7	10.48	155.2	6.79
200	200.8	11.51	214.8	16.46
250	258.9	14.60	260.9	14.40
315	299.3	22.63	295.9	17.29
400	414.5	22.00	467.6	26.40
500	512.9	28.70	500.5	25.00
630	639.0	20.70	634.0	43.20

agreement between different sets of sieves it is therefore necessary to calibrate them and thenceforth to monitor them to detect signs of wear.

One way of standardizing a single set of sieves is to analyze the products of comminution. It is known that the products are usually log-normally distributed hence if the distribution is plotted on a log-probability paper a straight line should result. The experimental data are fitted to the best straight line by converting the nominal sieve aperture to an effective sieve aperture.

The traditional way of determining the median and spread of aperture sizes for a woven wire sieve is to size a randomly selected set of apertures using a microscope. Due to the method of manufacture the measurements for the warp and weft will tend to differ. The limiting size may also be determined by using spherical particles. These are fed on to the sieve which is shaken and the excess removed. Many spheres will have jammed into the sieve cloth and may be removed for microscopic examination. In such an examination Kaye *et al.* [40] showed that both methods yielded similar data for a 65 mesh Tyler sieve, with 90% of the apertures falling between 0.91 and 1.07 of the nominal size. Kaye recommends monitoring sieves using glass beads every few months to find out whether the sieve apertures are deteriorating or enlarging.

Stork Screens measure apertures and screen wire dimensions using wax impressions and the impressions are examined with an automatic image analyzer.

Sieves may also be calibrated by a counting and weighing technique applied to the fraction of particles passing the sieve immediately prior to the end of an analysis. These will have a very narrow size range and the average particle size may be taken as the cut size of the sieve. A minimum number (n) of particles need to be weighed to obtain accurate volume diameters (d_v); let this weight be m and the particle density be ρ , then:

$$d_v = \left(\frac{6m}{\rho n} \right)^{1/3} \quad (4.7)$$

Particles larger than 250 μm can be easily counted by hand and, if weighed in batches of 100, d_v is found to be reproducible to three significant figures. For particles between 100 and 250 μm in size it is necessary to count in batches of 1000 using a magnifier. For sizes smaller than this the Coulter Principle can be used to obtain the number concentration in a known suspension. An alternative procedure using tacky dots has also been described [41]. Sieve analyses are then plotted against volume diameter in preference to the nominal sieve diameter. The method is tedious and time consuming and BCR [42] have prepared quartz samples by this method which may be used as calibration material. The quartz is fed to a stack of sieves and the

analytical cut size is read off the cumulative distribution curve of the calibration material. A method for measuring accurately the aperture and wire diameter using wax impressions has also been described [43].

4.7 Sieving errors

Hand sieving is the reference technique by which other sieving techniques should be judged. For instance, in the French standard NFX 11-57 [1, p.45] it states:

If sieving machines are used, they must be built and used in such a way that the sieve analysis must, within the agreed tolerances, agree with the analysis obtained by hand sieving.

The apertures of a sieve may be regarded as a series of gauges which reject or pass particles as they are presented at the aperture. The probability that a particle will present itself to an aperture depends upon the following factors:

- *The particle size distribution of the powder.* The presence of a large fraction of near-mesh particles reduces the sieving efficiency. An excess of fines also reduces sieving efficiency. It is recommended that fines should be removed before carrying out the sieve analysis. This is effected by pre-sieving, by hand, on the finest sieve to be used in the subsequent analysis. If this is not done, the fines will have to pass through the whole nest of sieves, thus prolonging the analysis and increasing the risk of high powder loss. Since small particles often adhere to large ones it may be necessary to carry out this operation by wet sieving.
- *The number of particles on the sieve (load).* The smaller the sieve loading the more rapid the analysis; too low a load however leads to errors in weighing and unacceptable percentage losses.
- *The physical properties of the particles.* These include adhesion; stickiness due to the presence of water, e.g. high humidity, cohesion, i.e. the tendency of particles to stick together to form granules and other surface phenomena. Brittle particles are best sieved using a gentle sieving action, as is found with the air jet sieve and sonic sifter. Granule formation can be reduced by coating the powder to reduce cohesivity.
- *The method of shaking the sieve.* Sieve motion should minimize the risk of aperture blockage and preferably include a jolting action to remove particles that have wedged in the sieve mesh.
- *Particles shape.* Elongated particles sieve more slowly than compact particles.
- *The geometry of the sieving surface.* e.g. fractional open area.

Table 4.3 The effect of sieving time and load on the amount passing a 200 mesh sieve

Sample weight (W) (g)	Sieving time (t) in minutes			
	5	10	20	40
	Percentage retained on sieve (P)			
500	83.6	80.7	76.5	73.8
250	67.2	64.3	61.6	57.8
125	58.6	58.0	55.2	53.2
62.5	56.6	55.0	53.2	52.3

Whether or not the particle will pass the sieve when it is presented at the sieving surface will then depend upon its dimensions and the angle at which it is presented.

The size distribution given by the sieving operation depends also on the following variables.

- *Duration of sieving.* The sieving time is closely related to sieve loading, a reduction in the latter resulting in a reduction in the former.
- *Variation of sieve aperture.*
- *Wear.*
- *Errors of observation and experiment.*
- *Errors of sampling.*
- *Effect of different equipment and operation.*

The effects of sieving time and sieve loading were investigated by Shergold [44]. The tests were carried out with 14, 52 and 200 mesh sieves using samples of sand specially prepared so that 50% of each sample could pass through the appropriate sieve. Some of the results using the 200 mesh sieve are given in Table 4.3.

These results are of the form $P = k \ln t$. Shergold showed that the smaller the sieve aperture, the greater the effect of overloading and the greater the discrepancies between the results for different loadings. He also showed that, although in general there is no end-point for sieving, the approach to the true percentage is faster for small apertures. Since it is evident that a reduction in sieve loading is more effective than prolonging the sieving, he recommended that the sample should be as small as is compatible with convenient handling 100–150 g for coarse sand and 40–60 g for fine sand with a sieving time of 9 min.

Heywood [45] also investigated the effect of sample weight on sieving time using 20, 50 and 100 g samples of coal dust on 60, 100, 150 and 200 mesh sieves. He found that neither the time required to attain the end-point of 0.1% per min nor the residual percentage on the sieve was affected by the weight of the sample.

Table 4.4 Aperture errors as a percentage of nominal apertures

Different sieves, different methods	8.30
Different sieves, same method	3.71
Same sieve, same method	
<i>Machine sieving</i>	0.61
<i>Hand sieving</i>	0.80

Other variables that have been investigated include sieve motion [46,47] percentage open area [48], calibration [49–51], static [52], humidity [53], and accuracy for a particular application [54–58].

Heywood [57], for example, describes experiments carried out at seven laboratories, in which 50 g samples of coal dust were sieved on BS sieves of 72, 100, 150 and 200 mesh. The average percentage retained on a specified sieve in all the trials was taken to correspond to the nominal sieve aperture, whilst the percentage retained on that sieve for a single trial was taken to correspond to an effective sieve aperture. From a graph of the cumulative percentage passing through the sieve against the nominal sieve aperture, an effective sieve aperture may be read. Heywood found that the average passing through the 52 mesh sieve ($295\text{ }\mu\text{m}$) was 76.9%. In a particular analysis 74% passed through the sieve making the effective aperture $280\text{ }\mu\text{m}$, an aperture error of $15\text{ }\mu\text{m}$. Heywood, by averaging over all the sieves, arrived at the following values for the standard deviation of aperture errors expressed as a percentage of the nominal aperture (Table 4.4).

Although differences between analyses are inevitable, standardization of procedure more than doubles the reproducibility of a sieving operation. Sieve calibration increases this even further. A useful statistical analysis of Heywood's data may be found in Herdan [59].

4.8 Methods of sieving

Large-scale sieving machines, requiring a charge of 50 to 100 kg of powder, are used for the coarsest size range. There are a range of commercial sieve shakers available for medium sized aperture sieves and they usually classify the powder into five or six fractions, with a charge of 50 to 100 g.

Dry sieving is used for coarse separation but other procedures are necessary as the powder becomes finer and more cohesive. Machine sieving is performed by stacking sieves in ascending order of aperture size and placing the powder on the top sieve. The most aggressive action is performed with Pascal Inclyno and Tyler Ro-tap sieves, which combine a gyratory and jolting movement, although a simple vibratory action may be suitable in many cases. Automatic machines are also

Table 4.5 Amount of sample required for a sieve analysis on an 8 in diameter sieve

(a) Based on particle density

Density (g cm ⁻³)	1.5	1.5–3.0	+3
Sample weight (g)	25	50	100

(b) Based on median diameter

Median, (mm)	> 2	2–1	1–0.5	0.50–0.25	0.25–0.075	< 0.075
Sample weight (g)	500	200	100	75	50	25

available which use an air jet to clear the sieves or ultrasonics to effect passage through the apertures. The sonic sifter combines two actions, a vertically oscillating column of air and a repetitive mechanical pulse. Wet sieving is frequently used with cohesive powders.

4.9 Amount of sample required

In determining the amount of sample to be used, it is necessary to consider the type of material, its sievability, and the range of sizes present [60]. Two opposing criteria must be met; it is necessary to use sufficient material for accurate weighing and a small enough sample that the sieving operation is completed in a reasonable time. The natural tendency is to use too large a sample though, in practice, the smaller the sample, within limits, the more reproducible the data.

As a rough guide, the amounts recommended for 8 in diameter sieves are given in Table 4.5a; alternatively the sample weight may be based on the median particle size (Table 4.5b), but this neglects to take into account that the narrower the distribution, the smaller the sample required [61]: A more detailed table is presented in [1].

4.10 Hand sieving

Hand sieving is time consuming but necessary for dependable dry sieving data. A representative sample is obtained and the whole of the sample used in the analysis. The preferred method of sampling is with

a spinning riffler or, failing that, a chute splitter. Coning and quartering induces segregation and should never be used with free-flowing powders. The smallest aperture sieve to be used should be rested on a catch pan, the tared sample placed on the mesh and the whole sealed with a lid. The sieve should be slightly inclined to the horizontal and rapped with a cylindrical piece of wood about 20 cm long and 3 cm in diameter; this should be wrapped in duct tape to eliminate splintering. (The heel of the hand is recommended in some standards and is an acceptable alternative if the hand can take it!). The rate of tapping should be about 150 per min and the sieve should be rotated 1/8 of a turn every 25 raps. After about 10 min the residue is transferred to the coarsest sieve which is nested in a second catch pan for subsequent weighing. It is suggested that white card be placed on the bench (approximately 60 cm square) so that accidental spillage may be recovered. The process is repeated in 5 min cycles until less than 0.2% of the original charge passes through the sieve. The powder is not normally removed from the sieve unless excessive blinding is occurring; both the sieve and the residue are weighed and the residual weight determined. At the end of the sieving operation the sieve is upturned on a white sheet of paper and the fine particles adhering to it removed with a soft brush and added to the sieve residue.

The process is repeated with sieves of increasing fineness and the residue weights collated. Finally, the process is repeated with the finest sieve and the fines are added to the dust collected initially. Brushing is not recommended for sieves with aperture less than 200 μm due to the possibility of damage. Sieves should be washed and dried after use. Ultrasonics should be used to remove particles clogging the apertures or these may be leached out if this can be done without damage to the sieve.

The results may be expressed in terms of the nominal size, although it is preferable to use calibrated sieves. A reference set of sieves should be used after every fiftieth analysis for comparison purposes in order to detect wear. In essence, the smaller the sieve loading, the more rapid is the sieving operation; the low weights however lead to errors in weighing and intolerable percentages losses. Table 4.5 gives the recommended volume loading for various sieves in order to minimize errors and obtain reproducible data.

It is recommended that, for a dry sieving operation, the fines be removed prior to the sieve analysis. This is effected by pre-sieving, usually by hand, on the finest sieve to be used in the subsequent analysis. If this is not done the fines have to pass through the whole stack of sieves, thus increasing the time of the sieving operation and increasing the risk of high powder loss. Since small particles often adhere to large ones, this pre-sieving may be carried out wet using water (with wetting agent if necessary) or, if necessary, some other liquid in which the powder is insoluble.

Sieve motion should minimize the risk of aperture blockage and preferably include a jolting action to remove particles that are wedged in the sieve mesh.

The time of sieving is closely related to sieve loading, a reduction in the latter resulting in a reduction of the former. It is usual for routine analysis to machine sieve for 20 min.

If more accurate data are required it is preferable to sieve for 10 min and weigh the residues. Repeat 2 min sieving should then be carried out until the amount passing any given sieve is less than 0.2% of the initial load. Care should be taken, with brittle material, that particle breakage does not occur. Granular particles pass through the sieve more rapidly than elongated particles although spherical particles are inclined to block the apertures.

Some materials tend to form granules when sieved; this effect can often be reduced by coating the particles in order to reduce cohesiveness. Powders may, for example, be shaken in a container with 1% fatty acid (stearic acid is often used) or fumed silica. Alternatively the powder may be sieved wet. The addition of 0.1% sub-sieve carbon black has been found useful (although rather messy) for eliminating electrostatic charge.

Brittle powders are best sieved using a gentle sieving action, as is found, for example, with the Air Jet Sieve or the Sonic Sifter.

For reliable data around 5% of the sample should be retained on the coarsest sieve and a similar amount should pass through the finest. Unless the size distribution is narrow alternate sieves (a root two progression) is recommended.

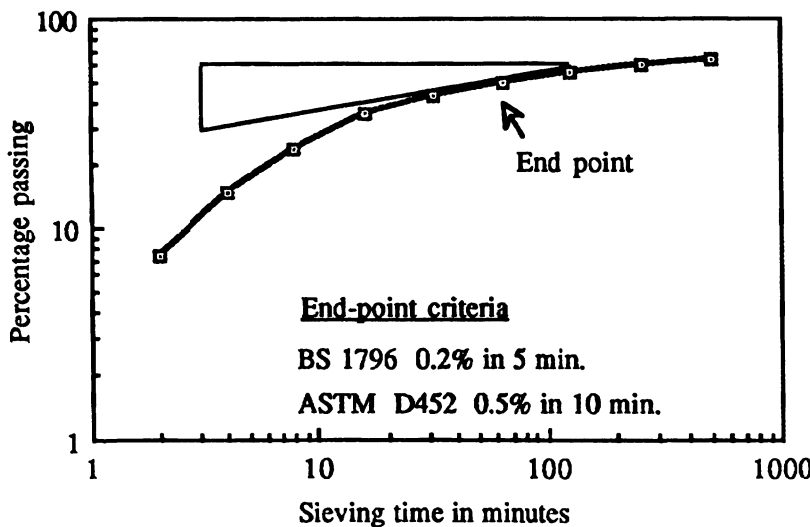


Fig. 4.7 Amount passing through a sieve as a function of time.

4.11 Machine sieving

Machine sieving is carried out by stacking the sieves in ascending order of aperture size and placing the powder on the top sieve. A closed pan, a receiver, is placed at the bottom of the stack to collect the fines and a lid is placed at the top to prevent loss of powder. A stack usually consists of five or six sieves in a root two progression of aperture size. The stack is vibrated for a fixed time and the residual weight of powder on each sieve is determined. Results are usually expressed in the form of a cumulative percentage of the nominal sieve aperture.

For routine control purposes it is usual to machine sieve for 20 min, after which time the sieving operation is deemed to be complete. In BS 1796 it is recommended that sieving be continued until less than 0.2% of the sample passes through in any 2 minute sieving period. In ASTM 452, a 20 min initial sieving period is recommended followed by 10 min periods during which the amount passing should be less than 0.5% of the total feed (Figure 4.7). For coarse aggregates sieving is deemed complete when the rate falls below 1% per min (ASTM C136).

It is generally recommended that if losses during sieving exceed 0.5% of the total feed, the test should be discarded. Preliminary hand sieving on the finest sieve should be carried out for the removal of dust; this dust would otherwise pass through the whole nest of sieves and greatly prolong the sieving time; it would also percolate between sieves in the nest and increase powder loss.

In BS 1796, which applies to the sieving of material from 3350 to 53 µm in size, it is suggested that the sieving operation be carried out in 5 min stages at the end of which the sieves should be emptied and brushed in order to reduce aperture blockage. Test sieving procedures are also described in ISO 2591-1973, Zurich.

The sieving action of many commercial machines is highly suspect and frequently subsequent hand sieving will produce a sieving rate far greater than is produced on the machine. The best type of sieving action is found with the types of shakers exemplified by the Pascal Inclyno and the Tyler Ro-tap which combine a gyratory and a jolting movement, although the simpler vibratory sieves may be suitable in specific cases. ASTM B214 suggest 270 to 300 rotations per min for granular materials combined with 140 to 160 taps to reduce blinding of sieve apertures. Tyler also market a sieve enclosure to reduce noise levels from approximately 85 dB to 60 dB.

Modifications to the methods may be necessary for materials that are not free flowing, are highly hygroscopic, very fragile, have abnormal particle shapes or have other properties which cause difficulty in sieving. For example, in ASTM C92 the fines are first removed by washing through the finest sieve; the residue is then dried and analyzed in the dry state.

4.12 Wet sieving

4.12.1 Manual

About 1 g of powder is dispersed in 1 liter of liquid and this is poured through a sieve in a support stand. The suspension passing through is channeled with a funnel into a second container. For woven wire and coarse micromesh sieves, the sieves may be mechanically rapped to facilitate sieving. The residual powder is then rinsed off the sieve and weighed or the pre-tared sieve is dried and weighed. With fine micromesh sieves an ultrasonic probe may be necessary and the sieving liquid must have a low surface tension, e.g. acetone, or it will not pass through the sieve apertures. The procedure is then repeated with sieves of increasing fineness.

An alternative procedure is to rest a micromesh sieve on a support in a container of water so that the mesh is submerged. About 1 g of powder is added and the bath subjected to 80 kHz ultrasonic vibrations at 40 W. Sieving intervals are 5 min and the operation is deemed complete when no further powder can be seen passing through the sieve.

Ultrasonic agitation is also required for cleaning fine micromesh sieves. Veco recommend 15 to 20 s at a time in a low power 40 kHz

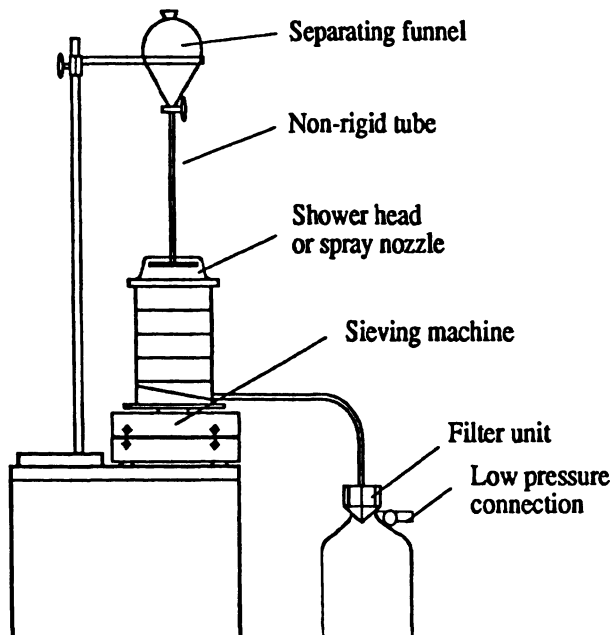


Fig. 4.8 The Retsch wet sieving machine.

ultrasonic bath containing an equal volume mixture of isopropyl or ethyl alcohol and water with the sieve in a vertical position.

Several methods of wet sieving using micromesh sieves have been described. Mullin [62] uses an 80 kHz, 40 W ultrasonic bath in which the micromesh sieve rests on a support which, in turn, rests on a beaker in the bath. Sieving intervals are 2 min with an initial load of 1 g, sieving continues until no further powder can be seen passing through the sieve. Colon [63] rinses the fines through the sieve aperture with a suitable liquid after 0.5 to 1 g has been dispersed in a small volume of the liquid. Sieving continues by moving the sieve up and down in a glass beaker filled with the same liquid so that the direction of flow through the sieve is continuously reversed. If necessary, ultrasonics may be used.

After a standardized time the operation is repeated using a second beaker containing fresh sieving liquid. Sieving is deemed complete when the amount passing through the sieve is visibly negligible.

4.12.2 Wet sieving by machine

Automated wet sieving has been proposed by several authors. In most methods a stack of sieves is filled with a liquid and the sample is then fed into the top sieve. Sieving is accomplished by rinsing, vibration, reciprocating action, vacuum, ultrasonics or a combination [1]. Commercial equipment is available in which the sample is placed in the top sieve of a stack of sieves and sprayed with water whilst the stack is vibrated (Figure 4.8).

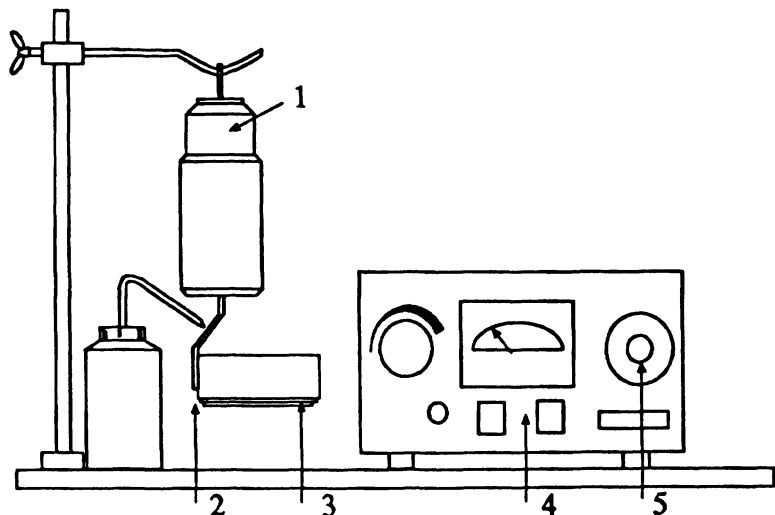


Fig. 4.9 The Alpine wet sieving device.



Fig. 4.10 The Hosokawa Mikropul Micron Washsieve.

A wet sieving device for the size range 10 to 100 µm which includes a sieve vibrator of variable amplitude is commercially available (Figure 4.9). The device consists of a variable-amplitude vibrator (1) with support (2), microsieve (3), regulator with voltmeter for adjusting amplitude (4) and timer (5).

The Hosokawa Mikropul Micron Washsieve is one version of a wet sieving process where water is sprayed on to the surface of a vibrating sieve (Figure 4.10). The machine consists of a sprinkler section, a sieving section and an electromagnetic section. The sprinkler rotates through the force of water to give an even spray whilst the sieve is vibrated to prevent blockage.

The Gallenkamp Gallie-Porritt apparatus (BS 4398) consists of a metal funnel terminating in a short cylindrical outlet in which a wire sieve cloth is soldered. Water, at a pressure greater than two bar, is supplied by a nozzle to discharge a spreading jet through the sieve. A similar arrangement is provided for another tube to give a gentle stream of water to keep the level of the water in the funnel constant throughout the test. About 25 g of powder is slurried and introduced into the funnel at the commencement of the test which continues until the water issuing from the apparatus is clear. The residual mass is determined in order to find the mass percentage undersize.

4.13 Air-jet sieving

The principle of operation of this instrument (Figure 4.11) is that air is drawn upwards, through a sieve, from a rotating slit so that material on

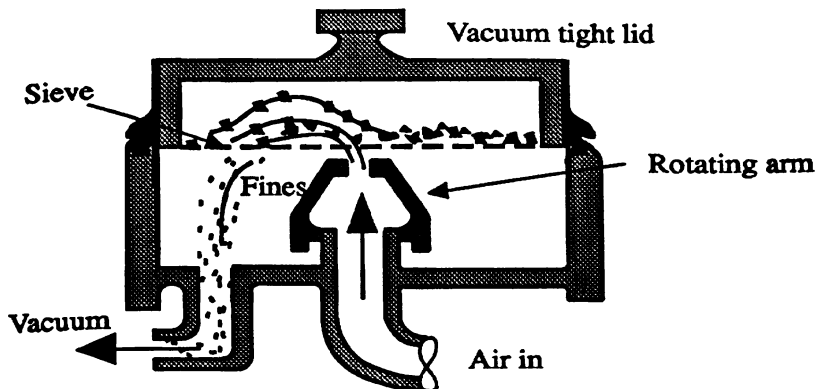


Fig. 4.11 Mode of action of the Alpine Air Jet Sieve

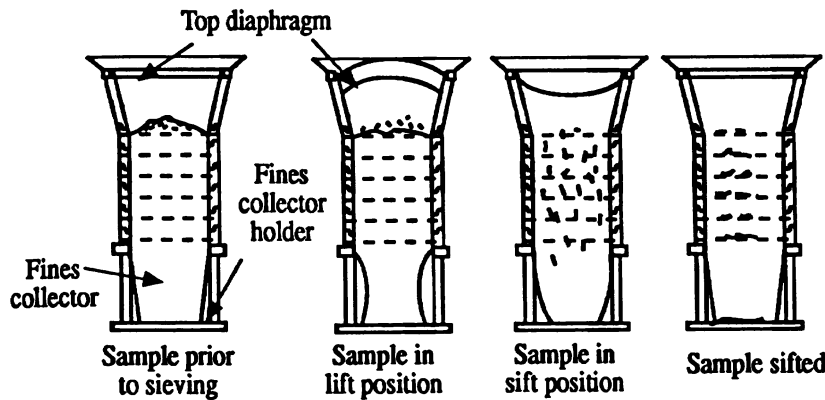


Fig. 4.12 Mode of action of the Sonic Sifter.

the sieve is fluidized. At the same time a negative pressure is applied to the bottom of the sieve which removes fine particles to a collecting device (a filter paper). With this technique there is a reduced tendency to blind the apertures, and the action is very gentle, making it suitable for brittle and fragile powders. Sieving is possible with some powders down to 10 µm in size but with others balling occurs.

The reproducibility is much better than by hand or machine sieving. Size analyses are performed by removal of particles from the fine end of the size distribution by using single sieves consecutively.

The end point of sieving can be determined by microscopic examination of the cleanliness of the sample or by adopting the same criteria as are used in conventional dry sieving. Since only one sieve is in operation at any one time, a full analysis may be unduly protracted

although with sieves coarser than 30 µm the run time is less than 3 min. Sieving is more protracted with finer mesh sieves, and a sieving time of 20 min is usual with a 1g load on a 3 in diameter 20 µm sieve. Similar instruments are marketed by Alpine, Micron Powder Systems and by MicroPul.

4.14 The Sonic Sifter

The ATM Sonic Sifter is produced as a laboratory and as an industrial model. It is claimed to be able to separate particles in the 2000 to 20 µm size range for most materials and 5660 to 5 µm in some cases. It combines two motions to provide particle separation, a vertical oscillating column of air and a repetitive mechanical pulse. The Sonic Sifter moves the air in the sieve stack (Figure 4.11). The oscillating air sets the sample in periodic vertical motion, which reduces sieve blinding and breaks down aggregates and yet produces very little abrasion, thus reducing sieve wear and particle breakage. The Gilson GA-6 Autosiever uses a unique double tapping action together with sonic sifting. The GA-6 features a memory for storing up to 10 programs.

A downward air flow has been found to improve sieving rate for 10, 25 and 45 µm electroformed sieves using a sonic sifter operating at 107 dB and 78 Hz [64]. The sieving rate also increased with decreasing feed rate especially for sub-10 µm sieves [65].

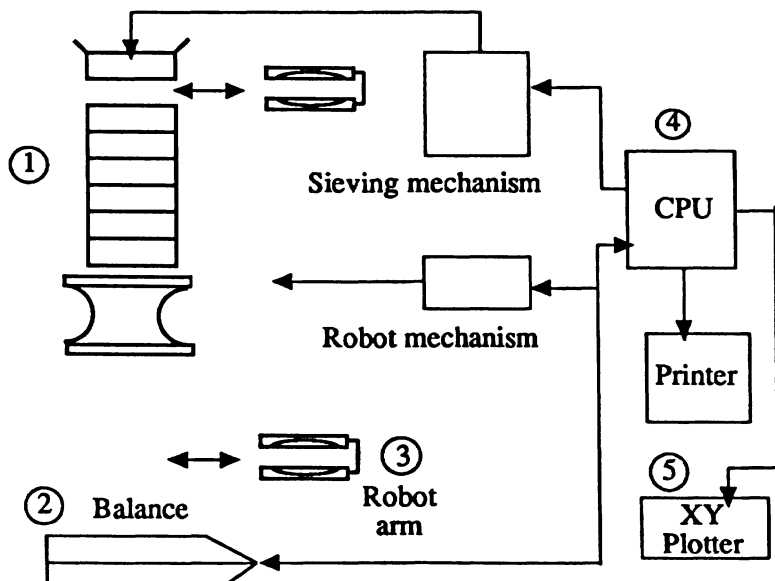


Fig. 4.13 The Seishin Robot Sifter

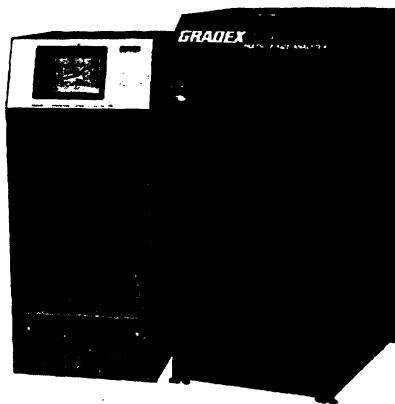


Fig. 4.14 The Gradex particle size analyzer.

4.15 The Seishin Robot Sifter

The Seishin Robot Sifter is an automated version of the ATM in that it includes a robot arm which transports the empty sieves to a balance where they are weighed and the data stored. At the end of this operation a nest of sieves have been assembled on the balance ready to receive a sample of powder on the top sieve. The robot arm then transfers the nest of sieves to the sieving position where sieving is automatically performed. Upon completion of sieving the sieves are transferred to the balance and re-weighed. The data is stored in a CPU and can be printed out as required (Figure 4.13).

4.16 Automatic systems

4.16.1 The Gradex particle size analyzer

Gradex use an octagonal two-compartment drum which can be arranged with up to 14 testing sieves (Figure 4.14). The operator selects the preset cycle for the sample to be analyzed and then loads the sample into the drum, via a feed chute, on to the sieve having the smallest opening. The operator then initiates the automatic cycle which imparts a reciprocating motion to the drum, separating the smallest size fraction from the sample. At the completion of the cycle for this separation, the reciprocating motion stops and the material which passed through the sieve is weighed. The sample then passes to the next coarsest sieve and the operation is repeated. Up to six samples can be loaded into an automatic dispenser on top of the analyzer.

The cycle continues for each sieve in the cycle and the material passing through each sieve is accumulated on an electronic scale. A computer reads and stores the weight of each fraction, then tares the balance before the cycle proceeds to the next sieve. The computer uses this data to calculate then print out the size distribution. When the Autotime computer controlled cycle is selected the analysis is stopped when the throughput rate decreases to a set value. Test times vary from 5 to 15 min depending on the analysis required [16].

4.16.2 Labcon automatic sieve system

The Labcon P114 computer system consists of an Epsom Pine computer mounted in a purpose made portable case containing the necessary power supplies and interface components to allow control of a sieve shaker and electronic balance. Firmware in Epsom is included to provide a variety of methods of data handling and presentation procedures.

4.17 Ultrasonic sieving

The Retsch ultrasonic sieving apparatus was developed for accurate sieving with micromesh sieves in the 5–100 µm range. The high intensity ultrasonic energy (50 W) produces small bubbles which continuously collapse and reform. The resulting cavitation keeps the particles in constant motion and simultaneously prevents blocking of the mesh. Sieve loading is 100 to 500 mg unless the sub-5 µm fraction is small, in which case it can be increased to around 2 g.

The sieves are held in the stack and sealed from each other with radial packing rings. Gravitational action carries the suspension through the stack through progressively smaller meshes.

The Vibrosonic sieve employs ultrasonic vibration of the separator mesh for industrial separation at high rates down to 400 mesh.

4.18 The sieve cascadograph

This technique was designed to classify particles according to shape and to provide a shape distribution profile for powders having a narrow size distribution [66].

The cascadograph consists of a stack of sieves of the same nominal aperture size in a shaking device (a Tyler Ro-Tap sieve shaker). Each stack consists of twenty 8 in diameter sieves specially made by the Newark Wire Cloth Company; Newark sieve cloth is claimed to have very uniformly sized apertures and a low tendency to 'blind'.

The narrow size distribution is prepared by pre-sieving for 1 h and then washing to remove fines. The feed for the 100 mesh cascadograph is the 100 to 120 mesh pre-sieved fraction with a maximum loading of 2.5 g.

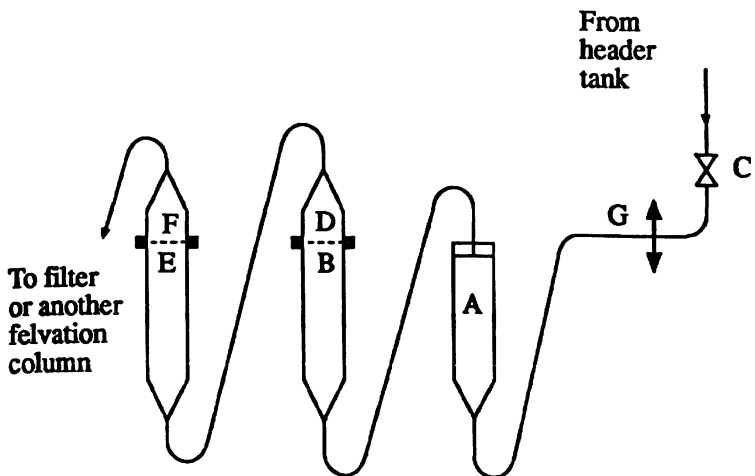


Fig. 4.15 Felvation apparatus. A = predisposition unit, B and E = felvation columns, C = needle valve, D and F = sieving surfaces, G = pulsator

Samples are removed from the cascadograph after 20, 40 and 80 s with subsequent time doubling until completion. A plot of weight fraction removed against sieving time plotted on a log scale provides a shape signature of the powder.

This was extended to continuous sieve cascadography to generate narrow distributions of spherical particles [67,68]. Theoretically, classification by sieving gives a size range of 1.2:1, whereas the new process can reduce this to a 1% variation. It is claimed to be economical with operating costs of less than a dollar per pound [69].

4.19 Felvation

The term felvation has been applied to a technique for grading powders using an elutriation process, with the sieves acting as stops for the coarse powder in suspension [70]. The apparatus used by Burt [71] is shown in Figure 4.15.

The powder to be classified is dispersed in unit A, which is connected to the felvation column B. A needle valve C is opened to allow liquid from the header tank to carry suspended particles into the conical base of the column, where they are fluidized. The flow rate is increased gradually until the finer particles are elutriated up the column to D, which consists of 1/2 in square or 3/4 in round micromesh or woven wire sieve cloth. The particles continue into the next felvation column E, where they meet, and if fine enough pass through, the sieving surface F. The flow rate is increased in steps until larger and

larger particles are elutriated and continued until the ascending particles are too large to pass through the sieves. The end point is when the liquid above the sieves becomes clear. The powder passing the finest sieve is collected on a suction filter and the various fractions are contained in the bodies of the appropriate columns.

Burt used 0.5 to 1.0 g samples for the micromesh sieves and found that the efficiency increased with decreasing sample size and then only when three felvation units were used. Separation efficiency increased if the fluid flow was pulsed two or three times a second so a pulsator was added to the equipment. The technique was found to be unsuitable with micromesh sieves, which were too fragile, but was more successful with woven wire sieves. The technique was not proposed as an alternative to standard sieving methods, but may be useful if only small quantities are available, or with hazardous materials, where small samples are desirable for safety reasons. The technique has also been used to grade 5000 g samples [71] in the size range 45 to 64 µm.

4.20 Self organized sieves (SORSI)

This system was developed in an attempt to eliminate some of the problems associated with nest sieving and to automate the process [72,73]. A hexagonal sieving chamber is supported on discs and rotated as shown in Figure 4.16. A steady stream of powder is fed to the entry port and as the sieve rotates the powder is gently moves across the surface; as the sieve rotates further, the powder is picked up by a vane and dumped out of the other side of the sieve. The mesh is automatically cleaned by an air jet every cycle in order to eliminate blinding and, while in a vertical position, it is interrogated by a laser beam to see if there are any damaged, distorted or blinded apertures.

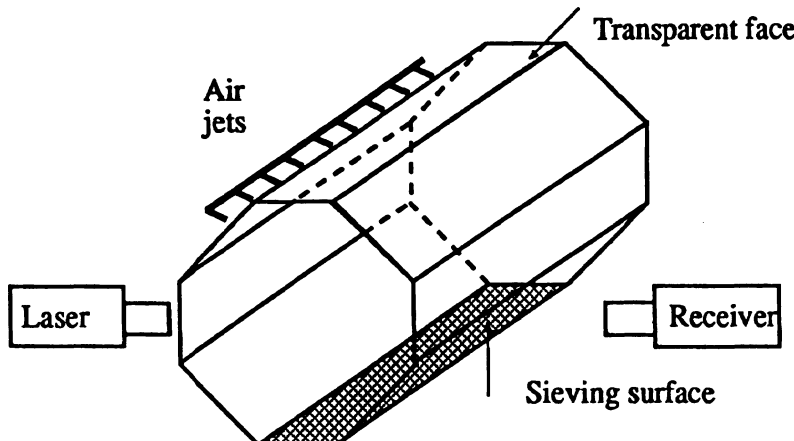


Fig. 4.16 Self-organized sieves.

A very low rate of feed and a series of mesh sizes can be used in sequence, and the fractions passing the sieves can be collected and weighed automatically to give a continuously generated sieve analysis of the powder.

Kaye postulated that partitioning of sieves should improve performance [74]. For new sieves the system isolates the effects of extremes of aperture size to give a distribution more nearly related to nominal size than a conventional sieving operation. The better mechanical support should also reduce wear and tear. Kaye suggests the reduction of an 8 in diameter sieve to a honeycomb of 0.5 in square partitions.

A variation of this system is the installation of 0.5 in diameter sieves mounted on a spinning riffler to obtain small representative powder samples, which can be sieved *in situ* without removing the miniature sieves from the riffler system [75]. By mounting several different aperture sieves around the riffler, a confederation of miniature sieves could replace nest sieving.

4.21 Shape separation

Wire mesh screens have been used as a length classifier of fibrous aerosols [76]. Glass fiber aerosols were sieved through a nest of sieves and the length distribution of the sieve residues decreased with decreasing aperture size. The rate of passage through the sieves depended only on the ratio of fiber length to aperture size. This rate was simulated using a Monte Carlo method and the experimental data were in good accord with theory. If a log-normal distribution is assumed for fiber length and the rate of passage through the sieves determined for a few sieves a fiber length distribution can be obtained using a calibration chart.

Kaye and Yousufzai [40] discuss the use of trapped particles, i.e. the particles blinding the sieve mesh at the completion of sieving, for determination of elongation ratio. A general formula was developed [77], on the probability of particles of different shape passing through a sieve, and the formula has been applied to spherical and needle shaped particles.

A set of sieves with rectangular apertures were used in combination with a set of sieves with square apertures to separate according to shape. The separation was superior to that obtained using a vibrating deck [78].

4.22 Correlation with light scattering data

In many industries particle size measurement has been carried out using sieves and these are being increasingly replaced by light scattering instruments. In order to correlate with historic data banks some

manufacturers have software to manipulate the data so as to present the size distribution in terms of sieve diameter.

Tests carried out on pneumatically conveyed salt particles showed that Insitec data gave size distributions that were over 30% coarser than sieve data, the difference being attributable to particle shape effects. The results for both instruments showed that the particles attrited with number of passes through the system, with the Insitec being more sensitive than sieving [79].

4.23 Conclusions

According to Heywood [80] sieving is the Cinderella of particle size analysis methods; it does most of the hard work and gets little consideration. This was reiterated by Leschonski [81] in 1977 who also quotes the chairman of the Institution of Mining and Metallurgy as stating, in 1903, that screening is not a scientific means of measurement.

However, measuring particle size distributions by sieving is simple and inexpensive and can give reproducible results, even when using different sets of sieves, if proper care is taken. Although most of the problems encountered in sieving have been known for years and solutions proposed, reproducibility is rarely achieved, owing to the failure to take advantage of this knowledge.

For accuracy it is necessary that the sieves be calibrated and, if the sieves are dedicated to a single powder, the calibration should be carried out with the powder under test. It is also necessary that the sieves be checked on a regular basis using a calibration powder so that worn sieves can be rejected. Normally, if a sieve analysis is plotted on log-probability paper, a smooth curve results; any points lying off the curve should be viewed with suspicion.

For reproducibility a standard operating procedure should be adopted. Table 4.6 illustrates the reproducibility that can be attained using calibrated sieves. The data is taken from the certification report on reference materials of defined particle size issued by the Commission of the European Communities and refers to data generated by four laboratories with BCR 68.

Table 4.6 Particle size distribution of BCR 68 by four laboratories

Equivalent volume diameter (μm)	Mass percentage undersize			
	Lab. 1	Lab. 2	Lab. 3	Lab. 4
160	4.7	4.4	4.3	4.4
250	21.9	24.6	23.0	24.5
320	44.0	45.4	44.5	47.6
400	68.6	70.0	70.6	66.9
500	89.6	88.6	87.7	88.5
630	96.8	98.1	97.0	96.0

References

- 1 Heywood, H. (1970), *Proc. Particle Size Analysis Conf.*, ed M.J. Groves and J.L. Wyatt-Sargent, Soc. Analyt. Chem., 156, 177
- 2 Rittinger, P.R. von (1887), *Aufbereit.*, 222 and 243, 156
- 3 Rudolph, A., Peters, C. and Schuster, M. (1992), *Aufbereit.-Tech.*, 3, 384–6, 389–91, 156
- 4 British Standard 1796 Part 1, (1989), (identical with ISO 2591–1) *Methods using test sieves of woven wire cloth and perforated metal plate*, 157
- 5 Leschonski, K. (1977), *Proc. Particle Size Analysis Conf.*, Chem. Soc., Analyt. Div., ed M.J. Groves, publ. Heyden, London, pp. 205–217, 158
- 6 Miwa, S. (1984), *Shikizai Kyokaishi*, 57(16), 334–341, 158
- 7 Miwa, S. (1984), *Funtai to Kogyo*, 16(1), 21–25, 158
- 8 ASTM, E-11-87 *Standard specification for wire-cloth sieves for testing purposes*, 158
- 9 British Standard 410 (1986), *Specification for test sieves*, 158
- 10 ASTM E323-80, (Reapproved 1990), *Standard specifications for perforated plate sieves for testing purposes*, 158
- 11 Bates, R.H. (1981), *Proc. Filtech Conf.*, 299–308, Uplands Press, Croydon, U.K., 158
- 12 Wahl, W. (1976), *Ger. Offen.*, 2 413 521, 158
- 13 Stork Brabent, B.V. (1975), *Neth. Appl.*, 74 07348, 158
- 14 Lauer, O. (1966), *Grain size measurement on commercial powders*, Alpine A.G., Augsburg, Germany, 159
- 15 ASTM E161-87 (Reapproved 1992), *Standard specification for precision electroformed sieves (square aperture)*, 159, 160, 161
- 16 Daescher, M.W., Sebert, E.E. and Peters, E.D. (1958), *Symp. Particle Size Measurement*, ASTM Sp. Publ. 234, 26–56, 159, 182
- 17 Zwicker, J.D. (1966), Report No. AW-FR-2-66, Aluminum Company of Canada Ltd., Arvida, Canada, 157, 180
- 18 Colon, F.J. (1965), *Chem. Ind.*, 206, Feb., 160
- 19 Serkowski, S. and Pautowski, S. (1988), *Polish Pat.* 153 683, June, 160
- 20 Sundukov, V.K., Chechetkin, A.Y. and Zhukov, A.N. (1993), *USSR Pat.* SU 1,788,095 (Cl C25D1/108), Jan., 160
- 21 Niklas, U. (1990), *Sonderb. Prakt. Metallogr.*, 21, 55–60, 160
- 22 Thuis, H.H.W. (1990), (Stork Screens B.V.), *Int. Appl.* WO 90 06 381 (Cl 23F1/04), June, 160
- 23 Stork Screens (1982), *Neth. Appl.* NL 82 04 381 (Cl C25D1/08) June, 160
- 24 Daescher, M.W., Siebert, E.E. and Peters, E.D. (1958), *Symp. Particle Size Measurement*, ASTM Sp. Publ. No. 234, 26–56, 160
- 25 Bernhardt, C. (1982), *Chem. Tech.*, Leipzig, 34(10), 507–511, 160

- 26 Crawley, D.F.C. (1968), *J. Scient. Instrum.*, 1 Series 2, 576–578, 161
27 Daescher, M.W. (1969), *Powder Technol.*, 2(6), 349–355, 161
28 Rosenberg, L.D. (1960), *Ultrasonic News*, 4(16), 161
29 Besancon, P., Chastang, J. and Lafaye, A. (1993), *Part. Part. Charact.*, 10, 222–225 161
30 ASTM-11-87, (1987), *Standard specification for wire-cloth sieves for testing purposes.*, 162
31 STP 447B, (1985) Manual on Testing Sieving Methods, Available from ASTM, 1916 Race St., Philadelphia, PA 19103, 162
32 British Standard 410, (1986), *Specification for test sieves.*, 162
33 ATM Test Sieves Inc. (1991), publ. Particle Post November, 163
34 Whitby, K.T. (1958), *Symp. Particle Size Measurement*, ASTM Sp. Publ. No 234, 3–25, 163
35 Kaye, B.H. (1962), *Powder Metall.*, 10, 199–217, 166
36 Jansen, M.L. and Glastonberry, J.R. (1968), *Powder Technol.*, 1, 334–343, 166
37 Gupta, V.S., Fuerstenan, D.W. and Mika, T.S. (1975), *Powder Technol.*, 11(3), 257–272, 166
38 Leschonski, K. (1970), *Proc. Particle Size Analysis Conf.*, ed M.J. Groves and J.L. Wyatt-Sargent, Soc Anal. Chem. 167
39 Ilantzis, M.A. (1961), *Ann. Inst. Tech. Batim. Trav. Publics.*, 14(161), 484, 167
40 Kaye, B.H. and Yousufzai, M.A.K. (1992), *Powder and Bulk Eng.*, 2, 29–35, 168, 185
41 Allen, T. (1994), *Powder Technol.* 79, 61–68, 168
42 Community Bureau of Reference (BCR), Commission of the European Communities, Directorate General for Science, Research and Development, 200 rue de la Loi, B-1049, Brussels, 168
43 Calboreanu, G. (1991), *Trans. Am. Foundrymen's Soc.*, 99, 111–116, 169
44 Shergold, F.A. (1946), *Trans. Soc. Chem. Eng.*, 65, 245, 170
45 Heywood, H. (1945/46), *Trans. Instn. Min. Metall.*, 55, 373, 170
46 Fahrenwald, A.W. and Stockdale, S.W. (1929), *U.S. Bureau of Mines Investigation* 2933, 171
47 Kaye, B.H. (1962), *Powder Metall.*, 10, 199–217, 171
48 Weber, M. and Moran, R.F. (1938), *Ind. Eng. Chem. Anal. Edn.*, 19, 180, 171
49 Carpenter, F.G. and Dietz, V.K. (1950), *J. Res. Natl. Bureau Stand.*, 47, 139, 171
50 Moltini, E. (1956), *Ind. Mineraria (Rome)*, 7, 771, 171
51 Carpenter, F.G. and Dietz, V.K. (1950), *J. Res. Natl. Bureau Stand.*, 45, 328, 171
52 Allen, M. (1958), *Chem. Eng.*, 65, 19, 176, 171
53 Fritz, S.S. (1937), *Ind. Eng. Chem.*, 9, 180, 171
54 MacCalman, D. (1937), *Ind. Chem.* 13, 464, 171

- 55 MacCalman, D. (1938), *Ind. Chem.* 14, 64, 171
 56 MacCalman, D. (1939), *Ind. Chem.* 15, 161, 171
 57 Heywood, H. (1956), *Instn Min Metall. Bull.*, also *Inst. Min. and Met.* (1946), 55, 373, 477, 171
 58 Ackerman, L. (1948), *Chem. Eng. Min Rev.*, 41, 211, 171
 59 Herdan, G. (1960), *Small Particle Statistics*, p121, *Butterworths*, 171
 60 Tyler Rotap operating instructions., 172
 61 Test Sieving Manual, Endecotts, London, 172
 62 Mullin, J.W., (1971), *Chem. Ind.*, 50, 1435–1436, 177
 63 Colon F.J. (1970), *Proc. Soc. Anal. Chem.*, 7(9), 163–164, 177
 64 Yamamoto, H., Utsumi, R. and Kushida, A. (1986), *Nagoya, Kogyo Gijutsu Shikensho Hokoku*, 35(5), 208–213, 180
 65 Yamamoto, H., Utsumi, R. and Kushida, A. (1986), *Nagoya, Kogyo Gijutsu Shikensho Hokoku*, 35(4), 159–164, 180
 66 Kaye, B.H. (1978), *Powder Technol.*, 19(3), 121–123, 182
 67 Meloy, T.P., Clark, N.N., Durmey, T.E. and Pitchumani, B. (1985), *Chem. Eng. Sci.*, 40(7), 1077–1084, 183
 68 Durmey, T.E. and Meloy, T.P. (1985), *Int. J. Mineral Proc.*, 14, 313–317, 183
 69 Meloy, T.P. and Williams, M.C. (1991), *Particle Size Analysis*, *Proc Conf.*, Anal. Div. Royal Soc. Chem. eds N.G. Stanley-Wood and R. Lines, Sp. Publ. 102, 514–521, 183
 70 Kaye, B.H. (1966), *Symp. Particle Size Analysis*, *Soc. Analyt. Chem.*, London, 183
 71 Burt, M.W.G. (1970), *Proc. Soc. Anal. Chem.*, 7(9), 165–168, 184
 72 Kaye, B.H. (1977), *Dechema Monogram*, 79, 1589–1615, Part B, 1–19, 184
 73 Kaye, B.H. (1977), *Proc. Powder Technol. Conf.*, *Powder Advisory Center*, Chicago, 184
 74 Kaye, B.H. (1978), *Powder Technol.*, 19, 121–123, 185
 75 Kaye, B.H. and Clark, C.G. (1985), *Proc. Conf. Particle Size Analysis*, pp. 439–447, Bradford, UK, ed P.J. Lloyd, publ. John Wiley & Sons Ltd., 185
 76 Myojo, T. (1991), *J. Soc. Powder Technology, Japan*, 28(8), 495–500, 185
 77 Kutepov, A.M. and Sokolov, N.V. (1983), *Teor. Osn. Khim. Tekhnol.* 17(4), 510–518, 185
 78 Whiteman, M. and Ridgeway, K. (1986), *Drug Dev. Ind. Pharm.*, 12(11–13), 1995–2013, 185
 79 Holve, D.J. (1994), *Powder and Bulk Eng.*, 8(82), 186
 80 Heywood, H. (1970), *Proc. Particle Size Anal. Conf.*, Bradford, Soc. Analyt. Chem., pp. 1–18, 186
 81 Leschonski, K. (1977), *Proc. Particle Size Anal. Conf.*, Anal. Div. Chem. Soc., Bradford, publ. Heyden., 186

Fluid classification

5.1 Introduction

Fluid classification is a process for separating dispersed materials, based on the movement of the suspended particles to different points under the effect of different forces. The fluid is usually water or air and the field force gravity, centrifugal or coriolis. The other forces of importance are the drag forces due to the relative flow between the particles and the flow medium, and the inertia forces due to accelerated particle movement. The classification process is defined in terms of sorting and sizing. The former includes processes such as froth flotation where particles are separated on the basis of chemical differences and classification based on particle density. The latter, which is covered here, is based only on differences in particle size.

The results of classification processes may be presented as size distributions, the accuracies of which depend on the sharpness of cut. In an ideal system the cut size is well defined and there are no coarse particles in the fine fraction and vice versa. In practice, however, there is always overlapping of sizes. The cut size may be predicted from theory but this usually differs from the actual cut size due to the difficulty of accurately predicting the flow patterns in the system. It is therefore necessary to be able to predict the future performance of classifiers based on their past performance.

5.2 Assessment of classifier efficiency

Consider a single stage of a classifier where W , W_c , W_f are the weights of the feed, coarse stream and fine stream respectively; $F(x)$, $F_c(x)$, $F_f(x)$ are the cumulative fraction undersize of feed, coarse and fine respectively; x is particle size. Then:

$$W = W_c + W_f \quad (5.1)$$

$$W \frac{dF(x)}{dx} = W_c \frac{dF_c(x)}{dx} + W_f \frac{dF_f(x)}{dx} \quad (5.2)$$

The total fine efficiency may be defined as:

$$E_f = \frac{W_f}{W} \quad (5.3)$$

and the total coarse efficiency as:

$$E_c = \frac{W_c}{W} \quad (5.4)$$

And $E_f + E_c = 1$

The total efficiency has no value in determining the effectiveness of a classification process since it only defines how much of the feed ends up in one or other of the two outlet streams and not how much of the desired material ends up in the correct outlet stream. To discover this, it is necessary to determine the grade efficiency which is independent of the feed, provided the classifier is not overloaded.

$$\text{Grade efficiency} = \frac{\text{amount of desired material in product of size } x}{\text{amount of desired material in feed of size } x}$$

$$\text{Coarse grade efficiency} = \frac{\text{amount of coarse product of size } x}{\text{amount of feed of size } x}$$

$$G_c(x) = W_c \frac{dF_c(x)}{dx} + W \frac{dF(x)}{dx}$$

$$G_c(x) = \frac{W_c}{W} \frac{dF_c(x)}{dF(x)}$$

$$G_f(x) = \frac{W_f}{W} \frac{dF_f(x)}{dF(x)} \quad (5.5)$$

Similarly the fine grade efficiency is defined as:

$$G_f(x) = E_f \frac{dF_f(x)}{dx} \quad (5.6)$$

which, from equations (5.2) and (5.4) may be written:

$$G_c(x) = 1 - G_f(x) \quad (5.7)$$

Table 5.1 Example of grade efficiency calculation

Mean size (\bar{x}) μm	Size limits (x) μm	$F(x)$ (%)	$F_c(x)$ (%)	$f(x)$ (%/ μm)	$E_c * f_c(x)$	$G_c(x)$ (%)
	0.71	0.00				
0.77	0.84	0.01	0.00	0.075	0.000	0.20
0.92	1.00	0.03	0.00	0.125	0.000	0.32
1.09	1.19	0.07	0.00	0.211	0.001	0.51
1.30	1.41	0.14	0.00	0.311	0.002	0.80
1.54	1.68	0.28	0.00	0.523	0.006	1.22
1.83	2.00	0.51	0.01	0.723	0.013	1.83
2.18	2.38	0.91	0.03	1.057	0.029	2.70
2.59	2.83	1.55	0.07	1.422	0.055	3.89
3.08	3.36	2.54	0.16	1.850	0.102	5.51
3.67	4.00	4.02	0.35	2.326	0.178	7.65
4.36	4.76	6.12	0.71	2.775	0.289	10.4
5.19	5.66	8.99	1.38	3.189	0.443	13.9
6.17	6.73	12.77	2.53	3.532	0.643	18.2
7.34	8.00	17.52	4.38	3.732	0.873	23.4
8.72	9.51	23.26	7.19	3.792	1.116	29.4
10.37	11.31	29.93	11.24	3.705	1.347	36.4
12.34	13.45	37.34	16.68	3.462	1.525	44.1
14.67	16.00	45.26	23.58	3.111	1.628	52.3
17.45	19.03	53.38	31.83	2.682	1.635	61.0
20.75	22.63	61.36	41.09	2.217	1.544	69.6
24.68	26.91	68.89	50.88	1.759	1.372	78.0
29.34	32.00	75.71	60.63	1.340	1.148	85.8
34.90	38.05	81.64	69.76	0.979	0.905	92.4
41.50	45.25	86.58	77.80	0.686	0.670	97.6
49.35	53.82	90.53	84.38	0.461	0.461	100.0
58.69	64.00	93.57	89.45	0.299	0.299	100.0
69.79	76.11	95.80	93.17	0.184	0.184	100.0
83.00	90.51	97.38	95.80	0.110	0.110	100.0
98.70	107.6	98.45	97.58	0.062	0.062	100.0
117.38	128.0	99.15	98.75	0.034	0.034	100.0
139.58	152.2	99.59	99.48	0.018	0.018	100.0
166.00	181.0	99.85	99.92	0.009	0.009	100.0
197.40	215.3	100.00	100.00	0.004	0.004	100.0

These equations are used to evaluate the grade efficiency of a classifier provided the total efficiency and the size distribution of two of the streams are known. Results are usually plotted as grade efficiency curves of $G_c(x)$ or $G_f(x)$ against x . Since the classifier separates on the basis of Stokes diameter, it is preferable to carry out the size determinations on the same basis.

Table 5.1 presents the data for the grade efficiency plots of Figure 5.1. Column 1 gives the medians and column 2 the size limits of the ranges; columns 3 and 4 give the mass percentage undersize of the feed and the coarse stream (data for the fine stream are not necessary since the size distribution of the fines can be deduced from these data); column 5 gives the mass frequency distribution for the feed [$f(x) = dF(x)/dx$]; column 6 gives the feed fraction that ends up in the coarse stream and column 7 gives the coarse grade efficiency. These data form the basis of Figures 5.1. It is preferable to know the total coarse efficiency as a check against the derived value from Figure 5.1b but this is not absolutely essential.

The grade efficiency curve is best determined by plotting $F_c(x)$ against $F(x)$ and differentiating [Figure 5.1b] since this allows experimental errors to be smoothed out. The tangent at $F_c(x) = 100\%$ in Figure 5.1b has a slope of $(dF_c(x)/dF(x)) = 100/60$ hence, from equation 5.5, $E_c = 60/100$. Since this tangent merges with the curve at $x = 58 \mu\text{m}$ all particle coarser than $58 \mu\text{m}$ are collected with the coarse fraction. Differentiating this curve at selected values of $F(x)$ and multiplying by 60 gives $G_c(x)$, the relevant diameters being determined from Table 1. The 50% size on the grade efficiency curve is called the *equiprobable* size since particles of this size have an equal chance of being in either the coarse or the fine stream; for this example $e = 16.7 \mu\text{m}$. Figure 5.1a shows how the feed is split between the coarse and fine fraction i.e. $f_f(x) + f_c(x) = f(x)$.

The grade efficiency is often expressed as a single number. This number is known as the sharpness index, ψ , and is a measure of the slope of the grade efficiency curve:

$$75\psi 25 = \frac{x_{75}}{x_{25}} \quad (5.8)$$

where x_{75} and x_{25} are the particle sizes at which the grade efficiency is 75% and 25% respectively. For perfect classification $\psi = 1$, while values above 3 are considered poor. Alternatively $10\psi 90$ has been used.

These ratios are not always adequate to define the sharpness of cut. In many cases it is important to keep the amount of fines in the coarse or the amount of coarse in the fines as small as possible. For these cases a

measure of the effectiveness of a separation process is given by the following:

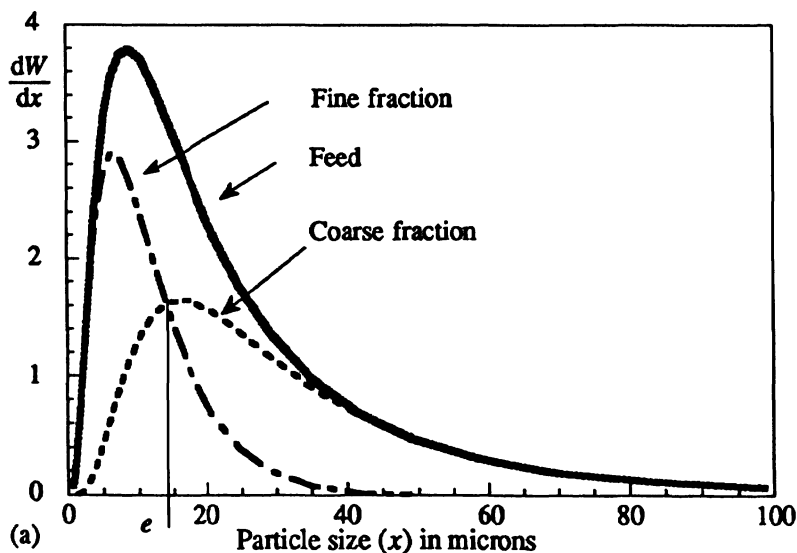
For the coarse yield

$$\psi_c = \frac{\text{weight of particles coarser than } e \text{ in the coarse fraction}}{\text{weight of particles coarser than } e \text{ in the feed}}$$

$$\psi_c = E_c \frac{\frac{x_{\max}}{\sum F_c(x)}}{\frac{e}{\sum F(x) - e}} \quad (5.9)$$

Similarly for the fine yield

$$\psi_f = E_f \frac{\frac{x_{\min}}{\sum F_c(x)}}{\frac{e}{\sum F(x)} - x_{\min}} \quad (5.10)$$



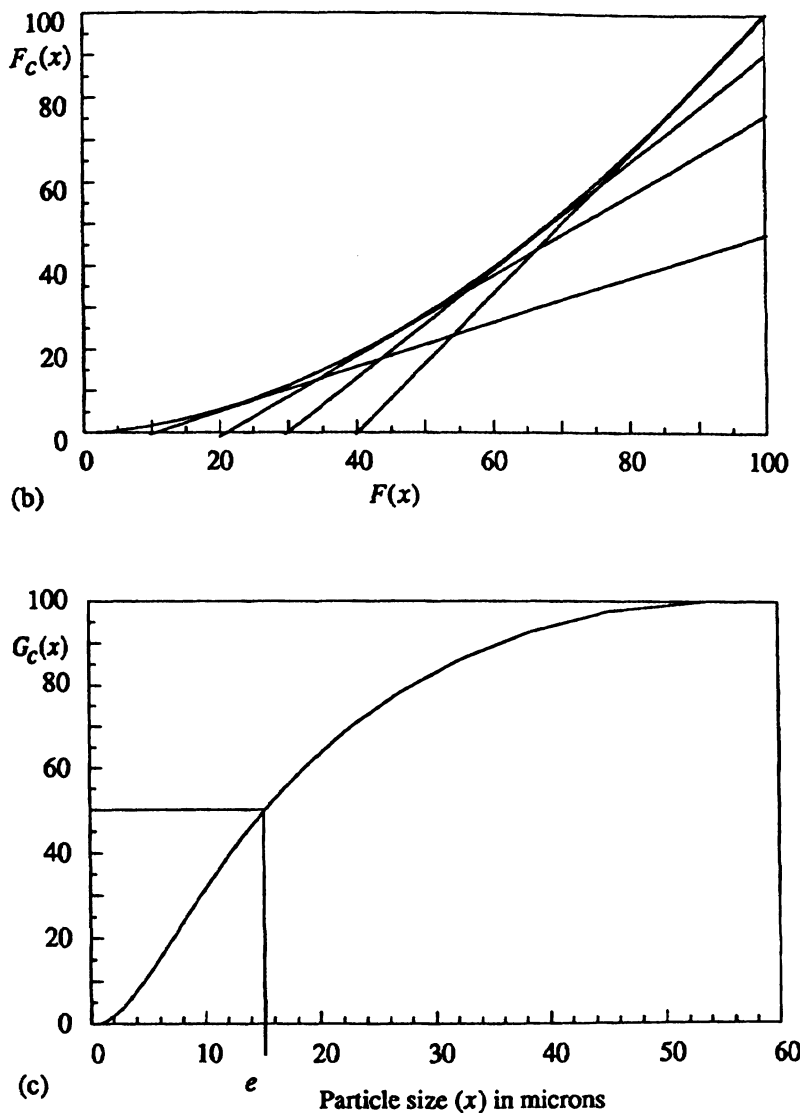


Fig. 5.1 Graphical determination of grade efficiency curve.

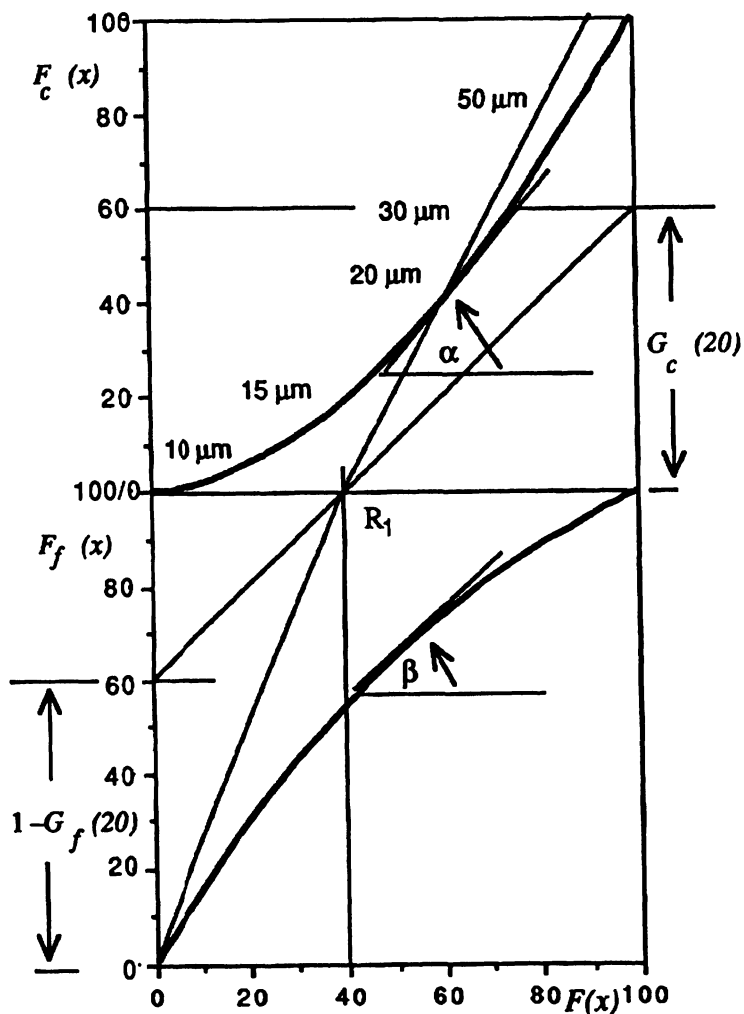


Fig. 5.2 An example of square diagrams.

The grade efficiency can be calculated directly from cumulative size distribution data using a simple geometric construction. The method consists of plotting a square diagram of $F_c(x)$ against $F(x)$ directly above a square diagram of $F_f(x)$ [which will also be against $F(x)$ (Figure 5.2)].

Consider the coarse versus feed diagram. Equation (5.6) can be written:

$$G_c(x) = E_c (\tan \alpha)_x \quad (5.11)$$

For large x , (coarse sizes), $G_c(x) = 1$ and:

$$(\tan \alpha)_{x \rightarrow \infty} = \frac{1}{E_c} \quad (5.12)$$

Equations (5.6) and (5.7) can be combined to give:

$$G_c(x) = 1 - E_f \frac{dF_f(x)}{dF(x)}$$

$$G_c(x) = 1 - (1 - E_f)(\tan \beta)_x \quad (5.13)$$

Consider the fines versus feed diagram. At small sizes $G_c(x) = 0$ and:

$$\tan(\beta)_{x \rightarrow 0} = \frac{1}{1 - E_c} \quad (5.14)$$

Hence, a tangent through $F_c(x) = F(x) = 100\%$ intersects the $F(x)$ axis at the point where $F(x) = 1 - E_c (= 40\%)$.

Plotting the two square diagrams as shown in Figure 5.2, using the data presented in Table 5.1, the total efficiency is represented by a single point R_1 and its straight line connections to $F_c(x) = 100\%$ for coarse and $F_f(x) = F(x) = 0$ for fines.

Some classifiers give grade efficiency curves where the grade efficiency does not reach the x -axis but runs parallel to it at a constant value τ . The corrected curve is given by:

$$G'_c(x) = \frac{G_c(x) - \tau}{1 - \tau} \quad (5.15)$$

In the limit at small sizes, as x approaches 0, $G'_c(x)$ approaches τ .

5.3 Systems

Classifiers may be divided into two categories, counter-flow equilibrium and cross-flow separation.

Counter-flow can occur either in a gravitational or centrifugal field: the field force and the drag force act in opposite directions and particles leave the separation zone in one of two directions according to their size. At the 'cut' size, particles are acted upon by two equal and opposite forces, hence stay in equilibrium in the separation zone. In gravitational systems these particles remain in a state of suspension, while in a centrifugal field the equilibrium particles revolve at a fixed radius, which is governed by the rate at which material is withdrawn from the system. They would therefore accumulate to a very high concentration in a continuously operated classifier, if they were not distributed to the coarse and fine fractions by a stochastic mixing process.

In a cross-flow classifier, the feed material enters the flow medium at one point in the classification chamber at an angle to the direction of fluid flow and is fanned out under the action of field, inertia and drag forces. Particles of different sizes describe different trajectories and so can be separated according to size.

5.4 Counter-flow equilibrium classifiers in a gravitational field – elutriators

Elutriation is a process of grading particles by means of an upward current of fluid, usually air or water. The grading is carried out in one or a series of containers (Figure 5.3), the bodies of which are

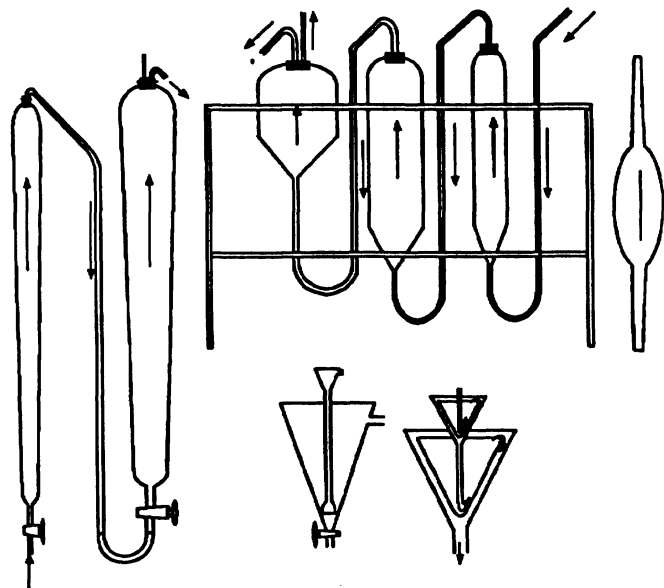


Fig. 5.3 Various types of gravitational elutriators.

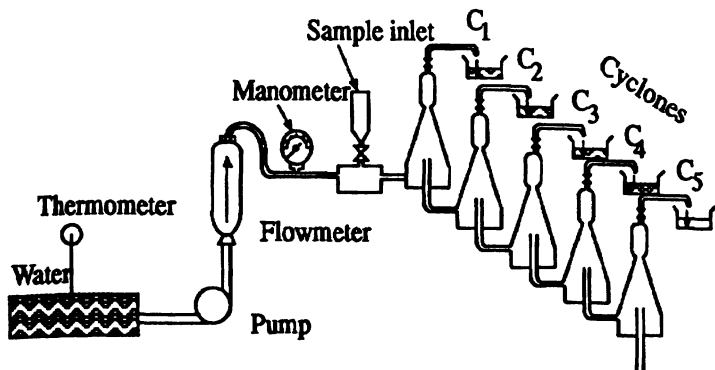


Fig. 5.4 Principle of the Warmain Cyclosizer.

cylindrical and the bases an inverted cone. The cut size is changed by altering the volume flow rate and the cross-sectional areas of the elutriation chambers. Water was used as the flow medium in some of the early elutriators. These instruments suffered from flocculation problems, and took several hours to generate a size distribution; they are no longer manufactured.

In air elutriators, air containing particles sweeps up through the system at a preset flow rate. Particles with a settling velocity lower than the air flow rate are carried out with the air stream, whereas larger particles are retained in the elutriation chamber. The Analysette 8 had a classifier chamber only 1 cm high sitting below a conical section [1].

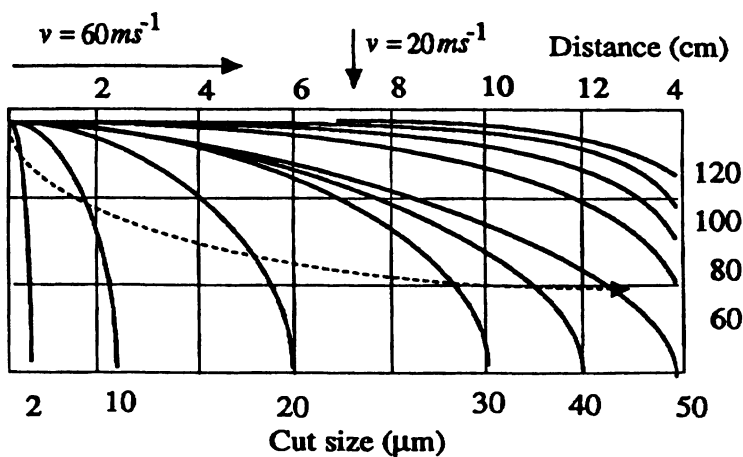


Fig. 5.5 Particle trajectories in a cross-flow classifier --->-- path of the photometer

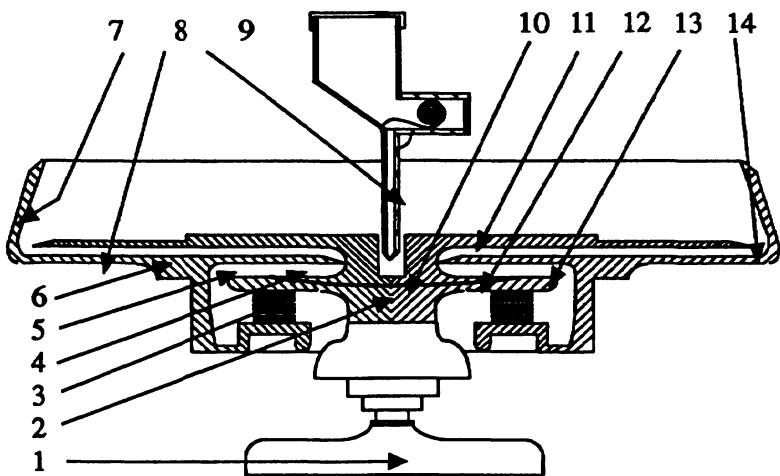


Fig. 5.6 Simplified schematic diagram of the Bahco microparticle classifier showing its major components; 1, electric motor; 2, threaded spindle; 3, symmetrical disc; 4, sifting chamber; 5, container; 6, housing; 7, top edge; 8, radial vanes; 9, feed point; 10, feed hole; 11, rotor; 12, rotary duct; 13, feed slot; 14, fanwheel outlet; 15, grading member; 16, throttle.

Powder spread on a filter paper resting on a porous plate became fluidized when pressure was applied below the plate. Fine particles were entrained in the air, whose velocity increased when it reached the conical section, so that the particles were carried away leaving the coarse fraction behind (see BS 3406, Part 3, (1963) reconfirmed (1983), Air Elutriation Methods).

The elutriation process is time consuming with an ill-defined cut size and has been largely supplanted by micromesh sieving. For a full description of these instruments readers are referred to earlier editions [2].

5.5 Cross-flow gravitational classification

5.5.1 The Warmain Cyclosizer

The Warmain Cyclosizer [3] is a hydraulic cyclone elutriator (Figure 5.4). Using inverted cyclones as separators with water as the flow medium, samples of between 25 to 200 g are reduced to five fractions having cut sizes (for quartz) of 44, 33, 15 and 10 µm. The cyclones are arranged in series and during a run the oversize for each cyclone is trapped and subjected to elutriating action for a fixed time period. At the end of a run the trapped materials are extracted by opening the

valves at the apex of each cyclone in turn and, after decantation, the solids are recovered by filtration and evaporation.

5.5.2. The Humboldt particle size analyzer TDS

This instrument [4] combines classification with particle size analysis. The material is fed into the classifying chamber with the aid of a special feeder and injector at rates between 40 and 60 g min⁻¹. At the outlet of the injector the particles enter a high speed air stream which breaks up any agglomerates. An acceleration channel forms the suspended stream into a flat jet which enters the separation chamber at an average speed between 20 and 80 m s⁻¹. Cross-flowing separation air rapidly forces the fine particles downwards whereas the coarser particles tend to fly straight on. Whilst separation proceeds a photometer scans the classification zone to generate a concentration profile in 5 s (Figure 5.5).

5.6 Counter-flow centrifugal classifiers

The Bahco Classifier is a centrifugal elutriator (Figure 5.6). The sample is introduced into a spiral air current created by a hollow disc rotating at 3500 rpm. Air and dust are drawn through the cavity in a radially inward direction against centrifugal forces. Separation into different sizes fractions is made by altering the air velocity which is effected by changing the air inlet gap by the use of spacers. Since no two instruments perform identically, instrument calibration is necessary; 5 to 10 g of powder are required for the sample which can be graded in the size range 5 to 100 µm [5].

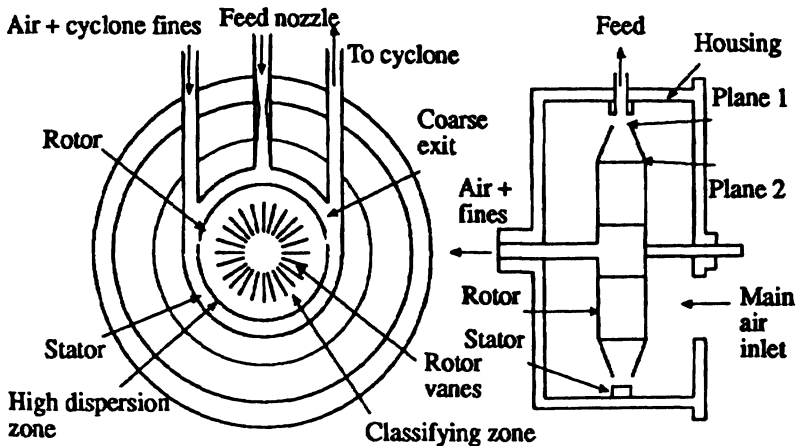


Fig. 5.7 The Donaldson Acucut laboratory classifier.

5.7 Cross-flow centrifugal classifiers

The principle of the Donaldson Acucut is illustrated in Figure 5.7. A vaned rotor produces a centrifugal field while, at the same time, air is drawn into the center of the rotor [6,7]. All but about 5% of the air intake, induced by a positive displacement pump downstream of the classifier, enters the classification zone through a very narrow gap formed between the rotor and the stator. This leads to a very high turbulence in the pre-classification zone. The material enters the classifier through a venturi type nozzle with the remaining 5% of air. Between planes 1 and 2 the ratio of centrifugal force to drag force is kept very nearly constant by a diverging radial cross-section. This zone is the classification zone. The smaller particles are carried out through the middle and the larger ones move towards the stator, where they undergo disaggregation until they reach the exit. The cut size of these machines ranges from 0.5 to 50 μm .

5.8 Zig-zag classifiers

Several versions of the Alpine Multi-plex classifiers are available (Figure 5.8) and these may be categorized as gravitational or centrifugal counter-flow classifiers [8]. A feed rating worm (b) feeds the unclassified material (c) into a classifying chamber. Radially arranged blades on the outer face of the classifier rotor (d) speed the inflow of material up to the peripheral velocity of the rotor suspending it, extra air being admitted through (e). The dust-air mixture is then sucked in to the zig-zag shaped rotor channels where classification takes place. Fine material is sucked into the classifier center (g), where it leaves via a cyclone. The coarse material (f) is expelled by centrifugal force. At the periphery it is flushed by the incoming air before being discharged. The gravitational instrument operates in the 1 to 100 μm size range and the centrifugal from 0.1 to 6 μm .

5.9 Cross-flow elbow classifier

In the cross-flow air classifier (Figure 5.9) the main air is introduced at (a₁) and secondary air at (a₂). Both streams are bent round a solid wall (b) and the resulting flow follows the bend without leaving the wall or forming vortices. The so-called Coanda effect helps to maintain the flow round the bend for approximately 90° and this is enhanced by the application of suction.

5.10 Fractionation methods for particle size measurement

Sub-micron particle sizing can be divided into two categories; non-fractionation and fractionation methods. The most commonly employed non-fractionation method is radiation scattering and

absorption, which include light attenuation, quasi-elastic light scattering and diffraction. Although suitable for rapid determination of an average particle size or an estimate of the size distribution of broad size distributions, these methods are not capable of high resolution. The shortcomings of the non-fractionation techniques have led to an interest in fractionation methods [9].

Commercially available fractionation methods include hydrodynamic chromatography (HDC), field flow fractionation (FFF) and disc centrifugation (DSC). One advantage of fractionation methods over non-fractionation methods is that the particles are separated physically according to size, prior to detection, which allows much higher resolution in determining the size distribution [10].

HDC and FFF are based on the separation by size of colloidal particles when they travel in Poiseuille flow through a narrow conduit. The larger particles travel faster than the smaller ones in HDC whilst the opposite occurs in FFF. Although FFF exhibits high efficiency of size separation, it is necessary to know the particle density in order to determine the particle size distribution, whereas HDC is density independent.

5.11 Hydrodynamic chromatography

In hydrodynamic chromatography (HDC) colloidal particles in a dilute suspension are separated by passing them through non-porous packing. Particle separation occurs due to a hydrodynamic interaction between the particles and the velocity profile near solid surfaces.

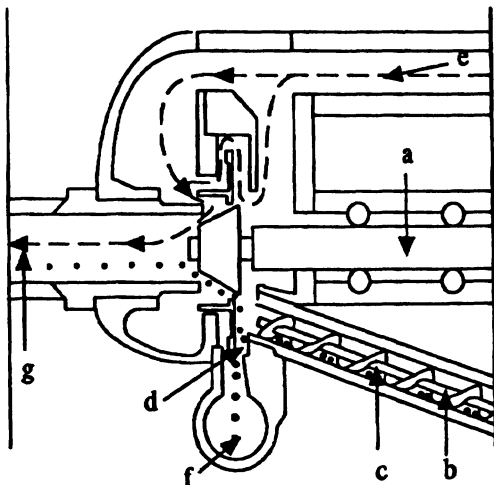


Fig. 5.8 The Alpine zig-zag centrifugal laboratory classifier.

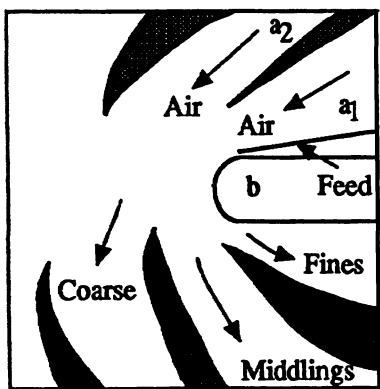


Fig. 5.9 Principle of the cross-flow elbow classifier.

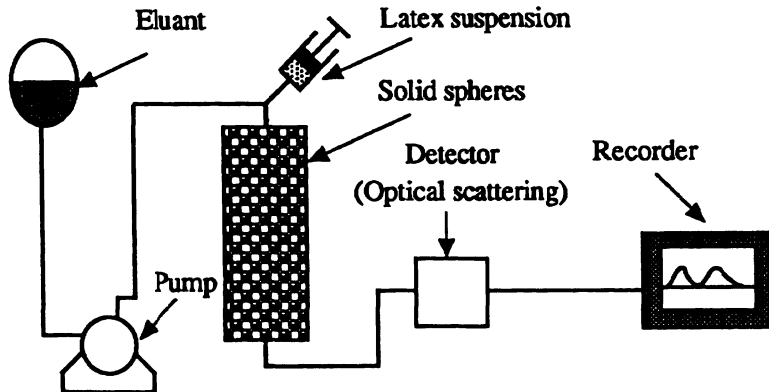


Fig. 5.10 Experimental arrangement for HDC experiment.

Particles with diameters ranging from 50 to 500 nm elute from the separating chromatographic column within 10% of void volume. Large particles interact with faster streamlines than smaller ones and are eluted first. HDC is a fast technique but its resolution is low. Another limitation is a commonly observed phenomenon of particle retention by the packing material, which leads to inaccuracies in the calculated size distribution [11].

The basic equipment consists of a column packed with stationary, solid beads in the size range 10 to 50 μm [12,13] (Figure 5.10). Alternatively a long narrow capillary can be used as the separating medium [14]. An aqueous solution is pumped through the column at a known flow rate. Approximately 0.2 mL of suspension, containing about 0.01% polymer, is injected into the solution and the particles are

sensed at the column exit by an ultraviolet detector. If a marker dye, e.g. potassium dichromate, is injected with the suspension it is found that larger particles elute before the smaller and the dye is the last to elute. Thus, the velocity of a particle through the column increases with increasing particle size. The explanation for this is that the fluid velocity is highest at the center of the streamlines and large particles, because of their size, are confined to high velocity regions. Small particles, on the other hand, can sample the lower velocities near the wall. Brownian motion ensures that the particles sample all the available radial positions (Figure 5.11). A typical calibration chromatogram is shown in Figure 5.12.

An instrument, which operated in the size range 30 to 1577 nm., was marketed as the Micromeritics Flow Sizer 5600 but it is no longer available. It was automated with operating programs on floppy discs and a data terminal was included. Calibration was effected with monosize latexes.

HDC suffers from poor resolution and particle size discrimination. In principle, accurate particle size determinations are possible but require special software with correction for the extensive band dispersion [13].

The superimposition of a steric exclusion effect on HDC by the use of porous media causes particle retardation and the resolution increases. This is known as porous wall hydrodynamic chromatography [15]. By operating at low ionic strength and high zeta potential, the double layer repulsion force predominates over the van de Waals attraction force and particles are repelled from solid surfaces. In such cases the rate of transport of particles through the column is enhanced; again, large particles are eluted before small ones. This is known as enhanced electrostatic chromatography.

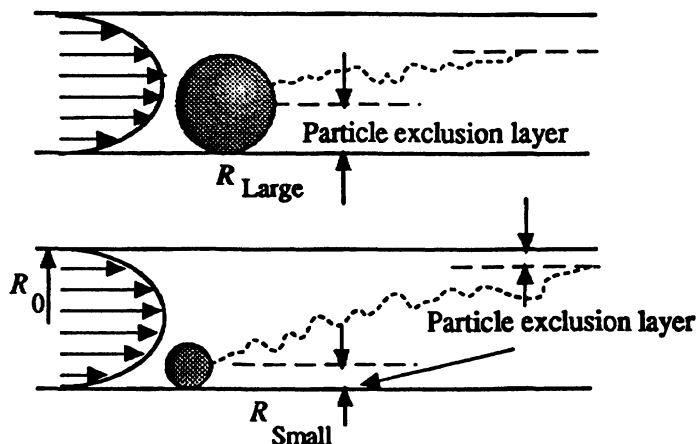


Fig. 5.11 Capillary model of hydrodynamic chromatography separation.

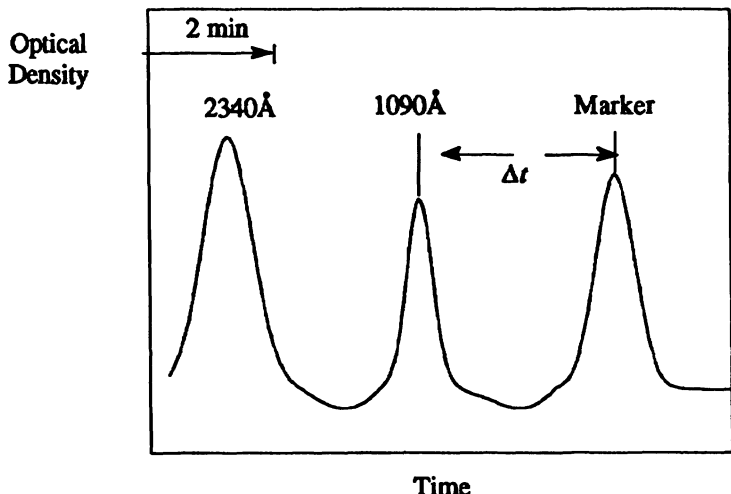


Fig. 5.12 Typical HDC calibration chromatogram using latex spheres. The marker is used to define the emergence of the elute. Particle velocity increases with particle size.

With potential barrier chromatography, the double layer is suppressed by the use of high ionic strength and the van de Waal's attractive force predominates. Large particles, due to their greater attraction to the packing, are retarded more than small ones and elute later.

In size exclusion chromatography the packing is made up of particles having closely controlled pore size distributions. These selectively retard polymer molecules in solution with sizes small enough to enter the pores. Large particles flow through the voids between the particles and are eluted first [16,17].

5.12 Capillary hydrodynamic fractionation

When rigid spheres are transported in Poiseuille flow through a straight cylindrical tube, they undergo radial displacement and move in trajectories parallel to the tube axis at fixed distances between the axis and the wall. The term capillary hydrodynamic fractionation (CHDF) was coined to describe the inertial hydrodynamic focusing of particles into annular rings, the radial position of which are a function of particle radius [18]. The capillaries can be up to 200 ft long with an internal diameter of 0.015 in to fractionate particles in the 0.5 to 30 μm size range. The resolution is higher than that of HDC with comparable analysis time. CHDF has also been used to characterize mini-emulsion stability and droplet size [19].

A set of capillary tubes is used to perform separation of particles in the 0.0015 to 1.1 μm size range. In Poiseuille flow the velocity profile is parabolic and the particles close to the wall travel more slowly than those near the center. Since the larger particles are excluded from the regions near the wall, they attain greater velocities than those of the smaller particles. As a consequence, their average velocity will exceed the average velocity of the eluant and also that of the smaller particles. Separation of particles based solely on hydrodynamic effects was first discussed in 1970, [20,21] and the analytical separation was later documented [22-25].

A full analysis of the efficiency of particle separation in CHDF gives the appropriate criteria for the development of a steady state radial concentration profile [26]. It has also been shown that the molecular weight and concentration of non-ionic surfactants adsorbed on latex particles have a significant effect on their separation factor [27]. The application of CHDF to mixtures of monodisperse particle samples, with diameters ranging from 20 nm to 1000 nm, has been described. The distributions were compared to distributions obtained by electron microscopy. HDC and SFFF and gave comparable results [28]. CHDF has also been used for the characterization of the size and stability of mini droplets of oil (50-500 nm) [29].

CHDF-1100 by Matec uses CHDF to obtain high resolution particle size distributions in the size range 0.015-1.1 μm and is capable of resolving size differences as small as 10% in diameter within that range. The analysis is particle density independent and a run takes less than 10 min. The system consists of modular type components, including a solvent delivery pump, pressure gauge, high pressure safety release valve, prefilter, sample injection valve, separation microcapillary, ultraviolet flowthrough detector, microcomputer and printer. The injected samples of less than 0.1 ml are at a volume concentration of 1 to 3%. After injection the output of the detector, which measures the UV light absorbed and scattered by the particles, is monitored. The output is used to determine the relative amount of different size modes present and is precalibrated. Approximately one minute after the sample injection a marker is injected. The use of marker allows accurate measurement of particle flow rate from which particle size can be calculated.

5.13 Capillary zone electrophoresis

A wide range of ionizable species can be separated by capillary zone electrophoresis (CZE) with high resolution. In CZE small fused silica or glass capillaries are used as the separating medium [30,31]. Capillary forces between a buffer and the capillary wall stabilize a liquid buffer in which the separation occurs, eliminating the need for a semi-rigid gel that is used in conventional slab-gel electrophoresis. The very narrow capillaries permit the use of very high voltages (30

kV) with resultant small electric currents. Joule heating is rapidly dissipated from the narrow capillary while permitting rapid separations. Since the process takes place in a capillary which is transparent to ultra-violet light, a portion of the capillary can be used as an optical measurement cell thus permitting on-line detection [32].

Electrical conductivity has also been used in a capillary system for drop-size concentration measurement [33].

5.14 Size exclusion chromatography

This is an effective and relatively simple method for characterizing silica sols and other colloids [34]. It has also been used to determine the particle size distributions of polymer latices [35,36]. Separations are performed in a column packed with particles having pores substantially of the same size. A carrier liquid is passed through the column; as a mixture of colloidal particles passes through the bed, the larger ones exit first since they are too large to sample the pore volume. Intermediate sized colloids enter the pores and are retained according to the volume that can be accessed by the colloid; the smaller the colloid, the larger the volume that can be accessed and the greater the delay.

The limitation of SEC is that calibration standards are required and silica sols larger than about 60 nm cannot be analyzed. The method has lower resolution and particle discrimination than FFF methods, which results in poorer analytical precision.

5.15 Field flow fractionation

Field flow fractionation (FFF) comprise a group of classification methods in which particles with different properties are eluted from the classifier at different times. The elution time depends upon the applied force field, the most common being sedimentation. While gravity has had limited use for particles larger than a micron, the sedimentation force is usually generated in a centrifuge. In FFF a narrow plug of suspension is introduced into a flow stream of carrier liquid that sweeps the sample into a long flat, ribbon like channel. When the sample reaches the channel, flow is stopped momentarily and a force field applied under which large particles accumulate into thinner, more compact layers at the outer wall, whereas small particles form thicker, more diffuse layers.

The particles do not, however, touch the wall because shear-induced hydrodynamic lift forces oppose the driving force of the field [37]. Because of their smaller sizes the centers of the smaller particles approach the wall more closely than the centers of the larger particles. The larger particles sample higher velocity streams than the smaller ones and are eluted first. The different velocities, as indicated by the length of the arrows in Figure 5.16, give rise to the separation. This

mechanism is applicable in the size range 1–100 µm where Brownian effects are negligible. Giddings *et al.* [38] showed that, using a gravitational field, it was possible to resolve seven polystyrene latexes in 3 min.

As a result of its versatility, FFF in one form or another has been applied to the characterization of particles or molecules whose sizes range over 5 orders of magnitude from particles as small as 0.005 µm to as large as 500 µm [39]. The total mass range covered is over 15 decades. Most of the reported data are for aqueous suspensions; non-aqueous suspensions have also been used [40, p.199].

Materials analyzed by FFF range from high density metals and low density latex microspheres to deformable particles such as emulsions and biological cells. The particles need not be spherical since separation is based on effective particle mass.

The degree of compression of the layer and its interaction with the field determines the differential migration and separation of the particles. At the outlet end of the channel the particles pass through a detector which is used to determine the relative concentrations of the separated fractions. The determination of concentration is usually based on light scattering by the particles as they pass through the flow cell of a chromatographic ultraviolet detector. The measured concentration versus elution time is converted into a size distribution using instrument software.

The force field can be gravitational, centrifugal, thermal, electrical or magnetic but not all of these have been commercialized. An overview of particle separation and size characterization by FFF has been presented by Giddings and his co-workers [41]. In this they describes how it works, the applicable size range, the properties that can be characterized and the underlying theory together with a number of applications.

5.15.1 Sedimentation field flow fractionation

Sedimentation field flow fractionation (SFFF) is one of a number of field flow fractionation methods that were originally devised by

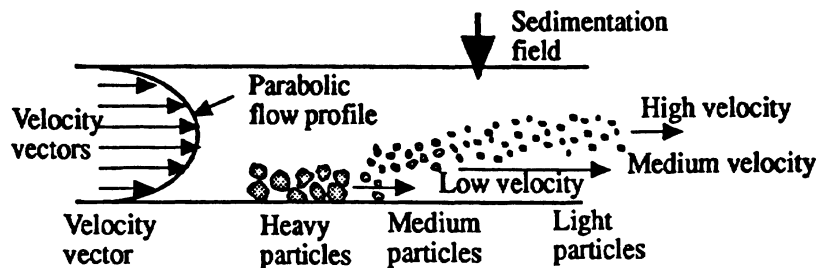


Fig. 5.13 Centrifugal sedimentation field flow fractionation.

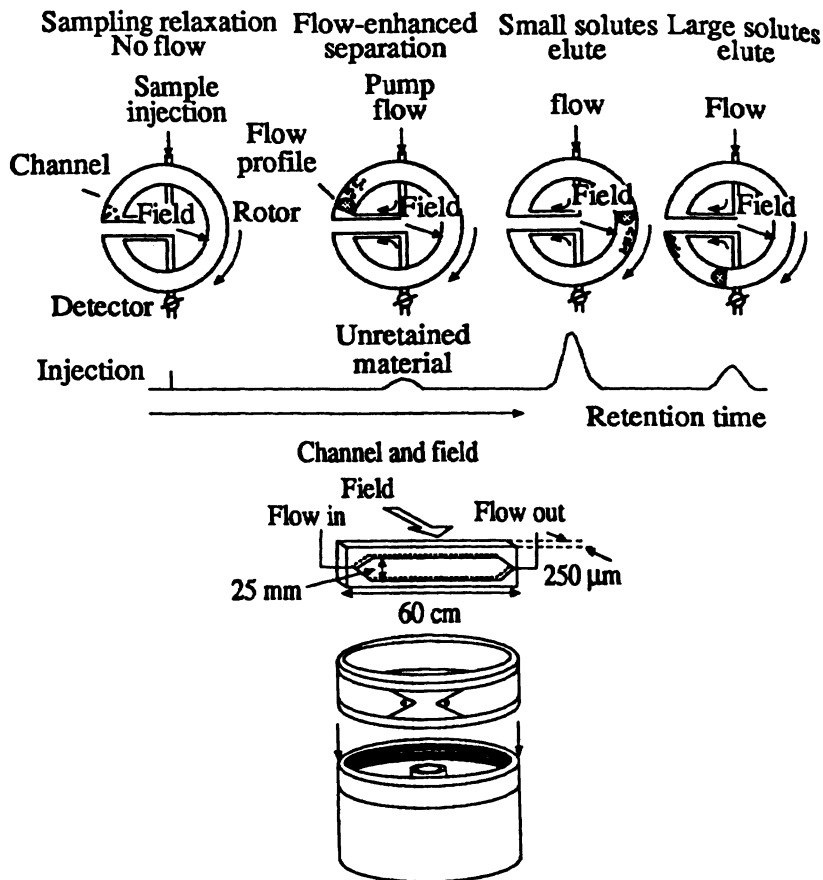


Fig. 5.14 Dupont SFFF equipment schematic.

Giddings [42,43]. In (SFFF) a centrifugal field is applied. Large particles accumulate in thin compact layers at the wall and small particles form more diffuse layers (Figure 5.13).

Interaction with the streamlines of fluid passing through the channel separates the thicker, more diffuse fine particle layer, eluting it first [44]. SFFF separations are carried out in very thin open channels, shaped like a ribbon, that are suspended in a centrifuge. Liquid mobile phase is delivered at a constant flow rate through a sampling loop containing the powder to be analyzed. The sample is swept from this loop into the channel within the centrifuge. Following separation in the channel, the sample flows back through the seal into a detector (typically a turbidimeter) which is used to determine the relative concentrations of the separated fractions. Since the retention time can

be related with particle properties, including size, the detector signal at any time indicates the relative amount of particulate material having a specific value of the relevant property. A computer controls the pump output, sample valve actuation and rotor speed. It also acquires data from the detector and transforms this output to a true concentration profile. A plot of detector signal against time called the fractogram then provides the information necessary to generate the corresponding distribution curve.

This method has an extraordinary ability to probe aggregation phenomena and to track particle size distribution changes caused by aggregation in colloidal samples [45].

15.2 Time-delayed exponential SFFF

In the Dupont SFFF (Figure 5.14) a Sorvall centrifuge is used to contain the SFFF rotor and develop the necessary centrifugal field. The speed of the motor is allowed to decay exponentially in order to speed up the analysis. Mobile phase is pumped through a rotating seal into the rotor. The separating channel is formed between two parallel surfaces 250 μm apart housed in a titanium rotor that can operate at up to 32,000 rpm. Particle sizes or molecular weights are determined from the output of a pre-calibrated UV spectrophotometer.

With the liquid mobile phase off and the channel rotating at an appropriate speed, the sample mixture is injected into the channel. The channel is rotated in this mode for a relaxation or pre-equilibrium period that allows the particles to be forced towards the accumulation wall at approximately their sedimentation equilibrium position. Particles denser than the mobile phase are forced towards the outer wall. Diffusion opposite to that imposed by the centrifugal force causes the particles to establish a specific mean thickness near the accumulation wall as a function of particle mass. Liquid mobile phase is then restarted with a parabolic velocity front. Small particles are engaged by the faster moving central streamlines and are eluted first. Large particles near the wall are intercepted by the slower streamlines and are eluted later. Thus particles are eluted from the channel in order of increasing mass.

Constant force field provides for highest resolution of particles in the sample with resulting highest precision. However characterization of samples with wide size distributions is difficult and time consuming. Force field programming [46,47] removes these limitations to ensure that the entire distribution can be analyzed in a convenient time. In time delayed exponential decay the initial force field is held constant for a time equal to τ and after this the force field is decayed exponentially with a time constant τ . In this mode, a log-linear relationship is obtained of particle mass against retention time. This simple relationship permits a convenient calculation of the quantitative information needed for the sample. Retention time is given by:

$$t_R = 3\tau \ln \frac{d_p}{\beta} \quad (5.16)$$

$$\beta = \left(\frac{4.2kT\tau}{t_0 W \omega_0^2 r \Delta\rho} \right) \quad (5.17)$$

where:

- τ = time of initial force field and delay constant;
- W = channel thickness;
- $\Delta\rho$ = density difference between the particle and the liquid;
- t_0 = solvent marker retention time;
- $\omega_0^2 r$ = centrifugal force field;
- d_p = particle diameter;
- k = Boltzmann's constant;
- T = absolute temperature.

A typical fractogram is shown in Figure 5.15. The instrument operates in the size range 0.01 μm to 1.0 μm . In summary, flow chromatographic methods offer the advantage of both separation and size analysis of fine particles and macromolecules. Separation is relatively gentle, and has application in the biological sciences. The driving force can be centrifugal as described here or electrical, thermal or magnetic; while many methods are still classed as academic, sedimentation field flow fractionation is commercially available. The

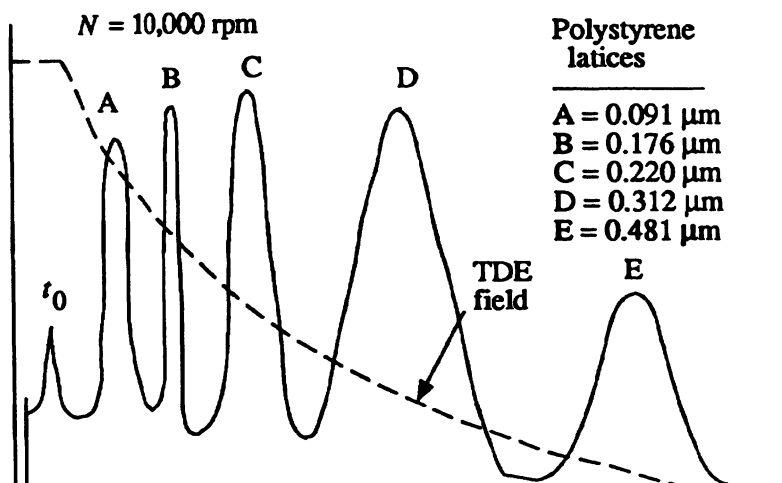


Fig. 5.15 A typical SFFF fractogram.

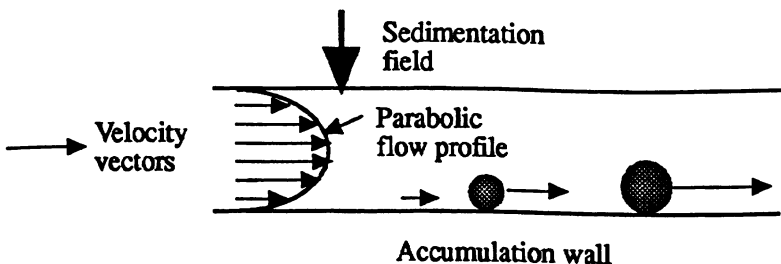


Fig. 5.16 Sedimentation/steric field flow fractionation.

former, because of a packed column system, has less flexibility in the size analysis of broad industrial and biological particle systems, whereas the latter, by virtue of open channel separation, has greater potential.

At low ionic strengths in the eluant, the retention of SFFF deviates from the prediction of standard theory, resulting in an underestimation of particle size due to particle-particle interaction and a modified theory has been proposed [48]. The influence of zone broadening on the measured particle size distribution has also been investigated [49].

5.15.3 Thermal field flow fractionation

In thermal field flow fractionation (TFFF) a temperature gradient is applied. The primary potential advantage of this technique is that it can be used to size particles in the range 0.01 μm to 0.001 μm , an order of magnitude smaller than SFFF.

Fractionation market a TFFF polymer fractionator channel module with 286/16 MHz IBM compatible PC, super VGA color monitor workstation to include data acquisition software, hardware and data analysis software. A linear UV detector and single channel high performance pump are optional.

5.15.4 Magnetic field flow fractionation

In magnetic field flow fractionation the separation depends upon how strongly particles are attracted to one pole of a magnet [50].

5.15.5 Flow field flow fractionation

When a simple cross-flow of carrier liquid is used, the method is known as flow FFF and this has been represented as having the widest range of application of any single FFF technique [51,52].

This technique has been used to separate and characterize particles in the 0.01 to 50 μm size range, using the normal mode for the size range 0.01 to 2 μm and a steric-hyperlayer mode for particles larger than 0.3 μm [40].

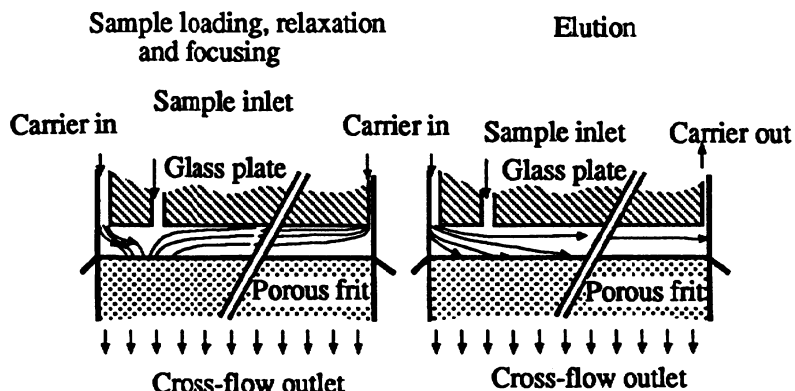


Fig. 5.17 Asymmetrical channel for flow field fractionation.

In this method the sample flow is perpendicular to the flow of the mobile phase [53]. This is accomplished in a rectangular channel of which one or both walls is a semi-permeable membrane so that solvent can flow through the membranes but particles are retained within the channel. Alternatively a narrow tubular porous channel can be used [54]. The remainder of the apparatus is similar to that described above. A more advantageous design [55] is shown in Figure 5.17, in which a single membrane is used as the accumulation wall and a flat glass plate is used at the top of the channel. The force field is created by flow through the bottom membrane. The mobile phase is introduced at one end and, due to loss of solvent through the porous frit, the liquid velocity decreases as it proceeds down the channel thus generating an asymmetrical velocity profile. A range of particle sizes from 10 to 1000 nm can be characterized in 0.5 to 1 hour [56] but the equipment is not yet commercially available.

In an evaluation of these two techniques, to measure the particle size of paint components having a broad size range, Schauer [57] states that they each have their own merits. In the case of symmetrical FFF, the set-up for the channel flow and cross-flow is simpler, thinner channels can be used and the distinct fractionation in the steric hyperlayer can be achieved. The characteristics of asymmetrical FFF are the simpler construction of the fractionating channel, the superior focusing and the minimization of zone broadening in the channel. Of the two he prefers the latter.

5.15.6 Steric field flow fractionation

When particle diameters reach the layer thickness the zone as a whole will sample faster flow lines and the particle velocities will depend on how far they extend into the faster flow lines. The elution order

becomes reversed under these circumstances and the larger particles elute first. Because the particle extends through liquid layers of different velocities, a lift force operates to raise the particles into the higher velocity streamlines. The first SFFF separations took place in flat horizontal channels with gravity as the field [58,59] and dense particles tended to be retained (Figure 5.16). Fractionation time is reduced by centrifugation; by performing the fractionation in channels spun to a field of 15 times gravity, the lift forces generated by very high channel flows could be offset by the increased settling forces.

5.16 The Matec electroacoustic system EAS-8000

It has long been recognized that dispersion properties can be a strong function of particle concentration and there is an increasing interest in obtaining direct analysis of particle size and zeta potential in non-dilute systems. The EAS-8000 measures the electrokinetic properties of concentrated dispersions and the Acoustosizer measures particle size and zeta potential over a wide concentration range. The ESA is used for routine characterization, as an aid in the preparation of high solids dispersions for coatings and castings and for characterizing non-aqueous liquid toners used in electrostatic imaging.

5.17 Continuous split fractionation

A split-flow separation cell is a thin (generally sub-millimeter) rectangular channel in which various physical forces are utilized to drive components across the thin dimension of the channel, generally from one major wall towards the opposite wall [60,61]. At the same time, a film of fluid flowing lengthwise through the channel causes the rapid displacement of entrained components. By positioning a flow splitter at the downstream end of the channel, the suspended material can be separated into two substreams containing particles of different sizes. The separation process is characterized by a high resolving power, a high speed, a relatively simple theoretical description, and a great deal of versatility resulting from the large variety of driving forces and flow configurations that can be used. The methodology differs from field flow fractionation (FFF) in that it can be used for continuous split fractionation (CSF) whereas FFF is limited to batch operations. A comparison between the two techniques has been published [62,63].

A number of different driving forces have been used to implement CSF including gravitational sedimentation [64], diffusive transport [65,66], electrically driven transport [67] and hydrodynamic lift forces [68].

The concept of utilizing hydrodynamic lift forces in the transport mode is illustrated in Figure 5.18. This figure represents the relevant features of separation viewed from one edge of the channel. The

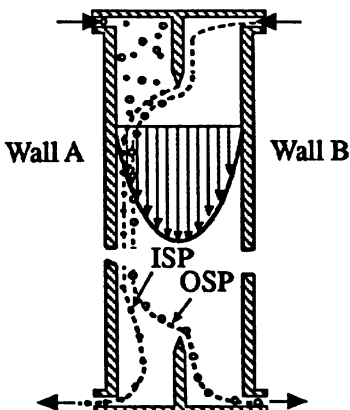


Fig. 5.18 Edge view of split cell. Carrier flow is in the downward direction. A representation of the parabolic velocity profile across the cell thickness, and the position of the inlet and outlet splitting planes (ISP and OSP) are shown.

system is characterized by an inlet splitter that serves to compress the incoming feed particles into a narrow band near wall A. The thin particle-containing lamina formed just beyond the inlet splitter is subject to loss of material by various transport processes including sedimentation, diffusion and lift forces. The first can be eliminated by turning the channel on one end and the second is negligible for particles larger than about a micron. Large particles are driven more rapidly from wall A than small particles by lift forces. A full description of the procedure may be found in [66], where its use is described for classifying polystyrene particles in the 1 to 60 μm size range together with separation of red blood cells from serum. Typically cells have dimensions 330 μm thickness, 2 cm breadth and lengths from 2 to 10 cm.

5.18 Classification by decantation

In this method a homogeneous suspension is allowed to settle for a predetermined time. The supernatant liquid is then decanted and replaced by fresh dispersing liquid and the suspension re-agitated. The process is repeated until the supernatant liquid is clear. The decanted liquid will contain only particles smaller than $D = k R(h/t)$ where h is the depth at which the liquid is siphoned off at times t and k is a constant. The process is repeated for shorter times so that the particles removed become progressively coarser. Herdan [69] suggested that six repeats would be sufficient to remove substantially all

the particles smaller than a selected size whilst Allen [70] found that 15 repeats were necessary to produce a clear supernatant.

Consider a vessel containing a depth h_1 of a homogeneous suspension, the siphoning off being at a depth h_2 . No particles coarser than $D = k\sqrt{h_2/t}$ will be removed. Particles of size xD , where $x < 1$, will have fallen a distance h in the same time where :

$$xD = k\sqrt{h/t}$$

Hence from these two equations:

$$x^2 = h/h_2.$$

The fraction F_1 of particles of size xD removed is:

$$F_1 = \frac{(h_2 - h)}{h_1} = (1 - x^2) \frac{h_2}{h_1}$$

The fraction of particles of this size still in suspension will be:

$$1 - F_1 = 1 - (1 - x^2) \frac{h_2}{h_1}$$

If the suspension is made up to its original volume, redispersed and a second fraction removed after a further time t , the fraction of particles of size xD removed will be:

$$F_2 = (1 - x^2) \frac{h_2}{h_1} \left[1 - \frac{h_2}{h_1} (1 - x^2) \right]$$

The fraction of these particles remaining in suspension will be:

$$1 - F_1 = \left[1 - \frac{h_2}{h_1} (1 - x^2) \right]^2$$

After n decantings the fraction still in suspension will be:

$$1 - F_1 = \left[1 - \frac{h_2}{h_1} (1 - x^2) \right]^n$$

Therefore, the fraction removed, F_r , is:

$$F_r = 1 - \left[1 - \frac{h_2}{h_1} (1 - x^2) \right]^n \quad (5.18)$$

The effect of the ratio (h_2/h_1) is negligible over a wide range compared with x hence there is little to be gained from making ($h_2 - h_1$) very small with consequent risk of disturbing the solids which have settled out. For example, if (h_2/h_1) is reduced from 0.9 to 0.8, the number of decantings to achieve the same separation will increase from n to m where :

Table 5.2 Reduction in the number of decantings, required to give the same degree of separation, as the ratio of decant height to suspension height increases from 0.8 to 0.9

Relative particle size (x)	0.1	0.2	0.3	0.4	0.5	0.6	0.7	0.8	0.9	0.95
Ratio increase of decants (m/n)	1.41	1.37	1.31	1.27	1.23	1.20	1.17	1.15	1.14	1.13

Table 5.3 Percentage of particles removed after a known number of decantings

Relative particle size	Number of decantings				
	1	2	4	8	16
0.1	89.10	98.81	99.99	100.00	100.00
0.2	86.40	98.15	99.97	100.00	100.00
0.3	81.90	96.72	99.89	100.00	100.00
0.4	75.60	94.05	99.65	100.00	100.00
0.5	67.50	89.44	98.88	99.99	100.00
0.6	57.60	82.02	96.77	99.90	100.00
0.7	45.90	70.73	91.43	99.27	99.99
0.8	32.40	54.30	79.12	95.64	99.81
0.9	17.10	31.28	52.77	77.69	95.02
0.95	8.78	16.78	30.74	52.04	77.00
0.98	3.56	7.00	13.51	25.20	44.05
0.99	1.79	3.55	6.97	13.46	25.11

$$\frac{m}{n} = \frac{\log[1 - 0.9(1 - x^2)]}{\log[1 - 0.8(1 - x^2)]} \quad (5.19)$$

Some values of the number of decantings required to achieve the same separation are presented in Table 5.2 and the percentages of various relative sizes removed are given in Table 5.3 for $h_2/h_1 = 0.9$. A large number of decantings are required to remove particles whose size is near the cut size. Hence the wider the size range of the original suspension, the fewer decantings required. Several descriptions of suitable apparatus have been described [71-74], including a fully automatic system [75].

References

- 1 Weilbacher, M. and Rumpf, H. (1968), *Aufbereit. Technik*, **9**(7), 323-30, 199
- 2 Allen, T. (1990), *Particle Size Measurement*, 4th ed., Chapman & Hall, 199
- 3 Kelsall, D.F. and McAdam, J.C.H. (1963), *Trans. Inst. Chem. Eng.*, **41**, 84, 94, 200
- 4 Leschonski, K., Metzger, K.L. and Schindler, U. (1977), *Proc. Particle Size Analysis Conf.*, ed. M.J. Groves, Chem. Soc., Anal. Div., publ. Heyden, 227-236, 201
- 5 Stein, F. and Corn, M. (1976), *Powder Technol.*, **13**, 133-41, 201
- 6 Lapple, C.E. (1970), Centrifugal Classifier, U.S. Patent 3 491 879, Jan., 202
- 7 Silva, S. de. (1979), Powtech 79, Birmingham, Inst. Chem. Eng. and Specialist Exhibitions Ltd., 202
- 8 Lauer, O. (1969), *Chem. Ing. Tech.*, **41**, 491-6, 202
- 9 Kirkland, J.J. (1990), *Ralph K. Ille Memorial Symposium*, Washington Aug., publ. Am. Chem. Soc. 123, 203
- 10 Ramos, dos, J.G., Mann, R.V. and Silebi, C.A. (1991), *Laboratory Products Technology*, **22**, 203
- 11 Ramos, J.G. dos and Silebi, C.A., (1992), *CHDF Application Note 501*, Matec Applied Sciences, 204
- 12 Small, H. (1974), *J. Colloid Interf. Sci.*, **48**, 147, 204
- 13 McGowan, G.R. and Langhorst, M.A. (1982), *J. Colloid Interf. Sci.*, **89**, 94, 204, 205
- 14 Silebi, C.A. and Ramos, J.G. dos (1989), *J. Colloid Interf. Sci.*, **130**, 4, 204
- 15 Nagy, D.J., Silebi, C.A. and McHugh, A.J. (1978), *ACS Conf., Florida*, 205
- 16 Kirkland, J.J. (1979), *J. Chromatogr.*, **185**(1), 273-288, 206
- 17 Singh, S. and Hamielec, A.E. (1978), *J. Liq. Chromatogr.*, **1**, 187, 206

- 18 Noel, R.J., Goodwin, K.M., Regnier, F.E., Ball, D.M., Orr, C. and Mullins, M.E. (1978), *J. Chromatography*, **166**, 373–383, 206
- 19 Miller, C.M., Venkatesan, J., Silebi, C.A. and Sudoi, E.D. (1994), *J. Colloid Interf. Sci.*, **162**, 11–18, 206
- 20 DiMarzio, E.A. and Guttman, C.M. (1970), *Macromol.*, **3**, 681, 207
- 21 Guttman, C.M. and Di Marzio, E.A. (1970), *Macromol.* **3**, 131, 207
- 22 Silebi, C.A. and Ramos, J.G. dos (1989), *J. Colloid Interf. Sci.*, **130**, 14, 207
- 23 Ramos, J.G. dos and Silebi, C.A. (1989), *J. Colloid Interf. Sci.*, **133**, 302, 207
- 24 Silebi, C.A. and Ramos, J.G. dos (1989), *J. Am. Inst. Chem. Eng.*, **35**, 1351, 207
- 25 Ramos, J.G. dos. and Silebi, C.A. (1990), *J. Colloid Interf. Sci.*, **136**, 3, 207
- 26 Ramos J.G. dos, Jenkins, R.D. and Silebi, C.A. (1991), *Particle Size Distribution II*, ed. T. Provder, Am. Chem. Soc., Am. Chem. Soc. Symp. Series, **472**, 264–278, 207
- 27 Venkatesan, J., Ramos, J.G. dos and Silebi, C.A. (1991), *Particle Size Distribution II*, ed. T. Provder, Am. Chem. Soc. Symp. Series **472**, 279–291, 207
- 28 Ramos, J.G. dos, and Silebi, C.A. (1991), *Particle Size Distribution II*, ed. T. Provder, Am. Chem. Soc. Symposium Series **472**, 292–307, 207
- 29 Miller, C.M., Ventatescan, C.A., Silebi, E.D., Sudal, E.D. and Asser, M.S. el (1984), *J. Colloid Interf. Sci.*, **162**, 11–18, 207
- 30 Jorgenson, J.W. and Lukacs, K.D. (1981), *Anal. Chem.*, **53**, 1298, 207
- 31 McCormick, R.M. (1988), *Anal. Chem.*, **60**, 2322, 207
- 32 Jorgenson, J.W. and Lukacs, K.D. (1981), *Anal. Chem.*, **53**, 3036, 208
- 33 Hocq, S., Milot, J.F., Gourdon, C. and Casamatta, G. (1994), *Chem. Eng. Sci.*, **49**(4), 481–490, 208
- 34 Yau, W.W., Kirkland, J.J. and Bly, D.D. (1979), *Modern Size Exclusion Chromatography*, John Wiley and Sons, Ch12 & 13, 208
- 35 Singh, S. and Hamielec, J. (1978), *J. Liqu. Chromatogr.* **1**, 187, 208
- 36 Kirkland, J.J. (1979), *J. Chromatogr.*, **48**, 273, 208
- 37 Williams, P.S., Moon, M.H. and Giddings, J.C. (1992), *Proc. Conf. PSA '91*, ed. N.G. Stanley-Wood and R. Lines, publ. Royal Soc. Chem., 280–289, 208
- 38 Giddings, J.C., Ratanathanawongs, S.K. and Moon, M.H. (1991), *Kona Powder and Particle*, No 9, 200–277, 209
- 39 Caldwell, K.D. (1984), *Modern Methods of Particle Size Analysis*, ed. H.G. Barth, John Wiley & Sons, 211–250, 209

- 40 Ratanathanawongs, S.K., Lee, I. and Giddings, J.C. (1991), *Particle Size Distribution II*, ed. T. Provder, Am. Chem. Soc. Symposium Series 472, 229–246, 209, 213
- 41 Giddings, J.C., Myers, M.N., Moon, M.H. and Barman, B.N. (1994), *Chem. Eng. Sci.*, 9(4), 481–490, 209
- 42 Giddings, J.C., Yang, F.J. and Myers, M.N. (1974), *Anal. Chem.*, 46, 1917, 210
- 43 Caldwell, K.D., Brimhall, S.L., Gao, Y. and Giddings, J.C. (1988), *J. Appl. Polymer Sci.*, 36, 703, 210
- 44 Kirkland, J.J. (1982), *Science*, 218, 8, 210
- 45 Barman, B.N. and Giddings, J.C. (1991), *Particle Size Distribution II*, ed. T. Provder, Am. Chem. Soc., ACS Symposium series 472, 217–228, 211
- 46 Kirkland, J.J., Yau, W.W., Doerner, W.A. and Grant, J.W. (1980), *J. Colloid Interf. Sci.*, 60, 574, 211
- 47 Kirkland, J.J., Rementer, S.W. and Yau, W.W. (1981), *Anal. Chem.*, 53, 1730, 211
- 48 Mori, Y., Kimura, K. and Tanigaki, M. (1991), *Proc. Second World Congress Particle Technology*, Kyoto, Japan, Part 1, 305–312, 213
- 49 Mori, Y., Kimura, K. and Tanigaki, M. (1992), *Proc. Conf. PSA '91*, ed. N.G. Stanley-Wood and R. Lines, publ. Royal Soc. Chem., 280–289, 213
- 50 Schunk, J. (1984), *Separation Science*, 19(10), 653, 213
- 51 Giddings, J.C. (1981), *Anal. Chem.*, 53, 1170A, 213
- 52 Wahlund, K.G. and Litzen, A. (1989), *J. Chromatogr.*, 461, 73, 213
- 53 Giddings, J.C. (1981), *Anal. Chem.*, 53, 1170A, 214
- 54 Granger, J. and Dodds, J. (1992), *Separation Science and Technol.*, 27(13), 1691–1709, 214
- 55 Wahlund, K.G. and Litzen, A. (1989), *J. Chromatogr.*, 461, 73, 214
- 56 Ratanathanawongs, S.K. and Giddings, J.C. (1993), Am. Chem. Soc. Symp. Ser., 521 (Chromatography of Polymers), 13–29, 214
- 57 Schauer, T. (1995), *6th European Symp. Particle Size Characterization*, Partec 95, Nürnberg, Germany, publ. NürnbergMesse GmbH.157–166, 214
- 58 Giddings, J.C. and Myers, M.N. (1978), *Sep. Sci. Technol.*, 13, 637, 215
- 59 Giddings, J.C., Myers, M.N., Caldwell, K.D. and Pav. J.W. (1979), *Sep. Sci. Technol.*, 14, 935, 215
- 60 Giddings, J.C. (1985), *Sep. Sci. Technol.*, 20, 749–768, 215
- 61 Giddings, J.C. (1988), *Sep. Sci. Technol.*, 23, 931–943, 215
- 62 Giddings, J.C. (1988), *Sep. Sci. Technol.*, 23, 931–943, 215
- 63 Giddings, J.C. (1986), *Chemical Separations*, 1, 3–20, ed. J.D. Navratil and C.J. King, Litarven, Denver, 215

- 64 Springston, S.R., Myers, M.N. and Giddings, J.C. (1985), *Sep. Sci. Technol.*, **20**, 749–768, 215
- 65 Williams, P.S., Levin, S., Lenczycki, T. and Giddings, J.C. (1992), *Ind. Eng. Chem. Res.*, **31**, 2172–2181, 215
- 66 Levin, S. and Giddings, J.C. (1991), *J. Chem. Tech. Biotechnol.*, **50**, 43–56, 215
- 67 Levin, S., Myers, M.N. and Giddings, J.C. (1989), *Sep. Sci. Technol.*, **24**, 1245–1259, 215
- 68 Zhang, J., Williams, P.S., Myers, M.N. and Giddings, J.C. (1994), *Sep. Sci. Technol.*, **29**(18), 2493–2522, 215
- 69 Herdan, G. (1960), *Small Particle Statistics*, Butterworths, 216
- 70 Allen, T. (1960), M.Sc. Thesis, London University, 217
- 71 Truog, E. et al (1936), *Proc. Soil Sci. Soc. Am.*, **1**, 10, 219
- 72 Davies, R.J., Green, R.A. and Donnelly, H.F.E. (1937), *Trans. Ceram. Soc.*, **36**, 181, 219
- 73 Birchfield, H.P., Gullaston, D.K. and McNew, G.L. (1948), *Analyt. Chem.*, **20**, 1168, 219
- 74 Johnson, E.I. and King, J. (1951), *Analyst*, **76**, 66, 219
- 75 Horsfall, F. and Jowett, A. (1960), *J. Scient. Instrum.*, **37**(4), 120, 219

Interaction between particles and fluids

6.1 Introduction

The interaction between particles and fluids is important in many industrial processes. The most relevant size distribution in such cases is, therefore, based on the sedimentation behavior of particles in fluids and the applicable size is the settling or Stokes diameter.

The simplest case to consider is the settling of a single homogeneous sphere, under gravity, in a fluid of infinite extent. Many experiments have been carried out to determine the relationship between settling velocity and particle size under these conditions and a unique relationship between drag factor (C_D) and Reynolds number (Re) has been found which reduces to a simple equation, known as the Stokes equation, at low Reynolds number.

At high velocities the drag increases above that predicted by Stokes' equation, due to the onset of turbulence, and particles settle more slowly than the law predicts. However, settling velocities can be related to particle diameters by applying Newton's equation which is available as an empirical relationship between C_D and Re .

The upper size limit for Stokes' equation is limited, due to the onset of turbulence, to Reynolds number less than 0.25.

Difficulties arise, however, with non-spherical particles which fall in random orientation in the laminar flow region but orientate themselves to give maximum resistance to drag in the turbulent region. Thus, in the laminar flow region a single particle will have a (usually narrow) range of settling velocities depending on its orientation whereas, once the boundary condition is exceeded, the measured size distribution becomes finer in a manner difficult to predict.

After agitation, a finite time is required before the particles commence to settle uniformly, but this is much greater than the time the particles are accelerating to a constant velocity, known as the terminal velocity, under a gravitational force.

If the concentration is monitored at a fixed depth below the surface, for an initially homogeneous suspension, it will remain constant until the largest particle in the suspension has fallen from the surface to the

measurement zone. The concentration will then fall, being at all times proportional to the concentration of particles smaller than the diameter given by Stokes' equation for that particular time and depth of fall.

Samples removed from this depth should not contain particles with diameters larger than the Stokes diameter. In practice this is not true, due to particle-particle interaction: pairs of equally sized spheres, for example, falling in close proximity will interfere with each other and fall with a different velocity to that predicted by Stokes' equation. For unequally sized particles the situation is more complex; the larger particle may actually pick up the smaller one so that it revolves round the larger one like a satellite. Assemblies of particles tend to diverge due to the rotation effect caused by the greater velocity of the streamlines on the envelope of the assembly. A cluster of particles may act as a single large particle of appropriate density and reduced rigidity and have a much greater velocity than that of the particles of which it is composed.

Interactions between particles are usually negligible provided the concentration is low. It is usually recommended that the volume concentration be less than 0.2%; if it is necessary to use a higher concentration it should be established that the measured size distribution is no finer than that obtained at the lower concentration.

At volume concentrations as low as 1% the suspension may settle *en masse* and the rate of fall of the interface gives an average size for the particles using a modified Stokes equation which is very similar to the permeametry equation for a fluid passing through a fixed bed of powder. This is in fact an analogous system in which a moving bed of particles is settling through a stationary liquid.

Settling velocities are also reduced due to the proximity of container walls, though this effect is usually quite small.

As particle size decreases, the particles move in a random manner due to molecular bombardment (Brownian or thermal diffusion) to give a variable settling rate for particles of the same size. Indeed, a proportion of the particles will actually rise during a time interval, although the concentration at a fixed depth will fall.

Impressed on this effect there are convection currents which may be set up by surface evaporation or temperature fluctuations. All sedimenting systems are basically unstable, due to the preferred paths up the sedimentation tank by the fluid displaced by the settling particles. This fluid tends to rise up the walls of the containing vessel, carrying with it some of the finer particles, and dissipate itself as convection currents at the top of the sedimentation column. This leads to an overestimation of the fines percentage in an analysis. For these reasons, for accurate analyses below about a micron, centrifugal techniques should be used.

Correction for the finite extent of the fluid is negligible in most cases and errors due to discontinuities in the fluid are only of importance for gas systems. Similarly the increased viscosity of a

suspension over that of a pure liquid has negligible effects at low concentrations. Reproducible data are possible at high Reynolds numbers, high concentrations and with sub-micron particles. These data may be highly inaccurate and in general precise values of erroneous sizes and percentage undersize are of limited worth.

6.2 Settling of a single homogeneous sphere under a gravitational force

6.2.1 Relationship between settling velocity and particle size

When a particle falls under gravity in a viscous fluid it is acted upon by three forces; a gravitational force W acting downwards; a buoyant force U acting upwards and a drag force F_D acting upwards. The resulting equation of motion is:

$$mg - m'g - F_D = m \frac{du}{dt} \quad (6.1)$$

where m is the mass of the particle, m' is the mass of the same volume of fluid, u is the particle velocity and g is the acceleration due to gravity.

Small particles accelerate rapidly to a constant or terminal velocity ($du/dt = 0$) and the drag force is balanced by the motive force. For a sphere of diameter D and density ρ_s falling in a fluid of density ρ_f , the equation of motion becomes:

$$F_D = mg - m'g$$

$$F_D = \frac{\pi}{6} (\rho_s - \rho_f) g D^3 \quad (6.2)$$

but, by definition:

$$C_D = \frac{\text{drag force}}{\text{cross-sectional area of the sphere} \times \text{dynamic pressure on the particle}}$$

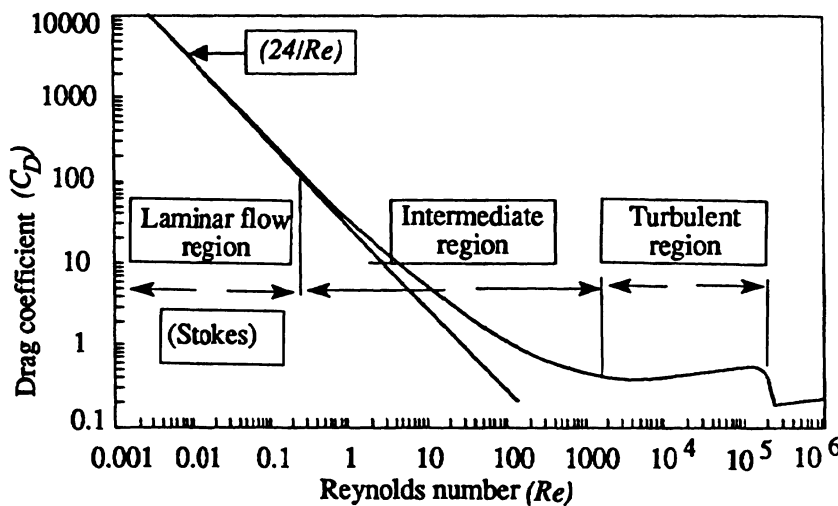
$$F_D = C_D \times \frac{\pi D^2}{4} \times \frac{\rho_f u^2}{2} \quad (6.3)$$

Combining equations (6.2) and (6.3) gives:

$$C_D = \frac{4}{3} \frac{(\rho_s - \rho_f)}{\rho_f} \frac{g D}{u^2} \quad (6.4)$$

Table 6.1 The experimental relationship between drag coefficient and Reynolds number for a sphere settling in a liquid [1].

<i>Re</i>	<i>CD</i>	<i>Re</i>	<i>CD</i>	<i>Re</i>	<i>CD</i>
0.01	2400	2	15	2 000	0.420
0.02	1200	5	7.12	5 000	0.410
0.05	484	10	4.35	10 000	0.420
0.08	304	20	2.74	20 000	0.450
0.10	244	50	1.56	50 000	0.480
0.20	123	100	1.10	100 000	0.480
0.50	51.4	200	0.808	200 000	0.440
0.80	33.3	500	0.568	500 000	0.200
1.00	27.2	1000	0.460	800 000	0.220

**Fig. 6.1** Experimental relationship between drag coefficient and Reynolds number for a sphere settling in a liquid.

Dimensionless analysis of the general problem of particle motion under equilibrium conditions gives a unique relationship between two dimensionless groups, drag coefficient (C_D) and Reynolds number (Re) where:

$$Re = \frac{\rho_f u D}{\eta} \quad (6.5)$$

and η is the viscosity of the fluid (Table 6.1).

The experimental relationship, for spheres, between the Reynolds number and the drag coefficient is shown in Figure 6.1. The graph is divided into three regions; a laminar flow or Stokes region, an intermediate region and a turbulent flow or Newton region. In the laminar flow region the drag on the particle is due entirely to viscous forces within the fluid. As the Reynolds number increases, eddies build up behind the particle thus increasing the drag. Further increase in Reynolds number leads to fully turbulent motion.

6.2.2 Calculation of particle size in the laminar flow region

From Figure 6.1 it can be seen that, as the Reynolds number approaches zero, $C_D Re$ approaches 24, i.e. in the limit:

$$C_D = \frac{24}{Re} \quad (6.6)$$

Combining equation (6.3), (6.5) and (6.6) gives, for low Reynolds numbers:

$$F_D = 3\pi D \eta u \quad (6.7)$$

Inserting equation (6.7) in equation (6.2) gives the relationship between the particle diameter and its Stokes velocity:

$$D = \sqrt{\frac{18\eta u_{St}}{(\rho_s - \rho_f)g}} \quad (6.8)$$

where u_{St} is the terminal velocity for a sphere of diameter D in the laminar flow region.

Terminal velocities will be about 3.5% higher than predicted by Stokes' equation at $Re = 0.25$ and the derived diameter will be 1.7% smaller than the physical diameter. This difference will increase with increasing Reynolds number.

The assumptions made in the derivation of Stokes' law are:

- the particle must be spherical, smooth and rigid and there must be no slip between it and the fluid;
- the particle must move as it would in a fluid of infinite extent;
- the terminal velocity must have been reached;
- the settling velocity must be low so that inertia effects are negligible;
- the fluid must be homogeneous compared with the size of the particle.

6.3 Size limits for gravity sedimentation

The upper size limit by gravity sedimentation is fixed by the unreliability of measurements taken in the first 30 s of the analysis and by the breakdown in Stokes' law due to the onset of turbulence; the extent of this breakdown is well documented. The lower size limit is due to diffusional broadening (or Brownian diffusion) and is a matter of some debate. This diffusion is due to bombardment by fluid molecules which causes the particles to move about in a random manner with displacements in all directions, which ultimately exceed the displacements due to gravity. Brownian motion is not the only limiting criterion. Gravity sedimentation is inherently unstable, due to factors such as return flow and vibration, so should be used with caution for very fine powders.

6.3.1 Upper size limit

Stokes equation is usually considered valid for Reynolds numbers less than 0.25 and the correction term is neglected. Combining equations (6.5) and (6.8) and applying the condition that $Re = 0.25$ gives the upper size limit (upper critical diameter D_{uc})

$$D_{uc} = \left[\frac{4.5\eta^2}{\rho_f g(\rho_s - \rho_f)} \right]^{1/3} \quad (6.9)$$

For example, for silica ($\rho_s = 2500 \text{ kg m}^{-3}$) sedimenting in water ($\rho_f = 1000 \text{ kg m}^{-3}$, $\eta = 0.001 \text{ Pa s}$, $g = 9.81 \text{ m s}^{-2}$) the upper size limit is about 67.4 μm . The upper size limit for silica settling in air is about 33 μm .

More accurately, the following relationship is an empirical fit to experimental data for spherical particles, between drag coefficient and Reynolds number for Reynolds number between 0.01 and 1.0:

$$C_D = \frac{24}{Re} [0.998 + 0.15Re - 0.013Re^2] \quad (6.10)$$

The resultant errors at Reynolds numbers of 0.25 and 1.0 are given in Table 6.2 where % error is defined as $100[(D - D_{St})/D]$.

Since C_D and Re are functions of the two variables u and D , it is necessary to derive relationships which are functions of only one of these variables. $C_D Re^2$ is a function of D and Re/C_D is a function of u . C_D is determined using equation (6.10) so that $C_D Re^2$ and Re/C_D can be calculated. From these calculated values u and D are determined for the case of silica under the conditions quoted above, i.e. a spherical

Table 6.2 Differences between Stokes diameter (d_{St}) and true diameter for a sphere of diameter (D) at two values of Reynolds number

Re	CD	$CD Re^2$	Re/CD	D (μm)	(mm s^{-1})	d_{St} (μm)	u_{St} (mm s^{-1})	% Error
0.25	99.33	6.208	0.0025	68.14	3.67	66.99	3.80	1.69
1.00	27.24	27.240	0.0367	111.6	8.96	104.7	10.17	6.16

silica particle of diameter 68.14 μm will settle, under the conditions under consideration here and $Re = 0.25$, with a velocity of 3.67 mm s^{-1} instead of the 3.80 mm s^{-1} derived using Stokes' equation. Applying Stokes' equation, the Stokes diameter is 66.99 μm , an undersizing of 1.69%.

For $Re = 1$, sometimes quoted as the upper limit for the application of Stokes equation, a silica sphere of diameter 111.6 μm will settle with a velocity of 8.96 mm s^{-1} rather than the 10.17 mm s^{-1} obtained using Stokes equation; this will give a Stokes diameter of 104.7 μm and an undersizing of 6.16%. The effect is greater for non-spherical particles since they settle with random orientation in the laminar flow region but orientate to give maximum drag in the turbulent flow region.

The time required for a particle to reach its terminal velocity is negligible but excessively short sedimentation times should be avoided since concentration measurements fluctuate, due to the initial agitation, up to a time of about 30 s.

6.3.2 Lower size limit

Stokes' law breaks down for very small particles settling under gravity due to diffusional broadening (or Brownian diffusion). This diffusion is due to bombardment by fluid molecules, which causes the particles to move about in a random manner with displacements, in all directions, which ultimately exceed the displacement due to gravity settling.

The equations to quantify this effect were developed by Mason and Weaver [2] in 1924. For monosize distributions Brownian motion leads to broadened measured distributions [3] but the effect is reduced as the width of the distribution increases [4,5]. Chung and Hogg [6] carried out theoretical and experimental studies of clay particles using centrifugal and gravitational sedimentation. Agreement between theory and practice was not too good.

The root mean square displacement due to Brownian motion in the time interval t is [7, p. 412]:

$$\left| \Delta h_{diff}^2 \right| = \frac{2kTt}{3\pi\eta D} \quad (6.11)$$

where k is the Boltzmann constant ($1.3806 \times 10^{-23} \text{ J K}^{-1}$).

Thus the root mean square displacement in 1 s for a particle settling in water at an absolute temperature 300 K is 0.938 μm ; this is almost the same as the distance settled by a quartz particle (density 2650 kg m^{-3}) in 1 s (0.90 μm). A comparison of Brownian movement displacement and gravitational settling displacement is given by Fuchs [8].

For a size determination to be meaningful the displacement of the particles due to Brownian diffusion must be much smaller than their displacement due to gravity, hence the condition:

$$|\Delta h_{\text{diff}}| \ll h^2 \quad \eta_1 \ll \eta_2 \quad (6.12)$$

where h equals $u_{St}t$, so that, in combination with Stokes equation [Equation (6.8)]:

$$D_{\min}^5 \gg \frac{216}{\pi} \frac{kT\eta}{(\rho_s - \rho_f)^2 g^2 t} \quad (6.13)$$

or:

$$D_{\min}^3 \gg \frac{12}{\pi} \frac{kT}{(\rho_s - \rho_f)gh} \quad (6.14)$$

Thus, the lower size limit increases if the analysis time is reduced or the measurement height is decreased. A corollary to this is that analyses at different scan speeds will give different results. The measured distributions for monodisperse powders will be broadened, the effect increasing as the measurement time is reduced [9].

For an estimate of the lower size limit, the displacement of the smallest particle by Brownian diffusion should be at least ten times smaller than its settling distance [10]. Other criteria could be selected since the error is both a function of the size and the spread of the distribution; it is reasonable however, for the sake of simplicity, to stipulate that if more than 10% of the distribution is smaller than the lower size limit, gravitational sedimentation should not be used.

Correspondingly, equations (6.13 and 6.14) take the equality sign and their right hand sides are multiplied by 100: Equation (6.13) becomes:

$$D_{\min}^5 = 100 \frac{216}{\pi} \frac{kT\eta}{(\rho_s - \rho_f)^2 g^2 t} \quad (6.15)$$

For quartz and a run time of 30 min, $t = 1800$ s and $D_{\min} = 0.58 \mu\text{m}$: For a run time of 15 min, $t = 1800$ s and $D_{\min} = 0.66 \mu\text{m}$.

These values are much lower than those quoted in national standards (BS 3406 Part 2:1984, DIN 66111:1983, AFNOR, ASTM) which vary from 1 to 3 μm . However the calculated values are for the 10% undersize value rather than a higher valued 'average' size.

Example: For quartz particles settling in water:

$$\rho_s = 2500 \text{ kg m}^{-3}$$

Hence, in meters:

$$\rho_f = 1000 \text{ kg m}^{-3}$$

$$k = 1.38 \times 10^{-23} \text{ J K}^{-1}$$

$$T = 300 \text{ K}$$

$$D_{\min} = \frac{2.59 \times 10^{-6}}{\sqrt[5]{t}}$$

$$g = 9.81 \text{ m s}^{-2}$$

$$\eta = 8.905 \times 10^{-4} \text{ Pa s}$$

One common way of monitoring the changing concentration in a settling suspension is to scan upwards, from far below the top of the sedimentation column. Assuming the initial reading is taken at a depth of 2.5 cm at time $t = 10$ seconds, the maximum size, from Stokes equation, is 52.2 μm . Assuming a beam width of 100 μm , Heywood's criterion [1] is that the final measurement depth must be at least 0.7 μm . The logarithmic relationship between measurement height and time, using the above boundary conditions is:

For a scan time of 30 min

$$h = 0.0330 - 0.0080 \log(t) \quad (6.16)$$

and, for a scan time of 15 min:

$$h = 0.0342 - 0.0092 \log(t) \quad (6.17)$$

This hyperbolic scan compresses small diameters into shorter times, to give similar resolutions at all heights, hence is the preferred scanning procedure.

For sub-micron powders and monomodal log-normal parent distributions, calculations indicate that the measured distributions would be bimodal log-normal and broadened, i.e. indicating an excess of coarse as well as an excess of fines [11]. The error increases with decreasing size and decreasing spread (geometric standard deviation). The effect for a powder with a density of 4250 kg m^{-3} , a geometric mean of 0.228 μm and a geometric standard deviation of 1.30, is an excess of 13% at the 10% level and 10% at the 90% level. Brownian motion is normally negligible when compared with even the most

feeble convection currents [12, p. 16] and this further limits the smallest size at which gravitational sedimentation gives meaningful results.

Muta and Watanabe [13] examined samples extracted during Andreasen analyses and detected particles of 1 μm , for example, when Stokes' equation predicted a maximum size of 0.89 μm . They concluded that gravitational Andreasen sedimentation analysis was unsuitable for powders of wide size range containing sub-micron particles. They surmised that this may be due to re-distribution of fine particles caused by disturbance to the suspension in the course of long term sedimentation.

Allen [14] reported the presence of convection currents which appeared in sedimenting suspensions. He concluded that these were caused by a basic instability in sedimenting suspensions which determines the lower size for which gravitational sedimentation could be used. The liquid displaced by the sedimenting particles tended to flow towards the surface up the sides of the walls and stirrer. This he attributed to the lower velocity of particles near such vertical surfaces which generated a radial pressure gradient, causing the particles to rotate in such a way to cause such a flow. The effect is most apparent when there are large particles together with fines. The large particles initiated a return flow of about 15 $\mu\text{m s}^{-1}$, and particles in the vicinity of the walls, having a velocity smaller than this, are entrained and carried towards the surface.

Allen and Baudet [15] compared several centrifugal techniques with the Andreasen and the Sedigraph x-ray sedimentometer. As an example, for kaolinite, the centrifugal techniques gave the percentage smaller than 0.2 μm as 31 to 36.6; the Andreasen gave 48; the Sedigraph gave 80. The high percentage of fines as given by the Andreasen was attributed to the long settling times required. In the Sedigraph high concentrations were required, since the material is a poor x-ray absorber, and the high concentrations resulted in hindered settling. Other cases are known where Andreasen results are comparable with centrifugal results. For example, for quartz particles of size range 0.2 to 0.8 μm , the author has found that the Andreasen results, using a volume concentration of 0.2%, agree with pipette centrifuge results.

6.4 Time for terminal velocity to be attained

For laminar settling, equation (6.1) may be written:

$$\frac{\pi}{6}(\rho_s - \rho_f)gD^3 - 3\pi\eta Du = \frac{\pi}{6}\rho_s d^3 \frac{du}{dt} \quad (6.18)$$

Simplifying by putting $\rho = \frac{(\rho_s - \rho_f)}{\rho_s}$ and $X = \frac{18\eta}{\rho_s D^2}$

$$\frac{du}{dt} = \rho g - Xu$$

$$\int_0^t \frac{du}{(\rho g - Xu)} = \int_0^t dt$$

$$u = \frac{\rho g}{X} [1 - \exp(-Xt)] \quad (6.19)$$

As t approaches infinity, u approaches the Stokes velocity $u_{St} = \frac{\rho g}{X}$ as given in equation (6.8).

Theoretically a particle never reaches its terminal velocity but for practical purposes it can be assumed that the velocity is sufficiently near the terminal velocity for the error to be neglected. From equation (6.19) the velocity is 0.99 the terminal velocity when:

$$1 - \exp(-Xt) = 0.99$$

$$Xt = \ln(100)$$

$$t = \frac{4.6\rho D^2}{18\eta} \quad (6.20)$$

For spheres of density 2650 kg m^{-3} , in water $\eta = 0.001 \text{ Pa s}$ and in air $\eta = 18 \times 10^{-6} \text{ Pas}$, the times taken to reach 99% of the terminal velocity for particles of different diameters are shown in Table 6.3. From Table 6.3 it can be seen that the assumption that a particle from rest reaches its terminal velocity instantaneously does not introduce any appreciable errors.

The distance covered, h , during the acceleration time is given by integration of equation (6.19):

$$\int_0^h dh = u_{St} \int_0^t [1 - \exp(-Xt)] dt$$

Table 6.3 Time for particles to reach 99% of their terminal velocities

Diameter (μm)	Time (ms)	
	Water	Air
5	0.017	0.94
10	0.068	3.76
50	1.693	94.06

$$h = u_{St} t \left(1 - \frac{1}{Xt} [1 - \exp(-Xt)] \right) \quad (6.21)$$

At 99% of the terminal velocity $[1 - \exp(-Xt)] = 0.99$ as before and $Xt = 4.6$ making

$$h = 0.785 u_{St} t$$

Since t is very small, the distance fallen in achieving a velocity equal to 0.99 times the settling velocity is also very small at low Reynolds numbers.

6.5 Wall effects

When the fluid is contained in a vessel, the fluid streamlines about the particle impinge on the walls and reflect back on to the particle causing increased drag; also, since the fluid is stationary at the vessel walls, there is a distortion of the flow pattern which reacts back on the particle. Both effects increase the drag on the particle, leading to a low estimate of particle size. The modified form of equation (6.7) [16]:

$$F_D = 3\pi d \eta u \left(1 + k \frac{D}{L} \right) \quad (6.22)$$

where L is the distance from the center of the particle to the walls of the containing vessel.

For a single wall $k = 0.563$, for two walls $k = 1.004$ and for a circular cylinder $k = 2.104$. Each extra wall increases the drag by an approximately equal amount, thus the effect on a sphere in a cylinder is much the same over a large part of the central area.

Replacing equation (6.7) by equation (6.22) modifies Stokes' equation to give:

$$D = D_{St} \left(1 + k \frac{d}{L} \right)^{0.5} \quad (6.23)$$

where D is the true diameter of the spherical particle and D_{St} the diameter obtained using the unmodified Stokes equation. For a $100 \mu\text{m}$ sphere settling in a 0.5 cm diameter container ($L = 0.25 \text{ cm}$) the error in particle size is given by:

$$D = D_{St} \left(1 + 2.104 \frac{100 \times 10^{-6}}{0.25 \times 10^{-2}} \right)^{0.5}$$

$D = 1.041 D_{St}$, an error of 4%.

A sphere moving near a vertical wall will rotate, as if it were rolling on the wall, at an angular velocity given by [10]:

$$\omega = \frac{3u}{2D} \left(\frac{D}{L} \right)^4 \left(1 - \frac{3D}{4L} \right) \quad (6.24)$$

The modified form of equation (6.10) due to the bottom of the container is:

$$F_D = 3\pi d \eta u \left(1 + \frac{9}{16} \frac{D}{L} \right) \quad (6.25)$$

The correction term is negligible at a distance greater than 1000 diameters from the bottom and small (0.6%) for a distance of 50 diameters.

6.6 Errors due to discontinuity of the fluid

The drag factor needs to be modified, for particles settling in a gas, to take account of the molecular nature of the gas. At low pressures, if the mean free path of the gas molecules (λ) is much greater than the size of the particles, the resistance to particle motion is due to molecular bombardment by individual molecules acting independently. This is much smaller than the Stokes drag leading to increased velocity:

$$u = u_{St} \frac{4.49\lambda}{BD} \quad (6.26)$$

where B depends on the nature of the molecular reflections and lies between 1 and 1.4 [17].

At high pressures, for particles much larger than λ , the discontinuity effect gives rise to 'slip' between the particle and the gas leading to the following modification to the Stokes velocity:

$$u = u_{St} \left[1 + \frac{2\lambda}{D} \frac{(2-f)}{f} \right] \quad (6.27)$$

where f , the fraction of molecules undergoing diffuse reflection at the particle surface, is of the order of 0.9.

Cunningham [18] introduced a correction for slip of the form:

$$u = u_{St} \left[1 + \frac{2A\lambda}{D} \right] \quad (6.28)$$

where A is approximately equal to unity. Experimental data, analyzed by Davies [19], gave the more accurate empirical equation:

$$u = u_{St} \left\{ 1 + \frac{\lambda}{D} \left[2.514 + 0.800 \exp \left(-0.55 \frac{D}{\lambda} \right) \right] \right\} \quad (6.29)$$

For air at 20°C and a pressure of 1 atmosphere, $\lambda = 6.62 \times 10^{-8}$ m.

With d in μm , equation (6.29) becomes:

$$u = u_{St} \left\{ 1 + \frac{1}{D} [0.1663 + 0.0530 \exp(-8.31D)] \right\} \quad (6.30)$$

Lapple [20] gives the following values of $2A\lambda/D$ for spherical particles in air at a temperature of 21°C:

D (μm)	0.1	0.25	0.5	1.0	10.0
$2A\lambda/D$	1.88	0.68	0.33	0.16	0.016

The correction is only of importance for sedimentation in a gas.

6.7 Viscosity of a suspension

When discrete particles are present in a fluid, they cannot take part in any deformation the fluid may undergo, and the result is an increased resistance to shear. Thus, a suspension exhibits a greater resistance to shear than a pure fluid. This effect is expressed as an equivalent viscosity of a suspension. As the concentration of solids increases, so the viscosity increases. Einstein [21] deduced the equation:

$$\eta_T = \eta(1 + kc) \quad (6.31)$$

where η is the viscosity of the fluid, η_T the viscosity of the suspension, c the volume concentration of solids and k a constant which equals 2.5 for rigid, inertialess, spherical particles.

The equation is found to hold for very dilute suspensions but requires modification for c greater than 1%. In the very dilute suspensions used in sedimentation analysis, the effect is smaller than errors inherent in the determination of η by conventional methods.

6.8 Non-rigid spheres

Non-rigid particles, e.g. liquid droplets, will deform in such a way that the drag will be reduced. The diameter calculated from the terminal velocity d_{St} will therefore be less than the true diameter D . It has been shown that the drag is:

$$F_D = 3\pi D \eta_2 u \left(\frac{3\eta_1 + 2\eta_2}{3\eta_1 + 3\eta_2} \right) \quad (6.32)$$

where η_1 and η_2 are the viscosities of the drop and fluid respectively.

For the case of a gaseous bubble rising slowly through a liquid, in the laminar flow region and $\eta_1 \ll \eta_2$.

$$F_D = 2\pi D \eta_2 u \quad (6.33)$$

This is identical to the drag force on a solid sphere at whose surface perfect slip occurs.

Comparing with Stokes' equation gives, for a droplet of diameter D :

$$d_{St} = D \sqrt{\frac{3\eta_1 + 3\eta_2}{3\eta_1 + 2\eta_2}} \quad (6.34)$$

For a raindrop falling in air; $\eta_1 = 10^{-3}$ Pa s ; $\eta_2 = 0.180 \times 10^{-3}$ Pa s making $d_{St} = 1.04D$.

Experimentally, small bubbles behave like solid spheres having terminal velocities closely approaching Stokes' which according to Levich may be attributed to impurities at the interface.

6.9 Non-spherical particles

6.9.1 Stokes region

Homogeneous symmetrical particles can take up any orientation as they settle slowly in a fluid of infinite extent. Spin-free terminal states are attainable in all orientations for ellipsoids of uniform density and bodies of revolution with fore and aft symmetry, but the terminal velocities will depend on their orientation. A set of identical particles will, therefore, have a range of settling velocities according to their orientation. This range is fairly limited [22], being less than 2:1, for discs and cylinders having length: diameter ratios up to 10:1.

Particles which are symmetrical in the sense that the form of the body is similarly related to each of three mutually perpendicular co-ordinate planes, as, for example, a sphere or a cuboid, not only fall stably in any orientation but fall with the same velocity in any orientation. An orienting force exists for less symmetrical particles.

Asymmetric particles, such as ellipsoids or discs, do not generally fall vertically, but tend to drift to the side. Thin, flat, triangular laminae fall edgewise unless equilateral. Few particles possess high symmetry and small local features exert an orienting influence.

Not all bodies are capable of attaining steady motion; with unsymmetrical bodies spiraling and wobbling may occur. For an

oblate spheroid [12, p. 144] of eccentricity ϵ and equatorial diameter a , the maximum drag force is:

$$F_D = 3\pi a \eta (1 + 0.2\epsilon) u \text{ for } \epsilon \text{ tending to 0} \quad (6.35)$$

For a sphere of equal volume to the above oblate spheroid

$$F_D = 3\pi a \eta (1 + 0.33\epsilon) u \quad (6.36)$$

Hence a sphere of equal volume has a smaller resistance than the spheroid; the same is also true for a sphere of equal surface.

A prolate spheroid, settling with its axis of revolution parallel to the direction of motion, behaves as a long thin rod when the major diameter a greatly exceeds the equatorial diameter [7, p. 156]. For this limiting case:

$$F_D = \frac{2\pi a \eta u}{(\ln(a/b) + 0.1935)} \quad (6.37)$$

Because of the logarithmic term the drag changes but slowly with the ratio of major to minor axes.

A thin circular disc of diameter a , thickness b , will have both a horizontal (u_h) and a vertical velocity (u_v) component with an angle (ϕ) between the normal to the plane of the disc and the vertical (Figure 6.2).

$$u_h = \frac{\pi abg \Delta\rho}{128 \eta} \sin 2\phi \quad (6.38)$$

$$u_v = \frac{\pi abg \Delta\rho}{128 \eta} (5 - \cos 2\phi) \quad (6.38)$$

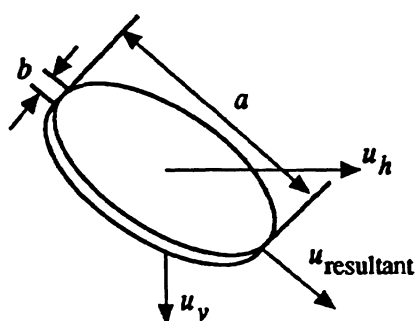


Fig. 6.2 Direction of motion of a disc settling in a fluid.

If β is the angle between the downward vertical and ϕ the direction of motion of the disc then:

$$\tan \beta = \frac{\sin 2\phi}{5 - \cos 2\phi}$$

This angle is a maximum when the disc orientation is $\phi = 39.2^\circ$, $\beta = 11.5^\circ$ corresponding to a maximum ratio of horizontal to vertical velocities of 0.204.

When $\phi = 0^\circ$, the disc will fall with its face horizontal and the drag force will be:

$$F_D = 8a\eta u \quad (6.39)$$

When $\phi = 90^\circ$, the disc will fall with its face horizontal and the drag force will be:

$$F_D = \frac{16}{3}a\eta u. \quad (6.40)$$

Averaging over all orientations:

$$F_D = 6a\eta u. \quad (6.41)$$

Thus, if the average Stokes diameter is taken as unity the measured diameter range will be from 0.94 to 1.15. With $b = 0.1a$, the values of the constants change only slightly (e.g. the constant in equation (6.39) changes from 8 by 0.4%).

Pettyjohn and Christiansen [23] made an extensive experimental study of isometric particles and proposed the following relationship:

$$d_{St}^2 = \left(0.843 \log \frac{\varphi}{0.065} \right) d_v^2 \quad (6.42)$$

where, the sphericity, is the ratio of the surface area of a sphere of the same volume as the particle to the surface area of the particle:

$$\varphi^2 = d_v^2 / d_s^2 \quad (6.43)$$

Hawksley [17] showed that this was equivalent to stating that the drag diameter closely approximates the surface diameter.

For non-spherical particles, equation (6.3) becomes:

$$F_D = C_D \left(\frac{\pi d_d^2}{4} \right) \left(\frac{\rho_f u^2}{2} \right) \quad (6.44)$$

where d_d , the drag diameter, is the diameter of the cross-sectional area of the particle perpendicular to the direction of motion. The modified form of equation (6.2) is:

$$F_D = \frac{\pi}{6} (\rho_s - \rho_f) g d_v^3 \quad (6.45)$$

where d_v is the volume diameter.

The modified Stokes' equation is therefore:

$$d_{St} = \sqrt{\frac{18 \eta u}{(\rho_s - \rho_f) g}} \quad (6.46)$$

where d_{St} , the Stokes diameter, is:

$$d_{St} = \sqrt{\frac{d_v^3}{d_d}} \quad (6.47)$$

For non-re-entrant particles the mean drag diameter is the same as the surface diameter and Stokes diameter is defined as:

$$d_{St} = \sqrt{\frac{d_v^3}{d_s}} \quad (6.48)$$

Since the drag diameter is otherwise indeterminable, it is usual in practice to assume that, in the Stokes region, it is equal to the surface diameter. This holds at low Reynolds numbers but as Reynolds number increases, $d_d > d_s$.

6.9.2 Transition region

In the transition region particles fall with their largest cross-sectional area horizontal. Hawksley proposed that the C_D - Re relationship be used with the following definitions:

$$C_D = \frac{4}{3} \phi \frac{(\rho_s - \rho_f) \rho_f d_v g}{u^2} \quad (6.49)$$

$$Re = \frac{1}{\sqrt{\phi}} \frac{u d_v \rho_f}{\eta} \quad (6.50)$$

It is more convenient to extend Heywood's technique [1] to non-spherical particles than to use these equations. $C_D Re^2$ is evaluated in terms of volume diameter d_v and, if this is known, the free-falling velocity u_f may be determined. Heywood determined u for particles of different projected area diameters d_a as seen in a microscope. The volume of such particles are given by:

$$V = \alpha_{v,a} d_a^3$$

Hence modified values of Pd_a and u/Q were determined for various values of $\alpha_{v,a}$. These values may be used to determine the settling velocities of non-spherical particles in the transition zone and vice versa.

Figure 6.3 displays the relationship between drag coefficient and Reynolds number for particles of different shapes. As the velocity increases the particles tend to rotate to give maximum resistance to drag.

Haider and Levenspiel [24] presented the following empirical equation relating drag coefficient and Reynolds number for spherical and non-spherical particles, where Reynolds number is based on volume diameter:

$$C_D = \frac{24}{Re} \left(1 + A Re^B \right) + \frac{C}{1 + \frac{D}{Re}} \quad (6.51)$$

The values of the constants are given in Table 6.4 and apply for $Re < 25000$. Squires and Squires [25] studied 18 discs, in both vertical and horizontal orientation, having a range of diameter to thickness ratios. A detailed report on these and other studies has been presented by Ganser [26].

Table 6.4 Best values of parameters for some regular shapes

Shape	ψ	A	B	C	D
Sphere	1.000	0.1806	0.6459	0.4251	6880.5
Cube	0.906	0.2155	0.6028	0.8203	1080.8
Octahedron	0.846	0.2559	0.5876	1.2191	1154.1
Cube	0.806	0.2734	0.5510	1.4060	762.39
Tetrahedron	0.670	0.4531	0.4484	1.9450	101.18

ψ is Wadell's sphericity factor.

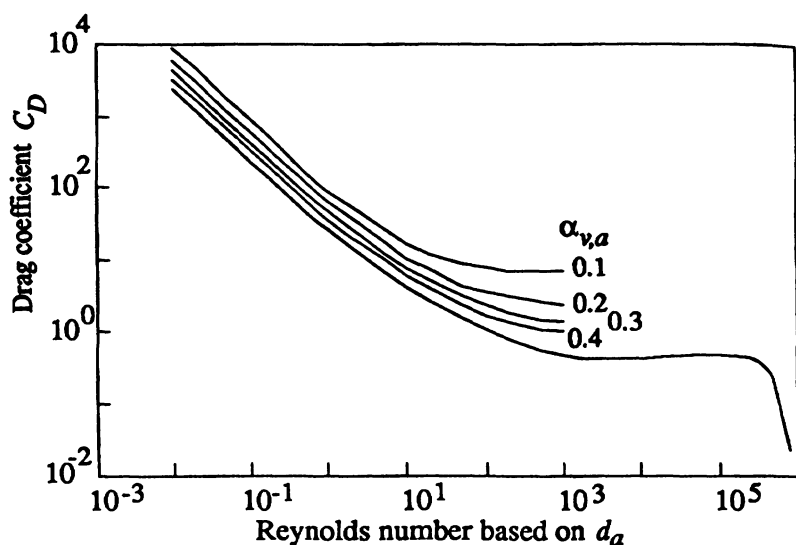


Fig. 6.3 Drag coefficient versus Reynolds number for particles of different volume shape coefficients by microscopy ($\alpha_{v,a}$) compared with data for a sphere.

6.10 Relationship between drag coefficient and Reynolds number in the transition region

Both equations (6.4) and (6.5) contain D and u and need to be expressed in terms of a single variable in order to determine D if u is known or u if D is known.

Several attempts at theoretical solutions of the relationship between C_D and Re (Equation (6.4)) have been made. Oseen [27] partially allowed for inertial effects to obtain:

$$C_D = \frac{24}{Re} \left(1 + \frac{3}{16} \frac{1}{Re} \right) \quad (6.52)$$

The equation is more complicated than Stokes', and in practice is found to be equally inaccurate, since the second term overcorrects Stokes' equation and gives a value of C_D as much in excess as Stokes' is too low.

Proudman and Pearson [28] pointed out that Oseen's solution could only be used to justify Stokes' law and not as a first order correction. They obtain a first order correction:

$$C_D = \frac{24}{Re} \left(1 + \frac{3}{16} Re + \frac{9}{20} Re^2 \ln Re \right) \quad (6.53)$$

Goldstein [29] solved the equation without approximation and obtained:

$$C_D = \frac{24}{Re} \left(1 + 0.188 Re - 1.48 \times 10^{-2} Re^2 + 3.46 \times 10^{-3} Re^3 - 8.57 \times 10^{-4} Re^4 \right) \quad (6.54)$$

Schillar and Nauman [30] fitted an empirical equation to the experimental values and obtained for $Re < 700$:

$$C_D = \frac{24}{Re} \left(1 + 0.15 Re^{-0.687} \right) \quad (6.55)$$

A comparison between these equations and experimental data is presented in Figure 6.4. Davies [31] analyzed the published data and expressed the result in the form of Re as a function of $C_D Re^2$ which is suitable for calculating the velocity when the diameter is known.

For $Re < 0.4$ or $C_D Re^2 < 130$:

$$Re = \frac{C_D Re}{24} - 2.34 \times 10^{-4} (C_D Re^2)^2 - 2.202 \times 10^{-6} (C_D Re^2)^3 - 6.91 \times 10^{-9} (C_D Re^2)^4 \quad (6.56)$$

For $3 < Re < 10^4$; $100 < C_D Re^2 < 4.5 \times 10^7$:

$$\log(Re) = -1.29536 + 0.986 \log(C_D Re^2) - 0.046677 \log(C_D Re^2)^2 - 0.0011235 \log(C_D Re^2)^3$$

A method for simplifying the calculation was proposed by Heywood [1] who used the dimensionless groups:

$$C_D Re^2 = \frac{4 \rho_f (\rho_s - \rho_f)}{3 \eta^2} g D^3 = P^3 D^3 \quad (6.58)$$

$$\frac{Re}{C_D} = \frac{3}{4} \frac{\rho_f^2}{(\rho_s - \rho_f) \eta g} u^3 = Q^3 u^3 \quad (6.59)$$

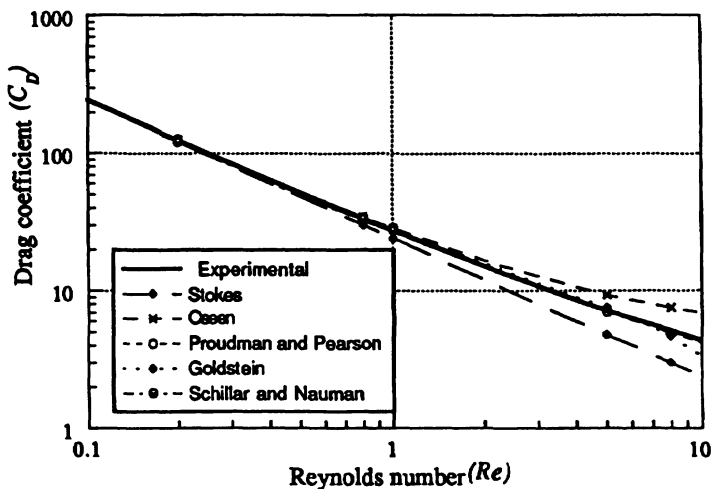


Fig. 6.4 Comparison between equations relating drag coefficient to Reynolds number and experimental data.

Experimental data were embodied in tables presenting $C_D Re^2$ in terms of $Re C_D^{-1}$ and vice versa. Since the former expression is independent of velocity and the latter is independent of particle diameter, the velocity may be determined for a particle of known diameter and the diameter determined for a known settling velocity. Heywood also presented data for non-spherical particles in the form of correction tables for four values of volume-shape coefficient from microscopic measurement of particle projected areas.

Pettyjohn and Christiansen [23] restricted their calculations to Stokes regime ($Re \leq 0.25$) and defined the Stokes shape factor (K_1) from equations (6.4) and (6.5) where:

$$C_D = \frac{4(\rho_s - \rho_f)gd_v}{3\rho_f u^2} = \frac{24}{Re K_1} \quad (6.60)$$

The middle expression is the formula for the drag when a particle of volume diameter d_v and density ρ_s settles with velocity u in a fluid of density ρ_f with acceleration due to gravity g . The right-hand expression is the usual equation for Stokes' law for a sphere ($K_1 = 1$) modified for non-spherical shapes ($K_1 \neq 1$).

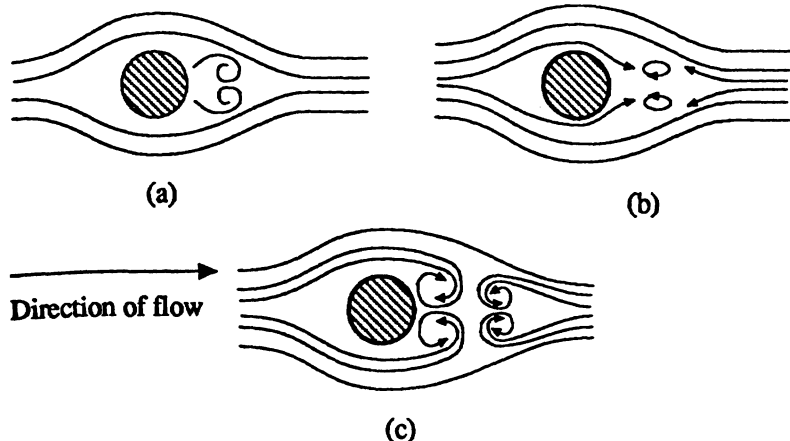


Fig. 6.5 Formation of vortices behind a spherical particle as the relative velocity between the fluid and the particle increases.

6.11 The turbulent flow region

For low Reynolds number, the drag is due mainly to viscous forces and the streamlines about a settling particle are all smooth curves. With increasing Reynolds number, the boundary layer begins to detach itself from the rear of the particle and form vortices (Figure 6.5a). Further increases in C_D causes the vortices to increase in size and move further downstream (Figure 6.5b). At very high Reynolds numbers, the wake becomes fully turbulent and the vortices break up and new vortices are formed (Figure 6.5c). For $Re > 500$, $C_D = 0.44$ and is roughly constant.

This effect can be demonstrated with a table tennis ball. If this is immersed in water, and released from a position near the surface, it will break through the surface at a high velocity, whereas if it is released several inches below the surface it will barely penetrate it. In the first case the ball's momentum is low but its velocity is high; in the second

Table 6.5 Ratios of drag force for pairs of spheres and single spheres falling (a) parallel, and (b) perpendicular to their line of centers, where L is the center to center separation of spheres of diameter D .

L/D	1	2	3	4	5	6	7
(a)	0.65	0.73	0.80	0.83	0.86	0.90	0.91
(b)	0.70	0.83	0.87	0.91	0.93	0.94	0.95

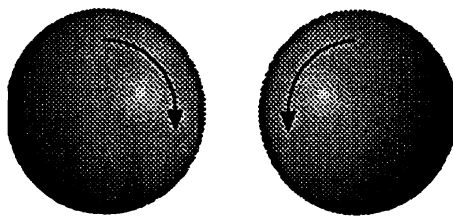


Fig. 6.6 Direction of rotation of two spheres falling close together.

case the momentum is high but the velocity is low. Since momentum is the product of mass times velocity, the mass in the second case must be greater than the mass in the first case. The increase in mass is due to the water contained in the turbulent eddies behind the ball adhering to it as it breaks through the surface.

6.12 Concentration effects

Stokes equation applies to the settling of a single spherical particle. This requirement is never fulfilled in sedimentation analyses where particles are separated by finite distances and mutually affect each other. In order to reduce interaction effects as much as possible it is recommended that a volume concentration no greater than 0.25% should be used. If it is necessary to use a higher concentration analyses should be carried out at two different concentrations in order to determine if the concentration effects are negligible.

Most of the theoretical work on particle-particle interaction has been limited to the study of pairs of spheres. If the particles are close together they may behave as a single particle and a correction applied, provided that their center-to-center distance is small. As the center-to-center distance increases, their separate effects must be considered, together with field reflections from the container walls. The net effect in the first case is a reduction in drag on the individual particles so that they fall with a greater terminal velocity than for a single sphere. Happel and Brenner [7, p. 27] plot the ratio of the drag force exerted on either sphere to that exerted on a single sphere, against L/D , the ratio of inter-particle separation (spheres touching when $L = D$), and against particle diameter for the cases where spheres are falling (a) parallel, and (b) perpendicular to their line of centers. The results are shown in Table 6.5. Particles settling side by side will also rotate as shown in Figure 6.6.

For all practical purposes the interaction becomes negligible for separations greater than about 10 diameters (0.3% by volume assuming a perfect dispersion). For more than two spheres, interaction becomes more complex; assemblies of spheres will diverge more slowly, that is repel each other, due to the rotation effect. For three identical spheres in a vertical line, with the top two closer together so that they fall more

rapidly, the center sphere will join forces with the lower sphere and, leaving its original companion behind, fall as a doublet [32]. A large sphere, falling in a vertical line close to a small sphere, can pick it up so that it revolves as a satellite. For two identical spheres, falling in the same vertical line, the retardation on the leading sphere is smaller than that on the leading sphere so that they will move towards each other [27].

It is important to distinguish between two cases; an assembly of particles which completely fills the fluid, and a cluster of particles. The descent of a single particle creates a velocity field which tends to increase the velocity of nearby particles. To balance this, the downward motion of the particle must be compensated for an equal volume upflow. If the particles are not uniformly distributed, the effect is a net increase in settling velocity, since the return flow will predominate in particle sparse regions. On the other hand, a system of uniformly distributed particles will be retarded to much the same extent.

A cluster of particles in an infinite fluid can be treated as a single large particle of appropriate density and reduced rigidity, that is as a liquid drop. A very large increase in settling rate could arise which is important at low concentrations.

For a dilute assembly of uniform spheres of diameter D , the settling velocity is retarded by a factor:

$$\frac{u_h}{u} = \frac{1}{1+1.3(D/L)} \quad (6.61)$$

where u_h is the settling velocity of a particle in the presence of other particles, u is the free-falling velocity and L is the inter-particle separation.

In a simple cubic assembly the volume concentration is given by

$$c = \frac{\pi}{6} \left(\frac{D}{L}\right)^3$$

hence:

$$\frac{u_h}{u} = \frac{1}{1+1.61c^{1/3}} \quad (6.62)$$

Famularo [33] investigated the problem further and found values of the constant for different assemblies as follows: cubic, 1.91; rhombohedral, 1.79; random, 1.30. Burgers [34] considered a random assembly of particles and replaced the second term in the denominator with $6.88c$. The numerical constant has been questioned by Hawksley [17 P. 131], who suggested that in practice the particles will accelerate to an equilibrium arrangement with a reduced constant of 4.5. The form of expression has also been criticized by Happel and Brenner [7, p. 236]:

Maude and Whitmore [35] suggest that:

$$\frac{u_h}{u} = (1 - c)\beta \quad (6.63)$$

where $4.67 \geq \beta \geq 4.2$ for $Re < 1$ and β is a function of particle shape and size distribution. Richardson and Zaki [36] also propose a relationship similar to this with $\beta = 4.65$.

For $0.6 < \varepsilon < 0.95$, where the porosity $\varepsilon = 1 - c$ Brinkman [37] proposed:

$$\frac{u_h}{u} = 1 + \frac{3}{4}(1 - \varepsilon) \left(1 - \sqrt{\frac{8}{1 - \varepsilon}} - 3 \right) \quad (6.64)$$

Steinour [38] developed, on theoretical grounds, a modification of Stokes' law which resulted in the equation:

$$\frac{u_h}{u} = \frac{\varepsilon^3}{1 - \varepsilon} \theta(\varepsilon) \quad (6.65)$$

Steinour, working with tapioca in oil and spherical glass beads in 0.1% aqueous sodium hexametaphosphate, reported that $\theta(\varepsilon)$ was sensibly constant over the range $0.3 < \varepsilon < 0.7$ giving:

$$\frac{u_h}{u} = 0.123 \frac{\varepsilon^3}{1 - \varepsilon} \quad (6.66)$$

He also derived a general expression for $\theta(\varepsilon)$:

$$\theta(\varepsilon) = \left(\frac{1 - \varepsilon}{\varepsilon} \right) 10^{-A(1 - \varepsilon)} \quad (6.67)$$

Substituting in equation (6.65) gives:

$$\frac{u_h}{u} = \varepsilon^2 10^{-A(1 - \varepsilon)} \quad (6.68)$$

Steinour obtained the result $A = 1.82$ from the slope of a plot of $\log(u_h/u)$ against ε .

Powers [39] found that in order to represent his experimental data he had to introduce a factor w_i to compensate for the liquid dragged down by the settling particles. His final equation was:

$$u_h = \frac{(\rho_s - \rho_f)g}{5\eta S_v^2} \frac{(\varepsilon - w_i)^3}{(1 - \varepsilon)}$$

For spherical particles, $S_v = 6/D$, hence:

$$\frac{u_h}{u_{St}} = 0.10 \frac{(\varepsilon - w_i)^3}{(1 - \varepsilon)} \quad (6.69)$$

Steinour [38] defined the immobile liquid per unit total volume as $a(1 - \varepsilon)$, where $a = w_i/(1 - w_i)$. To correct equation (6.66) ($\varepsilon - a(1 - \varepsilon)$) must be substituted for each value of ε giving:

$$\frac{u_h}{u} = 0.123 \frac{[\varepsilon - a(1 - \varepsilon)]^3}{(1 + a)(1 - \varepsilon)} \quad (6.70)$$

In terms of w_i this becomes:

$$\frac{u_h}{u} = 0.123 \frac{(\varepsilon - w_i)^3}{(1 - w_i)^2 (1 - \varepsilon)} \quad (6.71)$$

Similarly substitution into equation (6.68) gives:

$$\frac{u_h}{u} = \frac{(\varepsilon - w_i)^2}{(1 - w_i)^2} 10^{-1.82} \left[\frac{(1 - \varepsilon)}{(1 - w_i)} \right] \quad (6.72)$$

Bed expansion in particulate fluidization may be described by the Richardson-Zaki equation [36]

$$\frac{L^2}{t} = \frac{r}{K^2} \frac{\gamma_{LA} \cos(\theta)}{2\eta} u_h = u_i \varepsilon^n \quad (6.73)$$

where u_h is the superficial gas velocity and n is an exponential parameter given by:

$$n = (4.45 + 18 \frac{D}{D_B}) Re^{-0.1} \quad (6.74)$$

for $1 < Re < 200$, u_i is the extrapolated value of u_h at $\varepsilon = 1$ and is related to the terminal velocity u_{St} by:

$$\log u_{St} = \log u_i + \frac{D}{D_B} \quad (6.75)$$

where D = particle diameter and D_B = bed diameter [40].

These relationships have also been applied to sedimentation where the problem of dealing with particles which are aggregated into sedimentation units with properties similar to flocs has been recognized [41]. Such units effectively immobilize a relatively large volume of fluid, thus reducing the apparent porosity. In this situation Scott [42] replaced ε in equation (6.73) by an 'effective' porosity.

$$u_h = u_{St}(1 - kc)^{4.65} \quad (6.76)$$

where c is solids concentration and k is the volume of aggregates per unit weight of solid, $k = 1/(1 - w_i)$.

Equation (6.76) is also applicable to rough irregular particles [43], in which a layer of fluid may be considered to be immobilized in the surface irregularities. The linear rate of settling of the interface (u_h) increases with increasing initial liquid volume fraction (ε). Additionally, since $(1 - \varepsilon)$ decreases to zero as (ε) increases, a plot of $u_h(1 - \varepsilon)$ against ε will pass through a maximum at a porosity ε_1 . The quantity $u_h(1 - \varepsilon)\rho_s$ is known as 'solid flux' and indicates the mass transfer of solid per unit cross-section per unit time down the sedimentation column.

Applying this concept to equation (6.76) a graph of 'solid flux' against porosity has a slope with $D \ll D_B$ so that $u_i = u_{St}$.

$$u_h(1 - \varepsilon)\rho_s = u_{St}((1 - \varepsilon)\rho_s\varepsilon^n) \quad (6.77)$$

For maximum mass transfer

$$\frac{d}{d\varepsilon}(u_h(1 - \varepsilon)\rho_s) = 0 \quad (6.78)$$

Defining this point as ε_1 , gives $\varepsilon_1 = [n/(n+1)]$ so that the Richardson-Zaki equation takes the form:

$$u_h = u_{St}\varepsilon^{(n/(n+1))} \quad (6.79)$$

The physical significance of n , as a function of the porosity at which solids flux is a maximum was pointed out by Davies *et al.* [44]. In a later paper [45] they propose a relationship of the form:

$$u_h = u_{St}10^{-bc} \quad (6.80)$$

$$u_h = u_{St} 10^{-bc\rho_s(1-\varepsilon)} \quad (6.81)$$

where ρ_s is the density of the solids. For ε tending to unity this is equivalent to Steinour's equation (7.55).

Differentiating equation (6.81) gives [46]:

$$\varepsilon_1 = 1 - \frac{1}{2.303b\rho_s} \quad (6.82)$$

This is equivalent to equation (6.79); ε_1 may be determined from a plot of $\log u_h$ against c .

Equation (6.81) is criticized by Dixon *et al.* [47] as being equivalent to equation (6.73) at low concentrations and incorrect at high concentrations; they also criticize the use of equation (6.82) to evaluate ε_1 . In a reply Davies and Dollimore [48] defend their approach.

6.13 Hindered settling

At very low concentrations particles settle singly and, under laminar flow conditions, Stokes' law is valid. At higher concentrations particle-particle interaction occurs which, on average, should lead to reduced settling rates. At very high concentrations particles tend to settle *en masse*, and the rate of fall of the interface (u_h) is given by equations of the form presented in the preceding section. With closely graded powders, the interface between suspension and clear liquid is sharp, becoming more diffuse for powders with a wide size range which, in some cases form more than one interface. This phenomenon is due to fines being swept out of the bulk of the suspension by return flow of liquid displaced by the sedimenting solids: These form a suspension of fines over the main suspension; the fines supernatant being, in turn, subject to hindered settling. Multiple interfaces may form and persist until, at some critical condition, mechanical interlocking occurs [49]. The equations developed to represent such systems have much in common with permeametry equation developed to describe the flow of fluid through a fixed bed of powder.

6.13.1 Low concentration effects

Several investigators have shown that settling rates for selected particles increases with concentration, when the concentration is low, and this is probably due to particle-particle interaction. Kaye and Boardman [50] visually determined the velocities of 900 μm red glass marker spheres, in the presence of glass spheres of diameter 850, 400 or 100 μm , settling in a 62 mm tube filled with liquid paraffin. A maximum settling rate of 1.6 times the value found in very dilute suspensions was

reported at volume concentrations around 1%, after which the ratio decreased. Twenty measurements were carried out for each experimental point and considerable scatter was found, particularly around the maximum values. It was also found that this enhancement was greatest for powders having a narrow size range. Johne [51] used 200 μm glass spheres in a 35 mm diameter tube filled with 148 cP motor oil. The sedimentation velocity was determined by following a single 200 μm radioactive marker sphere. A maximum settling rate 2.4 n times the values found in very dilute suspensions was reported at volume concentrations around 1%.

Koglin [52] continued Johne's work with an emphasis on wall effects and attributed the difference between the two earlier investigations to these effects. Since Boardman visually determined the settling time between two marker lines on the sedimentation tube, he selected particles in the center of the tube, whereas Johne's method was non-selective.

The increasing rate of sedimentation at increasing concentrations, in the low concentration region, was also demonstrated by Jovanovic [53] who showed that the weight-mean diameter of aluminum powder, as determined with a Sartorius balance, increased as the powder volume concentration was increased from 0.02% to 0.05%. This he attributed to particle agglomeration. Barford [54] carried out similar experiments with polishing powders in the 15 to 30 μm size range. The maximum settling rate found was 1.12 to 1.40 times the Stokes rate at volume concentrations between 0.1% and 0.2% and this he attributed to cluster formation. Jayaweera *et al.* [55], in experiments with collections of 2 to 7 mm spheres, also found settling rates higher than the Stokes velocity for a single sphere.

Davies and Kaye [56] used a Cahn sedimentation balance to investigate cluster formation and found that, for a powder having a narrow size range, cluster formation was not eliminated at volume concentrations as low as 0.47%; for a powder having a wide size range it was not important at volume concentrations as high as 0.414%.

The laws of probability predict that, even in dilute suspensions, the unequal distribution of particle separation will result in cluster formation giving rise to enhanced settling. It is therefore desirable to use as low a concentration as is feasible when carrying out sedimentation size analysis.

6.13.2 High concentration effects

Several investigations have been carried out on the settling behavior of spherical particles in concentrated suspensions [7, p. 413] with best agreement with equations of the form (6.63). Equations similar to (6.64) indicate too high a concentration dependency on settling rate. Apparatus for carrying out hindered settling experiments [57] was

described in 1960, modified apparatus [58] was described in 1970 and experimental procedure [59] in 1977.

There are various ways of dealing with experimental data [45,60]:

1. Apply equation (6.66) combined with Stokes equation to find an 'uncorrected particle radius'.
2. Apply equation (6.71) and plot $[u_h(1-\varepsilon)]^{1/3}$ against ε to find w_i and equation (6.65) to find and a 'corrected particle radius'.
3. Apply equation (6.68) and plot (u_h / ε^2) against ε .
4. Plot $\log u_h$ against c and extrapolate to zero concentration.

Dollimore and Heal [61] applied method 2 to determine the thickness of the film on the outside of the particles. Ramakrishna and Rao [62] criticize this approach and prefer method 3. In a later discussion [63] they stated that their criticism was because equation (6.71) was being used outside its range of validity (i.e. at $\varepsilon > 0.8$) and in this region equation (6.68) must be used. Pierce [64], in the same discussion, suggested the use of equation (6.66).

Dollimore and co-workers [44] in later investigations, found wide variations in A and $\theta(\varepsilon)$. Dollimore and Horridge [65] found $A = 20.2$ for china clay; Thompson [cit. 44] found $24.3 < A < 36.6$ for calcium carbonate in aqueous sodium chloride; Dollimore and Owens [66] found $A = 81$ and $A = 206$ for non-porous silica in water and *n*-heptane respectively.

General conclusions are that, at low concentrations, hindered settling is more likely with high polarity systems, particularly high polarity solids [43]; it is more likely with dense solids in viscous liquids; the stability of some systems is due to the presence of electrical double layers: Davies and Dollimore [67] conclude that:

$$\text{hindrance} = \frac{\left. \begin{array}{l} \text{surface density of charge on particle;} \\ \text{particle density; liquid viscosity} \end{array} \right\}}{\left. \begin{array}{l} \text{difference in viscosity between suspension and} \\ \text{bulk liquid; the cation - stability constant} \end{array} \right\}}$$

Sarmiento and Uhlherr [68] also considered temperature effects on settling behavior and suggest that at low concentrations the change in settling velocity with temperature change can be predicted solely from the change in viscosity of the suspending liquid; at high concentrations this is no longer possible since the floc characteristics undergo change. Changes in sediment volume has also been used to predict particle size [10,41].

The general conclusions that can be drawn are that settling behavior is extremely complex in the high concentration region and several

equations may apply according to the range of porosity considered and the presence or absence of flocculation. The determined particle size decreases with the addition of dispersing agents and it is suggested that the size so determined is floc size [69]. The technique is therefore a useful and simple one for determining floc size.

6.14 Electro-viscosity

Charged particles in weak electrolytes have associated with them an electrical double layer. When these particles settle under gravity the double layer is distorted with the result that an electrical field is set up which opposes motion. This effect was first noted by Dorn [70] and was studied extensively by Elton *et al.* [71–74] and later by Booth [75, 76].

For a spherical particle of diameter D , the electrical force F_E is equal to the product of the electrical field E and the charge q . For a surface charge per unit area σ the force on the sphere is $D^2\sigma E$. If the sum of this force and the viscous force is set equal to the gravitational force, equation (6.6) is modified to:

$$\dot{u}_{St} = \frac{(\rho_s - \rho_f)gD^2}{18\eta} - \frac{D\sigma E}{3\eta} \quad (6.83)$$

That is, Stokes velocity is diminished by the term $(D\sigma E/3\eta)$.

The specific conductivity of a solution (k) is equal to the current density divided by the electrical field. For N spheres of diameter D per unit volume of suspension:

$$k = \frac{pD^2\sigma N}{E} \dot{u}_{St} \quad (6.84)$$

But N is equal to the total weight of particles in suspension (m) divided by the volume of suspension V and the weight of a single particle.

$$N = \frac{m/V}{\frac{\pi}{6}\rho_s D^3} \quad (6.85)$$

Substituting in equations (6.83) and (6.84) and rearranging gives:

$$\dot{u}_{St} = \dot{u}_{St} \left(1 + \frac{2m\sigma^2}{\rho_s \eta V k} \right) \quad (6.86)$$

Pavlik and Sansone [77] found that the size distribution of spherical particles, in the size range 5 to 40 μm , obtained by sedimentation in double-distilled deionized water plus a wetting agent was significantly different from that obtained in 0.1N KCl plus a wetting agent. Coulter Counter data agreed with the latter data. These results were later confirmed [78]. The electro-viscous effect needs to be eliminated, for Stokes' law to apply, by the addition of non-ionic sedimentation liquids.

The magnitude of this effect was determined [79] for a 0.1% suspension of 1.10 μm polystyrene settling in water. For a zeta potential of 50 mV the electric field strength is 1 mV cm^{-1} making the correction term negligible at a volume concentration of 0.04%.

6.15 Dispersion of powders

6.15.1 Dry powder dispersion

Dry powders are made up of primary particles which stick together to form clumps. If the forces holding the primary particles together are weak, the clumps are defined as *agglomerates*; strongly bonded clumps are called *aggregates*. If the particle size distribution of a powder is to be determined in a dry state, the amount of energy employed is critical. In order to determine the size distribution of products held together by weak bonds, such as fertilizer granules, gentle treatment is required. The same is true for weak crystals which will either *attrit*, i.e. asperities removed due to collision, or *comminate*, i.e. break into pieces. For pigments, such as titanium dioxide, high shear forces are required to break down the flocs, but they must not be so great that the aggregates are broken down. Quality granules have a defined size range, fines, which form dust, and coarse lumps are detrimental to the final product, and the determined size distribution should reflect this. Similarly for pigments, particles much smaller than the wavelength of light have low hiding power and particles coarser than about a micron generate surface irregularities which affect surface gloss. In order to predict end-use properties, the dispersing procedure should not destroy the coarse aggregates or generate fines, but should be vigorous enough to break down the agglomerates.

The demarcation between individual particles and groups of particles is often very blurred. In some systems there are aggregates which are tightly bound together with some chemical bonding or sintering, and strong mechanical forces are required to break the bonds; these aggregates may be associated with agglomerates which are weakly bound together. In others there may be a continuous gradation in the strength of clumps.

Several of the manufacturers of low angle laser light scattering instruments (LALLS) have developed dry powder feeders. The Sympatec Rodos and the Aerisizer dry powder dispenser are particularly suitable for dispersing fine cohesive powders.

6.15.2 The use of glidants to improve flowability of dry powders

Glidants are often added to powders, which are to be analyzed in the dry state, in order to improve their flow properties [80,81]. Various mechanisms have been proposed to explain their mode of action:

- Reduction of interparticle friction by coating the particles.
- Reduction of surface roughness.
- Reduction of interparticle attraction by creating a physical barrier between particles.
- Reduction of static electrical charge on particles.

An optimum concentration of glidant exists for most systems and amongst the techniques to estimate this concentration are angles of repose [82], flow through an orifice [85] vibrating funnel [83] and bulk density.

These additives are particularly useful for micromesh sieving and classification. In the absence of other data a mass concentration of about 1% is used. Fatty acid (usually stearic), fine silica (Aerosil 2000 from Degussa, Frankfurt, Germany), purified talc and magnesium stearate are used. York [84] examined three typical glidants with lactose mixtures using the Jenike shear cell [85] to assess flowability and found that fine silica produced the greatest increase in flowability, while magnesium stearate and purified talc gave smaller increases. All three systems indicated an optimum mass concentration (1.75%, 2.25% and 0.85% respectively). He also concluded that the angle of internal friction is not a useful indicator of flowability.

6.15.3 Wet powder dispersion

In many particle size analysis procedures it is necessary to incorporate the powder into a liquid or the sample may be provided in slurry form. In the latter case it is necessary to know whether it is desirable to determine the size distribution as delivered or whether loosely bound flocs need to be broken down. In many cases, drying a suspension and redispersing the powder will alter the resulting size distribution.

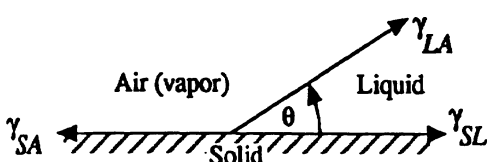


Fig. 6.7 The spreading of a liquid on the surface of a solid.

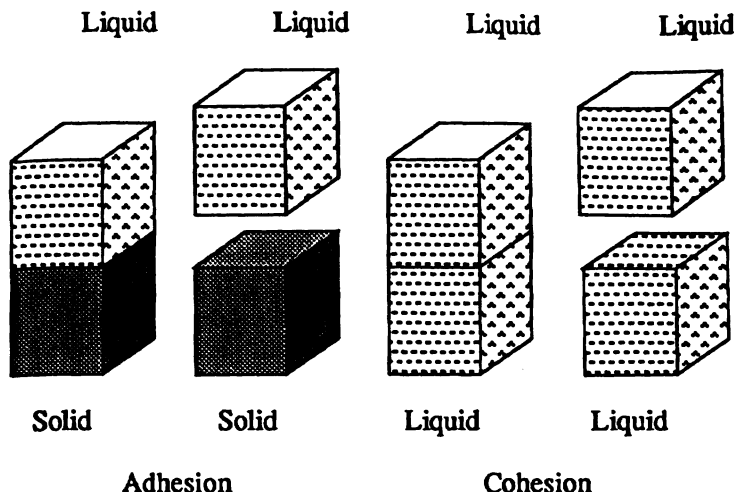


Fig. 6.8 Work of adhesion and work of cohesion.

Starting with a dry powder and a liquid medium, three stages in the dispersing process may be distinguished. First there is the process of wetting which is defined as the replacement of the solid-air interface by a liquid-air interface. Second there is the process of deagglomeration of the particle clusters and finally there is the process of dispersion stabilization [86].

6.15.4 Role of dispersing agents

The molecules of a dispersing agent adsorb on to the particle surface to change particle-particle interaction. This may be accomplished by (1) the adsorption of a strongly hydrated hydrophilic colloid thus increasing the affinity of the particle to water so that it exceeds any mutual attraction between particles, (2) the adsorption of an ionic electrolyte to create strong mutual repulsion on the particle surface and (3) the adsorption of a non-ionic polymer of sufficient chain length to create steric hindrance i.e. preventing the particles from entering each other's attractive field. A discussion on the selection of dispersing agents and the optimum concentrations to be used has been published [87]. For a fuller discussion of dispersion, readers are referred to Nelson [88].

6.15.5 Wetting a powder

If liquid is placed on a solid it will spread if (Figure 6.7) [89]:

$$\gamma_{SA} > \gamma_{SL} + \gamma_{LA} \cos(\theta) \quad (6.87)$$

where γ_{SA} , γ_{SL} , γ_{LA} are the interfacial tensions between the solid and the liquid, solid and air and liquid and air, and θ is the angle of contact between the solid and the liquid. (γ_{SA} and γ_{LA} will fall rapidly to γ_{SV} and γ_{LV} as the solid surface becomes saturated with vapor but, for simplicity, the former suffixes will be retained.)

The spreading coefficient is defined as:

$$S_{LS} = \gamma_{SA} - \gamma_{SL} - \gamma_{LA} \quad (6.88)$$

The liquid will spread on the surface if the spreading coefficient is positive, i.e. the liquid will wet the solid.

The work of adhesion is defined as the work necessary to separate unit area of interface between two phases (Fig. 6.8).

$$W_A = \gamma_{SA} + \gamma_{LA} - \gamma_{SL} \quad (6.89)$$

The work of cohesion is defined as the work necessary to separate unit area of one phase

$$W_C = +2\gamma_{LA} \quad (6.90)$$

Hence the spreading coefficient may be defined as:

$$S_{LS} = W_A - W_C \quad (6.91)$$

and, if positive, infers a greater affinity between the liquid and solid than between the liquid and itself.

The energy of immersion is defined as the surface energy loss per unit area of surface on immersion:

$$W_i = \gamma_{SA} - \gamma_{SL} \quad (6.92)$$

Combining equations (6.87) and (6.89) gives:

$$W_A = \gamma_{LA} - (1 + \cos(\theta)) \quad (6.93)$$

The ease of displacement of air from the surface of the powder is enhanced if W_A is increased. This is frequently accomplished by the use of surfactants to reduce the contact angle θ to zero if possible. At equilibrium, from equation (6.87):

$$\cos(\theta) = \frac{\gamma_{SA} - \gamma_{SL}}{\gamma_{LA}} \quad (6.94)$$

The addition of surfactant usually causes a reduction in γ_{LA} and, if absorbed, a reduction in γ_{SL} . Both effects lead to better wetting. The change in γ_{SA} is negligible in most cases so the dominating factor is γ_{LA} , the surface tension of the liquid phase.

6.15.6 Determination of contact angle (θ)

The difficulty in the use of these equations in practice is the experimental one of determining θ for fine powders. Bartell and Walton [90] developed a method in which a pressure was applied to prevent liquid from penetrating a plug of powder. The required pressure is given by the Laplace equation:

$$\Delta P = \frac{2\gamma_{LA} \cos(\theta)}{r} \quad (6.95)$$

For a liquid which wets the solid:

$$\Delta P = \frac{2\gamma_{LA}^0}{r} \quad (6.96)$$

where γ_{LA}^0 indicates the interface between the liquid and its saturated vapor, so that:

$$\cos(\theta) = \frac{\Delta P}{\Delta P_0} \left(\frac{\gamma_{LA}^0}{\gamma_{LA}} \right) \quad (6.97)$$

The principle of this method is to obtain the effective capillary radius r using a non-wetting liquid and repeat the measurement with a wetting liquid. The method is difficult to use and the following simpler method has been described [91]. The distance of penetration L in time t in a horizontal capillary, or in general when gravity can be neglected, is given by the Washburn equation [92]:

$$\frac{L^2}{t} = \frac{r\gamma_{LA} \cos(\theta)}{2\eta} \quad (6.98)$$

where η is the viscosity of the liquid. For a packed bed of powder this becomes:

$$\frac{L^2}{t} = \frac{r}{K^2} \frac{\gamma_{LA} \cos(\theta)}{2\eta} \quad (6.99)$$

where the bracketed term is an unknown factor dependent on the packing. If several liquids are used with the same powder, uniform high values of (r/K^2) are found and it is assumed that these correspond to $\cos(\theta) = 1$. This factor is then used to obtain values of θ for other liquids.

Heertjes and Kossen [93] present a full discussion of their techniques together with descriptions of the required apparatus and experimental procedure. They considered both the above methods unsuitable for the determination of $\cos(\theta)$ and proposed a new method, the $h-e$ method. Briefly this consists of determining the height of a drop of liquid placed on top of a cake of the compressed powder previously saturated with the liquid. The theory was presented in an earlier paper [94].

An analysis has been presented [95] on the wetting of fine powders by aqueous solutions of anionic wetting agents in terms of adhesion tension, spreading coefficient and capillary forces involved in the displacement of air from externally wetted aggregates. This study revealed how the film preceding the bulk liquid can retard or markedly accelerate the submersion of powder in a liquid.

6.15.7 Deagglomerating wetted clumps

The next stage in the dispersion process is the breakdown of agglomerates. For easily wetted material, penetration of liquid into the voids between particles may provide sufficient force to bring about disintegration. Often however, mechanical energy is required and this is usually introduced by spatulation or stirring, though the use of ultrasonics is now widely practiced.

For powders which are difficult to disperse, the dispersing liquid (e.g. 0.1% sodium hexametaphosphate in distilled water) may be added to the powder to form a paste. More liquid is added to this paste while it is sheared using a flexible spatula so that it becomes a slurry and eventually a suspension. Care needs to be taken, with this procedure, to ensure that aggregates and particles are not fractured.

Clumps of particle may contain occluded air which is difficult to displace; this is best dealt with by adding the liquid whilst the powder is under vacuum.

6.15.8 Suspension stability

The stability of the wetted, dispersed system depends on the forces between particles. The random motion of particles brings them into close contact and, under certain circumstances, causes them to flocculate. The frequency of collisions depends upon the concentration, viscosity and temperature. Whether two approaching particles will combine or not depends on the potential barrier between

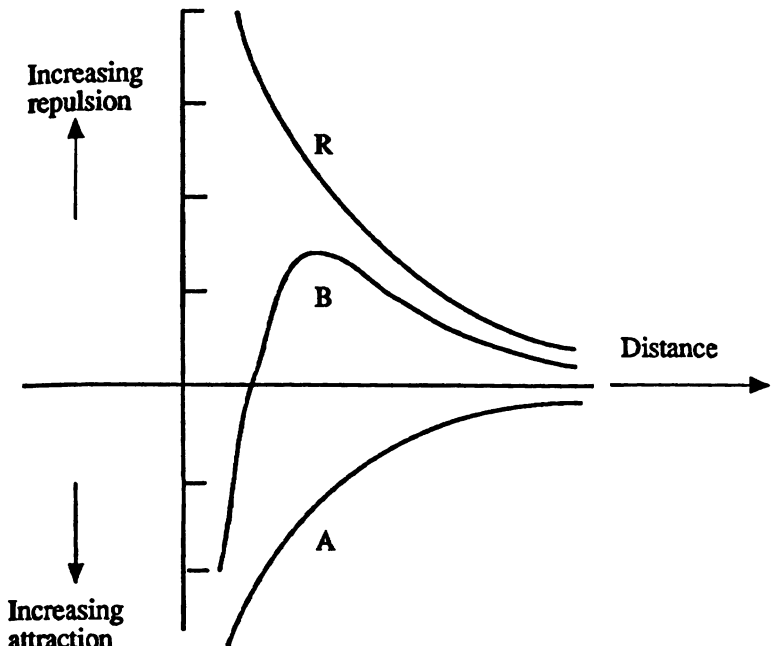


Fig. 6.9 Net interaction potential between particles: A, force of attraction, R, force of repulsion, B, resultant force.

them. The potential energy can be considered to consist of two terms, an attractive London-van der Waals force and a repulsive force due to the electrical double layer which surrounds particles. This double layer consists of an inner layer of ions at the surface of the particle and a cloud of counter-ions surrounding it. The sum of the two potentials generate an increasing repulsive force as the particles move closer together which reaches a maximum, or potential barrier, before decreasing and becoming an attractive force. If the potential barrier exceeds $15 kT$, where k is the Boltzmann constant and T is absolute temperature, the system is stable [96, p. 192]. With large particles the net potential energy curve may show a minimum at appreciable distances of separation (Figure 6.9).

This concept cannot account for the action shown by many non-ionic, surface-active agents, and in these cases it has been suggested that the size of the agent could lead to repulsion due to steric hindrance, i.e. the molecules extend so far out into the media that two approaching particles do not get close enough to flocculate.

In non-aqueous media of low dielectric constant ionic charge stabilization is unlikely to be very important. In such cases stabilization depends on steric or entropic repulsion and polymeric agents are

preferred against the long-chain paraffin types which are so successful in aqueous media.

In practice it is necessary to decide whether an agent is required to wet out the solid so that it will disperse in the liquid concerned or whether the problem is one of stabilization. The minimum of wetting agent to ensure adequate dispersion is added. Any combination which causes foaming should be rejected or used in combination of an anti-foaming agent such as fumed silica. The present state of the art is such that dispersing agents are chosen almost at random, but with some knowledge of the surface chemistry involved [97].

6.15.9 Tests of dispersion quality

A simple test for wetting efficiency is to make up suspensions using the same concentration of powder but different agents and allow the suspension to settle out. About a gram of powder dispersed in 10 mL of liquid is suitable. Slow settling, a clear interface between the clear liquid and the turbid lower layers and a small depth of sediment indicate the best agent or, if several concentrations of the same agent are being tested, the best concentration [98,99]. It is important that no vibration be imparted to the containers during settlement which may take several hours.

Another test for the degree of flocculation of a paste is to measure the difference between the smear and flow points. The test is made by adding known quantities of dispersing medium to a known weight of powder and working it in with a spatula. The difference is noted between the amount required to smear and to flow; the better the dispersion, the smaller the difference [100].

It has been found that for pigments in solvents, a high dielectric constant leads to a more dispersed system. In general, polar liquids disperse polar solids and non-polar liquids disperse non-polar solids. For polar solids suspended in non-polar liquids, it is possible to use the difference in polarity to anchor a stabilizing molecule to the powder surface. The effectiveness is characterized by the heat of wetting, which can be determined by calorimetry.

For sub-micron metallic powders, precoating with gelatin aids dispersion in aqueous systems. Coating of commercial powders in order to stabilize them is widely used e.g. aluminum oxide coated titanium dioxide. In such cases the interfacial properties will be those of the coating rather than those of the bulk powder.

Many weird and wonderful methods for obtaining stable, well-dispersed systems have been proposed. Some of the more valuable are incorporated into National Standards for particle systems. A more general one is to be found in BS 3406 [100] and a working group is currently preparing an international standard.

Effectiveness of deflocculants in dilute suspensions may be studied by light absorption. If the optical density of an agitated suspension

falls with time this is an indication of either flocculation or dissolution, whereas an increasing optical density indicates breakdown of flocs.

Dilute suspensions may be studied using the Coulter principle. It is sometimes found that the count level at the lower sizes decreases with time and this may be attributed to flocculation or dissolution. A problem arises in that the suspending liquid needs to be electrically conducting and one would expect this to reduce the potential energy barrier and decrease suspension stability [101].

A microscope examination should always be carried out. A thick paste should be made up as described earlier and a drop removed; this should be diluted to a reasonable concentration by the incorporation of more liquid. A drop of this should be placed on a microscope slide, without a cover slip, and examined for signs of agglomeration or break-up of aggregates. Particles smaller than a few microns will vibrate in a random manner due to thermal jostling (Brownian motion). Note what happens when particles collide; in a good dispersion they repel each other; in a poor dispersion they form flocs. Although a visual examination of particles is always useful as an indication of particle size, a false impression may be obtained as to their state of dispersion due to the wide difference in environment between this testing situation and the actual analysis.

Dispersion of magnetic suspensions may be effected by subjecting the suspension to a high frequency magnetic field [102]. For the Autometrics PSM 200, 400 Hz was selected at a peak field strength of 800 Oersted [103].

A range of non-ionic fluorochemical surfactants (FC-170C, FC-433, FC-430, FC-431) manufactured by 3M Corporation has been found to be particularly useful for dispersing sub-micron powders. The addition of 0.01% of any of these surfactants to water reduces the interfacial tension from $7.2 \times 10^{-6} \text{ N m}^{-1}$ (72 dyn cm^{-1}) to $2.5 \times 10^{-6} \text{ N m}^{-1}$. FC-430 is a 100% active, viscous liquid, FC-431 is a solution of 50% active solid in ethyl acetate. These surfactants exhibit good solubility in most liquids.

The final criterion is the practical test; if size analyses are carried out with two systems, provided there is no dissolution, the one showing the finer distribution having the best dispersion.

Koglin [104] has reviewed the methods of assessing the degree of agglomeration in suspension. He states that the only direct method is microscopy. Estimates of degree of flocculation are possible by rheological properties or sediment volume. The Coulter principle is only suitable for aggregates since flocs disintegrate due to the shear experienced as they pass through the aperture. He states that the degree of agglomeration can be determined by comparing the size distribution of the agglomerated suspension with the size distribution of a completely dispersed system. The methods he used are photo-sedimentation and the sedimentation balance; the review cites 57 references.

Dispersion of pigments is often effected by prolonged milling [105–107]. It is argued that pigment is made up of agglomerates which are readily reduced to their constituent aggregates (1–20 µm in size). These aggregates may be further reduced to primary crystals (0.3–1 µm) with the application of considerably more force. Further reduction to crystallites is effected by crystal fracture (0.001 – 0.6 µm). Milling times of around 20 h are required to attain stable conditions.

References

- 1 Heywood, H. (1962), *Proc. Symp. Interaction Particles and Fluids*, Inst. Chem. Eng. London, 189, 226, 231, 241, 243
- 2 Mason, M. and Weaver, W. (1924), *Phys. Review*, 23, 412–426, 229
- 3 Berg, S. (1958), *Symp. Particle Size Measurement*, ASTM Pub. 234, 143, 229
- 4 Okuyama, K., Kousaka, Y., Miyazaki, T. and Yoshida, T. (1977), *J. Chem. Eng. Japan*, 10, 46, 229
- 5 Moore, D.W. and Orr, C. (1973), *Powder Technol.*, 8, 13, 229
- 6 Chung, H.S. and Hogg, R. (1985), *Powder Technol.*, 41, 211–216, 229
- 7 Happel, J. and Brenner, H. (1965), *Low Reynolds number Hydrodynamics*, Prentice Hall, 229, 238, 246, 247, 252
- 8 Fuchs, N.A. (1964), *Mechanics of Aerosols*, Trans., (ed. C.N. Davies), Pergamon, Oxford, 230
- 9 Bernhardt, C. (1992), *Particle Size Analysis*, ed N.G. Stanley-Wood and R.W. Lines, 477–487, Proc. Conf., Royal Soc. Chem., Bradford, U.K., 230
- 10 Brugger, K. (1976), *Powder Technol.*, 14, 187–188, 230, 235, 254
- 11 Allen, T. and Nelson, R.D. Jr (1995), *6th European Symp. Particle Characterization*, Nürnberg, publ. NürnbergMesse GmbH, 143–156, 231
- 12 Boothroyd, R.G. (1971), *Flowing Gas Solids Suspensions*, Chapman & Hall, London, 232, 238
- 13 Muta, A. and Watanabe, S. (1970), *Proc. Conf. Particle Size Analysis*, Bradford, U.K., eds M.J. Groves and J.L. Wyatt-Sargent, Soc. Anal. Chem., pp. 178–193, 196, 197, 232
- 14 Allen, T. (1970), *Proc. Conf. Particle Size Analysis*, Bradford, U.K., eds M.J. Groves and J.L. Wyatt-Sargent, Soc. Anal. Chem., discussion, pp. 194, 195, 198, 232
- 15 Allen, T. and Baudet, M.G. (1977), *Powder Technol.*, 18, 131–138, 232
- 16 Lorentz, H. (1906), *Abh. u. Th. Phys.*, 82, 541, 234
- 17 Hawksley, P.G.W. (1951), BCURA (*British Coal Utilization Research Assoc.*) Bull., 15, 4, 235, 239, 247
- 18 Cunningham, E. (1910), *Proc. Royal Soc.*, A83, 357, 235

- 19 Davies, C.N. (1954), *Proc. Phys. Soc.*, **57**, 259, 235
 20 Lapple, C.E. (1950), *Perry's Chemical Engineering Handbook*, 235
- 21 Einstein, A. (1911), *Ann. Phys. Leipzig*, **19**, 289, 34, 591, 235
 22 Heiss, F. and Coull, J. (1952), *Chem. Eng. Progr.*, **48**(3), 133–140, 237
- 23 Pettyjohn, E.S. and Christiansen, E.B. (1948), *Chem. Eng. Progr.*, **44**, 157, 239, 244
 24 Haider, A. and Levenspeil, O. (1989), *Powder Technol.*, **58**, 63, 241
- 25 Squires, L. and Squires, W. Jr (1937), *Trans. Am. Inst. Chem. Eng.*, **33**, 1, 244 (1993), *Powder Technol.*, **77**, 143–152, 241
 26 Ganser, G.H. (1993), *Powder Technol.*, **77**, 143–152, 241
 27 Oseen, C.W. (1927), *Neuere Methoden und Ergebnisse in der Hydrodynamik*, Leipzig Akademische Verlag, 242, 247
 28 Proudman, I. and Pearson, J.R.A. (1957), *J. Fluid Mech.*, **2**, 237, 242
- 29 Goldstein, S. (1938), *Modern Developments in Fluid Dynamics*, Clarendon Press, 243
 30 Schillar, L. and Nauman, A.Z. (1933), *Ver. dt. Ing.*, **77**, 318, 243
 31 Davies, C.N. (1947), *Trans. Inst. Chem. Engrs.*, Suppl. **25**, 39, 243
- 32 Kynch, G.J. (1959), *J. Fluid Mech.*, **5**, 193, 247
 33 Famularo, J. (1962), *Eng. Sci. Thesis*, New York Univ., 248
 34 Burgers, A.M. (1941), *Proc. K. Ned. Akad. Wet.*, **44**, 1045, 248
 35 Maude, A.D. and Whitmore, R.L. (1958), *Br. J. Appl. Phys.*, **4**, 47, 248
 36 Richardson, J.F. and Zaki, W.N. (1954), *Chem. Eng. Sci.*, **3**, 65, 248, 249
 37 Brinkman, H.C. (1947), *Appl. Sci. Res.*, **A1**, 27, 248
 38 Steinour, H.H. (1944), *Ind. Eng. Chem.*, **36**, 618, 840, 901, 248, 249
 39 Powers, T.C. (1939), *Proc. Am. Concr. Inst.*, **35**, 465, 249
 40 Capes, C.E. (1974), *Powder Technol.*, **18**, 283–284, 250
 41 Michaels, A.S. and Bolger, J.C. (1962), *Ind. Eng. Fund.*, **1**(24), 250, 254
 42 Scott, K.J. (1968), *Ind. Eng. Fund.*, **7**, 484, 250
 43 Whitmore, R.L. (1957), *J. Inst. Fuel*, **30**, 238, 247, 250
 44 Davies, L., Dollimore, D. and Sharpe, J.H. (1976), *Powder Technol.*, **13**, 123–132, 251 253
 45 Davies, L., Dollimore, D. and McBride, G.B. (1977), *Powder Technol.*, **16**, 45–49, 250, 253
 46 Davies, L. and Dollimore, D. (1977), *Powder Technol.*, **19**, 1–6, 251
 47 Dixon, D.C., Buchanon, J.E. and Souter, P. (1977), *Powder Technol.*, **18**, 283–284, 251

- 48 Davies, L. and Dollimore, D. (1977), *Powder Technol.*, 18, 285–
287, 251
- 49 Davies, R. and Kaye, B.H. (1971/2), *Powder Technol.*, 207–222,
251
- 50 Kaye, B.H. and Boardman, R.P. (1962), *Proc. Symp. Interaction
between Fluids and Particles*, Inst. Chem. Eng, London, 251
- 51 John, R. (1966), *Diss. Karlsruhe*, (1965), 252
- 52 Koglin, B. (1970), *Proc. Conf. Particle Size Analysis*, eds. M.J.
Groves and J.L. Wyatt-Sargent, Soc. Anal. Chem., Bradford,
U.K., 223–235, 252
- 53 Jovanovic, D.S. (1965), *Kolloid Z., Polymere*, 203(1), 42–56,
252
- 54 Barford, N. (1972), *Powder Technol.*, 6(1), 39–44, 252
- 55 Jayaweera, K.O.L.F., Mason, B.J. and Slack, B.W. (1964), *J.
Fluid Mech.*, 20, 121–128, 252
- 56 Davies, R. and Kaye, B.H. (1970), *Proc. Conf. Particle Size
Analysis*, eds. M.J. Groves and J.L. Wyatt-Sargent, Soc. Anal.
Chem., Bradford, U.K., 223–235, 252
- 57 Dollimore D. and Griffiths, D.L. (1960), *Proc. 3rd Int. Cong.
Surface Activity*, Cologne, V.2, Section B674, 252
- 58 Christian, J.R., Dollimore, D. and Horridge, T.A. (1970), *J.
Phys. E*, 3, 744, 253
- 59 Sarmiento, G. and Uhlherr, P.H.T. (1977), *Proc. 5th Australian
Chem. Eng. Conf.*, Canberra, 296, 253
- 60 Dollimore, D. and McBride, G.B. (1970), *Proc. Conf. Particle
Size Analysis*, ed. M.J. Groves and J.L. Wyatt-Sargent, Soc.
Analyst. Chem., Bradford, U.K., 223–235, 253
- 61 Dollimore, D. and Heal, G.R. (1962) *J. Appl. Chem.*, 12, 455,
253
- 62 Ramakrishna, V. and Rao, S.R. (1970), *J. Appl. Chem.*, 15, 473,
253
- 63 Ramakrishna, V. and Rao, S.R. (1970), *Proc. Conf. Particle Size
Analysis*, eds M.J. Groves and J.L. Wyatt-Sargent, Soc. Analyst.
Chem., Bradford, U.K., 223–235, 253
- 64 Pierce, T.J. (1970), *Proc. Conf. Particle Size Analysis*, eds. M.J.
Groves and J.L. Wyatt-Sargent, Soc. Analyst. Chem., Bradford,
U.K., 223–235, 253
- 65 Dollimore, D. and Horridge, T.A. (1971), *Trans. Br. Ceram.
Soc.*, 70, 191, 253
- 66 Dollimore, D. and Owens, N.F. (1972), *Proc. 6th Int. Cong.
Surface Activity*, Zurich, 253
- 67 Davies, L. and Dollimore, D. (1978), *Powder Technol.*, 19, 1–6,
253
- 68 Sarmiento, G. and Uhlherr, P.H.T. (1979), *Powder Technol.*, 22,
139–142, 254
- 69 Dollimore, D. (1972), *Powder Technol.*, 8, 207–220, 254

- 70 Dorn, E. (1880), *Wied. Ann.*, 10, 46, cit. Adamson, H.A. (1934),
Electokinetic Phenomena, Chem. Catal. Co. N.Y., 254
- 71 Elton, G.A.H. (1948), Electroviscosity, 1, *Proc. Royal Soc.*,
A194, 259, 254
- 72 Dulin, C.I. and Elton, G.A.H. (1952), *J. Chem. Soc.*, 286, 254
- 73 Elton, G.A.H. and Hierschler, F.F. (1954), *Br. J. Appl. Phys.*,
Suppl. 3, S60, 254
- 74 Elton, G.A.H. and Hierschler, F.F. (1962), *J. Chem. Soc.*, 2953,
254
- 75 Booth, F. (1950), *Proc. Royal Soc.*, *A203*, 533, 254
- 76 Booth, F. (1954), *J. Chem. Phys.*, 22, 1956, 254
- 77 Pavlik, R.E. and Sansone, E.B. (1973), *Powder Technol.*, 8,
159–164, 255
- 78 Sansone, E.B. and Civic, T.M. (1975), *Powder Technol.*, 12(1),
11–18, 255
- 79 Siano, D.B. (1979), *J. Colloid Interf. Sci.*, 68(1), 111–127, 255
- 80 Jones, T.M. (1969), *Symp. Powders*, Soc. Cosmetic Chem.,
Dublin, 256
- 81 Peleg, M. and Mannheim, C.H. (1973), *Powder Technol.*, 7, 45,
256
- 82 Pilpel, N. (1970), *Mfg. Chem. Aerosol News*, 4, 19, 256
- 83 Gold, G. et al. (1966), *J. Pharm. Sci.*, 55, 1291, 256
- 84 York, P. (1975), *Powder Technol.*, 11, 197–198, 256
- 85 Jenike, A.W. (1961), *Bull. 108*, Eng. Exp. St., Utah State Univ.,
256
- 86 Parfitt, G. (1977), *Powder Technol.*, 17(2), 157–162, 257
- 87 Gabrys-Deutscher, E. and Leschonski, K. (1995), *6th European
Symp. Particle Size Characterization*, Partec 95, Nürnberg,
Germany Publ. NürnbergMesse GmbH, 225–234, 257
- 88 Nelson, R.D. (1988), *Dispersing Powders in Liquids*, Elsevier,
257
- 89 Adamson, A.W. (1963), *Physical Chemistry of Surfaces*, Wiley,
N.Y., 257
- 90 Bartell, F.E. and Walton, C.W. (1934), *J. Phys. Chem.*, 38, 503,
259
- 91 Crowl, V.T. and Wooldridge, W.D.S. (1967), *Wetting*, SCI
Monograph No. 25, 200, 259
- 92 Washburn, E.D. (1921), *Phys. Rev.*, 17, 374, 259
- 93 Heertjes, P.M. and Kossen, N.W.F. (1966), *Powder Technol.*, 1,
33–42, 260
- 94 Kossen, N.W.F. and Heertjes, P.M. (1965), *Chem. Eng. Sci.*, 20,
593, 260
- 95 Carino, L. and Mollet, H. (1975), *Powder Technol.*, 11, 189–
194, 260
- 96 Crowl, V.T. (1967), *Pigments, An Introduction to their Physical
Chemistry*, ed. D. Patterson, Elsevier, 261

- 97 Bryant, D.P. (1968), *Proc. Soc. Anal. Chem.*, 5(8), 165–166,,
262
- 98 Rossi, C. and Baldocci, R. (1951), *J. Appl. Chem.*, 1, 446, 262
- 99 Buzagh, A. von (1937), *Colloid Systems*. 262
- 100 British Standard, BS3406, *Recommendations for gravitational liquid sedimentation methods for powders and suspensions*,
262
- 101 Groves, M.J. (1968), *Proc. Soc. Anal. Chem.*, 5(8), 166–168,
263
- 102 Hartig, H.E., Oristad, N.I. and Foot, N.J. (1951), Univ. Minn.
Mines Exp. St., Info. Circular No. 7, 263
- 103 Hathaway, R.E. and Guttrals, D.L. (1976), *Can. Min. Metall.
Bull.*, 69, 766, 64–71, 263
- 104 Koglin, B. (1977), *Powder Technol.*, 17(2), 219–227, 263
- 105 Karpenko, I., Dye, R.W. and Engel, W.H. (1962), *TAPPI*, 45(1),
65–69, 263
- 106 Carr, W. (1970), *JOCCA*, 53, 884, 264
- 107 Carr, W. (1977), *Powder Technol.*, 17(2), 183–190, 264

Sedimentation theory

7.1 Powder density

The *effective density* of a particle is the particle mass divided by the volume of liquid it displaces (Archimedes density). Its *true density* is the particle mass divided by the volume it would occupy if it were compressed so as to eliminate all the pores and surface fissures. Its *apparent density* is its mass divided by its volume, excluding open pores but including closed pores.

Quoted density values in standard reference works are of the materials *true density*. If density is determined using a gas pycnometer, the volume measured would include closed pores but exclude open pores i.e. the measured density would be the *apparent density*. If the suspending liquid penetrates all the cracks and fissures on the particle surface, the measured volume would be the same as that determined by gas pyknometry but the total mass would be greater due to the included liquid which will remain with the particle as it falls in the liquid, hence its sedimentation density will be intermediate between the apparent density and the true density and greater than the effective density. These differences are usually not highly significant for coarse particles unless they are highly porous.

In density determination the volume of fluid, displaced by a known weight of powder, is determined. Since weight can be measured accurately, the problem is that of accurate determination of volume. With pycnometers (or density bottles) the fluid is a liquid, usually water with surfactant, unless the powder is water miscible. With gas pycnometers the fluid is usually dry air or helium.

The usual methods for determining density using a liquid pycnometer bottle are described in British Standards, BS 733 and BS 3483. Essentially, the pycnometer bottle is weighed empty (M_1), then full of liquid (M_2), next about one third full of powder (M_3) and finally the bottle is topped up with water to the fill mark (M_4). Great care is required in this final step that the liquid is fully wetted and all the air removed. Variations in recorded weight also arise depending on how much liquid escapes when the ground glass stopper is inserted in the liquid filled container. Wilkes and Allen [1] found that using this

procedure with BCR 66 quartz gave a density of 2630 kg m^{-3} which was reproducible to $\pm 10 \text{ kg m}^{-3}$.

By taking extra-ordinary care, e.g. letting the bottle, after it had been filled, stand in a constant temperature bath 2°C above ambient temperature until the liquid no longer escaped through the capillary; topping up the bottle plus powder under vacuum and taking each reading ten times. they determined the density and standard deviation to be: $2613 \pm 0.0013 \text{ kg m}^{-3}$. Repeat measurements gave 2615 and 2612 kg m^{-3} .

If liquids other than water are used they should have a low evaporation rate under vacuum and a high boiling point ($>170^\circ\text{C}$); aromatic or aliphatic compounds are suitable. The use of oil presents a particular problem in that it is difficult to ensure that the outside of the bottle is completely oil free.

Burt *et al.* [2] consider the liquid pyknometer method to be unsuitable for powders which are predominantly smaller than $5 \mu\text{m}$ due to absorbed gases present on their surface. In order to remove these gases, the powder may need treatment at high temperature or under high vacuum. For particles with rough surfaces it is also possible that air trapped within surface pits and cracks cannot easily be removed. They propose the use of a centrifugal pyknometer in which a suspension, prepared in the usual way for sedimentation analysis, is placed and centrifuged and the density determined. The density so obtained is slightly lower than that obtained by other methods.

A special apparatus has been described which is claimed to be simpler to operate than most other methods for the determination of the apparent density of porous carbons [3]. The apparatus is designed so that the solid can be thoroughly outgassed so that degassed dilatometric liquid can be brought into contact with it without exposing the latter to the atmosphere. Other procedures involve the use of mercury [4] to determine envelope volume and volatile liquids to determine pore structure [5].

May and Marienko [6] used a 1 cm^3 micropyknometer, with ethylene glycol as the fill liquid, for measuring the density of small amounts of material. Stein *et al.* [7] found this method time consuming and difficult and developed a method in which air was used as the fill 'liquid'. Their micropyknometer had a 2 mm bore stem, accurately calibrated with mercury, at 0.30 and 0.50 cm^3 . A known weight of powder was placed in the pyknometer and the neck sealed with a mercury plug. This was forced down to the 0.50 cm^3 level in a pressure chamber at pressure P_1 and then to the 0.30 cm^3 level at pressure P_2 . The volume of powder (V) is given by:

$$V = \frac{P_2(0.30) - P_1(0.50)}{P_2 - P_1} \quad (7.1)$$

The volume of powder could be determined to $\pm 0.5 \text{ mm}^3$ corresponding to an accuracy of $\pm 3\%$ for a 25 mg sample of density 1500 kg m^{-3} .

Gas pyknometers are commercially available and a description of these has been presented by Thudium [8]. He criticizes instruments in which the measurement consists of an absolute volume change or a variable containing the absolute volume change [9] since the relationship between the measured parameter and particle volume is nonlinear. In instruments having only one chamber,[10,11] or having one chamber as pressure reference only,[12] every fluctuation in temperature gives an error of measurement. In systems having two chambers only differences between the two chambers gives an error.

Essentially, the two chamber instruments [13] consist of two cylinders, containing linked pistons on a screw thread, separated by a diaphragm linked to a volume readout. When a handle is turned, the pistons are driven into the cylinders until the measurement piston hits a stop, at zero reading. With powder in the measurement cylinder, the reference cylinder will record a volume when the measurement cylinder hits the stop. Thudium criticizes this type of pyknometer [8] on the grounds that if the pressure was reduced, rather than increased, the large volume change could be reduced by 50%; moreover, sorption effects would also be reduced. An instrument embodying these recommendations was described by Hänel [14], who also described a micropyknometer with expansion using a micrometer syringe, thus reducing the pressure change to less than 10 mbar.

Thudium was particularly interested in micropyknometers for measuring volumes smaller than 5 mm^3 and considered that the best to be one described by Hänel [14] which would measure a volume of 20 to 40 mm^3 with an accuracy of $\pm 10\%$.

7.2 Liquid viscosity

The viscosity of the suspending medium should have a value that fulfills the following conditions.

1. The largest particle in the suspension should settle under laminar flow conditions, i.e. the Reynolds number should be less than 0.25.
2. The free-falling velocity of the largest particle should be restricted so that it takes at least 1 min for it to reach the measurement zone.

For the first condition, the relationship between Stokes diameter and viscosity is given by inserting a value $Re = 0.25$ in Stokes equation giving:

$$\eta = \sqrt{\frac{(\rho_s - \rho_f) \rho_f g d_{St}^3}{4.5}} \quad (7.2)$$

For a particle of density $\rho_s = 2700 \text{ kg m}^{-3}$ and size $75 \mu\text{m}$, settling in a suspending medium of density $\rho_f = 1000 \text{ kg m}^{-3}$, the required viscosity $\eta = 0.00125 \text{ Pa s}$. Alternatively, for comparison purposes, a frequency may be plotted against free-falling diameter.

7.3 Resolution of sedimenting suspensions

The size range of particles within a detector is controlled by the height of the detector beam (δh) hence the measurement gives the concentration between an upper and lower size limit.

Assuming Stokes' law to apply, equation (6.8) may be written as:

$$D^2 = k \left(\frac{h}{t} \right) \quad (7.3)$$

Differentiating with respect to h with t constant:

$$2D \left(\frac{dD}{dh} \right)_t = \frac{k}{t} = \left(\frac{D^2}{h} \right)$$

The size resolution is given by:

$$\frac{\Delta D}{D} = \frac{\Delta h}{2h} \quad (7.4)$$

For a hydrometer where $\Delta h = h$, when $50 \mu\text{m}$ particles are at a measurement depth of 10 cm, the bottom of the hydrometer bulb is at a depth of 15 cm and the top is at a depth of 5 cm, so that particles of size $35.4 \mu\text{m}$ will be entering the measurement zone and particles of size $70.7 \mu\text{m}$ will be leaving it. If the weight frequency of particles in the 35.4 to $50 \mu\text{m}$ range is balanced by the weight frequency in the 50 to $70.7 \mu\text{m}$ range, the effect is balanced out, otherwise a bias results. The effect of such a bias is to mask peaks in a multi-modal distribution.

If the thickness of the measurement zone is less than one sixth of the settling depth, the size resolution of around 8% leads to tolerable errors.

7.4 Concentration changes in a suspension settling under gravity

Let a mass $m_s = \rho_s v_s$ of powder be dispersed in a mass $m_f = \rho_f v_f$ of fluid, ρ and v being density and volume respectively. Initially the concentration will be uniform and equal to:

$$C(h,0) = \frac{\text{mass of powder}}{\text{volume of powder} + \text{volume of fluid}}$$

$$C(h,0) = \frac{m_s}{v_s + v_f} \quad (7.5)$$

where $C(h,0)$ is the concentration at depth h , time $t = 0$.

Consider a small horizontal element at depth h . At the commencement of sedimentation the particles leaving the element are balanced by the particles entering it from above. When the largest particles present in the suspension leave the element, after settling from the surface, there are no similar particles entering to replace them. The concentration will then fall and become equal to a concentration smaller than that of d_{St} , where d_{St} is the size of the particle that settles at a velocity of h/t . The concentration of the suspension at depth h at time t may be written:

$$C(h,t) = \frac{m'_s}{v'_s + v_f} = \frac{d_{St}}{\int F(d)dd} \quad (7.6)$$

where m'_s is the mass and v'_s is the volume of solids in a volume v_f of fluid at a depth h from the surface of the suspension at time t from the commencement of sedimentation.

$$C(h,0) = \frac{m_s}{v_s + v_f} = \frac{d_{\max}}{\int F(d)dd} \quad (7.7)$$

From equations (7.5–7.7):

$$\frac{C(h,t)}{C(h,0)} = \frac{\frac{m'_s}{m_s}}{\frac{d_{\max}}{\int F(d)dd}} = \frac{\frac{d_{St}}{d=d_{\min}}}{\frac{d_{\max}}{\int F(d)dd}} \quad (7.8)$$

It is assumed that the difference between v_s' and v_s is negligible compared with v_f .

Thus a graph of $100 \frac{C(h,t)}{C(h,0)}$ against d_{St} gives the percentage undersize Stokes diameter by weight.

7.5 Relationship between density gradient and concentration

Let $\phi(h,t)$ be the density of the suspension at depth h and at time t . Then:

$$\phi(h,t) = \frac{m_s' + m_f}{v_s + v_f}$$

$$\phi(h,t) = \frac{\rho_s v_s' + \rho_f v_f}{v_s + v_f}$$

$$\phi(h,t) = \frac{\rho_f(v_s' + v_f) + (\rho_s - \rho_f)v_s'}{v_s + v_f}$$

$$\phi(h,t) = \rho_f + \frac{(\rho_s - \rho_f)}{\rho_s} \frac{m_s'}{v_s + v_f}$$

$$\phi(h,t) = \rho_f + \frac{(\rho_s - \rho_f)}{\rho_s} C(h,t)$$

Also

$$\phi(h,0) = \rho_f + \frac{(\rho_s - \rho_f)}{\rho_s} C(h,0)$$

Therefore

$$\frac{C(h,t)}{C(h,0)} = \phi = \frac{\phi(h,t) - \rho_f}{\phi(h,0) - \rho_f} \quad (7.9)$$

where ϕ is the mass fraction undersize d_{St} .

A plot of $100 \frac{\phi(h,t) - \rho_f}{\phi(h,0) - \rho_f}$ against d_{St} gives a cumulative mass percentage undersize curve.

7.5.1 Hydrometers

The changes in density of a settling suspension may be followed with a hydrometer, a method widely used in soil science and in the ceramic industry. A suspension of known concentration is made up and the hydrometer inserted. Some operators leave the hydrometer in the suspension throughout the analysis and some remove it after each reading and replace it slowly before the next. Objections can be raised to either procedure since, in the former, particles settle on the hydrometer causing it to sink to a lower level than it would otherwise sink whereas, in the latter, the suspension is disturbed after each reading. To minimize errors some operators reshake the container after each reading.

With the hydrometer immersed, its weight W equals the weight of suspension displaced. Let the length of stem immersed in clear suspending liquid be L , i.e. the same as would be immersed at infinite time; the length immersed at the commencement of the analysis be L_0 and the length immersed at time t be L_t . Then, at the commencement of the analysis:

$$W = V\phi(h,0) + 100 \frac{\phi(h,t) - \rho_f}{\phi(h,0) - \rho_f} \quad (7.10)$$

At time $t = \infty$ (clear liquid in the container)

$$W = V\rho_f + L\alpha\rho_f \quad (7.11)$$

During the analysis, at time t

$$W = V\phi(h_t, t) + L_t\alpha\rho_2 \quad (7.12)$$

where V is the volume of the hydrometer bulb, α the cross-sectional area of the stem and h_t the depth of the hydrometer bulk at time t .

Since the density of the suspension around the stem (ρ_1, ρ_f, ρ_2) varies negligibly compared with the variation in L equation (7.9) can be written:

$$\phi = \frac{L_t - L}{L_0 - L} = \frac{w_t - w}{w_0 - w} \quad (7.13)$$

where w is the specific gravity marked on the hydrometer stem.

If the suspension is made up of W gram of powder making up 1 L of suspension, equation (7.12) can be written:

$$\phi = \frac{1000}{W} \frac{\rho_s(\rho_t - \rho_f)}{(\rho_s - \rho_f)} \quad (7.14)$$

where ρ_t is the density of the suspension at time t .

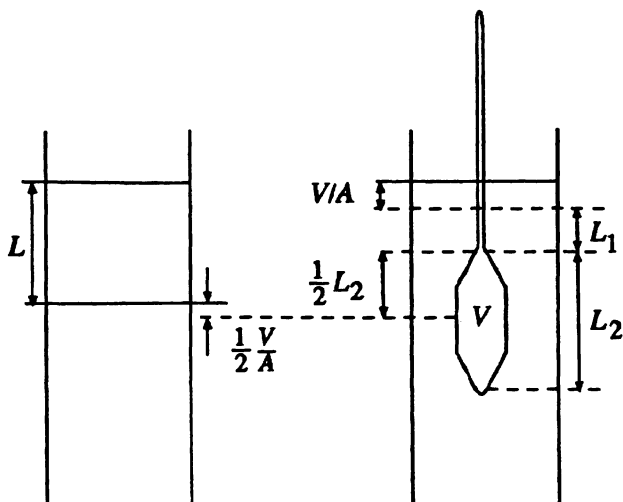


Fig. 7.1 Depth of immersion using a hydrometer.

With the hydrometer technique, both density and depth of immersion vary with each reading. If the temperature is maintained constant at the hydrometer calibration temperature the density may be read directly from the hydrometer stem otherwise a correction needs to be applied.

The chief difficulty lies in determining the point of reference below the surface to which this density refers, for when the hydrometer is placed in the suspension the liquid level rises in the container, thus giving a false reference point (Fig. 7.1). If the cross-sectional area of the container is A , the depth to be used in Stokes equation, from geometrical considerations, is:

$$L = L_1 + \frac{1}{2} \left(L_2 - \frac{V}{A} \right) \quad (7.15)$$

This simple formula has been challenged by several workers who claim that corrections have to be applied for the density gradient about the bulb and the displacement of suspension by the stem. Johnson [15], for example gives the sedimentation depth as:

$$L = L_1 + \frac{1}{2} \left(L_2 - \frac{V}{A} \right) - 0.5 \text{ cm} \quad (7.16)$$

The method for carrying out an hydrometer analysis is given in BS 1377 [16].

7.6 Theory for the gravity photosedimentation technique

7.6.1 The Beer - Lambert law

Consider a sedimentation container of width L measured in the direction of the light beam, containing the suspension of powder under analysis.

Let the incident light intensity falling on an element of thickness ∂L be I and the emergent light flux be $I - \partial I$. If the area of the light beam is A , the reduction in flux due to the presence of particles may be attributed to a fall in the overall intensity of the light beam or a reduction in the area of the light beam (Figure 7.2).

The emergent flux may be written:

$$(I - \partial I)A = (A - \partial A)I$$

$$\frac{\partial I}{I} = \frac{\partial A}{A} \quad (7.17)$$

where ∂A is the effective cross-sectional area of particles in the beam perpendicular to the direction of propagation. The equation holds provided that the beam of light becomes homogeneous again between adjacent particles.

Let there be n_x particles of diameter d_x in unit mass (1 kg) of powder and let the powder concentration in suspension be c (kg m^{-3}); then, at time t the following expression holds.

$$\partial A = cA\partial L \sum_{x=\min}^{x=St} K_x k_x n_x d_x^2 \quad (7.18)$$

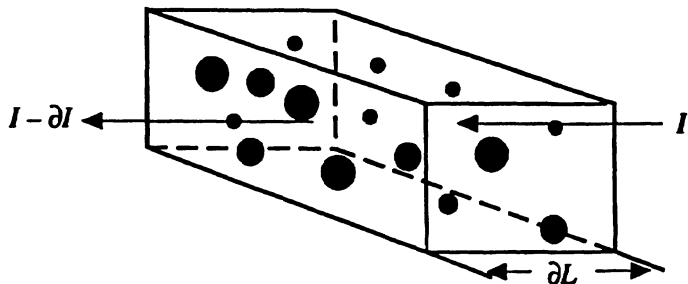


Fig. 7.2 For a light beam of cross-sectional area A intersecting a suspension the reduction in light flux, ∂I is proportional to the cross sectional area of particles in the beam ∂A .

where k_x is a shape coefficient ($k_x = \pi/4$ for spheres) d_{min} and d_{St} are the diameters of the smallest and largest particles in the beam at time t and K_x is the extinction coefficient for a particle of diameter d_x .

The extinction coefficient is defined as:

$$K_x = \frac{\text{light obscured by a particle of size } d_x}{\text{light which would be obscured if the laws of geometric optics held}} \quad (7.19)$$

From equations (7.17) and (7.18)

$$\frac{I_t}{I_0} = c \int_0^L dL \sum_{x=\min}^{x=S_t} K_x k_x n_x d_x^2 \quad (7.20)$$

Integrating for time t gives:

$$\ln\left(\frac{I_0}{I_t}\right) = -cL \sum_{x=\min}^{x=S_t} K_x k_x n_x d_x^2 \quad (7.21)$$

where I_0 is the emergent light intensity with clear liquid in the beam and I_t is the emergent light intensity at time t .

The optical density (E_t) of the suspension at time t is defined as:

$$E_t = \log\left(\frac{I_0}{I_t}\right)$$

$$E_t = cL(\log_{10} e) \sum_{x=\min}^{x=S_t} K_x k_x n_x d_x^2 \quad (7.22)$$

Consider a small change (ΔE_x) in the optical density as the sedimentation time changes from t to $t + \Delta t$ so that the average Stokes diameter in the beam is d_x .

$$\frac{\Delta E_x}{K_x} = cL(\log_{10} e) k_x n_x d_x^2 \quad (7.23)$$

The cumulative distribution undersize by surface, assuming that K is constant for the restricted size range under consideration, is:

$$\frac{\sum_{x=0}^{x=S_t} n_r d_x^2}{\sum_{x=0}^{x=\max} n_r d_x^2} = \frac{\sum_{x=0}^{x=S_t} \frac{\Delta E_x}{K_x}}{\sum_{x=0}^{x=\max} \frac{\Delta E_x}{K_x}} \quad (7.24)$$

It is therefore necessary to know how K varies with d in order to determine the size distribution. If this correction is not applied the method is only valid for comparison purposes. Theoretical values of K may be used but this will also introduce errors, since the effective K values depend upon the optical geometry of the system. Calibration may also be against some external standard.

The cumulative distribution undersize by weight is given by:

$$\frac{\sum_{x=0}^{x=S_t} n_r d_x^3}{\sum_{x=0}^{x=\max} n_r d_x^3} = \frac{\sum_{x=0}^{x=S_t} \frac{\Delta E_x d_x}{K_x}}{\sum_{x=0}^{x=\max} \frac{\Delta E_x d_x}{K_x}} \quad (7.25)$$

The surface area of the powder is derivable from the initial concentration of the suspension and the maximum optical density (E_{max}):

$$S = \alpha_{s,x} n_x d_x^2$$

Combining with equation (7.23), bearing in mind that n_x is the number of particles of size d_x in unit weight ($W = 1$) of powder:

$$S_W = \frac{\alpha_s}{c L \log_{10} e} \sum_{x=0}^{x=\max} \frac{\Delta E_x}{K_x} \quad (7.26)$$

where α_s is the surface shape coefficient, which may be assumed constant for a powder having a narrow size range.

Integrating equation (7.26):

$$S_W = \frac{\alpha_s}{k K_m L \log_{10} e} \frac{E_{max}}{c} \quad (7.27)$$

where K_m is the mean value for the extinction coefficient. For non-re-entrant (convex) particles, the ratio of the surface and projected area

shape coefficients (α_s/k) is equal to 4. For re-entrant particles, the surface obtained by making this assumption is the envelope surface area. Equation (7.27) simplifies to:

$$S_W = \frac{9.2}{K_m L} \frac{E_m}{c} \quad (7.28)$$

7.6.2 The extinction coefficient

The extinction coefficient varies with the optical properties of the solid and liquid which make up the suspension. Knowing these properties, it is possible to generate a relationship between the extinction coefficient and particle size using Mie or a boundary condition theory. Since unit area of $0.2\text{ }\mu\text{m}$ TiO_2 cuts off 10 times as much light as unit area of $0.1\text{ }\mu\text{m}$ TiO_2 , (Figure 7.3), if no correction is applied the measured distribution will be heavily weighted towards the coarser particles. The relationships hold for an infinitely small solid angle between the detector and the suspension so a correction for the geometry of the analyzer may be required. Alternatively the instrument may be calibrated against some external standard. If no correction is made for variation in extinction coefficient ($K = 1$) the derived distribution is only a size dependent response and the method becomes a fingerprint method (i.e. useful for comparison purposes only).

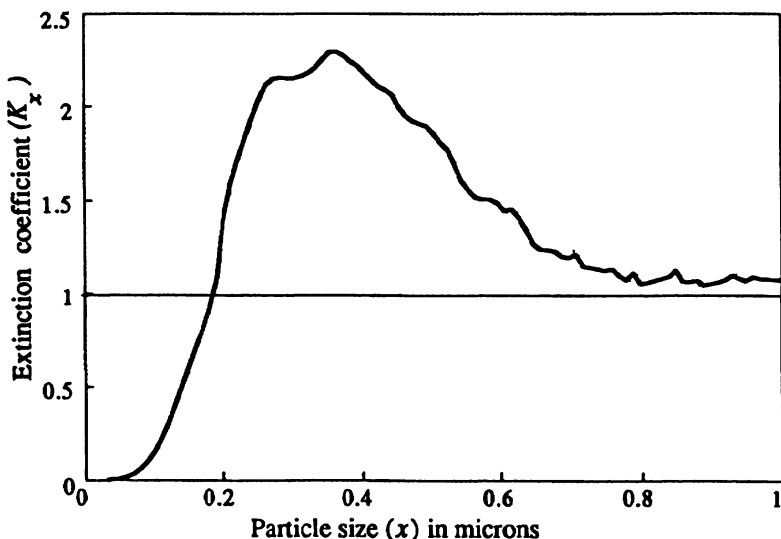


Fig. 7.3 Extinction curve for titanium dioxide in water for white light.

7.7 Theory for concentration determination with the x-ray gravitational sedimentation technique

A natural extension to the use of visible radiation is to use x-rays. In this case the x-ray density is proportional to the weight of powder in the beam. The Beer-Lambert law takes the form:

$$I = I_0 \exp(-Bc) \quad (7.29)$$

where B is a constant related to the atomic number of the powder in suspension, c is the powder concentration, I is the emergent flux with suspension in the beam and I_0 is the emergent flux with clear suspension liquid. E , the x-ray density, is defined as:

$$E = \log_{10} \left(\frac{I}{I_0} \right) \quad (7.30)$$

For powders of low atomic number, c needs to be high to obtain a large enough signal. Thus for silica powders, atomic number 13, a volume concentration of around 3% may be necessary and this can lead to hindered settling.

7.8 Theory for mass oversize distribution determination for cumulative, homogeneous, gravitational sedimentation

The theory given below was developed by Oden [17] and modified by Coutts and Crowthers [18] and Bostock [19]. Consider a distribution of the form:

$$W = \int_{d_{St}}^{d_{\max}} f(d) dd$$

where W is the mass percentage having a diameter greater than Stokes diameter. The weight percentage P which has settled out in time t is made up of two parts; one consists of all the particles with a falling speed equal or greater than v_{St} , the other consists of particles with a smaller falling speed which have settled out because they started off at some intermediate position in the fluid column (Fig. 7.4). If the falling velocity of one of these particles is v , the fraction of particles of this size which will have fallen out at time t is vt/h , where h is the height of the suspension. Hence:

$$P = \frac{\int_{d_{St}}^{d_{\max}} f(d) dd}{d_{St}} + \int_{d_{\min}}^{d_{St}} \frac{vt}{h} f(d) dd \quad (7.31)$$

Differentiating with respect to time and multiplying by t :

$$t \frac{dP}{dt} = \int_{d_{\min}}^{d_{St}} \frac{vt}{h} f(d) dd \quad (7.32)$$

i.e.

$$P = W + t \frac{dP}{dt} \quad (7.33)$$

Since P and t are known it is possible to determine W using this equation. It is preferable, however to use the equation in the following form [20]:

$$P = W + \frac{dP}{d \ln t} \quad (7.34)$$

Several methods of applying this equation have been suggested. The most obvious is to tabulate t and P and hence derive dP/dt and finally W . Alternatively, P may be plotted against t and tangents drawn. A tangent drawn at point (P_r, t_r) will intercept the abscissa at W_r , the weight percentage oversize d_r . Another method is to tabulate P against t at times such that the ratio of (t/dt) remains constant, i.e. at time intervals in a geometric progression; a simple expression relating W and P then develops [21,22].

Many powders have a wide size distribution and, in such cases, the time axis becomes cramped at the lower end or unduly extended at the upper end; in such cases equation (7.33) should be applied. Evaluation proceeds from a plot of P against $\ln t$; tangents are drawn every half-unit of $\ln t$; the point where the tangent cuts the ordinate line one $\ln t$ unit less than the value at which it is tangential gives the weight percentage oversize W at that value [19].

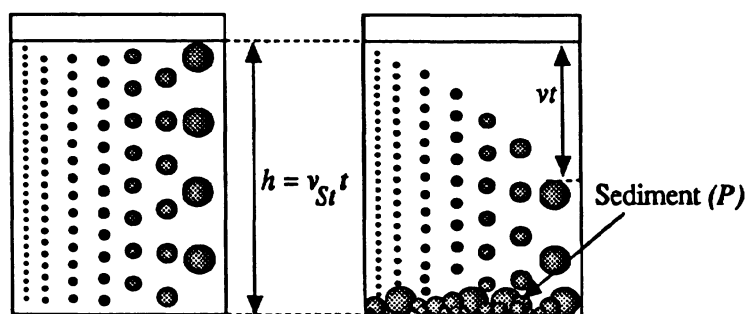


Fig. 7.4 Homogeneous, cumulative, gravitational sedimentation theory.

7.9 Stokes equation for centrifugal sedimentation

7.9.1 General theory

A particle settling in a centrifugal field is acted upon by a drag force and a centrifugal force. The force balance in the laminar flow region is given by:

$$\frac{\pi}{6}(\rho_s - \rho_f)d_{St}^3 \frac{d^2r}{dt^2} = \frac{\pi}{6}(\rho_s - \rho_f)d_{St}^3 \omega^2 r - 3\pi\eta d_{St} \frac{dr}{dt} \quad (7.35)$$

where:

r = distance from the axis to the particle;

$\frac{dr}{dt}$ = outward velocity of the particle;

ρ_s, ρ_f = density of the particle and suspension medium;

η = coefficient of viscosity of the medium;

d_{St} = Stokes diameter of the particle;

ω = speed of rotation of the centrifuge in radians per second.

At the terminal velocity ($dr/dt^2 = 0$) this equation becomes:

$$3\pi\eta d_{St} \frac{dr}{dt} = \frac{\pi}{6}(\rho_s - \rho_f)d_{St}^3 \omega^2 r$$

$$\frac{dr}{dt} = u_c = \frac{(\rho_s - \rho_f)d_{St}^2 \omega^2 r}{18\eta} \quad (7.36)$$

Thus, the settling velocity is not constant as in gravitational sedimentation but increases with increasing radius.

Comparing with Stokes equation for gravitational settling (settling velocity under gravity = u_{St}):

$$u_c = \frac{\omega^2 r}{g} u_{St} = G u_{St} \quad (7.37)$$

where G , the separation factor, is a measure of the increased rate of settling in a centrifugal field.

7.10 Stokes diameter determination for cumulative and incremental line-start techniques

Rewriting equation (7.36) in integral form:

$$\begin{aligned} \int_{S}^r \frac{dx}{x} &= \int_0^{d_{St}} \frac{(\rho_s - \rho_f)}{18\eta} d^2 \omega^2 dt \\ \ln\left(\frac{r}{S}\right) &= \frac{(\rho_s - \rho_f)}{18\eta} d_{St}^2 \omega^2 t \\ d_{St} &= \sqrt{\frac{18\eta \ln(r/S)}{(\rho_s - \rho_f) \omega^2 t}} \end{aligned} \quad (7.38)$$

where t is the time for a particle of Stokes diameter d_{St} to settle from the surface of the fill liquid at radius S to measurement radius r , which, for cumulative techniques, is equal to R , the distance from the axis to the inside radius of the centrifuge.

7.10.1 Incremental, line-start, centrifugal technique

Since all the particles emanate from the same starting point the Stokes diameter is determined using equation (7.38).

7.10.2 Homogeneous, cumulative, centrifugal technique

In this case all particles greater than d_{St} will have reached the bottom of the sedimentation cell [equation (7.38) with $r = R$].

7.10.3 Sedimentation distance small compared with distance from centrifuge axis

The simplest procedure with a homogeneous, centrifugal system is to make $r - S$ small compared with S and assume that the particles fall with constant velocity. Equation (7.36) becomes:

$$u_c = \frac{(\rho_s - \rho_f) d_{St}^2}{18\eta} \omega^2 \left(\frac{r+S}{2} \right) \quad (7.39)$$

This approach has been used by several investigators and applies to the Alpine sedimentation centrifuge and the Mikropul.

7.11 Line-start technique using a photocentrifuge

7.11.1 Introduction

Photocentrifuges are available in both disc and cuvet configuration. The former are normally used in the line-start mode and the latter in the homogeneous mode. The line-start mode has a much higher resolution than the homogeneous mode so that multimodal distributions are closely defined. The homogeneous mode can be run using a gradient procedure, with acceleration over time, which greatly speeds up the analysis.

Both modes suffer the disadvantage that the laws of geometric optics do not apply, and the correction required can introduce large errors, especially with size distributions having a wide size range. For the examination of paint pigments, end-use properties may be more closely related to the attenuation curve than the derived size distribution. It is therefore arguable that the measured relationship between attenuation and Stokes diameter should be used to define the powder rather than size distribution.

7.11.2 Homogeneous mode

(a) *Stokes diameter determination:* For a constant (centrifuge) speed operation equation (7.38) is applied. In the gradient mode ω is replaced by an expression relating centrifuge speed with time.

(b) *Mass frequency undersize determination:* Equations (7.25) is applied.

7.11.3 Line-start mode

(a) *Stokes diameter determination:* Equation (7.38) is applied.

(b) *Mass frequency undersize determination:* In the line-start mode the disc is filled to a known (surface) radius with clear fill liquid whilst the centrifuge is spinning. A small amount of buffer liquid is added and, finally, about 0.25 cm^3 of suspension. The surface radius, S , is taken as the interface between the suspension layer and the buffer layer. The position of a particle of Stokes diameter d_{St} will change with time according to equation (7.38):

$$r = S \exp((kd_{St}^2)t) \quad (7.40)$$

where

$$k = \frac{(\rho_s - \rho_f)}{18\eta} \omega^2$$

A wedge shaped detector window (with radial sides, circular inner and outer sides), centered on r and spanning r_1 to r_2 where $r_2 > r_1$, will view an annular section of the disc. At time $t = 0$ there is only clear liquid in the window. As time progresses, the largest particles present in the suspension will enter the window and at time t the diameter of the particles at the center of the window will be:

$$d_{St} = \sqrt{\frac{k}{t} \ln \frac{r}{S}} \quad (7.41)$$

The suspension in the window will contain particles with diameters in the size range $d_1 = d_{St}(1-\beta)$ to $d_2 = d_{St}(1+\theta)$ where d_1 is the diameter of the particle just entering the window and d_2 the diameter of the particle just leaving it:

$$\begin{aligned} d_{St}(1-\beta) &= \sqrt{\frac{k}{t} \ln \frac{r_1}{S}} \\ d_{St}(1+\theta) &= \sqrt{\frac{k}{t} \ln \frac{r_2}{S}} \end{aligned} \quad (7.42)$$

If we substitute to eliminate d_{St} we find that β and θ are dependent only on geometric factors and not on material properties.

$$\beta = 1 - \sqrt{\frac{\ln\left(\frac{r_1}{S}\right)}{\ln\left(\frac{r}{S}\right)}} \quad \theta = \sqrt{\frac{\ln\left(\frac{r_1}{S}\right)}{\ln\left(\frac{r}{S}\right)}} - 1 \quad (7.43)$$

If the detector window is fixed, both r_1 and r_2 will remain constant during a run, so that β and θ will be constants independent of time. Note that while the ratio of d_1/d_2 remains constant with time the difference between d_1 and d_2 decreases since the value of d_{St} decreases with time [$d_2 - d_1 = d_{St}(\theta + \beta)$, i.e. the difference is proportional to the Stokes diameter].

The number fraction of particles in the field of view is given by:

$$f(d) = \int f(N) dd_{St,r} \quad \begin{matrix} r = (1+\theta) \\ r = (1-\beta) \end{matrix} \quad (7.44)$$

$$\text{where } f(N) = \frac{dN}{dd}$$

Using a general series expansion, the solution to this equation takes the form [23]:

$$f(d) = (\beta + \theta) \sum_j g_j d_{St}^{j+1} \quad (7.45)$$

Thus, the fraction of particles in the field of view varies in a complex fashion with d_{St} .

Intuitively one would expect the optical density to be proportional to the projected area of the particles in the light beam. Published solutions state that the amount of light cut off is proportional to particle volume [24-26] for line-start and to particle surface for homogeneous mode.

The conclusion drawn from equation (7.45) is at odds with published data on polystyrene latices and silver bromide, in which a volume proportionality is found [27,28]. However these distributions were narrow, and with narrow distributions the difference between volume and surface distributions are small. The conclusion is also at variance with data published on BCR 66 quartz powder, ranging in size from 0.3 to 3 μm . In this case the median for the attenuation curve was 1.52 μm which reduced to 1.14 μm with extinction factor correction [29], and a correction of this magnitude could hide the effect.

Photosedimentation yields an attenuation curve; particles at the fine end of the distribution at say 0.1 μm , obscuring the light by perhaps one twentieth of their geometric area whereas at the coarse end, say 1 μm , the ratio can be greater than two. The correction for extinction coefficient modifies the shape of the curve considerably, making decisions as to correct theory to apply difficult. The unmodified attenuation curve may be more relevant to end-use properties, for organic pigments for example, than the derived size distribution and extinction curve corrections should be applied with caution.

7.12 Theory for mass oversize distribution determination for cumulative, homogeneous, centrifugal sedimentation

Equation (7.40) may be written (for $r = R$):

$$S = R \exp(-kd_{St}^2 t) \quad (7.46)$$

At the end of time t , all particles greater than d_{St} will have reached the bottom of the container. In addition, partial sedimentation will have taken place for particles smaller than d_{St} . For each of these smaller sizes, a starting point x_0 exists, beyond which all the smaller particles will have reached R where, from equation (7.40):

$$x_0 = R \exp(-kd^2 t) \quad (7.47)$$

The volume fraction of suspension lying between R and x_0 for shallow bowl or flat sector shaped tubes is equal to:

$$\frac{R^2 - x_0^2}{R^2 - S^2} = \frac{R^2}{R^2 - S^2} [1 - \exp(-2kd^2 t)] \quad (7.48)$$

If the particle size distribution is defined such that the weight fraction in the size range d to $d + \delta d$ is $f(d)dd$ then the weight of particles with diameters greater than d_{St} that have completely settled is:

$$W = \int_{d_{St}}^{\infty} f(d) dd$$

The weight fraction of particles smaller than d_{St} which have completely settled is:

$$I = \frac{R^2}{R^2 - S^2} \int_0^{d_{St}} [1 - \exp(-2kd^2 t)] f(d) dd$$

The total weight fraction deposited is:

$$P = W + \frac{R^2}{R^2 - S^2} \int_0^{d_{St}} [1 - \exp(-2kd^2 t)] f(d) dd \quad (7.49)$$

The weight fraction oversize can be determined if the weight fraction deposited is measured for different values of the variables S , R and t .

Similarly, the weight fraction of particles still in suspension at time t will consist of particles smaller than d_{St} that have originated in the volume between the surface S and radius x_0 . By comparison with equations (7.48) and (7.49), this fraction is:

$$(1 - P) = (1 - I) = \int_0^{d_{St}} \frac{x_0^2 - S^2}{R^2 - S^2} f(d) dd$$

$$(1-P) = \frac{R^2}{R^2 - S^2} \int_0^{d_{St}} [\exp(-2kd^2 t) - \exp(-2kd_{St}^2 t)] f(d) dd$$

$$(1-P) = \frac{1}{1 - \exp(-a)} \int_0^{d_{St}} \left[\exp\left(\frac{-ad^2}{d_{St}^2}\right) - \exp(-a) \right] f(d) dd \quad (7.50)$$

where $a = 2 \ln\left(\frac{R}{S}\right)$

7.13 Theory for mass oversize distribution determination for incremental, homogeneous, centrifugal sedimentation

7.13.1 General theory

The largest particle, of Stokes diameter d_{St} , present in the measurement zone at time t and radius r will have originated from the surface at radius S . From equation (6.78) the following relationship holds:

$$\left(\frac{r}{S}\right) = \exp\left[\frac{(\rho_s - \rho_f)}{18\eta} d_{St}^2 \omega^2 t\right] \quad (7.51)$$

$$\left(\frac{r}{S}\right) = \exp[kd_{St}^2 t] \quad (7.52)$$

where $k = \frac{(\rho_s - \rho_f)}{18\eta} \omega^2$

Particles in the measurement zone of size d_i will have originated from radius r_i where $r > r_i \geq S$ and:

$$\left(\frac{r}{r_i}\right) = \exp(kd_i^2 t) \quad (7.53)$$

The particles originally at radius r_i , in an annular element of thickness Δr_i move in diverging (radial) paths and at radius r occupy an annular element of thickness Δr . There will be a fall in the concentration of particles of this size in the measurement zone therefore, since the same number of particles will occupy a greater volume.

The fractional increase in volume is given by:

$$\frac{r\Delta r}{r_i \Delta r_i} = \left(\frac{r}{r_i} \right)^2 \quad (7.54)$$

since, from equation (7.53), $\Delta r/\Delta r_i = r/r_i$.

For a polydisperse system with a weight fraction in the size range d to $d + dd$ of $f(d)dd$, the concentration dQ of this weight fraction at r is given by:

$$dQ = \left(\frac{r_i}{r} \right)^2 f(d) dd$$

hence:

$$dQ = \int_0^{d_{St}} \left(\frac{r_i}{r} \right)^2 f(d) dd \quad (7.55)$$

Combining with equation (7.46) gives:

$$Q(d_{St}) = \int_0^{d_{St}} \exp(-2kd_i^2 t) f(d) dd \quad (7.56)$$

Substituting for k from equation (7.52):

$$Q(d_{St}) = \int_0^{d_{St}} \exp \left[-2 \left(\frac{d_i}{d_{St}} \right)^2 \ln \left(\frac{r}{S} \right) f(d) \right] dd \quad (7.57)$$

Various solutions to these equations have been proposed. In the variable time method the concentration is measured as a function of $\omega^2 t$ and all other variables are kept constant. For scanning systems both $\omega^2 t$ and r vary and in pipette withdrawal systems $\omega^2 t$ and S vary.

7.13.2 Variable time method

Differentiation of equation (7.14) gives:

$$\frac{dQ}{dd} = \exp(-2kd_i^2 t) f(d)$$

where

$$f(d) = \frac{dF(d)}{dd}$$

The boundary conditions are that $Q = 1$ when $t = 0$ for all r_i ; $Q = 0$ when $r_i = S$ for $t > 0$; with the additional condition that $F(d) = 0$ when $d_{St} = 0$. Thus:

$$F(d_{St}) = \int_0^{d_{St}} \exp(-2kd^2t) dQ \quad (7.58)$$

$$F(d_{St}) = \int_0^{d_{St}} \left(\frac{r_i}{S} \right)^2 dQ$$

d_{St} is the diameter of the particle that settles from the surface, radius S , to the measurement radius r in time t . The expression was first developed by Berg [30] and later by Kamack [31].

If Q is plotted as a function of $y = ((r_i/S)^2 t'$ with $t' = \omega^2 t$ as parameter, a family of curves is obtained whose shape depends on the particle size distribution function. The boundary conditions are that $Q = 1$ when $t' = 0$ for all r_i (i.e. the suspension is initially homogeneous) and $Q = 0$ for $r_i = S$ when $t' > 0$ (i.e. the surface region is particle free as soon as the centrifuge bowl spins). Hence all the curves, except for $t' = 0$, pass through the point $Q = 0$, $r_i = S$, and they will all be asymptotic to the line $t' = 0$, which has the equation $Q = 1$. Furthermore, from equation (7.58) the areas under the curves are each equal to $F(d_{St})$.

Let Q_1 be the smallest experimentally determined concentration so that $t_1 > t_2 > t_r$ and let Q be determined at a fixed sampling distance r for various values of t' . Then one point is known on each curve in addition to the common point $y = 1$, $Q = 0$. Such a set of points are illustrated by the black circles in Fig. 7.5. To each point corresponds a known value of d_{St} obtained from equation (7.38). Further, the area included between each curve, the concentration axis and the ordinates $Q = 0$ and Q_{St} is equal to $F(d_{St})$. Thus $F(d_{St})$ is approximated by the trapezoidal rule for, first of all, $F_1 = 0.5(1 + y)Q_1$. Now considering the curve for t'_2 , a point can be found on it corresponding to d_1 , i.e. a point such that the area under the curve up to this point is F_1 , which is

now known. If the ordinate at this point is called y_{12} and the abscissa F_{12} , then by equation (7.38):

$$d_1 = \sqrt{\frac{9\eta \ln y_{12}}{(\rho_s - \rho_f) \omega^2 t_2}}, \quad \text{and} \quad d_2 = \sqrt{\frac{9\eta \ln y}{(\rho_s - \rho_f) \omega^2 t_2}} \quad (7.59)$$

$$\text{so } y_{12} = y^{(d_1/d_2)^2}$$

Equating areas:

$$(1+y)Q_1 = (1+y_{12})Q_{12} = 2F_1 \quad (7.60)$$

so both y_{12} and Q_{12} are known. Applying the trapezoidal rule:

$$F_2 - F_1 = \frac{1}{2}(y + y_{12})(Q_2 - Q_{12}) \quad (7.61)$$

Substituting for Q_{12} from equation (7.61):

$$F_2 = \frac{1}{2}(y + y_{12})Q_2 + \left[1 - \frac{y + y_{12}}{1 + y_{12}} \right] F_1 \quad (7.62)$$

Proceeding in a like manner gives the general formulae:

$$F_n - F_{n-1} = \frac{1}{2}(y + y_{n-1,n})(Q_n - Q_{n-1,n}) \quad (7.63)$$

$$F_{n-1} - F_{n-2} = \frac{1}{2}(y_{n-1,n} + y_{n-2,n})(Q_{n-1,n} - Q_{n-2,n}) \quad (7.64)$$

and so on. By considering this series of equations with successive elimination of the Q functions, there is obtained a general equation in recursive form:

$$F_i = \frac{1}{2}(y + y_{j-1,i})Q_i + \sum_{j=1}^{i-1} \left[\left(\frac{y + y_{j-1,i}}{y_{j+1,i} + y_{j,i}} \right) - \left(\frac{y + y_{j-1,i}}{y_{j,i} + y_{j-1,i}} \right) \right] F_j \quad (7.65)$$

$$\text{where } y_{i,j} = y^{(d_i/d_j)^2} \quad (7.66)$$

$$d_n = \sqrt{\frac{9\eta \ln y}{(\rho_s - \rho_f) \omega^2 t_2}} \quad (7.67)$$

$$i = 1, 2, 3, \dots, m; y_{0,i} = 1$$

Equations (7.65) are a set of linear equations which express the desired values of F_i explicitly in terms of the measured values of Q_i . The coefficients of the equations depend upon the values of d_i

(corresponding to the value of t_i at which the concentrations are measured; more exactly, the coefficients depend on the ratios of the values of d_i , as shown in equation (7.66). Consequently, if the values of d_i are chosen in a geometric sequence when making particle size analyses, the coefficients are considerably easier to calculate and the equations themselves are also simplified. A ratio of $\sqrt{2}$ is recommended. The coefficients depend also on the values of y_i , that is, the dimensions of the centrifuge bowl employed.

Example: Variable time method

$$\begin{aligned} r &= 7.00 \text{ cm} & \rho_s &= 2650 \text{ kg m}^{-3} \\ S &= 4.304 \text{ cm} & \rho_f &= 1000 \text{ kg m}^{-3} \\ N &= 1500 \text{ rpm } (\omega = 50\pi \text{ rad s}^{-1}) & \eta &= 0.001 \text{ Pa s} \end{aligned}$$

In Table 7.1 particle size is determined using equation (7.67) and measured concentration is converted to mass undersize using equation (7.65). In order to carry out this conversion it is necessary to determine y values [equation (7.66)]; this is facilitated in this example by recording concentrations in a 2:1 size progression so that the y

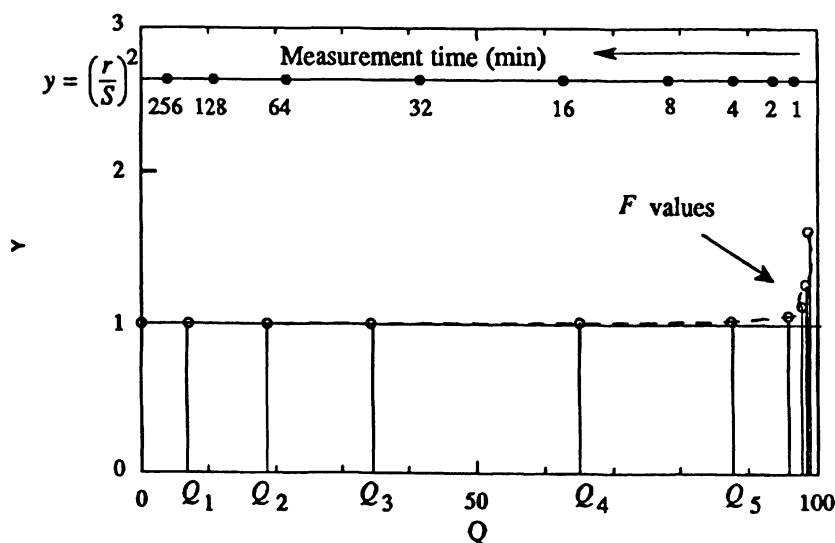
Table 7.1 Mass percentage undersize determination for homogeneous, incremental centrifuge technique (variable time method)

<i>i</i>	Time (min) (60 <i>t</i>)	Size (μm) d_{St}	Measured (%) conc. (Q)	Mass % undersize (F)
1	256	0.118	3.8	6.9
2	128	0.167	10.8	18.7
3	64	0.237	21.6	34.5
4	32	0.335	41.7	65.5
5	16	0.473	62.7	88.4
6	8	0.669	78.2	97.3
7	4	0.947	87.9	99.4
8	2	1.339	93.6	100.0
9	1	1.893	96.7	100.0

Table 7.2 Tabulated F and Q values for homogeneous, incremental centrifuge technique (variable time method)

$Q_{1,2}$	5.27	$Q_{2,3}$	14.23	$Q_{3,4}$	27.18			
$Q_{1,3}$	6.09	$Q_{2,4}$	16.32	$Q_{3,5}$	30.59	$Q_{4,5}$	51.93	
$Q_{1,4}$	6.51	$Q_{2,6}$	17.49	$Q_{3,6}$	32.44	$Q_{4,6}$	58.24	$Q_{5,6}$ 74.18
$Q_{1,5}$	6.72	$Q_{2,8}$	18.10	$Q_{3,7}$	33.46	$Q_{4,7}$	61.75	$Q_{5,7}$ 80.94
$Q_{1,6}$	6.83	$Q_{2,9}$	18.41	$Q_{3,8}$	33.96	$Q_{4,8}$	63.59	$Q_{5,8}$ 84.70
$Q_{1,7}$	6.88	$Q_{2,10}$	18.57	$Q_{3,9}$	34.14	$Q_{4,9}$	64.45	$Q_{5,9}$ 86.56
$Q_{1,8}$	6.90			$Q_{3,10}$	34.35	$Q_{4,10}$	65.01	$Q_{5,10}$ 87.63
$Q_{1,9}$	6.92							
$Q_{1,10}$	6.92							
Q_1	3.80	Q_2	10.80	Q_3	21.60	Q_4	41.70	Q_5 62.70
F_1	6.93	F_2	18.73	F_3	34.48	F_4	65.49	F_5 88.43

$Q_{6,7}$	86.94							
$Q_{6,8}$	91.87	$Q_{7,8}$	93.33					
$Q_{6,9}$	94.44	$Q_{7,9}$	96.20	$Q_{8,9}$	96.62			
$Q_{6,10}$	95.86	$Q_{7,10}$	97.79	$Q_{8,10}$	98.30	$Q_{9,10}$	98.62	
Q_6	78.20	Q_7	87.90	Q_8	93.60	Q_9	100.0	Q_{10} 100.0
F_6	97.25	F_7	99.36	F_8	99.98	F_9	100.0	F_{10} 100.0

**Fig. 7.5** Theoretical diagram for homogeneous, incremental centrifuge technique (variable time method).

values are in a $\sqrt{2}:1$ progression. Q values (Table 7.2) are then determined using equation 7.63. In Fig. 7.5 the black circles are the measured concentrations at a fixed measurement and surface radius and the white circles give the calculated concentration gradient for $i = 9$.

7.13.3 Variable inner radius (pipette withdrawal)

The Ladal pipette centrifuge was developed as a centrifugal version of the Andreasen gravitational pipette [32].

(a) *Stokes diameter determination* Let the time of the first withdrawal be t_1 ; the largest particle present in the withdrawn sample at this time will have fallen from the surface at radius S to the measurement zone at radius r . Equation (7.47) will apply and may be written:

$$d_1^2 t_1 = k \ln \frac{r}{S} \quad (7.68)$$

The liquid level will then fall to S_1 , where:

$$S_1^2 - S^2 = \frac{v}{\pi h} \quad (7.69)$$

where v is the volume extracted (10 cm^3) and h is the thickness of the centrifuge bowl (1.02 cm). The fall in the inner radius can therefore be determined:

$$\Delta S_1 = S_1 - S \quad (7.70)$$

Let the time for the second withdrawal be t_2 ; then the largest particle present in the withdrawn sample will have fallen from S to x_{12} in time t_1 , a distance Δx_{12} due to the withdrawal of the first sample and from $x_{12} + \Delta x_{12}$ to r in a time $t_2 - t_1$. Hence:

$$d_2^2 t_1 = k \ln \frac{x_{12}}{S} \quad (7.71)$$

$$d_2^2 (t_2 - t_1) = k \ln \frac{r}{x_{12} + \Delta x_{12}} \quad (7.72)$$

Adding equations (7.71) and (7.72) gives:

$$d_2^2 t_2 = k \ln \frac{r}{S} \left(1 + \frac{\Delta x_{12}}{x_{12}}\right)^{-1} \quad (7.73)$$

Repeating this gives, for the n th withdrawal:

$$d_n^2 t_n = k \ln \frac{r}{S} \left[\left(1 + \frac{\Delta x_{1,n}}{x_{1,n}} \right)^{-1} \left(1 + \frac{\Delta x_{2,n}}{x_{2,n}} \right)^{-1} \dots \left(1 + \frac{\Delta x_{n-1,n}}{x_{n-1,n}} \right)^{-1} \right] \quad (7.74)$$

This differs from the variable time equation in that the Stokes diameter reduces more rapidly thus, effectively, making this technique into a scanning technique.

(b) *Mass frequency undersize determination* Let the final sample withdrawn be of concentration Q_1 and let the surface be at S_1 immediately prior to this withdrawal, then:

$$F_1 = \frac{1}{2} (1 + y_1) Q_1 \quad (7.75)$$

where:

$$y_1 = \left(\frac{r}{S_1} \right)^2 \quad (7.76)$$

$$F_1 = \frac{1}{2} (1 + y_{12}) Q_{12} \quad (7.77)$$

and:

$$y_{12} = y_2^{(d_1/d_2)^2} \quad (7.78)$$

Hence, by the trapezoidal rule:

$$F_2 - F_1 = \frac{1}{2} (y_2 + y_{12}) (Q_2 - Q_{12}) \quad \text{where } y_2 = \left(\frac{r}{S_2} \right)^2$$

Substituting for Q_{12} gives:

$$F_2 = \frac{1}{2} (y_2 + y_{12}) Q_2 + \left[1 - \frac{y_2 + y_{12}}{1 + y_{12}} \right] F_1 \quad (7.79)$$

Proceeding in a like manner gives the general formula:

$$F_n - F_{n-1} = \frac{1}{2} (y_n + y_{n-1,n}) (Q_n - Q_{n-1,n})$$

By successively eliminating the Q functions, this gives a general equation in recursive form as before:

$$F_i = \frac{1}{2} (y_i + y_{i-1,i}) Q_i + \sum_{j=1}^{i-1} \left[\frac{y_i + y_{i-1,i}}{y_{j+1,i} + y_{j,i}} - \frac{y_i + y_{i-1,i}}{y_{j,i} + y_{j-1,i}} \right] F_j \quad (7.80)$$

where $y_i = \left(\frac{r}{S_i} \right)^2$ and $y_{i-1,i} = y_i^{(d_{i-1}/d_i)^2}$

7.13.4 Variable measurement radius (scanning x-ray centrifuge)

This instrument was developed as a centrifugal version of the gravitational instrument in order to reduce the measurement time and measure down to smaller sizes [33,34].

(a) Stokes diameter determination Equation (7.38) is applied in the form:

$$d_{St}^2 = k \ln \left(\frac{r_i}{S} \right) \quad (7.81)$$

where r_i is a variable.

(b) Mass frequency undersize determination Equation (7.80) is applied where $y_i = (r_i/S)^2$ and $y_{j,i} = y_i^{(d_j/d_i)^2}$.

References

- 1 Wilkes, R. and Allen, T. (1990), *Particle Size Measurement*, p.252–254, Chapman & Hall, 277
- 2 Burt, M.W.G., Fewtrel, C.A. and Wharton, R.A. (1973), *Powder Technol.*, 8, 223–230, 278
- 3 Dollimore, D. et al. (1970), *J. Phys. E.*, 3, 465–466, 278
- 4 Bond, R.L. and Spencer, D.H.T. (1957), *Proc. 1st Ind. Conf. Ind. Carbon and Graphite, Soc. Chem. Ind.*, London, pp. 231–251, 278
- 5 Spencer, D.H.T. (1967), *Porous Carbon Solids*, (ed. R.L. Bond), Academic Press, N.Y., pp. 87–154, 278
- 6 May, I. and Marienko, J. (1966), *Am. Mineral.*, 51, 931–934, 278
- 7 Stein, F., Pankala, S. and Buchino, J. (1971/2), *Powder Technol.*, 7, 45, 278

- 8 Thudium, J. (1976), *J. Aerosol Sci.*, 7(2), 167–174, 279
9 Krutzch, J. (1954), *Chemiker-Zeitung*, 78, 49, 279
10 Baranowski, J. (1973), *Ochrona Powietrza*, 2, 30, 279
11 Juda, J. (1966), *Staub*, 26, 197, 279
12 Hänel, G. (1972), Bestimmung Physikalischer Eigenschaften Atmosphärischer Schwebetulchen als Funktion der Relativen Lufteuchtigkeit, Diss. Universität Mainz, 279
13 Müller, G. (1964), *Methoden der sedimentuntersuchung*, E. Schweltzerbartsche Verlagbüchhandlung, Stuttgart, 279
14 Keng, E.Y.H. (1969/70), *Powder Technol.*, 3, 179–180, 279
15 Johnson, R. (1956), *Trans. Ceram. Soc.*, 55, 237, 284
16 British Standard 1377 (1961), *Methods of testing soils for civil engineering purposes*, 285
17 Oden, S. (1916), *Kolloid Z.*, 18, 33–47, 289
18 Coutts, J. and Crowthers, E.M. (1925), *Trans. Faraday Soc.*, 21, 374, 289
19 Bostock, W. (1952), *J Sci. Instrum.*, 29, 209, 289, 291
20 Gaudin, A.M., Schumann, R. and Schlechter, A.W. (1942), *J. Phys. Chem.*, 46, 903, 290
21 Stairmand, C.J. (1947), *Symp. Particle Size Analysis*, Inst. Chem. Eng., 25, 110, 290
22 Kim, S.C., Schltzer, G. and Palik, E.S. (1967), *Powder Technol.*, 1, 54–55, 290
23 Nelson, R.N. Jr, Khalili, M. and Allen, T. (1995), *Poranal, Symp. Particle Size Analysis and Powder Technology*, Hungary, June, 295
24 Treasure, C.R.G. (1964), *Whiting and Industrial Powders Research Council*, Welwyn, England, Tech. Paper no 50, 295
25 Coll, H. and Haseler, S.C. (1984), *J. Colloid Interf. Sci.*, 99(2), 591–592, 295
26 Devon, M.J., Meyer, E., Provder, T., Rudin, A. and Weiner, B.B. (1990), *Particle Size Distribution II, Assessment and Characterization*, Am. Chem. Soc. Symposium Series 472, Ch. 10, 295
27 Oppenheimer, L.E. (1983), *J. Colloid Interf. Sci.* 92(2), 350–357, 295
28 Coll, H. and Searles, C.G. (1987), *J. Colloid Interf. Sci.*, 115(1), 121–129, 295
29 Weiner, B.B., Fairhurst, D. and Tscharnuter, W.W. (1991), *Particle Size Distribution II*, Am. Chem. Soc., Ch. 12, ed. T Provder, 295
30 Berg, S. (1940), *Ingen. Vidensk. Skr. B*, Number 2, 299
31 Kamack, H.J. (1951), *Anal. Chem.*, 23(6), 844–850, 299
32 Allen, T. and Svarovsky, L. (1975), *Dechema Monogram*, Nurenberg, Numbers 1589–1615, 279–292, 303
33 Allen, T. (1992), *Centrifuge particle analyzer*, U.S. Patent 5,095,451, 305

- 34 Allen, T. (1992), *Proc. Conf. Particle Size Analysis*, PSA 91, Loughborough University, Leicester, Analyt. Div. Royal Soc Chem., publ. Heyden, 305

Sedimentation methods of particle size measurement

8.1 Introduction

Gravitational sedimentation methods of particle size determination are based on the settling behavior of a single sphere, under gravity, in a fluid of infinite extent. Many experiments have been carried out to determine the relationship between settling velocity and particle size and a unique relationship has been found between drag factor and Reynolds number. This relationship reduces to a simple equation, the Stokes equation, which applies at low Reynolds numbers. Thus at low Reynolds numbers the settling velocity defines an equivalent Stokes diameter which, for a homogeneous spherical particle, is its physical diameter.

At low Reynolds number flow is said to be laminar i.e. the fluid flow lines around the particle are unbroken. As the Reynolds number increases, turbulence sets in leading to increased drag on the particle so that it settles at a lower velocity than predicted by Stokes' equation.

It therefore follows that, if the settling velocity of a homogeneous, spherical particle is known, then its particle size can be deduced.

The drag force on a particle is orientation dependent, hence non-spherical particles settling with their largest cross-sectional area perpendicular to the flow direction will settle more slowly than similar particles settling with minimum area perpendicular to flow. It follows that an assembly of identical non-spherical particles, settling under laminar flow conditions, will have a range of settling velocities according to their orientation.

Table 8.1 Principles of sedimentation techniques

Suspension type	Measurement principle	Force field
Homogeneous	Incremental	Gravitational
Line start	Cumulative	Centrifugal

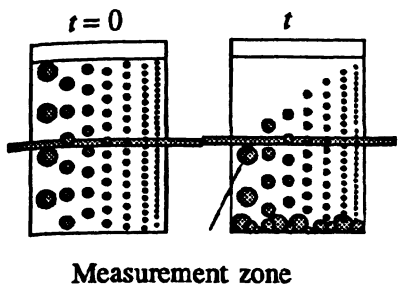


Fig. 8.1 Homogeneous, incremental, gravitational sedimentation.

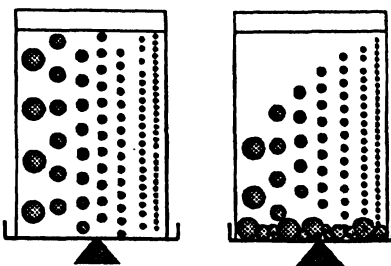


Fig. 8.2 Homogeneous, cumulative, gravitational sedimentation.

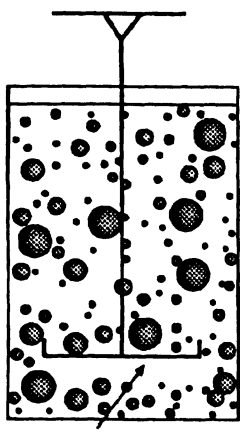


Fig. 8.3 Balance pan in suspension.

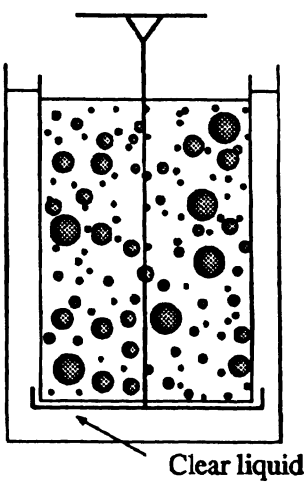


Fig. 8.4 Balance pan in clear liquid.

Sedimentation techniques can be classified according to the principles outlined in Table 8.1. Table 8.2 lists the various procedures that have been developed according to the principle applied. Techniques in current use are described here; descriptions of techniques which are now no longer used can be found in an earlier edition [1]. Sedimentation theory is covered in Chapter 6. Analytical procedures for some of these techniques are covered more fully in BS 3406 [2,3].

In the homogeneous, incremental, gravitational technique the solids concentration (or suspension density) is monitored at a known depth below the surface for an initially homogeneous suspension settling

Table 8.2 Commercial sedimentation particle size analyzers

Homogeneous, incremental gravitational sedimentation	Homogeneous, cumulative, gravitational sedimentation
Andreasen pipette	Oden Balance
Leschonski pipette	Svedberg and Rinde automatic recording sedimentation beam balance
Fixed depth pipette	Cahn balance
Side-arm pipette	Gallenkamp balance
Wagner photosedimentometer	Mettler H20E balance
EEL photosedimentometer	Sartorius Recording Sedibel balance
Bound Brook photosedimentometer	Palik torsion balance
Seishin Photomicrosizer	Kiffer continuous weighing chain link balance
Ladal wide angle scanning photosedimentometer	Rabatin and Gale spring balance
Paar Lumosed	Shimadzu balance
ICI x-ray sedimentometer	ICI sedimentation column
Ladal x-ray sedimentometer	BCURA sedimentation column
Micromeretics Sedigraphs 5000 & 5100	Fisher Dotts apparatus
Quantachrome Microscan	Decanting
X-ray sedimentometer	β -Back-scattering
Hydrometers	
Divers	
Suito specific gravity balance	
Line-start, incremental, gravitational sedimentation	Line-start, cumulative, gravitational sedimentation
MSA analyzer	Werner and Travis method
	Granumeter
	Micromerograph
	MSA analyzer
Homogeneous, incremental centrifugal sedimentation	Homogeneous, cumulative, centrifugal sedimentation
Simcar centrifuge	Alpine centrifuge
Ladal pipette centrifuge	Hosokawa Mikropul
Ladal x-ray centrifuge	Sedimentputer
Brookhaven scanning x-ray centrifuge	
Brookhaven BI-DCP, disc photocentrifuge	
Kaye disc photocentrifuge	
Coulter photofuge Technord photocentrifuge	
Horiba cuvet photocentrifuges	
Seishin cuvet photocentrifuge	
Shimadzu cuvet photocentrifuge	
	Line-start, incremental, centrifugal sedimentation
	Joyce-Loebl disc photocentrifuge
	Brookhaven BI-DCP, disc photocentrifuge
	Line-start, cumulative, centrifugal sedimentation
	MSA analyzer

under gravity. The concentration will remain constant until the largest particle present in the suspension has fallen from the surface to the measurement zone (Figure 8.1). At the measurement zone the system will be in a state of dynamic equilibrium since, as particles leave the zone, similar particles will enter it from above to replace them. When the largest particle present in the suspension settles through the measurement zone, the concentration will fall since there will be no particles of this size above the zone. Thus the concentration will be of particles smaller than the Stokes diameter and a plot of concentration against Stokes diameter is, in essence, the mass undersize distribution.

In the homogeneous, cumulative, gravitational technique the rate at which solids settle out of suspension is determined for an initially homogeneous suspension settling under gravity (Figure 8.2). This technique is typified by the sedimentation balance in which the balance pan can be in the suspension (Figure 8.3) or suspended in a clear liquid (Figure 8.4). With the former set-up, correction has to be made for the particles which do not fall on the pan; errors are also introduced since the particle free zone below the pan leads to convection currents. The latter technique also suffers from problems due to the motion of the pan as particles settle on it. In this system, the amount settled out consists of two parts, all particles larger than Stokes diameter and a fraction of particles smaller than this. The amount undersize is determined by carrying out an integration of the second fraction.

With the incremental, gravitational, line start technique (Figure 8.5) the suspension is floated on top of a container of clear liquid and, provided the particles fall independently, the largest particles present in the suspension will reach the measurement zone first and the measured concentration will be the concentration of this size band in the measurement zone. This technique can also be used in the cumulative mode (Figure 8.6).

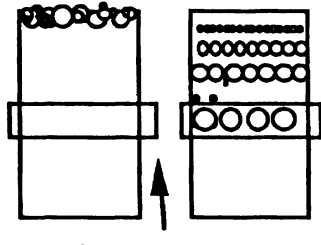


Fig. 8.5 Line-start, incremental gravitational sedimentation.

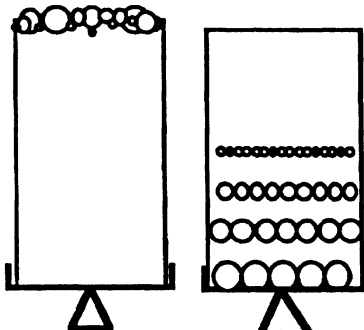


Fig. 8.6 Line-start, cumulative gravitational sedimentation.

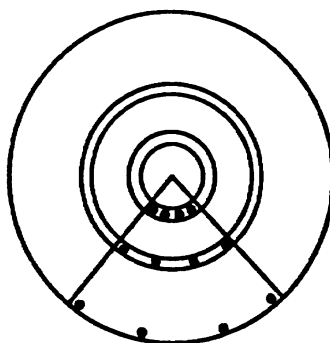


Fig. 8.7 Homogeneous, incremental, centrifugal sedimentation (the radial dilution effect).

In homogeneous, incremental, centrifugal techniques (Figure 8.7) matters are more complex. The particles move in radial paths, hence the number of particles smaller than Stokes diameter entering the measurement zone is less than the number leaving, so that the measured concentration of these particles is smaller than their original concentration. This problem does not occur with centrifugal line start methods at a fixed measurement radius.

In this presentation some of the methods for sedimentation particle size analysis in current use are described. Although operating procedures are not covered here it is stressed that two factors, more than anything else, lead to incorrect analyses. The first is incorrect sampling, since analyses are carried out on from a tenth of a gram up to a few grams and these samples must be representative of the bulk for the analyses to be meaningful. The second is dispersion: it has been said rightly that the most important factor in obtaining accurate sedimentation data is dispersion – the second most important factor is dispersion and the third is also dispersion!

8.2 Homogeneous incremental gravitational sedimentation

8.2.1 The pipette method of Andreasen

In the pipette method (Figure 8.8), concentration changes occurring within a settling suspension are followed by drawing off definite volumes, at predetermined times and known depths, by means of a pipette. The method was first described in 1922 by Robinson [4] who used a normal laboratory pipette. Various modifications were later suggested which complicated either the operating procedure or the apparatus [5]. Andreasen was the first to leave the pipette in the sedimentation vessel for the duration of the analysis. The apparatus

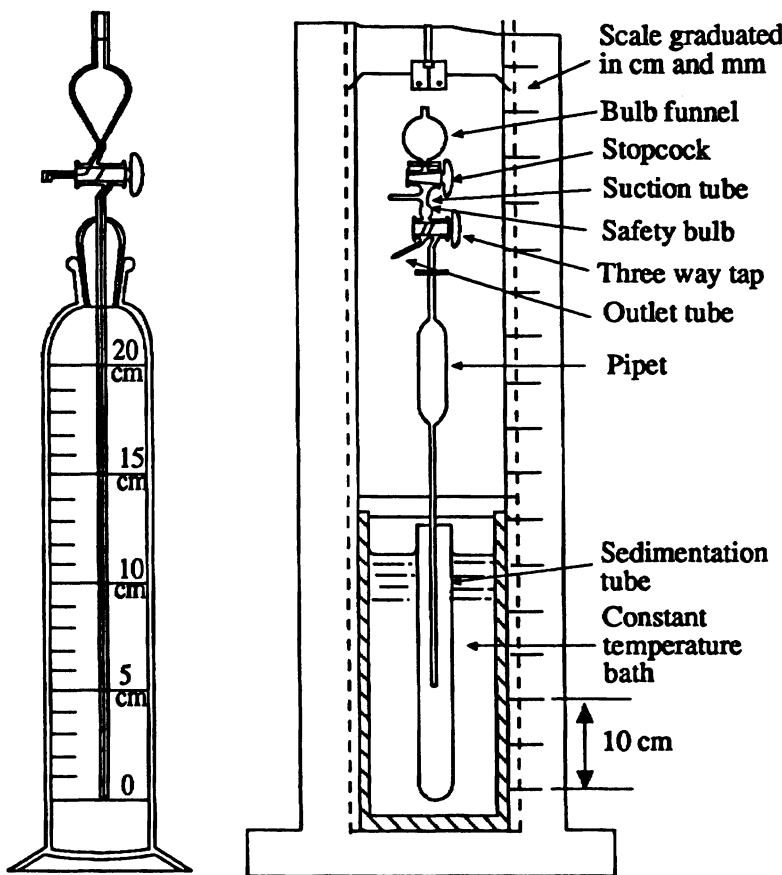


Fig. 8.8 (a) The fixed position pipette; **(b)** the variable height pipette.

described by Andreasen and Lundberg [6] is the one in general use today.

Although, theoretically, errors can be reduced by the use of more complicated construction and operation, it is highly debatable as to whether this is worthwhile for routine analyses since conventional apparatus is reproducible to $\pm 2\%$ if operated with care [7].

This technique is a standard procedure since both the Stokes diameter and the mass undersize are determined from first principles. The method is versatile, since it can handle any powder which can be dispersed in a liquid, and the apparatus is inexpensive. The analysis is however time consuming and operator intensive.

8.2.2 The photosedimentation technique

The photosedimentometer combines gravitational settling with photoelectric measurement. The principle of the technique is that a narrow horizontal beam of parallel light is projected through the suspension at a known depth on to a photocell. Assuming an initially homogeneous suspension, the attenuation at any time will be related to the undersize concentration.

Superficially, the attenuation is related to the random projected areas of the particles. The relationship is more complex than this however, due to the breakdown in the laws of geometric optics and complex diffraction, scattering, interference and absorption effects have to be considered. For small particles, an amount of light flux, equal in magnitude to that incident upon the particle, is diffracted away from the forward direction (Figure 8.9), making their effective obscuration area twice their projected area. As the particle size increases, the diffracted light is contained in an decreasing solid angle in the forward direction so that, no matter how small the light detector, most of the diffracted light is accepted and the effective obscuration area becomes the same as the projected area. For partially transparent particles some of the incident light is absorbed and some refracted to cause interference in the transmitted beam.

It cannot therefore be assumed that each particle obstructs the light with its geometric cross-sectional area. These effects are compensated for by inclusion of an extinction coefficient (K) in the equation, making the apparent area K times the geometric area.

Early experimenters [9,10] were either unaware of, or neglected, this correction. Some research workers used monochromatic light and determined K theoretically [8,11]; others used empirical calibration by comparison with some other particle sizing technique. Rose and Lloyd [12] attempted to define a universal calibration curve; Allen [13,14]

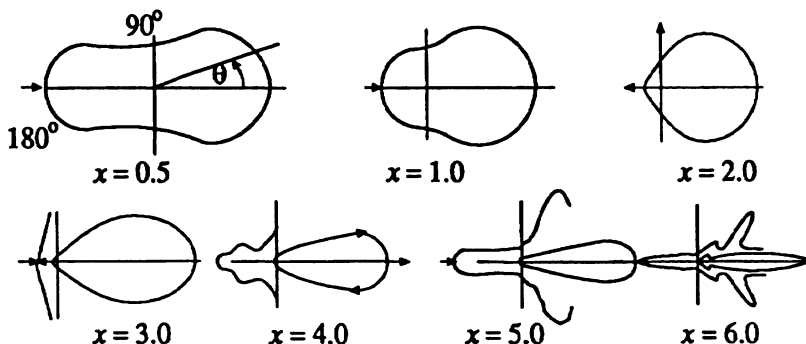


Fig. 8.9 Polar light scattering diagrams [8]. The outer curve magnifies the inner by a factor of 10 in order to show fine detail. $x = (\pi D / \lambda)$ where D = particle diameter and λ is the wavelength of light.

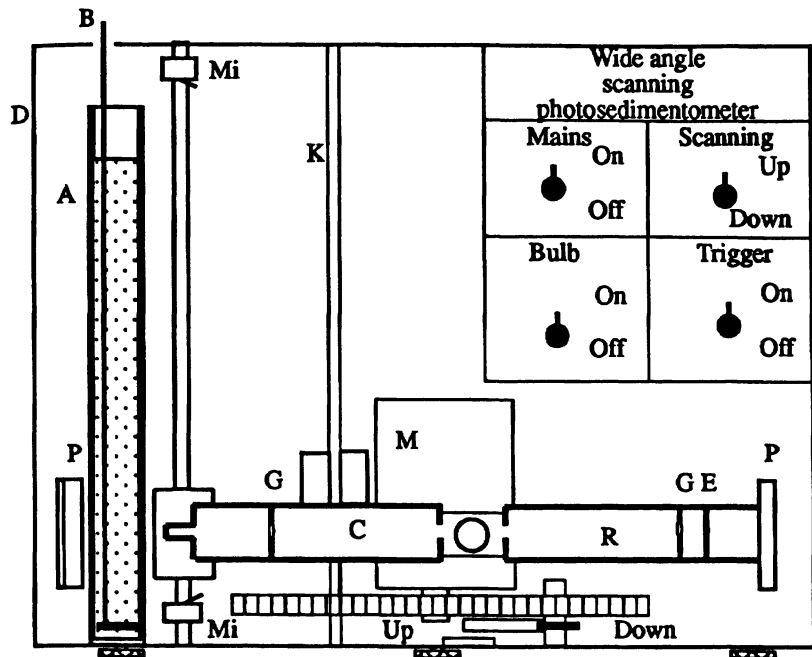


Fig. 8.10 The Ladal Wide Angle Scanning Photosedimentometer
 A, sedimentation tank; B, stirrer; C, collimator; D, light proof box; E, variable aperture; G, lenses; K, drive screw; L, light source; M, motor; Mi, microswitches; P, photocells.

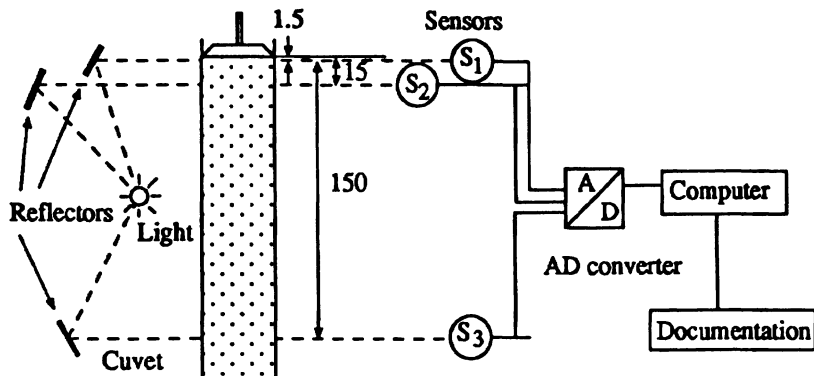


Fig. 8.11 The Paar Lumosed, depth of beams are marked in mm.

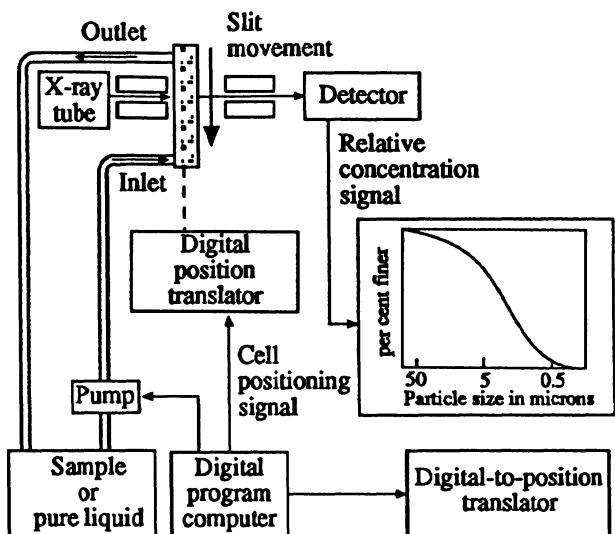


Fig. 8.12 The Micromeritics Sedigraph.

(Figure 8.10) designed a wide angle scanning photosedimentometer (WASP) which accepted forward scattered light so that K was constant down to a size of around 3 μm . Weichert determined a relative extinction coefficient by the use of different wavelengths and speeded up the analysis by the use of different settling heights [15].

Commercial equipment presently available ranges from the PAAR Lumosed (Figure 8.11), which operates in the gravitational size range with three light sources at different depths to speed up the analysis [16], to a range of photocentrifuges which also operate in the centrifugal mode. With these instruments a K factor, obtained either theoretically or experimentally, can be inserted in the software algorithm.

8.2.3 X-ray sedimentation

A natural extension to the use of white light is to use x-rays, in which case the x-ray attenuation is directly proportional to the atomic mass of the suspended particles in the beam, i.e. the mass undersize.

Brown and Skrebowski [17] first suggested the use of x-rays for particle size analysis and this resulted in the ICI X-ray sedimentometer [18,19]. Other instruments were developed by Kalshoven [20] and Oliver *et al.* [21]. In 1970 Allen and Svarovsky [22-24] developed an instrument in which the traditional x-ray tube was replaced by an isotope source.

Several commercial instruments utilizing these principles were developed. The Micromeritics' Sedigraph 5000 (Figure 8.12) was

based on the paper by Kalshoven [20]. The Quantachrome Microscan reduced the time for an analysis by a factor of about two and the Sedigraph 5100 was designed as a faster version of the 5000. Allen and Svarovsky's design was incorporated in the Ladal X-ray gravitational sedimentometer and the x-ray centrifugal sedimentometer, which are no longer commercially available. A later design of Allen's is available as the Brookhaven BI-XDC.

8.2.4 Hydrometers and divers

The changes in density of a sedimenting suspension may be followed with a hydrometer (Figure 8.13), a method still used in the ceramic industry. The method is open to several objections not least being the high concentration required in order to obtain accurate readings.

The resolution, see Section 7.3, is particularly poor for the hydrometer method of size analysis where the height of the measurement zone is of the same magnitude as the depth of immersion in the suspension. Despite these objections the instrument is useful for control purposes with wide size range continuous distributions.

Divers (Figure 8.14), overcome many of the objections associated with the hydrometer technique. These miniature hydrometers were developed by Berg [25] for use with both gravitational and centrifugal sedimentation, but have never been widely used. Basically, divers are small objects of known density which are immersed in the suspension so that they find their density level.

Berg's divers for example, were hollow glass containers which contained mercury to give the desired density. The density was then adjusted to the desired value by etching with hydrofluoric acid. Various modified divers were later developed, the final ones, by Kaye and James [26], being metal coated polythene spheres which were located with search coils.

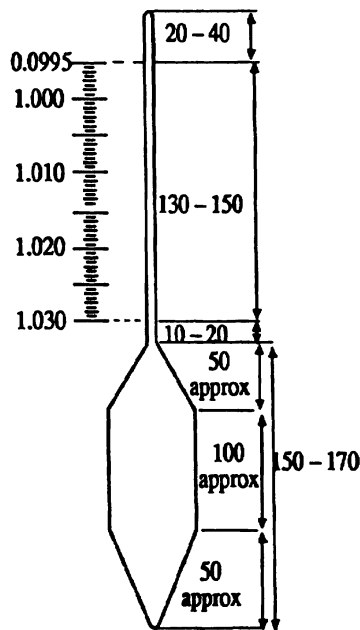


Fig. 8.13 Hydrometer
(Calibration in g ml^{-1} at 20 °C.
All dimensions in mm).

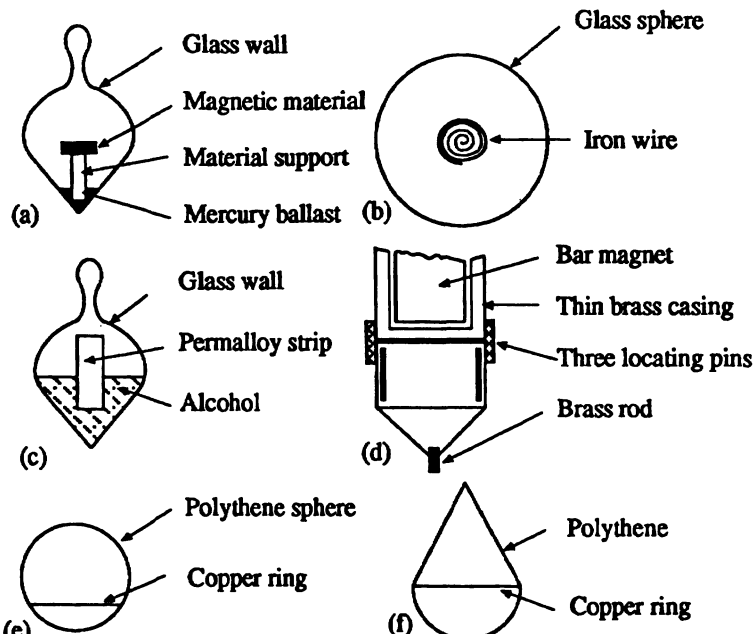


Fig. 8.14 Divers [(a) and (b)] Berg [25], gravitational and centrifugal [(c) and (d)] Jarrett and Heywood [27], (e) and (f) Kaye and James [26], (see reference 1).

8.3 Homogeneous cumulative gravitational sedimentation

8.3.1 Introduction

The principle of this method is the determination of the rate at which particles settle out of a homogeneous suspension. This may be done by extracting the sediment and weighing it; allowing the sediment to fall on to a balance pan or determining the weight of powder still in suspension by using a manometer or pressure transducer.

One problem associated with this technique is that the sediment consists both of oversize (greater than Stokes diameter) and undersize particles so that the sedimentation curve of amount settled (P) against time (t) has to be differentiated to yield the weight (W) larger than Stokes diameter.

$$W = P - t \frac{dP}{dt} \quad (8.1)$$

Several balance systems, based on this equation, have been described.

8.3.2 Balances

In the Gallenkamp balance [28,29] the pan is placed below a sedimentation chamber with an open bottom and the whole assembly is placed in a second chamber filled with sedimentation liquid so that all the powder falls on to the pan. The weight settled is determined from the deflection of a torsion wire, and either the run continues until all the powder has settled out of suspension or a second experiment is carried out to determine the supernatant fraction. Problems arise during the charging operation with leakage into the clear water reservoir and particle adhesion to the premixing tube.

In the Sartorius balance [30–32] the pan is suspended in the suspending liquid and a correction has to be applied for the particles which fall between the rim of the pan and the sedimentation vessel. In this instrument, when 2 mg of sediment has deposited, electronic circuitry activates a step by step motor which twists a torsion wire to bring the beam back to its original position. A pen records each step on a chart. The manufacturers suggest that about 8% of the powder does not settle on the pan. Leschonski [33] and Leschonski and Alex [34] reported losses of between 10% and 35%, depending on the fineness of the powder; the difference was attributed to the pumping action of the pan as it rebalances.

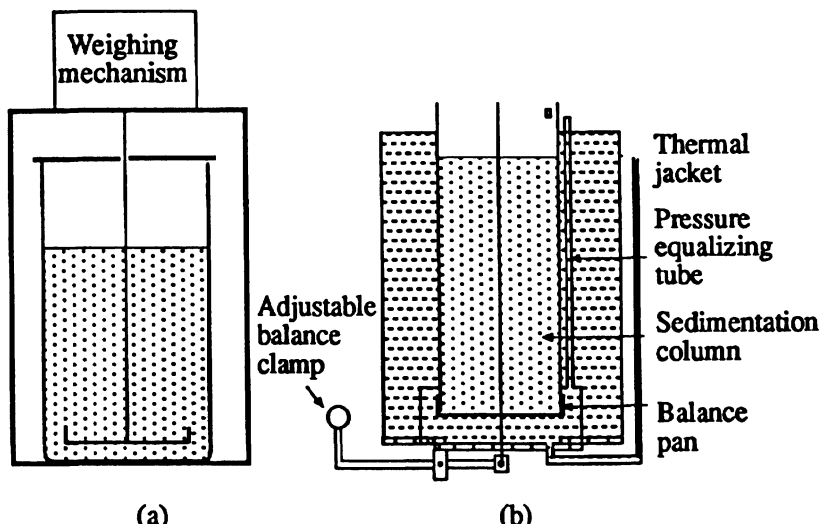


Fig. 8.15 (a) Sedimentation balance with pan in the suspension. (b) Sedimentation balance with pan in clear liquid (Leschonski modification of the Sartorius balance).

Leschonski modified the instrument (Figure 8.15) by placing the pan at the bottom of a sedimenting column surrounded by a second column of clear liquid so that all the powder settled on to the pan. This eliminated powder losses and resulted in more accurate analyses [31].

The manufacturers of the Cahn micro-balance make available an accessory to convert it into a sedimentation balance [35]. The balance pan is immediately below the sedimentation cylinder in order to eliminate convection currents. Shimadzu also make a beam balance [36] which operates using a simple compensating system which is prone to considerable error.

8.3.3 Sedimentation columns

Sedimentation columns (ICI, BCURA) have also been described in which the sediment is extracted, dried and weighed. A full description of these and other sedimentation columns may be found in [1].

8.4 Line-start incremental gravitational sedimentation

8.4.1 Photosedimentation

The Horiba cuvet photo(centri)fuge has been operated in this mode [37] but is not recommended since it is very difficult to make up a stable two-layer system in a cuvet.

8.5 Line-start cumulative gravitational sedimentation

8.5.1 Introduction

If the powder is initially concentrated in a thin layer floating on the top of a suspending fluid, the size distribution may be determined by plotting the fractional weight settled against the free falling diameter.

8.5.2 Methods

Marshall [38] was the first to use this principle. Eadic and Paync [39] developed the Micromerograph, the only method in which the suspending fluid is air. Brezina [40,41] developed a similar water based system, the Granumeter, which operated in the sieve size range, and was intended as a replacement for sieve analyses.

The Werner and Travis methods [42,43] also operate on the layer principle but their methods have found little favor due to the basic instability of the system; a dense liquid on top of a less dense liquid being responsible for a phenomenon known as streaming in which the suspension settles *en masse* in the form of pockets of particles which fall rapidly through the clear liquid leaving a tail of particles behind.

Whitby [44] eliminated this fault by using a clear liquid with a density greater than that of the suspension. He also extended the size range covered by using centrifugal settling for the finer fraction. The apparatus enjoyed wide commercial success as the (Mines Safety Appliances) MSA Particle Size Analyzer, although it is less widely used today [45]. The MSA analyzer can be operated in the gravitational mode, although it is more usually used in the centrifugal mode. Several papers have been published on applications of this equipment.

The line-start technique has also been used to fractionate UO_3 particles by measuring the radioactivity at the bottom of a tube, the settled powder being washed out at regular intervals without disturbing the sediment [46].

8.6 Homogeneous incremental centrifugal sedimentation

8.6.1 Introduction

Gravitational sedimentation techniques have limited worth for particles smaller than about a micron due to the long settling times required. In addition most sedimentation devices suffer from the effect of convection, diffusion and Brownian motion. These difficulties may be reduced by speeding up the settling process by centrifuging the suspension.

One of the complications that arises is that particle velocity is not only dependent on particle size as in gravity sedimentation, but also depends upon the radial position of the particle. The radial velocity may be written as:

$$v = \left(\frac{\ln(r/S)}{t} \right) \quad (8.2)$$

where t = time, r = radial position of the particles, S = radial position of the surface of the suspension.

In long arm centrifuges ($r-S$) is made much smaller than r or S so that the velocity may be assumed constant.

Correction is also necessary for radial dilution effects. Particles of narrow size range centered on x_r , originating from radius r and occupying an initial volume of $2\pi rh\Delta r$, will occupy a volume of $2\pi Rh\Delta R$ at the measurement radius R . The relationship between the concentration at the starting radius (the initial concentration in the suspension) and the concentration at the measurement zone is given by the ratio of these volumes:

$$\frac{F(x_r)}{Q(x_r)} = \frac{R\Delta R}{r\Delta r} \text{ which can be shown to equate to } \left(\frac{R^2}{r^2} \right)$$

and it can be shown that:

$$\int_0^{x_{\max}} F(x) dx = \int_0^{x_{\max}} \int_{r=R}^S \left(\frac{R}{r}\right)^2 Q(x) dx \quad (8.3)$$

This is solvable, for fixed R by an equation developed by Kamack [47,48], for a variable surface radius (S) by a modified equation developed by Allen and Svarovsky [49], and for variable R by an equation developed by Allen [50].

8.6.2 The Simcar pipette disc centrifuge

The Simcar centrifuge was developed by Slater and Cohen [51] to conform with Kamack's theory and was, in essence, a centrifugal version of the gravitational pipette. One problem with this instrument was the amount of suspension required (about 2.5 L of liquid containing about 5 g of powder) so that the liquid level did not alter appreciably during an analysis. The amount removed at each withdrawal was variable and about 40 ml, hence the error due to assuming a constant liquid level (S) increased as more samples were withdrawn.

Since no correction was available for the fall in surface with each extraction, it was inadvisable to withdraw more than four samples in each analysis. The analysis was carried out in duplicate to give eight points on the distribution curve, a single evaluation from about 5 μm to 0.2 μm taking up to a full day.

Concentrations were determined by drying and weighing. Using the modified equation to take into account the changing liquid level would allow more data points to be taken in a single run.

8.6.3 The Ladal pipette disc centrifuge

This pipette centrifuge (Figure 8.16) was designed by Allen and Svarovsky [52] to operate with a reduced volume of suspension (150 mL) and a modified Kamack equation which reduced the measurement time down to about an hour. At 500 rpm the measured size range for quartz is approximately 8 μm to 0.8 μm in 1 h and these sizes are halved if the speed is doubled.

8.6.4 The Ladal x-ray disc centrifuge

This is an extension of the Allen and Svarovsky [53] x-ray gravitational sedimentometer. The x-rays are generated by an isotope source and, after passing through the suspension, they are detected by a scintillation

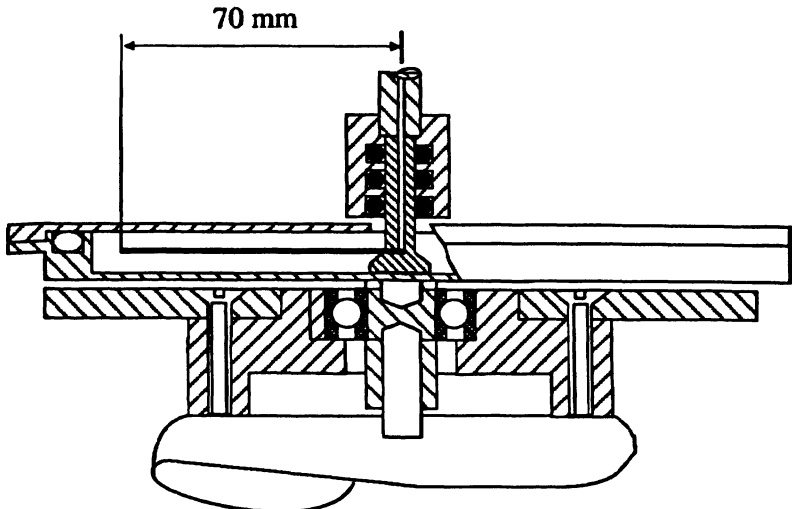


Fig. 8.16 Line diagram of the Ladal pipette centrifuge.

counter. The signal is then processed to generate the size distribution. The attenuation is proportional to the mass concentration at the measurement radius which has to be converted to the size distribution using the Kamack equation. A size range of about 8:1 is covered in about an hour.

8.6.5 The Du Pont/Brookhaven scanning x-ray disc centrifugal sedimentometer (BI-XDC)

This is an extension of the Allen and Svarovsky [53] x-ray gravitational sedimentometer. The x-rays are generated by an isotope source and, after passing through the suspension, they are detected by a scintillation counter. The signal is then processed to generate the size distribution. The attenuation is proportional to the mass concentration at the measurement radius, which has to be converted to the size distribution using the Kamack equation. A size range of about 8:1 is covered in about an hour.

This instrument was designed by the writer and a colleague [50,54] to fill a need for fast, reproducible sedimentation analyses in the sumicron size range. The heart of the instrument is a hollow, x-ray transparent, disc which, under normal operating conditions, contains 20 mL of suspension at a concentration of around 0.2% by volume.

The speed is selectable in the range 750 to 6000 rpm. The default condition is for the source and detector to remain stationary for 1 minute at a radial position of 48.00 mm and then to scan towards the surface. Total run time is normally 8 min. A commercial version is

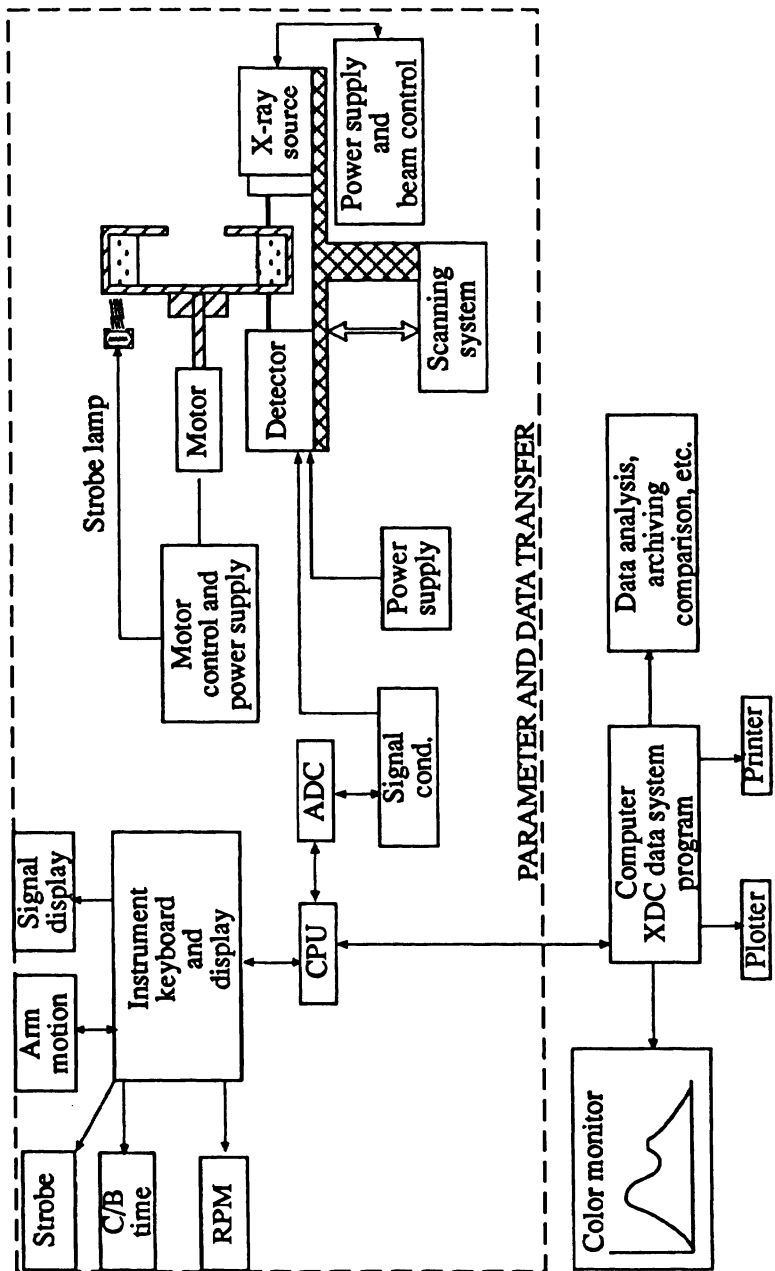


Fig. 8.17 The DuPont/Brookhaven x-ray scanning centrifuge.

available from Brookhaven as the BI-XDC (Figure 8.17). The instrument can operate in the gravitational or centrifugal mode and the analyses can be blended to cover a total size range of 0.05 µm to over 100 µm. A size range of 15:1 is covered in a standard 8 min analysis.

8.6.6 The BI-DCP disc (photo)centrifuge particle size analyzer

The technology that Brookhaven developed for the x-ray centrifuge has been transferred to their photocentrifuge. The revised software is for analysis by the homogeneous start technique plus a scanning head detector. The high resolution line-start technique can be used, but this is not amenable to scanning since the low concentrations necessarily employed generate a noisy baseline. An additional benefit of the new software is that it allows for particles whose density is lower than that of the surrounding liquid, thus making it suitable for emulsion sizing.

8.7 Cuvet photocentrifuges

In these instruments (Figure 8.18) the disc is replaced with a rectangular cell containing a homogeneous suspension. Unless corrections are applied for radial dilution effects and the breakdown in the laws of geometric optics, the derived data are suitable only for comparison purposes. For example, a 50:50 mixture of 0.25 and 0.60 µm spherical silica particles was recorded as 54.4:45.6 with no correction for radial dilution, and this increased to 70:30 without extinction coefficient correction with the smaller particles grossly

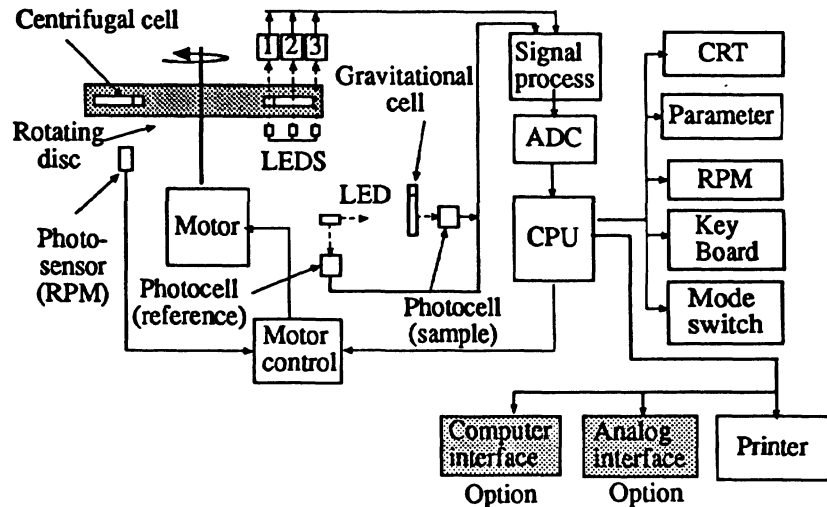


Fig. 8.18 Block diagram of the Horiba cuvet photocentrifuge.

under-counted. A computer program to correct for the light scattering of small particles reduces these errors [55]

Using the manufacturers correction for light scattering was found to be unsatisfactory[56]. It was also found that the light scattering correction was strongly affected by the shape of the particles [57]. An alternative procedure is to use several wavelengths and deconvolute the resulting set of linear equations that develop in order to find the size distribution. This has been used by Niemann and Weichert who used a modified Phillips – Twomey algorithm [58,59].

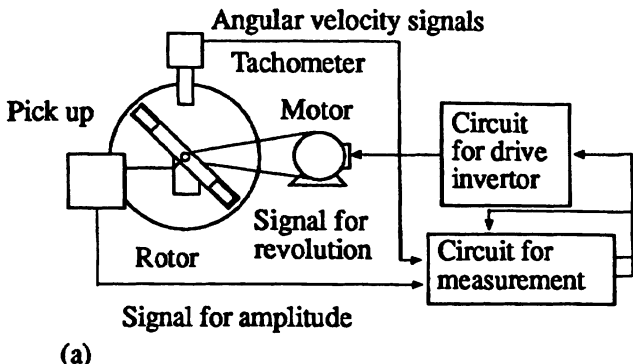
Their photocentrifuge used white light from a short arc xenon high pressure lamp. Two light beams are generated, one passing through the suspension at a depth of 2 mm and the other at a depth of 20 mm. Four cuvets are used, two containing clear liquid and two containing suspension. The light beams are collected with fiber optic guides after passing through the cuvets and then separated into four wavelengths. Additional photodetectors monitor the intensity of the lamp at the same four wavelengths. The speed of the wheel accelerates continuously over 20 minutes to a final speed of 3,000 rpm and maintained at this speed until all the particles have settled. This system enables a broad size distribution from below 0.05 μm to 10 μm (e.g. quartz in water) to be analyzed in 30 min.

Instruments are available from Horiba, Seishin and Shimadzu. They can be run in the gravitational, centrifugal or gradient mode. In the gradient mode the centrifuge accelerates over the analysis time to reduce the measurement time. The simpler instruments operate at constant speed and an analysis can take 45 min, which can be reduced to a few minutes in the more sophisticated versions. The Horiba CAPA-700 covers the size range 0.01 to 300 μm , automatically selecting the best of five operating conditions, involving the three modes enumerated above, at centrifuge speeds from 300 to 10,000 rpm. The CAPA-300 is a more economical version covering the size range 0.04 to 300 μm . Seishin offer three versions of their micron photo sizers covering the size range 0.1 to 500 μm , the SKC-2000, the SKC-3000 and the SKC-5000. The Shimadzu SA-CP3 operates at 120, 240 or 480 rpm and in any of four modes to cover the size range 0.02 to 150 μm . The SA-CP4 operates in the range 500 to 11,000 rpm to cover the size range 0.01 to 500 μm .

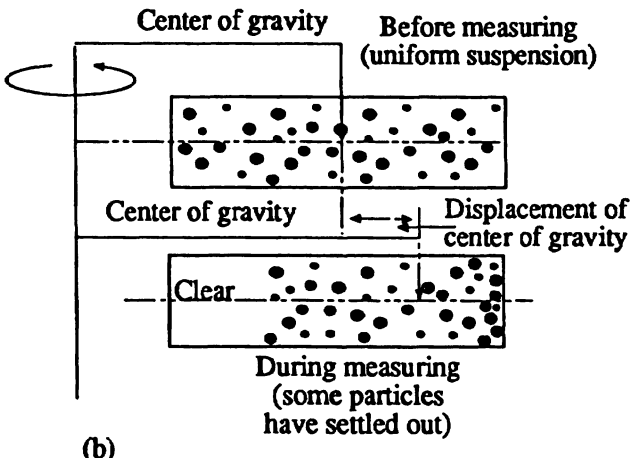
8.8 Homogeneous cumulative centrifugal sedimentation

8.8.1 Methods

The Hosokawa Mikropul Sedimentputer [60–62] has a sealed suspension in a cell which is rotated. As the particles settle, out the center of gravity changes, which creates an in-balance which causes the cell to vibrate (Figure 8.19). By detecting the amplitude and angular velocity of the vibration the size distribution is obtained.



(a)



(b)

Fig. 8.19 The Mikropul Sedimentputer. (a) Schematic of the system.
 (b) The settling of particles causes the center of gravity to shift.

Muschelknautz designed a centrifuge in which the displacement of two diametrically opposed bodies floating in a dispersion was measured [63–66]. The bodies are fixed on a common rod and are immersed at different depths in two chambers. The differential force yields the size distribution.

The Alpine sedimentation centrifuge is a long-arm centrifuge of diameter 400 mm with a 50 mm high measuring cell. The rate at which sediment settles out is determined by measuring pressure changes at the bottom of the cell using a diaphragm arrangement.

8.9 Line-start incremental centrifugal sedimentation

8.9.1 Disc photocentrifuges.

The first disc photocentrifuge was developed by Kaye [67]. In this instrument, concentration changes within a suspension are followed using a white light beam. The instrument is usually used in the line-start mode and intuitively, one would expect that attenuation would be proportional to the projected area of the particles in the beam so that the curve of attenuation against Stokes diameter would be a differential surface distribution. However, Treasure [68] derived a relationship which showed that the attenuation, due to the finite width of the light beam, was proportional to the volume (mass) of particles in the beam [69,70].

In the line-start mode it is necessary to use a spin liquid which is denser than the suspension, otherwise the suspension can break through the interface and settle *en-masse* in a phenomenon known as streaming. In order to eliminate this effect a buffer layer technique is often used (Figure 8.20). The spin liquid may consist of 15 mL of 10% aqueous glycerol on which is floated 0.5 mL of water. An interface forms between the two liquids and this is broken up by a momentary change in the speed of the centrifuge. 0.25 mL of dilute suspension is then introduced; this tends to break through the air-water interface and spread out on the diffuse interface between the buffer liquid and the spin liquid, which is the starting radius for the subsequent sedimentation process [71]. If streaming persists it may be eliminated by using much smaller volumes of buffer liquid and suspension, e.g. 0.1 mL. Coll and Searles [72] used 20 mL of sucrose solution topped by 1 mL of *n*-dodecane to prevent evaporation. Several injections of 0.25 mL of colloid sample ($\approx 0.01\%$) were then injected through the oil layer. In the external gradient method a hypodermic syringe is used to form the gradient. For spin conditions requiring 15 mL of aqueous spin fluid exactly 15 mL are drawn into a 25 mL syringe. Air bubbles are

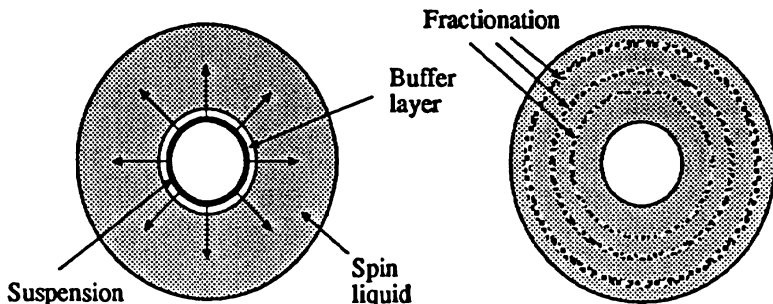


Fig. 8.20 The line-start technique.

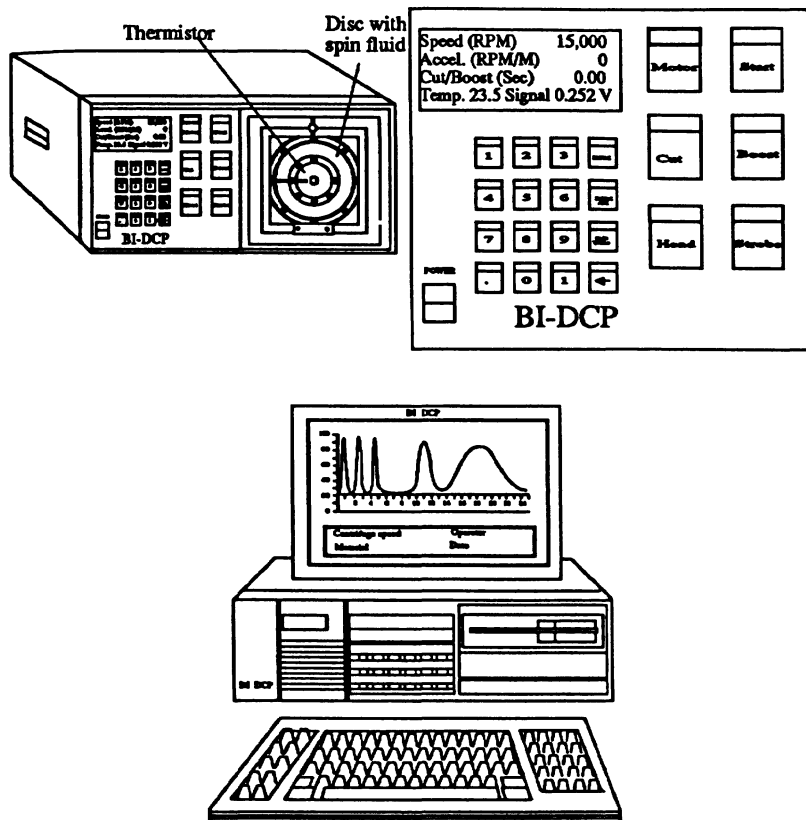


Fig. 8.21 The Brookhaven disc photocentrifuge.

expelled and, with the needle pointing down, an additional 1mL of methanol is drawn in and the entire volume injected into the disc. Finally 1 mL of a suspension containing < 0.5% by volume solids in an 80:20 water/methanol solution are added. An application of this technique is described by Devon *et al.* [73]. A density method with correction for light scattering has also been published [74].

It must be stressed that the raw curves are not size distributions and calibration is required to convert to absolute values [75]. The importance of the correction for the breakdown in the laws of geometric optics is stressed by Weiner *et al.* [76] who show excellent agreement between theory and experiment when this is done correctly. This method has been used to characterize void-containing latex particles [77]. Commercial versions are available from Joyce-Loebl and from Brookhaven (Figure 8.21).

8.10 Line-start cumulative centrifugal sedimentation

8.10.1 MSA analyzer

The MSA analyzer (Figure 8.22) operates in this mode [78]. Objections that can be leveled at this technique are:

- The amount of sediment is determined by the height of the sediment and, since the settled volume is not independent of size, errors are introduced.
- The lower part of the sedimentation cell has sloping walls hence some particles adhere to this section and others slide down the sloping walls into the measurement zone hence large particles are frequently found at a level where only small particles should be present.

One would expect that the large particles would carry some small particles with them so that the sediment would not be stratified into size bands but would contain small particles mixed in with the large ones. Zwicker [79] found the method highly unsatisfactory and recommended that it should no longer be used.

The problems associated with the use of cylindrical tubes, i.e. particles striking the walls of the tube and sticking or agglomerating and reaching the bottom more rapidly than freely sedimenting particles, has been recognized for many years. Berg's solution [25] was to construct sector-or conoidal shaped tubes (Figure 8.23).



Fig. 8.22 MSA special centrifuge tube.

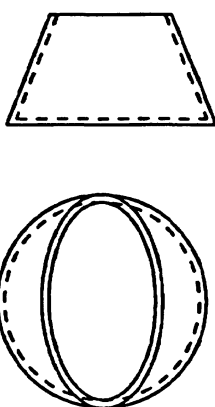
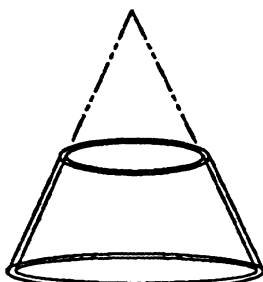
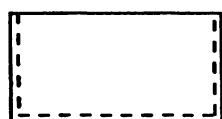


Fig. 8.23 Berg's conoidal centrifuge tubes.



8.11 Particle size analysis using non-invasive dielectric sensors

The use of capacitance measurement is based upon the principle that the concentration changes as particles settle through a suspension and will alter the effective dielectric constant between the sensing electrodes. A complete capacitance transducer consists of capacitance sensing electrodes together with capacitance sensing electronics, which is essentially a capacitance to voltage converter.

The analyzer described by Simons and Williams [80] consisted of an array of eight pairs of capacitance electrodes mounted vertically down the side of a sedimentation tube of length 26 cm and diameter 2.5 cm. The electrodes were embedded in acrylic and flush mounted to the inside wall of the tube.

Soda glass spheres at a volume concentration of 1.65%, in size ranges from 20 to 60 μm and 2 to 18 μm , gave results comparable with Andreasen and Elzone.

8.12 Conclusions

Sedimentation techniques are widely used for particle size analysis since the determined size distribution relates to unit operations such as classification. The distribution also relates to many end-use properties such as the hiding power and gloss of pigments. Thermal diffusion limits the use of gravity sedimentation to powders containing a limited amount of sub-micron material, but the technique is extended into the sub-micron size range with the use of centrifuges.

Gravitational and centrifugal sedimentation using a pipette is attractive due to its versatility and low capital cost, but the analysis requires a skilled operator and is time consuming.

Mass distributions are also determinable using x-ray systems which are available as gravity and centrifugal sedimentometers. These are essential where speed and running costs are more important than capital costs.

Photosedimentometers are also available for gravitational and centrifugal sedimentation. Centrifugal photosedimentometers are available with disc and cuvet cells. The former are usually used in line-start mode which gives high resolution, whereas the latter operate in the homogeneous mode. These instruments need to be calibrated for the breakdown in the laws of geometric optics. The modified distribution greatly alters the raw curve for sub-micron powders with a wide size range, thus limiting the accuracy of this technique. Accuracy is not always important; detecting changes which may affect powder handling or final product may be all that is necessary.

References

- 1 Allen, T. (1990), *Particle Size Measurement*, Chapman & Hall, 4th ed., 301, 312,
- 2 British Standard 3406 (1984), *Determination of particle size distribution*, Part 2, 301
- 3 British Standard 3406 (1985), *Determination of particle size distribution*, Part 6, 301
- 4 Robinson, G.W. (1922), *J. Agr. Sci.*, 12(3), 306–321, 304
- 5 Andreasen, A.H.M. (1928), *Kolloid Beith*, 27, 405, 304
- 6 Andreasen, A.H.M. and Lundberg, J.J.V. (1930), *Ber. Dt. Keram. Ges.*, 11(5), 312–323, 306
- 7 Allen, T. (1969), *Powder Technol.*, 2(3), 132–140, 306
- 8 Vouk, V. (1948), PhD Thesis, London University, 306
- 9 Jarrett, B.A. and Heywood, H. (1954), *Br. J. Appl. Phys.*, Suppl. No. 3, S21, 306
- 10 Morgan, V.T. (1954), *Symp. Powder Metall.*, Iron and Steel Inst. Preprint Group 1, 33–38, 306
- 11 Lewis P.C. and Lothian, G.F. (1954), *Br. J. Appl. Phys.*, Suppl. No. 3, S571, 306
- 12 Rose, H.E. and Lloyd, H.B. (1946), *J. Soc. Chem. Ind.*, 65, 52, 306
- 13 Allen, T. (1968), *J. Powder Technol.*, 2, 132–140, 306
- 14 Allen, T. (1968), *J. Powder Technol.*, 2, 141–153, 306
- 15 Weichert, R. (1981), *Proc. Particle Size Analysis Conf.*, Soc. Analyt. Chem., Loughborough, U.K., 303–310, ed. T. Allen and N.G. Stanley-Wood, publ. John Wiley, 308
- 16 Staudinger, G., Hangl, A. and Peschtl, P. (1986), *Proc. Partec*, Nuremberg, 308
- 17 Brown, J.F. and Skrebowski, J.N. (1954), *Br. J. Appl. Phys.*, Suppl. No 3, S27, 308
- 18 Conlin, S.G. et al. (1967), *J. Sci. Instrum.*, 44, 606–610, 308
- 19 Nonhebel, G. ed. (1964), *Gas Purification Processes*, Newnes, 308
- 20 Kalshoven, J. (1967), *Proc. Particle Size Analysis Conf.*, Soc. Anal. Chem., London, 308, 309
- 21 Oliver, J.P., Hicken, G.K. and Orr, C. (1969), U.S. Patent 3,449,567, 308
- 22 Allen, T. (1970), Br. Patent, 1764/70 3, 308
- 23 Allen, T. and Svarovsky, L. (1970), *J. Phys E*, 3, 458–460, 308
- 24 Allen, T. and Svarovsky, L. (1970), *Proc. Particle Size Analysis Conf.*, Bradford, Publ. Soc. Anal. Chem., 308
- 25 Berg, S. (1940), *Ingen Vidensk.*, Skr. B., No 2, Phys. Suppl. No. 3, S27, 309, 310, 322
- 26 Kaye, B.H. and James, G.W. (1962), *Br. J. Appl. Phys.*, 13, 415 258, 309, 310

- 27 Jarrett, B.A. and Heywood, H. (1954), *Br. J. Appl. Phys.*, Suppl. No. 3, S21, 310
- 28 Bostock, W. (1952), *J. Sci. Instrum.*, **29**, 209, 311
- 29 Cohen, L. (1952), *Instrum. Pract.*, **13**, 1036, 311
- 30 Gerstenberg, H. (1957), *Chem. Eng. Tech.*, **8**, 589, 311
- 31 Bachman, D. (1959), *Dechema Monograph*, **31**, 23–51, 311, 312
- 32 Gerstenberg, H. (1959), *Dechema Monograph*, **31**, 52–60, 311
- 33 Leschonski, K. (1962), *Staub*, **22**, 475–486, 311
- 34 Leschonski, K. and Alex, W. (1970), *Proc. Int. Symp. Particle Size*, Bradford, 236–254, publ. Soc Anal. Chem. ed. M.W.G. Groves and J.L. Wyatt-Sargent, 311
- 35 Kaye, B.H. and Davies, R. (1970), *Proc. Conf. Particle Size Analysis*, Bradford, 207–222, publ. Soc Anal. Chem. ed. M.W.G. Groves, and J.L. Wyatt-Sargent, 312
- 36 Suito, E. and Arakawa, M. (1950), *Bull. J. Chem. Res., Kyota University*, **23**, 7, 312
- 37 Hoffman, R.L. (1991), *J. Colloid Interf. Sci.*, **143**, 232, 312
- 38 Marshall, C.E. (1930), *Proc. Royal Soc.*, **A126**, 427, 312
- 39 Eadie, F.A. and Payne, R.E. (1954), *Iron Age*, **174**, 99, 312
- 40 Brezina, J.J. (1969), *Sediment. Petrol.*, **16**27–1631, 312
- 41 Brezina, J. (1970), *Proc. Conf. Particle Size Analysis*, Bradford, 255–266, publ. Soc Anal. Chem., ed. M.W.G. Groves, and J.L. Wyatt-Sargent, 312
- 42 Werner, D. (1925), *Trans. Faraday Soc.*, **21**, 381, 312
- 43 Travis, P.M. (1940), *ASTM Bull.*, **29**, 102, 312
- 44 Whitby, K.T. (1955), *Heat. Pip. Air Cond.*, Jan., Part 1, 231, June, Part 2, 139, 313
- 45 Whitby, K.T., Algren, A.B. and Annis, J.C. (1958), *ASTM Spec. Publ.* **234**, 117, 313
- 46 Imris, P. and Landsperky, H. (1956), *Silikaty*, **9**(4), 313,
- 47 Kamack, H.J. (1951), *Anal. Chem.*, **23**, 6, 844–850, 314
- 48 Kamack, H.J. (1972), *Br. J. Appl. Phys.*, **5**, 1962–1968, 314
- 49 Allen, T. and Svarovsky, L. (1976), *Dechema Monograph*, Nuremberg 1975, Nos. 1589–1615, 215–221, 314
- 50 Allen, T. (1991), *Proc. Int. Symp. Particle Size Analysis*, Publ. Royal Soc. Chem., ed. N.G. Stanley-Wood, and R. Lines, pp. 498–513, 314, 315
- 51 Slater, C. and Cohen, L. (1962), *J. Scient. Instrum.*, **39**, 614, 314
- 52 Allen, T. and Svarovsky, L. (1972), *Proc. Soc. Anal. Chem.*, **9**(2) 38–40, 314
- 53 Allen, T. and Svarovsky, L. (1974), *J. Powder Technol.*, **10**, 1/2, 23–28, 314, 315
- 54 Allen, T. (1992), US Patent 5,095,451, 315
- 55 Bowen, P., Dirksen, J.A., Humphry-Baker, R. and Jelinek, R. (1993), *Powder Technol.*, **74**, 67–71, 318
- 56 Bowen, P., Herard, C., Humphry-Baker, R. and Jelinek, L. (1994), *Powder Technol.*, **81**, 235, 318

- 57 Bowen, P., Humphry-Baker, R. and Eriksson, P-A. (1996), *5th World Congr. of Chem. Eng.*, San Diego CA, 6, pp. 518–523, publ. Amer. Chem. Soc. 318
- 58 Niemann, J. and Weichert, R. (1995), *4th International Congress Optical Particle Sizing*, Partec 95, Nurenberg, Germany, 375–385, publ. NürnbergMesse, GmbH, 318
- 59 Niemann, J. and Weichert, R. (1995), *Part. Part. Syst. Charact. J.*, 289–294 318
- 60 Kaya, N., Yokoyama, T. and Arawaka, M. (1986), *Partec*, Nurenberg, publ. NürnbergMesse , 318
- 61 Arakawa, M., Shimomura, G., Imamura, A., Yawaza, N., Kaya, N. and Kitai, H. (1984), *J. Soc. Powder Technol., Japan*, 21, 768, 318
- 62 Kaya, N., Yokoyama, T. and Arakawa, M. (1990), *Proc. Second World Congress Particle Technol.*, Sept., Kyoto, Japan, 518–525, Soc. Powder Technol. Japan , 318
- 63 Muschelknauts, E. (1974), Ger. Offen., 2 324 421, 319
- 64 Muschelknauts, E. (1967), *Verh. dt. Ing. Z.*, 109, 17, 757–61, 319
- 65 Muschelknauts, E. (1976), *Dechema Monogram*, 79, Nr. 1589–1615, Nurenberg, Part B, 267–278, 319
- 66 Muschelknauts, E. (1993), *Int. Chem. Eng.*, 33(3) 426–438, 319
- 67 Kaye, B.H. (1962), British Patent 895 222, 320
- 68 Treasure, C.R.G. (1964), Tech. Paper No 50, Whiting and Industrial Powders Research Council, Welwyn, U.K., 320
- 69 Coll, H. and Haseler, S.C. (1984), *J. Colloid Interf. Sci.*, 99, 591, 320
- 70 Devon, M.J., Meyer, E., Provder, T., Rudin, A. and Weiner, B.B. (1991), *Particle Size Distribution II*, ed. T. Provder, Amer. Chem. Soc. ACS Symposium Series 472, 154–168, 320
- 71 Jones, M.H. (1969), US Patent 3, 475,968, 320
- 72 Coll, H. and Searles, C.G. (1987), *J. Colloid Interf. Sci.*, 115(1), 121–129, 320
- 73 Devon, M.J., Provder, T. and Rudin, A. (1991), *Particle Size Distribution II*, ed T. Provder, Am. Chem Soc., 134–153, 321
- 74 Hansen, F.K. (1991), *Particle Size Distribution II*, ed T. Provder, Am. Chem Soc., 169–183, 321
- 75 Allen, T. (1988), *Powder Technol.*, 50, 3,193–200, 321
- 76 Weiner, B.B., Fairhurst, D. and Tscharnter, W.W. (1991), *Particle Size Distribution II*, ed T. Provder, Am. Chem Soc., 134–153, 321
- 77 Cooper, A.A., Devon, M.J. and Rudin, A. (1989), *J. Coating Technol.*, 61, 769, 321
- 78 ASTM C678–75 (Reapproved 1991), *Standard test method for determination of particle size of alumina or quartz using centrifugal sedimentation*, 322
- 79 Zwicker, J.D. (1972), *Powder Technol.*, 6, 133–138, 322
- 80 Simons, S.J.R. and Williams, R.A. (1992), *Powder Technol.*, 73, 85–90, 323

Stream scanning methods of particle size measurement

9.1 Introduction

It is convenient to divide particle size measurement techniques involving the interaction between particles and an external field into two categories, stream scanning and field scanning. In the former, particles are examined one at a time and their interaction is taken as a measure of their size whereas, in the latter, the interaction of an assembly of particles is interpreted in terms of the size distribution of the assembly.

The most widely used stream scanning technique employs the Coulter principle (Figure 9.1a), where the interrogating field is electrical and particle size (volume) is proportional to the change in the electrical impedance as the particles pass through the field. Particle projected area can be measured by the amount of light cut off as a particle passes through a light beam (Figure 9.1b). With a rotating or scanning beam, smaller in size than the particles, the pulse length is a measure of a random chord length (Figure 9.1c). If the incident beam is absorbed in a light trap the light scattered in the forward direction (Figure 9.1d) or at right angles (Figure 9.1e) is size dependent. The signal is greatly enhanced with the aid of an elliptical mirror (Figure 9.1f). Scanning beams, in concert with back-scattering detectors, are also used for chord size determination (Figure 9.1g). These can be used with fairly high concentration slurries since the beam does not have to traverse the suspension. Interferometers (Figure 9.1h) operate as a function of phase shift between a split laser beam, one passing through the particle and the other through the surrounding liquid. If particles are accelerated through a nozzle, the time it takes them to pass through two laser beams is a measure of aerodynamic size (Figure 9.1i). In the phase Doppler method (Figure 9.1j) particle size is determined from the interference pattern as a particle passes through the intersection of two laser beams.

Stream scanning is generally limited to low concentration suspensions, and is best suited to the determination of particle size distribution by number and contamination monitoring. The Coulter

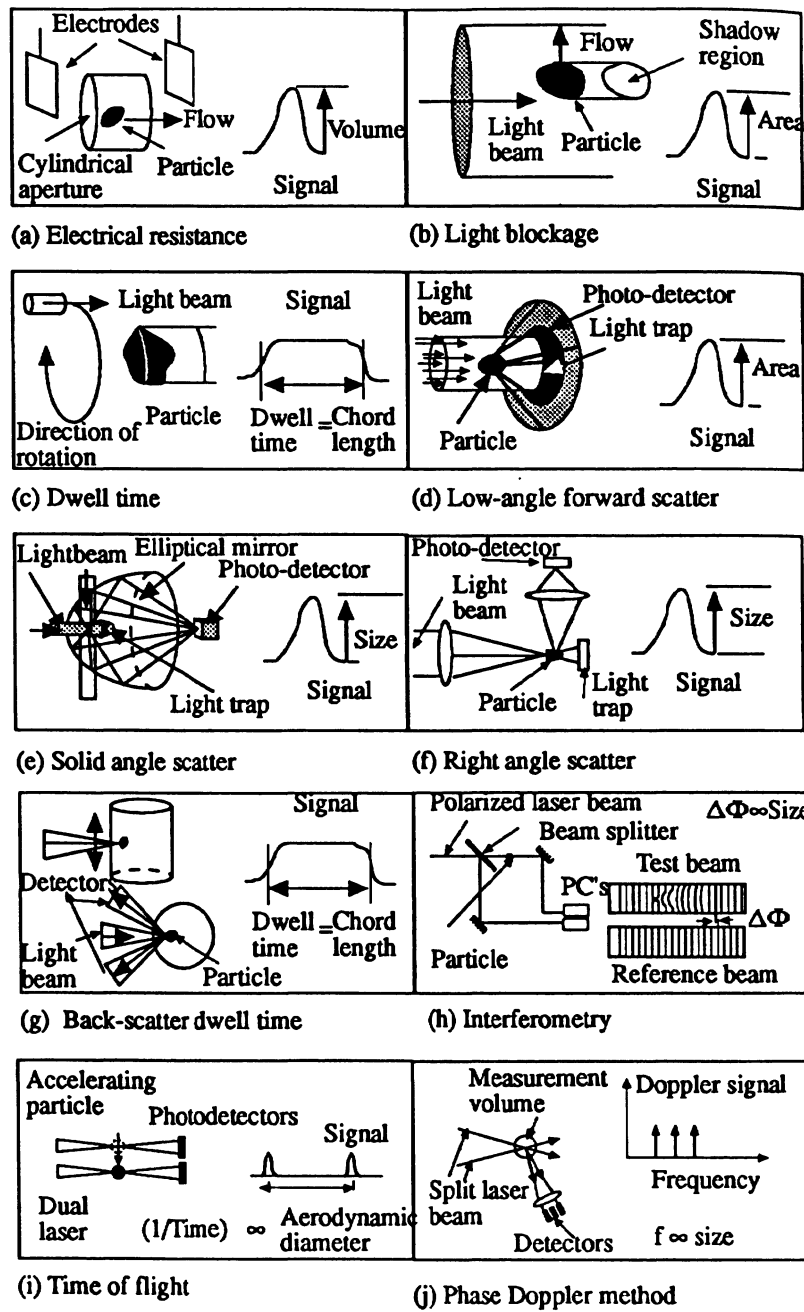


Fig. 9.1 Principles of streaming systems.

principle has been routinely used to monitor particulates in injectable solutions in Britain since the 1973 edition of the British Pharmacopoeia but the Hiac/Royco is preferred because it is faster. The United States Pharmaceutical method, USP XXII (1988), for determining particulates in injectable solutions is based on microscopy and suffers several disadvantages [1]. The Hiac/Royco light blockage method is allowed in USP XXI (1985) for the evaluation of particle burden in large volume dextrose solutions.

Conversion of number distribution to mass (volume) distribution can result in gross errors unless the width of the distribution is narrow. For example, if the range is 10:1 the omission of a single 10 unit particle (volume = 1000) is equivalent to the omission of 1000 one unit particles. In order to obtain accurate volume distribution data it may therefore be necessary to size millions of small particles in order to get a statistically acceptable count at the coarse end of the distribution.

9.2 The electrical sensing zone method (the Coulter principle)

9.2.1 Introduction

The Coulter technique is a method of determining the number and size distribution of particles suspended in an electrolyte by causing them to pass through a small orifice on either side of which is immersed an electrode. The changes in electrical impedance as particles pass through the orifice generates pulses whose amplitudes are proportional to the volumes of the particles. The pulses are fed to a pulse height analyzer where they are scaled and counted.

The Coulter principle was patented in 1949 [2] and described in 1956 [3] as a method for counting and sizing blood cells but was soon extended to a wide range of particulate material [4,5]. Since analyses may be carried out rapidly with good reproducibility using semi-skilled

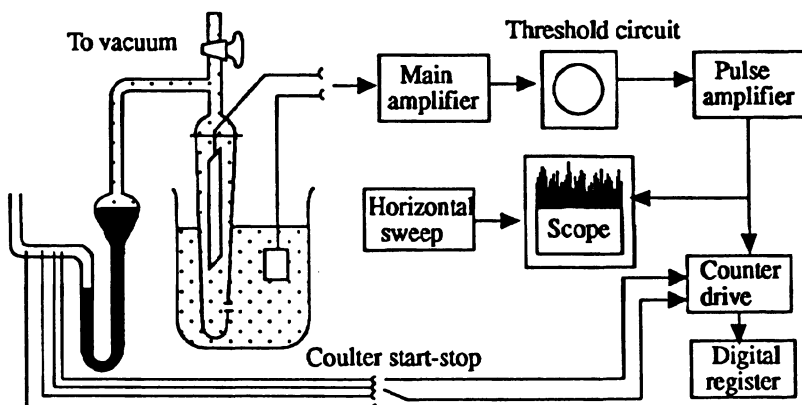


Fig. 9.2 Line diagram of the Coulter Counter.

operators the method has become very popular in a wide range of industries. In a recent Coulter bibliography, 1432 industrial references and 436 pharmaceutical references are cited [6].

9.2.2 Operating principle

The operating principle of the instrument may be followed by referring to Figure 9.2. The sample to be analyzed is dispersed in an electrolyte which is placed in a beaker. The glass sample tube, on either side of which there is a platinum electrode, is immersed in the electrolyte. A controlled vacuum initiates flow through a sapphire orifice let into the glass tube and unbalances a mercury siphon. The instrument can then operate in one of two modes.

- 1 The system may be isolated from the vacuum source by closing tap A and flow continues due to the balancing action of the mercury siphon. The advancing column of mercury activates a counter by means of start and stop probes placed so that a count is carried out whilst a known volume of electrolyte (0.05 mL, 0.50 mL, 2.0 mL) passes through the orifice.
- 2 Data may be acquired in a preset count mode in which counting is initiated manually and ends when the preset count number (up to 1 million) has been reached.

A current passing through the orifice, between the two electrodes, enables the particles to be sensed by the momentary changes in the electrical impedance as they pass through the aperture as each particle displaces its own volume of electrolyte within the aperture itself.

These changes in impedance are detected and presented as voltage pulses, the heights of which are proportional to the volumes of the particles producing them. The particle generated pulses are amplified, sized and counted and, from the derived data, the particle size distribution is determined.

Particle size analysis may be performed in the overall size range of 0.6 to 1200 μm . To achieve this, a number of different sensors (aperture tubes) are required. The operating range of each sensor is from around 2% to 60% of the orifice diameter, e.g. from 2 to 60 μm for a 100 μm aperture tube. Smaller particles generate pulses which are lost in electronic noise generated within the aperture and in the electronic circuitry. Larger particles give increasingly non linear response and tend to block the aperture if they are greater than about half the aperture diameter. For powders with a wider size range, an extrapolation or a two tube technique may be necessary. Alternatively the Coulter analysis can be combined with some other technique, e.g. the coarse end of the distribution can be analyzed by sieving and the two analyses combined. Care should be taken with powders having a wide size range since the uncounted fraction may form a substantial part of the distribution.

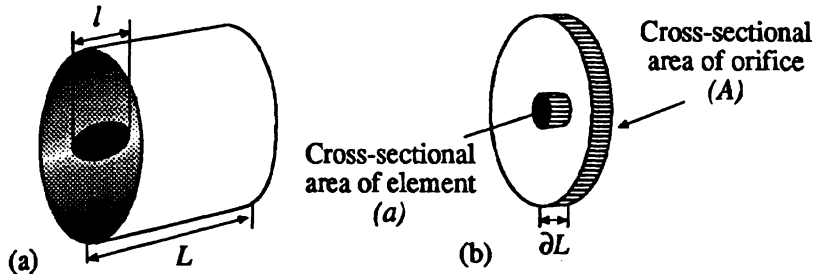


Fig. 9.3 The passage of a particle through the orifice of a Coulter Counter.

9.2.3 Theory for the electrical sensing zone method

The basic assumption underlying the Coulter principle is that the voltage pulse generated when a particle passes through the aperture is directly proportional to particle volume. The relationship between particle size and instrument response may be determined using a simplified theory. Figure 9.3a shows a particle passing through the orifice and Figure 9.3b shows an element of the particle and orifice.

The resistance of element without a particle

$$\partial R_0 = \rho_f \partial l / a$$

The resistance of element, with a particle included, is that of two resistors in parallel

$$\left[\frac{1}{\partial R} = \frac{1}{\partial R_1} + \frac{1}{\partial R_2} \right]$$

so that:

$$\partial R = 1 / \left(\frac{A - a}{\rho_f \partial l} + \frac{a}{\rho_s \partial l} \right) \quad (9.1)$$

where ρ_f , ρ_s , are the resistivities of the fluid and particle respectively, A is the cross-sectional area of the orifice, a is the cross-sectional area of the particle and V is the volume of the particle. Thus the change in resistance of the element due to the presence of the particle $\partial(\Delta R)$ is given by:

$$\partial(\Delta R) = \partial R_0 - \partial R$$

$$\partial(\Delta R) = \frac{-\rho_f a \partial l}{A^2} \left(1 - \frac{\rho_f}{\rho_s}\right) \frac{1}{\left[1 - \left(1 - \frac{\rho_f}{\rho_s}\right) \frac{a}{A}\right]} \quad (9.2)$$

The external resistance of the circuit is sufficiently high to ensure that a small change ΔR in the resistance of the orifice due to the presence of a particle will not affect the current I ; the voltage pulse generated is therefore $I\Delta R$.

In practice it is found that the response is independent of the resistivity of the particle. If this were not so, the whole technique would break down since a different calibration factor would be required for each electrolyte-solid system. This independency is attributed to oxide surface films and ionic inertia of the Helmholtz electrical double layer and associated solvent molecules at the surface of the particles, their electrical resistance becoming infinite [7].

The terms involving (ρ_f/ρ_s) may therefore be neglected and the preceding equation becomes

$$\partial(\Delta R) = \frac{\rho_f a \partial l}{A^2(1-a/A)} \quad (9.3)$$

The response therefore, is not proportional to the volume of the particle, but is modified by the a/A term. For rod shaped particles whose length is smaller than the aperture length, this leads to an oversizing of about 6% in terms of the diameter at the upper limit of each aperture with distortion of the measured size distribution [8,9]. This error decreases as a/A decreases.

For spherical particles of diameter $d = 2b$, the change in resistance due to an element of thickness dl at a distance l from the center of the sphere may be determined and this can be integrated to give the resistance change due to the particle [9–11]:

$$\Delta R = -\frac{2\pi^2\rho_f}{A} \int_0^b \frac{(b^2-l^2)}{(1-\pi(b^2-l^2)/A)} dl$$

$$\Delta R = \frac{8\rho_f d^3}{3\pi D^4} \left[1 + \frac{4}{5} \left(\frac{d}{D} \right)^2 + \frac{24}{35} \left(\frac{d}{D} \right)^4 + \frac{169}{280} \left(\frac{d}{D} \right)^6 + \dots \right] \quad (9.4)$$

This gives a limiting value of two thirds the Maxwellian value. Recognizing this, Gregg and Steidley [11], multiplied their solution by three halves. This procedure has been questioned [10].

The complete solution is:

$$\Delta R = -\frac{4\rho_f}{\pi D} \left[\frac{\sin^{-1}(d/D)}{1-(d/D)^2} - \frac{d}{D} \right] \quad (9.5)$$

This equation may be written:

$$\Delta R = -\frac{\rho_f v}{A^2} F \quad (9.6)$$

Hence, the instrument response is proportional to the volume of the sphere modified by the function F . This equation results from a simple integration of the area available for conduction. De Blois and Bean [10] derived an approximation for F which employs the solution to Laplace's equation for a sphere in an infinite medium, using only those streamlines which do not cross the sphere wall:

$$F_1 = 1 + 1.268 \left(\frac{d}{D} \right)^3 + 1.17 \left(\frac{d}{D} \right)^6 \dots \dots + \dots \quad (9.7)$$

De Blois and Bean derived the following equation as the best fit to their experimental results:

$$F_2 = 1 + 0.73 \left(\frac{d}{D} \right) \quad (9.8)$$

Smythe [12, cited in 13,14], solved the problem numerically, by using an integral formula, to derive:

$$F_3 = \frac{2}{3} C_0 \left(\frac{d}{D} \right) \quad (9.9)$$

with C_0 determined to an accuracy of 1 part in 10^7 for diameter ratios from 0.1 to 0.95.

Grover *et al.* [15] reported measurements on polystyrene spheres and pollen using the equation:

$$F_4 = 1 + \frac{2}{3} \left(\frac{d^3}{D^2 L_e} \right) + \frac{2}{3} \left(\frac{d^3}{D^2 L_e} \right)^2 \dots + \dots \quad (9.10)$$

where L_e is the effective length of the aperture; in the previous derivations the length was considered infinite.

Anderson and Quinn [12] compared the above equations and concluded that F_4 agrees well with experimental results at small $(d/D)^3$. F_1 does not coincide with F_4 as $(d/D)^3$ approaches unity and F_3 converges with the numerical results as $(d/D)^3$ approaches unity.

The initial experimental data by de Blois and Bean were with PVC spheres down to 0.09 μm in diameter using a pore in a plastic sheet for an orifice. They concluded that the technique was applicable down to 0.015 μm . In a later paper[16] they reported measurements down to a diameter of 0.06 μm , using a pore in a Nuclepore filter, and also measured the osmotic velocity of the liquid in the pore.

The error in assuming a linear relationship between resistivity change and particle volume for spherical particles is about 5.5% for $(d/D) = 0.40$. The principle may therefore be applied to higher ratios of (d/D) than 0.40 provided corrections are applied and aperture blockage does not become too troublesome. For non-spherical particles F is modified by the inclusion of a shape factor [12]. In general, as the ratio of (d/D) increases, the resistance pulse generated is greater than predicted by assuming proportionality and oversizing of the larger particles occurs.

9.2.4 Effect of particle shape and orientation

It has been claimed that particle shape, roughness and the nature of the material has little effect on the analysis [17], but there is considerable evidence that the size measured is the envelope of the particle. Comparison with other techniques gives good agreement for homogeneous spherical particles; for non-spherical particles results may differ [18,19]. For porous particles the measured volume may be several times the skeletal volume, and the apparent volume for flocs will be greater than the volume of the particles that make up the flocs [20]. Since flaky particles rotate as they pass through the sensor, the measured volume is the volume swept out by the particle and this can also lead to oversizing. With extreme shapes such as rods this may cause a change in size distribution, as apertures of different sizes are used, if the whole of the rod cannot be accommodated in the sensing zone. It has been reported that silica containing large pores can be undersized by as much as 100% due to pore filling by the electrolyte[21]. For these reasons it is worthwhile to calibrate the analyzers with the test material or carry out a mass balance routinely.

9.2.5 Pulse shape

Pulses deviate from the ideal, single modal shape when they are generated from coincident particles. These pulses take on a variety of shapes always of longer duration and often having multiple peaks [22]

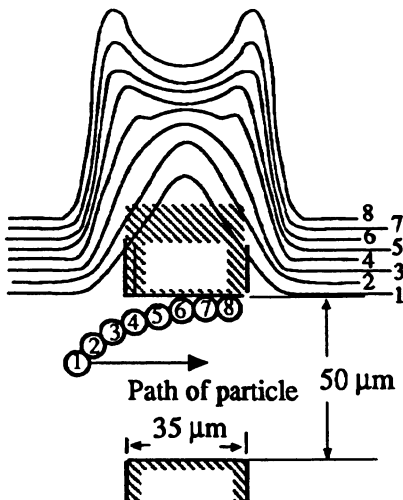


Fig. 9.4 Shape of pulses generated by particles not passing centrally through the aperture.

conducted experimental studies of the pulses generated in the aperture and determined that the potential field was dense at the inlet and outlet edges. Particles traveling parallel to and near the walls pass regions of high potential gradient and generate M-shaped pulses (Figure 9.4). This does not affect the analysis of powders having a wide range of particle size but grossly skews narrow distributions to generate too coarse an analysis. A partial correction is to use an 'edit' switch so that such grossly distorted pulses are not counted (Figure 9.5), but this can lead to the rejection of considerable information and is not necessarily free of bias. A better solution is to reshape the pulses electrically so as to provide information from them all. A full correction is to force the particles into a central streamline using 'hydrodynamic focusing' (Figure 9.6) [24].

9.2.6 Effect of coincidence

Two types of error arise due to more than one particle being in the measurement zone at any one time.

- **Primary Coincidence.** Two or more particles in the measurement zone give rise to two or more overlapping pulses. Depending on their proximity and electrical resolution, these pulses may not be resolved, leading to loss of count.
- **Secondary Coincidence.** Two or more very close particles, which individually give rise to pulses below the threshold level, may

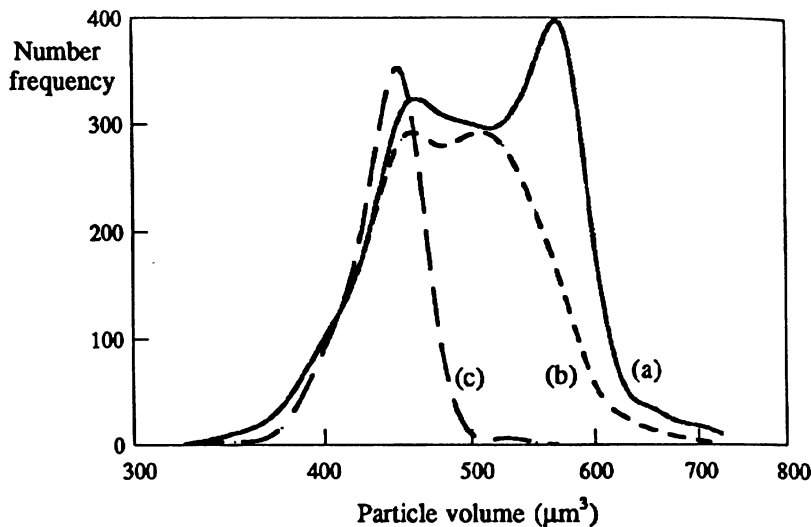


Fig. 9.5 Effect of edit on 10 μm latex; 256 channel windowed data
 (a) edit off, (b) edit on (c) focused (after Elkington and Wilson) [23].

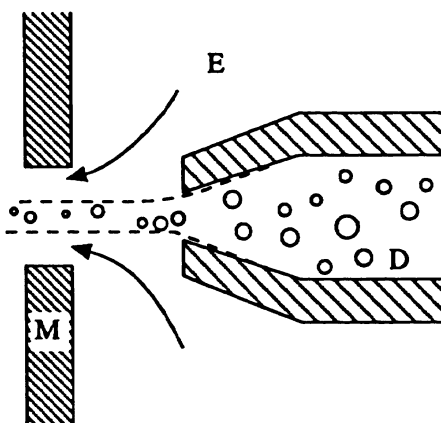


Fig. 9.6 Hydrodynamic focusing. Suspension is focused on the axis of the measurement opening M with a probe D. The suspension streams through the axis after dilution with particle free electrolyte E.

collectively generate a pulse above the level. Thus if the concentration is too high, oversize particles begin to appear.

A coincidence correction can be applied for primary coincidence but it is preferable to use a concentration so low that this effect is negligible. Under this condition, secondary coincidence errors are also reduced.

The correction yields the following relationship between true count N and observed count n :

$$n = \left(\frac{v}{s} \right) \left[1 - \exp \left(-\frac{s}{v} N \right) \right]$$

giving:

$$N = n + \left(\frac{s}{2v} \right) n^2 \quad (9.11)$$

where v is the monitored volume for each count and s is the sensing zone volume.

The manufacturers propose the more convenient empirical equation:

$$N = n + pn^2 \quad (9.12)$$

where p , the coincidence factor, can be calculated from:

$$p = 2.5 \left(\frac{D}{100} \right)^3 \left(\frac{500}{v} \right) \times 10^{-6} \quad (9.13)$$

D is the aperture diameter in micrometers and v the volume of the suspension in microliters monitored for each count. The factor 2.5 was determined experimentally using a 100 μm diameter aperture tube 75 μm long with $v = 500 \mu\text{L}$. For tubes with apertures smaller than 70 μm , the length to diameter ratio is greater than 0.75 and Auerbach's equation based on the electrical resistance of a tube of length L and diameter D should be used:

$$p = \pi D^2 \left(L + \frac{0.8D}{V_0} \right) \quad (9.14)$$

where V_0 is the volume of the aperture.

9.2.7 Multiple aperture method for powders having a wide size range

(a) General

If the size range of the powder is too wide to be covered by a single orifice, two or more aperture tubes should be used. As a general rule, if there is more than 2% of the distribution in the smallest size interval it is advisable to use a smaller orifice to determine the fine end of the distribution.

An orifice should first be selected to give zero count in the top size channel and a smaller orifice should then be selected to size the fine end of the distribution. The ratio of the orifice diameters should be less than 5:1 to ensure that the overlapping counts will match. An analysis is first carried out with the large aperture tube using a known volume of electrolyte; in order to facilitate calculation of dilution factors it is recommended that the weight of the beaker and the suspension be determined prior to the analysis. For an instrument that can provide a number count, the dilution factor can be calculated by counting the diluted suspension using the large aperture tube at two size settings at around one third of the orifice size. The ratio of this count, corrected for coincidence, to the corrected count on the original suspension, is the dilution factor.

(b) Sieving technique

After analysis with the large aperture tube the weight of residual suspension is determined. The suspension is then poured through a micromesh sieve with openings approximately half the diameter of the orifice of the smaller aperture tube. The filtrate is collected in a clean, weighed beaker. The suspension beaker is next rinsed with clean electrolyte and the rinsings poured through the sieve and collected. The dilution factor is calculated from the weights of the original and final suspensions.

(c) Sedimentation technique

An analysis is carried out using the larger aperture tube as before. Using Stokes' equation, the time is calculated for particles coarser than the upper size limit for the smaller aperture tube to settle below the orifice. After this time has elapsed, an analysis is carried out with the smaller aperture tube, after diluting if necessary.

With multichannel models it is necessary to calibrate the two aperture tubes so that the channel size levels coincide. The two sets of data should coincide in the overlap region to generate the combined analysis. An application of multiple aperture technique, using wet sieving to remove oversize, has been described for fly ash in the size range 1 to 200 µm [25].

9.2.8 Calibration

Calibration is usually effected with the use of narrowly classified (monosize) spherical latex particles. Rapid calibration may be made by observing the threshold level (t) required to screen out the single height pulses displayed on the oscilloscope. More accurately, a full count is taken at a visually determined threshold level of $0.5t$ and an oversize count at threshold setting $1.5t$: the threshold setting, to give a count equal to half the difference between these two counts, is used for calibration purposes. Calibration may also be made using powders under test provided the size range remains within the range of a single aperture tube. This procedure is a primary calibration procedure and is recommended in a recent standard as being superior to latex calibration [26]. This procedure cannot be used with the Coulter Multisizer due to count loss. A recent paper reported a count loss of over 30% which generated a mass loss of over 15%, which implies that the loss was preferentially of fines [27].

The volume of particles in a metered volume of suspension is:

$$v_p = \frac{vw}{V_s \rho_s} \quad (9.15)$$

where: v = metered suspension volume, V_s = total suspension volume, w = total weight of the powder and ρ_s = particle density.

9.2.9 Carrying out a mass balance

Although it is common practice to calibrate the Coulter Counter using a standard powder, it is possible to calibrate the instrument with the powder being examined. This is the preferred British standard method [26]. It is reiterated that this procedure cannot be carried out with the some instruments due to count loss. Essentially one balances the volume of particles passing through the measuring aperture with the known volume in the measurement sample. This serves a multiple purpose in that

- It indicates if part of the distribution has been missed. This occurs if the size range of the powder is greater than the detection range of the aperture. This is not always obvious from the appearance of the determined distribution. In particular, one mode of a bimodal distribution could easily be lost;
- Particle dissolution or growth is detected;
- It checks on the accuracy of the calibration and exposes measurement errors.

This procedure should be used as routine since it indicates whether all the powder is accounted for and allows for correction for powder outside the measuring range of the aperture used. In an extreme case it

Table 9.1 Mass balance calculation with BCR 66 using a Coulter Counter TAII

Upper size level (μm)	Mean count (N)	Mean size (μm) (d_v)	Oversize volume (μm^3) (v_m)	Uncorrected volume % oversize	Corrected volume % oversize
6.35	0	5.66	32	0.02	0.02
5.04	2	4.49	118	0.08	0.07
4.00	33	3.56	850	0.56	0.47
3.17	346	2.83	4 518	2.96	2.49
2.52	2 245	2.24	15 698	10.27	8.63
2.00	9 620	1.78	37 456	24.51	20.6
1.59	31 620	1.42	69 913	45.76	38.4
1.26	85 824	1.12	109 798	71.86	60.4
1.00	162 216	0.89	137 705	90.12	75.7
0.79	244 819	0.71	152 795	100.00	84.0

Column 1 gives the Coulter upper size

Column 2 gives the coincidence corrected oversize count by Coulter Counter, (N).Column 3 gives the Coulter size (volume diameter, d_v), these are the geometric mid-points of the size rangesColumn 4 gives the oversize volume ($v_m = \pi/6 \sum \Delta N d_v^3$)

Column 5 gives the uncorrected volume percentage oversize

Column 6 gives the corrected mass balance volume % oversize

From equation (9.15), the volume of material in the metered volume:

$$v_p = \left(\frac{0.1912}{100} \right) \left(\frac{1}{200} \right) \left(\frac{0.08}{2.62} \right) = 1.82 \times 10^{-4} \text{ mm}^3$$

$$\text{Hence: measured percentage} = \frac{152.8}{1.82} = 84.0\%$$

Data

$$D = 30 \mu\text{m}$$

$$w = 0.1912 \pm 0.001 \text{ g}$$

$$v_1 = 100 \pm 0.5 \text{ cm}^3$$

$$v_2 = 1.00 \pm 0.01 \text{ cm}^3$$

$$V_s = 200 \pm 0.5 \text{ cm}^3$$

$$v = 0.050 \pm 0.001 \text{ cm}^3$$

$$\rho_s = 2.62 \pm 0.01 \text{ g cm}^{-3}$$

Thus, 16% of the sample is smaller than the lower limit for the 30 μm aperture tube.**Coincidence correction.** From equation (9.12) $N = n + pn^2$

$$\text{where } p = 2.5 \left(\frac{D}{100} \right)^3 \left(\frac{0.5}{v} \right) = 0.675$$

has been found that less than 5% of the total distribution was being measured and decisions were made based on these incorrect distributions. Alternatively, if the whole size range cannot be covered using a single aperture tube, a two tube technique is required. This is not possible if the fraction unaccounted for is below the limit of the technique and the alternative mass balance procedure, as used with BCR 66 standard quartz powder, is as follows.

Disperse w gram of powder in $v_1 \text{ cm}^3$ of liquid. Pipette out $v_2 \text{ cm}^3$ of suspension and add it to electrolyte to make up $V_s \text{ cm}^3$. Determine the corrected Coulter count on a metered volume of $v \text{ cm}^3$.

There is often no indication that an undersize fraction has been missed hence it is usually worthwhile to carry out a mass balance routinely in order to check that no error has occurred. The check will also highlight odd behavior such as particle swelling or dissolution. This is important if the analysis is carried out using a saturated solution, as in the case of crystals in their mother liquor, but is also important for detecting the loss with slightly soluble powders. For accurate data, the Coulter count needs to be corrected for coincidence (i.e. two particles in the sensing zone at the same time).

The metered volume is guaranteed to within $\pm 2\%$ for the 2 mL volume only, hence it is necessary to calibrate if one of the other volumes is used. Calibration is effected by making a particle count, with a powder whose size range lies wholly in the range of the aperture tube in use, using the 2 mL volume and comparing this with a count using the metered volume being used.

For ease of calculation a volume balance is shown in Table 9.1 rather than a mass balance.

9.2.10 Oversize counts on a mass basis using the Coulter Counter

In many powder additives the presence of oversize particles results in faults in the finished product. A technique has been developed [28] for determining the number concentration of these oversize particles using the Coulter Counter Multisizer II.

The normal procedure for determining the number oversize is to carry out a mass balance and present the derived Coulter data graphically as counts/gram against particle size. The problem with using this procedure is that, in some cases, there are only one or two oversize particles in the presence of millions of smaller ones. It is therefore necessary to filter out many of the smaller particles and carry out a count on the oversize residue. This poses problems in that some oversize particles may be lost in the process and, even more likely, large contaminant particles may be introduced in the filtration process.

A precision transparent sieve with $\pm 2\%$ tolerance, introduced by Collimated Holes Inc., was tested as a simple alternative to straightforward Coulter counting and gave good, reproducible results when used in combination with a specially designed filter holder to

reduce contamination. This sieve has an additional advantage in that it can be examined under a microscope to determine the nature of the oversize particles. A mass balance carried out as described above indicated that, for the published example, at 15.87 μm the raw oversize count, averaged for four runs and corrected for background, was 68 with a standard deviation of 2.44. Without filtering, the observed count was of the order of one or two with little statistical validity.

Dividing by the weight of powder in the measurement sample (5.165×10^{-4} g) gives a total count of 1.317×10^5 particles g^{-1} with a standard deviation of 0.047×10^5 particles g^{-1} .

The true count is the observed count \pm the uncertainty defined as twice the standard deviation divided by the observed count.

$$\text{True count} = (1.32 \pm 0.07) \times 10^5 \text{ particles } \text{g}^{-1}.$$

The analytical error of around 3% needs to be added to this to give the overall uncertainty:

$$\text{True count} = (1.32 \pm 0.15) \times 10^5 \text{ particles } \text{g}^{-1}.$$

The data are presented in Figure 9.7. The graph is linear on a log-linear scale and indicates a high probability of an oversize count of 10,000 particles g^{-1} at the 33 μm level.

9.2.11 Apparatus

The Coulter Counter model TA11 operates in the overall size range of 0.6 to 1200 μm . For volume (weight) data the distribution is presented in 16 size channels. Number distribution can also be presented using an optional population count accessory (PCA1). An optional accessory, the Channelyzer (C256), provides 64, 128 or 256 channel high resolution data for narrow range material.

Data may be presented graphically in a cumulative or differential mode; a full tabular printout is also available.

A computer interface may be fitted to the PCA1 to incorporate the Coulter Accucomp data handling system. A free standing interface is also available to convert data to RS232C or IEEE-488 computer code.

The Coulter Counter ZM is a dual threshold system which operates in the overall size range of 0.4 to 800 μm . Manual threshold settings limits counting to one size range for each run (instead of 16 as with the TA11) but the size levels can be pre-selected. This instrument can also be used with the C256.

The Coulter Multisizer IIE delivers fast accurate sizing in the size range 0.4 to 1200 μm at up to 5000 counts per second. It provides size distribution in 256, 128, 64, 32 or 16 channels. Built in cursors allow users to electronically isolate sub-populations of interest in histograms

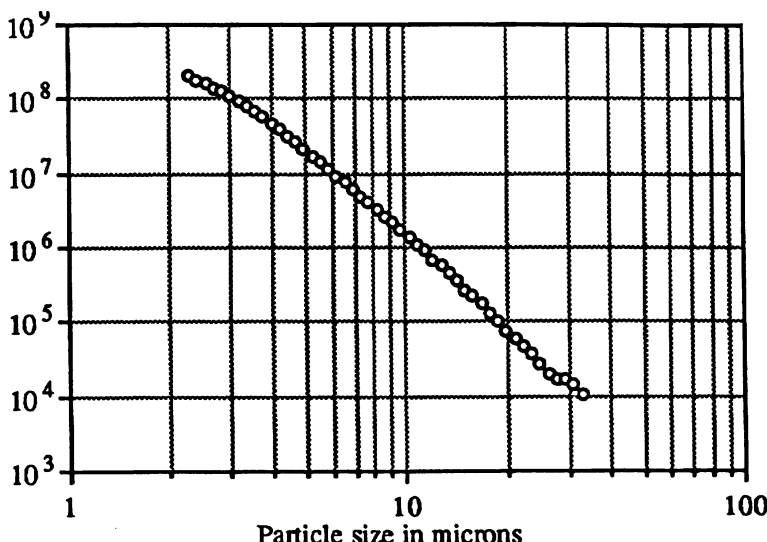


Fig. 9.7 Oversize count for BCR 70 by Coulter Multisizer after filtering through a 15 μm precision transparent sieve.

displayed on a monitor. The resolution can then be expanded to increase the instrument's resolution up to 25,600 channels for greatly improved resolution of narrow or mixed populations of particles. Sophisticated editing circuitry minimizes errors by removing misshapen pulses caused by non-axial or coincident passage of particles through the aperture.

The Coulter Counter Model D industrial is a low cost unit designed to work in the 1 to 112 μm size range.

The Coulter Z1 operates in the 1 to 120 μm size range. Metered volumes include 100 μL , 500 μL and 1000 μL . The mercury manometer is replaced with an oil displacement pump.

Particle Data market a similar range of instruments under the trade mark Elzone. Their product line is listed below with brief notes on their principal differences.

PC Series are dual threshold instruments which accept all accessories and options, completely operated by PC-AT micro-computer (IBM or compatible). The 282PC has dual sample stands and automatic valving and orifice clearance; the 280PC is similar but has only one sample stand.

180 Series have an integral micro-computer and mini-terminal, dual R232 output, and are field upgradable with plug-in components. The 180XY has 164 kbyte memory and up to 256 channel size analysis; the 180+ has 96 kbyte memory and up to 64 sequence channel size

analysis; the 180 has 64 kbyte memory and up to 9 sequence channel size analysis.

Model 180 is a single threshold cell counter (display only) and up to 9 sequence channel size analysis.

Special hardware accessories include mercury free (timed) sampling, choice of sample agitation means, enclosing shield against hazardous samples or excessive noise, flow through and direct input sample cells.

Software provides special data conversions (e.g. crystallization), particle length analysis and user selected printout formats.

The systems detect and clear aperture blockages automatically and resume data collection without operator intervention. Coincidence is corrected for automatically to allow a 20-fold increase in sample concentration. This is particularly useful when measuring coarse material, greatly reducing the analysis time. Dual sample stands eliminate changing glassware and/or electrolyte for different materials or size ranges. This facility is helpful for analyzing wide size distributions requiring data blending and for preparing one sample while the previous one is running.

The Signet ATS200 is a low cost instrument using aperture tubes from 20 µm to 300 µm in diameter although larger apertures are available on request. This instrument differs from others in that, in the 30 µs it takes for a particle to traverse the aperture, it is measured 30 to 60 times to give higher precision. The instrument is equipped with two apertures. This allows the operator to examine an unknown substance with the larger aperture and make the determination if the smaller aperture is required for precise analysis. The ATS200 continuously monitors the voltage across the aperture to give fast detection of aperture blockage and subsequent automatic backflushing. This feature enables the instrument to be used in an on-line mode. The measurement cycle takes approximately 9 s to complete.

9.2.12 Limitations of the method

The primary limitation of this technique is the need to suspend the powder in an electrolyte. For powders insoluble in water a 0.9% saline solution is often used and dispersion effected using ultrasonics. The manufacturers also provide a list of electrolytes for use with water soluble materials but these can cause cleaning difficulties.

The narrow size range covered using one aperture tube may necessitate the use of a two tube procedure which can be onerous. For a powder having a wide size range, the large particles may cause troublesome aperture blockage with the smaller aperture. One procedure to cope with this is to sieve out the coarse particles prior to the analysis using the smaller aperture and the second procedure is to allow the coarse particles to sediment out below the aperture level.

Particles which do not pass along the axis of the cylindrical aperture generate mis-shapen pulses which can greatly deform narrow size distributions. This effect can be reduced by editing out the mis-shapen pulses or using a technique known as hydrodynamic focusing in which the particles are fed through the central streamline.

9.2.13 Coulter Multisizer mass balance calculation for BCR 70 standard quartz powder

With most electrical sensing zone apparatus the volume of the measured particles is determined by multiplying the number of particles, corrected for coincidence, counted in each size interval by the mean volume for that interval.

The final value of $\Sigma \Delta N \bar{V}$ represents the total sample volume analyzed (in relative units if \bar{V} is in relative units) in the volume of suspension metered by the manometer.

The total mass of particles in the metered volume is m_A , given by the equation:

$$m_A = \pi K_d^3 \rho \Sigma \Delta N \bar{V} \quad (9.16)$$

where K_d is the diameter calibration constant and ρ the powder density.

This is equivalent to:

$$m_A = \frac{\pi}{6} \rho \Sigma \Delta N d_v^3 \quad (9.17)$$

where d_v is the volume diameter.

Since the total mass of sample used, m , is known, the mass m_T of sample in the manometer metered volume, v , is given by:

$$m_T = \frac{mv}{V_T} \quad (9.18)$$

where V_T is the total volume of electrolyte solution used.

Example

For ease of calculation a volume balance is shown in Table 9.2 rather than a mass balance.

Column 1 gives the Coulter size (volume diameter d_v), these are the mid-points of the size ranges,

- Column 2 gives the cumulative (raw) undersize count by Coulter Counter (n),
 Column 3 gives the cumulative undersize count corrected for coincidence errors (N),
 Column 4 gives the relative number (ΔN).

A dilution step is usually required in order to generate a representative analytical sample from the measurement sample obtained from the sample splitting operation. m_T is determined from the known tared mass m of density ρ g cm⁻³ dispersed in V cm³ of liquid from which Δv cm³ is extracted and added to V_L cm³ of electrolyte. If the metered volume is v then:

$$m_T = \frac{m}{V} \left(\frac{\Delta v}{V_L + v_1} \right) \quad (9.19)$$

The numbers in the size intervals given in column 4 are converted to volumes in column 5 and accumulated in column 6. Assuming homogeneity the volumes can be assumed proportional to weights and the cumulative weight distribution generated, column 7. (Note that these should not be plotted against column 1 but against the upper size limit e.g. the second smallest size range, in μm , is $\sqrt{1.35 \times 1.43} = 1.39$ to $\sqrt{1.43 \times 1.51} = 1.47$ centered on 1.43).

Coincidence Calculation

$$N = n + pn^2 \text{ where } p = 2.5 \left(\frac{D}{100} \right)^3 \left(\frac{500}{v} \right) \times 10^{-6}$$

Aperture diameter $D = 70 \mu\text{m}$:

Metered volume $v = 2000 \mu\text{L}$

Hence, $p = 0.2144 \times 10^{-6}$ making:

$$N = n + 0.2144 \left(\frac{n}{1000} \right)^2$$

Mass Balance Calculation

0.1219 g of powder of density 2.619 g cm⁻³ was dispersed in 100 cm³ of filtered 0.1% w/v sodium hexametaphosphate solution. 1.00 cm³ of this suspension was added to 150 cm³ of electrolyte. The count was carried out on 2.00 cm³.

Table 9.2 Mass balance calculation for the Coulter Multisizer

Size (μm) (d_v)	Cum. number (n)	Corrected cum. number (N)	Number in size interval (ΔN)	Volume diff. ΔV_A [$=(\pi/6)\Delta N d_v^3$]	Cum. volume $\Sigma \Delta V_A$	Cum. weight %
1.43	0	0	0	0	0	0.0
1.51	4 213	4 217	4 217	7 602	7 602	0.0
1.60	7 548	7 560	3 343	7 170	14 772	0.0
1.69	10 094	10 116	2 556	6 459	21 231	0.0
1.79	12 232	12 264	2 148	6 451	27 682	0.1
1.89	14 039	14 081	1 817	6 424	34 106	0.1
1.99	15 702	15 755	1 674	6 906	41 012	0.1
2.11	17 257	17 321	1 566	7 703	48 714	0.1
2.23	18 768	18 844	1 523	8 841	57 556	0.1
2.35	20 301	20 389	1 546	10 504	68 060	0.1
2.49	21 838	21 940	1 551	12 537	80 596	0.1
2.63	23 502	23 620	1 680	16 004	96 600	0.2
2.78	25 482	25 621	2 001	22 508	119 108	0.2
2.94	27 964	28 132	2 510	33 403	152 511	0.3
3.11	31 083	31 290	3 158	49 746	202 257	0.4
3.29	35 523	35 794	4 503	83 971	286 228	0.5
3.47	41 352	41 719	5 925	129 623	415 851	0.8
3.67	49 173	49 691	7 973	206 351	622 202	1.2
3.88	59 005	59 751	10 060	307 675	929 877	1.7
4.10	70 330	71 390	11 639	420 016	1 349 893	2.5
4.34	82 772	84 241	12 850	550 027	1 899 920	3.5
4.59	95 760	97 726	13 485	682 796	2 582 716	4.8
4.85	108 856	111 396	13 670	816 596	3 399 312	6.3
5.13	120 217	123 315	11 919	842 535	4 241 846	7.9
5.42	132 237	135 986	12 671	1 056 310	5 298 156	9.8
5.73	143 507	147 922	11 936	1 175 788	6 473 944	12.0
6.05	153 710	158 775	10 853	1 258 400	7 732 344	14.3
6.40	163 316	169 034	10 259	1 408 113	9 140 457	16.9
6.76	171 748	178 071	9 038	1 461 825	10 602 283	19.6
7.15	179 493	186 400	8 328	1 593 922	12 196 205	22.6
7.56	186 223	193 657	7 258	1 641 949	13 838 154	25.6
7.99	192 179	200 096	6 439	1 719 761	15 557 914	28.8
8.44	197 735	206 117	6 020	1 895 190	17 453 104	32.3
8.93	202 706	211 515	5 398	2 012 634	19 465 739	36.1
9.44	207 150	216 349	4 834	2 129 430	21 595 168	40.0
9.97	211 055	220 604	4 255	2 207 973	23 803 141	44.1
10.54	214 570	224 440	3 836	2 351 624	26 154 765	48.4
11.14	217 655	227 811	3 371	2 440 024	28 594 789	53.0
11.78	220 397	230 810	2 999	2 567 338	31 162 127	57.7
12.45	222 775	233 414	2 604	2 631 086	33 793 213	62.6
13.16	224 957	235 806	2 391	2 853 811	36 647 023	67.9

Table 9.2 (cont.) Mass balance calculation for the Coulter Multisizer

Size (μm) (d_v)	Cum. number (n)	Corrected cum. number (N)	Number in size interval (ΔN)	Volume diff. ΔV_A [= $(\pi/6)\Delta N d_v^3$]	Cum. volume $\Sigma \Delta V_A$	Cum. weight %
13.91	226 815	237 844	2 038	2 871 924	39 518 947	73.2
14.70	228 266	239 436	1 593	2 648 781	42 167 728	78.1
15.54	229 379	240 658	1 222	2 401 553	44 569 281	82.6
16.43	230 275	241 643	984	2 285 783	46 855 064	86.8
17.36	230 896	242 325	682	1 869 320	48 724 384	90.3
18.35	231 354	242 828	503	1 628 576	50 352 959	93.3
19.40	231 610	243 110	281	1 075 821	51 428 780	95.3
20.50	231 786	243 303	193	872 782	52 301 561	96.9
21.67	231 885	243 412	109	579 918	52 881 479	98.0
22.91	231 945	243 478	66	415 331	53 296 811	98.7
24.22	231 982	243 519	41	302 622	53 599 433	99.3
25.60	231 993	243 531	12	106 241	53 705 674	99.5
27.06	232 003	243 542	11	114 068	53 819 742	99.7
28.60	232 006	243 545	3	40 402	53 860 144	99.8
30.23	232 009	243 548	3	47 711	53 907 855	99.9
31.95	232 012	243 552	3	56 327	53 964 182	100.0
33.77	232 013	243 553	1	22 171	53 986 353	100.0
35.70	232 013	243 553	0	0	53 986 353	100.0
37.74	232 013	243 553	0	0	53 986 353	100.0

From Table 9.2, the measured volume analyzed in the suspension metered by the manometer is:

$$v_A = 53,986,353 \mu\text{m}^3$$

The volume calculated from the amount of powder used is:

$$v_T = \left(\frac{0.1219}{100} \right) \left(\frac{1}{150} \right) \left(\frac{2.00}{2.619} \right) = 62,059,310 \mu\text{m}^3$$

The uncertainty in this value is given by:

$$\frac{\Delta v_M}{v_M} = \frac{\Delta m}{m} + \frac{\Delta V}{V} + \sum \frac{\Delta v}{v} + \frac{\Delta \rho}{\rho}$$

$$\frac{\Delta v_M}{v_M} = \frac{0.0002}{0.1098} + \frac{0.2}{100} + \left(\frac{0.01}{1.0} + \frac{2}{150} + \frac{0.02}{2.00} \right) + \frac{0.0065}{2.619}$$

$$\frac{\Delta v_M}{v_M} = 0.040 = 4.0\%$$

The difference between the metered volume and the total volume in the metered sample is 15%. This difference has been shown to be due to count loss with the Coulter Multisizer [27]. A similar run using the Coulter TAII gives a 100% mass balance.

The 2.00 cm³ volume is certified as being accurate to $\pm 2\%$. If some other manometer volume were used it should be calibrated against the certified one. (It would be ideal if the 2.00 cm³ volume was also checked.)

The mass percentage analyzed by the counter is:

$$P = 100 \left(\frac{m_A}{m_T} \right) \quad (9.20)$$

9.3 Fiber length analysis

This is of fundamental importance in the pulp and paper industry which uses a light obscuration method – the Kajaani FS-200. This instrument is also used in the chemical industry for measuring the length of man-made fibers.

The Advanced Fiber Information System (AFIS) [29] contains a mechanism for opening a hand fed ribbon of fibers so that individual fibers can be presented aerodynamically to an electro-optical system for measuring fiber length. Length measurements for 10,000 individual fibers can be obtained in 5 min.

The assumption made when the instrument was first developed was that the variability in speed of the fibers, as they passed through the sensor, was small and could be assumed constant [30]. Analysis showed that this assumption was incorrect and a later instrument included a sensor to measure fiber speed [31]. Since the fibers are aligned with flow, the pulse length is a measure of fiber length and the pulse height is a measure of fiber width. The results showed excellent agreement with Suter-Webb measurements. The AFIS is widely used for cotton fiber measurement in the dry state.

Workplace exposure to asbestos fibers is usually assessed by personal sampling on a membrane filter which is subsequently examined using phase contrast or electron microscopy. Lilienfeld *et al.* [32] described an instrument that monitors asbestos fiber concentration in sampled air by laser light scattering from fibers oscillating in phase with an electric field and this instrument has also been used to monitor silicon carbide dust [33]. Light scattering has also been used to detect fibers in air down to 1 μm [34] and magnetically aligned fibers on a membrane filter [35]. Rood [36] aligned fibers using a simplified Prodi instrument, then passed them through a corona discharge so that a downstream precipitator deposits the fibers on to a removable glass slide where they retain their alignment. He then used the difference in

light scattered parallel to and perpendicular to flow in order to determine fiber length distribution.

The Coulter principle has been applied to fiber length determination [37,38]. This approach is interesting in that the pulse duration is a measure of fiber length and pulse height is a measure of fiber volume, hence an estimate can be made of fiber thickness. A modification of this procedure involved a flow collar upstream of the sensing zone to provide alignment of the fibers with the aperture axis [39-41]. Elzone used a long flow tube upstream of the sensing zone to provide laminar flow and fiber alignment [42]. This flow is caused to join a clear liquid sheath which centralizes the fibers in the aperture.

9.4 Optical particle counters

Optical particle counters have been used for many years in the stream scanning mode to determine particulate contamination levels in liquids. Particle size may be determined in one of the following ways:

- by the amount of light cut off by a particle as it passes through a sensitive zone in a light beam;
- by collecting and measuring the light it scatters over a specific solid angle in the forward direction;
- by collecting and measuring the light it scatters over a specific solid angle at an angle to the incident beam (usually a right angle);
- by measuring the phase shift as a particle passes through the beam;
- by measuring the 'time of flight' between two laser beams.

Optical particle counters are available which range from simple to highly sophisticated, together with considerable design differences to cater for the wide range of applications. Instrument response depends on particle size, particle shape, particle orientation, the wavelength of light, liquid flow rate and relative refractive index between the particle and its surroundings. In addition, the amount of light collected is determined by the geometry of the collecting system. The efficiency of the photodetector will further determine the degree to which the light pulses can be converted to electronic signals that can be detected [43]. Differentiation between particles of similar sizes is hampered by pick-up of stray light which causes noise. Stray light is light which is reflected from internal surfaces of the sensor which falls on the detector. This phenomenon is less of a problem with properly designed off-axis detectors than with coaxial systems.

The relationship between particle size and scattered light intensity at any angle may be obtained for spheres and simple shapes using Mie theory. The scattered intensity does not necessarily increase monotonically with particle size at all angles. To maintain a monotonic increase in scattering cross-section with size, small angles or small

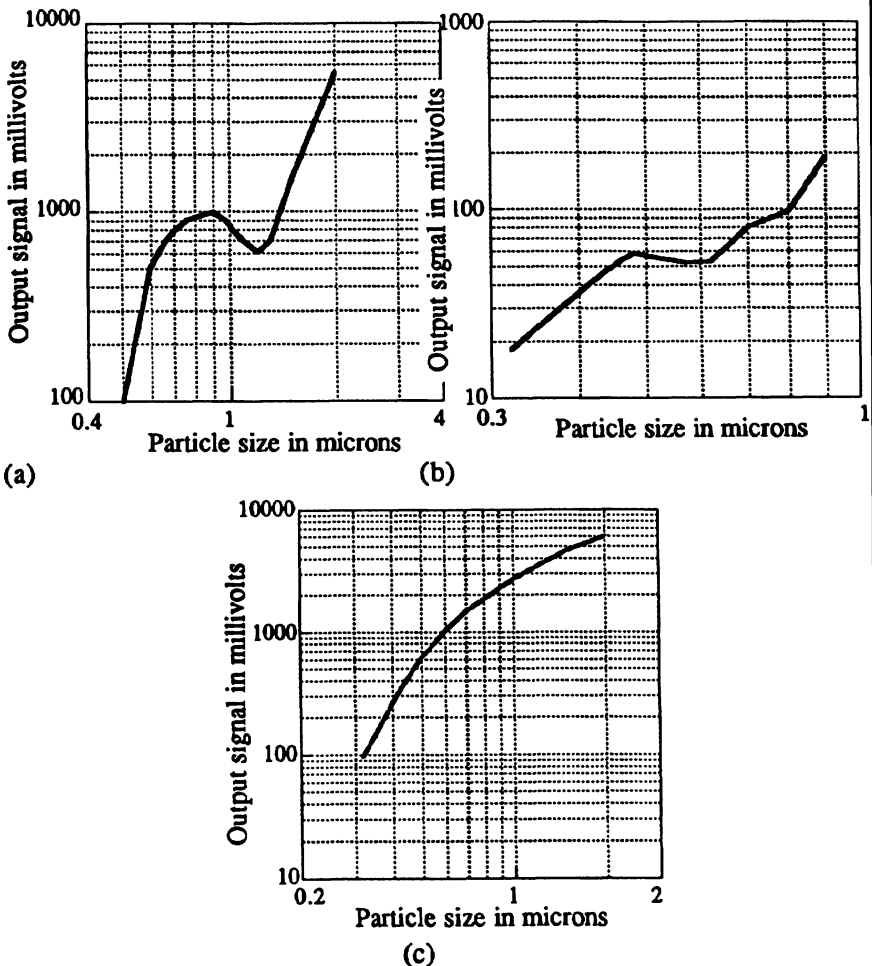


Fig. 9.8 Calibration curves for light scattering instruments after Chandler [43]. (a) Simple coaxial system, (b) simple off axis system, (c) Climet elliptical mirror system.

differences in refractive index should be used. The main disadvantage of low angle scattering is that the background scatter from the cell walls is higher than with 90° scatter and the main advantage is improved size resolution. A further advantage of low angle configurations is that the intensity is less dependent on relative refractive index than 90° scatter. Large collection angles damp out fluctuations which occur with a single

well defined angle. These instruments cover the size range 0.05 µm to 30 µm with a dynamic range varying from 20:1 at the small end to 40:1 for particles bigger than about half a micron.

Simple collecting systems generate a non-monotonic response in the sub-micron size range. Figure 9.8a shows a calibration curve for a co-axial collection system which illustrates this feature. Between the sizes 0.8 µm to 1.8 µm the calibration curve changes direction so that the same output signal occurs for as many as three different particle sizes. For this reason this type of system is limited to instruments with common size thresholds at 0.3 µm, 0.5 µm and 5 µm. Any size threshold between 0.8 µm and 1.8 µm is ambiguous. Figure 9.8b shows the calibration curve for an off-axis collection system where the output signal for a 0.49 µm particle is exactly the same as that for a 0.61 µm particle. Figure 9.8c shows the calibration curve for the Climet elliptical mirror system. Its most distinct advantage over other systems is its high degree of monotonicity. Its disadvantage is that a large detector is required to collect light properly from particles at the extreme edge of the view volume and this drives up the price.

Older systems tended to use white light illumination, later ones use gas lasers or solid state laser diodes. Laser diodes are smaller and more robust than gas lasers, resulting in smaller instruments. Their spatial properties have increased the sensitivity of particle sensors by a factor of two enabling dynamic size ranges of 700:1. Fast analog to digital conversion now counts every particle in semi-concentrated suspensions and provides 64 000 channels of particle size information [44]. The wavelength of white light ranges from 400 nm to 800 nm, helium-neon is 633 nm and solid state 780 nm. This variation results in differences in measured size when particles with a difference in refractive index from the calibration material are analyzed. Although the instruments are usually factory calibrated it is hardly surprising that instrument to instrument variability is high.

Volumetric sensors examine the entire stream of liquid passing through the flow cell at relatively low flowrates. *In situ* sensors focus the light on only a small portion. Focusing intensifies the illumination resulting in lower detection limits. Volumetric sensors can detect particles as small as 0.2 µm while *in-situ* sensors can get down to 0.05 µm. The sensitivity of volumetric sensors is limited since the amount of scattered light varies as the sixth power of particle size, hence a 0.1 µm particle scatters 1/64 of the light scattered by a 0.2 µm particle. Light scattered from the interface between the sensor wall and the fluid also reaches the detector to give a noisy base line.

With the light blockage technique (Figure 9.9), a narrow area of uniform illumination is established across the flow channel of the sensor so that the passage of a small particle causes an amount of light, proportional to the cross-sectional area of the particle, to be cut off. For a larger particle, having a diameter comparable with the width of

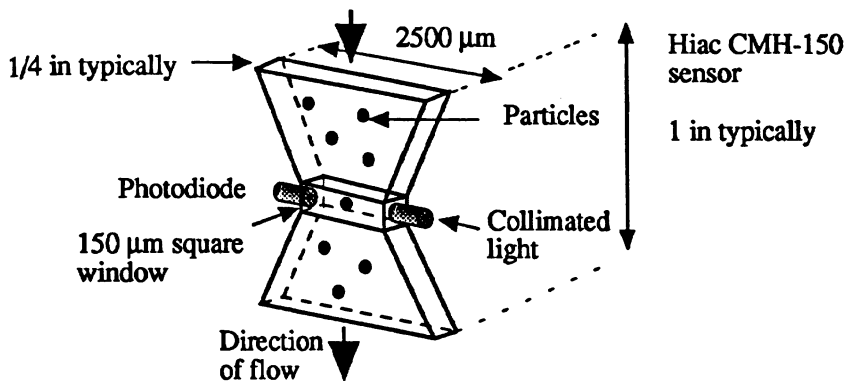


Fig. 9.9 Light blocking principle (Hiac/Royco).

the illuminated zone, the dependence of pulse height on particle diameter is linear. In both cases the pulse height increases monotonically with particle diameter. Light blockage sensors are available for a variety of size ranges from 1 µm to 3 mm with a dynamic range for each sensor of 100:1 or less. This is the method of choice for sizing above a micron or so since the instrument response is less affected by variations in relative refractive index and particle morphology, whereas light scattering provides the higher sensitivity required for smaller particles.

Basic commercial counters usually pick up the light scattered in the forward direction and great care is taken to damp out the direct beam; greater sensitivity is obtained by incorporating a light collecting device such as an elliptical mirror. These instruments find a ready market in measuring low level contamination in pharmaceutical suspensions such as intravenous liquids, for contamination measurements in industrial liquids, and are being increasingly used for on-line process monitoring. Often, two versions of an instrument are manufactured, one for measuring particles in suspension and the other for measuring particles in air. Knollenberg and Veal [45] discuss operation, design and performance of optical counters in general and a review of extinction optical particle counters has been presented by Sommer [46 (cit. 47)].

Light obscuration particle counters determine particle size from the projected areas of particles, giving information on only two dimensions. Umhauer [48,49] determines three projected areas of each particle by measuring in three mutually orthogonal directions. An application of this system to agglomerates of two to four spheres has been reported [50]. Hydrodynamic focusing is found to reduce errors when measuring the size of particles in light scattering and phase Doppler instruments as well as electrical sensing zone instruments [51].

9.4.1 Aerometrics Eclipse particle size analyzer

The Eclipse is a white light blockage system designed for both liquid and gas systems. The probe head includes a light source, flow cell and photodiode. The processor can accommodate two heads covering the size ranges: 2–100 µm, 20–1000 µm and 50–2500 µm. The flow cells are compatible with most liquids and can be specially adapted for high pressure environments.

9.4.2 Hiac/Royco

Hiac/Royco manufacture two counters which are compatible with a wide range of samplers. The 4100 series microprocessor based counter produces particle count data simultaneously in six channels; this is expanded to thirty two channels with the 4300 series counter. Detection limits range from 0.25 to 25 µm for air samplers and 0.5 to 9000 µm for liquid sensors. A range of sensors are available for liquid systems, each one covering a 50:1 size range.

The particles to be counted are suspended in a liquid having a refractive index different from the particles. The particles are then forced through a sensor containing a small rectangular cell with windows on opposite sides. A collimated beam of light from a high intensity, quartz halogen lamp is directed through the stream of liquid on to a sensor. The particles pass through the sensor in random orientation and produce pulses proportional to their average projected area. These pulses are scaled and counted. The sub-micron size range is covered using near-forward laser light scattering. The shear forces in the sensing zone are small enough for the instrument to be used for sizing flocs [52].

The 4100 series are for liquid-borne systems. Systems 4101 and 4102 are for airborne monitoring using models 1100 and 1200 airborne sensors respectively.

The Hiac/Royco Optisizer [53] is a single particle counting system which operates with composite scattering/extinction sensors, a 64 000 channel high speed digital counter, an automatic sample dilution system and a software package. The software controls the counter/sampler and acquires, archives and reduces the data. Particles smaller than 3 µm are measured by near-forward scattering and those above 3 µm by light extinction. Combining the two optical sizing techniques into a single sensor allows sizing over a dynamic range exceeding 700:1. The model HPS-200 uses a He-Ne laser and covers the size range 0.2 µm to 200 µm; the model HPS-350 uses a laser diode and covers the size range 0.7 µm to 350 µm.

Hiac/Royco also offer the Dynacount laser diode sensors for liquids with a dynamic range of greater than 150:1 at number concentration levels up to 12000 mL⁻¹. HRLD-150 covers the size range of 1 to 150 µm at particle concentrations up to 12,000 mL⁻¹, and flow rates from

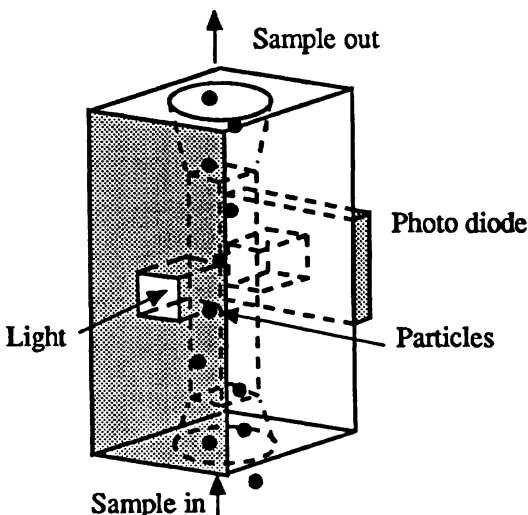


Fig. 9.10 The Kratel liquid-borne sensing cell.

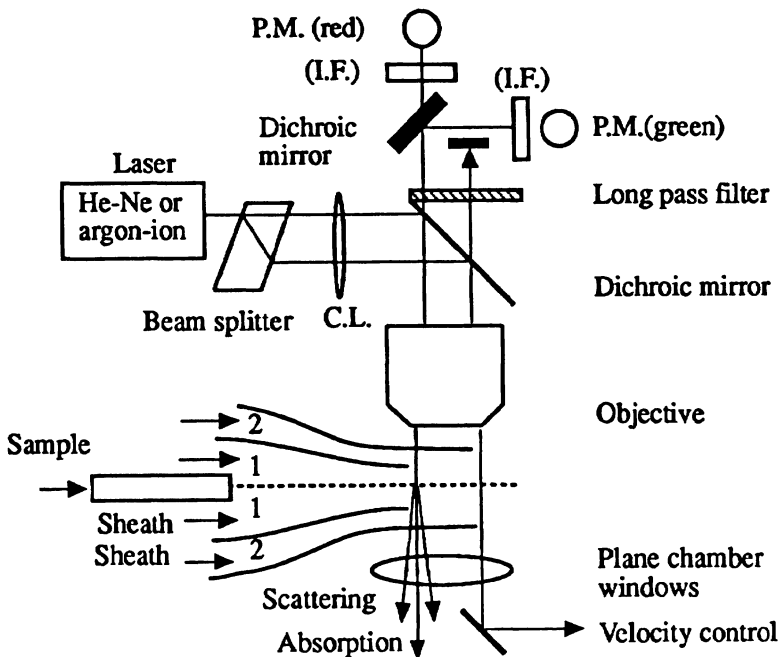


Fig. 9.11 The Kratel Partograph.

10 to 75 mL min⁻¹. HRLD-400 covers the size range of 2 to 40 µm at particle concentrations up to 8,000 mL⁻¹ and flow rates between 10 and 200 mL min⁻¹.

The Hiac/Royco Models 8000 and 8000S eight channel particle counters can control two to four sensors. In combination with ancillary samplers and sensors they can be used, for example, for small or large volume batch systems and also for submicron batch systems.

9.4.3 Kratel Partascope

The basic Partascope (Figure 9.10) operates using a light blocking detection system. Sensors are available, each one covering a 50:1 size range, to give an overall size range of 1 to 8000 µm. Data are presented in 4, 8, 16 or 32 channels using a multichannel analyzer module and this can be expanded to 64 channels using a computer. As with Hiac/Royco, a range of samplers are available. A sub-micron sensor is also available for the size range of 0.4 to 20 µm using near-forward laser light scattering.

9.4.4 Kratel Partograph

The Partograph (Figure 9.11) measures size, extinction, light scattering and fluorescence of particles. Hydrodynamic focusing is used to allow single particle centering in the beam. The optical design allows the simultaneous measurement of the particle size by forward and right angle light scattering as well as an extinction measurement. Particle size is also determined by time of flight from pulse width. Size range covered is 0.5 µm to 200 µm at concentrations up to 10⁷ particles mL⁻¹ at flow rates of 10-50 µL min⁻¹.

9.4.5 Climet

Climet manufacture a range of instruments for liquid-borne and air-borne particle counting. The CI 200 series collect forward scattered light at angles, relative to the incident radiation, from 15° to 105°. The sample volume is located at the primary focal point of an elliptical mirror and the scattered light is picked up by a photomultiplier located at the secondary focal point (Figure 9.12).

The CI 220 Liquid Particle Analyzer counts particles drawn from a syringe. Four size ranges are available via panel switches: 2 to 20, 5 to 50, 8 to 80 and 20 to 200 µm.

The CI 221 On-Line Monitor is designed for high purity liquids for counting particles in the size range 2 to 200 µm for flow rates of 120 to 750 mL min⁻¹. Particle concentrations up to 100 particles mL⁻¹ can be handled directly. Higher concentrations are sampled at proportionately lower flow rates down to 120 mL min⁻¹.

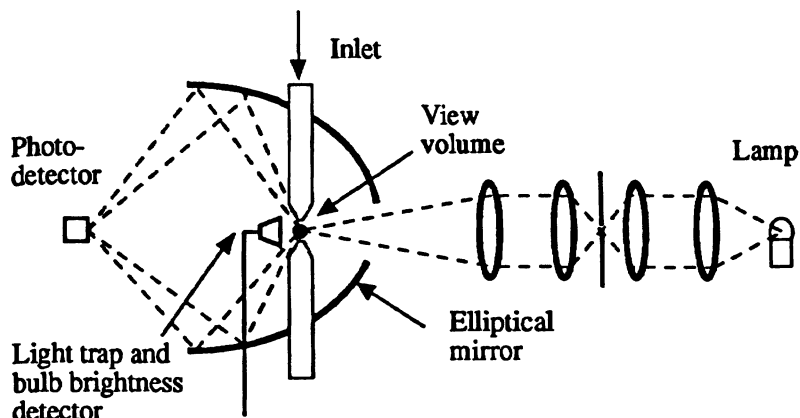


Fig. 9.12 The Climet elliptical mirror optical system.

The CI 1000 operates using light obscuration with white light and a fiber optics bundle for light collimation. Sensors are available in a variety of sizes from 1 to 1000 μm , each one encompassing a 50:1 dynamic range. The sampler accommodates sample sizes from 0.1 to 500 mL. The electronic module contains the electronic components for particle counting, data display and printing. Data are stored in 3000 size ranges simultaneously and can be recovered in six size ranges for display and printing. Other size ranges can be recovered by resetting the size thresholds.

Table 9.3 Particle Measuring Systems' instruments

The Micro-Laser Particle Spectrometer Data System will support simultaneous operation of any two of the following PMS liquid systems:

- The Laser Spectrometer Probe Electronics System
- The Liquid Point of Use System (CLPOU)
- The Liquid Batch Sampling System (LBS)
- The Corrosive Liquid Sampling System (CLS-700)
- The Automatic Parenteral Sampling System (APS)
- The Hydraulic Fluid Sampling System (HFS)
- The Laser Hydraulic Fluid Sampling System (LHFS)
- The Facility Monitoring System (FMS)

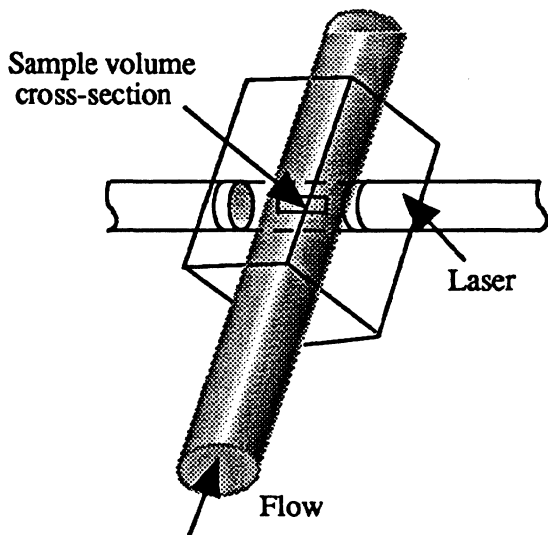


Fig. 9.13 Particle Measuring Systems' liquid-borne sensor cell.

9.4.6 Particle Measuring Systems

Particle Measuring Systems (PMS) manufacture a range of laser based particle sizing instruments. These are based on volumetric or *in situ* sampling. The former perform particle sizing on the whole of the fluid passing through them and have relatively low flow rates. Sizing may be accomplished using either light obscuration or light scattering. Volumetric sampling may be continuous or batch; batch sampling is accomplished using a liquid sampler to deliver a sample from a vial, bottle or tank to the sensor; continuous sampling is accomplished by measuring a side-stream flow from the primary line. *In situ* sensors accommodate a wide range of flow rates and perform the measurements directly in-line with the main flow of fluid (Figure 9.13). Particle sizing is accomplished using light scattered from particles within an optically defined area. The ratio between this area and the flow cross-sectional area yields the fraction sampled. Particles are classified into either 8 or 16 size intervals. Table 9.3 lists the PMS instruments.

The CLS-700 was developed for batch sampling process chemicals at temperatures up to 150 °C. Up to 15 sizing thresholds are available from 0.2 to 5 µm.

Simultaneous multipoint measurements at 0.3 µm, 0.4 µm, or 0.5 µm can be made. Right angle scattering instruments are more size sensitive to particle size than forward scattering instruments but also

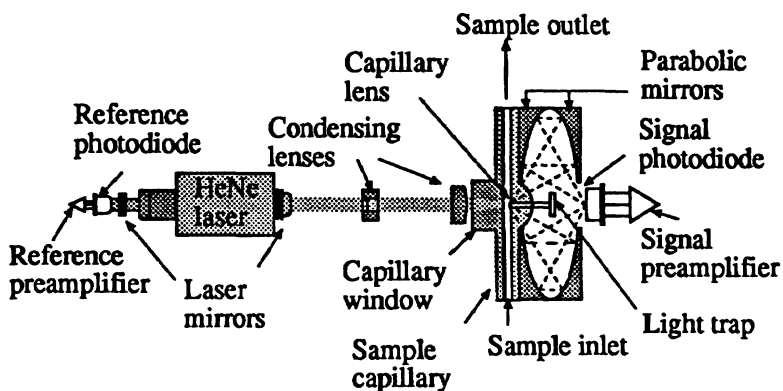


Fig. 9.14 Particle Measuring Systems' Liquid Volumetric Probe, designed for continuous monitoring of process waters, product liquids and semiconductor chemicals.

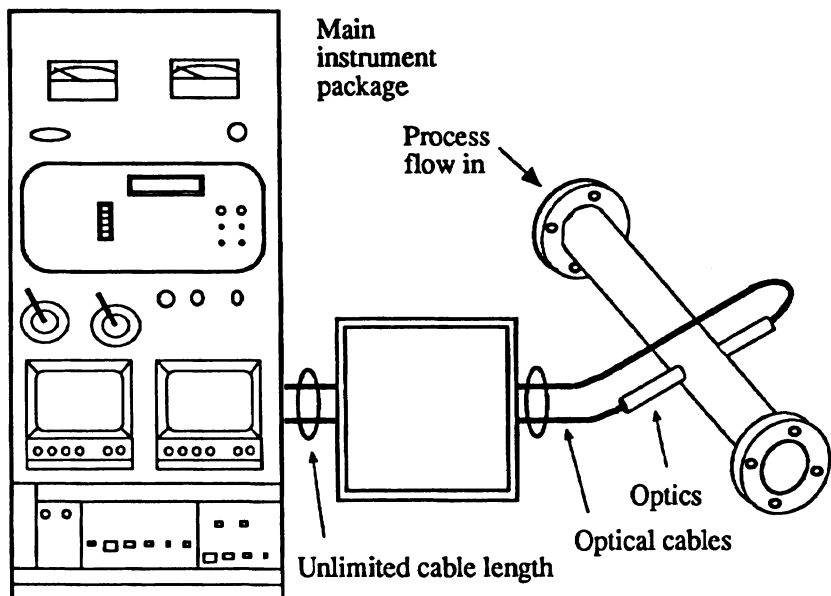


Fig. 9.15 The Flowvision Analyzer.

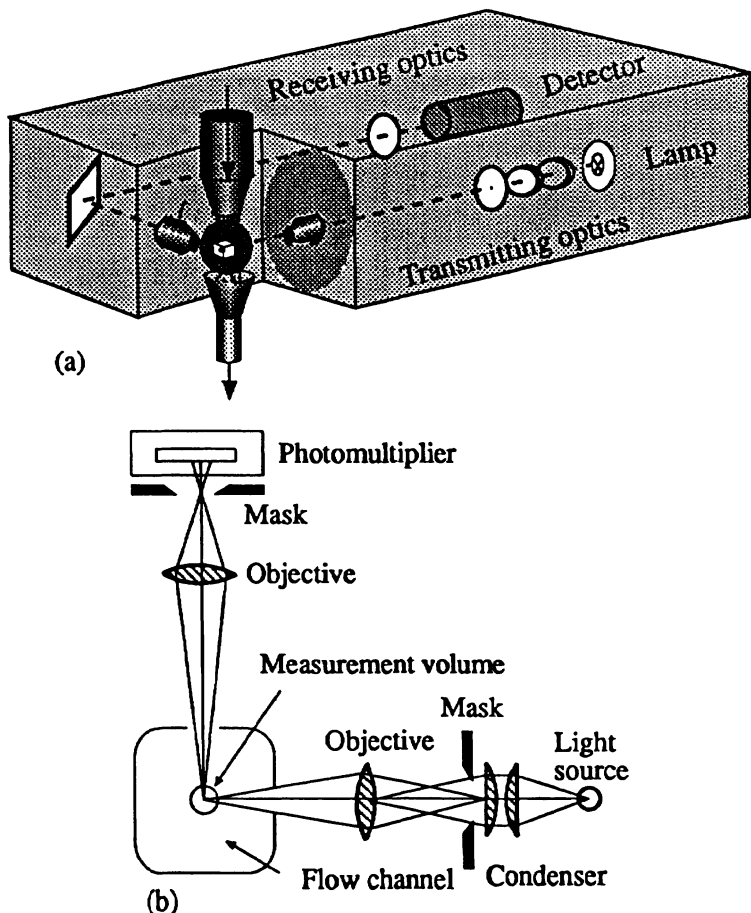


Fig. 9.16 (a) Block diagram of the Polytec HC Particle Counter (b) optics of Polytec HC white light counter.

have greater sensitivity to refractive index. For this reason most liquid counters are designed to pick up light scattered in the forward direction. Sensitivity is greatly improved with the use of parabolic mirrors (Figure 9.14).

9.4.7 Flowvision

The Flowvision Analyzer uses fiber optics to channel white light through a flowing liquid. As particles pass through the light beam they generate images which are converted to video and then analyzed using a high speed digital computer (Figure 9.15). The computer first

enhances the image and then classifies according to size. Particles are detected in the size range 2 to 1000 μm ; the optimum range for sizing is 25 to 600 μm .

9.4.8 Polytec HC (high concentration) optical counter

The Polytec HC series is for counting and size analysis of particles, droplets and bubbles in gases or liquids in the size range 0.4 to 300 μm . The HC system uses a white light source and a relatively large aperture which smoothes out irregularities in the intensity of the transmitted beam. The near linear relationship between intensity and particle size provides sufficient resolution to allow classification of the particles into 128 size channels in a size range of 30:1 at number concentrations up to 10^5 mL^{-1} and at a velocity of 0.1 m s^{-1} to 10 m s^{-1} . A correction can be applied for coincidence errors.

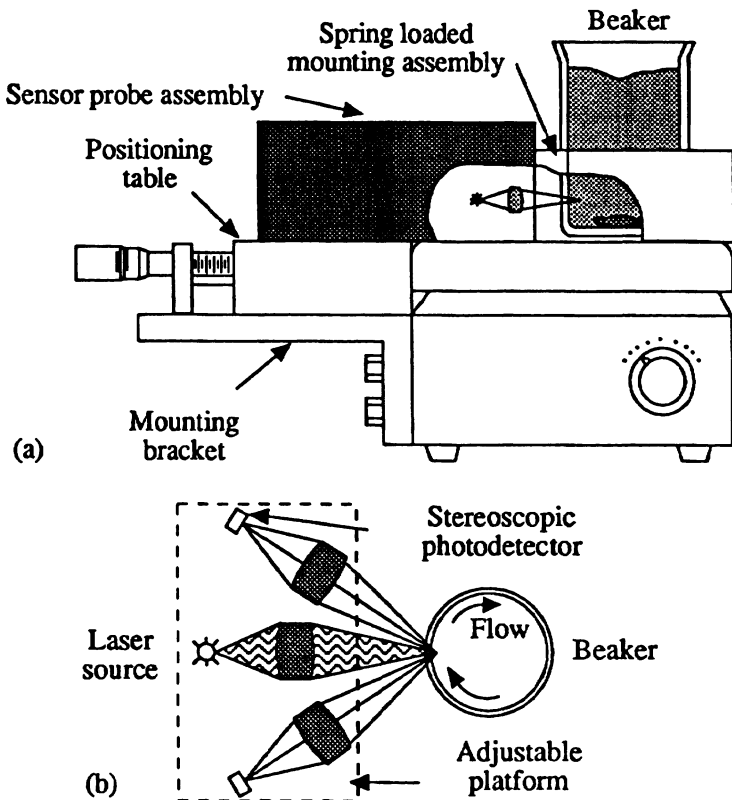


Fig. 9.17(a) Sampling configuration using standard glass beakers on a magnetic stirrer plate (b) The Lasentec Lab-Tec 100 measuring geometry.

The optical design of the HC system (Figure 9.16) defines a small rectangular measurement volume, at right angles to the flow direction, by imaging rectangular apertures with the transmitting and receiving optics. A particle passing through the illuminated measurement volume scatters light which is focused on to a photodetector. Each optical signal is converted into an electrical pulse which is processed electronically.

9.4.9 Lasentec

Lasentec's Lab-Tec 100 uses a scanning infrared laser beam to measure the particle size distribution of particles in suspension. The beam is highly focused and illuminates individual particles in its path (Figure 9.17a). The back-scattered light pulses are picked up by a non-scanning stereoscopic detection system (Figure 9.17b). The size of each particle is determined by measuring the time that the particle is in the beam hence the size is recorded as a random chord length. The laser diode and detectors are stationary while the lens, which focuses the light beam, is vibrated normal to the laser detector plane. The vibrating action causes the beam spot (focal point) to be scanned up and down normal to the direction of fluid flow. The beam amplitude is 3 mm and measurements are carried out in the central 1.5 mm where the velocity is maintained constant; since the frequency is 400 Hz the scan rate is 1.2 m s^{-1} . The technology is available for in-line and laboratory use and, since the focal point is only about a millimeter in front of the window, can operate with very high (40% by volume) concentration slurries [54].

The on-line version [55], the Partec 200 (Figure 9.18), gives a reasonably constant response over a range of 5–30% by volume. The Partec 200 gives much coarser data than the Lab-Tec 100, together with a lower count at similar concentrations. This can be attributed to the reflected light being collected by the same optics that are used to focus the light i.e. both the source and detector move in unison. Thus a much smaller volume around the focal point is investigated on reflection. The beam moves in a circular path compared to the vertical vibrations of the laboratory system and different hardware is used to determine the pulses [56]. The size range of 1.9 to 1000 μm is covered in a $\sqrt{1.5}$ progression of sizes.

The Labtec 1000 is the current laboratory instrument which covers the size range from 0.7 to 250 μm in 28 size channels. The data are generated as 'scanned counts', an empirical frequency distribution created from classification of chords from randomly oriented particles. Software can convert these chords to a spherical equivalent distribution on the assumption that the chords were generated from an assembly of spherical particles: this software contains a filter system to reject improbable data which would tend to skew the distribution to a coarser size. A discrimination loop sorts impulse for short rise times; only

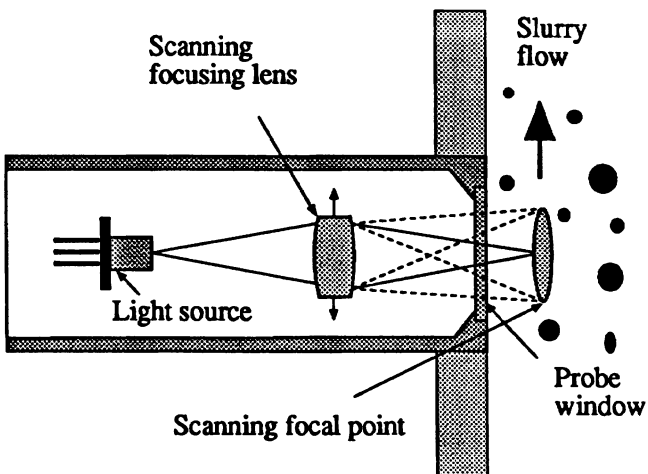


Fig. 9.18 Optical arrangement of the Lasentec Par-Tec 200/250.

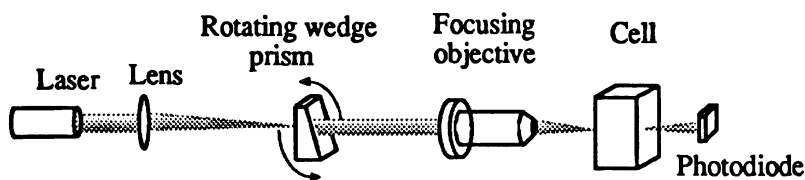


Fig. 9.19 The laser optic measuring system of the Galai Particle Analyzer.

pulses from particles that pass directly through the focal spot have short rise times and will be accepted. Other conversions are also available, including calibration against known standards. Monnier *et al.* investigated the influence of variables such as temperature, stirrer speed, focal point, concentration and the position of the focal point, on the measured size distribution and concluded that the most important, especially for small sizes, was the focal point position. They concluded that, due to this, it was not suitable for precise analyses [57].

9.4.10 Galai CIS

The Galai CIS-1 Model 2010 (Figure 9.19) scans the sample with a shaped and focused laser beam using a rotating wedge prism [58]. The time spent by the scanning beam on a particle is interpreted as particle size. A CCD TV microscope is incorporated into the basic unit, permitting the operator to observe the sample whilst it is being

measured. The images can be enhanced, processed and analyzed to obtain an independent measure of size distribution, particle shape and state of dispersion. The instrument operates in the size ranges 0.7 to 150, 2 to 300, 5 to 600 and 12 to 1200 μm . Interchangeable sample cells allow a wide variety of sample presentations; these consist of a spectrophotometer cell, a microscope slide, a liquid flow-through cell, an aerosol flow through cell and a thermo-electric cooled flow-through cell.

The Galai CIS-100 combines particle size analysis with dynamic shape characterization, covering the size range from 0.5 to 3600 μm in 300 discrete size intervals by changing a single lens. The Galai Video Microscope uses a synchronized strobe light and a black and white CCD camera to capture images at 1 or 30 times per second. The included software automatically analyses up to 30 000 particles with up to 1800 non-overlapping particles per frame. The measurement cell modules comprise systems for dry powders, aerosols, fibers in laminar flow and cells for particles in regular and opaque liquids.

The Galai Dynamic Shape Analyzer DSA-10 is a complete shape characterization system for particles in motion. All particles are classified by maximum and minimum diameters, area and perimeter, aspect ratio, shape factor and more. A video microscope camera synchronized with a strobe light takes still pictures continuously of particles in dynamic flow, generating shape information on tens of thousands of particles, in the 1 to 6,000 μm range in minutes.

The Galai CIS-1000 is an on-line particle size analyzer. A bypass from the process line feeds the sample into the sensor unit where it is sized and either drained off or fed back to the line. Full compatibility with the laboratory instrument is maintained since it uses the identical combination of laser based time of transition particle sizing using the 1001 sensor and dynamic shape analysis using the 1002 sensor. The size range covered is from 2 μm to 3600 μm with measurement of size, area, volume, shape, concentration and estimated surface area with a cycling time of 300 s.

9.4.11 Spectrex Prototron

The Spectrex Prototron uses near-forward scattering from a revolving laser beam (900 rpm.) for particle sizing and counting of *in-situ* and flowing liquids [59]. A He-Ne laser beam is focused to a small, well-defined volume (10 mL) within the liquid. Total particle count within the range 0.5 to 100 μm can be determined in less than a minute. Readout is in 1 μm steps from 0.5 to 17 μm and in five channel steps from 17 to 100 μm . Distribution may be presented on a number or a volume basis.

The SPC-410 combines the Prototron with an Apple computer for greater flexibility. A small vial attachment permits inspection of vials

and ampoules down to 5 mL size at concentrations up to 1000 particles mL⁻¹.

The Spectrex SPC-510 (Figure 9.20) uses both diffuse vertical illumination for visual identification of large particles and a scanning laser for detection of small particles. The instrument is widely used for quantitative particle counts in bottles [60] including *in situ* examination of bottled beer [61].

The Spectrex ILI-1000 Particle Counter combines the Prototron with a Particle Profile Attachment (multichannel analyzer). The instrument has been used [62] for examining volcanic ash. AC Fine Dust was used for calibration in eight 5 µm steps, which indicated that accurate data was obtained for sizes above 2 µm. It has also been shown to correlate well with the more tedious filtration and counting method for large volume parenteral liquids [63]. Although semi-transparent containers or liquids reduce the amount of transmitted light flux, the instrument gives valid data for particulates in oil [64].

9.4.12 Spectrex PCT-1 laser particle counter

The PCT-1 is a compact liquid particle counter designed specifically to monitor real-time particle counts in ultra-pure water. The water to be monitored is fed to a rectangular cross-section pyrex glass cell (Figure 9.21) and illuminated by a He-Ne laser at right angles to the direction of liquid flow. When a particle passes through the sensing zone, a pulse of scattered light is emitted and detected by a photomultiplier positioned at right angles to both the laser beam and liquid flow direction. Two channels of information are generated; total count coarser than 0.11 µm and counts above 0.2, 0.3, 0.5 or 0.7 µm as set in a four position switch. Measuring time is selectable from 1 second to 1 h.

9.4.13 Procedyne

The Procedyne PA-110 [65] uses a high intensity focused laser beam to scan a flowing suspension via an oscillating mirror, thus scanning the suspension horizontally and vertically (Figure 9.22). As particles interrupt the beam a pulse is generated at a photodiode, the length of which is related to particle size. The instrument is designed for the on-line analysis of process slurries at a sampling rate of 250 cm³ s⁻¹ with a maximum mass concentration of 2% and a particle size range of 3 to 2000 µm. There are five memory registers, four calibrated for particle size and the fifth for total particle count. Hinde [66] reported on the use of the instrument for controlling mill circuits with disappointing results.

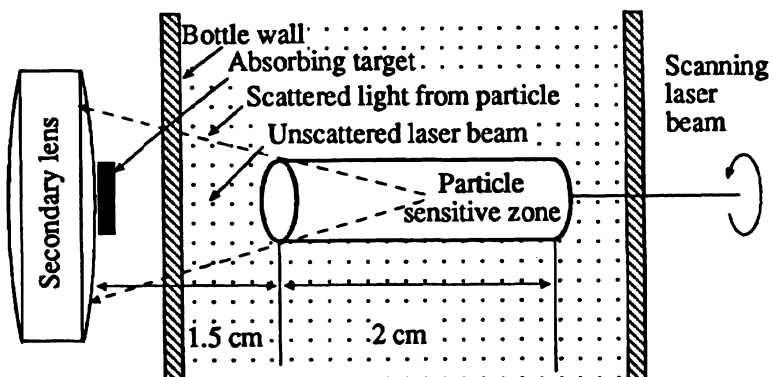
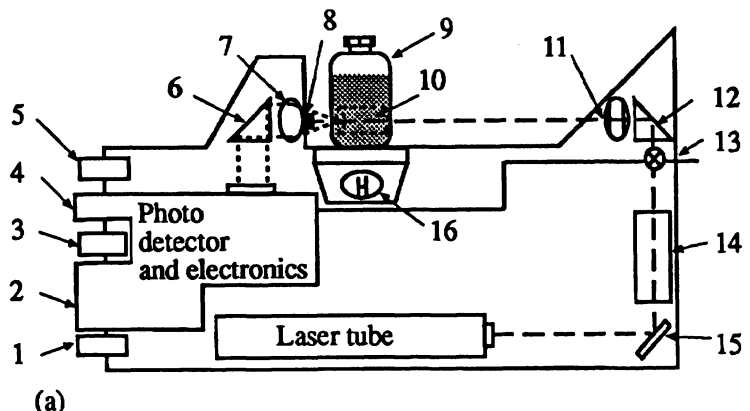


Fig. 9.20 The Spectrex SPC-510, (a) schematic of particle counter, (b) laser beam optics. 1 on-off switch, 2 digital readout, 3 count button, 4 threshold setting dial, 5 illuminate button, 6 prism, 7 secondary lens, 8 target, 9 bottle, 10 sensitive zone, 11 scanning laser beam, 12 prism, 13 beam splitter and beam strength monitor, 14 scanner, 15 mirror, 16 lamp.

9.4.14 Kane May

Kane May manufacture a series of instruments based on the light blocking principle. These consist of an on-line sampler, a small volume sampler and a large volume sampler. Each sensor operates over a size range of 75:1 using a variety of sensors and data may be processed into up to 10 size channels.

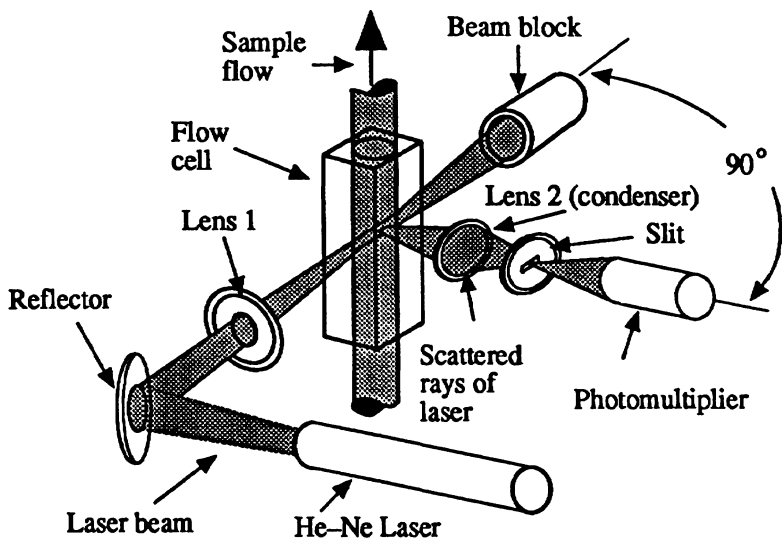


Fig. 9.21 Spectrex PCT-1, principle of measurement.

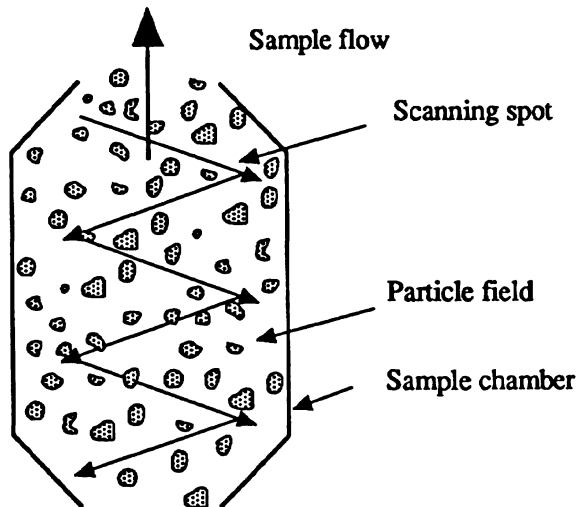


Fig. 9.22 Sample chamber of the Procedyne Analyzer.

9.4.15 Met One

The Met One 210 Liquid Particle Counter is used to measure particles in clean fluids used in electronic, pharmaceutical and other manufacturing processes. It classifies particles in six size ranges in the 0.4 to 25 μm size range using laser diode based forward light scattering. Maximum count rate is 8000 particles per minute at a fluid flow rate of 100 mL min⁻¹.

The Met One 2500 batch sampling system is computer controlled for greater flexibility. Flowrate and sample volume are controlled automatically to ensure precise particle counting and sizing of liquidborne particles. The sampler comes with either a 500 mL or 1000 mL sample capacity and uses either light scattering or light extinction sensors. The system's software displays and prints average counts per mL for up to sixteen size ranges in both graphic and numeric format. Sensors are available for various size ranges from 0.5 to 400 μm .

9.4.16 Erdco Acoustical Counter

Audible sounds may be produced by particles exiting from a high-velocity laminar flow tube into a low velocity tube. The phenomenon was first reported by Langer [67] and has since been investigated by others [cit.68], the latest in a paper by Langer [69]. The sensing zone of the Erdco counter is a capillary at the exit of a glass tube. As particles enter this section they interact with the boundary layer, resulting in a toroidal vortex which moves as a shock wave which is reflected back on the capillary. The pressure wave is detected by a transducer at the outlet of the capillary, whose displacement is measured by an optical probe (Figure 9.23). The displacement is proportional to particle size, which is measurable down to 4 μm .

9.4.17 Micro Pure Systems acoustic particle monitors (Monitek)

Monitek's system uses a focused acoustical beam to sense discontinuities in a flowing liquid and can detect the size and amount of suspended solids, entrained gases, fibrous material in any liquid, or oil droplets in water. The sensor mounts in-line without restricting the process flow and the acoustical beam is focused to a point approximately 0.8 to 1.5 in from the sensor tip. The high frequency is generated by a piezoelectric crystal which acts both as a transmitter and receiver. The transmitter emits hundreds of pulses per second and monitors the echoes; this high sampling rate makes the instrument's insensitive to liquid flowrate. The amplitude of the echo is size sensitive so that a lower limit size threshold can be set; this limit can range from 0.2 μm to a few millimeters.

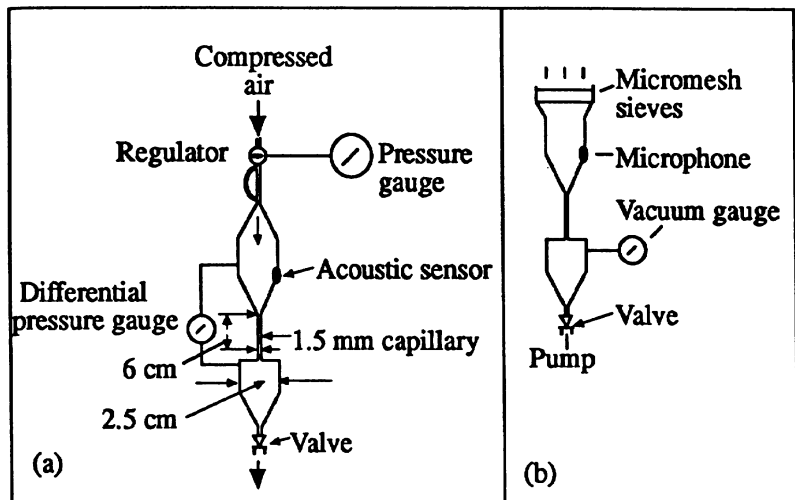


Fig. 9.23 The Erdco Acoustical Counter. (a) pressure mode, (b) vacuum mode with sieves to control size.

9.4.18 Rion Laser Based Liquidborne Particle Counter

The Rion Counter uses an optional sampler and 'sideways' scatter to allow off-line, on-line and automatic measurement down to $0.2 \mu\text{m}$ using a range of configurations. A range of sensors are available for use with either corrosive or aqueous liquids.

9.4.19 Faley Status 8000

Faley Status make several particle counters, mainly for airborne particles, however the model 8000 measures particles in non-corrosive liquids from 1 to $150 \mu\text{m}$, using either of two available sensors based on the light extinction principle. Counts are collected in up to six preset particle sizes

9.4.20 Kowa Nanalyzer™ PC-30 and PC-500

The PC-500 uses a He-Ne source and 90° light scattering to size from $0.1 \mu\text{m}$ in the ranges: 0.1 to $0.2 \mu\text{m}$, 0.2 to $0.5 \mu\text{m}$ and $+0.5 \mu\text{m}$ at a flow rate of 20 mL min^{-1} . and a maximum pressure of 70 psi. The axis of the measuring cell is parallel to the flow path and a mask placed in front of the photomultiplier precisely defines the measuring area. The image of the mask area is centered on the laser focus where beam intensity is constant in order to ensure even spatial sensitivity across the

measuring area. Moreover, with detection occurring along the flow path, particles flow through the mask image, so that the measuring area is not only precisely defined but also of equal size for all particle diameters. This configuration guarantees accurate measurement of particle size and concentration in each size range. The analyzer is intended for use with clear chemical liquids.

The PC-30 is of similar design and intended for monitoring ultra clean water. It classifies particles in the size ranges, 0.08 to 0.1 μm , 0.1 to 0.15 μm , 0.15 to 0.2 μm and +0.2 μm in concentrations of less than 30 particles mL^{-1} . Particles are sized according to Mie theory.

9.4.21 Malvern Autocounters

Malvern Autocounters [70] use light extinction sensors for particle measurement. Although designed primarily for counting particles in hydraulic and fluid power systems the ALPS 150H can be used for any liquid samples. Eight size thresholds are available in the 2 to 100 μm , 3 to 150 μm or 5 to 250 μm range with automatic verification to principal contamination standards. The flowrate can be adjusted between 1 and 30 mL min^{-1} with particle counts up to 10,000 mL^{-1} . Simple, in-field calibration is an important feature of all models of this instrument.

The ALPS 100 system liquid particle counter is a modular system which can be used with an autosampler for multiple samples or with an on-line sampler for direct measurement of flowing liquids. It can be used with sample volumes down to 0.5 mL and uses a built-in multi-channel analyzer to perform size distribution analyses of low concentration dispersions. Suitable for both aqueous liquids or solvents, it measures up to 50 size bands in the 2 to 100 μm or 3 to 150 μm size range with output from a built-in thermal printer or external dot matrix printer.

The Autocounter 300A Air Particle Counter is designed for general cleanroom and environmental monitoring. It is a 0.3 μm to +5 μm , 1 cfm (cubic feet per minute) laser particle counter with eight preset or user defined size thresholds.

9.4.22 Particle Sizing Systems Accusizer™ 770

This consists of a patented autodilution stage, optical sensor, pulse height analyzer/counter (PHA), systems computer/processor and software control. The autodiluter performs a continuous dilution of the concentrated sample suspension prior to its passage through the optical sensor. The PHA module continuously monitors the pulse rate during autodilution and when it falls below the coincidence level (typically 10,000 particles per second for particles smaller than 100 μm) the PHA unit starts to collect data. The resulting size distribution is displayed in real time as absolute counts versus diameter for each diameter channel

(8 to 512) logarithmically displayed over the total size range covered by the sensor (e.g. 1.5 to 400 μm). Additional derived distributions are calculated from the measured number distribution. A later version covers the size range 0.5 to 2500 μm using multiple sensors with analytical times of less than 5 min.

The autodilution system is shown in Figure 9.24. A few drops of concentrated liquid suspension containing several grams of powder are manually mixed into the mixing chamber. Filtered diluent is caused to flow into the mixing chamber, the resulting positive pressure causing some of the suspension to exit through the sensor at a rate of 25-100 mL min^{-1} . The PHA starts counting when the count rate falls to 20,000 s^{-1} [71,72].

9.4.23 AWK-electronic sieve analyzer

The AWK analyzers measure vibratory fed dry powders in the size range of 20 μm to 10 mm and drops in the 30 μm to 3 mm range at a rate of up to 10,000 particles per second. The analysis system consists of a sensor comprising measurement optics, control electronics and a personal computer which is connected to the sensor via a parallel or serial interface and undertakes evaluation and data display. The measuring principle is based on a combination of light scatter and obscuration. The measurement time is selectable in 0.01 s steps up to 10 min and the generated pulses are classified into 32 size categories for final presentation in 8, 16 or 32 channels.

9.4.24 PMT universal size distribution measuring systems

PMT (Partikel Messtechnik) manufacture a range of microprocessor controlled 16 and 32 channel analyzers. The RBG-1000 is a dry powder dispersing system covering the size ranges 1.5 μm to 500 μm and 20 μm to 2000 μm . Adry system, with on-line capability, is also available for granules and free flowing powders covering the micron size ranges, 20–2000, 80–8000, 200–15000. The SAS sampling system covers the same size ranges as the RBG-1000 but is intended for suspensions and emulsions; this can also be used on-line.

The PMT-2120 counter uses light blockage and can count up to 3,000 particles per second. It covers the size range 1–12,000 μm with selectable 16 or 32 channels.

9.4.25 Carty Vision System

This in-line system uses lighted video images and a microprocessor-based image analysis system to visually verify particle size, length, width and distribution. The microprocessor can monitor up to eight applications under process conditions with a lower limit of 1 μm .

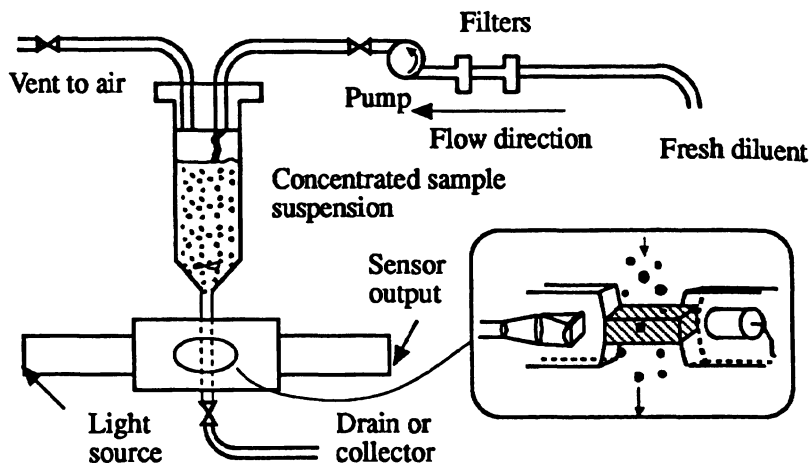


Fig. 9.24 Schematic diagram of the Particle Sizing Systems Accusizer 770 autodilution apparatus and optical particle counter.

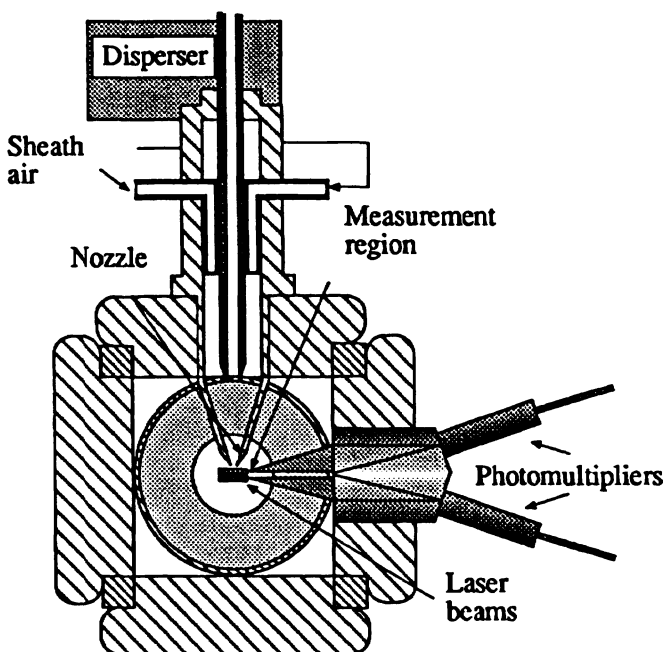


Fig. 9.25 Amherst Aerosizer.

9.4.26 Contamination Control Systems

The AWK is a powder and drop size analyzer operating over the size range 20 μm to 10 mm for powders and 30-30000 μm for drops. The measurement principle is based on a combined light scatter and light obscuration process. Particles crossing the measurement cell produce an impulse of height proportional to size. The impulses are examined to eliminate 'bad' signals and this automatically eliminates coincident pulses. The data can also be processed to give an equivalent sieve distribution.

9.5 Aerodynamic time-of-flight measurement

9.5.1 Amherst API Aerosizer

Time-of-flight aerosol beam spectrometry was first described by Dahneke in 1973 [73] and resulted in the Amherst Aerosizer [74]. The basic principle of the API analyzer is the precise laser based measurement of a particle's aerodynamic time of flight. Particles to be measured are first suspended in air using a disperser. The suspension expands through a nozzle into a partial vacuum and accelerates through a measurement region (Figure 9.25). The smaller the particle, the faster the acceleration. The particle's velocity is measured by passing two laser beams through the measurement region. As particles pass through the beams they scatter light which is picked up and converted to electrical signals by two photomultipliers. One photomultiplier detects light as the particle passes through the first beam and the other detects light as it passes through the second beam. The time between the two events (time-of-flight) is a measure of particle size. Particles are measured, with 500 channel resolution, at rates up to 100,000 per second in the size range 0.2 to 200 μm . The optional AeroDilution model enables high concentrations of powders and aerosols to be analyzed. Since only a small sample is required (typically 0.1 g) it is particularly useful for expensive or research material. The Aero-breather has been developed for sampling dry powder inhalers. An evaluation of the instrument has been carried out by Barr and Cheng [75]. The instrument has been used to monitor mixing structure of cohesive dry powders [76].

9.5.2 The TSI Aerodynamic Particle Sizer APS 33B

The time of flight of individual particles is measured in an accelerating flow field (Figure 9.26). Airborne solids and non-volatile liquids are counted and sized at number concentrations up to 600 cm^{-3} at 0.5 μm and 45 cm^{-3} at 30 μm , and sorted into 58 size channels. The aerosol is

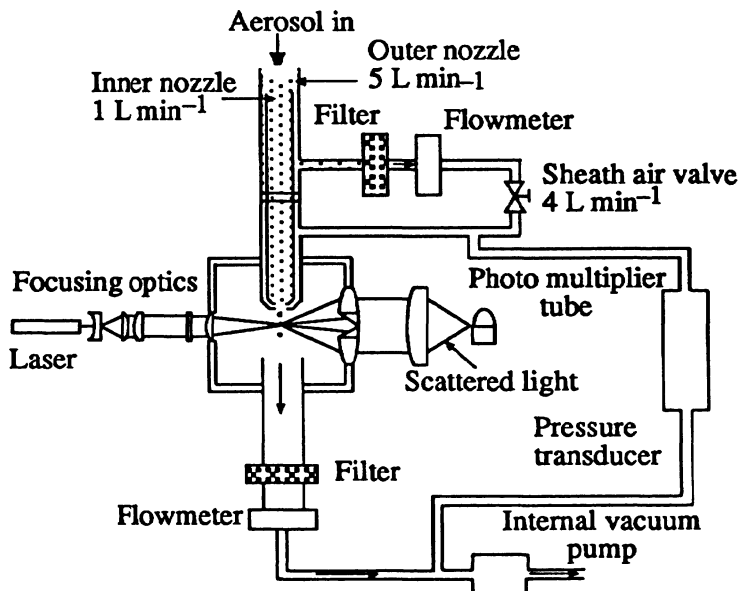


Fig. 9.26 Schematic of the APS showing the accelerating nozzle and the two spot laser velocimeter.

sampled into an inner tube, surrounded by a sheath of filtered air and accelerated through a nozzle. Two timers are used, a 2 ns resolution timer for sizes from 0.5 to 15 μm and a 66.67 ns timer for sizes from 5 to 30 μm . A full description of the equipment is given in a paper by Blackford *et al.* [77]. Although designed for the size range 0.5 to 30 μm its overall efficiency falls from 95% for 3 μm particles down to less than 45% for particles smaller than 10 μm [78].

The Model 3433 small scale powder disperser breaks up agglomerated powder, by lifting particles from a turntable, and feeds them to the APS. TSI also manufacture a fluidized bed aerosol generator to generate high concentration aerosols.

9.6 Laser phase/Doppler principle

The phase/Doppler technique simultaneously measures particle velocity, size and flux and may be considered an extension of laser Doppler velocimetry (LDV). The basic principle is as follows. A measuring volume containing a system of plane fringes, resulting from constructive and destructive interference, is formed at the intersection of two laser beams. A particle crossing this volume produces a signal of periodic intensity with a Gaussian envelope. The particle velocity is directly related to the frequency of this signal and the particle size is determined from the phase difference in the signals collected from two

different observation angles. The technique was introduced by Durst and Zare [79] and improved by others [80-83].

The standard phase Doppler anemometer (PDA) requires an excessively large angle between the laser beams and yet the system response is non-monotonic and results in large uncertainties in the measurement. By employing planar layout the beam angle is kept smaller than 10° and the fluctuations in the response curves are significantly suppressed [84].

A history of the development of the phase Doppler particle sizing velocimeter has been presented by Hirleman [85].

9.6.1 BIRAL PD-Lisatek and L2F

In the PD-Lisatec a measuring volume with a Gaussian distribution (that is without real fringes) is generated and the velocity and phase information is derived using sophisticated patented polarization techniques. The optical processing employed directly filters the signal and removes the Gaussian envelope. This allows the dynamic range for velocity measurements to be greatly increased from a usual 5:1 or 10:1 to at least 30:1. The instrument covers the size range from 1 μm to several mm at flow rates from 1 cm s⁻¹ to 500 m s⁻¹. It was developed by the Industrial Optics Group at AEA Technology who have published over 50 papers on this subject.

Laser two focus velocimetry is applied in the BIRAL L2F. The measurement volume is formed by focusing two laser beams to two small waists of about 10 μm diameter. The result is a light gate operating with concentrations orders of magnitude greater than possible with the LDV system. Particle velocity is determined by the time it takes the particle to pass from one beam waist to the other.

9.6.2 Hosokawa Mikropul E-Spart Analyzer

Characterization of electrostatic charge and aerodynamic size of particles is of critical importance in many electrokinetic processes [86]. A number of instruments are available that can characterize aerodynamic size distribution of particles. Likewise, instruments are available to estimate the net average electrostatic charge of particles. However, the choice of instruments for real-time simultaneous measurement of aerodynamic size and electrostatic charge distribution of particles on a single particle basis is limited. The Electrical Single Particle Aerodynamic Relaxation Time (E-SPART) Analyzer simultaneously measures size in the range from submicron to 100 μm and particle charge distribution from zero to saturation levels [87-89].

The operating principle depends upon the phenomenon that when an airborne particle is subjected to an oscillatory external force, such as acoustic excitation, the resultant oscillatory motion of the particle lags behind the external driving field. The particles vibrate at the same

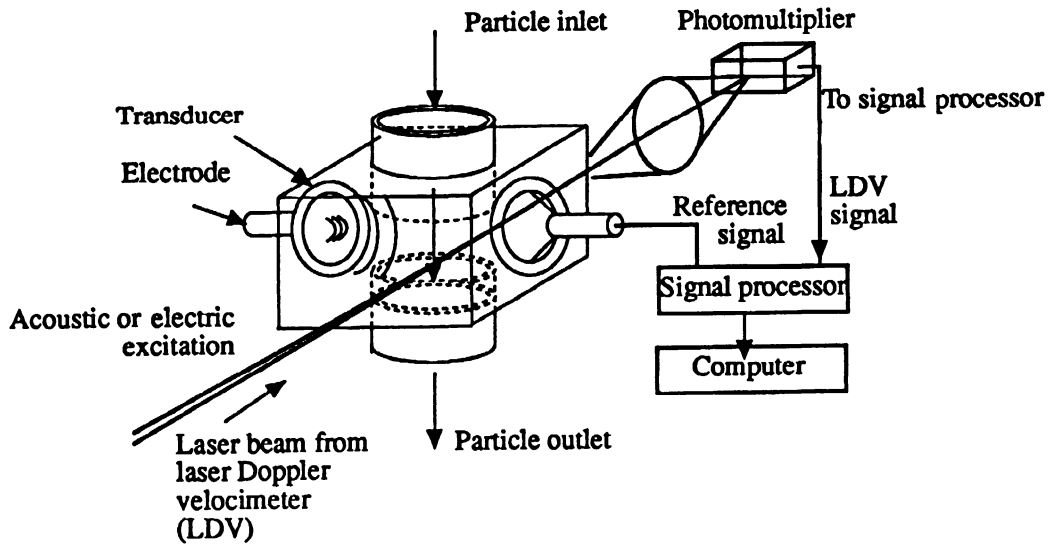


Fig. 9.27 Schematic of the E-Spart relaxation cell. Individual particles are subjected to acoustic and/or electric excitation and the resultant response is measured by LDV to determine aerodynamic size and electrostatic charge.

frequency as the acoustic field but with a phase lag due to particle inertia. The larger the particle the greater the phase lag, which can therefore be related to particle size. To determine this phase lag, the analyzer uses a differential laser Doppler velocimeter (LDV) to measure the velocities of individual particles subjected to a combination of an acoustic and a DC electric field. Simultaneously a charged particle will have its vertical position shifted by the electric field by an amount related to the charge. The maximum count rate varies from 10 to 2,000 particles per second depending on particle size which, typically, can range from 0.3 μm to 75 μm .

The particles are sampled in a laminar flow field through the LDV sensing volume. As each particle passes through the sensing volume it experiences the acoustic excitation and the superimposed DC electric field in a direction perpendicular to the direction of the laminar air flow. A typical sampling configuration is shown in Figure 9.27. A full description of the theoretical basis for the instrument has been published [90] together with some typical applications.

9.6.3 Aerometrics phase-Doppler particle analyzer (APDPA)

The Aerometrics phase-Doppler particle analyzer (APDPA), based on the Laser Doppler Anemometer (LDA), is used for complete analysis of two-phase flows containing particles, droplets or bubbles [91-93]. It consists of a laser based optical transmitter, an optical receiver, an electronic signal processor and a computer with software for data acquisition and analysis (Figure 9.28). Measurements are made at the intersection of two laser beams. As a particle passes through the probe volume (10^{-11} m^3) it scatters light from the beams and creates an interference fringe pattern. A receiving lens projects a portion of this fringe pattern on to three detectors. Each detector produces a Doppler burst signal with a frequency proportional to the particle velocity. The phase shift between the Doppler burst signals from the three detectors is proportional to particle size. The sample volume is determined simultaneously with particle size and velocity, which enables an accurate determination of number concentration. The transmitter and detector can be traversed together for spatial mapping of the flow field and particle size distribution. The instrument operates over the size range 0.5 to 10,000 μm in 50 uniform size classes, with a dynamic size range of 35:1 at each configuration. Velocities over 200 m s^{-1} can be measured at particle concentrations up to 10^6 cm^{-3} .

The optical system is available in both single component or dual component versions. The single component PDPA-1000 uses a HeNe laser, the dual component PDPA-2000 uses an Argon-ion laser for simultaneous measurement of two orthogonal velocities. Theoretical results and experimental comparisons have been presented by the manufacturers [94].

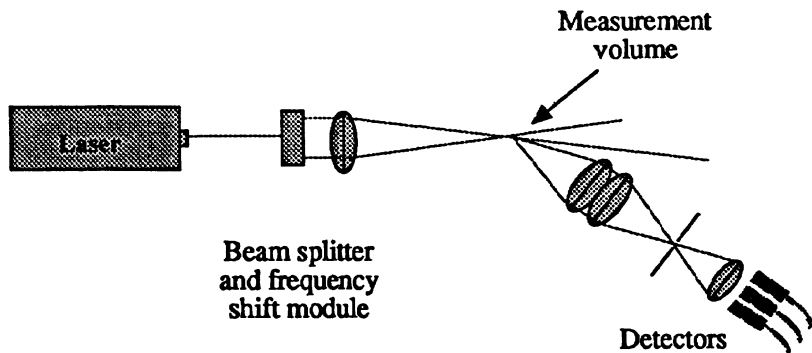


Fig. 9.28 Schematic of the Aerometrics phase-Doppler particle analyzer.

9.6.4 Dantec Particle Dynamic Analyzer

The Dantec Particle Dynamic Analyzer measures particle size, one to three velocity components and concentration using the phase/Doppler principle. The Doppler effect is a phase shift in light scattered from moving particles and incident illumination with the frequency shift being proportional to particle velocity. If a standard laser Doppler anemometer is combined with a second photodetector, the photodetector signals, under certain conditions, are a direct measure of particle size. A third photodetector is included to extend the dynamic range and, in two dimensional flows, a color separator and a fourth photodetector are added to allow two velocity directions to be measured. A fifth detector is needed for measurement of three dimensional flows.

Its applications include droplet sizing, spray characterization, fuel injectors and agricultural sprays. The size range covered is 0.5 to 10,000 μm with a dynamic range of 40:1 with the possibility of extending this by a factor of 2.5 by varying the aperture spacing. Velocity maximum is $>500 \text{ m s}^{-1}$; up to 3 components being measured using a combination of near forward scatter, near backward scatter and side scatter.

9.7 Interferometers

Unlike light scattering instruments, interferometers do not measure the scattered light, but the phase shift in light waves. They can distinguish between gas bubbles and particles because bubbles have a lower refractive index than the surrounding liquid and therefore produces phase signals of opposite polarity to those of particles. This makes these instruments particularly useful for examining the reagents used

for semiconductor cleaning since these reagents often have high vapor pressures and tend to form bubbles that can be counted as particles using light scattering or obscuration instruments.

Interferometers separate a laser beam into two beams and then recombine them to create a signal whose intensity depends on the phase difference between them. When a particle with a refractive index greater than that of the surrounding liquid passes through the beam the wave front is retarded and when a gas microbubble passes through it the wave front is advanced. The magnitude of the phase signal depends on particle size and the pulse can be calibrated with particles of known size.

Figure 9.29 is a schematic of a Mach Zehnder type interferometer the design of which allows for a polarized light beam to be split in two. The incoming beam with intensity I_0 is divided into two equally intense beam with a beam splitter. The beam following path 1 undergoes a 90° phase change and a second beam splitter combines beams 1 and 2 to form new beams A and B. The two beams are now 180° out of phase; when one is bright the other is dark. The intensities of the beams I_A and I_B are measured using separate detectors. Due to their inherent complexity, large size and susceptibility to vibration interferometers have remained laboratory and research tools.

9.7.1 The TSI Liquitrak™ interferometer

The TSI Liquitrak™ interferometer [95–97] uses a dual beam interferometer to detect slight differences in the refractive indices of

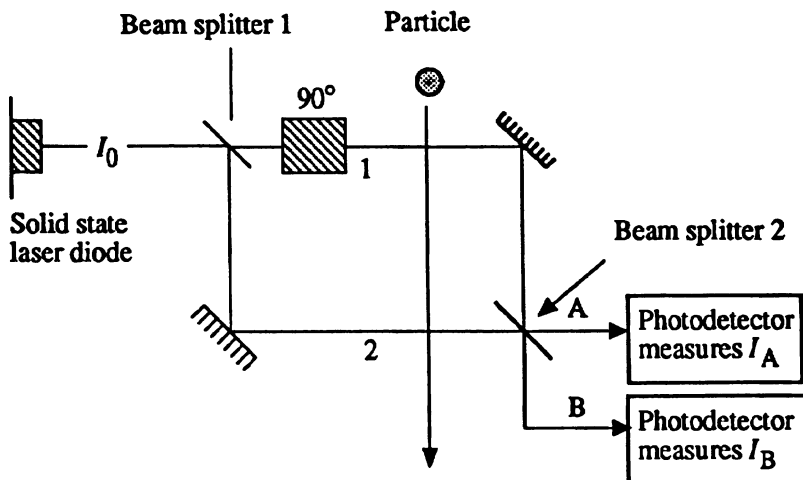


Fig. 9.29 Schematic diagram of a Mach Zehnder type interferometer.

particles relative to the surrounding media. It is less sensitive to vibration than the Mach Zehnder type of interferometer because it does not separate the two light beams. Instead the beams are overlapped and polarized at 90° to each other. Hence the beams do not interfere and are effectively separated from each other until combined by the second beam splitter. The narrow separation of the beams reduces vibration sensitivity dramatically because any vibration interference affects both beams equally.

The dual beam interferometer also has the advantage of allowing flow-rate measurement. The instruments flow-rate ranges from 4 to 40 mL min⁻¹ of which 1/200 is examined. Flow-rate is measured each time a particle signal is processed hence particle concentration can be measured in a fluctuating flow.

The interferometer has several advantages over dark field scattering instruments. Because it is a bright field instrument it is less sensitive to the stray light scattered by interfaces between the instrument's capillary cell wall and the liquid medium. The instrument can also identify signals created by bubbles thus avoiding false counts. It can also measure flow-rate and it is more sensitive to particles with a refractive index near that of the liquid than dark field instruments because it can look at forward light without noise interference from the incident laser beam.

A drawback is that its inspected volume is small (0.5%) compared to the full flow stream since a highly intensive beam is required in the viewing volume, rendering the instrument less useful for low concentration contamination measurements.

An evaluation of this procedure is available in recent articles by Blackford and Grant [98] and Grant [99] and the instrument is available from Thermal Systems Inc. as Model 7750.

9.8 Flow ultramicroscope.

In the flow ultramicroscope [100] dispersed particles are injected into a stream of liquid and hydrodynamically focused so as to pass through a laser beam. The scattering is detected by a photomultiplier and electronically processed as a series of pulse heights. The detector can be at right angles to the incident beam, with either a narrow or wide receiver angle, or forward angle scattering may be used. Since the scattered light intensity is highly dependent on particle size, the dynamic range of the photomultiplier can be exceeded by samples of relatively low polydispersity. The range is greatly increased by using a feedback system from the photomultiplier to the laser. The instrument measures number concentration and size distribution for spheres and particles of simple shapes in the size range 0.1 to 5 µm. Such an instrument has been used to measure particle flocculation [101].

9.8.1 ISPA image analysis system

ISPA 800 series characterizes the size and shape of 5 µm to 10 mm particles by measuring the projected areas of the particles in a strobed image. The unit, manufactured by Greenfield, can process 15 images per second and can analyze particles moving at 30 m sec⁻¹.

9.9 Measurement of the size distribution of drops in dispersions

The most common method is direct photography [102–105]. The method is simple, easy and accurate and covers a wide size range, controlled by microscope magnification, from a lower limit of 1 µm. The technique is only suitable for low concentration systems, particularly in the case of high opacity continuous phases. The procedure requires many pictures and lengthy analysis times. Direct image analysis of the data has met with limited success.

Light attenuation is a simple, widely used method for determining interfacial area, i.e. surface-volume mean diameter if droplet concentration is known but cannot be used for size distribution determination [106–108].

Light scattering has been used for measurement of small drop sizes below 10 µm in diameter [108] and also for drop sizes below 800 µm. Although on-line measurement is possible the technique is only suitable for volume concentrations below 0.05 [110].

Laser Doppler velocimetry (see section 9.6) has also been used for the measurement of a broad size range of drop sizes in solid–liquid and liquid spraying systems [111,112].

Drop size distribution in dilute suspensions of electrical conducting liquids may be determined using the Coulter principle but the need to add what may be undesirable conductive materials limits its applicability [113–115].

The use of chemical means to measure interfacial area has been used extensively for gas–liquid dispersions. Chemical reaction methods for determining the interfacial of liquid–liquid systems involve a reaction of a relatively unchanging dispersed-phase concentration diffusing to the continuous phase. The disadvantage of this approach is that the mass transfer can affect the interfacial tension, and hence the interfacial area [116–118].

Drop stabilization methods rely on the immediate stabilization of drops by encapsulation with thin polymer films or surfactants [119–121]: a photomicrographic method has been employed usually after encapsulation of drops. However this method cannot always be used due to incompatibility of the encapsulating materials with some systems. The method also has the disadvantage of the influence of the chemical treatment on drop size. A special sampling apparatus has been developed to withdraw a sample of dispersed phase from the mixing vessel to stabilize drops with a surfactant and to force the

dispersed sample through a capillary with a photometer assembly to measure both droplet size and concentration [122].

The capillary method employs a fine bore capillary of the order of the drop size for sampling from the liquid dispersion. As drops pass through the capillary they are transformed into cylindrical slugs of equivalent volume. A laser beam is split into two rays using a beam splitter and a plane mirror and the rays pass directly through the capillary precisely 0.1 mm apart. The emergent beam is collected by a $\times 10$ microscope objective lens and focused on to a photodiode. From the measurement of the passage time of a slug at one detector and its travel time between two detectors the velocity and diameter of the drop can be calculated. The method can be used to obtain broad drop size distributions in the range above 50 μm in real time and automatically [123-127].

The scintillation method uses short range radioactive particles for measuring interfacial area. This technique is limited by the necessity of high immiscibility between the phases as well as the availability of suitable isotopes and target materials [128].

The Lasentec particle/droplet size analyzer can be used for laboratory and in-line analysis, in the +1 μm size range, over a wide range of operating conditions.

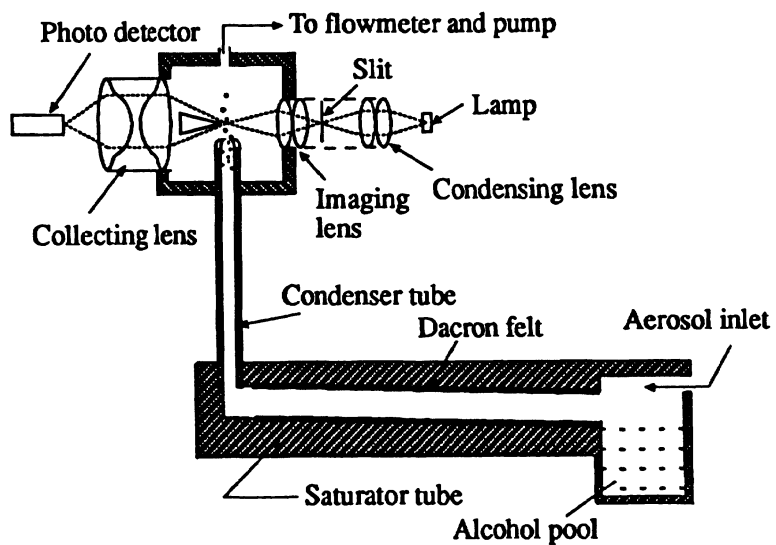


Fig. 9.30 Schematic of condensation nucleus particle counter.

9.10 Dupont electrolytic grain size analyzer

The EGSA provides a rapid (4 to 10 min) absolute measurement of the charge required to electrolytically reduce/oxidize AgX crystals. This electrolytic decomposition is singularly effective as a basis for measuring the particle size distribution of photographic emulsion grains since the charge is directly related to grain volume. Grains are electrolytically reduced as they are rotated under a measuring electrode and the generated pulses are sorted according to their integral size and stored in 256 logarithmically distributed channels. Three size ranges cover an overall range of 0.05 μm to 2 μm [129].

9.11 TSI condensation particle counter

This is an extremely sensitive instrument for counting sub-micron powders. An aerosol is drawn over a container of working fluid, usually alcohol (Figure 9.30). Vapor condenses on to the particles and they grow to about 10 μm in size so that they can be counted using light blockage or light scattering. After leaving the condenser the droplets pass through an optical detector that uses a 3 mW laser diode as its light source. Concentration less than 10^4 particles cm^{-3} are counted by the pulses generated as they pass through the light beam. Higher concentrations are measured by measuring the scattered light and comparing the intensity to predetermined calibration levels.

The TSI 3025A Ultrafine CPC continuously samples and counts particles from 0.003 μm to several microns in diameter at number concentrations up to 10^5 mL^{-1} ; the TSI 3022A CPC operates in the size range from 0.007 μm to several microns in diameter at number concentrations up to 10^7 mL^{-1} and the TSI 3010 CPC from 0.010 μm to several microns in diameter at number concentrations up to 10^4 mL^{-1} . Similar instruments are manufactured by GEC and RAC. A comparison between the TSI condensation particle counter and the TSI mobility aerosol spectrometer gives good agreement [130].

9.12 TSI diffusion battery

The motion of aerosol particles in the 0.005 to 0.2 μm diameter range is strongly affected by random collisions with gas molecules i.e. diffusion. As particles undergoing diffusion pass through a fine mesh screen some will collide with, and adhere to, the screen wires.

The TSI 3040, for example, captures a large fraction of the 0.005 μm particles on the first stage (Figure 9.31) the next stage captures a large fraction of the next size and so on. Finally the tenth stage removes a large fraction of the remaining 0.1 μm particles.

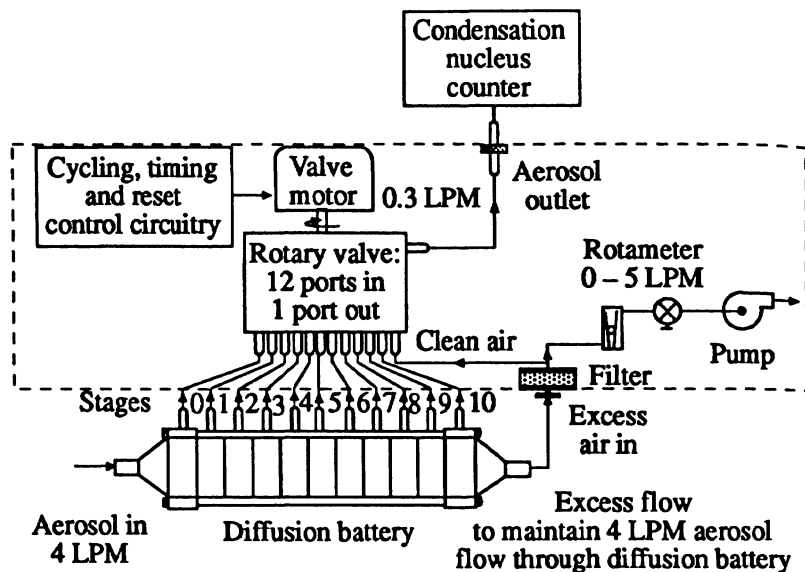


Fig. 9.31 TSI model 3040 diffusion battery with connection to TSI model 3042 switching set and TSI model 3020 condensation nucleus counter.

The instrument is designed for rugged application and is often used in conjunction with a continuous flow condensation nucleus counter. With particle number counts at each stage of the diffusion battery, a particle size distribution can be built up. The latest version of this instrument, the model 3931, covers the size range 0.005 μm to 0.2 μm .

9.13 TSI diffusional particle sizer

The Model TSI 3931 DPS uses Brownian motion to size particles in 11 stages from 0.007 to 0.2 μm in diameter. It is rugged and handles a broad concentration range from 0.1 to 10^7 particles cm^{-3} . Included in the DPS is a Model 3022A CPC and a diffusion battery.

9.14 Differential mobility analyzer (DMA)

A differential mobility analyzer fractionates charged particles according to their electrical mobility which is related to their particle size and charge. It consists of two concentric cylinders (Figure 9.32) with sheath air flowing in the annular space between them from the bottom to the top. The aerosol is introduced tangentially into a plenum chamber and exits through a slit to merge with the sheath air flow. Voltage is applied to the inner electrode to cause the charged particles to

migrate along a trajectory to the inner electrode. At the end of the inner electrode there is a small slit through which particles with the correct mobility exit.

9.15 Scanning mobility particle sizer (SMPS)

The scanning mobility analyzer measures airborne particles in the size range 0.01 to 1.0 μm . Two primary stages are used, the first to classify the particles and the second to count them. In the first stage aerosols are passed through a krypton-85 neutralizer which exposes the particles to high levels of both positive and negative ions. Subsequently, the particles acquire a charge distribution described by the Boltzmann equilibrium charge distribution equation. The charged aerosol is then passed through a laminar flow classifier in which a precise negative potential is maintained at the center electrode. The charged particles migrate to this electrode so that only a narrow range of particles pass through a slit near the bottom of the electrode for a given applied voltage. By varying the applied voltage, particles are classified over the entire range. The size-classified particles are then carried to a condensation particle counter where they are counted.

The SMPS measures the whole submicron particle size distribution in 2 to 3 min as compared to 30 min for the DMA.

The TSI 3934 SMPS replaces the TSI 3932 D(ifferential) MPS and is an order of magnitude faster than the earlier system, providing a

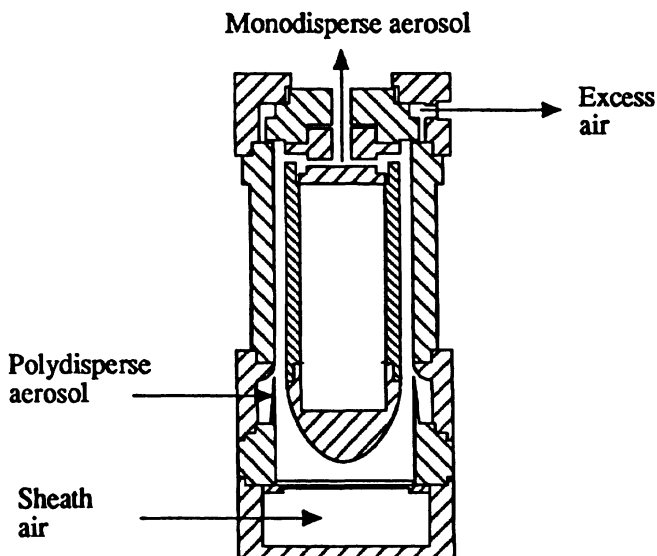


Fig. 9.32 Schematic diagram of the differential mobility analyzer [131].

complete scan in 60 s. It resolves sizes of stable aerosols over a total of 147 channels spanning the 0.005 to 1 µm diameter range. Three system configurations are available. All include a Model 3071A electrostatic classifier, a condensation particle counter and ancillaries. The 3934U is an SMPS with a 3022A CPC for ultrafine powders; the 3934C with a 3022A-S CPC is for high concentrations and the 3934L with a 3010-S CPC offers the lowest price and is suitable for low concentrations.

9.16 Atmospheric particle counters

Many of the procedures outlined above can be modified to measure atmospheric particles. These range from instruments designed to monitor and measure atmospheric pollution, control clean room environments, monitor and in some cases (e.g. where hazardous dust such as asbestos may be present) generate a concentration profile of atmospheric particles in a factory environment.

Fissan *et al.* compared four DMAs for nanometer aerosol measurement and transfer function evaluation [132]. Miller *et al.* compared the APS with the SMPS and conclude that these instruments can simultaneously measure particulate contamination in hot, moist process streams [133]. In a comparison between a TSI APS, Model 3310 and a modified Polytec HC 70 using mixtures of latex spheres, it was found that the resolution of the latter was inferior to that of the former but could be improved by calibration against the APS [134].

References

- 1 Groves, M.J. (1991), *Particle Size Distribution II*, ed. T. Provder, Am. Chem. Symp. No. 472, 123–131, 329
- 2 Coulter, W.H. (1953), US Patent No. 2,656,508. Appl. 1949, 329
- 3 Coulter, W.H. (1956), *Proc. Soc. Nat. Electronics Conf.*, 12, 1034, 329
- 4 Kubitschek, H.E. (1958), *Nature*, 182, 234–235, 329, 353
- 5 Kubitschek, H.E. (1960), *Research*, 13, 128, 329
- 6 Coulter Counter and other scientific instruments, Coulter Electronics, U.K., 332
- 7 Berg, R.H. (1958), *ASTM Sp. Publ.* 234, 332
- 8 Batch, B.A. (1964), *J. Inst. Fuel*, 455, 332
- 9 Allen, T. (1967), *Proc. Conf. Particle Size Analysis*, Loughborough, Soc. Analyt. Chem., London, 332
- 10 De Blois, R.W. and Bean, C.P. (1970), *Rev. Sci. Instrum.*, 41, 7, 909–916, 332, 334
- 11 Gregg, E.L. and Steidley, K.D. (1965), *Biophys. J.*, 5, 327, 332
- 12 Andersen, J.L. and Quinn, J.A. (1971), *Rev. Sci. Instrum.*, 42(8), 1257–1258, 332, 334
- 13 Smythe, W.R. (1961), *Phys. Fluids*, 4, 756, 333

- 14 Smythe, W.R. (1961), *Phys. Fluids*, **7**, 633, 333
 15 Grover, N.B. *et al.* (1969), *Biophys.*, **9**, 1398, 1415, 333
 16 De Blois, R.W., Bean, C.P. and Wesley, R.K.A. (1977), *J. Colloid Interf. Sci.*, **61**(2), 323–335, 334
 17 Eckhof, R.K. and Soelberg, P. (1967), *Beton tek. Publik.*, **7**(1), 334
 18 Schrag, K.R. and Corn, M. (1970), *Am. Ind. Hyg. Assoc. J.*, 446–453, 334
 19 Simecek, J. (1967), *Staub Reinhalt. Luft*, **27**, **6**, 33–37, 334
 20 Michael, A. *et al.* (1994), *Part. Part. Syst. Charact.* **11**, 391–397, 334
 21 Batch, B.A. (1964), *J. Inst. Fuel*, **45**, 55, 334
 22 Grover, N.B. *et al.* (1969), *Biophys. J.*, **9**, 1398, 1415, 334
 23 Thom, R. von, Hampe, A. and Sauerbrey, G. (1969), *Z. ges. Exp. Med.*, **151**(331), 336
 24 Elkington, D.A. and Wilson, R. (1985), *Proc. 5th Int. Conf. Particle Size Analysis*, Anal. Div. Chem. Soc., 509–526, ed. P.J. Lloyd, Wiley, U.K., 283, 336
 25 Ghosal, S., Ebert, J.L. and Self, S.A. (1993), *Part. Part. Charact.*, **10**, 11–18, 338
 26 British Standard, BS 3406: Part 5: 1983, *Determination of particle size of powders*, Recommendations for electrical sensing zone method (the Coulter principle), 339
 27 Rohricht, W., Khalili, M. and Allen, T. (1994), *Fine Particle Society Conf.*, New Brunswick, August, 339, 349
 28 Allen, T. (1992), *Part. Part. Syst. Charact.*, **9**, 252–258, 341
 29 Zellweger Uster, Inc., 456 Troy Circle, Knoxville, Tennessee 37919, 349
 30 Bragg, C.K. (1988), *Proc. 19th International Cotton Conference*, Bremen, Germany, Faserinstitut, Bremen e.V., 349
 31 Bragg, C.K. and Shofner, F.M. (1993), *Textile Res. J.*, **63**(3), 171–176, 349
 32 Lilienfeld, P., Elterman, P.B. and Baron, P. (1979), *Am. Ind. Hyg. Assoc. J.*, **40**, 270–282, 349
 33 Shenton-Taylor, T. and Iles, P. (1986), *Am. Occup. Hyg.*, **30**(1), 77–87, 349
 34 Al-Chalabi, S.A.M., Jones, A.R., Savaloni, H. and Wood, R. (1990), *Meas. Sci. Technol.*, **1**, 29–35, 349
 35 Timbrell, V. and Gale, R.W. (1980), *Biological Effect of Mineral Fibers I*, *ARC Sci. Publ.* No 30, 53–60, 349
 36 Rood, A.P. (1992), *Proc. Conf. PSA '91*, ed. N.G. Stanley-Wood and R. Lines, publ. Royal Soc. Chem., 236–245, 349
 37 Valley, R.B. and Morse, T.H. (1965), *TAPPI*, **48**, **6**, 372–376, 357
 38 Kominz, D.R. (1971), *Biophys. J.*, **2**, 47–65, 350
 39 Kahrn, R. (1974), *Powder Technol.*, **11**, 157–71, 350

- 40 Davies, R., Kahrn, R. and Graf, J. (1975), *Powder Technol.*, 12, 157-76, 350
- 41 Kahrn, R., Berg, R.H. and Davies, R. (1976), *Powder Technol.*, 13, 193-202, 350
- 42 Kahrn, R. and Berg, R.H. (1978), *Powder and Bulk Solids Handling Conf.*, Fine Particle Soc., Chicago, IL, 350
- 43 Chandler, D., (1992), *Filtration and Separation*, May/June 211-212, 351
- 44 Sarto, L. (1992), *Laboratory Equipment*, Dec. 8, 352
- 45 Knollenberg, R.G. and Veal, D.L. (1991), *Proc. 37th Annual Technical Meeting*, Institute of Environmental Sciences, May 6-10, San Diego, CA, 353
- 46 Sommer, H.T. (1990), *Swiss Contamination Control*, 3, 353
- 47 Liebermann, A. (1993), Private Communication, 353
- 48 Umhauer, H. (1992), *Proc. Conf. PSA '91*, ed. N.G. Stanley-Wood and R. Lines, publ. Royal Soc. Chem., 236-245, 353
- 49 Umhauer, H. (1992), Partec 92, *5th European Symposium Particle Characterization*, Nuremberg March, Preprints 2, 519-535, 353
- 50 Gutsch, A., Umhauer, H. and Loffler, F. (1994) *Proc. First Int. Part. Techn. Forum*, Denver, Am. Inst. Chem. Eng., 101-106, 353
- 51 Ovad, V.I. (1995), *Part. Part. Syst. Charact.* 12, 207-211 353
- 52 Akers, R.J., Rushton, A.G., Sinclair, I. and Stenhouse, J.I.T. (1991), *Proc. Int. Symp. Particle Size Analysis*, Publ. Royal Soc. Chem., ed. N.G. Stanley-Wood, and R. Lines, pp 498-513, 354
- 53 Sommer, H.T., Harrison, C.F. and Montague, C.E. (1991), *PSA '91 Particle Size Analysis Grou Conf.*, Loughborough, U.K., publ. Anal. Div. Royal Soc. Chem. 354
- 54 Allen, T. and Davies, R. (1988), *International Conference on Particle Size Measurement*, Guildford, Surrey, Royal Soc. Chem., Anal. Div., pub. Heyden, ed. P.G. Lloyd, 362
- 55 Hobbel, E.F., Davies, R., Rennie, F.W., Allen, T., Butler, L.E., Water, E.R. Smith, J.T. and Sylvester, R.W (1991), *Part. Part. Syst. Charact.*, 8, 29-34, 362
- 56 Allen, T., Hobbel, E.F., Davies, R. and Boughton, J.H. (1991), *Pharmtech. Conf.*, Brunswick, NJ, 362
- 57 Karasikov, N. and Krauss, M. (1989), *Filtration and Separation*, 121-124, 363
- 58 Monnier O., Klein, J-P., Hoff, C. and Ratsimba, B. (1996), *Part. Part. Syst. Charact.*, 13, 10-17, 363
- 59 Porter, M.C. (1975), *Proc. 7th Ann. Conf.*, Fine Particle Soc., August, Chicago, 364
- 60 Tate, C.H., Lang, J.S. and Hutchinson, H.L. (1977), *J. Am. Water Wks. Assoc.*, 69(7), 4245-4250, 365
- 61 Porter, M.C. (1974), *The Brewers Digest*, Feb., 365

- 62 Gooding, J.L. and Clanton, U.S. (1983), *Geophys. Res. Lett.*, **10**, 1033–1036, 365
- 63 Blanchard, J., Thompson, C.N. and Schwartz, J.A. (1976), *Am. J. Hosp. Pharm.*, **33**, 150–151, 365
- 64 Mathes, K.N. and Atkins, J.M. (1978), *I.E.E.E. International Symposium on Electrical Insulation*, 365
- 65 Ricci, R.J. and Cooper, H.R. (1970), *ISA Trans.*, **9**, 28–36, 365
- 66 Hinde, A.L. (1973), *J. S. Afr. Min. Metall.*, **73**, 8, 258–268, 365
- 67 Langer, G. (1965), *J. Colloid Sci.*, **20**, 6, 602–609, 368
- 68 Allen, T. (1990), *Particle size measurement*, Chapman & Hall (Methuen), 4th ed., 368
- 69 Langer, G. (1972), *Powder Technol.*, **6**, 5–8, 368
- 70 Parsons, D. (1992), *Filtration and Separation*, May/June, 206–208, 370
- 71 Nicoli, D.F., Chang, J.S., Wu, K., Hasapidis, K. and McKenzie, D.C. (1992), *International Labmate*, 17–21, 371
- 72 Nicoli, D.F., Chang, J.S., Wu, K., Hasapidis, K. and McKenzie, D.C. (1992), Partec, *5th European Symp. Particle Characterization*, Nurenberg, March, 371
- 73 Dahneke, B.E. (1973), *Nature (Physical Science)*, **244**, 54, 373
- 74 Dahneke, B.E. (1994), *Proc. First International Part. Techn. Forum.*, Denver, Am. Inst. Chem. Eng., Part 1, 54–58, 373
- 75 Barr, E.B. and Cheng, Y.S. (1993), *Particles in Gases and Liquids*, 3rd Symp., *Plenum Press*, 131–140, 373
- 76 Kaye, B.H. (1995), *6th European Symp. Particle Characterization*, Partec 95, Nurenberg, Germany, publ. NürnbergMesse GmbH, 421–426, 373
- 77 Kinney, P.D. and Pui, D.Y.H. (1995), *Part. Part. Syst. Charact.*, **12**, 188–193, 374
- 78 Blackford, D.B., Quant, F.R. and Gilmore, J.S. (1994) An improved aerodynamic particle size analyzer, available from TSI,
- 79 Durst, F. and Zare, M. (1975), *Proc. LDA Symposium*, Copenhagen, 403–429, 375
- 80 Bachalo, W.D. (1980), *Appl. Optics*, **19**, 363–370, 375
- 81 Bachalo, W.D. and Houser, M.J. (1984), *Optical Eng.*, **23**, 583–590, 375
- 82 Grehan, G., Gousebet, G., Naqwi, A and Durst, F. (1992), Partec, *5th European Symposium on Particle Characterization*, Nurenberg, March, Preprints 1, 309–317, 375
- 83 Aizu, Y., Domnick, J., Durst, F., Grehan, G., Onofri, F., Qiu, H., Sommerfeld, M., Xu, T-H. and Ziema, M. (1994), *Part. Part. Syst. Charact.*, **11**(1), 43–54, 375
- 84 Naqwi, A., Ziema, M. and Durst, F., (1992), Partec, *5th European Symposium on Particle Characterization*, Nurenberg, March, Preprints 1, 267–279, 375
- 85 Hirleman, D. (1996), *Part. Part. Syst. Charact.* **13**, 59–67, 375
- 86 Cross, J.A. (1987), *Electrokinetic processes, Principles, problems and applications*, Adams Hilger, England, 375

- 87 Mazumder, M.K., Ware, R.E. and Wilson, J.D. (1979), *J. Aerosol Sci.*, **10**, 561–569, 375
- 88 Mazumder, M.K., Ware, R.E., Yokoyama, T., Rubin, B. and Kamp, D. (1982), *Measurement of suspended particles by quasi-elastic light scattering*, B. Dahneke, ed., John Wiley and Sons Inc., New York, pp. 328–341, 375
- 89 Mazumder, M.K., Ware, R.E. and Hood, W.G. (1983), *Measurement of suspended particles by quasi-elastic light scattering*, B. Dahneke, ed., John Wiley and Sons Inc., New York, 375
- 90 Mazumder, M.K. (1993), *Kona, Powder and Particle*, No. 11, 105–118, Council of Powder Technology, Japan, 377
- 91 Bachalo, W.D. and Houser, M.J. (1984), *Optical Engineering*, **23**, 583–590, 377
- 92 Dodge, L.G. (1987), *Applied Optics*, **26**, 1328–1341, 377
- 93 Young, B.W. and Bachalo, W.D. (1988), Optical Particle Sizing, Theory and Practice, *Proc. Int. Symp. 1987*, Rouen, France, Plenum Press, New York, 483–487, 377
- 94 Rudoff, R.C., Sankar, S.V. and Bachalo, W.D. (1991), *Proc. Int. Symp. Particle Size Analysis*, publ. Royal Soc. Chem., ed. N.G. Stanley-Wood, and R. Lines, pp 498–513, 377
- 95 Batchelder, J.S. and Taubenblatt, M.A. (1991), *US Pat.* 5,037,202, 379
- 96 Batchelder, J.S., DeCain, D.M., Taubenblatt, M.A. et al. (1991), *US Pat.* 5,061,070, and Taubenblatt, M.A. (1991), *US Pat.* 5,037,202, 379
- 97 Batchelder, J.S. and Taubenblatt, M.A. (1991), *Appl. Optics*, **30**, 33, 4972–4979, 379
- 98 Blackford, D.B. and Grant, D.C. (1993), *Microcontamination*, **11**, 2, 27–32, 66–67, Feb., 380
- 99 Grant, D.C. (1993), *Microcontamination*, March, 37–44, 380
- 100 Cummins, P.G., Staples, E.J., Thompson, L.G., Smith, A.L. and Pope, L.J. (1983), *Colloid Interface Sci.*, **92**, 189, 381
- 101 Cummins, P.G., Smith, A.L., Staples, E.J. and Thompson, L.G. (1984), *Solid-liquid separation*, ed J Gregory, publ. John Wiley for Soc. Chem. Ind., London, Ch. 12, 381
- 102 Chen, T.M., and Middleman, S. (1967), *AIChE Journal*, **13**, 989, 381
- 103 Coulaloglou, C.A. and Tavlarides, L.L. (1976), *AIChE J.*, **22**(2), 289, 381
- 104 Hazett R.L., Sechter, R.S. and Agarwel, J.K. (1985), *Ind. Eng. Chem. Fund.*, **24**, 101, 381
- 105 Kirou, V., Tavlarides, L.L., Bonnet, J.C. and Tsouris, C. (1988), *AIChE J.*, **34**, 283, 381
- 106 Calderbank, P.M. (1958), *Trans. Inst. Chem. Eng.*, **36**, 443, 381
- 107 McLaughlin, C.M. and Rushton, J.H. (1973), *AIChE J.*, **19**, 817, 381

- 108 Hancil, V., Rodd, V. and Reznickova, R. (1986), *ISEC*, **81**, 381
109 Sullivan, D.M. and Lindsey, E.E. (1962), *Ind. Eng. Chem. Fund.*, **1**, 87–93, 381
110 Rebelein, F. and Blass, E. (1986), *ISEC '86*, **11**, 387, Munich, 381
111 Semiat, R. and Duckler, A.E. (1981), *ISEC '81*, **27**, 148, 381
112 Plawsky, J.L. and Hatton, T.A. (1986), *ISEC '86*, IV–89, Munich, 381
113 Sprow, F.B. (1967), *AIChE J.*, **13**, 5, 995, 381
114 Hoffer, M.S. and Reznick, W. (1975), *Chem. Eng. Sci.*, **30**, 473, 381
115 Tamano, K. (1986), *Inst. Chem. Eng.*, **26**, 698, 381
116 Nanda, A.K. and Sharma, M.M. (1966), *Chem. Eng. Sci.*, **21**, 707, 381
117 Fernandes, J.B. and Sharma, M.M. (1967), *Chem. Eng. Sci.*, **22**, 1267, 381
118 Puranik, S.A. and Sharma, M.M. (1970), *Chem. Eng. Sci.*, **25**, 257, 381
119 Madden, A.J. and McCoy, B.J. (1964), *Chem. Eng. Sci.*, **19**, 506, 381
120 Mylnek, Y. and Reznick, W. (1972), *AIChE J.*, **6**, 505, 381
121 Tanaka, M. (1985), *Can. J. Chem. Eng.*, **63**, 723, 381
122 Verhof, F.H., Ross, S.L. and Curl, R.L. (1977), *Ind. Eng. Chem. Fund.*, **16**, 371, 382
123 Janjua, K.M. (1982), PhD Thesis, Univ. of London, 382
124 Goldmann, G. and Blass, E. (1984), *CHISA '84*, **14**, 382
125 Pietzsch, W. and Blass, E. (1987), *Chem. Eng. Technol.*, **10**, 382
126 Bae, J.H. and Tavlarides, L.L. (1989), *AIChE J.*, **35**(7), 1073–1084, 382
127 Smith, T.N. (1974), *Chem. Eng. Sci.*, **29**, 583, 382
128 Mitsis, T.J., Plebuch, R.R. and Gordon, K.F. (1960), *AIChE J.*, **6**, 505, 382
129 Holland-Batt, A.B. and Sawers, J.R. (1973), *Photographic Sci. and Eng.*, **17**(3) 295–8, 383
130 Raes, F. and Plomp, A. (1983), *J. Aerosol Sci.*, **14**(3), 394–6, 383
131 Winkelmayr, W., Reischl, G.P., Linder, A.O. and Bemer, A. (1991), *J. Aerosol Sci.*, **22**, 289–296, 385
132 Fissan, H., Hummes, D., Stratman, F., Neumann, S., Pui, D.Y.H. and Chen, D. (1995), *6th European Symp. Particle Size Characterization*, Partec 95, Nuremberg, Germany, publ. NürnbergMesse, GmbH, 391–400, 386
133 Miller, S.J., Dunham, G.E., Laudal, D.L. and Heidt, M.K. (1995), *6th European Symp. Particle Size Characterization*, Partec 95, Nuremberg, Germany, publ. NürnbergMesse, GmbH, 401–409, 386
134 Heidenreich, S., Büttner, H. and Ebert, F. (1995), *6th European Symp. Particle Size Characterization*, Partec 95, Nuremberg, Germany, publ. NürnbergMesse, GmbH, 411–420, 386

Field scanning methods of particle size measurement

10.1 Introduction

Field scanning methods are those in which the size distribution of an assembly of particles is inferred from the interaction between the assembly and a measuring device. In the simplest systems, the powder (or slurry) is probed or classified in order to generate a single point on the distribution curve. For example, one might monitor the 100 mesh percentage oversize from a mill in order to control a continuous milling operation. If the percentage increases, the residence time in the mill is increased in order that the product size remains unchanged.

Field scanning instruments are ideally suited to on-line analysis. Rapid, minute by minute, control of crystal size from a crystallizer; granule size from a granulator, product size from a milling operation; particle size from a reactor etc. can yield enormous dividends in terms of less wastage (i.e. more material in specification) and superior product quality.

One problem associated with implementing this technology is the need to build an interface between the process and the measuring instrument. This often requires a dilution step which may alter the size of the particles. In the case of crystallizer control, for example, it may be necessary to remove two streams from the crystallizer and filter one so that the mother liquor can be used as the diluent.

Process streams often operate at high flowrates and these have to be split in order to obtain an acceptable flowrate in the measuring device. This sampling has to be carried out with care in order to minimize sampling errors. Ideally, the whole of the process stream would be examined. Inserting a probe directly into a process line is usually not feasible due to servicing and downtime problems. It is therefore preferable to use a side-stream which can be isolated from the process stream.

A sophisticated on-line analyzer can cost around \$100,000 and the interface can easily double this cost. However a 1% increase in yield can pay back this investment inside a year, making on-line size analysis very attractive. At the present time retro-active fitting of size analyzers

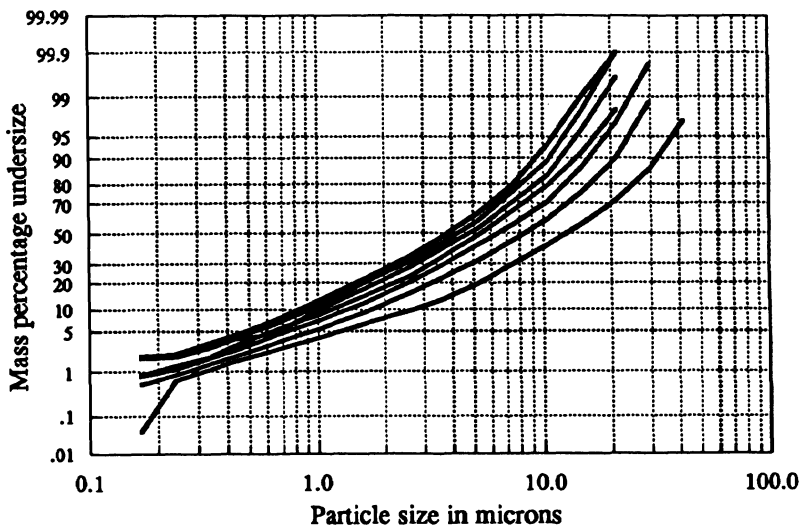


Fig. 10.1 Monitoring a sand milling operation using a Microtrac SPA. Samples were extracted at 2 hourly intervals.

is often necessary and one is often faced with space limitations. Designing these units into new process lines should greatly reduce cost and make their introduction more attractive.

10.2 Effect of comminution on particle size distribution

It is commonly found that comminution shifts the whole distribution to a finer size distribution, to form an homologous family of curves, and plotting particle size against milling time on a log-log scale generates a straight line. Figure 10.1 displays the results from a sand milling operation. These data are converted into a log frequency plot in Figure 10.2a and the changing percentile sizes are presented in Figure 10.2b. The distribution follows the well known type of comminution equation:

$$T = 127x^{-1.606} \quad (10.1)$$

which, on differentiation, becomes:

$$\frac{dT}{dx} = -\frac{204}{x^{2.6}} \quad (10.2)$$

This equation, relating milling time (which is equivalent to energy input, E) to particle size (x), has the same form as the relationships

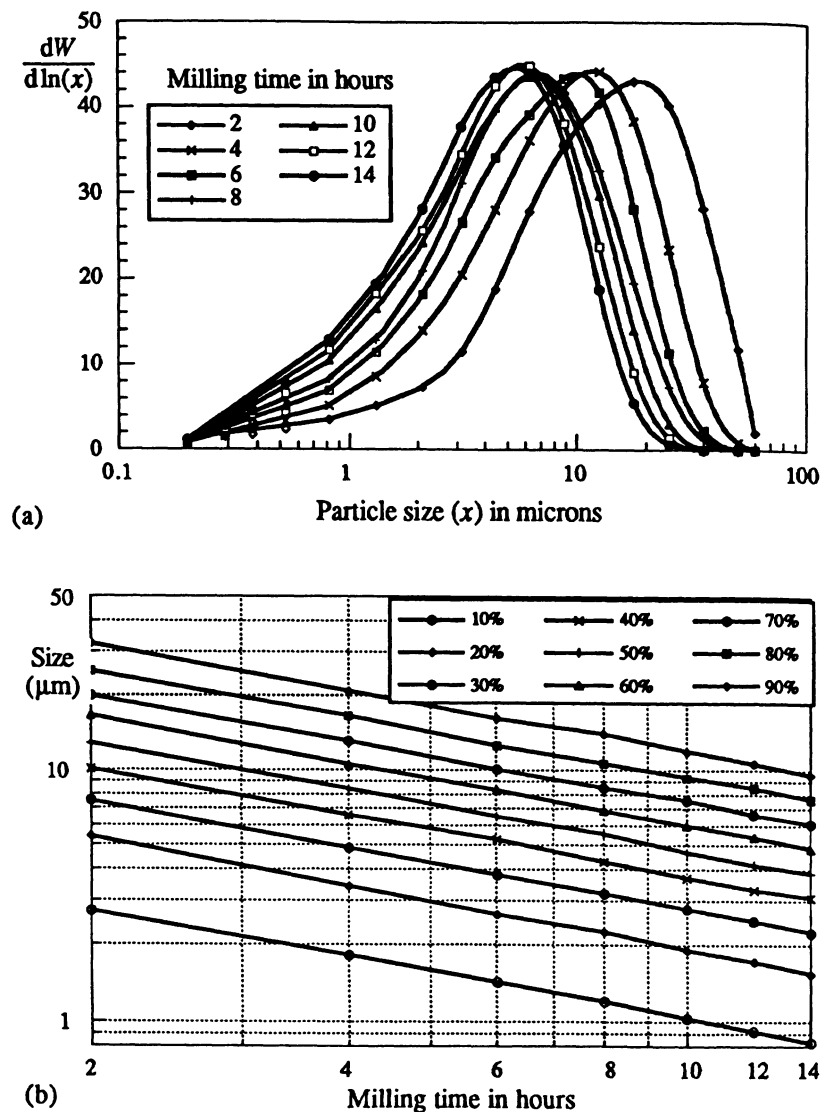


Fig. 10.2 Microtrac monitoring of a milling operation.

generated by Rittinger, Kick and Bond and discussed by Marshall [1].

The constant in the equation depends on the nature of the powder and its previous history, e.g. the initial size distribution, but the slope of the lines in Figure 10.2b depend only on the nature of the feed material

and the type of mill, i.e. the slope remains the same for repetitive operations using similar starting material.

Apart from the conclusion that the end point of a milling operation can be predicted, it may also be deduced that if a single point on the distribution curve is known, then the whole distribution can be found. This assumption led to the development of a range of single point particle size analyzers [2]. An alternative method for plotting such distributions is the Gaudin-Schuman plot where the cumulative weight finer than a given size is plotted against that size, with each scale on a logarithmic basis. For the majority of milled material the relationship between the two variables is linear except at the coarse end of the distribution. The distribution is characterized by two parameters; a distribution modulus, n (slope), and a size modulus, k . Again, n remains constant for consecutive grinding of the same material.

10.3 Single point analyzers

10.3.1 Static noise measurement

This technique has been applied to the measurement of the average size of milled silica powder (size range 2 to 5 μm) suspended in air [3]. A continuous sample is drawn from the product stream into a sampling probe and diluted with an air injector which also provides the driving force. The sample stream is then passed through a 'uni-flow' cyclone which splits the sample into two streams, a low concentration 'fines' stream and a high concentration 'coarse' stream. As the relative mass flow rates of the two streams depend strongly on the size distribution of the feed (at a given flow rate), an average size may be found from a measure of the two concentrations.

Most particles suspended in air carry an electric charge, particularly if they have passed through a highly turbulent process. A probe inserted into the stream will detect this charge as an AC voltage which is strongly dependent on concentration. The system was calibrated by feeding in samples of known mean sizes and recording the signals these generated for comparison with signals from unknown samples.

10.3.2 Ultrasonic attenuation.

The principle of this technique is that plane sound waves moving through a slurry are attenuated according to the size and concentration of the particles in the slurry, the spacing of the transmitter and receiver and other physical parameters in a predictable manner (Figure 10.3). In normal operation, two frequencies are used in order to isolate the size dependency from the concentration effect. The instrument, available as the Denver Autometrics PSM-100, 200, 300 and more recently 400, is pre-calibrated for the selected mesh size (100, 200, 300, 400) and the mesh read-out is proportional to the mass percentage less

than this size [4]. The instrument can operate at extremely high concentrations, up to 60% by weight, and has found its widest application in mineral processing plants for improved grinding circuit control. Since traces of air can lead to substantial attenuation losses a de-aerator is necessary and this increases the cost of the overall system considerably.

The attenuation is governed by the following equation:

$$I = I_0 \exp(-2\alpha x) \text{ for } \lambda \approx \pi D \text{ where } \alpha = f(c, D^3, \lambda), \quad (10.3)$$

λ is the wavelength of the sound wave, I_0 the incident intensity and I the transmitted intensity, c is the solids concentration in the slurry and D the particle diameter.

10.3.3 β -ray attenuation

The Mintex/RSM slurry sizer is based on the work of Holland-Batt [5–8] and has been subjected to rigorous investigation [9,10]. A slurry, having a weight concentration in the range 10% to 30%, flows through a rectangular tube at flow rates in the range 100 to 200 $\text{cm}^3 \text{s}^{-1}$, under a constant pressure head condition. In the center of the tube is a measuring cell fitted with windows and collimation plates top and bottom so that a β -ray transmission measurement can be made to quantify the concentration (Figure 10.4).

After passing through this section, the slurry flows through a single turn helix of the same dimensions. Centrifugal force causes the particles to separate according to size, the magnitude of the displacement being a function of size distribution. Two sets of windows and collimation slits are provided downstream of the helix to enable the solids concentration to be sensed. The source and detector are designed to traverse the cell so that they can be placed in any of four measuring positions.

A correlation exists between the solids concentration, the particle size represented by the percentage passing a 150 mesh sieve, and the difference reading between the two β -attenuation measurements and this is available in the form of a nomogram.

The signal from the scintillation counter can be used to control mill feed rate in order to compensate for changes in feed ore, grindability and feed particle size. Accuracies of 2% have been reported on Cornish granite, copper and iron pulps and nepheline systems in the size range 20 to 105 μm [11,12].

10.3.4 X-ray attenuation and fluorescence

This sensor (Figure 10.5) is based on the comparison of the absorption of two x-ray beams, one of which is sensitive and the other insensitive to variations in particle size [13–15]. Each sensing head is specific to a

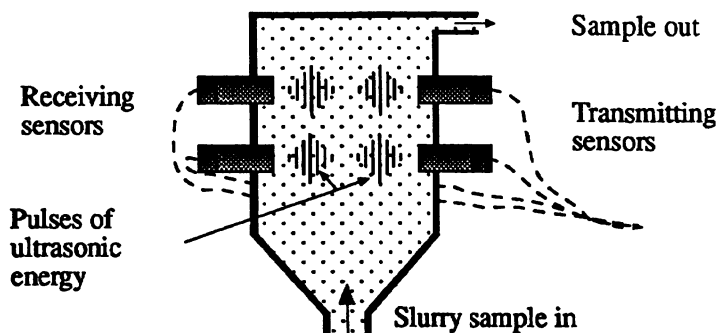


Fig. 10.3 The Autometric's PSM Analyzer.

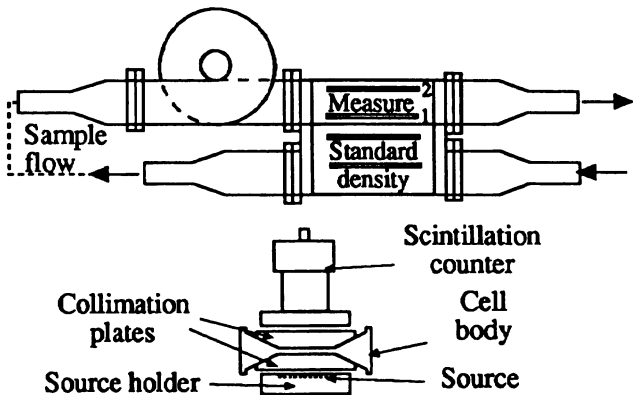


Fig. 10.4 The Mintex/Royal School of Mines slurry sizer.

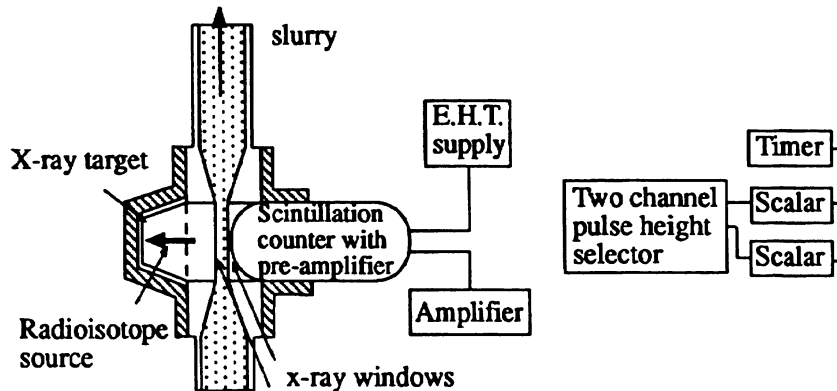


Fig. 10.5 Schematic diagram of the measuring head and associated electronics for the x-ray absorption particle size analyzer.

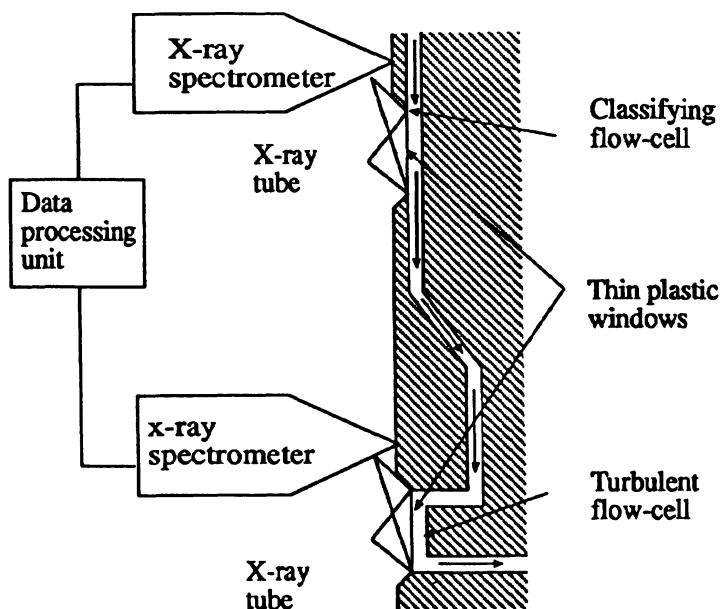


Fig. 10.6 Von Alfthan x-ray on-line size analyzer.

particular system since the relationship between the two beams is dependent on the composition of the solids in the slurry stream. The technique is limited to x-ray opaque material.

Von Alfthan [16] describes an on-stream x-ray fluorescence system which consists of two flow cells (Figure 10.6) through which the slurry passes. In the classifying flow cell, the slurry flows in a straight path behind a window; it then strikes an obstacle which causes slurry mixing as it enters a turbulent flow cell. The slurry in both cells is excited by x-rays and the resulting fluorescent radiation is a measure of particle size.

The system, sold as the Courier 300, measures both x-ray scattering and x-ray fluorescence and is primarily intended as a composition monitor. The measured data can be analyzed to give chemical composition, solids content and maximum particle size.

10.3.5 Counter-flow classifiers

Two instruments have been developed [17–20] for on-line measurement of flowing powders coarser than 100 µm in size. In the first instrument (Figure 10.7) a solid stream of particles from a process line is fed into an air elutriator which separates it into an oversize and undersize stream. The particle flow rate into the elutriator (F_{in}) is measured and the cut size for the elutriator adjusted so that the flow of

oversize particles out (F_{out}) equals 50% of the inlet flow. The elutriator cut size is then equal to the average size of the powder.

In the second instrument the flow rate is varied and the signal ratio of the two flowmeters (F_{out}/F_{in}) is inputted as the y-axis of an x-y recorder. The x-axis is reduced to the cut size for the elutriator. A sweep time of 40–60 s at flowrates of 2.4–3.0 g s⁻¹ gives a cumulative size distribution in the size range 100–700 µm.

10.3.6 Hydrocyclones

An ideal on-stream sizing device would sample the whole of the suspension and not include any special instrumentation. The nearest approach is to use a classifying hydrocyclone as these are easily installed and often form part of an industrial plant.

The method of using such a system depends upon the theoretical relationship between the size distribution of the feed with the weight of solids and the volume of water in the overflow. By measuring the flow rates and pulp densities, and assuming a size distribution law for the feed, a computer program can be written to give the modulus and index of the feed. Under normal operating conditions the present state of the theory of cyclone operation renders this impracticable [21], although it can be used under favorable conditions [22].

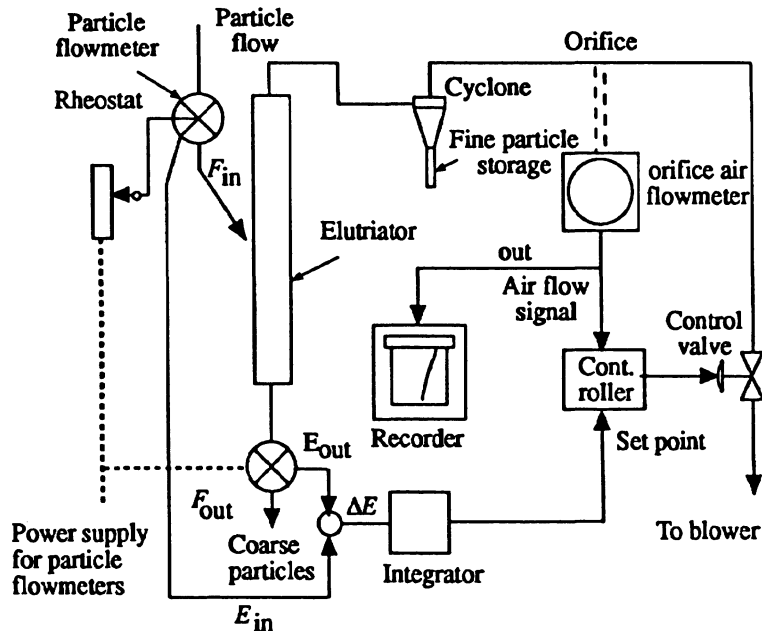


Fig. 10.7 Schematic diagram of an elutriator for determining average size.

Lynch *et al.* [23] proposed that the percentage less than some chosen mesh size in the cyclone overflow could be related directly to the D_{50C} parameter of the cyclone, provided that the size distribution of the feed to the cyclone does not change appreciably. This parameter is the size of classified particle which reports 50% to the overflow and 50% to the underflow and can be calculated from the operating parameters of the cyclone. In closed production circuits there may be marked changes in the size distribution of the cyclone feed and an empirical relationship has been developed [24].

The application of this technique requires very thorough analysis of the circuit and repeated checking of empirical equations. An alternative approach has been to accept the inherent difficulties of sampling and install smaller, more precise classifiers alongside the production classifiers [25]. The use of hydrocyclones for on-line analysis has also been investigated by Tanaka [26].

10.3.7 The Cyclosensor

This is a batch size analyzer [27] (Figure 10.8). An extremely dilute sample of milled ore is introduced, at a constant flow rate, to a coarse separator in the form of a tangentially fed cylindrical screen. The coarse fraction is allowed to settle and the fine fraction is further separated with an efficient hydrocyclone into a fine and a very fine

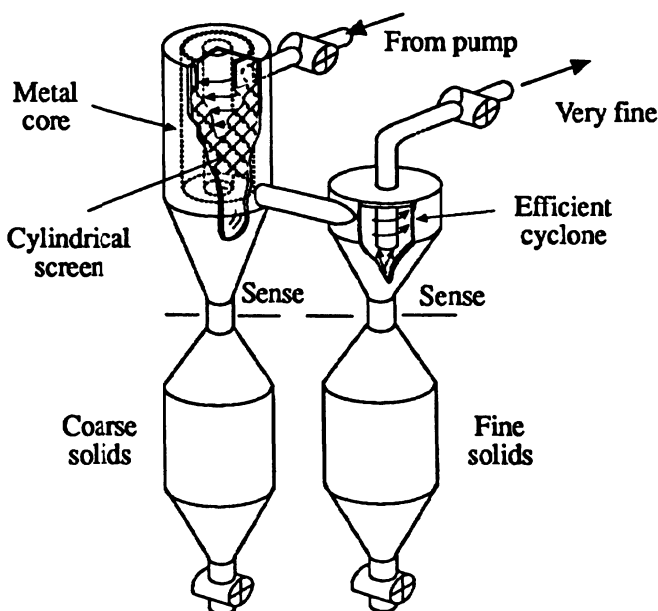


Fig. 10.8 The Cyclosensor.

fraction. The very fine fraction is discarded and the fine fraction is allowed to settle. The ratio of the times taken to fill the coarse and fine fraction collection vessels to indicated levels can be related directly to the particle size distribution. The cyclosensor has a sensitivity whereby a change of $\pm 1.8\%$ passing 100 mesh can yield a 7% change in the ratio of the settling times. The reproducibility is such that for the same feed rate of the same solids the ratio of times remains constant to better than 1% and an increase in feed rate of 30% has no effect on the ratio.

10.3.8 Automatic sieving machines

This automatic wet sieving machine (Figure 10.9) determines a single point on the size distribution curve in a few minutes without the need to dry samples [28,29]. The sieving vessel is first filled with slurry and topped up with water to a precise level to allow accurate determination of the mass of solids added (w_1) by application of Archimedes' principle. The fine fraction is next removed from the vessel through a discharge valve. Screening is hastened by propeller agitation and with ultrasonics to maintain the sieve mesh free of pegged material. The weight of the residue (w_2) is determined by further application of Archimedes' principle, and the fraction coarser than the screen size is given directly by (w_2/w_1) .

The ability to remove pegged material from the screen by the use of ultrasonics is of considerable importance. By this means, the open

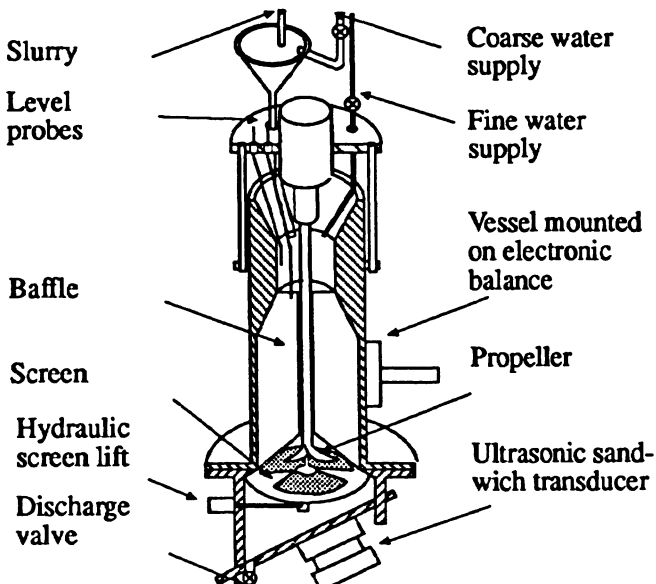


Fig. 10.9 Automatic wet sieving machine.

area of the screen can be held constant throughout the sieving process, and the ideal rate of sieving can be approached. It is of some interest to note that the rate of sieving under these conditions is found experimentally to be independent of the mass of solids to be sieved.

A simple theory has been developed to account for these results. If $w_i(t)$ is the weight of particles retained by the screen at any one time, which lies in the size range x_i to x_{i+1} , and if P_i is the rate of passage of unit mass of particles in this same size range through a sieve of aperture size a , and if first order kinetics on a mass basis are assumed, then:

$$\frac{dw_i}{dt} = -w_i P_i \quad (10.4)$$

Integrating and summing over all sizes gives an equation for $W(t)$, the total mass on the screen at time t :

$$W(t) = \sum_{i=1}^n w_i(0) e^{-P_i t} \quad (10.5)$$

or in integral form

$$W(t) = W(0) \int_0^{x_{\max}} e^{-P(x)t} \frac{dF(x)}{dx} dx \quad (10.6)$$

where x_{\max} is the maximum size of particle in the feed and $F(x)$ is the cumulative weight size distribution of the feed.

A suitable form for $P(x)$ has been given by Rendell [30]:

$$P(x) = b \left(\frac{a}{x} - k \right)^m \quad (10.7)$$

with k and m being constants close to 1 and 2 respectively; a being the screen aperture, in the same units as x , and b being a constant determined by the aperture shape, etc. Use of this function in equation (10.6) leads to a decrease in $W(t)$ with time very much as is found experimentally and the ratio $W(t)/W(0)$ is independent of $W(0)$.

It is interesting to note that the capacity of the rapid wet sieving device, expressed as screen charge mass per unit screen area, is more than an order of magnitude higher than that normally recommended for conventional dry test sieving. Comparisons with conventional sieving using a 'Ro-Tap' sieve shaker indicated that the accuracy of a laboratory manually operated device, at the 95% confidence level with

31 data points, was $\pm 2\%$ at 200 mesh with distribution moduli varying between 0.58 to 0.69 and oversize 200 mesh varying between 0 and 100%. Pulp densities were in the range of 10 to 30% by weight [25].

A description has been given of a technique using a two cell compartment divided by a screen [31]. The slurry density in the two compartments is determined using nuclear gauges to provide a single point on the distribution curve.

A fully automatic sieving machine which can determine seven points on the size distribution curve has also been described [32]. In this technique a pulsating water column was used with the application of ultrasonics and the charges were dried and weighed automatically.

10.3.9 Gas flow permeametry

Air, whose pressure varies sinusoidally with a specific amplitude and frequency, is forced through a moving bed of powder [17–20]. At a known height in the bed the attenuated and retarded air pressure is tapped by a pressure transducer, so that the amplitude and pressure drop are measured after being separated into the pulsating and steady flow components.

The amplitude attenuation of the pulsating pressure is related to bed porosity and specific resistance. Using the Carman-Kozeny equation, together with an analog computing circuit, after the system has been calibrated with materials of known porosity and permeability the average size of particle can be evaluated.

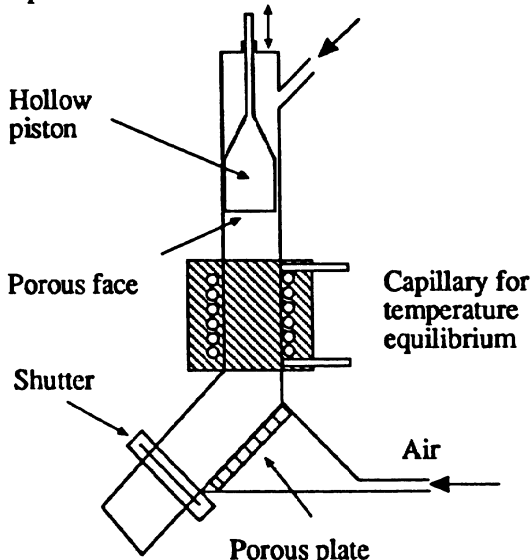


Fig.10.10 Cell for automatic determination of surface area [33].

The bed is packed from the top of a test cylinder and discharged by a vibratory feeder at the bottom after measurements have been taken. This enables a new bed to be packed and measured within minutes.

Air permeability has also been used to determine the surface area of cement [33]. A sample of cement is compressed by a porous piston into a cell. Air is passed through the bottom porous plate, through the sample and porous piston, into the atmosphere. The inlet pressure is automatically adjusted and recorded to give a known air flow rate and the surface area is evaluated from the inlet pressure. The cell is emptied automatically becoming ready for the next test (Figure 10.10).

Weiland [34] used a similar idea but based on the Blaine permeability method. An automatic weigher produced a packed bed of powder, of known voidage, in a standard cell. Air was drawn through the bed by the passage of water from one reservoir to another. After a certain volume of air had passed through the bed, measured by a certain volume of water flowing, the time required was converted to an electrical proportionality signal. The measurements were repeated every 4 min and the signals used to control the feeder to a grinding mill.

10.3.10 Correlation techniques

Correlation techniques can be used with signals from attenuation of radiation such as light and lasers but are mainly used for low concentration systems. The signals from two sensors in close proximity, situated in a flowing stream of slurry, are cross-correlated to give an autocorrelation function. Stanley-Wood *et al.* [35,36] found that this function obtained from alternating current transducers, initially designed to measure mass flow rate, gave a measure of the particle size of a sand/water mixture. A measure of mean size could be achieved by allowing the normalized signal from a correlator to be divided in two and passed through either high or low pass filters. This results in an inequality, due to variations in frequencies from large and small particles; the ratio of this inequality can be used to determine mean size after calibration. The particle size was between 70 and 2000 μm with a concentration between 10% and 30% by weight.

10.4 Low angle laser light scattering (LALLS)

10.4.1 Introduction

When light strikes a particle, some of it is absorbed, some is refracted, some diffracted and some transmitted (Figure 10.11). As a result, interference phenomena occur which give rise to scattering patterns with characteristic maxima and minima in intensity [37]. In order to describe fully the scattering pattern it is necessary to assume that the

particles are optically homogeneous and spherical and, in order to give independent, incoherent scattering, in a dilute random arrangement.

The scattering pattern is deconvoluted based on Mie or Fraunhofer theory to yield the unknown size distribution. Mie theory takes into account all the above conditions and requires a knowledge of both the real and imaginary (absorption) parts of the refractive index. Fraunhofer theory is limited to particles which are opaque or large compared with the wavelength of light. With Fraunhofer theory, only diffraction is considered, hence no knowledge of the particle refractive index is needed. The diffracted interference pattern is large compared with the geometric image, with smaller particles diffracting the light through larger angles than larger particles. The optical system is arranged on an optical bench whose length, therefore, needs to be greater for large particles than for small ones. An assembly of monosize, spherical particles gives an enhanced diffraction pattern. Azzopardi [38] states that this phenomenon was used for particle sizing more than 170 years ago and in 1918 a commercial instrument was developed for sizing blood cells [39,40].

Non-spherical particles are measured over all orientations and this causes a broadening in the measured size distribution. Textured particles tend to give enhanced weighting to the fine end of the distribution.

The measurement volume is controlled by the width of the laser beam (10–25 mm) and the path length in the sample cell. The number of large particles in a broad distribution is low, which requires an extended measurement time in order to obtain an accurate estimate of their frequency. Synthetic fibers have been found to give a bimodal log-normal distribution using LALLS and rod shaped particles a trimodal log-normal distribution (see Chapter 11). Other investigations of the response of LALLS to anisotropic particles have been carried out [41].

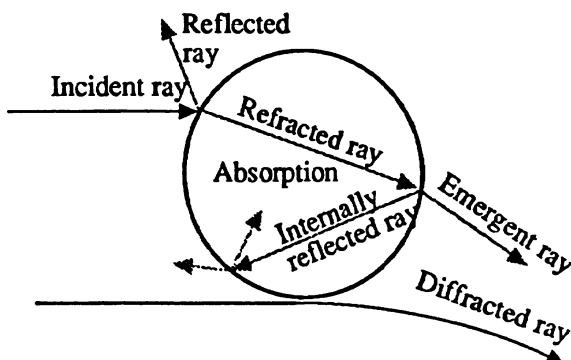


Fig. 10.11 Interaction of a ray of light with a spherical particle.

LALLS instruments collect light scattered from particles in a collimated laser beam by an array of detectors in the focal plane of the collecting lens. Early instruments used forward scattering angles up to 14° which limited the lower size to about a micron. Later instruments allowed angles up to about 40° through the use of converging incident beams and larger lenses, which extended the lower size to 0.1 μm. Some instruments incorporate additional information, such as polarization ratios and intensities at higher angles using extra detectors, in order to improve the characterization of particle size in the sub-micron size range with extension down as low as 0.04 μm. The optical system of the Helos acts as a telescope, which extends its upper size to 3,500 μm while retaining a lower size limit at the sub-micron level.

Samples may be introduced directly into the laser beam, as is the case with aerosols and metered dose inhalers, passed through a sample cell whose windows are transparent to the laser beam, or suspended in a cuvet under agitation. Dry powders are either blown through the beam or allowed to fall through it under gravity whereas particles in suspension are recirculated via a pump through the beam.

10.4.2 Theoretical basis for LALLS instruments

The angular distribution of light flux $I(\theta)$ for a single opaque spherical particle, as given by the Fraunhofer equation, is shown in equation (10.8) in terms of the Bessel function $J_1(\theta)$.

$$I(\theta) = I(0) \left[\frac{2J_1(\alpha\theta)}{\alpha\theta} \right]^2 \quad (10.8)$$

where $I(0)$ is the intensity of the incident beam, $\alpha = \pi D/\lambda$, D is the particle diameter and λ is the wavelength of light in the surrounding medium. For a distribution of particle sizes this becomes:

$$I(\theta) = I(0) \int_0^\infty \left(\frac{2J_1(\alpha\theta)}{\alpha\theta} \right)^2 f(D)dD \quad (10.9)$$

In early instruments, the detectors consisted of a series of half rings [42,43] (Figure 10.17) so that a matrix equation developed. Sliepcevich and co-workers [44,45] inverted this equation to obtain the particle size distribution. The equation was solved by assuming the distribution fitted a standard equation and carrying out an iteration to obtain the best fit. A matrix inversion was not possible due to the large dynamic range of the coefficients and experimental noise which could give rise

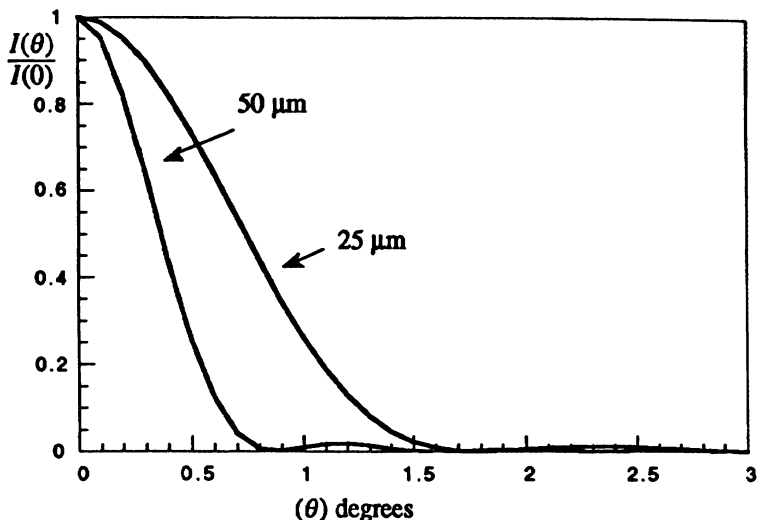


Fig. 10.12 The forward intensity distributions for single particles: note that 84% of the energy lies within the first minimum.

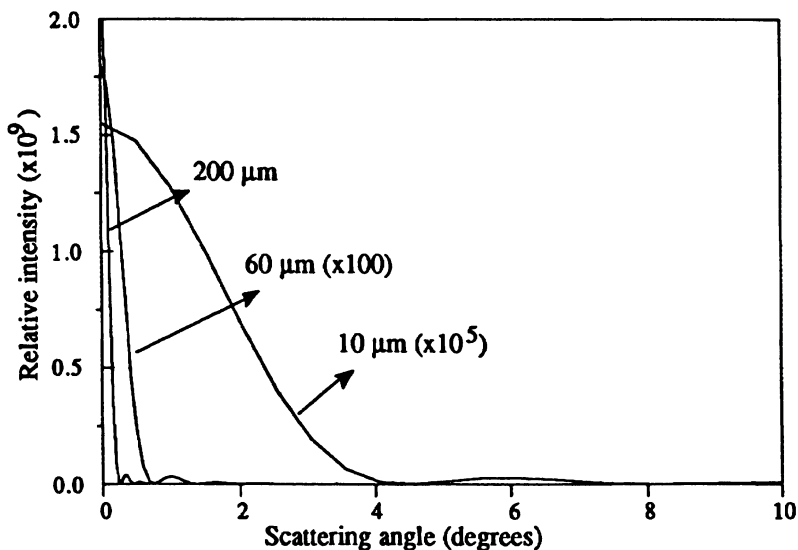


Fig. 10.13 Intensity distribution from three particles of size 10, 60 and 200 μm. The intensity scale is times 1 for the 200 μm particle, times 100 for the 60 μm particle and times 10^5 for the 10 μm particle [46].

to non-physical results. An inversion procedure which overcame these problems was developed by Philips [47] and Twoomey [48].

Boxman *et al.* suggest that more information can be obtained if the fluctuations in the signals from each detector are examined together with the mean values [49]. They note that this approach can identify whether the inaccuracy is due to insufficient sampling of the detector array or imperfections in the optical model.

Figure 10.12 presents a two dimensional graph of the pattern for latex beads in air ($\lambda = 1.55$) of diameter 50 and 25 μm . These curves are determined by the size parameter $\alpha = \pi D/\lambda$, where D is the particle projected area diameter in random orientation. The curve scale, on the vertical axis, decreases with increasing particle size, compressing to smaller angles, so that the large size results in a curve compressed by a factor of two compared to the 25 μm particles. Over a particle size range of 1000:1 the scale would change a thousand fold.

Figure 10.13 shows the relative intensities from three opaque particles in air of sizes 10, 60 and 200 μm ; this illustrates how the scattered flux in the forward direction falls off rapidly with decreasing particle size. The effect is also illustrated in Figure 10.14a together with the resulting diffraction pattern for a monosize distribution (Figure 10.14b).

Considerable differences exist between instruments, both in hardware and software, so that there is a lack of agreement in data generated by different instruments.

A commercially used means of measuring the scatter pattern is with a logarithmic line array detector, which has detector elements in a geometric size progression with each element larger than the preceding one by a constant multiple. The important feature of the logarithmically measured scatter pattern is that for two different particle sizes the shape of the elements remains the same but the position on the $\ln(\theta)$ axis is shifted. This shift invariant function $f(x)$ permits the use of iterative deconvolution to determine the particle size distribution from the scatter pattern measurement.

Typically, the pattern is measured 1000 times in 20s and the results averaged. Mathematically, a coordinate transformation converts the linear scatter function $I(\theta)$ to the logarithmic scatter function $f(x)$. This function is a convolution of the volume distribution of particles and the single sized shift invariant response functions for each size shifted according to the size. A method of solving the deconvolution is to divide the particles into size intervals and assume that each one will generate a diffraction pattern according to its average size, the intensity of which depends upon the number of particles in that size range. The diffraction pattern can then be manipulated by matrix methods to yield the size distribution. The measured data always contain random and systematic errors which have to be accounted for in the deconvolution step. Several mathematical procedures have been developed which can generate different solutions using the same initial data [50,51].

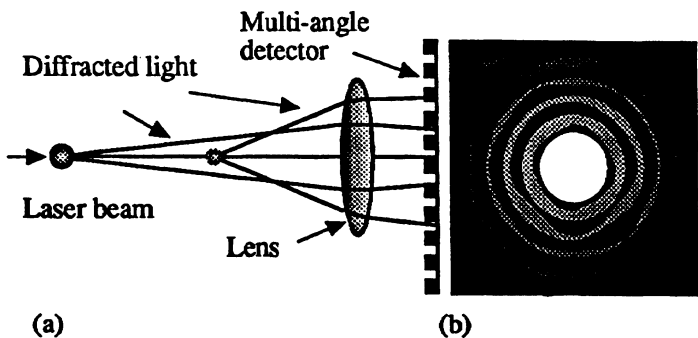


Fig. 10.14. (a) Particle size determines diffraction angle; (b) the diffraction pattern from a monosize distribution.

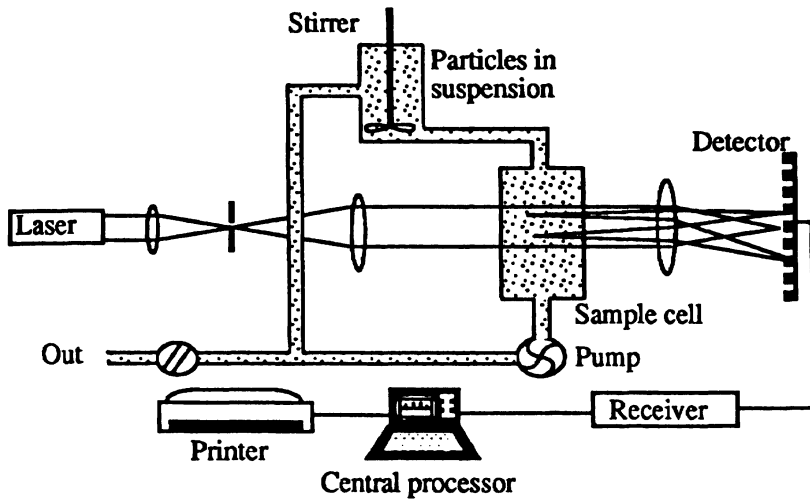


Fig. 10.15 The principle of low angle laser light scattering instruments.

The basic instrument consists of an analyzer that includes an optical bench that has a low-power visible wavelength laser, a lens train, a photodetector, a receiver and an amplifier/analog-to-digital converter linked to a microprocessor and monitor (Figure 10.15).

The possible size range of a LALLS instrument is linearly dependent on the wavelength λ and the focal length of the Fourier lens f . The lower limit for a He-Ne 632.8 nm source is 0.1 μm and this can be extended to 0.05 μm with a 325 nm He-Cd source; however this is 30 times more expensive. At the upper limit, a He-Ne laser at a

Table 10.1 Commercial low angle laser lightscattering instruments

Instrument	Size Ranges (μm)	Number of Intervals
Cilas 920, (U.S. agent, Quantachrome)	0.70 – 400	100
Cilas 940	0.50 – 2000	100
Cilas 1064	0.10 – 500	100
Coulter LS100Q	0.375 – 948	84
Coulter LS200	0.375 – 2000	92
Coulter LS230	0.040 – 2000	116
Fritsch Analysette 22 (U.S. agent, Gilson)	0.16 – 1250	62
Horiba LA-500	0.10 – 200	28,56
Horiba LA-700	0.04 – 262	32,64
Horiba LA-900	0.04 – 1000	74
Horiba LA-910	0.02 – 1000	80
Insitec ESPA systems	1.00 – 500	31
Jenoptic PSI-Z	8.00 – 2000	32
Leeds and Northrup Microtrac FRA (Upgraded to X100)	0.10 – 700	20
Standard Range Analyzer: SRA100	0.04 – 1000	
Series 9200; made up of: FRA; UPA ; SRA (Upgraded to Series 9300)	2 – 700	
Malvern Mastersizer E	0.10 – 600	100
Malvern Mastersizer S ; long bed	0.05 – 3500	100
Malvern Mastersizer S ; short bed	0.05 – 900	100
Malvern Mastersizer X; long bed	0.10 – 2000	100
Malvern Mastersizer X	0.10 – 600	100
Malvern Mastersizer Micro	0.30 – 300	32
Malvern Mastersizer Microplus	0.05 – 550	
Nitto LDSA-1300A	0.60 – 170, 0.9–255 1.80 – 510, 3.6–1020	
Nitto LDSA-2300	1.00 – 500	
Seishin SK Laser Micron Sizer PRO-7000	1.00 – 192	
Shimadzu SALD-1100	0.10–45; 1.0–	32
Shimadzu SALD-3001	150; 5–500; 0.10–2000	
Sympatec Helos Latest version has a stated upper size limit of 8750 μm .	0.10–35; 0.25– 87.5; 0.50–175; 0.50–350; 0.50– 875; 0.50–1750; 0.50–2625; 16– 3500	31



Fig. 10.16 Representation of a typical photosensitive silicon detector. The thin lines represent insulating gaps.

wavelength of 1152 nm extends the size limit to 6 mm. A discussion of the various alternatives has been presented by Witt and Röthele [52].

10.4.3 Commercial instruments

This principle has been applied by several instrument manufacturers (Table 10.1). A suspension of particles to be examined is illuminated by a low power laser. The scattered light is focused by a convergent optical system on to a multielement, solid state detector which usually consists of 32 semi-circular rings (Figure 10.16) or a linear array. An additional detector at the center is used to align the laser and measure the intensity of the unscattered light. The electrical output of the rings is proportional to the amount of light flux falling on them and the signals can be interrogated to obtain the size distribution generating them. A total size range of 0.1 μm to 3600 μm can be measured, though only a part of this range can be measured at one time. The measurable size range can be extended by the use of off-axes detectors and white light sources with 90° detection of polarized light.

The powder to be measured is dispersed in a bath, where it is stirred or/and ultrasonically agitated whilst being circulated through a glass measurement cell. The cell is illuminated with a laser beam and the forward scattered light is focused on the multielement detector with a Fourier transform lens. The signal which is derived from each detector element according to the intensity of the light falling on it is collected and digitized for high speed computer processing. Each instrument uses its specialized software to generate the size distribution from the signals and, since the algorithms differ, the size distributions generated also differ. Since one lens is only suitable for a limited range of particle sizes, several lenses are usually available to encompass a wider range. The technique can be used to analyze powders in suspension, liquids, droplets and particles dispersed in air.

The radial symmetrical diffraction pattern can be measured in other ways, for instance by a rotating optical filter with windows at different

radial distances, such as was used in the Microtrac Small Particle Analyzer [53].

Some instruments combine LALLS with 90° scattering at three wavelengths and orthogonal polarities to extend the size range to a lower size than is usually assumed possible for forward light scattering alone. Others use off-axis lasers and detectors to extend the size range.

Cilas 920 measures in the size range 0.7 to 400 µm without changing the optics. It includes accessories for measuring dry powders and automatic feed and analyses of up to 28 samples. It has the capability for displaying particles in the 10 to 400 µm range using a CCD camera.

Cilas 940 measures in the size range 0.5 to 2000 µm without changing the optics. It includes accessories for measuring dry powders and automatic feed and analyses of up to 28 samples. It has the capability for displaying particles in the 10 to 400 µm range using a CCD camera.

Cilas 1064 has high resolution, giving information over the size range 0.1 to 500 µm in one shot, due to a double sequenced laser system (two lasers at different incident angles) and 64 separate silicon detectors to give 100 size channels of data. The benefits of such a system include coverage of a wide size range with a small optical bench structure. The diffraction pattern is compared to a known powder and the size distribution calculated.

Coulter LS100 uses polarization intensity differential scattering (PIDS), a patented technology, to extend the lower limit to 0.1 µm and employs 126 detectors to measure the scattered light. Multiple optical trains and a wide angle detector array are used so that the instrument can simultaneously capture light diffracted at high angles from small particles and at small angles by large particles. Measurements from 0.1 to 1000 µm can be made in a single run [54].

Coulter LS 200 can measure particles from 0.375 to 2000 µm without changing optics or settings with a resolution into 116 size channels.

Coulter LS 230 has eight more detectors which extends the lower size limit down to 0.04 µm .

Ancillaries include a micro-volume module, a hazardous fluid module and a dry powder module. Their small volume module uses less than 125 mL of diluent. The micro volume module has a total volume of 12 mL: this has an internal stirring mechanism to keep particles suspended during analyses. The automatic hazardous fluids module can be supplied with a microtip eight power ultrasonic probe to keep the particles dispersed. The dry powder module analyzes both free flowing and cohesive powders covering the size range from 0.375 µm to 2000 µm.

Fritsch Analysette 22. The outstanding feature of this instrument is its convergent laser beam, with the broad measurement range of 0.16 to 1250 µm which can be covered in a single pass with no need to change

optical elements. Moreover, by moving the measurement cell in the beam the complete range can be divided into over 400 individual size ranges starting at 0.16 to 23.7 μm . The instrument is available in four versions; A(dvanced), C(onvenient fully automated), Economical) and P(rofessional).

Horiba LA-500 is an economical analyzer based on forward scattering Fraunhofer theory and covers the limited size range from 0.1 to 200 μm .

Horiba LA-700 is a more sophisticated instrument which employs side and back scattering detectors as well as forward scattering detectors. By using a tungsten lamp in conjunction with a He-Ne laser the lower limit is reduced to 0.04 μm to cover the range 0.04 μm to 262 μm with no change in lens.

Horiba LA-900 extends the upper range to 1000 μm by the use of a long focal length lens to cover the range 0.04 to 1000 μm with no need to change lenses.

Horiba LA-910 extends the lower size limit down to 0.02 μm . Small angle light intensity is measured using a condenser lens to condense the light on to a ring-type detector. Detectors are located at the side and rear to measure light scattered at larger angles. The measurable range is extended with the use of a short wavelength tungsten lamp in addition to the He-Ne laser beam. Up to three different dispersing media can be stored in the analyzer's reservoir unit which automatically injects the right amount of dispersant into the sample. It employs an auto-cycle agitation, ultrasonic dispersion, circulation and measurement. The auto sampler can make continuous measurement of up to 24 different samples. Minute quantities of material can be analyzed in the optional fraction cell. The unit includes a PowderJet dry feeder capable of feeding millimeter size powders and dispersing cohesive powders to sizes below 1 μm . Horiba claim a higher resolution than similar devices by using repetitive calculations instead of the more conventional matrix method.

Insitec EPSC is covered in detail in section 10.11. They are laser based instruments for in-line particle measurements which provide information on particle volume concentration and size distribution. Unlike other instruments operating on this principle, the EPSC can perform direct measurements of particle-laden gas flow stream provided the concentration is within operating limits.

Leeds and Northrup Microtrac SRA 100 (Standard Range Analyzer) is a low cost instrument which covers the size range of 2 to 700 μm using either a small volume (250 mL) recirculator or a dry powder feeder ($10\text{--}20 \text{ g min}^{-1}$).

Leeds and Northrup Microtrac FRA (Full Range Analyzer), has extended the lower size by using an off-axis low angle array with a separate collector lens in conjunction with the logarithmic line array detector.(Figure 10.17)

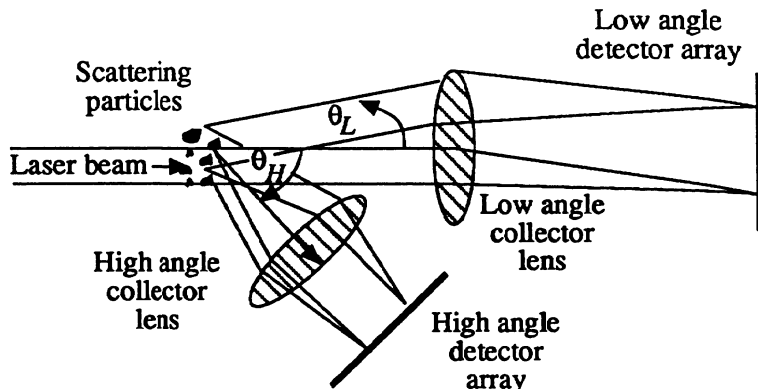


Fig. 10.17 Low angle on-axis and high angle off-axis array as used with the Microtrac Full Range Analyzer.

Leeds and Northrup Microtrac X100 system uses three lasers to measure scattered light at angles up to 160° with resolution from 0.04 to 1000 μm . The use of three lasers provides superior resolution in the sub-micron region so that modes smaller than 0.5 μm can be more readily detected and resolved. An automated small volume recirculator accessory provides efficient sampling. A photograph of this instrument is presented in Figure 10.18.

The Leeds and Northrup lower size limit is extended in the range 0.003 to 6.5 μm with the addition of the Ultrafine Particle Analyzer which operates using photon correlation spectroscopy in the controlled reference mode.



Fig. 10.18 The Leeds and Northrup Microtrac X100

There are two types of Mastersizer instruments; the Mastersizer Micro and the Mastersizer E, which are low cost instruments for repetitive analyses; and the modular series of Mastersizer S and Mastersizer X, the ultimate in resolution and dynamic size range, which are required when samples in the form of aerosols, suspensions and dry powders need to be measured. Mastersizer X provides a selection of small size ranges using a variety of interchangeable lenses whereas the Mastersizer S provides a wider dynamic size range covered in a single measurement. For powders which are to be suspended in a solvent, emulsions, suspensions and particles in liquids there are small volume cells which require as little as 15 mL of dispersant. Where a material is either valuable or toxic the Malvern Small Volume Flow Cell, with a sample volume of 50–80 mL and full sample recovery, can be used. The X-Y sampler is a 40 sample accessory for either dry or wet samples. Malvern also offer a free fall dry powder feeder, a dry powder feeder, an automated dry powder feeder and an aerosol mounting unit.

The Malvern lower size limit is extended to the range 0.01 to 3 μm with the addition of the Autosizer, which operates using fixed angle photon correlation spectroscopy, and this is extended to 0.001 to 5 μm with the more sophisticated System 4700.

Malvern Mastersizer X operates in the size range 0.1 to 2000 μm . A wide choice of modules can handle dry powders, suspensions, emulsions, aerosols and sprays in manual or fully automatic mode.

Malvern Mastersizer S uses Mie theory to cover the size range 0.05 to 900 μm using a single lens, and up to 3500 μm with an extended range system. Scattering angles from 0.01° to 150° are detected in order to cover this wide size range. The system handles measurements of particles, droplets or gas bubbles.

Mastersizer Micro, which uses a 'folded optics' configuration, is the most compact LALLS instrument presently available. In its basic form it has a size range of 0.3 to 300 μm but the *Mastersizer Microplus* extends this range to 0.05 to 550 μm . This instrument is intended where low sample throughput, a limited size range or well defined user needs makes the flexibility of the more sophisticated versions unnecessary.

Mastersizer E is a fixed configuration model to lower cost. A range of small volume accessories are available along with the standard Mastersizer E tank which is suitable for volumes of 1 L. The wide size range of 0.1 μm to 600 μm makes it ideal for routine analysis and quality control.

Earlier versions comprise the Series 2600 and 3600 and Mastersizer R/IP on-line particle size analyzer. The Malvern 2200 was a droplet and spray particle analyzer and the Fibersizer 600 was designed for fast automatic measurement of fibers in the 4 to 64 μm size range with a resolution of 0.25 μm .

Nitto LDSA-1300A covers the size range 1 to 2000 μm and the *LDSA-2300A* covers the size range 1 to 500 μm .

Seishin PRO-7000 laser micron sizer operates in the measurement range 1 to 192 μm with ancillaries for dry powder feeding and automated analyses on 20 samples. The PRO-8000 is an on-line system for either wet or dry processes.

Shimadzu Sald 1100 combines Mie, Fraunhofer and 90° scattering theory to cover three size ranges from 0.1 to 500 μm . The size range is extended to 2000 μm with the *Sald 3001*.

Sympatec Helos is a multi-range instrument from 0.1 to 3500 μm . The ancillary Rodos is a unique dispersing system for both cohesive and free-flowing dry powders [55]. The powder is fed from a hopper into a rotating channel where the excess is skimmed off and the remainder compacted. It is then transported into an eductor using suction and a rotating brush. Further dispersion can be carried out by impacting the powder against inclined targets in the eductor. The brush disperser has been compared with a pin mill disperser with sub-micron powder feed [56].

Ancillary Equipment: Most instruments are based on the analysis of circulating wet suspensions. This set-up is unsuitable for brittle material and many manufacturers provide agitator cells to reduce breakage. Waste disposal is a major problem with some materials and this is reduced by the use of small volume cells (< 125 mL). Cells are also provided for corrosive liquid systems. Instruments can be set up to analyze falling streams of dry powders; this is particularly suitable for brittle or soft (wet granules) materials. Deagglomerators are often provided for sticky dry powders.

LALLS are being used increasingly for rapid off-line and also on-line size analysis. The latter requires an automatic sampling device which takes part of the process slurry and dilutes it to the required concentration for the analyzer. The dilution unit can be quite complex; when the instrument is hooked up to a crystallization unit for example it is necessary to filter some of the mother liquor and use that as the diluent. The Mastersizer on-line analyzers, the MS200/IP series have the same 0.1-600 μm overall and sub-ranges as the laboratory analyzers. For a wider overall range the MS200/IP systems extend from 0.1 to 2000 μm . Sympatec manufacture an on-line system extending from 5 to 3500 μm or more. A cell has also been described for measuring the fines outlet in an air classifier [57].

The instruments tend to be easy to operate and yield highly reproducible data. Data presentation varies from instrument to instrument and generation to generation, each new model being a great improvement on its predecessor. The general tendency with non-spherical particles is to oversize the coarse end of the distribution and assign an excess of particles to the fine end and, in so doing, broaden the distribution. The instruments are particularly useful with powders that are difficult to disperse since such powders can be incorporated into a liquid containing a dispersant and close loop circulated whilst

undergoing ultrasonic probing. Analyses are taken every few minutes until the measured size distribution stabilizes.

As stated earlier, the mathematics of the single-event Fraunhofer diffraction of an on-axis laser beam by a sphere was used in the development of this technique [58]. The assumption of single scattering is adequate for accurate measurement so long as the light obscuration by the particle field lies within the range 5-50%. Although measurement at low concentration is desirable it is not always possible; with industrial sprays, for example, size measurements may have to be made for light obscuration values in the range 90-99%. The more that multiple scattering occurs, the more the particle size distribution is biased to smaller sizes if single event theory is wrongly used.

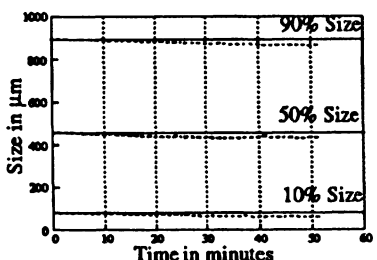
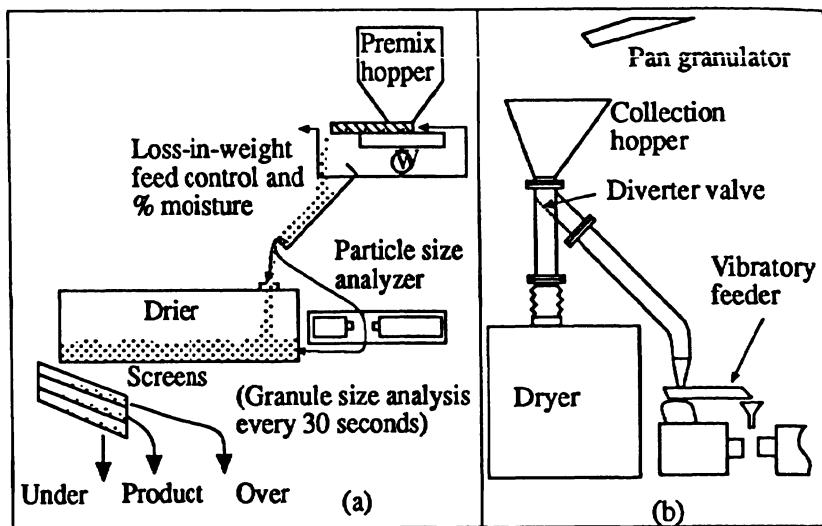
Comparison tests between the PSS Accusizer 770 (light blockage), API Aerosizer (time of flight) and LALLS instruments indicated that the LALLS instruments gave results which differ from each other and from microscopy whereas the other two instruments gave results in agreement with each other and with microscopy [59]. The effect of multiple scattering has been studied by several researchers [60,61]. Solutions, in the form of empirical equations, have been provided for Rosin-Rammler and log-normal distributions [62]. This has since been extended to a 'model-independent' case [63]. Fraunhofer theory does not apply if the refractive indices of the particles and the fluid are similar. Fraunhofer theory applies when a plane wave front of monochromatic light is diffracted by an opaque particle, much larger than the wavelength of light, and focused by a lens on to a detector. For low relative refractive indices it is possible for light to pass through the particle and the transmitted light then interferes with the diffracted light to produce the so-called 'anomalous diffraction patterns'. If no correction is applied an erroneously high percentage of small particles will be predicted. Experimental and theoretical verification of this effect has been reported [64]. An experimental study has also been carried out on the on-line monitoring of clear and opaque particles. [65]

The need for maintaining constant temperature was emphasized since this affects the length of the light path in the measurement cell and the particle. Considerations such as this are particularly important when studying crystal growth [66].

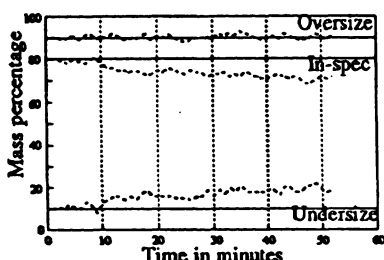
A standard test method for calibration verification of laser diffraction particle sizing instruments using photomask reticles has been introduced by the American Society for Testing and Materials [67-69]. The test sample consists of a two dimensional array of thin, opaque circular discs deposited on a transparent disc. The test method is designed to verify instrument performance on an ongoing basis, to compare one instrument performance with that of another and to provide error limits for the instrument tested.

Figure 10.19 illustrates the installation of a low angle laser light scattering instrument in a pan granulation process. A major problem in

retro-fitting equipment such as this is the dearth of suitable installation positions. In cases where there is insufficient room for a commercial sampler, a special unit has to be designed (Figure 10.19b). Since segregation is almost certainly present it is necessary to design a system that takes the whole of the stream for very short time intervals. This 'bite' is fed to a hopper and thence to the analyzer via a vibratory feeder such that the complete sample is fed through the system in about 20s. The sampler senses when the concentration is adequate and commences analyzing; when the concentration fell below the required level the analysis is terminated. During the measurement time several hundred analyses are carried out; the instrument generates a weighted average and stores the data.



(c)



(d)

Fig. 10.19 On-line installation of particle size analyzer.

In this illustration, six parameters were forwarded to the control room for display; the 10%, median and 90% sizes, the mass percentage within specification, the mass percentage oversize and the mass percentage undersize. Figure 10.19c and 10.19d show a process going out of spec. due to generation of excess fines. An increase in yield of 1% can be worth hundreds of thousands of dollars per year and pay-back is rapid. Using laboratory type equipment to measure the dried product gives a time lag of hours. Minute by minute control of such variables as the slope of the pan, the amount of water and the positions of the sprays maximizes the yield.

10.5 Optical incoherent space frequency analysis

The method for obtaining particle size distributions using optical incoherent space frequency analysis is detailed in [70,71] and has resulted in the development of a low price, robust, on-line dry powder measuring system, the Jenoptik PSI-Z, which covers 32 size intervals in the range 8 μm to 2 mm.

The basis of the method is to replace the coherent light source used in LALLS with an infinite number of point light sources which emit light in an incoherent way with respect to each other. The intensity of radiation resulting from this two dimensional radiator is measured using a point detector located on the optical axis. This is equal to the surface integral of the Fourier power spectrum and can be measured with the aid of wedge-ring detectors in a coherent optical set-up. In this way, the incoherent arrangement consists of several switchable two dimensional light emitters together with a single detector on the

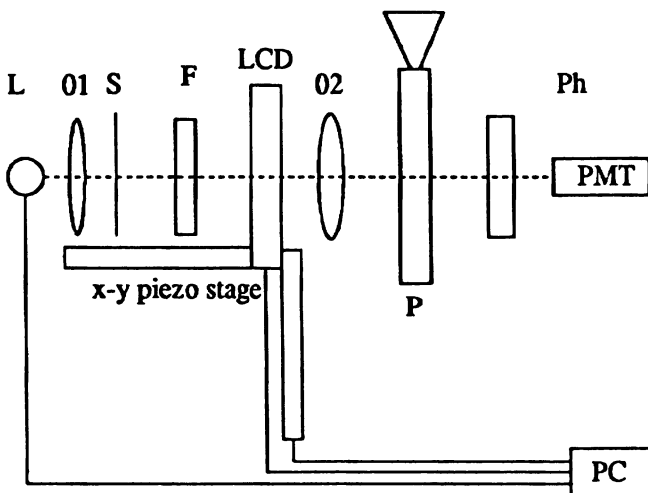


Fig. 10.20 Experimental set-up of PSI-Z.

optical axis. This allows the measurement of the same intensity characteristics as in a coherent arrangement.

Figure 10.20 shows the principle set-up. The incoherent light source consists of a 25 W halogen lamp L with voltage stabilization, including condensor system O1, diffusing screen S and filter F. The variable geometry, binary two-dimensional emitter consists of an addressable liquid crystal modulator (LCD) with back lighting. The structural organization of the transparent electrodes within the LC modulator can create ring segments with transmission controlled by the help of the corresponding voltage. The response time of the individual LC segments is less than 3 ms when the electrically controlled birefringence of liquid crystals is utilized [72]. A photomultiplier, with a micro pinhole in front of it, serves as a point light detector with diameter variable up to 300 μm with a resolution of 1.2 μm . The LCD modulator is projected on to the detector by transformer objective O2. A piezoelectric x-y stage adjusts the central segment of the LC modulator precisely on the micro-pinhole. The material is fed through the optical path with sample feeding device P.

A personal computer (PC) controls the measuring arrangement. The evaluation algorithm in the PC calculates the ring intensity values of the percentage of certain particle size classes by comparison between measured values and predetermined theoretical values. The intensity values are converted into a size distribution by an iteration process.

10.6 Small angle x-ray scattering (SAXS)

This effect depends upon the difference of electron density between particles and their surroundings, and the measured sizes are of primary particles rather than the external aggregate size. Thus samples are relatively easy to prepare and do not require pre-dispersion. The operating size range is from 1 to 300 nm and it breaks down at concentrations over about 3% due to inter-particle interference. A necessary requirement is near sphericity of the particles. The electron density also needs to be high. SAXS cannot distinguish between pores and particles and is therefore not suitable for porous particles. The theory is similar to that for LALLS, the forward scattered flux being related to the size and size distribution of the particles in an x-ray beam [73]. Two approaches have been described for calculating size distributions from SAXS data, the successive logarithmic graphical (SLG) [74,75] and the dividing distribution function (DDF) [76]. The method has been used extensively on metallic and ceramic powders, colloidal suspensions and precipitates.

10.7 Ultrasonic attenuation

In-line measurement of particle size distribution is essential in order to maximize production capacity and product quality. Ultrasonic

attenuation is emerging as a technique, with capabilities beyond those of light scattering, to fulfill this need. In addition to the needs of industry for compact, robust instrumentation, this method is capable of operating at high concentrations, thus eliminating the need for an expensive dilution step, which may alter the very properties one wishes to measure.

Originally developed as the PSM single point device (section 10.3.2), the scope of the technique has been greatly enhanced by the use of a range of frequencies to generate a series of relationships between particle size, mass frequency and wavelength. These can be solved by nonlinear mathematical programming techniques to generate the full particle size distribution. The program is linked to the PSM instrument via a computer based signal processor for on-line data analysis and graphics display and is marketed by Proassist as the SD-21.

The following expression is used for the attenuation (in decibels) $\alpha(D, \omega)$ due to a narrow size distribution of particles with a size D , solids concentration by volume c and distance between transmitter and receiver x :

$$\text{Total attenuation: } \alpha(D, \omega) = 22.05 \left[A + \frac{1}{B+C} \right] cx \quad (10.9)$$

$$\text{Viscous losses: } A = \frac{18v^2(1+v)(\rho-1)^2(\omega/v)}{81(1+v)^2 + v^2[9 + (\rho+0.5)]^2}$$

$$\text{Scattering losses: } B = \frac{12}{(\omega/v)^4 (D/2)^3}$$

$$\text{Diffraction phenomena: } C = (\omega/v)^3$$

$$\text{where } n = \frac{D}{2} \sqrt{\frac{\omega}{2k}}$$

- ω is the sonic wave frequency (s^{-1});
- k is the kinematic viscosity of water (Stokes);
- ρ is the density of the particles (gcm^{-3});
- v is the velocity of sound in water (cms^{-1});

Velocity differences between a viscous liquid and suspended particles result in a heat loss at the surface of each particle and therefore an absorption of energy. The viscous losses term can be derived from Stokes' equation for the effect of viscosity on a spherical pendulum

swinging in a viscous liquid. This term predominates when the ratio of λ to D is so high that particles do not follow the liquid movement.

The scattering losses mechanism is an apparent absorption of energy due to a redistribution of energy. Energy losses occur because of interference between radiated and scattered waves or simply because a scattered beam goes outside the wave path of the main beam and is not picked up by the detector. Essentially, in the diffraction region the wavelength is so small compared to particle diameter that sound behaves in the same way as light. Each particle casts a shadow so that the attenuation is proportional to the square of the particle diameter.

By superposition, the attenuation due to a polydisperse distribution is:

$$a_T(\omega) = \int_0^{\infty} \alpha(D, \omega) f(D) dD \quad (10.10)$$

This may be written in discrete form as:

$$a_T(\omega) = \sum_{i=1}^N \alpha(D_i, \omega) \Delta F_i \quad (10.11)$$

The problem reduces to finding the size distribution $f(D)$ and the solids concentration c given measurements of the total attenuation $a_T(\omega)$. The problem is difficult because of inherent instabilities in the inversion of the transform.

Herbst and Alba [77], in developing the Proassist, measured the attenuation of the sound at ten different frequencies from 0.5 MHz to 6 MHz to retrofit five points on the size distribution instead of only one. They discretized the above equation for narrow size fractions where ΔF_i is the fraction of particles in the narrow size range D_i to D_{i+1} and used a mathematical programming technique to find the set of fractions (i, \dots, N) and c which minimized the objective function ϕ where:

$$\phi = \sum_{j=1}^N [\alpha_{T_{\text{observed}}}(w_j) - \alpha_{T_{\text{theoretical}}}(w_j)]^2 \quad (10.12)$$

$$\phi = \sum_{j=1}^N [\alpha_{T_{\text{observed}}}(w_j) - \alpha_{T_{\text{theoretical}}}(w_j)]^2 \quad (10.13)$$

Alba [78] reported on an extension of this technology and termed it the Ultraspec™ particle size analyzer [79]. The prototype laboratory

analyzer covers the size range 0.01 μm to 1,000 μm at a volume concentration range of 0.1% to 70% employing a frequency band of 1MHz to 2000MHz. A mathematical model (Allegra-Hawley) predicts the attenuation of ultrasonic waves as a function of frequency for each particle size distribution and concentration. Some mechanical, thermodynamic and transport properties of both phases are needed. The relationship between the size, concentration and frequency is obtained from the solution of the ultrasonic wave propagation equations synthesized in matrix form [80]. The technique has been extended to measurement of undiluted emulsions [81] and an on-line system has also been tested [82]. The flow cell for the on-line system consisted of two transducers, one stationary and one that could be moved to give different acoustic path lengths. Three distinct concentration regimes were found. For concentrations below 5% by volume the attenuation at each frequency, from 2 to 50 MHz, was found to be proportional to slurry concentration. In the intermediate regime, 5 to 10% by volume, the observed attenuation was higher than expected. A third regime, at greater concentrations, was found to have attenuation significantly lower. Although the attenuation spectra could be predicted using the A-H model it was found necessary to assume a log-normal particle size distribution to determine the particle size from the attenuation data [83]. This system has been acquired recently by Malvern and a commercial version is envisaged.

The Pen Kem System 7000 Acoustopheretic Titrator, based on the measurement of colloidal vibration potential arising from the motion of suspended solids relative to the suspending medium when subjected to a sound field, was the first commercial instrument capable of monitoring zeta potential of concentrated solids.

The system was extended for the measurement of sub-micron particle size distributions in concentrated slurries [84] which resulted in a prototype instrument, the AcoustophorTM Penn Kem 8000 system. With this system the acoustic attenuation is measured at several discrete frequencies between 1 and 100 MHz. At these frequencies viscous energy dissipation of the sound wave is the dominant phenomenon for sub-micron, rigid particles. The authors claim that this system is capable of measuring particle size distributions in the size range 0.01 to 100 μm for slurry concentrations at volume concentrations as high as 50%. They report experimental work with an on-line system using titanium dioxide at volume concentrations from 3.5% to 42.3%. Quantitative comparison of data was carried out at eighteen frequencies and eleven concentrations by volume [85,86]. Theoretical work resulted in the development of a unified coupled phase model which successfully predicted the experimental data for suspensions, emulsions and aerosols [87].

To illustrate the capability of this instrument, two high purity alpha aluminas having log-normal distributions were analyzed separately and

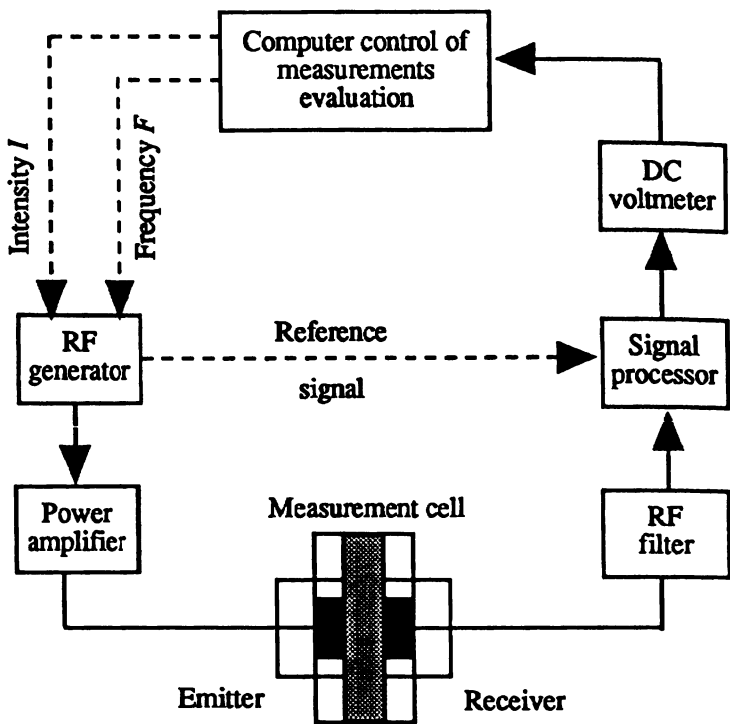


Fig. 10.21 Schematic representation of the experimental apparatus for ultrasonic spectroscopy.

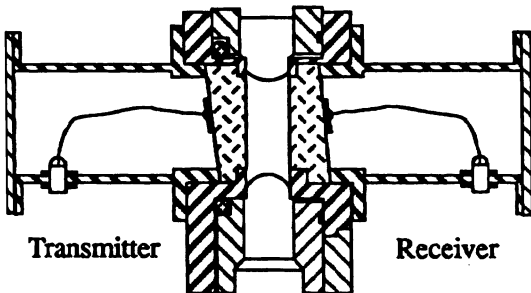


Fig. 10.22 Simplified presentation of the Sympatec Opus.

as a 50:50 mixture. Results clearly demonstrated the ability of this technique to resolve the original component distributions from a mixture of the two powders [88].

Riebel and Loeffler [89] obtained an acoustic attenuation spectrum with one transducer pair to infer the particle size distribution. Solids concentrations and particle size distribution were obtained using both

Phillips-Twomey algorithm and relaxation method. The PTA gives a least squares solution by simple linear matrix operations to yield a numerical inversion from the attenuation spectra to the size distribution and concentration. This works well in the presence of systematic errors such as concentration fluctuations whereas errors arising from inaccurate extinction data often give negative values. Iterative solution algorithms use a priori knowledge to correct for this. However Riebel and Loeffler showed that the relaxation method, though slow, gave the most reliable results but that its use on-line requires a larger computing capacity. Narrow and broad size ranges of glass beads were analyzed. They found that concentration effects were less important than with laser diffraction with little deviation from linearity until the volume concentration exceeded 10%. If results are plotted in terms of the surface-volume diameter, even fibers give good agreement with microscopy.

In later papers they extended the theory to cover multiple scattering effects [90,91]. They also investigated neural network recognition of particle size distributions by ultrasonic spectroscopy [92] for measuring high concentration suspensions. This work formed the basis for an on-line particle ultrasonic size analyzer (OPUS™) which is available from Sympatec (Figure 10.21).

The OPUS™ is based on ultrasonic attenuation in the regime where attenuation is proportional to the total projected area concentration of the particles and the attenuation is governed by the Lambert-Beer law. For this to be valid, the particles must be considerably larger than the wavelength of the incident radiation.

The Sympatec Opus (Figure 10.22) system uses 20 discrete frequencies in the 1.7 to 8 MHz range with typical measurement times of 2 to 5 min to cover the size range 5 µm to 3000 µm at volume concentrations from 1% to 40%.

Matec [93,94] in collaboration with the University of Sydney introduced the Acoustosizer™ ESA-8000, in which the sound waves are generated by the particles themselves as they are exposed to an alternating electric field. This phenomenon is called the ESA effect, an acronym for electro-acoustic size analyzer, and yields the average particle size (0.1 to 10 µm), breadth of distribution and zeta potential at volume concentrations from 1% to 40%.

Ultrasonic measurement has also been used to determine the particle size distribution in emulsions down to 20 nm in size. The attenuation was measured in the frequency range 100 kHz to 185 MHz with computer controlled small volume cylindrical resonators and computer assisted VHF and UHF pulse send-receive apparatus. Concentrated (25% w/v) aqueous emulsions of F-dimethyladamantane-trimethyl-bicyclononane, among others, were studied as well as perfluorochemical emulsions [95,96]. A comparison with x-ray sedimentation showed good agreement for nominal 1 µm silica.

10.8 Photon correlation spectroscopy (PCS)

10.8.1 Introduction

Particle sizing of sub-micron powders can be performed on a routine basis using photon correlation spectroscopy. The success of the technique is based mainly on the facts that it provides estimates of average size in a few minutes and that user-friendly commercial equipment is available. The technique is also referred to as quasi-elastic light scattering and dynamic light scattering [97].

The limitations of the technique are the need to use low concentrations in order to avoid multiple scattering, which results in too low an estimate of particle size, and the conflicting need for high concentrations in order that the number of particles in the measurement zone is sufficiently high for statistical significance. There are also reservations about its ability to separate accurately multimodal distributions and determine wide size distributions. Its strong point is the accuracy with which narrow size distributions may be determined on an absolute basis, i.e. without calibration, in only a few minutes.

10.8.2 Principles

The technique involves passing a collimated laser beam into a dilute suspension and measuring the radiation scattered at an angle θ (usually 90°) with respect to the incident beam (Figure 10.23). Particles in a fluid are in constant motion as a result of collisions with molecules of the suspending medium. As the particles become smaller the

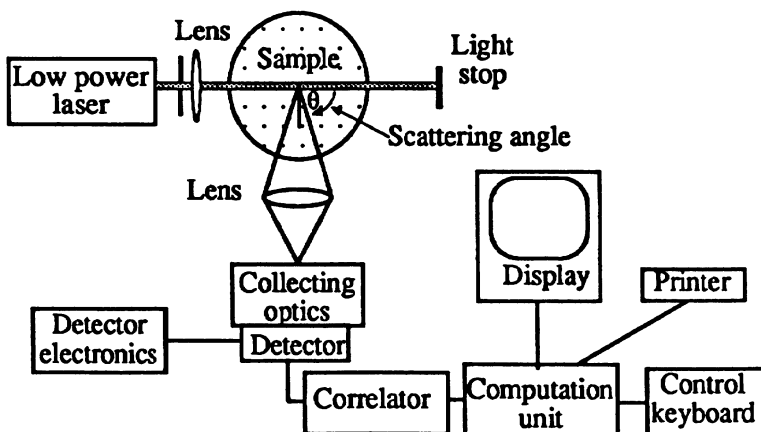


Fig. 10.23 Block diagram of a fixed angle photon correlation spectrometer.

movement becomes more rapid and gives rise to the phenomenon known as Brownian motion. The incident light is of wavelength λ whilst the scattered light is of wavelength $\lambda + \Delta\lambda$, where the frequency shift is an (optical) Doppler shift the magnitude of which depends upon the velocities of the particles and the angle of observation. The Doppler shifts are too small to be measured directly and are sensed from the interference of light scattered from pairs of particles and summed over the whole distribution. The velocity differences between the paired particles, ranging from a few microns to thousands of microns per second, generate beat frequencies ranging from 1 to 10,000 Hz.

The signal generated by the detector resembles a noise signal due to the constantly changing diffraction pattern caused by destructive and constructive interference as the particles change their position. Analysis of the intensity fluctuations yields a diffusion coefficient which is related to particle size.

The basic technique is only applicable to dilute suspensions where multiple scattering does not occur and is sometimes referred to as through sample dynamic light scattering however the introduction of the controlled reference method has extended it to more concentrated systems [98].

In the through sample technique the low frequency signal is deconvoluted using the autocorrelation function, whereas in the controlled reference method the signal is transformed into a frequency spectrum and the particle size determined from iterative deconvolution of the spectrum. This greatly simplifies photon correlation for process control since the remote sampling, dilution and wash cycles are eliminated. The signal is fed to a correlator and the autocorrelation function of the scattered intensity is interpreted in terms of average particle size and polydispersity index.

Multi-angle instruments are also available to generate the angular variation of scattered light intensity for derivation of molecular weight, radius of gyration, translational and rotational diffusion coefficients and other molecular properties. The additional data gathered simultaneously at a range of angles helps [99].

10.8.3 Through dynamic light scattering

The autocorrelation function of the scattered intensity $G(t)$ is defined as the product of the light intensity at the detector at time t and at a short time later $t + \tau$.

$$G(\tau) = \langle I(t) \cdot I(t + \tau) \rangle \quad (10.14)$$

where t is effectively zero for the commencement of an analysis. The symbol $\langle \dots \rangle$ refers to an average value of the product $I(t) \times I(t + \tau)$ for a large number of times τ .

The normalized first order autocorrelation function $G(\tau)$ can be calculated from the measured function:

$$G(\tau) = A + B \exp(-2\Gamma\tau) \quad (10.15)$$

where A and B can be considered as instrument factors with $B < A$.

The ratio B/A is often designated as the intercept, as a percent merit or as a signal to noise ratio

The decay rate Γ is linked to the translational diffusion coefficient D by:

$$\Gamma = K^2 D \quad (10.16)$$

The modulus of the scattering vector, K , is defined as:

$$K = \frac{4\pi n}{\lambda_0} \sin\left(\frac{\theta}{2}\right) \quad \omega_0 = \frac{8\pi kT}{3\lambda^2 \eta a} \quad (10.17)$$

where n = refractive index of liquid medium, λ_0 = wavelength of light in vacuum. Note that with PCS the diffusion coefficient D is determined and not the particle size. The latter quantity can only be determined by relating the diffusion coefficient to the particle size. There is no general relationship that applies to all situations and the frequently used Stokes-Einstein expression only applies to non-interacting, spherical particles.

$$D_0 = \frac{kT}{f_0} = \frac{kT}{3\pi\eta x} \quad (10.18)$$

where D_0 is the diffusion coefficient for a single particle in an infinite medium; T is the absolute temperature; k is Boltzmann constant; η is liquid viscosity; x is particle size (x is used in this section to avoid confusion with diffusion coefficient) and f_0 is the friction coefficient for a single particle.

10.8.4 Particle size

For homogeneous spherical particles, which are small compared to the wavelength of light, the average diffusion coefficient is the z average D_z . However the diameter calculated from this (x_m) is not a z average but a harmonic z average i.e. an average intermediate between the volume-moment and the z average [100].

$$G(\tau) = \int_{-\infty}^0 F(\Gamma) \exp(\Gamma t) d\Gamma \quad x_z = \left(\sum_i n_i x_i^7 / \sum_i n_i x_i^6 \right) \quad (10.19)$$

$$x_m = \left(1/x_z \right)^{-1} \quad (10.20)$$

so that:

$$x_m = \left(\sum_i n_i x_i^6 / \sum_i n_i x_i^5 \right) \quad (10.21)$$

where n_i represents the number of particles of diameter x_i .

10.8.5 Concentration effects

The particles must scatter independently, otherwise the diffusion coefficient, and particle size, cannot be determined unambiguously from the decay rate of the autocorrelation function. The net effects of multiple scattering are that the instrument factor B/A decreases, and the autocorrelation factor decays faster, leading to too low an estimate for particle size. Thus, multiple scattering limits the application of the technique to low concentration dispersions (< 0.01% by volume), although techniques have been developed to overcome this condition.

10.8.6 Particle interaction

Since most colloidal dispersions are stabilized by particle interactions, the use of equation (10.18) may lead to biased estimates of particle size which are often concentration dependent. The effect may be taken into account by expanding the diffusion coefficient to a concentration power series which, at low concentrations, gives:

$$D_c = D_0 (1 + k_D c) \quad (10.22)$$

The equation reduces to the Stokes-Einstein equation for spherical particles. Since the friction coefficient for a non-spherical particle always exceeds the friction coefficient for a spherical particle, over estimation of particle size will occur if equation (10.18) is applied.

The virial coefficient k_D is positive for repulsive particle interaction and negative for attractive interaction. Thus if particle interaction is neglected the apparent size will be concentration dependent, increasing with increasing concentration for attractive interactions and decreasing with repulsive interactions. In such cases the diffusion coefficient should be determined at a range of concentrations and D_0 determined by extrapolating to zero concentration.

The effect of particle interaction is proportional to the average interparticle distance which, for a fixed volume concentration, decreases with particle size. Hence the effect of interaction reduces as particle size increases. However, small particles scatter much less light than large particles and it is necessary to use a higher concentration for reliable PCS measurements. In these cases the concentration needs to be increased to volume fractions up to 0.1% and, again, particle sizes can only be determined from extrapolations to zero concentration.

10.8.7 Particle size effects

PCS relies on uneven bombardment of particles by liquid molecules which causes the particle to move about in a random manner and this limits the technique to particles smaller than 2 or 3 μm .

In order to avoid bias due to number fluctuations, it is necessary that there is at least 1000 particles present in the measuring volume and, for a typical value of the scattering volume of 10^{-6} cm^3 , effects of number fluctuations are to be expected for particle diameters greater than around 0.5 μm . Number fluctuations lead to an additional time decaying term in the autocorrelation function. Since the characteristic decay time of this additional term is usually much slower than the decay attributed to Brownian motion, the average particle size, which is proportional to the average decay time, will be overestimated if the effect of number fluctuations is neglected [101].

Loss of large particles due to sedimentation effects can usually be considered negligible. Stokes' law predicts that a 1 μm particle of density 3000 kg m^{-3} sediments in water at a rate of about $1 \mu\text{m s}^{-1}$ so that, in 3 min, there will be no particles larger than 1 μm at a depth of 0.2 mm below the surface. Since the measuring volume is usually situated several mm below the surface, this effect is only important for unduly protracted measurement times.

10.8.8 Polydispersity

For monodisperse samples, a plot of $G(\tau)$ against τ gives a straight line with a constant slope which is inversely proportional to particle size. For polydisperse samples, the relationship is multi-exponential and a plot of $G(\tau)$ against τ acquires curvature, the degree of which increases with increasing polydispersity [102].

The autocorrelation function for a polydisperse system represents the weighted sum of decaying exponential functions, each of which corresponds to a different particle diameter. For such a system:

$$G(\tau) = \int_{-\infty}^{0} F(\Gamma) \exp(-\Gamma\tau) d\Gamma \quad (10.23)$$

$F(\Gamma)$ is the normalized distribution of decay constants of the scatterers in suspension. Given $G(\tau)$ it is necessary to invert equation (10.23) in order to determine $F(\Gamma)$. Unfortunately, the inversion is ill-posed in that there are an infinite number of distributions which satisfy this equation within the experimental error to be found in $G(\tau)$. A large number of algorithms have been suggested for the inversion and an evaluation of their performance can be found in Stock and Ray [103].

The autocorrelation function can also be analyzed by the method of cumulants. In this approach $G(\tau)$ is fitted to a low order polynomial. For a third order cumulants fit:

$$G(\tau) = -\bar{\Gamma}\tau + \left(\frac{1}{2!}\right)\mu_2\tau^2 + \left(\frac{1}{3!}\right)\mu_3\tau^3 \quad (10.24)$$

An average particle size is obtained from the average decay rate $\bar{\Gamma}$ using equations (10.16 - 10.18) and an indication of spread (or polydispersity) is given by μ_2 .

An advantage of the cumulants approach is that it is computationally very fast. A chi-squared fitting error parameter serves to test whether the assumed Gaussian shape in diffusivities is reasonable. The calculated values of mean size and polydispersity are reasonable (chi-squared approaching unity) for approximately symmetrical distributions having a coefficient of variation within 25% of mean size.

Commercially available instruments usually employ both approaches. For highly skewed distributions or distributions having more than one mode, an inversion algorithm must be used [104], whereas for narrowly classified mono-modal distributions the cumulants approach is satisfactory.

The relative second moment, $K_2/\bar{\Gamma}^2$, a dimensionless quantity, is a measure of polydispersity. It is the intensity-weighted variance divided by the square of the intensity-weighted average of the diffusion coefficient distribution. The relative second moment is also called the polydispersity index which characterizes the spread of the decay rates and hence the spread of particle size about the average value.

Most inversion methods (e.g. Contin [105] and maximum entropy method [106], require prior knowledge of the distribution.

The singular value analysis and reconstruction method (SVR), reduces the inversion problem to a well conditioned problem, thus eliminating the need for prior knowledge [107].

Other methods of translating the polydispersity index into size distribution information have been proposed [108] but the reliability of the transformations are in question.

These procedures are detailed in a review, containing 67 references, by Finsey [109]. A later, excellent, review contains 292 references [110].

10.8.9 The controlled reference method

A laser beam is fed into an agitated measuring cell or flowing suspension using an optical wave guide. Particles within 50 µm of the tip of the wave guide (a fiber optic probe) scatter light, some of which is reflected back into the fiber and transmitted back through the guide. The reflected light from the interface between the guide tip and the suspension is also transmitted back. If these two components are coherent they will interfere with each other and result in a component of signal which has the difference or beat frequency between the reflected and scattered components. The difference frequencies are the same as the desired Doppler shifts. The received signal resembles random noise at the output of the silicon photodiode as a result of the mixing of the Doppler shifts from all the particles scattering the laser light. The photodiode output is digitized and the power spectrum of the signal is determined using fast Fourier transform techniques. The spectrum is then analyzed to determine the particle size distribution [111,112]. The controlled reference method has been shown to give a more constant measured size, over the concentration range 1 to 1,000 ppm, than the through dynamic method and has also been operated successfully with polystyrene at a concentration of 25% [113].

For a single particle size the power function takes the form of a Lorenzian function. The ω_0 term depends inversely on size so the power spectrum plots for different sizes show a shift to higher frequencies as the particle size decreases. In terms of the Brownian motion smaller particles move more rapidly than large ones. An assembly of particles will have a power spectrum $P(\omega)$ which is the sum of Lorenzian functions weighted by the volume concentration of each size (equation 10.23). An addition weighting occurs since the scattering efficiency $S(a)$ is size dependent. The analysis routine must deconvolute the combined power spectrum to determine the volume distribution. The optical properties of the particles and the suspending medium together with the viscosity and its temperature coefficient must be known.

$$P(\omega) = S(a) \frac{2\omega_0}{\omega^2 + \omega_0^2} \quad (10.25)$$

$$\omega_0 = \frac{8\pi kT}{3\lambda^2 \eta a}$$

η = viscosity; λ = wavelength in fluid; T = absolute temperature and a = particle radius.

One advantage of this system over conventional PCS is that since the light is reflected back rather than transmitted through the suspension, higher concentrations can be monitored.

Measurement of bimodality for mixtures of sizes ranging from less than 0.1 μm to sizes greater than 0.1 μm is difficult because of the rapid decrease in scattering efficiency as the size decreases. Broad distributions can be measured accurately.

10.8.10 Commercial equipment

Commercial particle sizing equipment usually operate at a fixed angle of 90° (Table 10.2). Multi-angle instruments generate two moments of the size distribution which renders direct evaluation of size distribution possible, provided a suitable model (e.g. log-normal) can be selected [114]. Multi-angle goniometers using different wavelengths increase flexibility.

Amtec spectrophotometers are designed to measure angular dependent intensity and correlation function either separately or concurrently. The photon correlation option enables sizing to be carried out from 5 nm to 3 μm . Rotation is continuously variable between 10° and 160° with angular resolution of 1/60° in the manual model and 1/100° in the step motor version.

Brookhaven BI-90 is designed for routine sub-micron particle sizing in quality control. Operation of the instrument is fully automatic and a series of repeat measurements including data processing can be set up easily. The *Brookhaven ZetaPlus* is an electrophoresis instrument with the capability of particle sizing by photon correlation spectroscopy. The *Brookhaven BI-200SM* is a multi-angle instrument which yields more information on particles and molecules.

Table 10.2 Commercial photon correlation spectroscopy equipment

Amtec	Multiangle
Brookhaven BI 90	Fixed angle
Brookhaven BI-200SM	Multi-angle
Brookhaven BI-Fogels	Fiber optics
Brookhaven 90 plus	Dual angle
Coulter N4	Fiber optics: multi-angle Optional
Leeds & Northrup UPA	Fiber optics
Malvern System 4700	Multi-angle
Malvern Autosizer Hi-C	Fiber optics
Malvern Autosizer	Fixed angle
Malvern Zetasizer 3	Multi-angle
Nicomp HNS - 90/TC 100	Fixed angle
Nicomp Model 270/370 (Hiac/Royco)	Fixed angle
Otsuka Photol DLS-700 (Munhall)	Fiber optics: multi-angle
Wyatt Technology Dawn	Multi-angle

Brookhaven 90 Plus sub-micron particle size instrument is a dual angle instrument with measurements at 15° and 90° to generate size distributions in the 10 nm to 1 µm size range together with zeta potential determinations.

Brookhaven BI-Fogels is designed for on-line process control using a fiber optic probe for remote sensing in colloidal dispersions at concentrations from 0.001% up to 40% by volume. Fiber optic sensing greatly simplifies the application of photon correlation spectroscopy to process control by eliminating the need for sample dilution and wash cycles. Since glass fibers are inherently rugged they may be used in hostile environments. In this instrument, visible light from a laser diode is transmitted into the sample via a monomode fiber and the scattered light is collected by a second monomode fiber at an angle of 153°. It is claimed that the troublesome homodyne signals that arise in single fiber optics design are eliminated by the use of two fibers [115,116]. The measurement range is 0.002 to 2 µm.

Brookhaven BI-200SM goniometer system is a precision instrument designed for macromolecular studies and sub-micron particle sizing. It is based on a special turntable to measure angular intensity and photon correlation measurements.

Coulter Model N4 system operates in the 3 nm to 3 µm size range, determining average particle size, standard deviation and diffusion coefficient, typically in 2 min. The instrument is also available with a detection option at seven angular positions which are selected automatically at a keystroke via a built-in keypad. This option gives extra information to enable concentration determination together with more accurate particle size analysis determination.

Malvern Autosizer Hi-C (Figure 10.24) operates in a similar manner to cover the size range 0.015 to 1 µm at solids concentrations from 0.01% to 50%. One reported application [117] was the measurement of casein micelles in cheese making as they grew in size from 200 to 1200 nm.

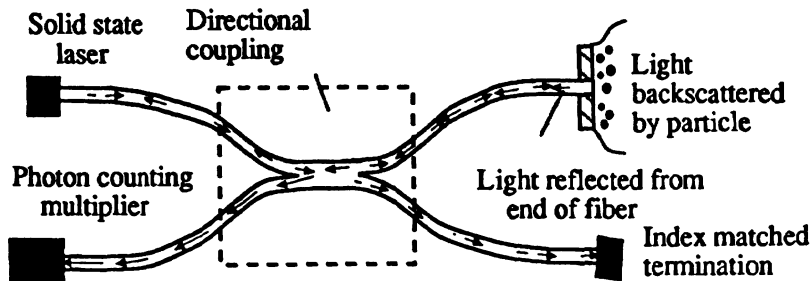


Fig. 10.24 The optical unit for the Malvern Autosizer Hi-C.

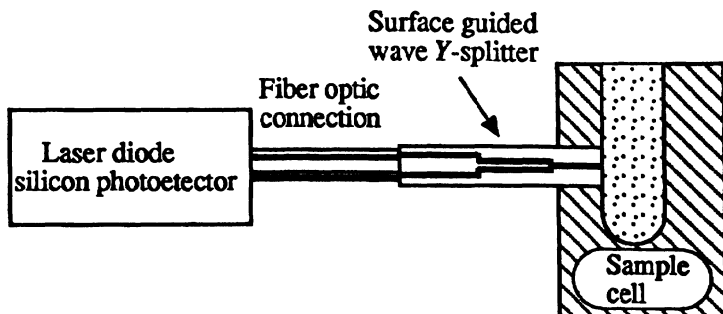


Fig. 10.25 Line diagram of the Leeds and Northrup Ultrafine Particle Analyzer (UPA).

Malvern System 4700 comprises a variable angle spectrometer with computer controlled automatic operation, combining photon correlation spectroscopy and angular intensity measurements with full Mie theory calculations to give accurate size distributions in the 1 nm to 5 μm size range.

Malvern Zetasizer II consists of a light scattering spectrometer and digital autocorrelator with integral microcomputer. In addition to measuring electrophoretic mobility—the movement of charged colloidal particles under the influence of an applied electric field—the Zetasizer II also determines particle size by Brownian motion. The Zetasizer III combines both photon correlation spectroscopy and angular intensity measurements with full Mie theory calculations to give accurate size distributions in the 3 nm to 3 μm size range.

Microtrac Series 9200 Ultrafine Particle Analyzer Model 9230 operates in the 0.003 μm to 6 μm size range (Figure 10.25) and gives reproducible results in the concentration range 2 to 2000 ppm (2%).

Nicomp Model 270 uses an analysis algorithm to mathematically invert the scattered light autocorrelation function, thereby obtaining a fresh estimate of the particle size distribution every 25 s.

Nicomp Model 370 combines automatic sample handling and dilution. A concentrated suspension is introduced into the instrument via a syringe or flexible sampling tube. This is automatically diluted to the appropriate concentration and sized.

Otsuka Photal is a dynamic light scattering spectrophotometer which provides sub-micron sizing in the 3 nm to 3 μm size range and also provides information on the shape of polymers.

Wyatt Technology manufacture over 30 *Dawn* instruments of varying degrees of sophistication. *Dawn Model F* simultaneously measures the intensity of light scattered at 15 angles which, together with the *Astra* menu driven software system, yields molecular weights and sizes.

10.8.11 Discussion

The basic theory and discussion of results are covered in papers by Thomas [118] who uses a Brookhaven Instrument Fiber Optics Quasi-Elastic Light Scattering System (BI-FOQELS) with dynamic light scattering obtained using the BI-DLS and diluted samples.

An autodilution unit has been described to analyze on-line particle growth during a polymerization process [119]. The results compared favorably with off-line dynamic light scattering and on-line turbidimetric data [120].

Several data analysis software packages are available and average sizes generated by these are not comparable [121–123].

De Jaeger *et al.* [124] carried out inter-laboratory tests using polystyrene latices with particle sizes ranging from 30 nm to 2 μm . They concluded that for diameters less than 0.5 μm reliable particle sizes can be obtained. In the range 0.5 to 1 μm this was only possible within a very narrow range of concentration. For the largest size investigated (about 2 μm) the measurements were less reliable.

10.8.12 Diffusion wave spectroscopy (DWS)

DWS addresses dynamic light scattering in the multiple scattering concentration range. Pine *et al.* [125] describe the theory for the technique and it has been applied to the determination of mean size and polydispersity [126,127]. The method has also been used for on-line measurement of concentrated suspensions [128].

10.9 Insitec Ensemble Particle Concentration Size (EPCS) Systems

The EPCS are laser based instruments for in-line particle measurements which provide information on particle volume concentration and size distribution. EPCS instruments are part of a larger group of electro-optical instruments (LALLS) whose principle of operation is based on light scattering from a group (or ensemble) of particles. Unlike other instruments operating on this principle, the EPCS can perform direct measurements of particle laden flow stream provided the concentration is within operating limits.

Insitec EPCS-P instrument is designed for in-line measurements in powder or spray processing systems under hostile conditions [129,130]. Applications include process powder sizing, mass emission monitoring and fossil energy combustors. It has a general capability from 1 to 500 μm at concentrations up to 1000 g m^{-3} . EPCS-P has a gas purged window with a 9 cm by 4 cm aerosol access region. The 5 mW He-Ne laser beam is approximately 1 cm in diameter. All particles in the beam, over the 9 cm length, scatter light into a logarithmically scaled solid state ring detector. Particle measurements are based on the

analysis of light scattered into each of the 32 detector rings from all particles in the laser beam.

Insitec EPSCS-F is designed for powders in the size range of 0.2 µm to 1000 µm [131]. Particle measurements are made at rates up to 500 per second with immediate display of particle size distribution and characteristic diameters. Specific values or points on the particle size distribution are continuously fed back to the user or to a process control system. Particles with different refractive indices and aspect ratios up to 2:1 can be measured.

The instrument consists of an optical head with a purge gas over the lenses to reduce coating by the powder stream, an interface box, computer and software. As particles pass through the laser beam, light scattered in the forward direction is collected by the receiver lens and focused on to an annular ring detector. The detector is scanned at high speed and the signal level on each of 32 rings is measured and stored. Once a sufficient number of detector scans are acquired the software uses a non-linear inversion technique to solve for the relative particle concentration. The size distribution is determined from theory defined by the relative refractive index between the particles and carrier with no assumptions on the shape of the distribution.

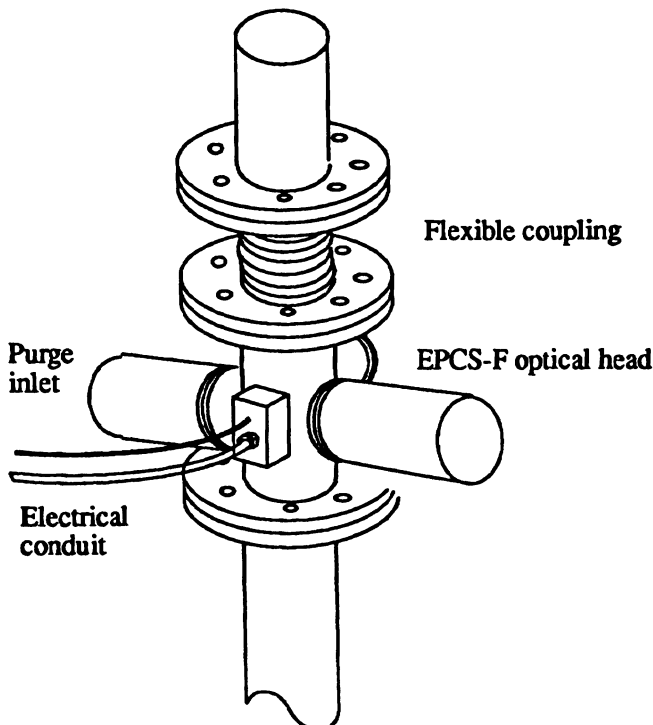


Fig. 10.26 EPSCS-F optical head installation.

Figure 10.26 shows the optical head inserted in the process line. The head is installed directly into the line, preferably via a flexible coupling for vibration isolation. The interface box is a NEMA 4.9 rated explosion proof enclosure, weighing 50 lb, which can be bolted to a wall or floor within 20 ft of the head.

The process control display into three sections. Six process control variable displays are shown at the top of the screen. Variable displays reflect the most recent measurements of the particulate. A time history of the point values for the process control variables is displayed on the lower portion of the screen. The third portion is the system status flags shown in the middle of the screen. The particle size distribution may also be viewed whilst in the process control mode but this can slow down the processing time considerably.

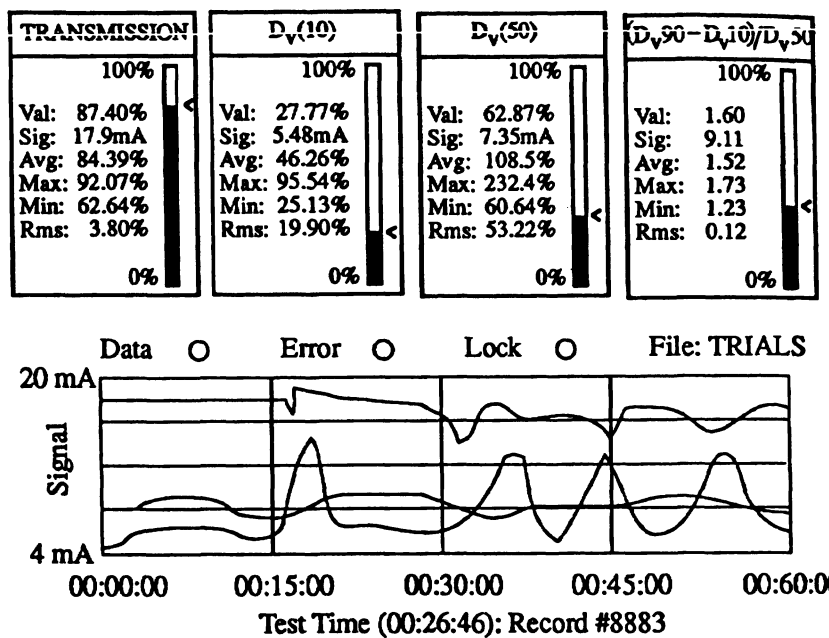


Fig. 10.27 EPICS process control display format.

Figure 10.27 depicts the screen. The six variable display boxes are positioned at the top of the screen and reflect the current values only. The process control plot shows a time history of all six variables. The window bar is on the bottom of the time axis and shows the relationship of the current window to the total planned duration of the test. System status flags on the left light up when the control and error flags are on. The error status shows the error number if it is active. The other flags are for display only and indicate the status of the program.

Discrete data point, extracted from the log file, can be viewed. The data can also be viewed in tabular form and as a size distribution curve. Data can also be integrated over any selected range. A Statistical Process Control (SPC) option enables the file data to be viewed in standard control chart format either as an X or R chart.

Various interface arrangements, including a direct in-line system and an eductor bypass, have been described [132]. A comparison between the Insitec ensemble sizer (field scanning system) and the Insitec single particle counter showed good agreement with gas atomized zinc powder [133]. The instrument has been used successfully to characterize the atomisation and dispersion of droplets and solids dispersed in a pneumatic transport device [134].

10.10 Turbo-Power Model TPO-400 in-line grain size analyzer

This instrument was developed for the cement industry by Nissin. At preset times it automatically samples a few kilograms of material and feeds it into a turbo classifier. The fines are fed into a micron line which determines the Blaine number for the powder.

10.11 Turbidity

Turbidity has been widely used for determining the particle size distribution (PSD) of particles in suspension, since it is experimentally simple, can be used over a wide size range and does not disturb the system under investigation. It is also fast, reproducible and inexpensive. Turbidity gives a measure of the attenuation of a beam of light passing through a suspension. Specific turbidity relates the PSD of a suspension to the turbidity (measured at a given wavelength) and the particle volume fraction c_v . For a suspension of spherical, non-absorbing, isotropic particles, in the absence of multiple scattering, specific turbidity (τ) is given by:

$$\tau = \frac{3}{2} c_v \int_0^{\infty} x^2 K\left(\frac{x}{\lambda_{\mu}}, \frac{n_p}{n_m}\right) f(x) dx$$

$$\tau = \frac{\int_0^{\infty} x^2 K\left(\frac{x}{\lambda_{\mu}}, \frac{n_p}{n_m}\right) f(x) dx}{\int_0^{\infty} x^3 f(x) dx} \quad (10.26)$$

where $f(x)$ is the normalized PSD. $K\left(\frac{x}{\lambda_m}, \frac{n_p}{n_m}\right)$ or K_{scat} is the scattering coefficient which is a function of $\alpha = (\pi x / \lambda_m)$, x is the particle diameter and $\lambda_m = \lambda_0 / n_m$ is the wavelength of light in the medium, λ_0 is the wavelength of the incident beam *in vacuo*, and $m = (n_p/n_m)$ where n_p and n_m are the refractive index of the particle and medium respectively.

PSD can be estimated from the turbidity at different wavelengths provided the other variables are known. Kourti *et al.* [135] assumed a log-normal PSD and observed that the parameters of the estimated distribution were so highly correlated that an infinite number of distributions could explain the data. However, all the alternative solutions were found to have the same weight average diameter.

With turbidity ratio, the ratio of the turbidities at two wavelengths, one of which is chosen as basis, is used. This has been successfully applied with large particles [136] ($0.65 < D < 1.3$) μm but is not applicable to smaller particles or for small values of m ($m < 1.15$) [137].

Equation (10.26) can be written in the form:

$$\tau = \frac{\pi}{4} \int_0^\infty K_{scat} x^2 f(x) dx \quad (10.27)$$

This is a Fredholm integral equation of the first kind where $f(x)dx$ is the number density of particles in the size range x to $x + dx$. The regularized solution to this equation has been applied to the measurement of both the moments and the size distributions of a wide range of latices [138].

The controversy over whether turbidity is capable of giving a true size distribution has been fully discussed by Kourti and MacGregor, who conclude that in many cases it can, and much of the controversy arises due to unjustified extrapolation from one regime to another [139].

Zollars [140] described an on-line turbidity system for the estimation of particle size distribution, refractive index and solids concentration. In a review and simulation of turbidimetric methods of on-line analysis Brandolin and Garcia-Rubio [141] state that this method is suitable only for mono-modal distributions. Turbidity has also been used on-line, in conjunction with an Anton Paar vibrating tube densitometer for measuring concentration, to determine the particle size distribution of polyvinyl acetate. Samples were withdrawn from the process line using a Bristol Engineering Isolock sampler and a dilution system. Turbidity measurements were carried out using a Bausch and Lomb Single Beam Spectronic 20 [142].

10.12 Transient turbidity

Transient turbidity is an optical technique for measuring magnetic particles [143,144]. It does this by aligning particles in an electric field, removing the field, and following their return to random orientation induced by Brownian motion. Their relaxation is measured by turbidity and this can be related to particle size distribution if assumptions are made about the particle geometry and the shape of the size distribution. The technique is rapid (less than a second) and reproducible. Its most serious limitation is that the specific conductance of the sample must be less than $100 \mu\text{mho cm}^{-1}$. Transient electrical birefringence operates in a similar manner.

10.13 Concentration monitors

Monitek instruments measure the concentration of suspended solids in a liquid by shining a light through the stream and detecting the amount of light that is scattered by the suspended solids. The scattered light is seen as turbidity hence the name *turbidimeters*. Suspended solids scatter light in all directions so that there are many potential viewing angles; 90° side-scatter instruments are called *nephelometers*. Forward scatter instruments sample a more representative cross-section of a process stream and can monitor a wide range of particle sizes from 0.01 to $100 \mu\text{m}$. For accurate measurement Monitek uses a ratio of forward scatter intensity where the scattered intensity is divided by the direct beam signal.

10.14 Shape discrimination

The information content of the uv/vis spectrum of sub-micron and micron size particles yields information on the size, chemical composition and shape of the particles [145]. The angular dependence of the scattered intensity is given by the Rayleigh-Gans-Debye (RGD) theory. The form factors for various particle shapes were calculated as a function of the angle of observation θ and wavelength λ of the incident light. Comparison of the scattering intensities for particles with different shapes showed that each differently shaped particle had a unique surface pattern thus suggesting the possibility of selecting combinations of λ and θ to enable shape discrimination.

References

- 1 Marshall, V.C. (1966), *Chem. & Process Eng.*, 47(4), 177–183, 394
- 2 Hinde, A.L. (1973), *IFAC Symp. Automatic Control in Mining, Mineral and Metal Processing*, Sydney, Aug. 13–17, Inst. J. Engrs., Australia, 45–47, 395

- 3 Svarovsky, L. and Hadi, R.S. (1977), *Proc. Particle Size Analysis Conference*, Analyt. Div. Chem. Soc., 395
- 4 Cushman, C.R. et al (1973), U.S. Patent No. 3,779,070, 396
- 5 Holland-Batt, A.B. (1968), *Trans. Inst. Min. Metall.*, Sect. C 77, 185-190, 396
- 6 Holland-Batt, A.B. (1968), *Trans. Inst. Min. Metall.*, Sect. C 78, 163-165, 396
- 7 Osborne, B.F. (1970), *ISA Conf.*, October, Philadelphia, Paper 844, 70, 396
- 8 Osborne, B.F. (1970), *Can. Inst. Metall. Bull.*, 65, 97-107, 396
- 9 Holland-Batt, A.B. and Birch, M.W. (1974), *Powder Technol.*, 10, 4/5, 189-200, 396
- 10 Holland-Batt, A.B. (1975), *Powder Technol.*, 11(1), 11-26, 396
- 11 Stanley-Wood, N.G. (1974), *Control Instrum.*, 42, 43, 45, 47, 396
- 12 Hinde, A.L. (1973), *J.S.Afr. Inst. Min. Metall.*, 73(8), 258-68, 396
- 13 Carr-Brion, K.G. (1966), *Analyst*, 91, 289-290, 396
- 14 Carr-Brion, K.G. and Mitchel, P.G. (1967), *J. Sci. Instrum.*, 44, 611, 396
- 15 Carr-Brion, K.G. (1968), *British Patent Appl.* 13598, 396
- 16 Alftahan, C. von (1973), *Dechema Monogram*, 1589-1615, 79, 1231-41, 398
- 17 Nakajima, Y., Gotah, K. and Tanaka, T. (1970), *IEC Fundamentals*, 9(3), 489-495, 398, 403
- 18 Nakajima, Y., Gotah, K. and Tanaka, T. (1971), *IEC Fundamentals*, 10(2), 318-320, 398, 403
- 19 Nakajima, Y., Gotah, K. and Tanaka, T. (1967), *IEC Fundamentals*, 6, 587, 398, 403
- 20 Tanaka, T. and Nakajima, Y. (1973), *Proc. Conf. Part. Technol.*, IITRI, Chicago, 398, 403
- 21 Joy, A.S. and Jenkinson, A. (1968), *Proc. Soc. Analyt. Chem.*, 5(5), 80-82, 399
- 22 Lynch, A.J. (1966), *Australian Mineral Ind. Res. Assoc., Progress Report Number 7*, 399
- 23 Lynch, A.J., Rao, T.C. and Whiten, N.J. (1967), *Proc. Austral. Inst. Min. Metall.*, 223, 71-73, 400
- 24 Draper, N. and Lynch, A.J. (1968), *Trans. Mech. Chem. Engng.*, Nov., 207-217, 400
- 25 Putman, R.E.J. (1973), *Min. Congr. J., S.Afr.*, 68-74, 393, 396
- 26 Tanaka, T. (1976), *Technocrat*, 9(9), 40, 400
- 27 Kelsall, D.F. and Restarick, C.J. (1971), *Proc. Symp. Automatic Control Systems in Mineral Processing Plants*, 400
- 28 Hinde, A.L. and Lloyd, P.J.D. (1975), *Powder Technol.*, 12(1), 37-50, 401
- 29 Hinde, A.L. (1973), *IFAC Symp. Automatic Control in Mining, Mineral and Metal Proc.*, Aug. 13-17, Sydney, Australia, Inst. Eng., 45-7, 401

- 30 Rendell, M. (1964), *Separation of particles by sieving and screening*, PhD Thesis, Univ. Coll. London, 402
- 31 Bartlett, R.W. and Chin, T.H. (1974), *Trans. Soc. Min. Engrs., AIME*, 256, 403
- 32 Schönert, K., Schwenk, W. and Steier, K. (1974), *Aufbereit Tech.*, 7, 368–372, 403
- 33 Papadakis, M. (1963), *Rev. Mat. Constr. Trav.*, 570, 79–81, 403, 404
- 34 Weiland, W. (1967), *Min. Proc.*, 8, Feb., 30, 404
- 35 Stanley-Wood, N.G., Lee, T. and Beck, M.S. (1973), *Proc. Soc. Anal. Chem.*, 10, 282, 404
- 36 Beck, M.S., Lee, T. and Stanley-Wood, N.G. (1973), *Powder Technol.*, 8, 85, 404
- 37 Hulst, H.C. van de (1957), *Light Scattering by Small Particles*, Wiley, 404
- 38 Azzopardi, B.J. (1991), *Particle Size Analysis Group, Anal. Div. Royal Soc. Chem. PSA '91 Conf.*, Loughborough, England, 405
- 39 Pijper, A. (1918), *Med. J. S. Africa*, 14, 211, 405
- 40 Pijper, A. (1947), *J. Lab. Clin. Med.*, 32, 857, 405
- 41 Gabas, N., Hiquily, N. and Lagueric, C. (1994), *Part. Part. Charact.*, 11(2), 121–126, 405
- 42 Swindenbank, J.H., Beer, J., Taylor, D.S., Abbot, D. and McCreath, C.G. (1976), *AIAA Paper No. 76–69*, 406
- 43 Comillault, J. (1972), *Appl. Optics*, 11, 265, 406
- 44 Boxman, A., Merkus, H., Verheijen, P.J.T. and Scarlett, B. (1991), *Appl. Optics*, 30, 4818–4823, 406
- 45 Gumprecht, R.O. and Sliepcevich, C.M. (1953), *J. Phys. Chem.*, 57, 90 and 95, 406
- 46 Chin, J.H., Sliepcevich, C.M. and Tribus, M. (1955), *J. Phys. Chem.*, 59, 841 and 845, 407
- 47 Phillips, B.L. (1962), *J. Assoc. Comp. Mach.*, 9, 84, 408
- 48 Twomey, S. (1963), *J. Assoc. Comp. Mach.*, 10, 97, 408
- 49 Boxman, A., Merkus, H.G., Verheijen, P.J.T. and Scarlett, B. (1978), *Proc. 2nd Int. Congr. on Particle Sizing*, Tempe, Ariz. 178, 408
- 50 Twomey, S. (1963), *J. Assoc. Comp. Mach.*, 10, 97–101, 408
- 51 Heuer, M. and Leschonski, K. (1985), *Part. Part. Charact.*, 2(1), 7–13, 408
- 52 Witt, W. and Röthele, S. (1995), *6th European Symp. Particle Size Characterization*, Partec 95, Nurenberg, Germany, publ. NürnbergMesse GmbH., 277–290, 411
- 53 Wertheimer, A. W. and Wilcock, W. L. (1994), *Measurement of particle distributions using light scattering*, Leeds and Northrup Company Advanced Technology Note 7501, 412
- 54 Bott, S.E. and Hart, W.H. (1991), *Particle Size Distribution II*, ed. T. Provder, Am. Chem. Symp. No 472, 106–122, 412

- 55 Leschonski, K., Röthele, S. and Menzel, U. (1984), *Part. Part. Charact.*, 1, 161–166, 416
- 56 Leschonski, K., Benker, B. and Bauer, U. (1995), *6th European Symp. Particle Size Characterization*, Partec 95, Nurenberg, Germany, publ. NürnbergMesse GmbH, 247–256, 416
- 57 Heuer, M. and Swechten, D. (1995), *6th European Symp. Particle Size Characterization*, Partec 95, Nurenberg, Germany, publ. NürnbergMesse GmbH, 301–314, 416
- 58 Swithenbank, J., Beer, J.M., Taylor, D.S. and McCreath, C.G. (1977), *Prog. Astronaut. Aeronaut.*, 53, 441–447, 417
- 59 Etzler, F.M. and Sanderson, M.S. (1995), *Part. Part. Syst. Charact.* 12, 217–224, 417
- 60 Hamida, A.A. and Swithenbank, J. (1986), *J. Inst. Energy*, 59, 101–105, 417
- 61 Hirleman, E.D. (1987), *Optical Sizing, Theory and Practice*, Proc. Int. Symp., Rouen, France, publ. Plenum Press, New York, 1988, 159–177, 417
- 62 Felton, P.G., Hamidi, A.A. and Aigal, A.K. (1985), Proc. 3rd Int. Conf. on Liquid Atomization and Spray Systems, Institute of Energy, London, 417
- 63 Cao, J., Brown, D.J. and Rennie, A.G. (1991), *J. Inst. Energy*, 64 (458), March, 26–30, 417
- 64 Brown, D.J., Alexander, K. and Cao, J. (1991), *Part. Part. Charact.* 8, 175–178, 417
- 65 Dobbs, C.L. and Sparks, R.G. (1993), *Particle Characterization*, 10, 227–294, 417
- 66 Brown, D.J. and Weatherby, E.J. (1989) *Industrial Crystal*, 87 Academia, Prague and Elsevier, Amsterdam, 411–414, 417
- 67 ASTM E1458 (1992), 417
- 68 Hirleman, E.D. (1983), 28th Int. Gas Turbine Conf., Am. Soc. Mech. Eng., N.Y., Paper 83-GT-232, 417
- 69 Hirleman, E.D., Felton, P.G. and Kennedy, J. (1992), PARTEC, 5th European Symp. Particle Characterization, Nurenberg, 655–671, 417
- 70 Reichel, F. and Löffler, W. (1994), *Int. J. Optoelectronics*, 9, 99–109, 418
- 71 Thorwirth, G. and Reinhold, B. (1990), *Laser und Optoelektronik*, 22, 64–69, 419
- 72 Reichel, F. and Hawlitschek, N. (1994), Proc. Opto, 94, ACS Organization GmbH, 95–103, 420
- 73 Lui, C.L. and Zhang, J.Y. (1990), *Powder Metall. Technol.*, 8, 199, 420
- 74 Zhang, J.Y. et al. (1974), *New Metallic Materials*, No. 2, 56 (Chinese), 420
- 75 Zhang, J.Y. and Lui, C.L. (1981), *Modern Developments in Powder Metallurgy*, 12, 47, 420

- 76 Zhang, J.Y. and Lui, C.L. (1981), *Modern Developments in Powder Metallurgy*, 12, 59, 420
- 77 Herbst, J.A. and Alba, F. (1987), *Particulate and multiphase processes*, 3, *Colloidal and Interfacial Phenomena*, 297–311, ed. T. Arriman and T.N. Veziroglu, 422
- 78 Alba, F. *private communication*, 422
- 79 Alba, F. (1992), *U.S. Patent 5,121,629*, 422
- 80 Allen, T., Hobbel, E.F., Davies, R. and Boughton, J.H. (1991), *Pharmtech Conference September* (1991), publ. Pharmaceutical Technology, August, 423
- 81 Alba, F., Dobbs, C.L. and Sparks, R.G. (1994), *First Int. Forum Particle Size Measurement*, Part 1, 36–45, Denver, Am. Inst. Chem. Engrs., 423, 431
- 82 Boxman, A., Scott, D.M. and Jochen, C.E. (1995), *6th European Symp. Particle Size Characterization*, Partec 95, Nürnberg, Germany, publ. NürnbergMesse GmbH., 37–46, 423
- 83 Scott, D.M., Boxman, A. and Jochen, C.E. (1995), *Part. Part. Syst. Charact.*, 12, 269–273, 423
- 84 Pendse, H.P. and Strout, T.A. (1990), *Sensors Expo West Proceedings*, 205B–1–7, 423
- 85 Pendse, H.P. and Sharma, A. (1993), *Part. Part. Syst. Charact.* 10 (5), 229–233, 423
- 86 Pendse, H.P. and Han, W. (1996), *The 5th World Congr. of Chem. Eng.*, San Diego CA, 6, 545–550, publ. Am. Inst. Chem. Eng., 423
- 87 Pendse, H.P. and Sharma, A. (1994), *First Int. Particle Technology Forum*, Part 1, 136–147, Denver, Am. Inst. Chem. Eng., 423
- 88 Hackley, V.A. (1996), *The 5th World Congr. of Chem. Eng.*, San Diego CA, 6, 557–562, publ. Am. Inst. Chem. Eng., 424, 425
- 89 Riebel, U. and Löffler, F. (1989), *European Symposium on Particle Characterization*, Nurenberg, Germany, April, 424
- 90 Riebel, U. and Kräuter, U. (1994), *Part. Part. Syst. Charact.*, 425
- 91 Kräuter, U. and Riebel, U. (1994), *First Int. Particle Techn. Forum*, Denver, Am. Inst. Chem. Eng., Part 1, 30–35, 425
- 92 Kräuter, U., Grammenoudis, P. and Riebel, U. (1995), *6th European Symp. Particle Size Characterization*, Partec 95, Nurenberg, Germany, publ. NürnbergMesse GmbH., 27–36, 425
- 93 O'Brien, R.W. and Cannon, D W., (1991), *202nd meeting, Am. Chem. Soc.*, New York, Aug, 425
- 94 Matec Applied Sciences, Hopkinton, Maryland 01748, 425
- 95 Barrett Gultepe, M.A., Gultepe, M.E., McCarthy, J.L. and Yeager, E. (1988), *Biomat., Art, Cells, Art, Org.*, 16(1–3), 691–692, 425
- 96 Barrett Gultepe, M.A., Gultepe, M.E., McCarthy, J.L. and Yeager, E. (1988), *Biomat., Art, Cells, Art, Org.*, 16(1–3), 693–694, 425
- 97 Weiner, B.B. (1991), *PSA '91, Particle Size Analysis Group, Analyt. Div. Royal Soc. Chem. Conf.*, Loughboroug, U.K., 426

- 98 Cloake, P. (1991), *Proc. Int. Symp. Particle Size Analysis*, publ. Royal Soc. Chem., ed. N.G. Stanley-Wood, and R. Lines, pp 498–513, 427
- 99 Cummins, P.G. and Staples, E.J. (1987), *Langmuir*, **3**, 1109–13, 427
- 100 Finsey, R. and De Jaeger, N. (1991), *Part. Part. Syst. Charact.*, **8**, 187–193, 484
- 101 Berne, B. and Pecora, A. (1976), *Dynamic Light Scattering*, Wiley, New York, 430
- 102 Finsey, R., Jaeger, N. de, Sneyer, S. and Geladé, E. (1992), *Part. Part. Charact.*, **9**, 125–137, 430
- 103 Stock, R.S. and Ray, W.H. (1985), *J. Polym. Sci., Polym. Phys.*, **23**, 1393, 431
- 104 Finsey, R., Jaeger, N. de and Sneyer, S. (1991), *Part. Part. Syst. Charact.*, **8**(9), 179–186, 427
- 105 Provencher, S. (1982), *Comput. Phys.*, **27**, 229, 431
- 106 Livesey, A., Licinio, P. and Delaye, M. (1986), *J. Chem. Phys.*, **84**, 5102, 431
- 107 Finsey, R., Groen, P. de, Deriemaeker, L., Geladé, E. and Joosten, J. (1991), *PSA '91, Particle Size Analysis Group, Analyt. Div. Royal Soc. Chem. Conf.*, Loughboroug, U.K., 431
- 108 Bertero, M., Boccacci, P., Moiri, C. de and Pike, E.R. (1989), *J. Aerosol Sci.*, **20**, 91–99, 431
- 109 Finsey, R. (1993), Kona, No. 11, 17–32, Council of Powder Technology, Japan, 431
- 110 Finsey, R. (1994), *Adv. Colloid Interf. Sci.*, **52**, 79–143, 431
- 111 Trainer, M.N., Freud, P.J. and Weiss, E.L. (1990), *Pittsburgh Conference Analytical Applied Spectroscopy, Symp. Particle Size Analysis March*, 432
- 112 Trainer, M.N., Freud, P.J. and Leonardo, E.M. (1992), *Am. Lab.*, **24**(11), 34, 36–38, 432
- 113 Plantz, P.E432 and Freud, P.J. (1995), *Powder and Bulk Eng.*, **9**(2), 36–45, 432
- 114 Thomas, J.C. (1987), *J. Colloid Interface Sci.*, **117**, 187–192, 432
- 115 Dhadwal, H., Ansari, R. and Meyer, W. (1991), *Rev. Sci. Instrum.*, **62**(12), 2963, 434
- 116 Dhadwal, H. et al. (1993), *S.P.I.E.*, **1884**, 16, 434
- 117 Horne, D.S. and Davidson, C.M. (1990), *Milchwissenschaft*, 434
- 118 Thomas, J.C. (1991), *Particle Size Distribution II*, ed. T. Provder, Am. Chem. Symp. No. 472, 98–105, 436
- 119 Kourti, T., MacGregor, J.F., Hamielec, A.E., Nicoli, D.F. and Eling, V.B. (1990), *Adv. Chem. Ser.*, **227** (Polym. Charact.), 105–39, 436
- 120 Nicoli, D.F., Kourti, T., Gossen, P.D., Wu, J.S., Chang, Y.J. and MacGregor, J.F. (1991), *Particle Size Distribution II*, ed. T. Provder, Am. Chem. Symp. No. 472, 86–97, 436

- 121 Meeren, P. van der, Vanderdeelen, J. and Baert, L. (1992), *Royal Soc. Chem., Special Publ.* 102, (Part. Size Analysis), 196–205, 436
- 122 Meeren, P. van der, Laethen, M. van, Vanderdeelen, J. and Baert, L. (1991), *J. Lipossum Res.*, 2, 23–42, 436
- 123 Meeren, P. van der, Vanderdeelen, J. and Baert, L. (1991), *PSA '91, Particle Size Analysis Group, Analyt. Div. Royal Soc. Chem. Conf.*, Loughborough, U.K., 436
- 124 Jaeger, N. de, Demayere, H., Finsey, R., Sneyer, S., Vanderdeelen, J., P. van der Meeren and Laethen, M. van (1991), *Part. Part. Syst. Charact.*, 8(9), 179–186, 436
- 125 Pine, D.J., Weitz, D.A., Zhu, J.H. and Herbolzheimer, E. (1990), *J. Phys. (Paris)*, 51, 2101–27, 436
- 126 Horne, D.S. (1990), *J. Chem. Soc., Faraday Trans.*, 86(7), 1149–50120, 436
- 127 Horne, D.S. (1989), *J. Phys. D, Applied Phys.*, 22, 1257–65, 432
- 128 Horne, D.S. (1991), *Proc. SPIE-Int. Soc. Opt. Eng.*, 1430, 166–80, 436
- 129 Holve, D.J. (1991), *Powder and Bulk Eng.*, 5(6), 15–16, 436
- 130 Harvill, T.L. and Holve, D.J. (1993), *Part. Part. Charact.*, 10(5), 262–265, 437
- 131 Holve, D.J. (1993), *Proc. Tech. Prog. Powder and Bulk Solids Conf. Exhib.*, 301–302, 437
- 132 Holve, D. and Harvill, T.L. (1995), *6th European Symp. Particle Size Characterization*, Partec 95, Nürnberg, Germany, publ. NürnbergMesse GmbH., 291–300, 439
- 133 Boyco, C.M., Tuyet, H.Le. and Henein, H. (1993), *Part. Part. Charact.* 10(5), 266–270, 439
- 134 Kourti, T., MacGregor, J.F. and Hamielec, A.E. (1991), *Particle Size Distribution II*, ed. T. Provder, Am. Chem. Symp. No. 472, 2–19, 439
- 135 Sunshine, G.A., Adeyayo, A. and Woznicki, B. (1996), *The 5th World Congr. of Chem. Eng.*, San Diego, CA, 6, 125–128 publ. Am. Inst. Chem. Eng., 439
- 136 Wallach, M.L., Heller, W. and Stevenson, A.F. (1964), *J. Chem. Phys.*, 68, 924, 439
- 137 Maxim, L.D., Klein, A., Meyer, M.E. and Kuist, C.H. (1969), *J. Polym. Sci. Part C*, 27, 195, 439
- 138 Brandolin, A., Garcia-Rubio, L.H., Provder, T., Khoeler, M.E. and Kuo, C. (1991), *Particle Size Distribution II*, ed. T. Provder, Am. Chem. Symp. No 472, 20–33, 1, 440
- 139 Kourti, T. and MacGregor, J.F. (1991), *Particle Size Distribution II*, ed. T. Provder, Am. Chem. Symp. No 472, 34–63, 440
- 140 Zollars, R.L. (1980), *J. Colloid Interf. Sci.*, 74, 163, 440
- 141 Brandolin, A. and Garcia-Rubio, L.H. (1991), *Particle Size Distribution II*, ed. T. Provder, Am. Chem. Symp. No. 472, 64–85, 440

- 142 Gossen, P.D. and Mac Gregor, J.F. (1993), *J. Colloid Interf. Sci.*, **160**, 24–38, 440
- 143 Paulson, C.M. (1972), *Eng. Res. Review*, **10**, 11, 441
- 144 Oakley, D.M. and Jennings, B.R. (1983), *Colloid and Interface Science*, **91**, 188, 441
- 145 Bacon, C. and Garcia-Rubio, H.S. (1996), *The 5th World Congress of Chem. Eng.*, San Diego, CA, 534–539, publ. Am. Inst. Chem. Eng., 441

Industrial applications of particle size measurement

11.1 Introduction

The Dupont Company has a group of some 35 individuals who comprise the Particle Science and Technology (PARSAT) core technology team. These individuals have acquired specialist knowledge in the key areas of this subject as indicated in Table 1.1. The particle size analyst is a key member of this team and some of his responsibilities are given in Table 1.1b

Table 1.1a Specialist areas in powder technology

- Particle manufacture, liberation; crystallization, chemical reaction;
- Particle size enhancement; granulation, tabletting, pelletization;
- Particle size reduction; comminution;
- Particle characterization; size and shape analysis, surface area and pore size determination;
- Sampling of powders and slurries;
- Dispersing powders in liquids and gases, interfacial phenomena;
- Fluid-solid separation, filtration, gas cleaning;
- Powder handling; mechanical, pneumatic and hydraulic conveying;
- Dust explosion hazards, environmental concerns;
- Powder characterization; shear strength, bulk density;
- Powder storage; hopper design, powder feeding;
- Powder sorting; screening, classification;
- Powder drying, fluidization;
- Powder mixing and blending;
- Powder coating.

Table 1.1(b) Responsibilities of a particle size analyst

- *Design of particles with good handling characteristics.* Particles that are fragile will break during handling; if this results in an unacceptable product it is necessary to generate stronger particles or gentler handling procedures.

- *Design of granules with acceptable bulk densities.* A limited range of bulk densities is acceptable in many consumer products.
- *Design of products with acceptable end-use properties.* Small differences in shape, size, size and porosity distribution can have considerable effect on end-use properties.
- *Sample selection procedures.* Analyses carried out on a few milligrams may affect the valuation of many tonnes. The size distribution may control the price valuation of a batch or, in the limit, whether it is accepted or rejected. Batches should be thoroughly mixed before samples are extracted and the rules of sampling should be obeyed. Continuous processes are best sampled on-line with due regard to the rules of sampling.
- *Process control.* Continuous processes are best controlled using on-line analysis with feedback. Batch processes can be controlled by representative sampling and, in comminution processes for example, extrapolation to the desired end-point.
- *Design of new products.* Traditionally processes are designed without regard to powder properties and this attitude needs changing. Making particles *right up front* can lead to considerable savings in plant design, down time, retrofitting, product quality and, the bottom line, *return on investment*.

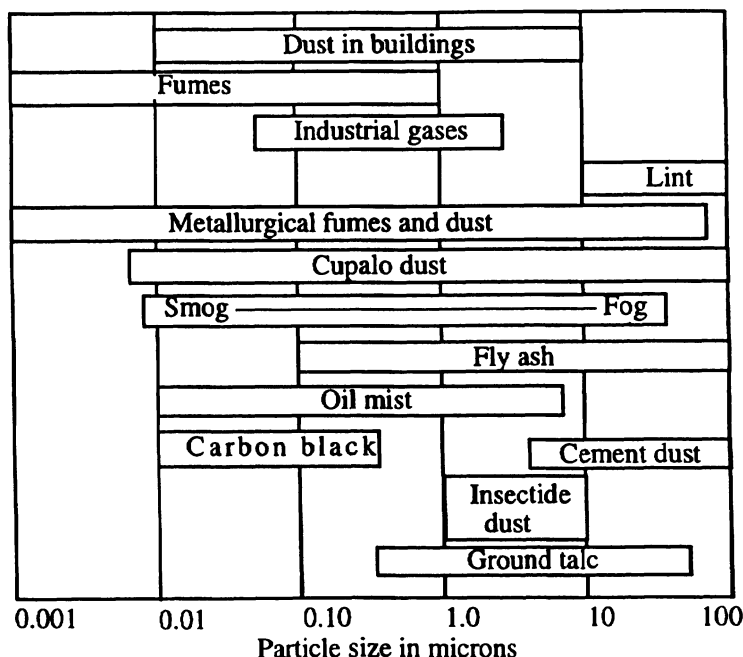


Fig. 11.1 Examples of contaminants classified according to size.

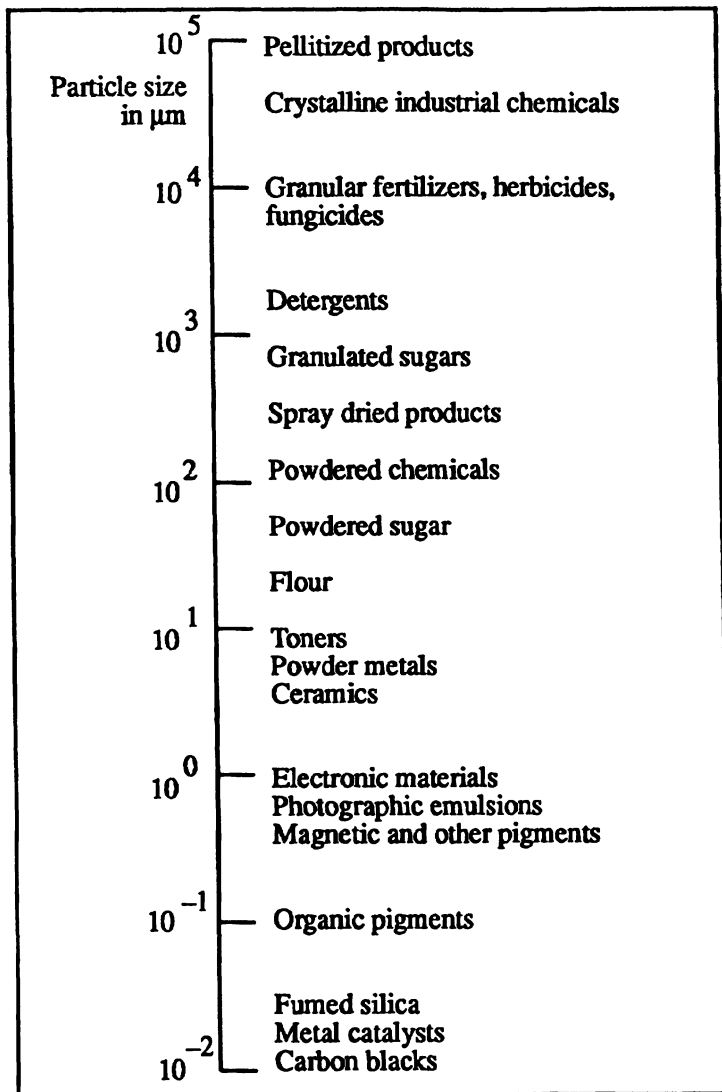


Fig. 11.2 Sizes of typical powder products.

Dupont is usually considered to be a chemical company but it is in fact a powder company. A review of Dupont products reveals that two thirds are sold as powders, slurries, crystals, granules, flakes, pellets, dispersions, etc., and a further 15% have particles added to impart a desired end-use performance [1].

A total of 80% of Dupont products therefore depend on particle technology, and particles have to be made in a form to optimize certain marketing criteria. As well as product requirements, particles are often present as contaminants and impurities.

Just as the measurement of temperature is central to the study of heat, so particle characterization plays a key part in the study of powders. Particle size, shape, surface area and pore size distribution affects such diverse variables as the efficacy of drugs, the life of catalysts, the hiding power and gloss of paints, the mechanical properties of powder compacts and the taste of chocolate. It also affects handling properties such as bulk density, flowability, settling rate, segregation potential, attrition during handling and shrinkage during sintering.

Figure 11.1 shows examples of contaminants classified in terms of their size distributions. Contaminants are seen to cover five orders of magnitude in size, and particle products typically cover seven orders (Figure 11.2).

Adjustment of granule size to give reproducible bulk density is essential, since containers that are only 90% full invite customer rejection and containers that fill to over 100% make packaging impossible.

Producing particles with no asperities is important in eliminating attrition and customer dissatisfaction due to dust production during use, e.g. no one wants to generate a cloud of dust when emptying washing powder into a washing machine.

Drugs ground fine may be toxic, the same formulation ground coarse may be inert. Coarse chocolate tastes gritty, fine chocolate tastes slimy; somewhere between these limits lies a desirable smooth taste.

Particles can be characterized on the basis of size, shape, surface, density, size distribution and pore size distribution. It is then often necessary to relate these primary parameters to the bulk properties of a powder.

In the examples which follow, the importance of good size distribution measurement is demonstrated for a variety of applications. It will be seen from these applications that resolution and detection in specific parts of the size distributions is required for certain end-use correlations, and this demands specific measurement requirements in instrumentation.

The particle size analyst is faced with a bewildering range of instrumentation and, although a manufacturer may push the claims of a particular instrument, it may not be suitable for the type of analysis required. Together with this, a single instrument is usually not sufficient for the wide range of problems associated with particle characterization. These points will be illustrated many times in this chapter.

11.2 Industrial diamonds

As advances in technology create increasing demands for ultra-tight dimensional tolerances, the role of super abrasives is becoming more important. One of these abrasives, DuPont diamond, is widely used for polishing sapphire, ferrites, ceramics, compacted diamond products, multiphase metallographic specimens and other very hard materials. Dupont Mypolex® is synthesized from graphite by transient pressures from 2 to 7 million psi, produced by the controlled detonation of chemical explosives.

The microcrystals so produced are approximately 10 nm in size and these bond together, in a random polycrystalline structure, so that they are equally strong in all directions. The blocky shape facilitates grading into narrow discrete size ranges by sedimentation, elutriation and other processes which depend on Stokes' law.

Customers pay a premium for this product since each grade is narrowly classified with no oversize particles to scratch the surface.

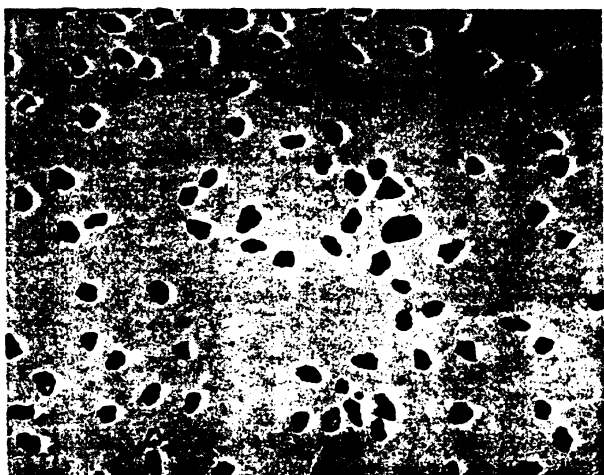


Fig. 11.3 A photomicrograph of graded industrial diamonds.

Particle sizes range from 60 μm (nominal) to 1 μm in traditional increments and from 1 μm to 0.125 μm in steps of 0.75 μm , 0.500 μm , 0.250 μm and 0.125 μm .

A characterization problem arises in that the product is not homogeneous, since a small quantity of graphite co-exists with the diamonds, with the two phases having the same size distribution by Stokes diameter due to the classification procedure employed in their production.

Figure 11.3 shows the uniformity of the 0.25 μm size diamonds in which a larger graphite particle can be seen which, if it were also a diamond, would render the batch unacceptable. A photocentrifuge, which uses a measuring principle based upon Stokes diameter, cannot differentiate between the two phases whereas sedimentation field flow fractionation, which is based on projected area diameter, generates a bimodal distribution.

Figure 11.4 illustrates the problem using a 60:40 mixture of diamonds and graphite; the coarse fraction by SFFF composed of the less dense graphite and the fine fraction being nominal 0.25 μm diamonds. The presence of a small amount of graphite in the finished product is advantageous in that it acts as a lubricant.

11.3 Control of oversize particles in film additives

In photography, particles are added to film to impart a surface friction effect and prevent a roll of film base unrolling on wind-up. Careful

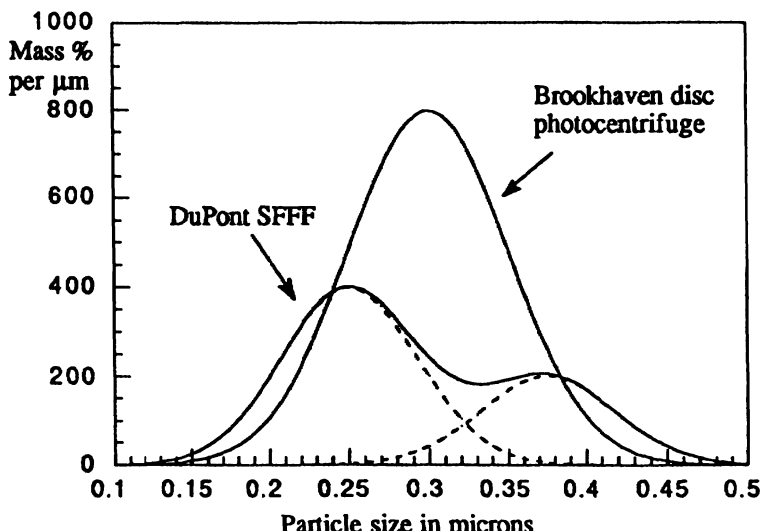


Fig. 11.4 Analyses of a mixture of industrial diamonds and graphite using two measurement methods.

choice of the additive is required, so that no large particles are present and stand out in the film, since these cause end-use problems. Quality is assessed using the Coulter principle, as this has been found to be the best way of determining the number of a few large particles in the presence of millions of small ones, but a sufficient sample needs to be examined to give a statistically acceptable count (Figure 11.5).

A mass balance is carried out by equating the measured volume of powder in the measurement sample with the known volume dispersed in the electrolyte. If the full size distribution is examined the agreement is usually better than 5%; in fact this is the preferred method of calibrating the instrument according to BS 3406 [2]. The Coulter TA II is preferred for this analysis, since it has been found that the Multisizer I cannot be used in this mode due to count loss in the pulse height analyzer, so that as many as 30% of the pulses are lost.

Polymer additives can contain over 10 trillion (10^{10}) particles of various sizes per gram of powder and around 40,000 may be coarser than 15 μm , i.e. oversize for a 3 μm coating thickness. This is equivalent to 1 oversize in 250,000 particles which is unacceptable for many products but difficult to quantify. At a covering of 1g for 13 m^2 , a film contains around 7.7×10^8 particles per m^2 of which, for this case, more than 3,000 are oversize.

Typically, less than a quarter of a million particles are counted by the Coulter Counter to give the oversize count which, for the above

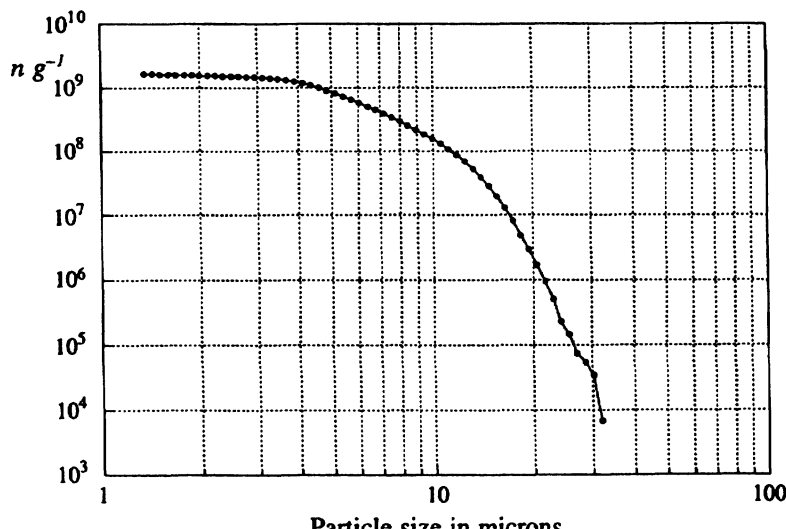


Fig. 11.5 Number oversize per gram distributions of BCR 67 using the Coulter Counter with mass balance.

example, would yield less than 1 ± 0.3 oversize particles. Pre-sieving techniques have been tried in order to reduce the number of undersize particles so that the oversize concentration is increased. These techniques have been found unreliable due to the difficulty of controlling cross-contamination.

A filtration technique was developed in which sample cross-contamination was reduced to an acceptable level by the use of a single container for the particle separation and subsequent number concentration measurement [3]. Precision Transparent Sieves™ (PTS) [4] are used in a specially designed holder for use with the Coulter



Fig. 11.6 Oblique view of $25\text{ }\mu\text{m}$ collimated holes, courtesy of Precision Collimated Holes Inc.

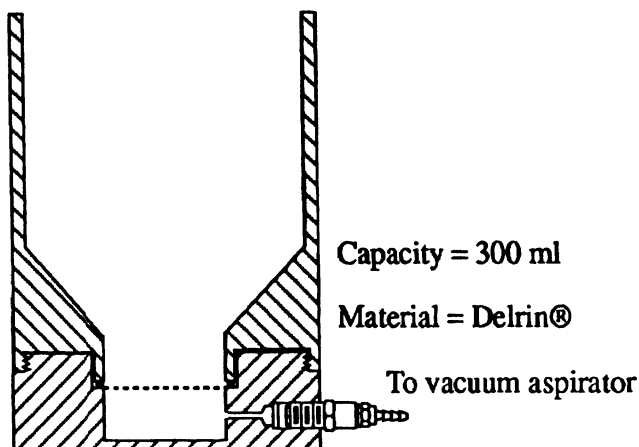


Fig. 11.7 Precision Transparent Sieve holder.

Counter. These PTS are made of uniform parallel holes in chemically stable, optically transparent glass discs. Standard holes diameters are 5, 10 and 25 μm but other sizes can be made. Figure 11.6 taken at a magnification of 500, shows an overhead view of a 15 μm PTS.

The holder is shown in Figure 11.7. In essence the sieve is clamped in the holder which is then filled with an electrolyte. Background counts yield zero oversize count, i.e. with a 15 μm PTS the count at 15 μm is zero. The powder is added and dispersed and vacuum is then applied. The procedure is repeated several times until most of the undersize particles have been removed. A known volume of electrolyte is then added, the residual articles re-dispersed and the oversize count determined. Since the filtration and counting are carried out in the same container, cross-contamination is minimized. An advantage of this procedure is that the particles are retained on the glass filter surface and so that they can be identified as either contaminants or aggregates.

11.4 Starry night

A problem in manufacturing photographic film, known as the starry night effect is due to the presence of oversize particles in the film overcoat (Figure 11.8). This is particularly troublesome with commercial film and x-ray enhancing film, where ultra-high quality is required. It is necessary to add particles to the film otherwise when it is rolled the touching faces will stick together (Figure 11.9). Present manufacturing processes are so fast that the undercoat is still soft when the top coat is added. If the particles are too big they penetrate the undercoat and displace the light sensitive particles. When the film is exposed to light this region becomes a bright spot on the negative, hence its name.

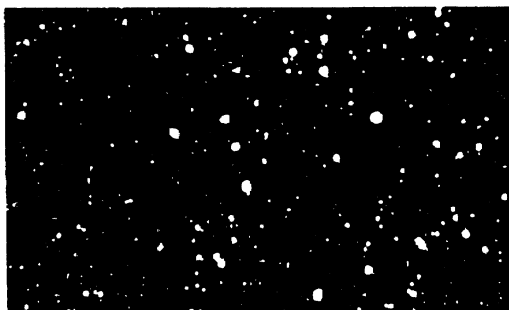


Fig. 11.8 The starry night effect.

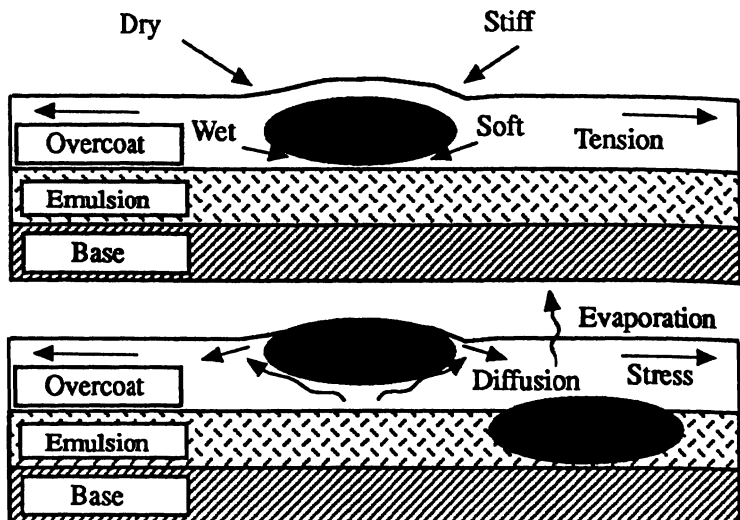


Fig. 11.9 The role of additives in film coating.

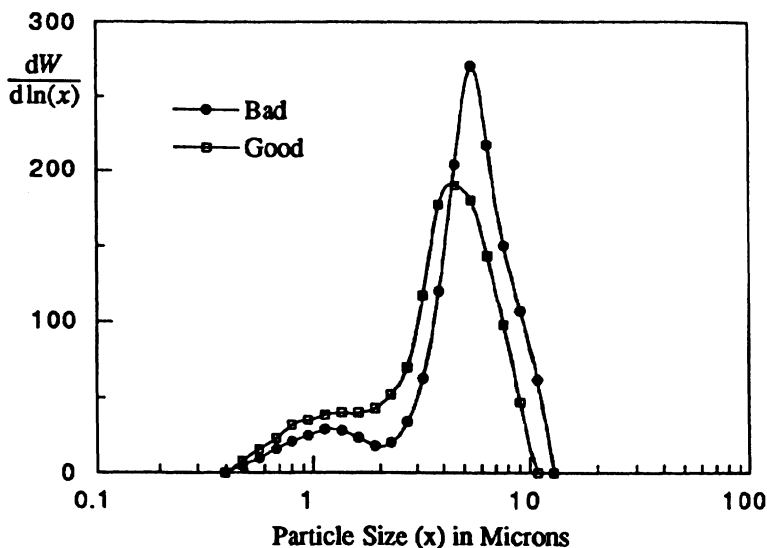


Fig. 11.10 Relative size distribution of good and bad adhesives.

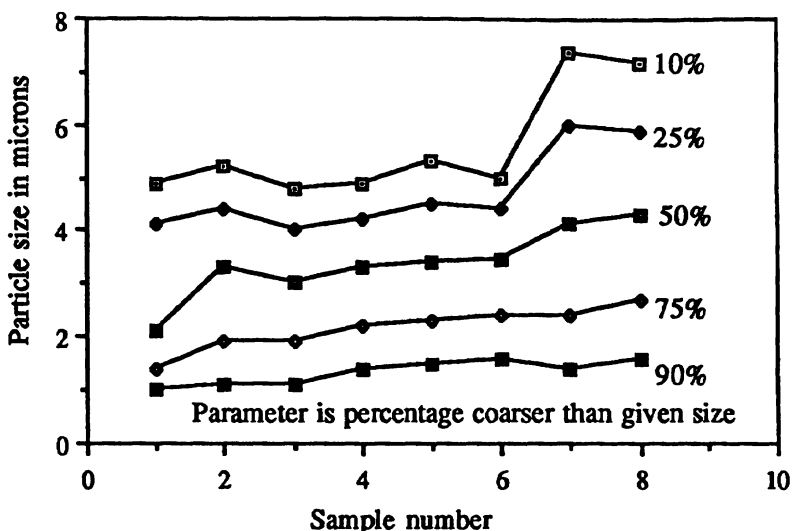


Fig. 11.11 The difference between good and bad film additives.

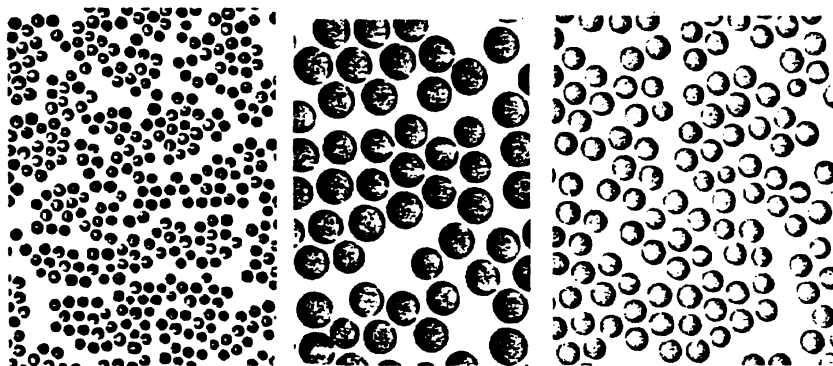


Fig. 11.12 Narrowly classified film additives.

11.5 Control of adhesive additives.

Oversize particles have a similar deleterious effect on the coating efficiency of adhesives. Figure 11.10 shows that the adhesive contains a bimodal distribution of particles; the one that coated poorly has more coarse particles than the one that was acceptable. This figure also illustrates the care needed in presenting data since a cumulative plot

masks the bimodality and indicates that the adhesive having the largest particulate median diameter has the superior coating property.

The presentation in Figure 11.11 shows samples 1 to 5 as overcoats containing a fine adhesive in increasing concentrations (0.068%, 0.136%, 0.212%, 0.425% and 0.637%); samples 6, 7 and 8 are a coarser additive at concentrations 0.068%, 0.212% and 0.425%.

It can be seen that the poorer quality of the latter is due to its larger particle size and that there is some increase in apparent size (flocculation!) with increasing loading.

Table 11.2 Typical micrograph data of relative mass percentages of metal oxide

Size (μm)	Sample designation												
	A	B	C	D	E	F	G	H	I	J	K	L	
0.15	1	1	0	1	0	0	0	0	1	0	0	0	
0.20	3	2	0	2	2	2	1	2	2	1	1	0	
0.30	6	5	6	6	4	4	3	4	3	3	3	1	
0.39	18	16	17	17	15	12	13	13	13	12	10	7	
0.55	32	28	33	29	28	26	30	27	27	27	26	20	
1.30	10	12	12	14	17	21	17	19	19	20	22	25	
2.20	0	0	0	0	5	6	6	7	7	7	7	16	
3.10	0	0	0	0	0	0	0	0	0	1	2	7	
4.40	0	0	0	0	0	0	0	0	0	0	0	0	



Fig. 11.13 Photomicrograph of oxides used for making video tape.

One way of eliminating oversize particles is by growing narrowly classified particles such as the 0.28, 0.55 and 0.75 μm spheres shown in Figure 11.12, each having a standard deviation of less than 0.04 μm .

11.6 Video-tape

Large particles or aggregates are a problem in video tape manufacture. Some oxides are acicular in shape, and size distributions are difficult to measure due to magnetic effects. Figure 11.13 shows a typical photomicrograph. Using continuous dispersion in conjunction with a special Microtrac procedure allowed comparison between samples. Table 11.2 shows typical data. Figure 11.14 shows a tape cross-section containing large aggregates capable of causing poor amplitude uniformity if not drop-outs.

11.7 Curve fitting

Oxide particles used in tape manufacture are of nominal face diameter 0.2 μm and length 0.5 μm and it was found that, using the curve fitting procedure outlined in Chapter 2, they generated a Microtrac SPA distribution similar to that shown in Figure 11.15. Since the algorithm used for converting the scattered light flux into a size distribution is based on spherical particles, it was deduced that the two finer modes referred to the particle dimensions and the third mode was due to aggregates. This was supported by the finding that the area under the two primary modes was directly related to product quality (Figure 11.16).

11.8 Effect of size distribution on filter efficiency

When demand increases for a particular product, plant personnel are often subjected to pressures to step up the rate of production and this may lead to unwanted side effects. Figures 11.17 illustrate the differences in the size distribution of a product pumped at different flow rates. Increasing the flow rate caused the slurry to plug on-line filters more rapidly. The differences are subtle: the main effect of increasing the flow rate is to decrease the size of the coarse mode (agglomerates) from 1.65 μm to 1.22 μm , and the spread, [geometric standard deviation (σ_g)] from 2.17 to 2.12. The fine mode remains substantially constant at $0.47 \pm 1 \mu\text{m}$ and the spread decreases from 1.39 to 1.38. The percentage under the fine mode remains constant at $58\% \pm 1\%$.

11.9 Predicting pigment gloss and hiding power

The magnitude of the tails of a particle size distribution is of fundamental importance in pigment production. Gloss is adversely

affected by the presence of a few large particles and hiding power increases as the fraction of small particles increases (Figures 11.18 and 11.19). Accurate simultaneous measurement of the coarse and the fine end of a sub-micron powder is a tough assignment for any instrument hence tailor made instrumentation is needed.



Fig. 11.14 Cross-section of a tape showing unwanted large particles.

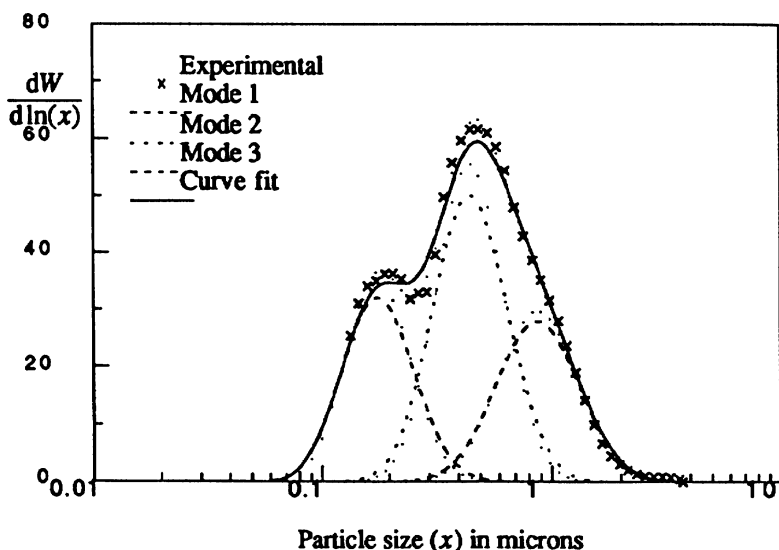


Fig. 11.15 Curve fitting a trimodal log-normal equation to Microtrac SPA data.

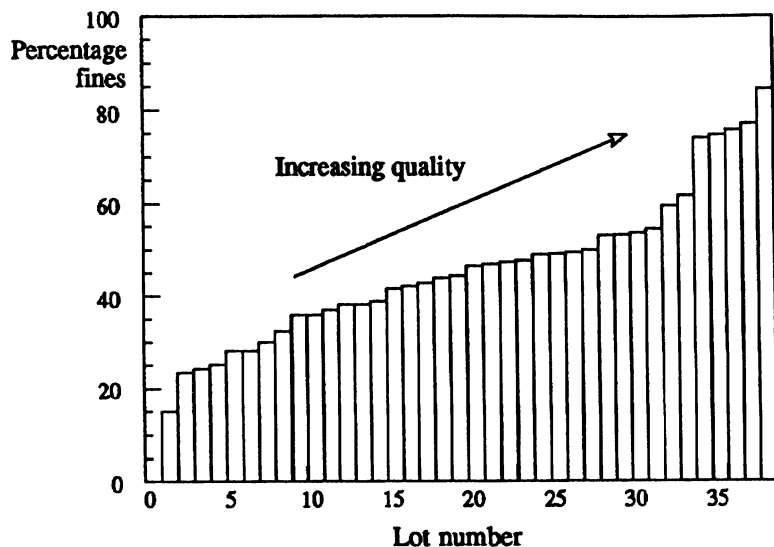
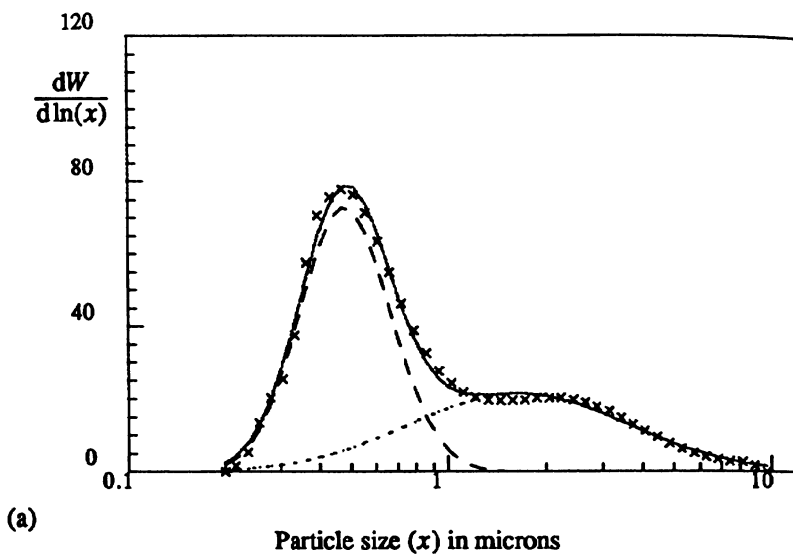


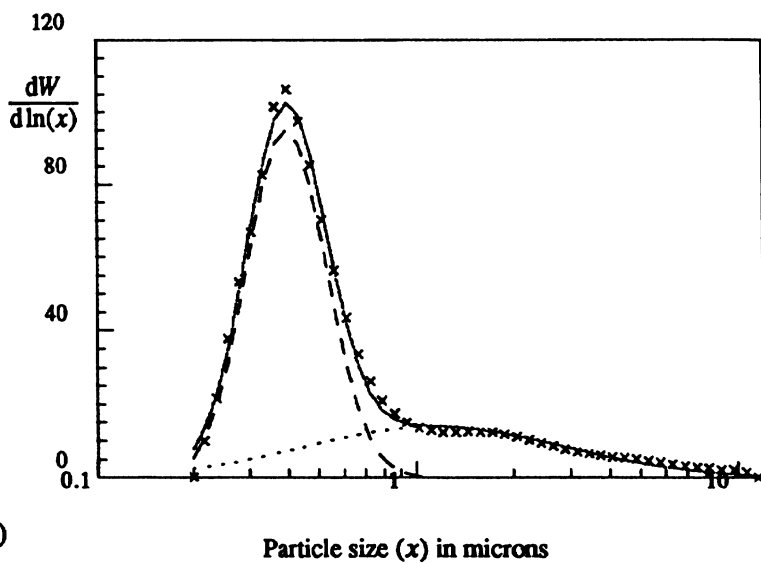
Fig. 11.16 Relationship between amount of product in the two fine modes of a trimodal distribution and product quality.

The problem becomes even more difficult when the pigment is dispersed and mixed with various additives to make a paint. It is necessary to ascertain whether poor gloss is due to the presence of large particles or to flocculation of the paint in formulation. To do this, it is necessary to analyze the state of the particles in the film itself using image analysis. Sample preparation is time consuming, and must be done correctly. Furthermore, since the particles are sub-micron, TEM or SEM images are needed. Figure 11.20 shows a typical photomicrograph of a paint film cross-section; comparison of different sections of the cross-section can be made to study sedimentation in a film and film quality.

Flocculation is indicated by the mass median diameter of the inter-particle distance, the larger the diameter the more the flocculation. Pigment crowding, illustrated by pigment volume concentration, has a profound effect on quality. Size analysis of pigments and paints involves accurate measurements of the tails of the distribution together with accurate measures of single and multi-particle groups. Sizing methods combine x-ray sedimentation with light scattering end-use and image analysis of paint cross-sections. These distinctly different physical principles combine to predict end-use performance.



(a)

Particle size (x) in microns

(b)

Particle size (x) in microns

Fig. 11.17(a) Size distribution of a slurry pumped at 25 g m^{-1}
(b) Size distribution of a slurry pumped at 100 g m^{-1} .

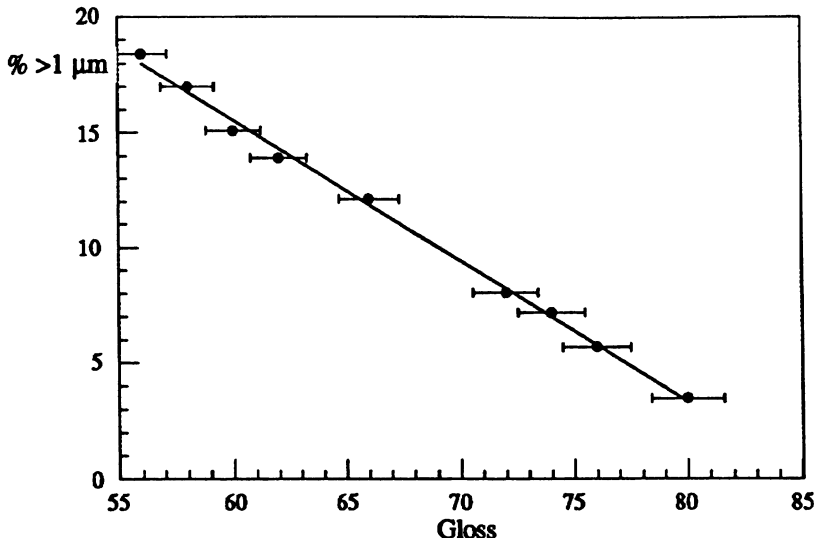


Fig. 11.18 Relationship between gloss and pigment size.

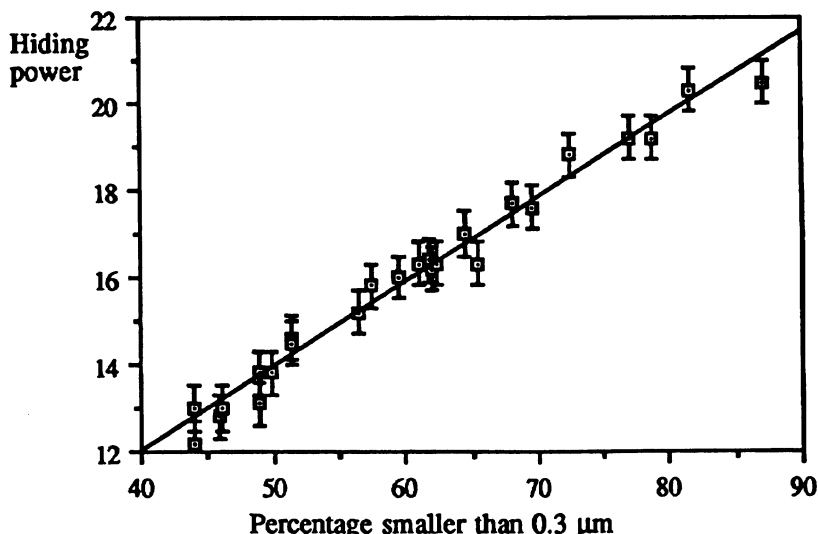


Fig. 11.19 Relationship between percentage smaller than 0.3 μm and pigment hiding power.

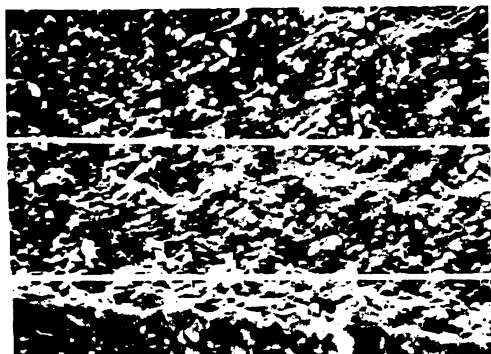


Fig. 11.20 Photo-micrographs of typical paint film.

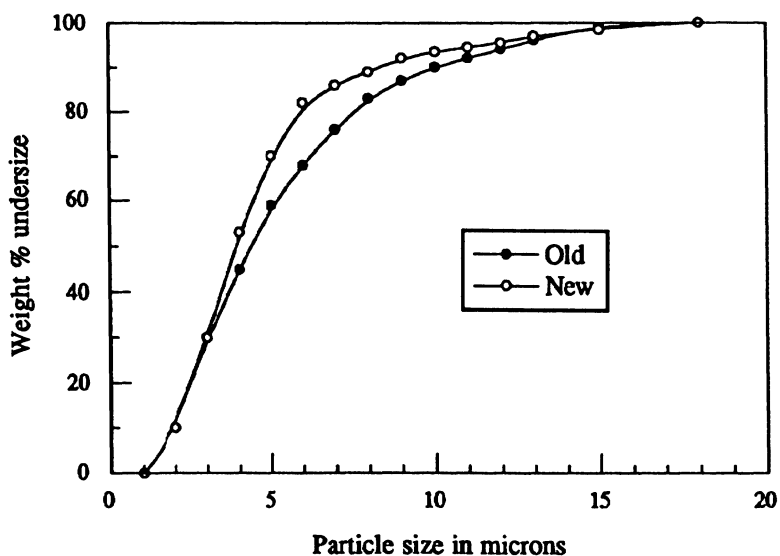


Fig. 11.21 Sedigraph size distributions of two additives for impact strength enhancement.

11.10 Strength of engineering plastics

Large particles are detrimental when powder is used to impart impact strength to engineering plastics, since they become crack initiators. Small differences in size distribution can markedly change impact strength. Figure 11.21 illustrates how a small reduction in the quantity of coarse particles leads to a new, improved product. Thus a knowledge of the optimum size distribution is necessary for good product control. The additive was measured by taking good and bad plastic, dissolving off the polymer and measuring the particle size distribution of the residue with the Sedigraph. This test enabled plant personnel to establish tight specifications on the additive particles per gram using the Coulter Counter and a sample on which a mass balance was carried out.

Sometimes it is possible to greatly inhibit crack propagation by introducing a bimodal size distribution (Figure 11.22); here the filling of inter-particle voids greatly increased crack resistance. Size distribution measurement helped to optimize the crack resistance by designing the particle distribution to minimize inter-particle voidage in the polymer matrix while eliminating the presence of crack initiating large particles.

11.11 Homogeneity control of ceramic paste

During the manufacturing of pastes, for use as dielectrics in electrical capacitors, the size and size distribution has to be carefully controlled since a small deviation from the ideal size causes defects due to porosity (Figure 11.23). Too fine a distribution causes blistering during

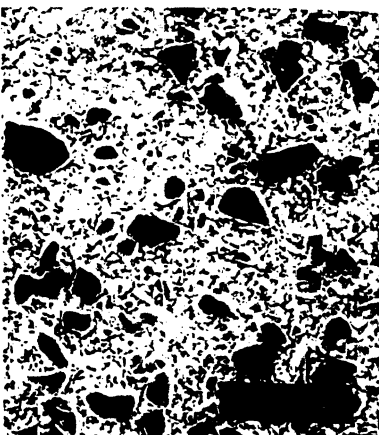
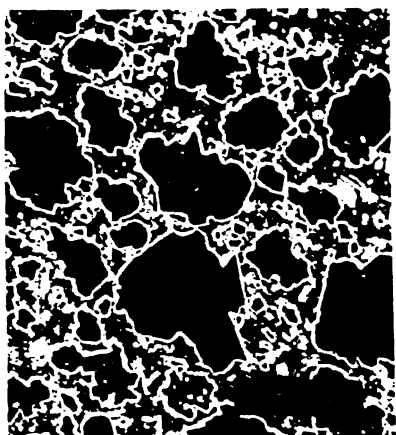


Fig. 11.22 Strength of plastics (a) is the original matrix which has low strength and (b) the high strength bimodal mixture.

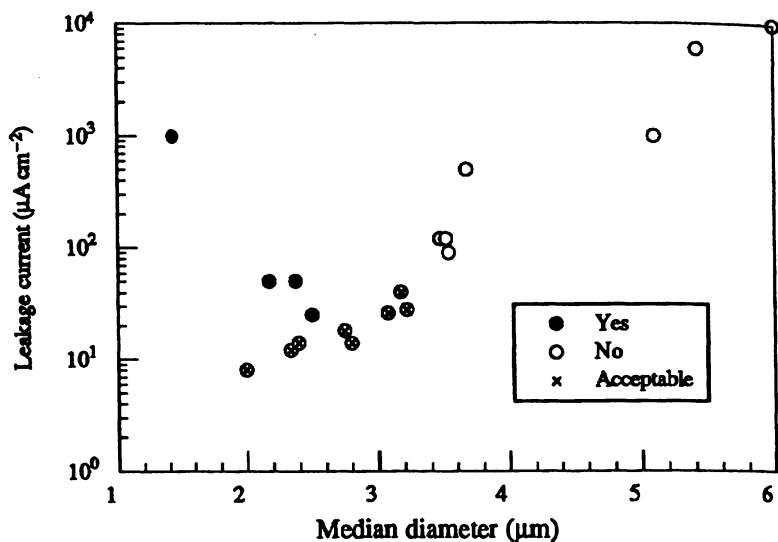


Fig. 11.23 Dielectric leakage current versus frit particle size.

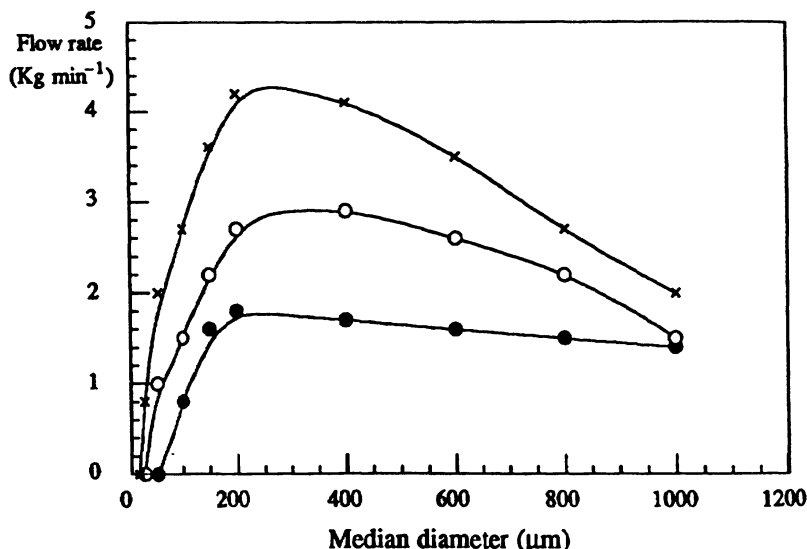


Fig. 11.24 Flowrate of three powders through a circular aperture.

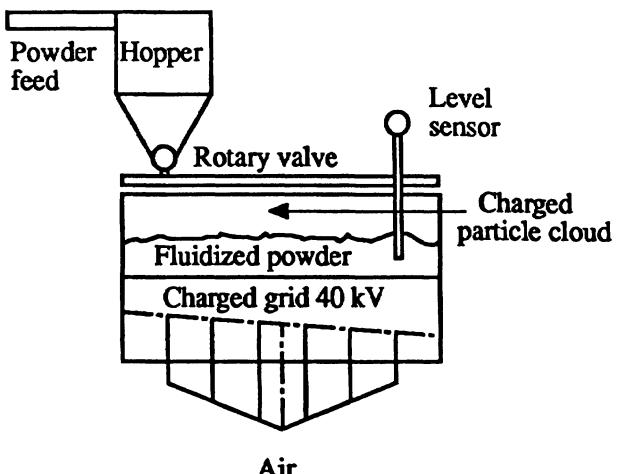


Fig. 11.25 Coater.

sintering and too coarse a distribution leads to electrical leakage. Interlot variability can be reduced by mixing and intralot variability by control of milling.

11.12 Flowability

An optimum granule size is essential for high flowrate pneumatic conveying. Figure 11.24 shows that flowrate through a circular aperture for three different powders correlates well with the Coulter Counter median diameter and shows a definite maximum around 250 µm.

Flowability of cohesive resins and polymers can be enhanced by the addition of flow aids such as hydrophobic silicas. For optimum end-use performance this has to be applied with the correct size of agglomerates. One example is a glass bottle coating operation which used a polymer powder. Hot bottles were passed through a cloud of polymer (Surlyn®) particles in the coater shown in Figure 11.25 in order to deposit a polymer skin on the exterior of the bottle. In order to work in the coater the powder had to remain fluidized for 4 to 6 h using a minimum air velocity. Of 10 million pounds made, only 2 million met these operating criteria. Hydrophobic silica was coated on to the polymer powder in a high intensity mixer and an optimum residence time and silica concentration defined (Figure 11.26) which gave both good flow and fluidity. Too much silica gave an unacceptable hazy appearance to the bottle. SEM photographs showed that the silica agglomerates on the resin surface had to be large enough to impart glidant properties to the powder but small enough not to be

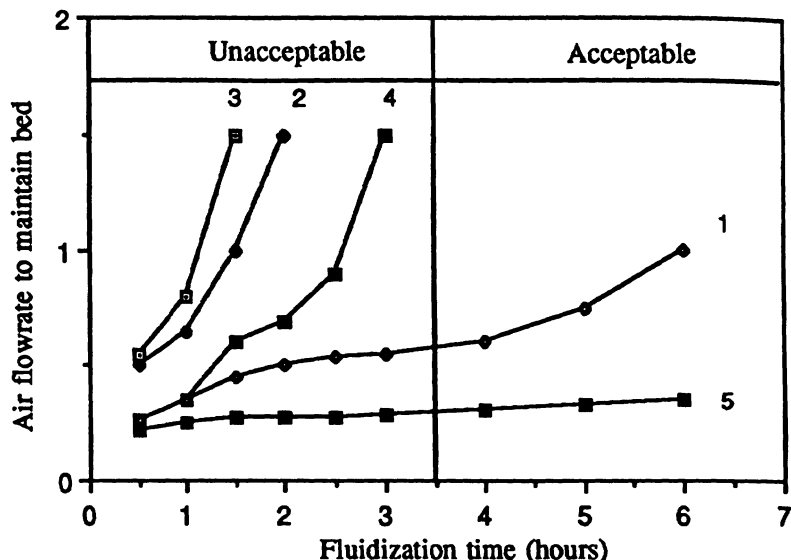


Fig. 11.26 Fluidity/fluidization time relationship.

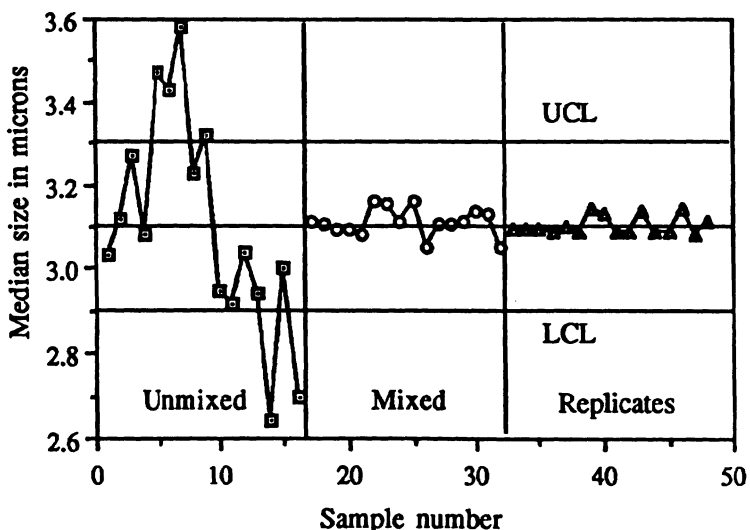


Fig. 11.27 Effect of mixing on powder homogeneity.

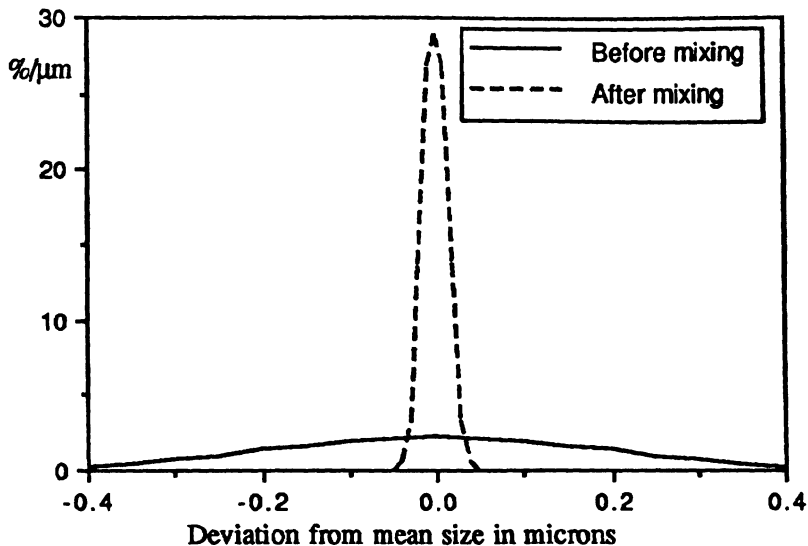


Fig. 11.28 Reduction of intralot variability by a factor of 14 with mixing.

removed by the action of the fluidized bed on the coater. Too small flowed poorly causing the bed to collapse; too large—aerated from bed: Just right—worked well became known as the Goldilock principle of flow aid addition. Careful addition of silica under high shear mixing produced optimum size agglomerates and converted 8 million pounds of out-of-specification powder into useful product.

11.13 Elimination of intra-lot variability by mixing

It is well known that free flowing powders tend to segregate, but not so widely recognized that cohesive powders may segregate during manufacture and need to be mixed prior to assay. Figure 11.27 gives the median sizes, generated using a Leeds and Northrup Small Particle Analyzer, of 16 samples taken at random from an unmixed batch of product together with 16 samples taken after mixing. The acceptance criterion was that one out of three sequential samples had to be within the upper (UCL) and lower (LCL) control limits. This resulted in acceptance of bad product and rejection of good. The standard deviation with replicate runs, i.e. 16 samples taken from a master dispersion using a single extracted sample, is the same order as the sampling errors. A more dramatic representation of the impact of mixing on product quality is given in Figure 11.28.

11.14 Mixing and segregation

Though mixing can be used effectively, the choice of an unsuitable mixer and bad subsequent handling can cause problems. Every powder analyst has seen examples of a mixing process followed by a segregation process e.g. a mixer emptying into a core flow hopper to form a heap of segregated powder within the hopper. Practices such as this can completely undo whatever good the mixer has done.

A powder is used in polymer filtration cartridges. For economy reasons the used filters are broken down and the powder reclaimed. This reclamation results in highly segregated material with wide variations in particle size distribution. This appears solvable by the use of a mixer. The choice of a mixer might appear simple at first sight but the constraints imposed on the mixing made the decision more difficult. Firstly, batches of 6000 lb were not uncommon; secondly, different size grades had to be mixed sequentially and, thirdly, it was important that the mixer did not generate fines during the mixing process.

The particles were very irregular in shape and were compressed into the filter cartridges at a pressure of several tons per square inch. Excessive fines caused large pressure drops across the filters during service and high starting pressure drops were linked to short life and inefficient service.

Uniformity of pressure from filters made from the same lot was another requisite, hence powders should not segregate during the time a lot was being used. To minimize this, lots consisted of 25 lb bags. Mixing therefore had to:

1. Mix 600 lb batches of material which had a tendency to segregate.
2. Minimize fines production.
3. Empty the mixer without segregation through a bagging system.
4. Bag 25 lb batches in such a way that they could be transported to the press without segregation.
5. Be homogeneous enough to produce filters having low starting pressures with little inter-pack variation.

Unfortunately, the most commonly used size fraction was also the worst for segregation and attrition. Sampling and size distribution measurements were carried out for a range of mixers: Figure 11.29 showing typical ribbon blender fines concentration, as a function of axial and radial mixing, at mixing times of 5 and 15 min and during emptying. Clearly fines were generated during mixing, and segregation occurred during discharge. A Nautamixer, on the other hand, mixed the material in 5 min with no noticeable attrition and, due to its mass flow hopper design, emptied with no segregation (Figure 11.30). Packing 25 lb bags tightly full from the Nauta discharge maintained

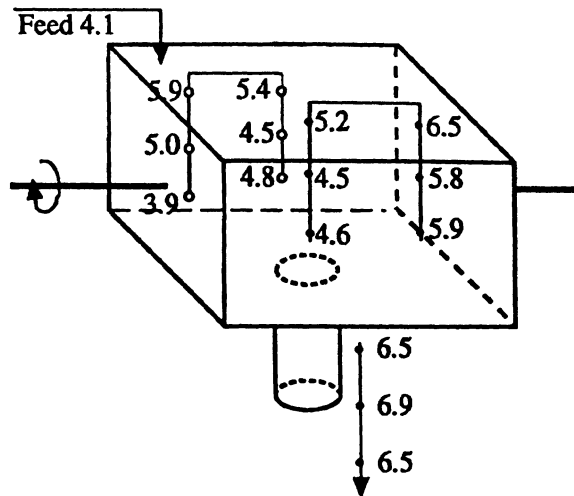


Fig. 11.29 Fines concentrations in a ribbon blender at three sampling locations, two mixing times and during emptying.

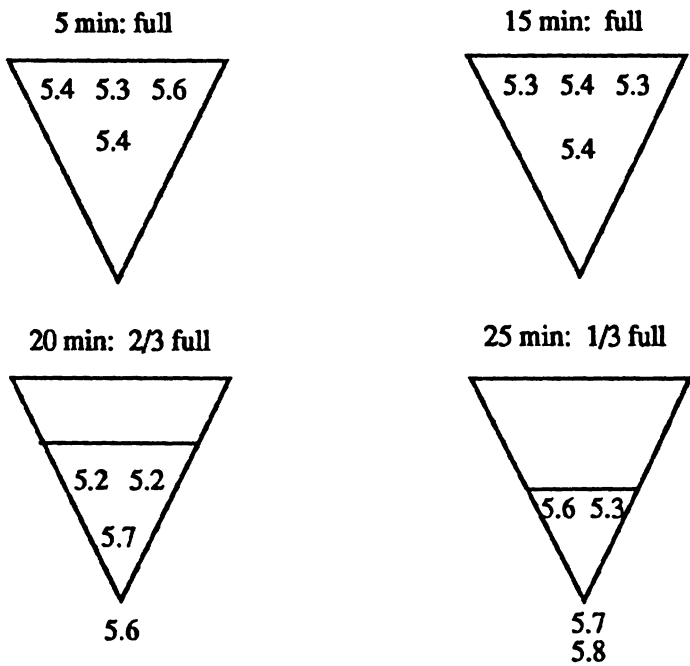


Fig. 11.30 Fines (%) distribution in a Nautamixer after mixing and during emptying.

Table 11.3 Shape data for abrasive grinding

Mill Type	Weight %	Elongation	Flakiness
Roll	28.4	1.71	1.57
	23.2	1.63	2.06
	48.4	1.57	2.03
Impact	93.1	1.34	1.35
	6.4	1.41	1.42
	0.5	1.57	2.23
Ball	63.1	1.49	1.47
	17.8	1.57	1.55
	19.1	1.63	2.58
Rod	96.1	1.47	1.37
	3.8	1.43	1.55
	0.1	1.50	1.70

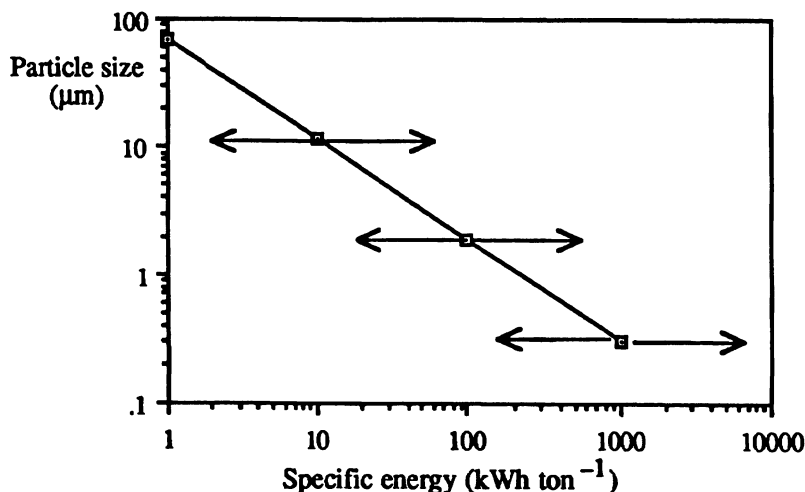


Fig. 11.31 Relationship between particle size and energy input to a mill.

homogeneity by rendering the powder grains immobile. Particle size distribution measurements identified possible segregation problems and made the choice of the best system possible for this particular application.

11.15 Comminution

There are few industrial processes that do not involve comminution, i.e. size reduction. It has been estimated that one twentieth of the artificially generated energy in the world is spent on particle comminution and an energy requirement of a fraction of a percent would save billions of dollars. This operation is used to:

- Decrease the size of material;
- Increase surface area;
- Free material from a matrix (beneficiation).

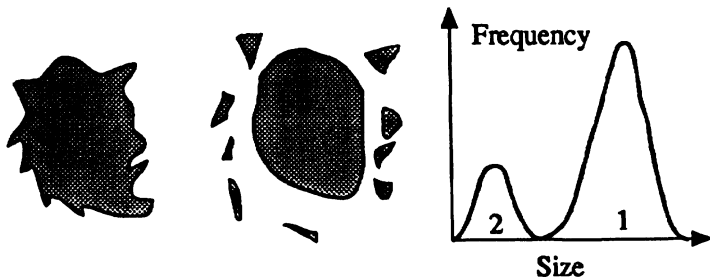


Fig. 11.32 An illustration of the concept of particle attrition.

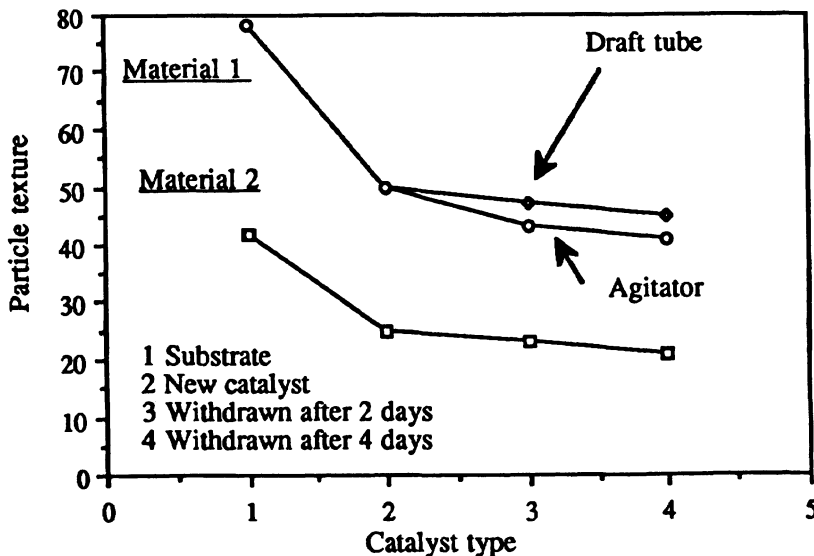


Fig. 11.33 Relationship between particle texture and energy input to a mill.



Fig. 11.34 Photograph of catalyst grains.

Choice of the correct machine can greatly reduce operating costs as is shown in Figure 11.31 where the spread of data points illustrates the effect of the grinding equipment on the mass median diameter. In Table 11.3 the choice of mill on the basis of yield in the optimum shape category to produce abrasives is shown. Elongation $E < 1.5$; flakiness $F = 1.35$ is demonstrated for a typical abrasive system. Size measurement and size production can never be made, in the absence of shape criteria.

Comminution is an example of wanted breakage whereas attrition is a special type of unwanted breakage in which protuberances are broken off the parent particles to generate a bimodal distribution to produce an undesirable dusty powder. Figure 11.32 illustrates this concept; the challenge is to find a method of accurately measuring the small fraction of fines generated.

11.16 Attrition

A product yield difference found using two catalysts was traced to a difference in the surface texture of the two materials. The material having a rough texture produced more fines than the smooth material and these reacted adversely downstream. Figure 11.33 shows attrition displayed in terms of particle texture, which was determined by shape analyses on catalyst support grains as shown in Figure 11.34. First there is a marked difference between the two substrates, demonstrated

by substrate 2 having a smoother texture than substrate 1. Secondly the rate of smoothing (i.e. attrition rate) is greater for substrate 1. Furthermore note the effect of agitator design; a draft tube system being gentler than an agitator.

11.17 Instrument evaluation

11.17.1 Introduction

The literature on the measurement of particle size distributions contains numerous references to anomalous results using identical powders. There are several possible explanations for these differences.

(a) The techniques may be measuring different size parameters

Particle size is not a unique property of a particle but depends upon the method of measurement. Diameters are only equivalent for spherical, homogeneous particles. However, for all but the most extreme of shapes, the differences between diameters measured by different techniques should be quite small.

(b) The amount of material assigned to a particular size range also depends upon the measurement technique

For example, the Coulter Counter counts the number of particles between two particle volumes; hence, the number of particles between two volume diameters is calculated. Errors arise in any technique in which particles are counted and the count converted to a volume (mass), unless the number counted is very large or the size range is very small. For example, the Coulter Counter spans a size range of 30 to 1 and the volume of a 30 μm particle is the same as the volume of 27,000 1 μm particles. Thus increasing the number detected in the top channel by a single particle is equivalent to increasing the count in the bottom channel by 27,000 particles. This error can be minimized by counting a sufficiently large number of particles in the top channel but this makes the total count excessively large.

In sedimentation techniques, suspension can be physically withdrawn and the weight of powder in the withdrawn sample determined by weighing. Alternatively, the weight can be deduced from the attenuation of an x-ray beam. In either case the mass oversize is proportional to the weight of powder in the sample.

Photosedimentometers use a light beam, but the interaction between particles and a light beam is so complex that accurate determination of the amount of powder in the beam is difficult. The situation is rendered more difficult when the suspension is sedimented in a centrifugal force field, with an initially homogeneous suspension, due to the problem of radial dilution; i.e. particles move away from each

other as they settle out on radial paths rather than the parallel paths followed with gravity sedimentation.

Particle size is determined using Stokes' equation, the Stokes diameter being the diameter of a sphere which settles at the same velocity as the particle under the same conditions. This is not a unique diameter for a particle since it depends on particle orientation during settling.

Low angle laser light scattering (LALLS) instruments generate classical black box data. The forward scattered light flux is relatively easy to calculate for a known system of opaque, spherical particles. Calculating the particle size distribution of partially transmitting, non-spherical particles from the measured light flux is an entirely different matter. Each manufacturer uses his own conversion algorithm, so each instrument generates a different size distribution. The differences here therefore can be considerable.

(c) The samples may not be identical

Powders have a natural tendency to segregate and, unless sampling is carried out with extreme care, samples can be widely disparate.

(d) The degree of dispersion may not be the same

Some powders are very easy to disperse whereas others pose considerable difficulty. Some powders increase in fineness with increasing energy input, seemingly without limit. (The limiting size may be the primary particle size but this is approached asymptotically.)

It is not uncommon to find that easily dispersed, identical samples analyzed on similar equipment generate different size distributions. These differences are attributable to incorrect operating procedures, poor calibration or differences between instruments. Operating conditions can also affect the results. For example, cuvet photocentrifuges can operate in two modes; constant speed or speed increasing with time, and the derived data are significantly different with the former being most accurate and reproducible. The resolution in sedimentation techniques is affected by the ratio of the height of the sampling zone to the height of fall and by the speed of the analysis if it is too fast. Errors also arise if gravity sedimentation is used for particles that are too large, due to the breakdown in Stokes' equation, or too small due to the onset of Brownian motion.

The criteria in selecting particle size measuring instruments are many and varied. Obviously the desired application is of paramount importance, whether the instrument is to be dedicated to one product or required for a range of materials. Two criteria, covered here, are reproducibility and accuracy. It is found sometimes, however, that even though an instrument has high reproducibility, similar instruments sitting side by side can give very different data.

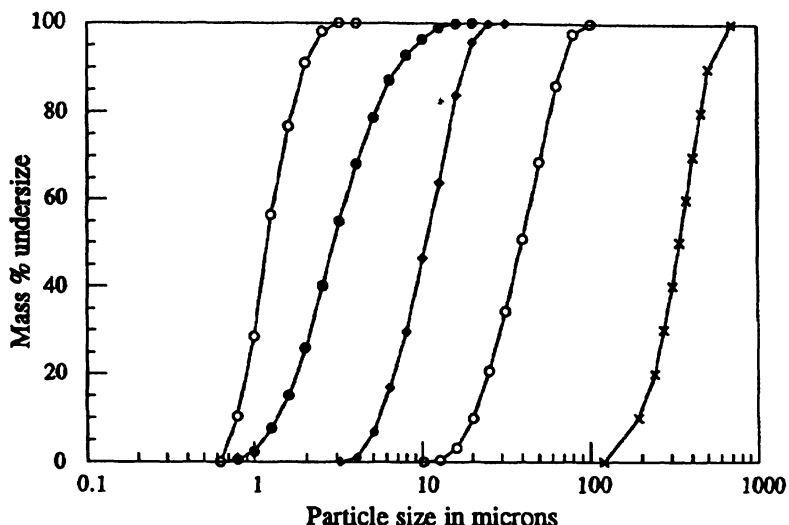


Fig. 11.35 Certification data on BCR powders.

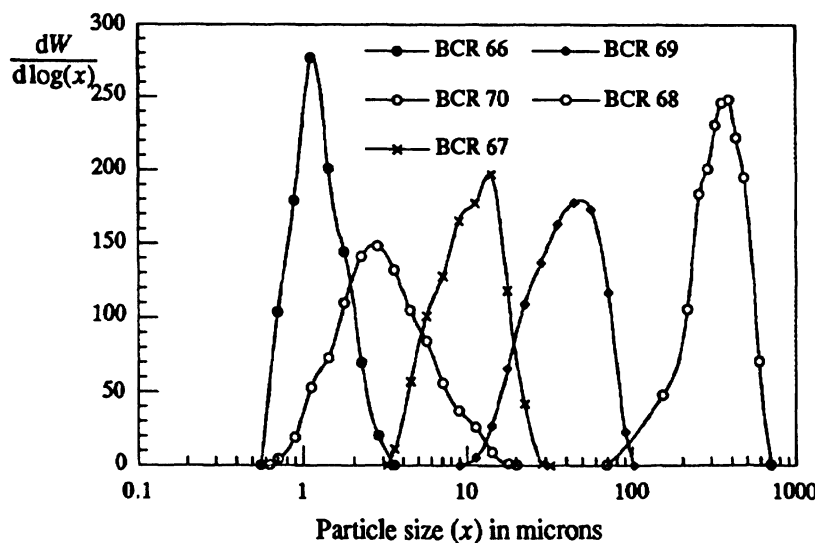


Fig. 11.36 Mass percentage frequency distribution of BCR standard powders.

Commercial instruments may be highly reproducible but inaccurate or accurate with poor reproducibility. Even instruments operating using the same physical principles can give widely different analyses. To help resolve these problems various instruments have been assessed for accuracy and reproducibility with respect to silica standards [5]. Accuracy is important in relating powder properties to particle size. Reproducibility is important in process control and should be high enough not to mask product differences. Instruments are always operated under optimum conditions, with the proviso that in some cases the analyses were carried out by the suppliers under supervision and they selected the operating conditions.

Other factors have to be considered when selecting an instrument, such as capital costs, running costs, ease of use (operator friendliness), speed, reliability, versatility, and operating size (and concentration) range, together with the manufacturer's back-up facilities for repairs and replacements.

11.17.2 Evaluation procedure

A particle size consultant is required to recommend instruments to his clients and these recommendations can be either subjective or objective. In order to be as objective as possible it is necessary to evaluate instruments, and for these instrument evaluation tests it is necessary to eliminate sampling and dispersion errors. This has been done by using four standard quartz powders (Figures 11.35, 11.36), certified by their Stokes diameters.

BCR 66, Size range 0.35 to 2.5 µm, density 2.62 g cm⁻³

BCR 70, Size range 0.5 to 12 µm, density 2.64 g cm⁻³

BCR 67, Size range 3 to 20 µm, density 2.65 g cm⁻³

BCR 69, Size range 12 to 90 µm, density 2.65 g cm⁻³

It is known that these powders disperse readily and the procedure employed to reduce sampling errors to a minimum was to extract measurement samples from an agitated master blend. Instruments have been evaluated on the basis of accuracy and reproducibility as defined below.

$$\bar{s} = \sum_{P=0}^{100} \frac{s\Delta P}{100}$$

11.17.3 Definition of accuracy

Experimental data has been quantified by introduction of two definitions.

Accuracy (*A*) is a measure of how closely the measured data reflects the standard silica data:

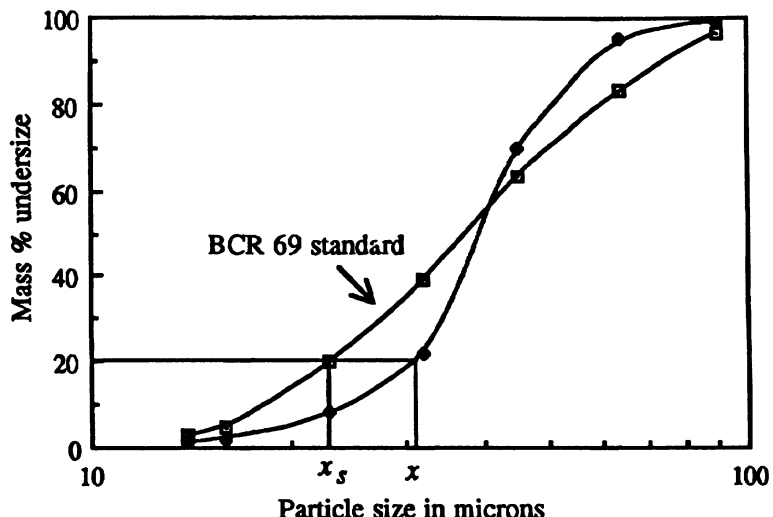


Fig. 11.37 Accuracy is defined as the percentage deviation of experimental data from standard data.

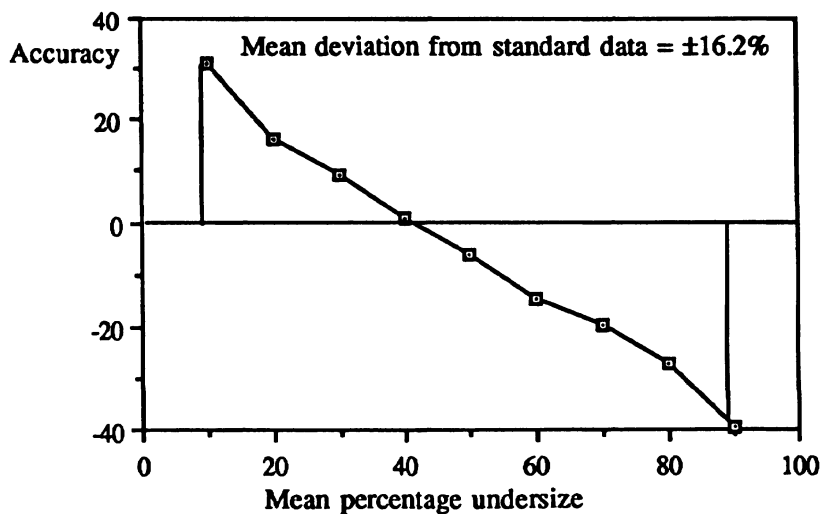


Fig. 11.38 Graphical description of mean accuracy.

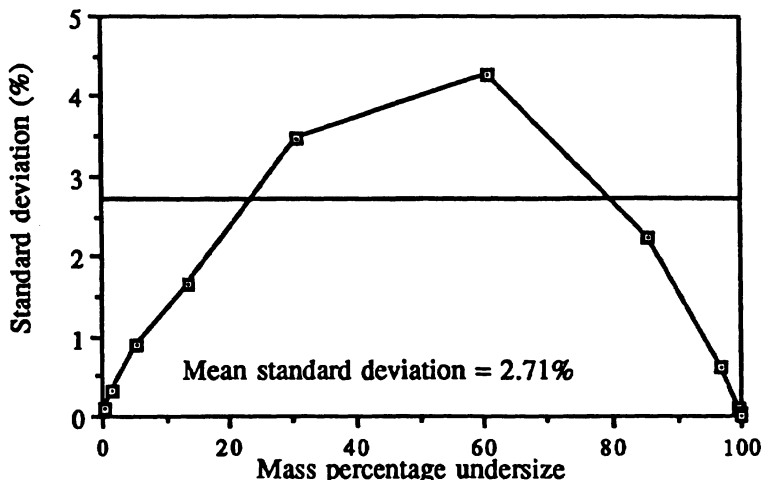


Fig. 11.39 Calculation of *mean reproducibility*.

$$A = 100 \frac{(x - x_s)}{x_s} \quad (11.1)$$

where x and x_s are the measured and standard sizes at the percentiles (Figure 11.37).

Since the differences between the measured and standard distributions are difficult to quantify at the extremes of the distribution, the mean accuracy has been defined as the average value of A between the percentiles for the standard powder from 10% to 90% (Figure 11.38), i.e.

$$\bar{A} = \sum_{P=10}^{P=90} \frac{A \Delta P}{80} \quad (11.2)$$

Thus $80\bar{A}$ is the area under the graph of A against P from $10 < P < 90$ and \bar{A} is the mean value of A (Figure 11.37) without regard to whether the error is negative or positive.

It is emphasized that high values for mean accuracy indicates that the measured diameter is very different from the standard (Stokes) diameter. Since the mean accuracy for the Coulter Counter is low this also indicates that the measured diameter differs widely from the volume diameter.

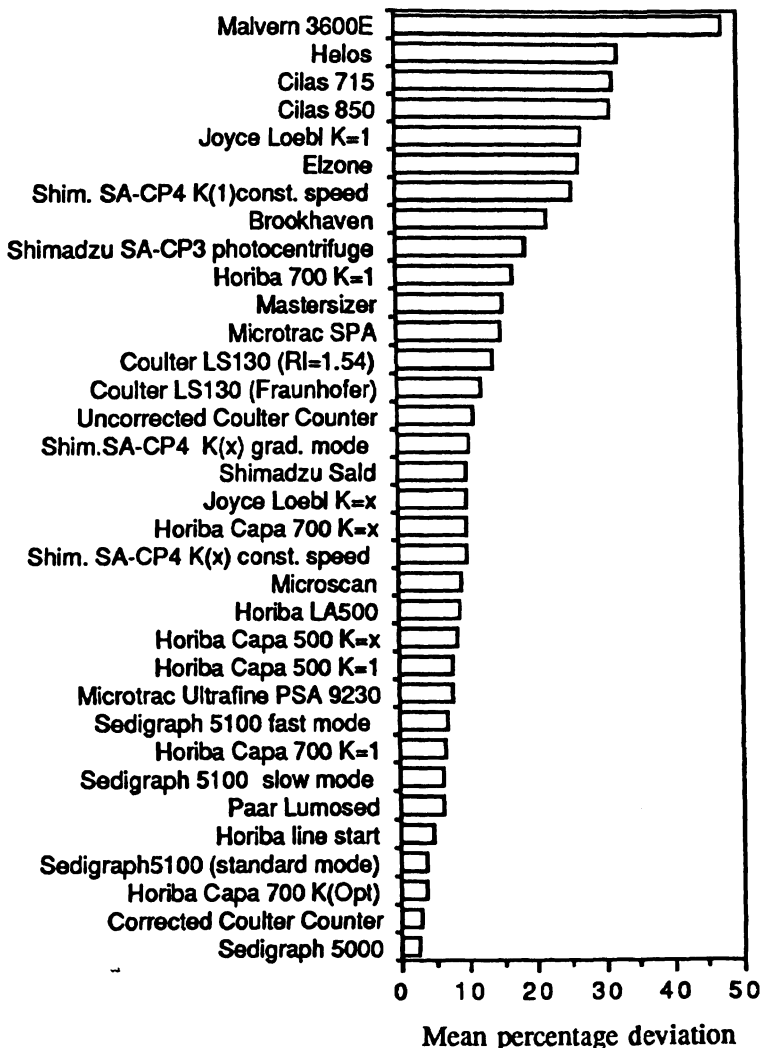


Fig. 11.40 Mean percentage deviation from standard BCR 66 data.

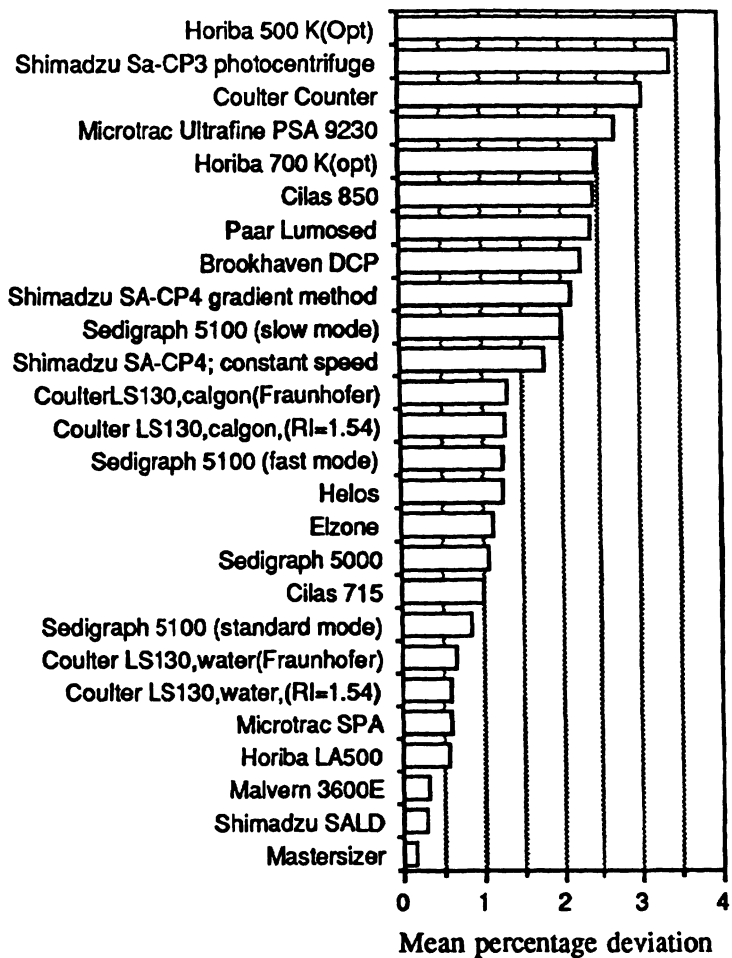


Fig. 11.41 Mean instrument reproducibilities for BCR 66.

11.17.4 Definition of reproducibility

Where feasible, instruments were run six times to assess reproducibility, which has been defined as average standard deviation \bar{s} where:

$$\bar{s} = \sum_{P=0}^{100} \frac{s\Delta P}{100} \quad (11.31)$$

100 \bar{s} being the area under the error curves (Figure 11.39).

Table 11.4 List of instruments examined

Brookhaven disc photocentrifuge
Brookhaven BI-XDC disc x-ray centrifuge
Cilas 715 (LALLS)
Cilas 850 (LALLS)
Coulter Counter, mass balance corrected (BCR 66)
Coulter LS130 (Fraunhofer Model)
Coulter LS130, refractive index (quartz) = 1.54)
Coulter Counter (uncorrected for undersize)
Elzone Electrical Sensing Zone
Galai
Horiba cuvet photocentrifuge Capa 700 $K=1$
Horiba cuvet photocentrifuge Capa 500 $K=1$
Horiba cuvet photocentrifuge Capa 500 $K=x$
Horiba cuvet photocentrifuge Capa 700 $K(\text{Opt})$
Horiba cuvet photocentrifuge Capa 700 $K=1$
Horiba cuvet photocentrifuge Capa 700 $K=x$
Horiba LA500 (LALLS)
Horiba cuvet photocentrifuge, line start
Joyce Loebl disc photocentrifuge, $K=1$
Joyce Loebl disc photocentrifuge, $K=x$
Ladal pipette centrifuge
Lasentec Lab-Tec 1000
Malvern 3600E (LALLS)
Malvern Mastersizer (LALLS)
Microtrac SPA (old model) (LALLS)
Microtrac SPA (1992 model) (LALLS)
Microtrac Ultrafine PSA 9230
Paar Lumosed photosedimentometer
Quantachrome Microscan x-ray sedimentometer
Sedigraph 5000 x-ray sedimentometer
Sedigraph 5100 (fast mode) x-ray sedimentometer
Sedigraph 5100 (slow mode) x-ray sedimentometer
Sedigraph 5100 (standard mode) x-ray sedimentometer
Shimadzu SA-CP4 $K(1)$ constant speed
Shimadzu SA-CP4 $K(x)$ constant speed
Shimadzu SA-CP4 $K(x)$ gradient mode
Shimadzu SA-CP3 photocentrifuge
Shimadzu Sald (LALLS)
Sympatec Helos (LALLS)

The deviations from standard data should be approached with caution. A big deviation does not mean that the instrument is in error, it just implies that a different parameter is being measured than by the standard technique (Andreasen).

11.17.5 Mean accuracy and reproducibility

Each instrument has been examined using whichever BCR powders lie in its measuring range. The data were then collected and presented for each instrument in the form of a data bank. The mean data have been extracted and the mean data for BCR 66 are presented here. Accuracy data are presented in Figure 11.40 and reproducibility data in Figure 11.41.

11.17.6 Discussion

Detailed data from the 1992 DuPont internal report are not presented here since instrument performance varies from year to year as the models change, though some general comments still apply. The reproducibility of laser light scattering instruments (LALLS) is around 0.2%, which is a factor ten times better than sedimentation and Coulter type instruments. The deviations from standard Andreasen sedimentation data are, however, around 10% to 20%, which is ten times worse. The general tendency of LALLS is to broaden the distribution, as postulated in chapter 10, reporting more fines and more coarse than the other instruments. The accuracy of x-ray sedimentation depends on the speed of the analysis as predicted by the discussion on thermal diffusion in Chapter 6. The accuracy of the Coulter Counter with BCR 66 improves from 11.2% to 2.9% when a mass balance correction is applied, thus underlying the role of this technique when some of the distribution is outside its normal operating range. The deviations of the photocentrifuges from the standard sedimentation data is around 8%, which is not unexpected when one considers the problems associated with the breakdown in the laws of geometric optics. Their reproducibilities are, not unexpectedly, similar to those of other sedimentation procedures.

11.18 Summary

The examples in this presentation are intended to demonstrate the need for physical characterization of powders in diagnosing particle product and process problems. There is a growing need for in-line and rapid off-line analyses and this technology is poised on the threshold of implementation. In the past, micron size powders were considered to be fine but the present trend is to finer ($0.1\text{ }\mu\text{m}$) and finer ($0.01\text{ }\mu\text{m}$) powders, particularly in the field of electronics, as printed circuits become miniaturized.

A particle size analysis method can be found for most applications but the instrument needs to be *selected*, not just applied because it happens to be in the laboratory. A decision must then be made as to which parameter is of importance to characterize the powder and finally

a method of data presentation must be found to highlight this parameter.

A final example to illustrate this point: Product quality suddenly deteriorated for no apparent reason although the Coulter size distribution by volume, centered around 15 µm, remained unchanged. A microscope examination showed that the particles were essentially around 1 µm in size and that the 15 µm particles were aggregates. Data presentation on a number basis rather than a mass basis highlighted this fact. The change in product quality arose due to a shift in the number distribution, not the mass distribution, and this was not detected initially due to the data presentation method.

The three important essentials with particle characterization are dispersion, dispersion, dispersion! Thus the microscope is probably the most important instrument in the laboratory, since it enables you to see the particles and assess their degree of dispersion. Even microscope examination needs to be approached with caution since the particles are in a different environment than when they are being analyzed.

References

- 1 Hobbel, E.F., Davies, R., Rennie, F.W., Allen, T., Butler, L.E., Waters, E.R., Smith, J.T. and Sylvester, R.W. (1991), *Part. Part. Syst. Charact.* **8**, 29–34 451
- 2 British Standard BS3406 Part 5 (1986). *The electrical sensing zone method of particle size measurement (The Coulter principle)*, 455
- 3 Allen, T. (1992), *Part. Part. Syst. Charact.*, **9**, 252–258, 456
- 4 Precision Collimated Holes Inc., 456
- 5 Allen, T. and Davies, R. (1988), *4th European Symp, Particle Characterization*, Nuremberg, Germany, pp 17–46, publ. NürnbergMesse, European Fed. Chem. Eng., 480

- Wu, K., 371 (9.71)
Wyckoff, R.W.G., 145 (3.83)
- Xu, T-H., 375 (9.83)
- Yamaguchi, K., 58 (2.17), 58
(2.19)
Yamamoto, H., 180 (4.64–65)
Yang, F.J., 210 (5.42)
Yau, W.W., 208 (5.34), 211
(5.46–47)
Yawaza, N., 318 (8.61)
Yeager, E., 425 (10.95–96)
Yokoyama, T., 318 (8.60, 8.62),
375 (9.88)
York, P., 256 (6.84)
Yoshida, T., 229 (6.4)
Young, B.W., 377 (9.93)
Yousufzai, M.A.K., 168, 185
(4.40)
- Yu, A.B. 81 (2.51, 2.54–55), 81,
84, 86 (2.53)
Yu, L., 133 (3.53)
- Zackariah, K., 147 (3.97)
Zaki, W.N., 248, 249 (6.36)
Zaltash, A., 62 (2.36)
Zare, M., 375 (9.79)
Zbuzek, B., 154 (3.75)
Zellweger Uster, Inc., 349 (9.29)
Zhang, J.Y., 215 (5.68), 420
(10.76)
Zhu, J.H., 436 (10.125)
Zhukov, A.N., 160 (4.20)
Ziema, M., 375 (9.83–84)
Zollars, R.L., 440 (10.1)
Zwicker, J.D., 157, 180 (4.17),
322 (8.79)

Subject index

The numbers shown in **bold** indicate that a section about the subject commences on that page.

- accuracy **480**
acoustic microscopes **129**
Acucut laboratory classifier **201**
adhesion, work of **258**
adhesive additives. **460**
Advanced Fiber Information System **349**
Aerometrics **374**; Eclipse particle size analyzer **354**
Aerosizer **413**
aerosol **112**; *sampling* **143**
air-jet sieving **178**
Alpine; **180**, *wet sieving device* **177**, *Multi-plex classifiers* **202**, *sedimentation centrifuge* **319**
American Innovision **139**
Amherst API Aerosizer **373**
amount of sample **172**
Amstrad personal computer **138**
Amtec **433**
Analysette 8 **199**
Analytical Measuring Systems **137**
Andreasen **232**, *analyses* **92**, **94**
anisotropic particles **405**
API Aerosizer **417**
apparent density **269**
Archimedean screws **17**
area **133**
arithmetic normal distribution **69**
Artek Omnicon **138**
asbestos **349**
asperities **59**
Astra **435**
ATM Sonic Sifter **180**
atmospheric particle counters **386**
attrition. **475**
auger; sampler. **11**, *process* **145**
autodilution **436**
automatic wet sieving machine **401**
automatic; sampler for belt conveyor. **9**, *wet sieving machine* **397**
Automatix **138**
Autometrics **26**
Autosizer Hi-C, System **4700** **434**,
average diameters; **50**, *means* **50**, *medians* **53**
AWK electronic sieve analyzer **371**
Bahco microparticle classifier **200**
balances; **311**, *Sartorius* **311**, *Cahn* **312**
Bausch & Lomb; **147** *ruled stage graticule* **137**
BCR powders **455**, **479**
BI-DCP disc (photo)centrifuge **317**
bimodal distributions;
intersecting log-normal **89**,
intersecting **93**, *non-intersecting* **93**
BIRAL PD-Lisatek **375**
Blaine permeability method **404**
Boeckeler **138**
Boltzmann constant **229**, **261**

- Bristol Industrial Research 372
 British Standard graticule 119,
 122
 Brookhaven; *disc*
 photocentrifuge. 321, *BI-90*,
 BI-200SM, *ZetaPlus* 433, *BI-*
 Foqels, 434
 Brownian motion 228, 229, 427
 Buehler 138
 buffer layer 320
 bulk density 452
 buoyant force 225
 β-ray attenuation 396
- Cahn; *micro-balance* 312,
 sedimentation balance 252
 calibration; 118, 339, 417, of
 image analyzers 128, of sieves
 167
 Carty Vision System 371
 capacitors 467
 capillary; *method* 382,
 hydrodynamic fractionation
 206, *zone electrophoresis* 207
 carbon films 143
 Carl Zeiss 140
 Carman-Kozeny 403
 Carr-Brion 397
 cascadograph 18
 catalyst 476
 cement 404
 centrifugal; *classification* 200,
 pyknometer 270, *sedimentation*
 283
 centrifuges; *Ladal pipette disc*
 295, *Horiba cuvet photo*, 312,
 long arm 313, *Brookhaven*
 scanning x-ray disc 315,
 Brookhaven disc
 photocentrifuge 321, *Seishin*
 412
 ceramic paste 467
 chemical analysis 145
 chromatography; *hydrodynamic*
 203, *size exclusion* 208
 chute splitter. 21, 22
 Cilas 412
- classification 93
 classifier efficiency 190
 classifiers; *grade efficiency* 191,
 192, *yield* 195, *counter-flow*,
 cross-flow 197, *gravitational*
 198, *centrifugal* 201, *Donaldson*
 Acucut laboratory 201, *zig-zag*
 202, *elbow* 204, *electrostatic*
 382
 Climet; 356, *elliptical mirror*
 system 352
 coarse grade efficiency 191
 coarse yield 194
 coater. 469
 coefficient of variation 103
 cohesion, work of 258
 coincidence. 335
 comminution 393, 475
 comparison tests 417
 Compic-Imaging System 138
 concentration effects; 246, 429,
 low 251, *high* 252, *monitors*
 441
 condensation particle counter
 386
 coning and quartering 7, 20
 constant volume sampler. 16
 contact angle 259
 contaminants 450
 Contamination Control Systems
 373
 controlled reference method 432
 correlation techniques 404
 Coulter; 455 *Counter* 137, *LS100*,
 principle 263, 327, 329, 350,
 Model N4 434
 counter-flow classifiers 398
 Courier 300 394
 Cross's slotted pipe slurry
 sampler. 25
 Cross-flow; *separation* 197,
 gravitational classification 200,
 centrifugal classifiers 202,
 elbow classifier 202, 204
 cross-sectional sampler 13
 crystal growth 417

- cumulative, homogeneous;
 centrifugal sedimentation 287,
 gravitational sedimentation 281
 curve fitting 94
 cuvet; 317, *photocentrifuge* 320
 Cyclosensor 400
- Dage-MTI camera model 70 137
 Dante 367
 Data Translation 139
 data interpretation 96
 Dawn 426, 435
 deagglomerating 260
 decantation 216
 density; distribution functions 82
 effective, true, apparent 269
 derived mean sizes 77
 diameter, Stokes 46, Feret 47,
 statistical 47, unrolled 47, Feret,
 Martins 49 Martin's 118,
 projected area 118, Feret 118,
 dielectric; 467, 468, *sensors* 323
 Differential mobility analyzer
 (DMA) 384
 diffraction gratings 141
 diffusion wave spectroscopy 436
 disc; *centrifugation* 203,
photocentrifuge 320
 discontinuity of the fluid 235
 dispersing; *agents* 257 *quality*
 262
 dispersion; *particle* 54, *dry*
powder 255, *wet powder* 256
 dispersions 378
 distributions; *bimodal*
intersecting log-normal, 89,
bimodal intersecting 93,
trimodal non-intersecting log-
normal 91, *bimodal non-*
intersecting 93, *means of* 101
 divers 309
 diverter valve sampler 18
 Donaldson Acucut laboratory
classifier. 201
 Doppler principle 372
 Dow Chemicals 141
- drag; *coefficient* 226, 242, *factor*
 223, 300, *force* 225
 drops in dispersions 381
 dry powder dispersion 255
 Du Pont/Brookhaven scanning x-
 ray disc centrifugal
 sedimentometer 315
 Du Pont; *SFFF* 210, */Brookhaven*
scanning x-ray disc centrifugal
sedimentometer 315, *electrolytic*
grain size analyzer 383
 dual beam interferometer 380
 Duke Scientific, 14
 Dynacount 354
 dynamic light scattering 426
- edit 336
 effective density 269
 electro-viscosity 254
 electroformed micromesh sieves
 159
 electrostatic classifier 386
 elutriator 399
 elutriators 198, 395
 Elzone 350
 emulsions 425
 enhanced electrostatic
 chromatography. 205
 Erdco Acoustical Counter 368
 errors 144
 external gradient method 320
 extinction coefficient 278, 306
 extinction optical particle
 counters 353
- Faley Status 369
 felvation 183
 Feret diameter 47, 49, 118
 Fffractionation 213
 fiber; 133, *length* 349,
magnetically aligned 349
 field flow fractionation; 203, 208,
sedimentation 458
 film additives 454
 filter efficiency 461
 fine grade efficiency 191,
 fine yield 194

- fixed position pipette 305
 flaky particles 334
 Flow Sizer 5600 205
 flow ultramicroscope 380
 flowability 256, 469
 Flowvision 360, 249
 fluidization 470
 focused 336
 force field programming 211
 form and proportions. 56
 Fourier analysis 58
 fractal; dimension 59, 130
 geometry, 59, 133
 fractionation; 202, capillary
 hydrodynamic 206, field flow
 208, sedimentation field flow
 209, 458, delayed exponential
 SFFF 211, magnetic field flow
 213, steric field flow 214
 fractogram 211, 212
 Fraunhofer theory 405
 Fritsch Analysette 22 412
 Full Range Analyzer, 414
 full-stream trough sampler. 15
- Galai CIS 363
 Gallenkamp; balance 311,
 Gallie-Porritt apparatus 178
 gas flow permeametry 403
 Gates-Gaudin-Schumann 101
 Genias™ particle sizing software
 133
 Gilson GA-6 Autosiever 180
 Glen Creston rotary divider 23
 glidants 256
 Global Lab Image 139
 globe and circle graticules 120
 golden rules of sampling 4
 grade efficiency 191, 192
 Grader 181
 Granumeter, 312
 graticule; linear eyepiece 118,
 British Standard 119, globe
 and circle 120, Bausch & Lomb
 ruled stage 137
 gravitational; elutriators 198,
 force 225
- gravity photosedimentation 277
 gray level shading 130
 gross sample 2
- Hamamatsu 139
 hand sieving 172
 Hawksley & Sons, 329
 Hiac PA 720 137
 Hiac/Royco 329, 354
 high concentration effects 252
 hindered settling 251
 Hitech Olympus Cue-3 139
 homogeneity 467
 homogeneous; mode 285,
 cumulative gravitationa
 lsedimentation 281, cumulative,
 centrifugal technique 284
 incremental centrifugal
 sedimentation 289
 Horiba; cuvet photo(centri)fuge
 312, 413
 Hosokawa Mikropul;
 Sedimentputer 318, E-Spart
 Analyzer 375
 Humboldt particle size analyzer
 TDS 201
 hydrocyclones 399
 hydrodynamic; chromatography
 203, focusing 336
 hydrometers; 275, and divers 309
 hyperbolic scan 231
- image, three dimensional 137
 in situ sensors 352
 incremental; line-start,
 centrifugal technique 284,
 homogeneous, centrifugal
 sedimentation 289
 industrial diamonds 453
 Insitec EPICS 413, 436
 instrument evaluation 477
 Interferometers 378
 ISPA image analysis system 381
- Kane May 366
 Köhler illumination 121

Kowa; *Nanalyzer* 369, *Optimed Inc.*, 369
 Kratel; *Partascope* 355,
Partograph 355

Lab-Tec 362
 Labcon 182
 laboratory sample 2
 Ladal pipette centrifuge
 Ladal; *pipette disc centrifuge*,
 295, 314, *x-ray disc centrifuge*
 314

Lambert-Beer law 277
 laminar flow region 227
 Lasentec 362
 laser phase-Doppler principle
 374

law of compensating errors 88
 Leco 139
 Leeds and Northrup Microtrac
 413

Leica Quantimet 139
 LeMont Oasys 139, Scientific
 147

light blockage 352
 light pen 133
 limit of resolution 114
 line-start mode , 285, 320
 linear eyepiece graticules 118
 log-normal distribution 72
 London-van der Waals force 261
 long arm centrifuges 313
 low angle laser light scattering
 404, *instruments* 406
 low concentration effects 251
 lower size limit 114, 229
 Lumosed 308

Mach Zehnder 379
 machine sieving 175
 Macintosh 138
 macroviewer 129
 Magiscan image analyzer 133
 magnetic field flow fractionation
 213
 magnetic suspensions 263
 magnetically aligned fibers 349

Malvern
 Malvern
 Malvern; *Autocounters* 370, *Full Range Analyzer* 409,
Mastersizer 415, *Autosizer Hi-C, System* 4700 434, *Ultrafine Particle Analyzer Model* 9230 435

Martin
 Martin's diameter 47, 49, 118
 mass balance 339, 455
Mastersizer 415,
Matec 207, electroacoustic system 215

mean; 50, *diameters, definitions of* 53, *free path* 235
 means of distributions 101
 Measuremouse 138
 median 50
 membrane filter 350
 Met One 368
 Micro Pure Systems 368
 Micromeretics Flow Sizer 5600 205

Micromerograph, 312
 MicroPul 180, *Micron Washsieve* 178

microsample splitter 116
 Microscal suspension sampler 27
 Microscan 309
 microscope
microscope; optical 113, *training of operators* 120, *acoustic* 129, *examination* 263, *transmission electron* 141, *scanning electron* 146, *scanning tunneling electron* 148

microscopy 46
 Microsoft 139
 Microtrac Analyzer, *Full Range, Standard Range, Ultrafine Particle*, 413, *Small Particle* 462

Mie theory 350
 Millipore pMC System 139
 Mintex 397
 Mintex/RSM slurry sizer 392

miscellaneous sampling devices 23
 mixing; 466, *mixing and segregation* 472
 mode 50
 Monitek 368 441
 morphology 112
 moving flap sampler 17
 MSA Particle Size Analyzer 313, 322
 multiple aperture method 338
 Myplex® 453

Nachet 139
 Nicomp Model 270 435
 Nitto 415
 non-ionic fluoroochemical surfactents 263
 non-rigid spheres 236
 non-spherical particles 237, 405
 normal law 69
 normal probability function 34
 number count 122
 number of samples required 28

Omega 139
 Omnimet 138
 Oncor 139
 on-line; *measurement* 398, *installation* 4148
 optical density 278
 optical incoherent space frequency analysis 419
 optical microscopy 113
 optical particle counters 350
 Optisizer 363
 Optoma 138, 139
 Optovar 133
 Osborne's rotating slot slurry sampler, sampling tank. 25
 oscillating hopper sample divider, 23
 oscillating paddle sample divider 23
 Otsuka Photol 435
 Outokumpu Imagist 140
 oversize particles 454

PAAR Lumosel 308
 paint pigments 50
 Par-Tec 363
 Particle Measuring Systems 358
 Particle Sizing Systems Accusizer 370
 particle size 428, particle; *morphology* 44, *size* 45, 117, 424, *diameters* 48, *dispersion* 54, *shape* 54, 334, *size effects* 428, *effects* 430
 Pascal turntable sample divider. 22
 Pen Kem System 7000
 Acoustopheretic Titrator 423
 perimeter 133
 permanent slides 116
 permeability 404
 phase Doppler method 327
 phi-notation 108
 photo-etching process 159
 photocentrifuge; 285, 454; *Horiba cuvet* 312, *cuvet* 317, *disc* 320
 photography 381
 photomask reticles 417
 photon correlation spectroscopy 426
 photosedimentation 263
 photosedimentation technique 306
 pipette method of Andreasen 304
 plane sections through packed beds 117
 PMT universal size distribution measuring systems 371
 point samplers 10
 polarization intensity differential scattering 412
 polydispersity 430
 Polytec HC 361
 porous particles 334
 porous wall hydrodynamic chromatography 205
 potential barrier chromatography, 206

- powder density 269
 Precision Transparent Sieves™ 341, 456
 primary coincidence. 335
 Proassist 421
 Procedyne 365
 Prodi instrument, 349
 projected area; 47, 118, diameter 49, shape coefficients 279
 PSM single point device 421
 PSS Accusizer 770 417
 pulse shape 334
 punched plate sieves 158
 pyknometry 269
- Quantimet, 128
 quantitative image analysis 128
 quasi-elastic light scattering 426
 Quickstep, 137
- replicas 145
 reproducibility, 484
 resolution of sedimenting suspensions 272
 resolving power 114
 Retsch; 182, *rotary sample divider* 21, *wet sieving machine* 176
 Reynolds number 223, 226, 242, 300
 Rion 369
 Roller 84
 Rosin-Rammler 83
 rotary sample divider 23; Retsch. 21
 roughness 59
 Ro-Tap' sieve shaker 402
 RSM slurry sizer 396
 rugosity 59
- sample; *reduction* 19, „*amount of* 172
 sampler for screw conveyor. 18
 sampling; *from falling streams* 1, *stored material* 4, *spear* 5, *from trucks and wagons* 5, *stored non-flowing material* 5, *spear*. 6, *stored free-flowing material*
flowing streams 8, *dusty material* 16, *from hopper*. 17
- Sartorius balance 311
 Scanning mobility particle sizer (SMPS) 385
 scanning; *electron microscopy* 146, *transmission electron microscope* 148, *tunneling electron microscope* 148, *x-ray centrifuge* 297
 scintillation method 382
 scoop sampling 19
 scoop suitable for sampling coal 9
- screw or drag conveyors 24
 secondary coincidence. 336
 Sedigraph 232, 308, 466
 sedimentation 338, *balance* 263, 312, *field flow fractionation* 209, 450, *balance* 263, *cumulative, homogeneous, gravitational* 281, *incremental, line-start, centrifugal* 284, *cumulative, homogeneous, centrifugal* 287, *incremental, homogeneous, centrifugal* 289
 sedimentation field flow fractionation 458
 Sedimentputer 318
 Seishin Robot Sifter 181, 416
 self organized sieves 184
 self-burrowing; *probes* 5, *sampler* 7
 shadowing techniques 145
 Shape separation 185
 shape; 334, 62, *factors* 56, 112, *coefficients* 55, 279, *regeneration* 58, *effect of (particle)* 99, *coefficients; projected area* 279, *surface* 279, *discrimination* 441
 Shakespeare Corporation's Juliet 140
 sharpness inde 193
 Shimadzu Sald 416
 side-wall sampling, 26

- sieves; *woven-wire and punched plate* 158, *electroformed micromesh* 159, *standard* 162, *warp, weft* 167, *calibration of* 167, *cascadograph* 182, *self organized* 184
 sieving 137, 338
 sieving machine; 159, *errors* 169, *hand* 172, *machine* 175, Retsch *wet* 176, *air-jet* 178, *ultrasonic* 182, *wet* 401
 size exclusion chromatography, 206, 208
 size limit; lower, upper 114, upper 228, lower 229
 slide valve sampler. 16
 slides, permanent, temporary 116
 sloping trough cutter. 24
 slurry sampling 24
 snorkel type point sampler. 10
 sonic sifter 180
 sorting by shape 62
 specific surface 62
 specimen preparation for TEM 142
 Spectrex Prototron 364
 sphericity 57
 spinning riffler 116
 spreading coefficient 258
 Standard Range Analyzer, 414
 standard deviations 102
 standard sieves 162
 starry night effect. 462
 static noise 395
 statistical diameter 47
 stereographic image 146
 steric exclusion 205
 steric field flow fractionation 214
 Stokes diameter 46
 stream sampling, cup 13
 strength of engineering plastics 467, *surface area* 279,
 surface; *texture* 130, *areas* 144, *shape coefficient* 279, *friction* 454
 surfactents, non-ionic
 fluoroochemical 263
 suspension sampler, Microscal 27
 suspension stability 260
 Svensson 59
 Sympatec; *Helos* 416, *Opus* 425
 table sampling 20
 temporary slide 116
 terminal velocity 227, 232
 test sample, 2
 texture; 59, *surface* 130
 textured particles 405
 thermal field flow fractionation 213
 thermal precipitation 144
 through dynamic light scattering 427
 time-delayed exponential SFFF 211
 tolerances 160, 163
 total fine efficiency 191
 Tracor Northern 140, 147
 transient turbidity 441
 transition region 240
 transmission electron microscopy 141
 traversing cutters 14
 true density 269
 TSI; *Aerodynamic Particle Sizer* 373, *Liquitrak™ interferometer* 379, *diffusional particle sizer* 381, *condensation particle counter, diffusion battery* 383, turbidity 439
 Turbo-Power Model TPO-400 439
 turbulent flow 245
 typical powder products. 451
 Ultrafine Particle Analyzer, 410, 435
 ultrasonic attenuation. 395, 420
 ultrasonic sieving 182
 ultrasonics 161
 Ultraspec 422
 unrolled diameter 47
 upper size limit 114, 228

- variable height pipette 305
variable time method 290
vertical pipe cutter. 24
Vezin samplers. 14
Vibrosonic sieves 182
Video Image Marker 138
video tape 461
viscosity; 271, *of a suspension*
 236
volumetric sensors 352
Von Alfthan 398
- Wadell's sphericity factor. 241
wall effects 234
Warmain Cyclosizer 200
warp 167
weft, 167
weight of sample 38
weight size determination 124
- Werner and Travis methods 312
wet powder dispersion 256
wet sieving 176
wide angle scanning
 photosedimentometer 308
work; *of adhesion, of cohesion*
 258
woven-wire sieves 158
Wyatt Technology 435
- x-ray attenuation and
 fluorescence 396
x-ray; *gravitational*
 sedimentation 281, *centrifugal*
 sedimentation 308
- Zeiss universal microscope 133
zig-zag classifiers 202